MARINE STRUCTURAL DESIGN

Functional requirements | Loads | Ultimate strength, Fatigue and frature | Structural reliability, Risk assessment

Limit-state design

$$R(f_k/y_m, \cdots,) > S(y_f Q_k)$$

Scantling ← Redesign

No

Final element evaluation

Yes

Finish

by
Yong Bai

MARINE STRUCTURAL DESIGN

MARINE STRUCTURAL DESIGN

YONG BAI

This Page Intentionally Left Blank

PREFACE

This book is written for marine structural engineers and naval architects, as well as mechanical engineers and civil engineers who work on structural design. The preparation of the book is motivated by extensive use of the finite element analysis and dynamic/fatigue analysis, fast paced advances in computer and information technology, and application of risk and reliability methods. As the professor of offshore structures at Stavanger University College, I developed this book for my teaching course TE 6076 "Offshore Structures" and TE6541 "Risk and Reliability Analysis of Offshore Structures" for M.Sc and Ph.D. students. This book has also been used in IBC/Clarion industry training courses on design and construction of floating production systems for engineers in the oil/gas industry.

As reliability-based limit-state design becomes popular in structural engineering, this book may also be a reference for structural engineers in other disciplines, such as buildings, bridges and spacecraft.

My former supervisors should be thanked for their guidance and inspiration. These include: Executive Vice President Dr. Donald Liu at American Bureau of Shipping (ABS), Professor Torgeir Moan at Norwegian University of Science and Technology (NTNU), Professor Robert Bea and Professor Alaa Mansour at University of California at Berkeley, Prof. Preben Terndrup Pedersen at Technical University of Denmark, Professor T. Yao at Osaka University and Professor M. Fujikubo at Hiroshima University. The friendship and technical advice from these great scientists and engineers have been very important for me to develop materials used in this book.

As manager of advanced engineering department at JP Kenny Norway office (now a section of ABB) and manager of offshore technology department at the American Bureau of Shipping, I was given opportunities to meet many industry leaders in oil companies, design/consulting offices, classification societies and contractors. From ISSC, IBC, SNAME, OMAE, ISOPE and OTC conferences and industry (ISO/API/Deepstar) committees, I learned about the recent developments in industry applications and research.

The collaboration with Dr. Ruxin Song and Dr. Tao Xu for a long period of time has been helpful to develop research activities on structural reliability and fatigue respectively. Sections of this book relating to extreme response, buckling of tubular members, FPSO hull girder strength and reliability were based on my SNAME, OMAE and ISOPE papers co-authored with Professors Preben Terndrup Pedersen and T. Yao and Drs. Yung Shin, C.T. Zhao and H.H. Sun.

Dr. Qiang Bai and Ph.D. student Gang Dong provided assistance to format the manuscript.

Professor Rameswar Bhattacharyya, Elsevier's Publishing Editor James Sullivan and Publisher Nick Pinfield and Senior Vice President James Card of ABS provided me continued encouragement in completing this book.

I appreciate my wife Hua Peng and children, Lihua and Carl, for creating an environment in which it has been possible to continue to write this book for more than 5 years in different culture and working environments.

I wish to thank all of the organizations and individuals mentioned in the above (and many friends and authors who were not mentioned) for their support and encouragement.

Yong BAI

Houston, USA

TABLE OF CONTENTS

Part II: Ultimate Strength

Part III: Fatigue and Fracture

Part IV: Structural Reliability

Part V: Risk Assessment

This Page Intentionally Left Blank

Part I: Structural Design Principles

This Page Intentionally Left Blank

Part I

Structural Design Principles

Chapter 1   Introduction

1.1   Structural Design Principles

1.1.1   Introduction

This book is devoted to the modern theory for design and analysis of marine structures. The term "marine structures" refers to ship and offshore structures. The objective of this book is to summarize the latest developments of design codes, engineering practice and research into the form of a book, focusing on applications of finite element analysis and risk/reliability methods.

The calculation of wave loads and load combinations is the first step in marine structural design. For structural design and analysis, a structural engineer needs to have basic concepts of waves, motions and design loads. Extreme value analysis for dynamic systems is another area that has gained substantial developments in the last decades. It is an important subject for the determination of the design values for motions and strength analysis of floating structures, risers, mooring systems and tendons for tension leg platforms.

Once the functional requirements and loads are determined, an initial scantling may be sized based on formulae and charts in classification rules and design codes. The basic scantling of the structural components is initially determined based on stress analysis of beams, plates and shells under hydrostatic pressure, bending and concentrated loads. Three levels of marine structural design have been developed:

- Level 1: Design by rules
- Level 2: Design by analysis
- Level 3: Design based on performance standards

Until the 1970's, structural design rules had been based on the design by rules approach using experience expressed in tables and formula. These formulae-based rules were followed by direct calculations of hydrodynamic loads and finite element stress analysis. The Finite Element Methods (FEM) have now been extensively developed and applied for the design of ship and offshore structures. Structural analysis based on FEM has provided results, which enable designers to optimize structural design. The design by analysis approach is now applied throughout the design process.

The finite element analysis has been very popular for strength and fatigue analysis of marine structures. In the structural design process, the dimensions and sizing of the structure are

strengthened, and structural analysis re-conducted until the strength and fatigue requirements are met. The use of FEM technology has been supported by the fast development of computer and information technology. Information technology is widely used in structural analysis, data collection, processing, and interpretation, as well as in the design, operation, and maintenance of ship and offshore structures. The development of computer and information technology has made it possible to conduct a complex structural analysis and process the analysis results. To aid the FEM based design, various types of computer based tools have been developed, such as CAD (Computer Aided Design) for scantling, CAE (Computer Aided Engineering) for structural design and analysis and CAM (Computer Aided Manufacturing) for fabrication.

Structural design may also be conducted based on performance requirements such as design for accidental loads, where managing risks is of importance.

1.1.2   Limit-State Design

In a limit-state design, the design of structures is checked for all groups of limit-states to ensure that the safety margin between the maximum likely loads and the weakest possible resistance of the structure is large enough and that fatigue damage is tolerable.

Based on the first principles, limit-state design criteria cover various failure modes such as:

- Serviceability limit-state
- Ultimate limit-state (including buckling/collapse and fracture)
- Fatigue limit-State
- Accidental limit-state (progressive collapse limit-state)

Each failure mode may be controlled by a set of design criteria. Limit-state design criteria are developed based on ultimate strength and fatigue analysis as well as use of the risk/reliability methods.

The design criteria have traditionally been expressed in the format of Working Stress Design (WSD) (or Allowable Stress Design, ASD), where only one safety factor is used to define the allowable limit. However, in recent years, there is an increased use of the Load and Resistance Factored Design (LRFD), that comprises of a number of load factors and resistance factors reflecting the uncertainties and safety requirements.

A general safety format for LRFD design may be expressed as:

$$S_d \leq R_d \tag{1.1}$$

where,

S_d $= \sum S_k \cdot \gamma_f,$ Design load effect

R_d $= \sum R_k / \gamma_m,$ Design resistance (capacity)

S_k $=$ Characteristic load effect

R_k $=$ Characteristic resistance

γ_f $=$ Load factor, reflecting the uncertainty in load

γ_m $=$ material factor $=$ the inverse of the resistance factor

Figure 1.1 illustrates use of the load and resistance factors where only one load factor and one material factor are used in the illustration for the sake of simplicity. To account for the

uncertainties in strength parameters, the design resistance R_d is defined as characteristic resistance R_k divided by the material factor γ_m. On the other hand, the characteristic load effect S_k is scaled up by multiplying a load factor γ_f.

The values of the load factor γ_f and material factor γ_m are defined in design codes. They have been calibrated against the working stress design criteria and the inherent safety levels in the design codes. The calibration may be conducted using structural reliability methods that allow us to correlate the reliability levels in the LRFD criteria with the WSD criteria and to assure the reliability levels will be higher or equal to the target reliability. An advantage of the LRFD approach is its simplicity (in comparison with direct use of the structural reliability methods) while it accounts for the uncertainties in loads and structural capacities based on structural reliability methods. The LRFD is also called partial safety factor design.

While the partial safety factors are calibrated using the structural reliability methods, the failure consequence may also be accounted for through selection of the target reliability level. When the failure consequence is higher, the safety factors should also be higher. Use of the LRFD criteria may provide unified safety levels for the whole structures or a group of the structures that are designed according to the same code.
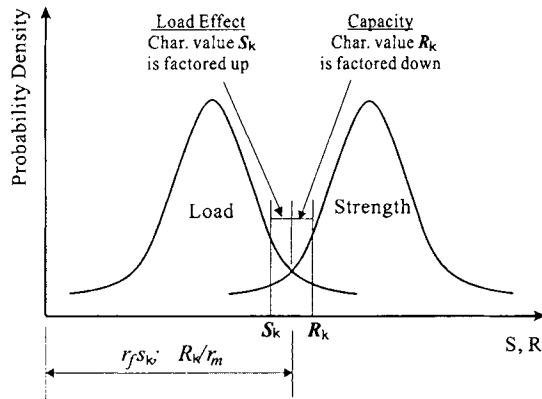
Figure 1.1   Use of Load and Resistance Factores for Strength Design

1.2   Strength and Fatigue Analysis

Major factors that should be considered in marine structural design include:

- Still-water and wave loads, and their possible combinations

- Ultimate strength of structural components and systems

- Fatigue/fracture in critical structural details.

Knowledge of hydrodynamics, buckling/collapse, and fatigue/fracture is the key to understanding structural engineering.

1.2.1   Ultimate Strength Criteria

Ultimate strength criteria are usually advocated in design codes for various basic types of the structural components such as:

- columns & beam-columns

- plates and stiffened panels

- shells and stiffened shells

- structural connections

- hull girders

An illustration of the Euler buckling strength is given in Figure 1.2 for pinned columns under compression. Due to combination of axial compression and initial deflection, the column may buckle when the axial compression approaches its critical value,

$$P_{CR} = \frac{\pi^2 EI}{l^2}$$
(1.2)

where l and EI are column length and sectional bending rigidity respectively. Due to buckling, the lateral deflection δ will increase rapidly.

Initiation of yielding usually occurs in the most loaded portion of the structural members. As the yielding portion spreads, the bending rigidity of the structural component decreases and hence buckling is attained. For structural members other than un-stiffened thin-walled shells, ultimate strength is reached when inelastic buckling occurs.

The design of components in ship and offshore structures is mainly based on relevant classification rules and API and ISO codes. The classification rules are applicable to ocean-going ships, mobile offshore drilling units (MODU) and floating structures. For offshore structural design, however, API and ISO codes are more frequently applied.
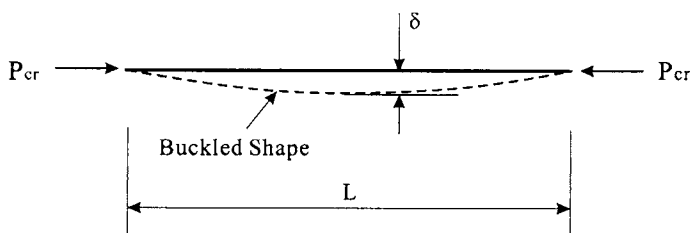
Figure 1.2   Buckling of Pinned Columns

It should be pointed out that final fracture is also part of the ultimate strength analysis. The assessment of final fracture has been mainly based on fracture mechanics criteria in British standard PD6493 (or BS7910) and American Petroleum Institute code API 579. In fact there is a similarity between buckling strength analysis and fracture strength analysis, as compared in the table below:

Table 1.1 Comparison of Buckling Strength Analysis and Fracture Strength Analysis

	Buckling Strength	Fracture Strength
Loads	Compressive/shear force	Tensile loads
Imperfection	Geometrical and residual stress due to welding etc.	Defects due to fabrication and fatigue loads
Linear Solution	Elastic buckling	Linear fracture mechanics
Design criteria	Curve fitting of theoretical equations to test results	Curve fitting of theoretical equations to test results

In general, the strength criteria for code development may be derived using the following approaches:

- to derive analytical equations based on plasticity, elasticity and theory of elastic stability,
- to conduct nonlinear finite element analysis of component strength,
- to collect results of mechanical tests,
- to compare the analytical equations with the results of finite element analysis and mechanical testing,
- to modify the analytical equations based on finite element results,
- to finalize the upgraded formulations through comparisons with numerical and mechanical tests,
- to further calibrate the derived strength equations on design projects.

From the above discussions, it is clear the theoretical knowledge and practical design experience are vital for the successful development of ultimate strength criteria.

As an alternative to criteria in rules and codes, mechanical testing and finite element analysis may be applied to determine the ultimate strength of structural components. For simple components, the prediction of finite element analysis and rule criteria is usually close to the results of mechanical testing. Hence, mechanical testing is now mainly applied to subjects on which less experience and knowledge have been accumulated.

Subjects that warrant future research on ultimate strength analysis include, e.g.

- development of strength equations for combined loads
- calibration of partial safety factors using risk assessment and structural reliability analysis
- standardization of the finite element models and benchmark of the models
- development of procedures for the determination of partial safety factors for finite element analysis and strength design based on testing

1.2.2 Design for Accidental Loads

The accidental loads that should be considered in the design of ship and offshore structures are e.g.:

- Ship collision and impacts from dropped objects offshore
- Ship grounding
- Fire/explosion
- Freak waves

The term "accidental loads" refers to unexpected loads that may result in a catastrophe causing negative economical, environmental, material consequences and the loss of human life. Extreme and accidental loads differ in the sense that the magnitude and frequency of the extreme loads can be influenced to a small extent by the structural design, whereas active controls may influence both the frequency and the magnitude of accidental loads.

The design for accidental loads includes determination of design loads based on risk consideration, prediction of structural response using rigid-plastic analytical formulation and/or non-linear FEM and selection of risk-based acceptance criteria. Traditionally rigid-plastic analytical formulation has been popular for design against accidental loads because large plastic deformation is usually the mechanism for energy absorption in accidents. In recent years, the nonlinear finite element analysis has been applied to simulate the structural behavior in accidental scenarios and to design the structure for the performance standards. Use of the finite element analysis enables us to deal with complex accidental scenarios and to better predict the structural response.

1.2.3 Design for Fatigue

Fatigue damage and defects may threaten integrity of the marine structures. This concern is aggravated as the cost of repair and loss of production increase. Fatigue design became an important subject due to use of higher strength materials, severe environmental conditions and optimized structural dimension. In recent years there is a rapid development in analysis technologies for predicting fatigue loading, cyclic stress, fatigue/fracture capacity and damage tolerance criteria. The fatigue capacities are evaluated using S-N curve approach or fracture mechanics approach. The S-N curves are established by stress controlled fatigue tests and may generally be expressed as:

$$N = K \cdot S^{-m} \tag{1.3}$$

where:

N = Number of cycles to failure

S = Stress range

m, K = Material constants depending on the environment, test conditions, etc.

The S-N curve approach is mainly applied in the design for fatigue strength, and it consists of two key components: determination of hot-spot stress and selection of appropriate S-N curves. A bi-linear S-N curve is shown in Figure 1.3 where on a log-log scale the x-axis and y-axis are number of cycles to failure and stress range respectively. The slope of the curve changes from m to r where the number of cycles is N_R ($= 5 \cdot 10^6$ for steel).

Discrepancy has been observed between the hot-spot stresses predicted by different analysts or in different analyses. It is therefore important to derive an optimum procedure and standardize the analysis procedure as part of the rules/code development. In recent years, there has been a rapid development in the standardization of the S-N curves. In this aspect, International Institute of Welding (IIW) has published a couple of new guidance documents on the selection

of S-N curves and the determination of hot-spot stress. In the IIW code, the S-N curves are named according to their reference stress range $\Delta\sigma_R$ that corresponds to $2 \cdot 10^6$ cycles.
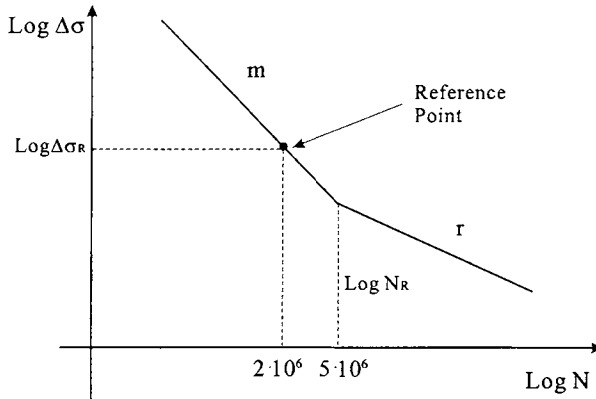
Figure 1.3   S-N Curves for Fatigue Assessment

With the increasing use of finite element analysis, a design approach based on the hot-spot stress will be more and more popular. The fatigue uncertainties are due to several factors such as

- selection of environmental conditions such as sea-states and their combinations

- extrapolation of fatigue stresses in the hot spot points

- selection of design codes such as the S-N curves and the stress calculations

- combination of wave-induced fatigue with the fatigue damages due to vortex-induced vibrations and installation

- selection of safety factors and inspection/repair methods

The accumulative fatigue damage for a structural connection over its life-cycle is usually estimated using Miners rule, summing up the damage due to individual stress range blocks.

$$D = \sum \frac{n_i}{N_i} \leq D_{allow} \tag{1.4}$$

where n_i and N_i denote the number of stress cycles in stress block i, and the number of cycles until failure at the i-th constant amplitude stress range block. D_{allow} is the allowable limit that is defined in design codes.

A simplified fatigue analysis may be conducted assuming stress ranges follow Weibull distribution. This kind of analysis has been widely applied in classification rules for fatigue assessment of ship structures. The Weibull parameters for stress distribution have been calibrated against in-service fatigue data for ships and more refined fatigue analysis. The value of the Weibull parameters may be found from classification rules, as a function of ship length and locations of interests. Alternatively, in offshore design codes API RP2A, a simplified fatigue analysis is proposed assuming the wave height follows Weibull distributions. The

Weibull parameter for wave heights may be found from API RP2A for Gulf of Mexico offshore.

There are three approaches for predicting accumulated fatigue damages accounting for wave scatter diagrams, namely:

- Frequency-domain (e.g. spectral fatigue analysis based on Rayleigh model or bi-model)

- Time-domain (which could account for non-linearities and contact/friction due to soil-structure interactions)

- A mixture of frequency-domain and time-domain approaches (e.g. use stress range spectrum from frequency-domain fatigue analysis and rain-flow counting approach to sum up the fatigue damages due to individual sea-states).

As an alternative to the S-N curve approach, fracture mechanics has now been used for evaluation of the remaining strength of cracked structural connections and in planning inspections of welded connections. There is an approximate linear relationship between the crack growth rate and ΔK on a log-log scale. This is generally characterized by the Paris equation:

$$\frac{da}{dN} = C(\Delta K)^m \tag{1.5}$$

where

$$\Delta K = K_{max} - K_{min} \tag{1.6}$$

K_{max} and K_{min} are the maximum and minimum values of the stress intensity factor, at the upper and lower limit stresses during a cyclic loading. The values of material properties C and m may be found from design codes for typical materials used in marine structures and other types of steel structures. The stress intensity factors may be available from handbooks for simplified structural and defect geometry's and loads.

1.3   Structural Reliability Applications

1.3.1   Structural Reliability Concepts

Component reliability concerns the failure probability modeled by a single limit-state function. It is a fundamental part of the structural reliability analysis since all marine structures are composed of their components.

The concept of structural reliability is illustrated in Figure 1.4, where load and strength are both modeled as random variables. Failure occurs when load exceeds strength. Denoting the probability density function for load and strength as $F_S(x)$ and $F_R(x)$ respectively, the failure probability may then be expressed as:

$$P_f = P(S \geq R) = \int_0^\infty F_S(x)F_R(x)dx \tag{1.7}$$
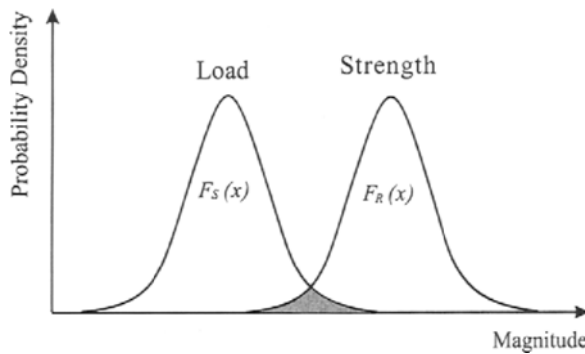
Figure 1.4   Structural Reliability Concepts

System reliability deals with the evaluation of failure probability where more than one limit-state function must be considered. There are two types of basic systems: series systems and parallel systems. A system is called a series system if it is in a state of failure whenever any of its elements fails. Such systems are often referred to as weakest-link systems. A typical example of this is marine pipelines and risers. A parallel system fails only when all of its elements fail.

Structural reliability analysis has been used to determine load combinations, derive design criteria, and plan in-service inspection.

The life-cycle cost of a marine structure consists of:

• Initial investment relating to the steel weight and manufacturing process

• Maintenance cost

• Loss caused by damage or failure – a risk resulted expenditure

Degradation or failure of a structural system may lead to a reduction/shut-down of the operation and loss/damage of the structure. The owner and the builder want a structure with a low initial cost, the highest possible operating margin, and an extendable operating period. A life-cycle cost model, based on probabilistic economics may be a useful tool to improve the design analysis, inspection, and maintenance.

This is further illustrated in Figure 1.5 where the total cost is the sum of the initial investment and maintenance cost plus the loss caused by structural damage/failure. The relationship between the reliability and cost is shown in this figure. A target reliability level may then be estimated based on cost optimization, if it is higher than the value required by legislative requirements.
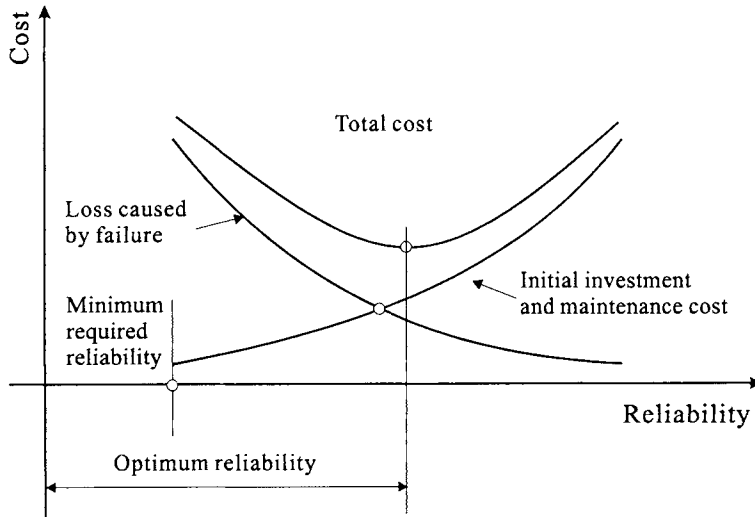
Figure 1.5   Target Reliability and Minimization of Life Cycle Cost

1.3.2   Reliability-Based Calibration of Design Factor

One of the structural reliability applications is the calibration of safety factors for structural design. The calibration process may help achieve a consistent safety level. The safety factors are determined so that the calibrated failure probability for various conditions is as close to the target safety level as possible. The following steps should be taken when conducting a reliability-based code calibration:

- Step 1: Identify potential failure modes for the given design case

- Step 2: Define design equations

- Step 3: Form limit-state functions

- Step 4: Measure uncertainties involved with random variables of the limit-state functions

- Step 5: Estimate failure probability

- Step 6: Determine target safety level

- Step 7: Calibrate safety factors

- Step 8: Evaluate the design results

The load and resistance factors (or safety factors) in the design criteria may be calibrated using risk/reliability methods.

1.3.3   Re-qualification of Existing Structures

Re-qualification of existing ship and offshore structures is one of the very important subjects for structures in operation. The re-qualification is conducted when the design environmental conditions have been changed, the structure has degraded due to corrosion, fatigue and possible impact loads.

Corrosion resulted defects may significantly reduce ultimate strength and fatigue strength of the structures. Various mathematical models have been developed to predict the future corrosion development in structures such as pipelines, risers and plating. Various methods have been applied by the industry to measure the amount, locations and shape of the corrosion defects, as all these are crucially important for strength and fatigue assessment.

In many cases, the use of nonlinear analysis of loads and structural response and risk/reliability methods is required to fully utilize the design margins. The re-qualification may be conducted using the strength and fatigue formulations, and the risk/reliability methods discussed in this book.

1.4 Risk Assessment

1.4.1 Application of Risk Assessment

Risk assessment and management of safety, health and environment protection (HSE) became an important part of the design and construction activities.

Use of risk assessment in the offshore industry dates back to the second half of the 1970s when a few pioneer projects were conducted, with an objective to develop analysis methodologies and collect incident data. At that time, the methodologies and the data employed, were those used for some years by the nuclear power industry and chemical industry.

The next step in the risk assessment development came in 1981 when the Norwegian Petroleum Directorate issued their guidelines for safety evaluation. These guidelines required that a quantitative risk assessment (QRA) be carried out for all new offshore installations in the conceptual design phase. Another significant step was the official inquiry led by Lord Cullen in the UK following the severe accident of the Piper Alpha platform in 1988. Lord Cullen recommended that QRAs be implemented into the UK legislation in the same way as in Norway nearly 10 years earlier.

In 1991, the Norwegian Petroleum Directorate replaced the guidelines for safety evaluation issued in 1981 with regulations for risk analysis. In 1992, the safety case regulation in the UK was finalized and the offshore industry in the UK took up risk assessments as part of the safety cases for their existing and new installations. In 1997 formal safety assessment was adopted by IMO as a tool to evaluate new safety regulations for the shipping industry.

1.4.2 Risk-Based Inspection (RBI)

Based on risk measures, the development of a system-level, risk-based inspection process involves the prioritization of systems, subsystems and elements, and development of an inspection strategy (i.e., the frequency, method, and scope/sample size). The process also includes making the decision about the maintenance and repair. The risk-based inspection method may also be applied for updating the inspection strategy for a given system, subsystem, or component/element, using inspection results.

The important features of the risk-based inspection method include:

- The use of a multidisciplinary, top-down approach that starts at the system level before focusing the inspection on the element levels;

- The use of a "living" process that is flexible, strives for completeness, and can be easily implemented;

- The use of qualitative and quantitative risk measures;

- The use of effective and efficient analytical methods, which provide results that are sound and familiar to inspection personnel.

A risk-based inspection approach may be developed based on evaluation of structural performance for fatigue/corrosion, fracture mechanics, corrosion engineering, structural reliability and risk assessment.

1.4.3   Human and Organization Factors

Statistics shows that over 80% of the failures are initially caused by the so-called human and organization factors. Figure 1.6 shows the interaction between the structure, human, organization and management system. Human behavior, organizational culture and management of HSE will all influence the structural safety.
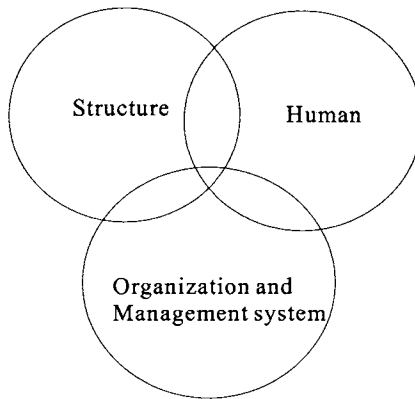
Figure 1.6   Human-Organization Factors (HOF) in Structural Safety

1.5   Layout of This Book

Risk-based limit-state design, combining probabilistic methods with FEM-based structural analysis, will be widely accepted and implemented by the industry for the cost-effective and safe design and operation of marine structures. The purpose of this book is to summarize these technological developments in order to promote advanced structural design. The emphasis on FEM, dynamic response, risk/reliability and information technology differentiates this book from existing ones.

Figure 1.7 illustrates the process of a structural design based on finite element analysis and risk/reliability methods.
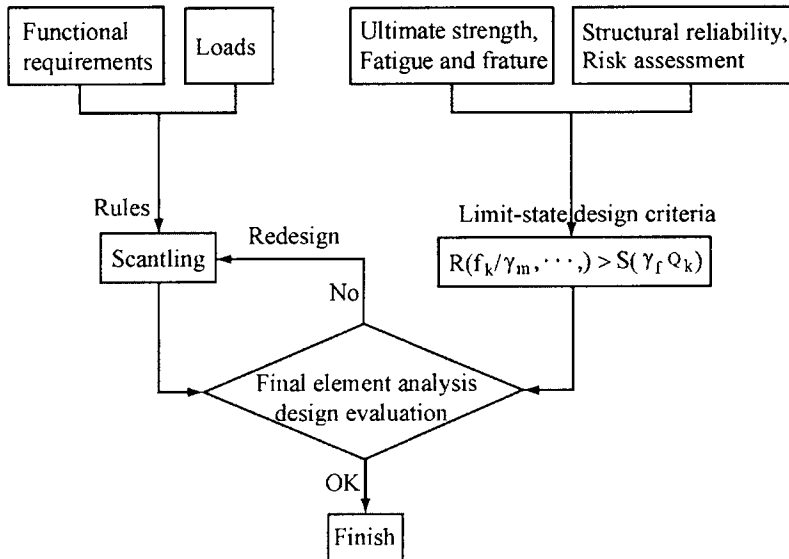
Figure 1.7   Modern Theory for Marine Structural Design

There are several well-known books on marine/offshore hydrodynamics, e.g. Bhattacharyya (1978), Sarpkaya and Isaacson (1981), Chakrabarti, (1987), Faltinsen (1990), CMPT (1998), Jensen (2001) and Coastal Engineering Manual (CEM, 2003). However, there is a lack of books on marine/offshore structural design, ultimate strength, fatigue assessment and risk/reliability analysis. In an integrated manner, the present book shall address modern theories for structural design/analysis, ultimate strength and fatigue criteria as well as the practical industry applications of the risk and reliability methods:

Part I - Structural Design Principles (Chaps. 1-7): summarizes the hydrodynamic loads for structural design of ship and offshore structures, and scantling of ship hulls. It also addresses the applications of the finite element technologies in marine structural design. The design by analysis procedure is also called the direct design method. Applications to practical design are discussed for ships, fixed platforms, FPSO, TLP, Spar and semi-submersibles.

Part II - Ultimate Strength (Chaps. 8-15): presents applications of buckling and plasticity theories, as well as nonlinear finite element formulations. The nonlinear finite element analysis may also be applied to the design of structures under accidental loads such as ship collisions, grounding, fires, and explosions.

Part III – Fatigue and Fracture (Chaps. 16-22): explains the fatigue mechanism, fatigue resistance, fatigue loads and stresses, simplified fatigue analysis, spectral fatigue analysis and fracture assessment. The basics of fatigue and fracture are provided for finite element analysts and structural engineers.

Part IV - Structural Reliability (Chaps. 23-28): provides simplified methods for the application of structural reliability theories for ships and offshore structures. Its objective is to explain complex theories in simplified terms. An outline of the analysis software and tools is given for readers to find references or more information.

Part V - Risk Assessment (Chaps. 29-34): summarizes recent industrial developments to facilitate the use of risk analysis when applied to measure and reduce risks in marine structures and their mechanical components. Risk analysis and human reliability are applied to justify and reduce risks to economy, the environment, and human life.

1.6   How to Use This Book

When this book was first drafted, the author's intention was to use it in teaching his course "Marine Structural Design (MSD)". However, the material presented in this book may be used for several M.Sc. or Ph.D. courses such as:

- Ship Structural Design,

- Design of Floating Production Systems,

- Ultimate Strength of Marine Structures,

- Fatigue and Fracture

- Risk and Reliability in Marine Structures.

This book addresses the marine and offshore applications of steel structures. In addition to the topics that are normally covered by civil engineering books on design of steel structures (e.g. Salmon and Johnson, 1995), this book also covers hydrodynamics, ship impacts and fatigue/fracture. Comparing with books on design of spacecraft structures (e.g. Sarafin, 1995), this book describes in greater details about applications of finite element methods and risk/reliability methods. Hence, it should also be of interests to engineers and researchers working on civil engineering (steel structures & coastal engineering) and spacecraft structures.

For more information on the use of risk/reliability-based limit-state design, reference is made to a separate book entitled "Pipelines and Risers" (Bai, 2001). Practical aspects for design and construction of floating production systems are addressed in Bai et al (2001).

1.7   References

1.   Bai, Y. (2001), *"Pipelines and Risers"*, Vol. 3 of the Elsevier Ocean Engineering Book Series, London, ISBN 0-08-043712-5.

2.   Bai, Y., Ayney, C., Huang, E., Maher, J., Parker, G., Song, R. and Wang, M. (2001), *"Design and Construction of Floating Production Systems"*, Course Notes for an Industry Training Course led by Yong Bai and Organised with Clarion Technical Conferences in Houston and IBC in London.

3.   Bhattacharyya, R (1978), *"Dynamics of Marine Vehicles"*, John Wiley & Sons, Inc.

4.   Chakrabarti, S.K., (1987), *"Hydrodynamics of Offshore Structures"*, Computational Mechanics Publications.

5. CMPT (1998), *"Floating Structures: A Guide for Design and Analysis"*, Edited by N. Baltrop, Oilfield Publications, Inc.

6. Faltinsen, O.M. (1990), *"Sea Loads on Ships and Offshore Structures"*, Cambridge Ocean Technology Series, Cambridge University Press.

7. Jensen, J. J. (2001), *"Load and Global Response of Ships"*, Elsevier Ocean Engineering Series, Vol.4.

8. Salmon, C.G. and Johnson, J.E. (1995), *"Steel Structures, Design and Behavior"*, 4th Edition, Harper Collins College Publishers.

9. Sarafin, T.P. (1995), *"Spacecraft Structures and Mechanism"*, Space Technology Series, Micrcosm & Kluwer Academic Publishers.

10. Sarpkaya, T and Isaacson, M (1981), *"Mechanics of Wave Forces on Offshore Structures"*, Van Nostrand Reinhold Co.

This Page Intentionally Left Blank

Part I

Structural Design Principles

Chapter 2   Wave Loads for Ship Design and Classification

2.1   Introduction

One of the major aspects of ship design is the calculation of wave-induced loads on the ship structure. The difficulty in calculating this load arises from the fact that the sea is highly irregular. Hence a number of techniques have been developed to tackle this problem. These techniques enable the sea waves be defined in a mathematical form and this may then be used to calculate the wave loads on the ship and ultimately the response of the ship to these loads.

When designing a ship, formulae provided by classification societies are used in order to calculate the wave loads and ship response. However, a ship designer ought to have some knowledge of the theory and techniques utilized for the statistical determination of wave loads. Novel ship designs also exist, which require an extensive statistical estimation of the wave loads to be undertaken in addition to using rule-based formulae alone.

As a basis for marine structural design, the objectives of this Chapter are threefold:

- Present various ocean wave spectra and wave statistics
- Discuss the wave-induced loads, slamming and green-water loads and hence the response of the ship
- Outline the design load calculations per ship classification rules.

For more information on wave loads acting on ship structures, reference is made to Bhattacharyya (1978), Hughes (1988) and Jensen (2001).

2.2   Ocean Waves and Wave Statistics

2.2.1   Basic Elements of Probability and Random Process

Obtaining ocean wave data requires the use of different elements of statistics and probability. Therefore, an introductory reference to statistics and probability is given prior to dealing with wave loads.

In statistics, a random variable X is an event or an outcome among all possible outcomes. If all possible outcomes form a continuous space, $-\infty < x < \infty$, and all events possible are a part of this space, then the probability density function of an event occurring is the probability that X lies within that portion of x. The probability density function is written as $p_x(x)$. Thus in Figure 2.1 the probability that X lies between x and x + dx, is $p_x(x)dx$. From this figure, we may also define the mean value μ_x as:

$$\mu_X = \int_{-\infty}^{\infty} x p_X(x) dx \qquad (2.1)$$

$$Var[X] = (\sigma_X)^2 = E\left[(X - \mu_X)^2\right] \qquad (2.2)$$

Another important aspect of statistics is the random process distribution, which describes the likelihood of occurrence of a random process. One of the most common random process distributions is the normal or Gaussian distribution. Typical examples of Gaussian distribution can be seen in Figure 2.2. One of the most important features of this Gaussian distribution is the fact that it may be described entirely in terms of two parameters: the mean value μ_X and variance σ_X^2.

The waves that make up a sea-state are normally described using two parameters, the significant wave height and the peak period. These two parameters follow a log-normal distribution which means that their natural logarithm $Z = \ln X$, follows a Gaussian distribution. The surface elevation at any point in the ocean is a random variable, which follows a Gaussian distribution with zero mean.
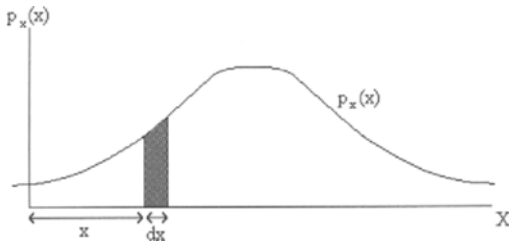
Figure 2.1   Probability Density Function
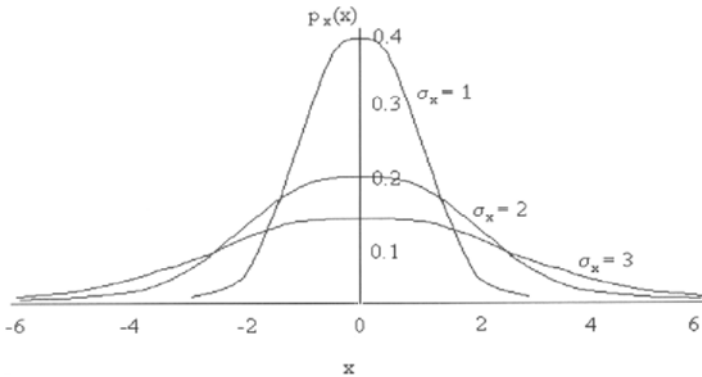
Figure 2.2   Gaussian Probability Density Function, (with $\sigma_x = 1$, 2, and 3, and with $\mu_x = 0$)

The parameters used to describe ocean waves are stochastic processes, which are continuous functions of time. Thus the measurements of the same parameter taken at different times could result in very dissimilar readings. The data regarding the parameters used to describe ocean waves, is collected by taking different samples over a period of time. For the validity of this data, it is essential to ensure that each sample is collected under similar conditions. In the case of ocean waves, a parameter such as sea elevation is influenced by a number of different variables, such as wind speed and wind direction. In order to be certain that these different variables remain relatively constant from sample to sample, the data is collected within a short observation period.

A random process is *stationary* if the statistical characteristics of the process do not change with time t. This means that the averages and moments of the stationary process are invariant over time. Ocean data is usually collected from samples spanning anywhere from 30 minutes to 3 hours, because during this period the data is considered stationary.

There are two different methods for defining averages of samples of a random process: the ensemble and the temporal. The ensemble average is the average taken over all of the samples at one instant in time. The temporal average is the average of a particular sample over time. In the case of random processes such as ocean waves, the time averages formed from a single sample over a given time interval are equal to the ensemble averages. This situation is known as an ergodic random process.

A random process may be characterized as a narrow-band or a wide-band process. In simple terms, a narrow-band process is made up of waves with frequencies lying within a narrow range, while a wide-band process consists of waves with widely varying frequencies. Ocean wave data shows that a fully developed, wind-generated, mid-ocean sea-state (i.e. with no growth or decay, and no coastal effects), is essentially narrow-banded. Of course, there are always wave components, which differ by having a high frequency, but these waves tend to be small in both height and length and have little effect on the ship. It is also interesting to note that a ship acts as a filter, only a narrow band of wave frequencies has an effect on the ship's motion and hull girder loads. Thus the ship's response is even more narrow-banded than the sea itself and this response is usually also characterized as a Gaussian and stationary process just like the ocean waves.

Chapter 24 of this book contains more information on random variable definitions.

2.2.2   Statistical Representation of the Sea Surface

This Section deals with the representation of a complete sea surface. Of course, we know that the sea surface is highly irregular and random under all sorts of conditions, calm or stormy weather. However, it has been found that this random process may be accurately represented by a series of different regular waves of varying heights, lengths, directions and phase that all superimposed on each other.

Three papers, which paved the way for further work on statistical representations of the sea surface, were published by Pierson (1952), St. Denis and Pierson (1953), and Pierson, Neumann, and James (1955). These papers proved that the sea surface could be represented by the superposition of a large number of regular sinusoidal waves of varying frequencies. A typical sinusoidal wave may be represented by the following:

$$\zeta(x,t) = a\sin(-kx - \omega t + \theta) \tag{2.3}$$

where,

a   = Wave amplitude

k   = $2\pi/\lambda$: wave number

λ = Wave length

ω = $2\pi/T$: wave ferquency

T   = Wave period

θ = Phase angle

Pierson, Neumann, and James (1955) also proposed that the surface elevation h(x,t) of an irregular sea could be represented as:

$$h(x,t) = \lim_{N \to \infty} \sum_{I=1}^{N} a_I \sin\left(-k_I x - \omega_I t + \theta_I\right)$$ (2.4)

A number of different procedures exist on to how to describe a sea surface. Jensen (2001) provides a detailed analysis for the description of surface waves.

2.2.3   Ocean Wave Spectra

A vast amount of data regarding ocean waves has been collected and measured throughout the years. This data is needed in order to define the sea-state where the ship is likely to sail. One of the most comprehensive collections of data regarding ocean waves was published by Hogben, Dacunha, and Olliver (1986). It tabulates the data from 104 ocean areas, known as Marsden areas, covering all major shipping routes.

The representation of the ocean data may be carried out in a number of different ways. Bretschneider (1959) proposed that the wave spectrum for a given sea-state could be described in terms of two parameters: the significant wave height (H_S) and the modal wave frequency (ω_M). The modal wave frequency is the peak frequency at which the wave spectrum's maximum height occurs. One of the most popular spectra in use is given by Pierson and Moskowitz (1964). This spectrum assumes a deep sea and a fully developed sea-state. For coastal waters, the Joint North Sea Wave Project (JONSWAP) spectrum is used as described by Hasselman (1973) and Ewing (1976).

Chakrabarti (1987) gave the mathematical descriptions for the various wave spectrums, such as

- Phillips
- Neumann Spectrum
- Pierson-Moskowitz Spectrum
- Bretschneider Spectrum
- ISSC Spectrum
- ITTC Spectrum
- Unified Form
- JONSWAP Spectrum
- Scott Spectrum
- Liu Spectrum

- Mitsuyasu Spectrum

- Ochi-Hubble Spectrum

The Pierson-Moskowitz (P-M) spectra for fully developed seas may be analytically expressed as:

$$S(\omega) = \frac{\alpha g^2}{\omega^5} \exp\left[-0.74\left(\frac{\omega V_w}{g} \right)^{-4} \right]$$ (2.5)

where,

$S(\omega)$ = spectral ordinate in $cm^2 sec$

g = acceleration of gravity in cm/sec^2

ω = frequency in radians/sec

$\alpha = 0.00810$

V_w = wind speed in cm/sec (19.5 m above the sea level)

The Bretschnerder spectrum is a two-parameter family that permits period and wave height to be assigned separately and has the form:

$$S(\omega) = 0.1687 H_s^2 \frac{\omega_s^4}{\omega^5} \exp\left[-0.675(\omega_s / \omega^4 \right]$$ (2.6)

where the two parameters A and B depend on the modal frequency ω_m and the variance, E.

$$\omega_s = \frac{2\pi}{T_S}$$ (2.7)

$$T_S = 0.946 T_0$$ (2.8)

where T_S and T_0 are significant wave period and peak period respectively. H_s is significant wave height. The JONSWAP spectrum can be written by modifying the P-M spectrum as:

$$S(\omega) = \frac{\alpha g^2}{\omega^5} \exp\left[-1.25(\omega / \omega_m)^{-4} \right] \gamma^{\exp\left[-\frac{(\omega - \omega_m)^2}{2\sigma^2 \omega_m^2} \right]}$$ (2.9)

where,

$\gamma = 3.3$

$\sigma = 0.07$ and 0.09 for $\omega < \omega_m$ and $\omega > \omega_m$ respectively

$\alpha = 0.076 \bar{x}^{-0.22}$

$$\omega_m = 2\pi \frac{3.5 \bar{x}^{-0.33} g}{V_{W10}}$$

V_{W10} = wind speed 10 m above the sea level

$$\bar{x} = \frac{gx}{V_{W10}^2}$$

x in the above equations denote fetch.

However, the Ochi 6-parameter spectrum provides a better method to represent all stages of development of a sea in a storm (Ochi, 1978). They start with a basic form as:

$$S(\omega) = \frac{\left(\frac{4\lambda+1}{4}\omega_m^4\right)^\lambda H_s^2}{4\Gamma(\lambda)\omega^{4\lambda+1}} \exp\left[-\frac{4\lambda+1}{4}(\omega_m/\omega)^4\right]$$ (2.10)

where $\Gamma(\lambda)$ is a gamma function and the parameter H_S is the significant wave height, λ is a shape parameter and the Ochi 6-parameter spectrum reduces to the Bretschnerder form when $\lambda = 1$. By adding two of these forms, Ochi (1978) obtained a six-parameter spectral form as:

$$S(\omega) = \sum_j \frac{\left(\frac{4\lambda_j+1}{4}\omega_{mj}^4\right)^{\lambda_j} H_{sj}^2}{4\Gamma(\lambda_j)\omega_j^{4\lambda_j+1}} \exp\left[-\frac{4\lambda_j+1}{4}(\omega_{mj}/\omega)^4\right]$$ (2.11)

where j =1, 2 stands for the lower- and higher-frequency components, respectively. The size parameters, H_{S1}, H_{S2}, ω_{m1}, ω_{m2}, λ_1 and λ_2 may be determined numerically to minimize the difference from a specific observed spectrum.

Figure 2.3 compares the Bretschneider wave spectrum with the JONSWAP wave spectra of various sharpness parameters (H_S and T_P are unchanged). Both Bretschneider and JONSWAP (γ=3.3) wave spectra are frequently used in the calculation of extreme values and fatigue damage.

Figure 2.4 shows the relationship between a time-domain solution of the waves (Eq. (2.3)) and the frequency-domain representation of the waves by a wave spectrum $S(\omega)$.

2.2.4   Moments of Spectral Density Function

The moments of a spectral density function $S(\omega)$ may be expressed as (Bhattacharyya, 1978),

$$m_n = \int_0^\infty \omega^n S(\omega) d\omega$$ (2.12)

where n is an integer. The zero moment, m_0, is the area under the energy density spectrum curve.

$$m_0 = \int_0^\infty S(f) df = \int_0^\infty S(\omega) d\omega$$ (2.13)

where f is the cyclic frequency, that is $2\pi\omega$. Hence the following relation may be derived.

$$S(f) = 2\pi\, S(\omega)$$ (2.14)

$$m_n(f) = \int_0^\infty f^n S(f) df = (2\pi)^{-n} m_n$$ (2.15)
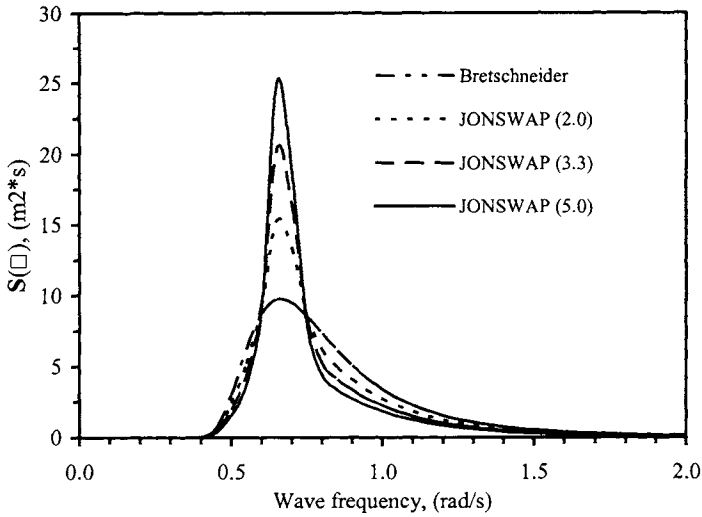
Figure 2.3 **Wave Spectral Density Functions** (H_S=8.5 m, T_P=9.5 sec, $m_0 \approx 4.4$)
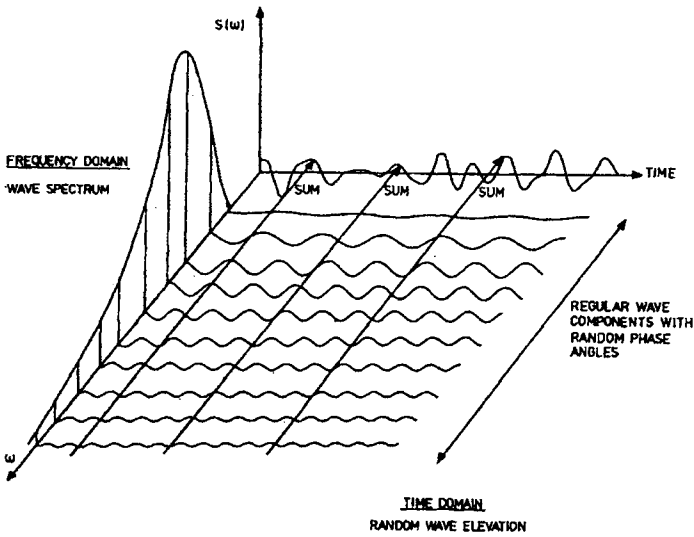
Figure 2.4 **Relations between Frequency-Domain and Time-Domain Representation of Waves in a Long-Crested Short Term Seastate (Faltinsen, 1990)**

2.2.5   Statistical Determination of Wave Heights and Periods

In the time-domain analysis, the significant wave height H_S is defined as the average height of the highest one-third of all waves, and it is also denoted as $H_{1/3}$.

$$H_{1/3} = \frac{1}{N/3} \sum_{i=1}^{N/3} H_i \tag{2.16}$$

where N is the number of individual wave heights and H_i is a series of wave height ranked from highest to lowest. In the frequency domain analysis, the significant wave height H_S is defined based on the zero moment, m_0, which is the area under the energy density spectrum curve.

$$H_S = 4\sqrt{m_0} \tag{2.17}$$

In the time-domain analysis, the root-mean-square (rms) wave height H_{rms} is defined as

$$H_{rms} = \sqrt{\frac{1}{N} \sum_{i=1}^{N} H_i^2} \tag{2.18}$$

In the frequency domain analysis, H_{rms} is defined as.

$$H_{rms} = 2\sqrt{2m_0} \tag{2.19}$$

In the time-domain analysis, the maximum wave height H_{max} is the largest value of the wave heights in a record. In the frequency domain analysis, the most probable maximum wave height H_{max} is defined by Longuet-Higgins (1952) for a narrow band of the wave spectrum as,

$$H_{max} = \left(\sqrt{\ln N} + \frac{0.2886}{\sqrt{\ln N}} \right) H_{rms} \tag{2.20}$$

In the time-domain analysis, the mean zero-upcrossing period $T_{0,2}$ is defined as the total length of time divided by the number of zero upcrossings in the record. The mean crest period $T_{0,1}$ is calculated as the total length of time divided by the number of crests in the record.

In the frequency domain analysis, the mean wave period is defined as

$$T_{0,1} = 2\pi \frac{m_0}{m_1} \tag{2.21}$$

$$T_{0,2} = 2\pi \sqrt{\frac{m_0}{m_2}} \tag{2.22}$$

2.3   Ship Response to a Random Sea

2.3.1   Introduction

The six degrees of freedom motions of ships nd floating systems are illustrated in Figure 2.5.

HEAVE
Y

YAW

SURGE
(C.G.) X
ROLL

PITCH

Z
SWAY
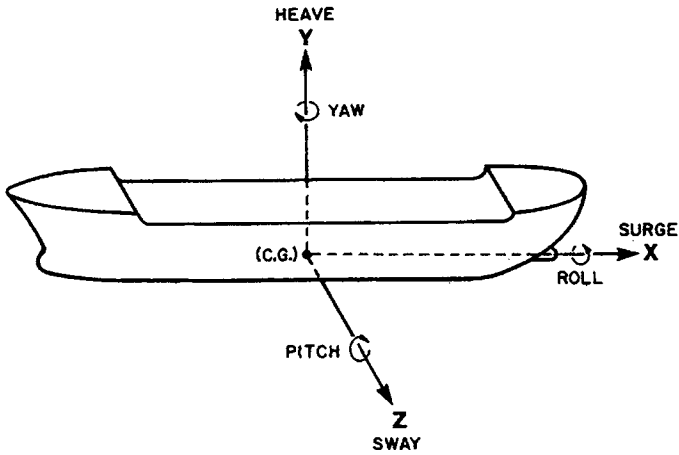
Figure 2.5   Six Degree of Freedom Motion of Ships and Floating Systems (Charkrabarti, 1987)

Once the data describing the sea-states encountered by a ship during its lifetime is available, the wave-induced loads on the ship structure and the ship response to such loads may be calculated. It is useful to classify the different forces that acting on a ship during its lifetime into four groups:

- The body forces such as weight and inertia

- The dynamic pressure on the ship's hull due to the incident and diffracted waves

- The inertial forces arising from the acceleration of the fluid (referring to both the sea and the liquids carried in tanks on the ship)

- The inertial and damping forces arising due to wave radiation from the ship

These forces are considered when building a ship-sea interaction model. This model is made up of a number of equations describing the waves, the motion of the ship, and the interaction between the two. The equations used are non-linear due to the random and irregular nature of the sea. This results in a very expensive and time-consuming analysis and methods are developed in order to simplify such an analysis.

Bhattacharyya (1978) gives an easy-to-follow discussion of the wave loads such as vertical/horizontal bending moments, shear forces and slamming loads. One of the most popular methods employed is a technique known as strip theory, which utilizes an assumption in order to simplify the ship-sea interaction model. The principal assumption made in the strip theory is that the ship is slender. The forces acting on the ship are then calculated separately on each segment using a two-dimensional flow theory neglecting the longitudinal component of relative velocity and any type of interaction between the different segments. The shear force and bending moment of the ship are then obtained by integrating the vertical forces of each segment along the length of the ship. The name 'strip theory' arises from the fact that the ship's hull is divided into a number of prismatic segments or strips. Strip theory originated from a linear theory of Korvin-Kroukovsky (1955), Gerritsma and Beukelman (1964). Strip theory is still widely applied due to its efficiency. However, its weaknesses include the lack of three-dimensional effects, the inability to account for the above-water hull form, the forward

speed corrections and the lack of viscous effects. All these methods assume the ship to be rigid beam. Bishop and Price (1979) developed a flexible beam strip theory that accounts for bending and shear stiffness of the hull when solving for compatibility between strips. This kind of theory can estimate the distortional higher frequency responses of a hull to slamming and whipping excitation. However, it is still linear analysis and extreme response is not well modeled.

2.3.2 Wave-Induced Forces

Jensen and Pedersen (1979) proposed a second order strip theory for hydro-elastic analysis in frequency-domain. Their theory is based on a perturbational expression of the hydrodynamic and the hydrostatic coefficients around the still water line and includes the incident pressure field from second order Stokes' waves. The equation used to evaluate the forces acting on a ship in such an analysis is similar to:

$$F(x,t) = F_H(x,t) + F_B(x,t) \tag{2.23}$$

The procedure for actually working out the above equation is rather complicated due to the non-linear nature of some of the parameters. The following explanation is only to give a basic understanding of the parameters present in Eq. (2.23).

The right hand side of Eq. (2.23) consists of two parts. The second part is the buoyancy force known as the Froude-Krylov buoyancy force:

$$F_B(x,t) = -\int_{-T}^{\eta} B(x,y) \left(\frac{\partial p}{\partial y} \right)_{y+V} dy \tag{2.24}$$

where,

B	= Breadth of the ship
y	= Distance along an axis starting from the bottom of the hull and moving vertically upwards
V	= Instantaneous vertical displacement of the hull
η	= Distance from the calm water surface to the local elevation of the ocean wave
x	= Distance along an axis starting from the aft of the ship and travelling forward along a horizontal axis
t	= Time
T	= Still-water draught
p	= Pressure given by Bernoulli's equation:

$$p(y,x,t) = \rho \left(\frac{\partial \phi}{\partial t} + gy + \frac{1}{2}(\nabla \phi)^2 \right) \tag{2.25}$$

where,

ρ	= Fluid density
ϕ	= Velocity potential which is made up of first- and second- order terms. The derivation of ϕ is well described by Jensen and Pedersen (1979)
g	= Acceleration due to gravity

The first part of the right hand side in Eq. (2.23) refers to the hydrodynamic forces acting on the ship:

$$F_H(x,t) = -\frac{D}{Dt}\left(m(x,\eta)\frac{D\eta}{Dt}\right) - N(x,\eta)\frac{D\eta}{Dt} \qquad (2.26)$$

where,

m = Added mass (due to the hydrodynamic load) per unit length

N = Damping force per unit length

D/Dt = Total derivative with respect to time t

In recent years, the diffraction and radiation theories based on panel methods became widely accepted (Faltinsen, 1990).

More recent advanced methods include fully nonlinear time-domain approaches. Cao et al (1991) used a desigularized method in which the source panels are located outside the fluid domain and thus the kernel in the governing integral equation is desigularized. The desingularized method was developed for more general boundary value problems of potential flows and was used in the time-domain computations of fully nonlinear waves. Jensen et al (2000) gave a detailed discussion of the different theories and comparisons with experiments on extreme hull girder loads. Beck and Reed (2001) gave a precise account of all fundamental theoretical developments in the field of sea-keeping over the past 50 years as well as the computational methods that currently in use.

The large amplitude motion programs FREDYN (De Kat and Pauling, 1989) and LAMP (Lin et al, 1997) may be used to calculate the extreme loads, capsizing, habitability and crew effectiveness. Other popular hydrodynamics codes include WAMIT (WAMIT, 1999), SWAN (Sclavounos et al , 1997).

2.3.3   Structural Response

Once the forces (or loads) acting on a ship are calculated, the hull girder response of the ship may be determined. In most cases, the hull girder analysis means calculating the longitudinal bending moment of the ship. It is performed by assuming the hull is rigid, e.g. no deformation. However, there are a number of cases in which the ship needs to be considered as a flexible beam, thus resulting in a more complicated solution that must include a hydroelastic analysis of wave-induced loads. Examples of cases when the ship is assumed flexible are:

(1)   When the ship's natural vibration is low enough to cause significant vibrations during its operational life.

(2)   When the ship's response to slamming and green water on deck needs to be investigated

The governing differential equation for the vertical deflection of a flexible beam subjected to a dynamic distributed load F(x,t) is:

$$EI\frac{\partial^4 v}{\partial x^4} + m_S\frac{\partial^2 v}{\partial t^2} - m_S r^2 \frac{\partial^4 v}{\partial t^2 \partial x^2} = F(x,t) \qquad (2.27)$$

where,

E = Young's Modulus

I = Moment of inertia for vertical bending

v = Hull girder deflection

m_S = Ship mass per unit length

r = Radius of gyration of the sectional mass m_S in rotation about a horizontal transverse axis through the section's center of mass

The theories and equations described in this Section are used to calculate the wave induced bending moment. This bending moment along with the stillwater bending moment, can help determine the longitudinal strength of the ship, which is applied during the scantling design of the ship. It would be useful to refer to Chapter 4 to obtain a description of bending moments and scantling design.

For stress analysis of ships (e.g. container ships), reference is made to Pedersen (1983)

2.3.4   Slamming and Green Water on Deck

So far only loads occurring at wave encounter frequency have been discussed. However, waves can also cause loads at much higher frequencies due to impacts between the ship's hull and the water surface, such as slamming and green water on deck. Slamming occurs when the forward part of the ship hits the water surface after a bow emergence. If the slam takes place with a relatively high velocity, there is a probability of damaging the ship, because a high impulsive load is created in the ship's bow structure. Green water on deck takes place when the deck becomes submerged under water. The water on the deck may cause structural damage to the deckhouse of the ship and to the deck facility and cargo. Both slamming and green water on deck are to be avoided as much as possible during a ship's lifetime due to the damage they may cause. The ship's speed is usually reduced or the heading is changed if such an action reduces the probability of slamming or green water on deck.

Both slamming and green water on deck loads are functions of the relative motion of the ship with respect to the sea. Two conditions need to be satisfied for slamming to occur at any section of the ship. First, the relative vertical motion, $\eta(x,t)$ should be larger than the draught at the section being considered. Also, the relative velocity, $D\eta/Dt$, must be larger than the threshold velocity v_0.

$$\eta_T \equiv \frac{D\eta}{Dt} = \frac{\partial \eta}{\partial t} - V\frac{\partial \eta}{\partial x} \geq v_o \qquad (2.28)$$

In a stationary stochastic seaway both η and η_T are normally distributed parameters with zero mean values. Thus, it is possible to determine the likelihood of slamming on the ship through the statistical probability of the occurrence of η and η_T. The resultant load can then be calculated and used in the ship design. The sectional force, $q_{SL}(x,t)$ associated with a slam, has been found to be approximately proportional to the square of the relative velocity η_T.

$$q_{SL}(x,t) = \alpha\eta_T^2 \qquad (2.29)$$

Eq. (2.29) may be included in Eq. (2.23), to account for all the wave loads experienced by a ship in a global wave load analysis. Eq. (2.29) is useful to describe what is known as bow flare slamming, that occurs when the bow flare of a ship hits the sea surface. Another type of slamming is bottom slamming where the flat bottom of a ship hits the water. This type of slamming cannot be described by Eq. (2.29), because bottom slamming is not directly related to the relative vertical motion and velocity of the ship, which are the two starting points of the

analysis leading up to Eq. (2.29). In the case of bottom slamming, empirical formulae are used, see Zhao and Faltinsen (1993).

For green water on deck to occur, the relative immersion of the section of the ship must be larger than the distance between the water level and the deck (freeboard). The actual force the green water exerts on the deck is difficult to assess because of the complicated flow of the water. Wang, Jensen, and Xia (1998) derived the following equation to calculate the sectional force, $q_{GW}(x,t)$ resulting from green water on deck:

$$q_{GW}(x,t) = -gm_{GW}(x,t) - \frac{D}{Dt}\left[m_{GW}(x,t)\frac{Dz_E}{Dt} \right] \tag{2.30}$$

where,

m_{GW} = Sectional mass of water on the deck

Z_E = Modified relative vertical motion depending on z and a parameter known as the Smith correction factor κ

The first term on the right hand side of Eq. (2.30) represents the gravity force, while the second term is analogous to a momentum slamming force. Eq. (2.30) may also be included in a global wave load equation, such as Eq. (2.23).

Green water has caused damage to bow super-structure and FPSO topsides along the length of the ship. A prediction theory for the green water on deck and the resulting green water loading have been developed by Zhou, De Kat and Buchner (1999). The green water or deck wetness slamming phenomena is highly non-linear. Wang, Leitch and Bai (2001) proposed the following design procedures for greenwater impact on FPSOs:

1) Estimate the possibility of greenwater occurrence using past experience and approximate methods. Ideally, some preliminary analysis using computer software should be done to get a more reliable estimation.
2) If the estimation indicates that greenwater likely to occur in a significant manner, model tests should be performed. Greenwater model tests can be arranged as part of global performance model testing program. The critical parameters should be identified during planning stage of the model tests. If the greenwater impact is judged to be a serious problem and must be designed on, height, occurrence frequencies and the impact pressure of greenwater should be carefully measured.
3) If the model tests do not or cannot cover sufficient number of the values of the identified critical parameters, some complementary numerical simulations using benchmarked software should be performed to identify the critical value of each critical parameter for design consideration.
4) Analyze the results of model tests and numerical simulations to judge if the greenwater needs to be dealt with in design and engineering. Risk analysis may be conducted to help decision making if the judgment is difficult make directly from the results of model tests and numerical simulation.
5) If it is found that greenwater must be considered, model test results should be used for design. In case no applicable model test results are available, the impact pressure can be calculated using some approximate formulas. For instance, the formulas summarized in reference 1 may be used to estimate the horizontal pressure of greenwater impact while classification societies rules may be used for calculation of the pressure vertically acting on vessel deck. Due to the complexity of greenwater analysis and the limitation of those

simple formulas, calculated results may be inaccurate.

6) If particular measures are required to prevent/reduce greenwater impact, past design experience can be used, including increasing freeboard, using better bow shape and flare, adding some protection measures, etc.

It should be noted that steps 1) through 3) may be replaced by a single step, i.e, sophisticated numerical analysis, if a reliable prediction method becomes available in future. Although great effort has been made in recent years to develop such methods, there is no method considered to be satisfactory. Therefore, use of model test results is recommended for design

A risk based approach may be more helpful for design decision making. The probability analysis presented in Wang, Leitch and Bai (2001) can be expanded and modified to form such a method. However, the probability (likelihood) of vessel heading involves a considerable quantity of analysis work and some model tests may also be required. In addition, the probability of vessel draft is also difficult to accurately determine because it is a function of production rate, offloading rate (and frequency) ballast plan and rate, etc.

2.4   Ship Design for Classification

2.4.1   Design Value of Ship Response

The ultimate goal of determining the wave loads and the ship's response to these loads is to obtain the design value of the ship's response. This involves making predictions of the worst seas in which the ship could encounter within its lifetime. There are four factors, which are going to influence the design value of the ship's response (Hughes, 1988):

- The severity of the sea-state, as characterized by the significant wave height, the frequency of occurrence, and the duration of each level of severity. This data is used to determine the ship's exposure time to each sea-state of different severity.

- The shapes of the wave spectra for each sea-state.

- The ship heading (direction) in a given sea-state.

- The ship speed for a particular heading and sea-state.

The overall aim is to determine the largest response value resulting from the worst combination of wave loads, which has a probability, α, of being exceeded during the ship's life. This design value α, is a risk parameter determined by the ship designer and is used to calculate the structural response of the ship. A typical value of α is 0.01.

There are two methods used to determine this design value as below.

The first method assumes that the largest waves appear in the most severe stationary sea-state, which the ship is likely to encounter. This is called the "design wave method". Thus, this wave value is used as the design value of the ship, along with a couple of less severe sea-states. This method may not be considered to be accurate, because a larger wave may be encountered in a less severe sea-state. However it is less time-consuming and is the preferred method unless a more accurate determination of the design value is required.

The second method requires that all possible sea-states, which the ship is likely to encounter in its lifetime, be evaluated. A complete analysis of all the sea-states is carried out and the

different sea-states are weighted according to the likelihood of being encountered by the ship. This method is computationally more expensive but is a more realistic analysis, see Chapter 4.

Once the method to be used has been chosen, and the design wave load is determined, the ship's required structural strength may be evaluated.

2.4.2 Design Loads per Classification Rules

General

Structural analysis may be divided into three parts:

- establishing the design load,
- defining the acceptance criteria,
- conducting the strength assessment.

It is relatively easy to establish the acceptance criteria thanks to many years of accumulated knowledge and expertise from owners, builders, class societies and researchers, see Part II and Part III of this book for more details. The strength assessment is also rather simple once the loads and acceptance criteria are defined. However, the most challenging task is to calculate the different loads that the ship is subjected to. This difficulty arises from the fact that the ship may be exposed to various sea and wave conditions, and different loading patterns of the cargo.

Classification societies have proven techniques for calculating the loads on a ship and evaluating the structural integrity of ship hulls.

Load Components

A detailed design consists of two steps:

- the nominal design for initial scantlings,
- a more detailed analysis where finite element analysis is used to evaluate the combination of a number of load cases and their effects on the ship structure.

In a ship structural design, three load components are considered:

- hull girder load, which consists of the still-water/wave induced bending moments and shear forces,
- external pressure, which consists of a static, hydrodynamic, and an impact slamming load,
- internal pressure caused by the liquids carried in tanks onboard the ship. This pressure depends on the hydrostatic pressure, the changes in pressure head due to pitching and rolling motions, and the inertial force of the liquid column resulting from accelerations of the fluid.

The following sub-sections describe the evaluation process of these different loads.

Hull Girder Loads

Wave data measured from the North Atlantic are used to determine wave loads. Thus, the nominal design value of a ship represents the long-term extreme value for the North Atlantic Sea in 20 years, which corresponds to a probability of exceedance of 10^{-8}. The global spectral ocean wave models provide data about different wave spectra and different wave heights.

The structural response to waves used in the global structural analysis of a ship is calculated based on the ship's Response Amplitude Operations (RAOs) when exposed to regular sinusoidal waves, for different wave headings and frequencies.

The structural integrity of the ship is assured by implementing a number of different combinations of loads, wave periods, and heading angles. For each situation, a number of load components are calculated, such as external wave pressure, acceleration of the liquid cargo and ballast tanks, accelerations at several stations along the ship's length, wave-induced bending and torsional moments together with the corresponding shear forces along the length of the ship, and the ship's motion in roll and pitch modes.

The short-term response of the ship is obtained through the evaluation of the seaway spectrum, which is assumed to be stationary in a period of a few hours. The long-term response and the probability of exceedance of the load are evaluated from the short-term prediction.

The hull girder loads are calculated from a number of components. The most significant of these components are the still-water moments and shear forces resulting from the weight of the ship, cargo, and buoyancy. The second major component of hull girder loads is, the dynamic-induced loads that include the vertical and horizontal bending moments, shear forces and torsional moment. These dynamic loads result from wave motions encountered by the ship.

The classification rules are used to determine the still-water bending moments and shear forces, as these are mainly dependent on the loading conditions of the vessel. A more detailed analysis is required when determining the dynamic aspects of the hull girder loads. Such analysis is based on the sea conditions that the vessel is bound to encounter over its lifetime. Normally, a 20-year service life is chosen and appropriate wave data is selected. The result of such an analysis determines the extreme values that are used to calculate a design value for the hull girder loads.

When determining the hull girder loads, the vertical bending moments and shear forces are calculated first. Then tables and other sources of data are used to calculate the ratio of vertical to horizontal bending moment and shear force. These ratios are mainly dependent on the ship's dimensions and loading conditions.

External Pressure

Determining the external pressure acting on a ship is a more complicated process than the calculation of hull girder loads. This is because the external pressure is influenced by a larger number of parameters such as hull form, wave motion characteristics, ship speed, heading angles in the sea, etc. The methods and theories used to determine the external pressure on a ship are usually based on a number of assumptions, such as having a wall-sided hull, small motions of the vessel, and being in an inviscid fluid. Thus, one has to be careful when predicting a value for the external pressure.

The external pressure on a vessel is determined by initially dividing the vessel into two parts. The pressures distributed over 40% of the length of the vessel, centered around the amidships are normally very similar from ship to ship. Thus, the calculation of the pressure in these regions is relatively straightforward and is done by applying the results of a complete seakeeping analysis of full form tankers and bulk carriers. Formulae are used for the pressure applied over the rest of the ship, since the pressure varies significantly from one ship to the next depending primarily on the hull form.

In a simplified form, the total external pressure P_E, on a ship may be expressed as (ABS, 2002):

$$P_E = \rho g(h_s + k_U h_{DE}) \tag{2.31}$$

where,

ρg = Specific weight of sea water

h_S = Hydrostatic pressure head in still water

k_U = Load factor

h_{DE} = Hydrodynamic pressure head induced by the wave

The pressure distribution may be predicted across a vessel in both a lengthwise and girthwise direction. Most of the data required in order to carry out such calculations are obtained from seakeeping analysis of ships.

Internal Tank Pressure

The internal pressure in a tank, which carries liquids onboard a ship, is made up of three parts:

- Hydrostatic pressure that is equivalent to ρgh,

- Changes in pressure head that are due to the pitching and rolling motions of the ship,

- Inertial force of the liquid column due to the accelerations caused by the motion of the ship.

The internal pressure in a tank is calculated by a series of formulae specific to the shape of the tank being analyzed. A number of different tank shapes exist, such as J-shaped, rectangular, and U-shaped. Other factors that affect the internal pressure are the amount of liquid carried in the tank, and the location and number of air pipes in the tank.

For example, a simplified formula used to determine the internal pressure in a liquid-carrying tank is as follows (ABS, 2002):

$$P_I = \rho g(\eta + k_U h_D) \tag{2.32}$$

where,

η = Local coordinate in vertical direction for tank boundaries measuring from the top of the tanks

k_U = Factor that takes into consideration the resultant acceleration of the liquid due to the ship's motion

h_D = wave-induced internal pressure head, including inertia force and added pressure head.

2.5   References

1.   ABS (2002), "Rules for Building and Classing Steel Vessels", American Bureau of Shipping.

2.   Bhattacharyya, R (1978), *"Dynamics of Marine Vehicles"*, John Wiley & Sons, Inc

3.   Bishop, R.E.D. and Price, W.G. (1979): *"Hydroelasticity of Ships"*, Cambridge University Press.

4.   Bretschneider, C. L (1959), "Wave Variability and Wave Spectra for Wind-Generated Gravity Waves", Beach Erosion Board, US Army Corps of Engineers, Technical Memorandum, No. 118.

5.   Cao, Y., Schultz, W.W. & Beck, R.F., (1991), "A Three-Dimensional Desingularized Boundaru Integral Method for Potential Problems", *Int. J. Num. Meth. Fluids*, 11, 785-803.

6.   Chakrabarti, S.K., (1987), *"Hydrodynamics of Offshore Structures"*, Computational Mechanics Publications.

7.   De Kat, J.O. and Pauling, J.R. (1989, "The Simulation of Ship Motions and Capsizing in Severe Seas", Trans. SNAME, 97, 139-168.

8.   Ewing, J. A. (1976), "Wave Prediction: Progress and Applications", Proc. of 6th International Ship Structures Congress, Boston.

9.   Faltinsen, O.M. (1990), *"Sea Loads on Ships and Offshore Structures"*, Cambridge Ocean Technology Series, Cambridge University Press.

10. Gerritsma, J. and Beukelman, W. (1964), "The Distribution of the Hydrodynamic Forces on a Heaving and Pitching Ship Model in Still Water", Fifth Symposium on Naval Hydrodynamics, Washington.

11. Hasselman, K., et al (1973), "Measurements of Wind-Wave Growth and Swell Decay During the Joint North Sea Wave Project (JONSWAP)", Deutsche Hydrographischen Zeitschrift, A8, 12.

12. Hogben, N., Dacunha, N. M. C. and Olliver, G. F. (1986), *"Global Wave Statistics"*, British Maritime Technology, Unwin Brothers Ltd., U.K.

13. Hughes, O.F. (1988), *"Ship Structural Design: A Rationally-Based, Computer-Aided, Optimisation Approach"*, SNAME.

14. Jensen, J. J. and Pedersen, P. T. (1979), "Wave-Induced Bending Moments in Ships – A Quadratic Theory", RINA, 121.

15. Jensen, J. J. (2001), *"Load and Global Response of Ships"*, Elsevier Ocean Engineering Book Series.

16. Korvin-Kroukovsky, B.V. (1955), "Investigation of Ship Motions in regular Waves", Trans. SNAME, 63, 386-435.

17. Lin, W.M., Shin, Y.S., Chung, J.S. and Salvesen, N. (1997), "Nonlinear Predictions of Ship Motions and Wave Loads for Structural Analysis", OMAE.

18. Longuet-Higgins, M.S. (1952) "On the Statistical Distribution of the Heights of Sea Waves", Journal of Marine Research, 11, pp.245-266.

19. Ochi, M. K. (1978), "Wave Statistics for the Design of Ships and Ocean Structures", Trans. SNAME, 86.

20. Pedersen, P. Terndrup (1983), "Beam Model for Torsional-Bending Response of Ship Hulls", Trans. RINA, Vol. 125, pp.171-182.

21. Pierson, W. J. (1952), "A Unified Mathematical Theory for the Analysis of Propagation and Refraction of Storm-Generated Ocean Surface Waves, Part I and II", New York University.

22.   St. Denis, M. and Pierson, W.J. (1953), "On the Motions of Ships in Confused Seas", Trans. SNAME, Vol. 61.

23.   Pierson, W. J., Neumann, G., and James, R. W. (1955), "Practical Methods for Observing and Forecasting Ocean Waves by Means of Wave Spectra and Statistics", Hydrographic Office Publication.

24.   Pierson, W. J. and Moskowitz, L. (1964), "A Proposed Spectral Form for Fully Developed Wind Seas Based on the Similarity of S. A. Kitaigorodskii", Journal of Geophysical Research, Vol. 69 (24).

25.   Sclavounos, P.D., Kring, D.C., Huang, Y.F., Mantzaris, D.A., Kim, S.G. and Kim, Y.W. (1997), "A Computational Method as an Advanced Tool of Ship Hydrodynamic Design", Trans. SNAME, 105, 375-397.

26.   WAMIT (1999), "WAMIT User Manual", www.wamit.com.

27.   Wang, Z., Jensen, J. J. and Xia, J. (1998), "Effects of Bow Flare Shape to the Wave Loads of a Container Ship", J. Society of Naval Architects of Japan, Vol. 166.

28.   Wang, M., Leitch, J. and Bai, Y. (2001), "Analysis and Design Consideration of Greenwater Impact on Decks and Topsides of FPSO", OTC 13208.

29.   Zhao, R. and Faltinsen, O. M. (1993), "Water Entry of Two-dimensional Bodies", J. Fluid Mech., Vol. 246.

30.   Zhou, Z., De Kat, J. O. and Buchner, B. (1999), "A Non-linear 3-D Approach to Simulate Green Water on Deck", Seventh International Conference on Numerical Ship Hydrodynamics, Nantes.

31.   Jensen, J.J., Beck, R.F., Du, S., Faltinsen, O.M., Fonseca, B., Rizzuto, E., Stredulinsky, D. and Watanabe, I. (2000), "Extreme Hull Girder Loading", ISSC Committee Report.

32.   Beck, R. and Reed, A.M. (2001), "Modern Computational Methods for Ships in a Seaway", SNAME Transactions.

This Page Intentionally Left Blank

Part I

Structural Design Principles

Chapter 3   Loads and Dynamic Response for Offshore Structures

3.1   General

One of the key issues in the design of offshore structures is to define the environmental conditions for the transportation route and installation site, and to determine the environmental loads acting on the structure for conditions such as transit, installation, operational extreme and survival. The parameters to be defined in the environmental conditions may be found from design codes such as API RP 2T, among of several other codes.

The prediction of extreme values is required for the structural strength evaluation. Various methods have been proposed for determining the extreme values, (Ochi, 1981, 1990). In this Chapter, both long- and short-term (surviving storm) wave data approaches are detailed.

The aim of this chapter is to give an overall picture of the environmental conditions and loads for offshore structural design, and to detail the recent developments in the prediction of extreme response. A systematic method for structural analysis of offshore structures has been developed to predict extreme response and fatigue assessment under wave loads.

Vibrations and the associated dynamic effects are also an important factor in structural design and vibration control. Basics of vibration analysis will be covered in an Appendix of this Chapter.

The contents related to extreme loads in this Chapter were modified from Zhao, Bai and Shin (2001).

3.2   Environmental Conditions

3.2.1   Environmental Criteria

The collection and selection of the environmental criteria for the design of offshore structures are the owner's responsibility. Statistical models are essential to adequately describe environmental conditions. All environmental phenomena of importance should be considered, such as wind, waves, currents, and tides. In general, environmental conditions as follows need to be considered in design (API RP 2T, 1997),

- wind
- waves
- currents
- Tide

- Ice

- Earthquake

- Marine growth

Some of the above mentioned items are detailed below.

Wind

Wind is a significant design factor. The wind conditions used in a design should be appropriately determined from collected wind data and should be consistent with other associated environmental parameters. Two methods are generally used to assess the effects of wind in design:

- Wind forces are treated as constant and calculated based on the 1-minute average velocity.

- Fluctuating wind forces are calculated based on a steady component, the 1-hour average velocity plus a time-varying component calculated from an empirical wind gust spectrum.

The choice of methods depends on the system's parameters and goals of the analysis. Either approach may give more severe load than the other, depending on the system's mooring and the wind spectrum used. The design wind speed should refer to an elevation of 10 meters above the still water level. Rapid changes of wind direction and resulting dynamic loads should be considered in the design of offshore structures.

Waves

Wind-driven waves are a major component of environmental forces affecting offshore structures. Such waves are random, varying in wave height/length, and may approach an offshore structure from more than one direction simultaneously. Due to the random nature, the sea-state is usually described in terms of a few statistical wave parameters such as significant wave height, spectral peak period, spectral shape, and directionality, etc.

The calculation of extreme wave loads and their load effects may be based on selected short-term sea-states. The overall objective of this approach is to estimate loads and load effects corresponding to a prescribed annual exceedance probability, e.g. 10^{-2} or 10^{-4}, without having to carry out a full long-term response analysis. This is the so-called design storm concept.

An appropriate formulation of the design storm concept is to use combinations of significant wave height and peak period along a contour line in the H_{m0} and T_P plane. Such a contour line can be established in different ways. The simplest way to establish the contour line at a probability level of 10^{-2} is to first estimate the 10^{-2} value of H_{m0} along with the conditional mean value of T_p. The contour line is then estimated from the joint probability model of H_{m0} and T_p with constant probability density. An example of such a contour line is shown in Figure 3.1. The estimation of the load effect at the probability level of 10^{-2} is then obtained by determining a proper extreme value for all seastates along the contour line and taking the maximum of these values.

Current

The most common categories of currents are:

- Tidal currents, which are associated with astronomical tides

- Circulation currents, which are associated with oceanic-scale circulation patterns

- Storm generated currents

- Loop and eddy currents
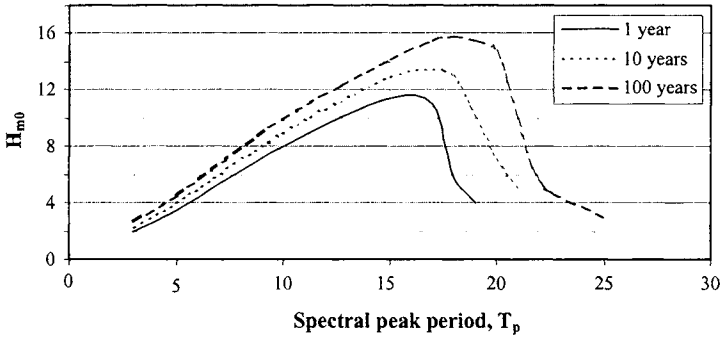
Figure 3.1   Example $H_{m0} - T_p$ Contour Lines

The vector sum of these currents is the total current. The variation of current speed and direction with elevations are represented by a current profile. The total current profile associated with the extreme storm sea-state should be specified for the design. In certain geographic areas, the current force can be one of the governing design loads. Consequently, selecting the appropriate current profile requires careful consideration.

Detailed description of environmental conditions related to wind and current may be found from Chakrabarti (1987) and CMPT (1998).

3.2.2   Regular Waves

Regular wave theories may be applied to describe the velocity and acceleration of the water particles. Commonly used wave theories include (Chakrabarti, 1987),

- linear airy wave theory (The small amplitude wave theory is the simplest and most useful of all wave theories.)
- Stokes finite amplitude wave theory
- Cnoidal wave theory
- Stream function wave theory
- Standing wave theory

3.2.3   Irregular Waves

A real sea does not possess the characteristic of a regular wave, but has an irregular form. The slowly varying local sea-state can reasonably be assumed stationary in a 'short' time interval, with an appropriate three-hour duration. A sea-state is usually described by a wave spectrum with significant wave height (H_S), and a characteristic period (T), such as peak period (T_P), or zero-crossing period (T_Z). One wave spectrum describes only a short-term sea-state. The statistical value based on a single short-term sea-state is referred to as short-term. When predicting extreme responses using the short-term methods, an 'extreme' storm wave spectrum based on long-term wave statistics is usually used as the short-term sea-state. Bhattacharyya (1978) gives a comprehensive discussion of the irregular waves and most probable largest wave amplitude.

3.2.4   Wave Scatter Diagram

Long-term descriptions are required to describe the variation of sea-states. The wave scatter diagram provides a joint probability table of significant wave heights and characteristic periods for a site. Beck et al (1989) outlined methods of collecting ocean wave data:

(a) Visual estimates of wave conditions (of heights and periods) by trained observers aboard weather ships: Hogben and Lumb (1967) collected log entries of some 500 British ships from 1953 to 1961 in oceans of worldwide.

(b) Point Spectra from wave measurements using a ship borne meter: Pierson and Moskowitz (1964) evaluated the wave generation process and fully developed spectra in particular.

(c) Directional spectra

(d) US Naval hindcast wave climatology: An alternative to wave data is to calculate a set of spectra from the comprehensive wind data that have been collected for years over the important trade routes worldwide, see e.g. Bales et al (1982).

Figure 3.2 compares contours of two wave scatter diagrams retrieved from a wave database for a site in the North Sea (W156) and a site in the Gulf of Mexico (W391). As observed, the wave environment at site W156 is much more severe than that at site W391. In order to obtain a wave scatter diagram, various short-term wave data that have been accumulated over a long period of time (for example, 10 to 20 years) and cover all sea-states defined by different combinations of pairs (H_S, T), are statistically averaged. The statistical value based on the long-term description of sea-states is referred to as long-term. The wave directional probability corresponding to each wave scatter diagram table should also be provided. Figure 3.3 shows the wave directional probability distributions at two grid zones, W156 and W391, with 24 equally divided directional divisions. The radius for each direction shown in Figure 3.3 describes the probability for that direction.
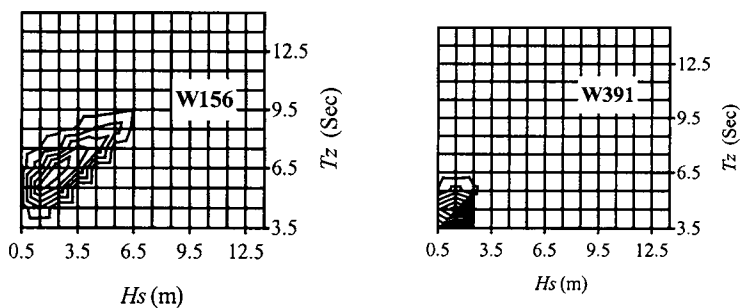
(a) A site in the North Sea   (b) A site in Gulf of Mexico

Figure 3.2   Graphic Comparison of Wave Scatter Diagrams for Two Locations (Zhao, Bai & Shin, 2001)
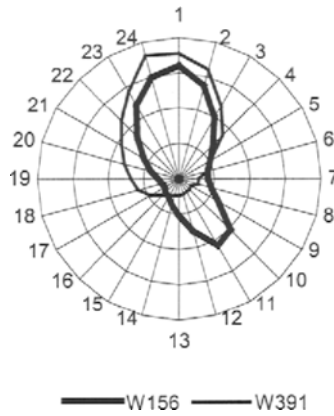
Figure 3.3   Wave Directional Probabilities (Zhao, Bai & Shin, 2001)
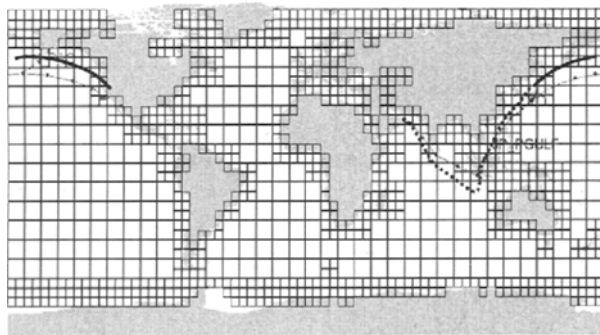
Figure 3.4   Wave grid of A Wave Database and Two Sample Service Routes (Zhao, Bai & Shin, 2001)

An example of a two-dimensional wave scatter diagram for the Northern North Sea is shown in Table 3.1.

A wave scatter diagram provides a long-term wave description for only one specific region. In order to assess the fatigue damage for a ship on past service, it is necessary to obtain additional wave information along the routes. For this purpose, a global wave database can be used, from which wave data for any wave zone on the service route can be retrieved.

Table 3.1   Wave Scatter Diagram, Representative Dat from the Northern North Sea (Faltinsen, 1990)

Significant wave height (m) (upper limit of interval)	Spectral peak period (s)																			
	3	4	5	6	7	8	9	10	11	12	13	14	15	16	17	18	19	21	22	Sum
1	59	403	1061	1569	1634	1362	982	643	395	232	132	74	41	22	12	7	4	2	2	8636
2	9	212	1233	3223	5106	5814	5284	4102	2846	1821	1098	634	355	194	105	56	30	16	17	32 155
3	0	8	146	831	2295	3896	4707	4456	3531	2452	1543	901	497	263	135	67	33	16	15	25 792
4	0	0	6	85	481	1371	2406	2960	2796	2163	1437	849	458	231	110	50	22	10	7	15 442
5	0	0	0	4	57	315	898	1564	1879	1696	1228	748	398	191	84	35	13	5	3	9118
6	0	0	0	0	3	39	207	571	950	1069	885	575	309	142	58	21	7	2	1	4839
7	0	0	0	0	0	2	27	136	347	528	533	387	217	98	37	12	4	1	0	2329
8	0	0	0	0	0	0	2	20	88	197	261	226	138	64	23	7	2	0	0	1028
9	0	0	0	0	0	0	0	2	15	54	101	111	78	39	14	4	1	0	0	419
10	0	0	0	0	0	0	0	0	2	11	30	45	39	22	8	2	1	0	0	160
11	0	0	0	0	0	0	0	0	0	2	7	15	16	11	5	1	0	0	0	57
12	0	0	0	0	0	0	0	0	0	0	1	4	6	5	2	1	0	0	0	19
13	0	0	0	0	0	0	0	0	0	0	0	1	2	2	1	0	0	0	0	6
14	0	0	0	0	0	0	0	0	0	0	0	0	0	1	0	0	0	0	0	1
15	0	0	0	0	0	0	0	0	0	0	0	0	0	0	0	0	0	0	0	0
Sum	68	623	2446	5712	9576	12 799	14 513	14 454	12 849	10 225	7256	4570	2554	1285	594	263	117	52	45	100 001

3.3 Environmental Loads and Floating Structure Dynamics

3.3.1 Environmental Loads

According to API RP 2T (1997), the environmental loads to be considered in the design of offshore structures include,

- wind forces
- current forces
- wave loads
- ice loads
- wave impact forces
- earthquakes
- accidental loads
- fire and blast loading

3.3.2 Sea loads on Slender Structures

For slender structures such as jackets, jack-ups, pipelines, risers and mooring lines, viscous flow phenomena are of importance. Wave loads on slender structures may be predicted using Morison equation, see Sarpkaya and Isaacson (1981) and Chakrabarti (1987). The Morison equation assumes the force is the sum of inertia and drag forces.

Vortex-induced vibration (VIV) occurs when the wave/current flow cause resonance with the natural frequency of the structure. For the design of pipelines and risers, it is necessary to account for the wave-induced fatigue and VIV induced fatigue (Bai, 2001).

3.3.3 Sea loads on Large-Volume Structures

When the size of the structure is comparable to the length of wave, the pressure on the structure may alter the wave field in the vicinity of the structure. In the calculation of wave forces, it is then necessary to account for the diffraction of the waves from the surface of the structure and the radiation of the wave from the structure if it moves (Charkrabarti, 1987).

First Order Potential Forces: Panel methods (also called boundary element methods, integral equation methods or sink-source methods) are the most common techniques used to analyze the linear steady state response of large-volume structures in regular waves (Faltinsen, 1990). They are based on potential theory. It is assumed that the oscillation amplitudes of the fluid and the body are small relative to cross-sectional dimension of the body. The methods can only predict damping due to radiation of surface waves and added mass. But they do not cover viscous effects. In linear analysis of response amplitude operator (RAO), forces and response are proportional to wave amplitude and response frequency are primarily at the wave frequency.

Second Order Potential Forces: The second order analysis determines additional forces and responses that are proportional to wave amplitude squared. The second order forces include steady force, a wide range of low frequency forces (which will excite surge, sway and yaw of a moored floating system) and high frequency forces (which will excite roll, pitch and heave springing of a TLP). The most common way to solve non-linear wave-structure problems is to

use perturbation analysis with the wave amplitude as a small parameter. The non-linear problem is solved in second-order (Faltinsen, 1990).

In addition to the boundary element methods, finite element methods or hybrid (BEM & FEM) methods are available to develop commercial codes for a body of general geometry's. Other special simplified methods have also been mathematically developed for specific geometries that are much more efficient. When viscous forces become important, a hybrid diffraction and Morison drag method is required in which the drag force calculation based on the undisturbed flow but a more elaborate approach is applied to account for the change in flow velocity due to diffraction.

In very deep seas various higher order wave loading effects also become very important (CMPT, 1998):

- Higher order potential flow and drag forces coupled with highly non-sinusoidal waves lead to ringing

- Impact of parts of the structure with water surface leads to bottom slamming and run up (on near vertical surfaces). The duration of slamming pressure at a specific location is of the order of milliseconds and the location of the peak pressure moves with time.

Bhattacharyya(1978) gives a comprehensive and easy to follow discussion of the wave loads, deck wetness and slamming, as well as the influence of slamming on the hull girder bending moment.

3.3.4   Floating Structure Dynamics

Dynamic response of an offshore structure includes the sea-keeping motion of the vessel in waves, the vibration of the structure, and the response of the moored systems. The response of an offshore structure may be categorized by frequency-content as below:

- **Wave-frequency response:** response with period in the range of 5 – 15 seconds. This is the ordinary see-keeping motion of a vessel. It may be calculated using the firs-order motion theory.

- **Slowly-varying response:** response with period in the range of 100 – 200 seconds. This is the slow drift motion of a vessel with its moorings. The slowly-varying response is of equal importance as the linear first-order motions in design of mooring and riser systems. Wind can also result in slowly-varying oscillations of marine structures with high natural periods. This is caused by wind gusts with significant energy at periods of the order of magnitude of a minute. Figure 3.5 shows wave frequency and slow-drift constituents for a floating system.

- **High-frequency response:** response with period substantially below the wave period. For ocean-going ships, high frequency springing forces arise producing a high-frequency structural vibration that is termed whipping (Bhattacharyya,1978). Owing to the high axial stiffness of the tethers, TLPs have natural periods of 2 to 4 seconds in heave, roll and pitch. Springing is a kind of resonance response to a harmonic oscillation (CMPT, 1998).

- **Impulsive response:** Slamming occurs on the ship/platform bottoms when impulse loads with high-pressure peaks are applied as a result of impact between a body and water. Ringing of TLP tethers is a kind of transient response to an impulsive load. The high-frequency response and impulsive response cannot be considered independently of the structural response. Hydroelasticity is an important subject.

Damping forces are important when a system is under resonant loading, which is cyclically applied at one of the system's natural frequencies. They consist of hydrodynamic damping, structural damping, soil/foundation damping etc.

The above is just a road map to floating structure dynamics because this book is devoted to structural design. Details of motion and load calculations are available from Bhattacharyya (1978), Beck et al (1989), Faltinsen (1990), and CMPT (1998).

Surge (m)

Time (s)
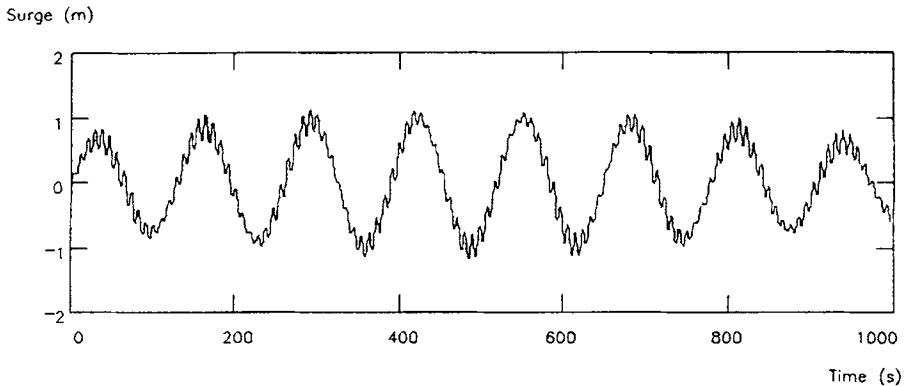
Figure 3.5   Surge Time-History of a Moored Vessel Showing Wave Frequency and Slow-Drift Constituemts (CMPT, 1998)

3.4   Structural Response Analysis

3.4.1   Structural Analysis

For structural analysis of FPSO, Zhao, Bai and Shin (2001) proposed a general procedure as follows:

1. Defining the major service profiles for a FPSO based on the operations that significantly affect the local deck and storage tank loads as well as the global motion responses. Typical operations include normal operation, storm survival condition, loading condition, and offloading condition.

2. Determining a series of static deck and tank loading patterns Λ_l based on the major service profiles.

3. Calculating global motion of the FPSO with mooring and riser systems and the hydrodynamic forces on the FPSO for each Λ_l,

4. Loading the hull-girder structure under each Λ_l, wave frequency and wave heading. The following components should be included (Zhao, 1996; ABS, 1992):

   • Static deck and internal tank loads

   • Static structural loads

   • Hydrostatic forces

- Hydrodynamic forces

- Motion induced hydrostatic restoring forces

- Motion induced structural inertial loads and internal tank sloshing loads

- Mooring and riser forces

- Shear forces, bending moments, and torsional moments like structural boundary conditions

5. Performing structural analysis to calculate stress FRF $H(\omega, \alpha_k, \Lambda_l)$ for each wave frequency ω, wave heading α_k, and loading pattern Λ_l. Each combination of $(\omega, \alpha_k, \Lambda_l)$ forms a different loading case in structural analysis. The finite element method or other simplified structural analysis can be applied for the various levels of analysis, see Chapter 6. For example, to analyze the strength of deck and bottom plating in the hull-girder strength level, calculations using vertical bending moment and sectional modulus can provide satisfactory results.

The following table provides an example of tank loading patterns (ABS, 1992):

Table 3.2 Tank Loading Patterns

No.	Tank loading description	
1	Homogeneous Full load	Design draft
2	Normal ballast load	Light draft
3	Partial load	33% full
4	Partial load	50% full
5	Partial load	67% full

The hydrodynamic force components consist of incident wave forces, diffraction wave forces, and motion-induced radiation forces (added mass and damping forces). The potential theory of fluid mechanics based on boundary element methods using source distributions, can be applied to numerically calculate the hydrodynamic forces. Currently, hydrodynamic analysis software, which use three-dimensional models (preferred) or two-dimensional strip methods, are widely applied. A detailed discussion of numerical techniques and other load effects (such as bow flare impact, bottom slamming, green water, ice loads, and accident loads), are beyond the scope of this chapter, and may be found from, e.g. Faltinsen (1990).

The wave heading α_k, is defined with respect to a FPSO (see Figure 3.6). Depending on the mooring type, the wave probability at direction α_k, needs to be converted into FPSO local coordinates. For example, if the turret-mooring system is adopted, the weather vaning should be considered, and some of the wave headings can be removed.
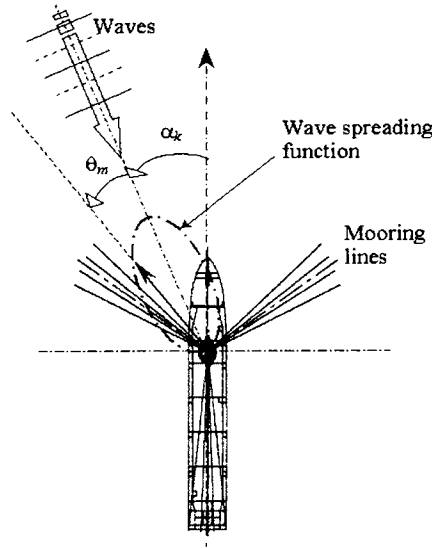
Figure 3.6   A FPSO System and Coordinates for Wave Directionality and Wave Spreading

3.4.2   Response Amplitude Operator (RAO)

A wave scatter diagram provides a long-term wave description for only one specific site. Determining the stress Frequency Response Function (FRF) or Response Amplitude Operator (RAO), H (ω; α_k, Λ_l) is one of the major efforts in the strength assessment, because it allows the transfer of the exciting waves into the response of structures. This concept of linear dynamic theory is applicable to any type of oscillatory "load" (wave, wind-gust, mechanical excitation, etc.) and any type of "response" (motion, tension, bending moment, stress, strain etc.).

For a linear system the response function at a wave frequency can be written as

$$\mathrm{Re}\,sponse(t) = RAO \cdot \eta(t)$$

where $\eta(t)$ denotes the wave profile as a function of time t. The RAO could be determined using theoretical computation or experimental measurement (Bhattacharyya, 1978). Almost all of the theoretical computation has neglected viscosity and used potential flow.

The structure may be envisaged in a general terms as a "black box", see Figure 3.7. The input to the box is time-history of loads and the output from a structural analysis is time-history of the response. The basic assumption behind the RAO concept is linearity, that allows superimpose the output based on superimpose of the input. In these situations, the response to regular oscillatory loading of any waveform can be obtained by expressing the load as a Fourier series, and then estimate the corresponding Fourier series of the response for each component. A typical RAO is shown in Figure 3.8, that is a roll RAO of a barge in beam seas. The RAO is given in degrees (or meters/ft) of motion amplitude, per meter (or ft) of wave amplitude and expressed as a function of wave period (second). The RAO may be calculated using the first order wave theory as wave frequency response.

Input time—history   Output time—history
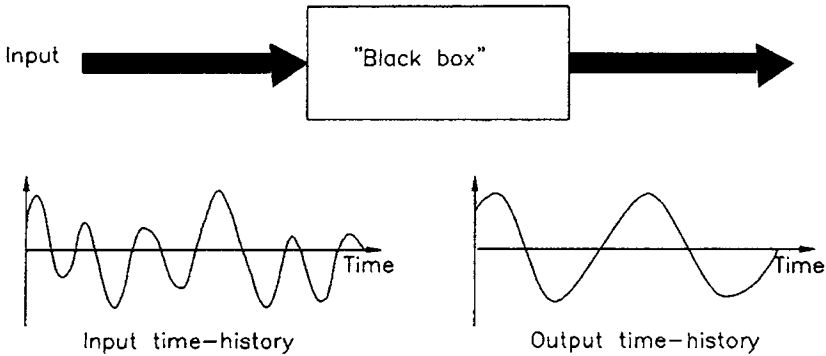
Figure 3.7   The Concept of RAO for a Structure (CMPT, 1998)
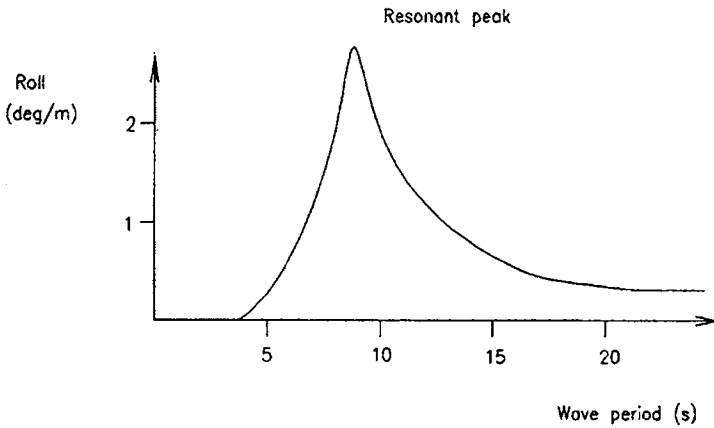
Figure 3.8   Typical RAO of Barge Roll Motion in Beam Seas (CMPT, 1998)

Another application of the RAO is to calculate loads in irregular waves. Bhattacharyya (1978) suggests that the total response of a vessel in an irregular seaway is the linear superposition of the response to the individual components that may be determined using RAO.

In the calculation of H $(\omega,\alpha_k,\Lambda_l)$, a suitable range of wave frequency, number of frequency points, and wave headings should be used. The commonly used parameters for an FPSO analysis are:

- Frequency range: $0.20 \leq \omega \leq 1.80$ rad/s

- Frequency increment: 0.05 rad/s

- Wave heading: 0° to 360° with 15° increment

If a finite element method is used, the pressure distribution needs to be mapped from a hydrodynamic model onto a finite element model with $N_A \times N_F \times N_H$ loading cases, where:

N_A = Number of loading patterns

N_F = Number of frequency points

N_H = Number of wave headings

Figure 3.9 shows a deck plating at the mid-section. The stress FRFs at twenty-four incident wave directions (refer to Figure 3.10) are calculated by using the 2D strip method. 3D hydrodynamic and FE method can be used for general structural details.
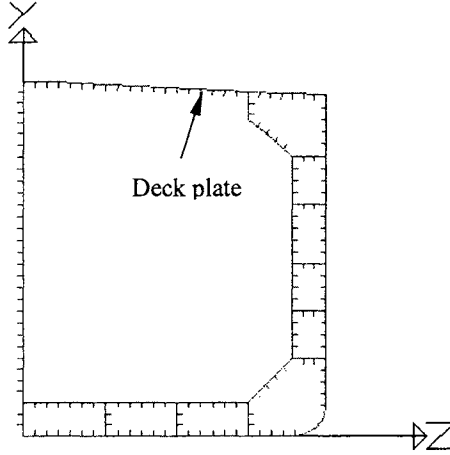
Figure 3.9   Deck Plating at the Mid Cross-section

The spectral density function of the response (stresses or loads) to a wave spectrum using the wave scatter diagram and the FRF, can be determined by:

$$\mathbf{S}_x^{ijkl}(\omega) = \sum_m \overline{H} \cdot H(\omega; \alpha_k + \theta_m, \Lambda_l) \mathbf{S}_w^{ij}(\omega, \theta_m) \tag{3.1}$$

where,

$\mathbf{S}_x^{ijkl}(\omega)$ = Spectral density function for response x

$\mathbf{S}_w^{ij}(\omega, \theta_m)$ = Wave spectral density function with wave spreading

$\Theta(\theta_m)$ = Spreading function

$$\mathbf{S}_w^{ij}(\omega, \theta_m) = \mathbf{S}_w^{ij}(\omega)\Theta(\theta_m) \tag{3.2}$$

where,

$s_w^{ij}(\omega)$ = Wave spectral density function specified by (H_S, T) and $\Theta(\theta_m)$ is expressed as:

$$\Theta(\theta_m) = C_n \cos^{2n}(\theta_m) \quad (|\theta_m| \leq \pi/2, \ n = 1,2,\ldots) \tag{3.3}$$

where,

$$C_n = \frac{\Gamma(n+1)}{\sqrt{\pi}\Gamma(n+\frac{1}{2})} = \frac{2^{2n}(n!)^2}{\pi(2n)!} \quad \text{where } \Gamma() \text{ is Gamma Function.}$$
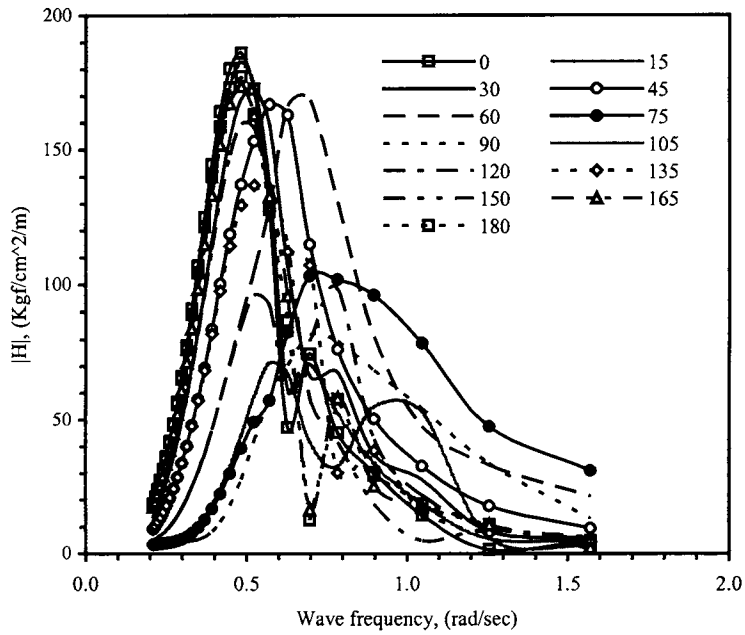
Figure 3.10   Comparison of Stress Frequency Response Functions at 13 Wave Directions (symmetric with respect to α=0° or α=180°) (Zhao, Bai & Shin, 2001)

Table 3.3 Comparison of Different Wave and Response Spectra (Zhao, Bai & Shin, 2001)

	Wave Spectrum				Response Spectrum	
	H_S (m)	T_P (Sec)	m_0 (m^2)	ε	m_0 $[kgf/cm^2]^2$	ε
JONSWAP (γ=3.3)	8.5	9.5	4.4	0.59	2.17×10^5	0.32
Bretschneider	8.5	9.5	4.4	0.59	2.33×10^5	0.36

Figure 3.11 demonstrates the stress spectral density functions at $\alpha_k = 0$. The bandwidth parameter ε of the response to JONSWAP and Bretschneider is shown in Table 3.3.
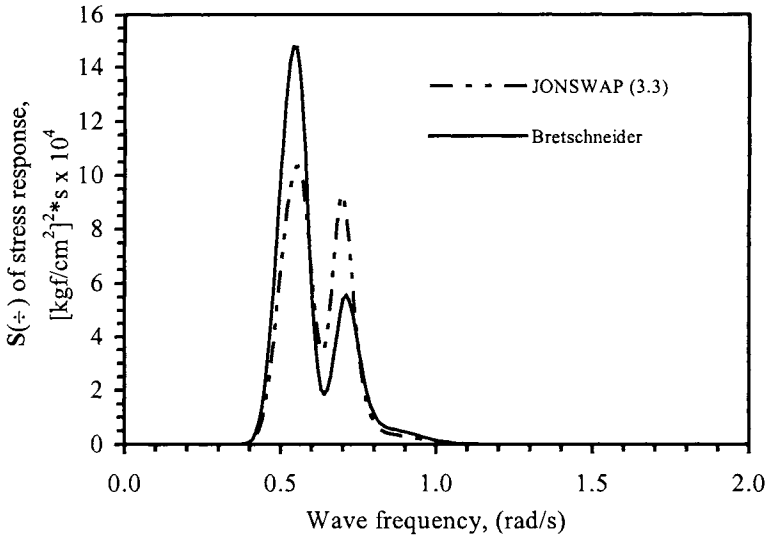
Figure 3.11   Stress Spectral Density Functions using the JONSWAP Spectrum (γ=3.3) and using the Bretschneider Spectrum (Zhao, Bai & Shin, 2001)

3.5   Extreme Values

3.5.1   General

Strength analysis generally involves assessing the yield, buckling, ultimate, and fatigue strengths, see PART II and PART III of this book. The yield, buckling, ultimate strength are directly related to the extreme values of stress response, which will be discussed in this Section.

Figure 3.12 illustrates the extreme response and strength assessment procedure, which uses short-term and long-term approaches. Ochi and Wang (1979, 1981) showed that both long- and short- term approaches predict very close extreme values. It seems that applying one approach is good enough. This is true only for ideal situations. In fact, using either approach cannot guarantee a conservative design in practice, for the following reasons:

*   It is impossible to predict extreme storm spectrum defined with a set of (H_S, T) exactly. For example, even with the same H_S, the characteristic wave period may be different depending on wave development stages or regions of a storm.

*   Structural response depends on both incident wave height and wave frequency. It is obvious that an extreme storm may not generate the largest structural response.

*   The currently used wave scatter diagram may be incomplete to cover all severe storms due to the lack of data, while the long-term extreme value predicted is sensitive to those storms.

Therefore, if possible, both short- and long-term approaches should be used to achieve a conservative design.

3.5.2   Short-Term Extreme Approach

The short-term extreme values can be estimated based on a known initial probability distribution of the maxima. For *a Gaussian random response with zero-mean*, the probability density function of the maxima (peak values) can be represented by the following Rayleigh distribution:

$$p(x) = \frac{x}{m_0} \exp(-\frac{x^2}{2m_0}) \qquad x \geq 0 \tag{3.4}$$

based on the assumption of a small bandwidth ε, where,

$$\varepsilon = \sqrt{1 - \frac{m_2^2}{m_0 m_4}}$$

m_0, m_2, and m_4 are the moments of response spectral density functions of zero-th, second, and fourth order, respectively.

The cumulative probability distribution is:

$$P(x) = \int_0^x p(\xi) d\xi = 1 - \exp(-\frac{x^2}{2m_0}) \tag{3.5}$$

The Probable Extreme Value (PEV) can be determined by:

$$x_{PEV} = \sqrt{2 \ln N} \sqrt{m_0} \tag{3.6}$$

Sometimes, the extreme response that is exceeded at a small possibility level α (risk parameter), can be expressed as (Bhattacharyya, 1978):

$$x_{ext}\big|_\alpha = \sqrt{2 \ln(N/\alpha)} \sqrt{m_0} \qquad \text{for } \varepsilon \leq 0.9 \tag{3.7}$$

where N, is the number of observations (or cycles) and x_{PEV} represents the value that may be exceeded once out of N observations. The chance for x_{PEV} to be exceeded is $1/\alpha$ times of that for $x_{ext}\big|_\alpha$ to be exceeded. $\alpha(\leq 1)$ is chosen at the designer's discretion, depending on the condition of application.

For a response spectrum with a finite ε, the probability density function of maxima in Eq. (3.4) can be represented as (Zhao, Bai & Shin, 2001):

$$p(x) = \frac{2}{1 + \sqrt{1 - \varepsilon^2}} \left[\frac{\varepsilon}{\sqrt{2\pi m_0}} \exp(-\frac{x^2}{2\varepsilon^2 m_0}) + \sqrt{1 - \varepsilon^2} \frac{x}{m_0} \exp(-\frac{x^2}{2m_0}) \phi(\frac{\sqrt{1 - \varepsilon^2}}{\varepsilon} \frac{x}{\sqrt{m_0}}) \right] \quad (x \geq 0) \tag{3.8}$$

in which $\phi(r) = \frac{1}{\sqrt{2\pi}} \int_{-\infty}^r \exp(-\frac{r^2}{2}) dr$.

Similar to Eqs. (3.6) and (3.7), the PEV of responses is given by:

$$x_{PEV} = \sqrt{2\ln\left(\frac{2\sqrt{1-\varepsilon^2}}{1+\sqrt{1-\varepsilon^2}}N\right)}\sqrt{m_0} \qquad \text{for } \varepsilon \le 0.9 \tag{3.9}$$

and the extreme response at possibility level α is:

$$x_{ext}|_\alpha = \sqrt{2\ln\left(\frac{2\sqrt{1-\varepsilon^2}}{1+\sqrt{1-\varepsilon^2}}\frac{N}{\alpha}\right)}\sqrt{m_0} \qquad \text{for } \varepsilon \le 0.9 \tag{3.10}$$
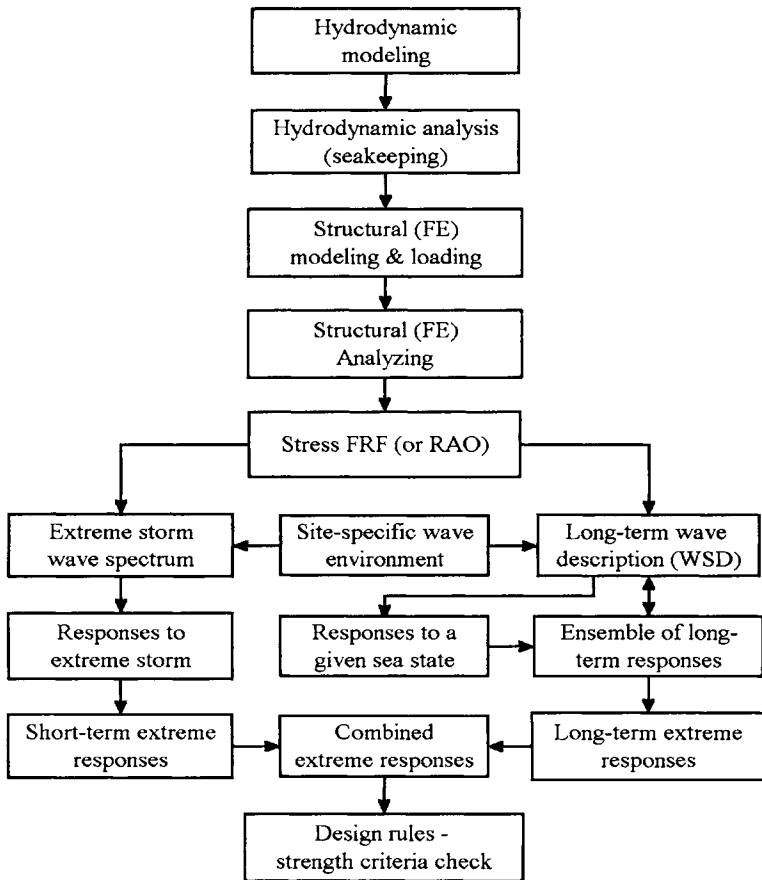
**Figure 3.12   Extreme Response and Strength Assessment Procedure
(Zhao, Bai & Shin, 2001)**

Ochi (1981) has shown that the expected number of positive maxima (peak values) for a short-term random process can be expressed as:

$$N = (60)^2 \frac{T_S}{4\pi} \cdot \frac{1+\sqrt{1-\varepsilon^2}}{\sqrt{1-\varepsilon^2}} \sqrt{\frac{m_2}{m_0}} \tag{3.11}$$

where T_S is the time length of wave data, unit of time in hours.

Figure 3.13 indicates the dependency of ε vs. spectral peak periods in a wave scatter diagram and describes the range of ε where the stress response is mostly between 0.25 and 0.40. Based on Eq. (3.11), the relative counting error, can be determined in case ε is ignored. For the wave conditions listed in Table 3.3, the relative counting errors are compared in Table 3.4. It is evident that ε can be easily close to 0.4, and an error of 5% to 10% could be introduced if ε is ignored. Therefore, it is suggested that a correction factor for ε be used.
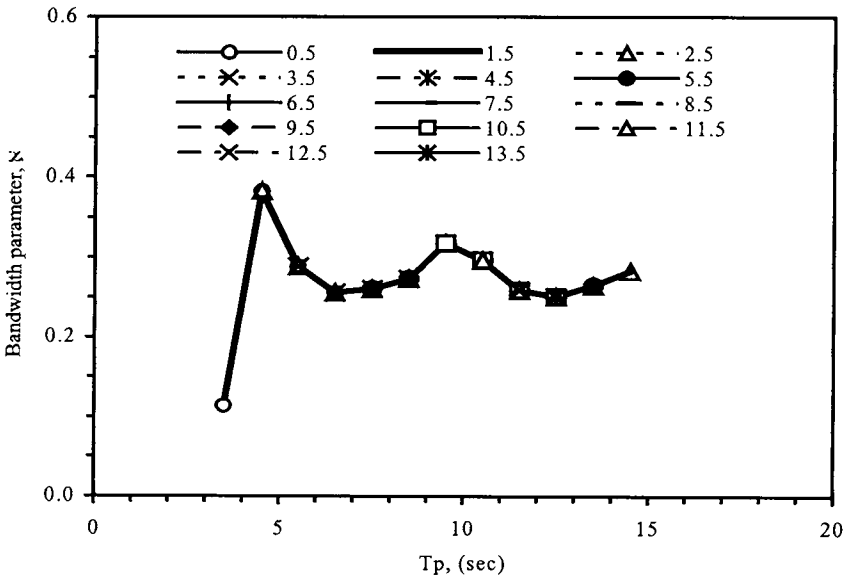
Figure 3.13   **Variation of Bandwidth Parameters of Stress Responses vs.**
T_P and H_S (Wave spectrum used: JONSWAP; Wave at
W156) (Zhao, Bai & Shin, 2001)

Table 3.4   **Comparison of Relative Counting Errors (Zhao, Bai & Shin,**
2001)

	Wave Spectrum		Response Spectrum	
	ε	Error	ε	Error
JONSWAP	0.59	11.8	0.32	2.7
Bretschneider	0.59	11.9	0.36	3.7

Using Eq. (3.11), Eqs. (3.9) and (3.10) can be rewritten as:

$$x_{PEV} = \sqrt{2\ln\left(\frac{(60)^2 T_S}{2\pi}\sqrt{\frac{m_2}{m_0}}\right)}\sqrt{m_0} \tag{3.12}$$

$$x_{ext}\big|_\alpha = \sqrt{2\ln\left(\frac{(60)^2 T_S}{2\pi\alpha}\sqrt{\frac{m_2}{m_0}}\right)}\sqrt{m_0} \tag{3.13}$$

Eqs. (3.12) and (3.13) are not directly dependent on ε.

When applying the short-term approach, a design wave spectrum of the extreme storm condition is usually combined with a long-term extreme value of H_S and T. Ochi's (1981) results indicate that the probability density function of (H_S, T) takes a bivariant lognormal distribution. A commonly used approach is to determine the long-term extreme value of H_S, and obtain T along with the conditional probability distribution $p(T|H_S)$, or using a simpler formula between H_S and T based on the wave steepness.

The long-term PEV of H_S with different return periods is listed in Table 3.5, where H_S is calculated by applying the long-term extreme approach discussed in the next Section. T_P is required in order to determine the extreme wave environment used in the short-term approach (two parameter wave spectra in this example). Table 3.6 lists the peak periods associated with H_S. The values of T_P are calculated by using $p(T|H_S)$ for confidence levels of 0.5, 0.75, 0.85, and 0.95, separately (Ochi, 1978). Each H_S and related T_P form a wave spectral family and they are used to determine the response spectrum, and finally the short-term extreme values.

Table 3.5   Extreme Significant Wave Height (Zhao, Bai & Shin, 2001)

Wave	H_S (m) with Return period		
	20 years	50 years	100 years
W156	17.0	18.2	19.1
W391	10.2	11.6	12.6

Table 3.6   Wave Spectral Family with Different H_S (Zhao、Bai&Shin、2001)

	H_S (m)			Weighting factor
	17.0	18.2	19.1	
T_P (sec)	13.1	13.4	13.5	0.0500
	13.8	14.1	14.3	0.0500
	14.8	15.0	15.2	0.0875
	15.7	16.0	16.2	0.1875
	16.6	16.8	17.0	0.2500
	18.4	18.7	18.9	0.1875
	19.7	19.9	20.1	0.0875
	20.7	21.0	21.2	0.0500
	22.1	22.4	22.6	0.0500

m_0 and m_2 need to be calculated properly when applying Eqs. (3.12) and (3.13). Table 3.7 compares the short-term extreme values obtained by two different methods. Method I, uses the weighting factors listed in Table 3.6 to calculate the mean values of m_0 and m_2, while method II uses each member of the spectral family in Table 3.6, and takes the maximum *i.e.*:

$$x_{PEV} = \max_j \{x_{PEV}(H_S, T_j)\} \tag{3.14}$$

The extreme values provided by the latter are up to 16% larger than those obtained using the former method. This is understandable, because the sample size (or exposure time) for the latter is relatively larger. In this example, extreme values for H_S with risk parameter $\alpha = 1$ are directly applied. Obviously, the final extreme values of responses are dependent on the designer's discretion and choice of H_S.

Table 3.7   Short-term Extreme Values of Dynamic Stresses for Deck Plates (Zhao, bai & Shin, 2001)

Method	Wave	Spectrum	Return period (years)		
			20	50	100
I	W156	JONSWAP	2021.0	2135.4	2139.6
	W156	Bretsch.	1991.9	2121.4	2156.2
	W391	JONSWAP	1288.6	1446.9	1527.6
	W391	Bretsch.	1211.0	1372.7	1467.4
II	W156	JONSWAP	2304.1	2468.7	2565.7
	W156	Bretsch.	2081.3	2226.6	2334.0
	W391	JONSWAP	1381.3	1568.0	1714.7
	W391	Bretsch.	1248.9	1412.8	1547.2

(stress in unit: Kgf/cm^2)

3.5.3   Long-Term Extreme Approach

A long-term initial cumulative probability distribution function $P(x)$ of responses is required when predicting a long-term extreme value. Although function $P(x)$ cannot be predicted explicitly due to the complications of the responses in various sea-states, it can be built up approximately through accumulations of various short-term statistical analysis. Generally, $P(x)$ can be of the form:

$$P(x) = 1 - \exp[-q(x)] \qquad (q(x) \geq 0) \tag{3.15}$$

Weibull distributions or log-normal distributions are commonly used for $P(x)$. The Weibull cumulative probability distribution function can be represented as:

$$P(x) = 1 - \exp[-(\frac{x-\gamma}{\beta})^m] \qquad (\beta, m > 0) \tag{3.16}$$

where parameters m, β, and γ can be determined from the observed data by the least-squares fitting method. Ochi (1981) also suggested to use a generalized form to achieve higher accuracy in the curve fitting:

$$q(x) = cx^m \exp(-\rho x^k) \tag{3.17}$$

where, c, m, ρ, and k are four constant parameters to be determined by nonlinear least-squared fitting:

$$Q = \ln[-\ln(1 - P(x))] = \ln c + m \ln x - \rho x^k \tag{3.18}$$

Once the mathematical expression of $P(x)$ in Eq. (3.15) is obtained, the long-term PEV can be determined by:

$$1 - P(x_{PEV}) = \frac{1}{N} \tag{3.19}$$

$$1 - P(x_{ext}|_\alpha) = \frac{\alpha}{N} \tag{3.20}$$

Here α, is the possibility level as in Eqs. (3.7) and (3.10) and N is the number of observations or cycles related to the return period. In the design of offshore structures, a return period of 100 years is widely used for estimating the long-term extreme values.

When the wave scatter diagram is applied, $P(x)$ from Eq. (3.15) can be obtained by using the definition of probability density function of maxima:

$$p(x) = \frac{\sum_{i,j,k,l} n_{ijkl} \Pr(w_{ij}) \Pr(\alpha_k) \Pr(\Lambda_l) p_{ijkl}(x)}{\sum_{i,j,k,l} n_{ijkl} \Pr(w_{ij}) \Pr(\alpha_k) \Pr(\Lambda_l)} = \frac{1}{\overline{N}_S} \sum_{i,j,k,l} n_{ijkl} \Pr(w_{ij}) \Pr(\alpha_k) \Pr(\Lambda_l) p_{ijkl}(x) = \frac{1}{\overline{f}_S} \sum_{i,j,k,l} f_{ijkl} \Pr(w_{ij}) \Pr(\alpha_k) \Pr(\Lambda_l) p_{ijkl}(x)$$

$$\tag{3.21}$$

where,

$Pr(w_{ij})$ = Normalized joint wave probability of $(H_S(i), T(j))$ or cell w_{ij} in Wave Scatter Diagram, $\sum_{i,j} \Pr(w_{ij}) = 1$

$Pr(\alpha_k)$ = Probability of wave in direction α_k, $\sum_k \Pr(\alpha_k) = 1$

$Pr(\Lambda_l)$ = Probability (or percentage) of loading pattern Λ_l during service, $\sum_l \Pr(\Lambda_l) = 1$

n_{ijkl} = Average number of responses in T_S corresponding to cell w_{ij} of Wave Scatter Diagram, wave direction α_k and loading pattern Λ_l. n_{ijkl} can be computed by Eq. (3.11)

f_{ijkl} = Average number of responses per unit of time of a short-term response corresponding to cell w_{ij}, wave direction α_k and loading pattern Λ_l, unit in 1/hour. $f_{ijkl} = n_{ijkl}/T_S$

$p_{ijkl}(x)$ = Probability density function of short-term response maxima corresponding to cell w_{ij}, wave direction α_k and loading pattern Λ_l. If the wave spreading (short-crest sea) effect is considered, it should have been included in the responses as shown in Eq. (3.8).

$\overline{N}_S$ = Long-term based, average number of observations of responses in T_S,

$$\overline{N}_S = \sum_{i,j,k,l} n_{ijkl} \Pr(w_{ij}) \Pr(\alpha_k) \Pr(\Lambda_l) = T_S \sum_{i,j,k,l} f_{ijkl} \Pr(w_{ij}) \Pr(\alpha_k) \Pr(\Lambda_l) \tag{3.22}$$

Denoting the long-term based average number of observations of responses in T_D by $\overline{N}_D$, then

$$\overline{N}_D = \frac{T'_D}{T_S}\, \overline{N}_S = T'_D\, \overline{f}_S \tag{3.23}$$

T_D = Duration of service, unit of time in years

T'_D = Duration of service, unit of time in hours

Figure 3.14 displays the long-term distribution P (x) of stress responses to waves W156 and W391. It is obvious that the wave environment is the dominant factor affecting the long-term probability distribution, since the effects of spectral shape are not significant.

After the mathematical formula of $q(x)$ in Eq. (3.17) has been determined by curve fitting using Eqs. (3.18) and (3.21), the extreme value can be calculated by Eq. (3.19) or (3.20). Figure 3.15 compares the long-term extreme values for waves W156 and W391 using the JONSWAP and Bretschneider spectra. The extreme values of stress dynamic components are listed in Table 3.8. The extreme values obtained by using the long-term approach are up to 9% larger than the short-term extreme values listed in Table 3.7. The long-term approach uses the probability distribution of responses, which can avoid the uncertainty caused by the choice of extreme H_S and associated wave spectral family (a series of T_P). Based on this point of view, the long-term approach is more reliable than the short-term approach under the given circumstances and with the same environmental information.
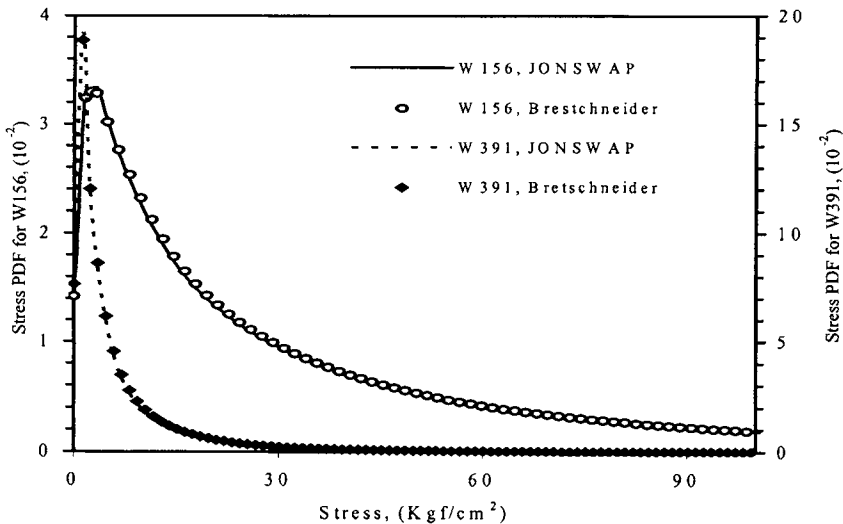
Figure 3.14   **Long-term Probability Density Function P(x) of Stress Responses for Deck Plate (Zhao, Bai & Shin, 2001)**

Table 3.8 Long-term Extreme Values of Dynamic Stress for Deck Plate (Zhao, Bai & Shin, 2001)

Wave	Spectrum	Return period (year)			Number of Cycles (1/ hour)
		20	50	100	
W156	JONSWAP	2476.9	2669.3	2818.2	509.2
W156	Bretsch.	2166.4	2328.0	2452.8	500.9
W391	JONSWAP	1751.6	1982.9	2169.9	694.0
W391	Bretsch.	1676.6	1899.1	2079.0	673.2

(stress in unit: Kgf/cm^2)
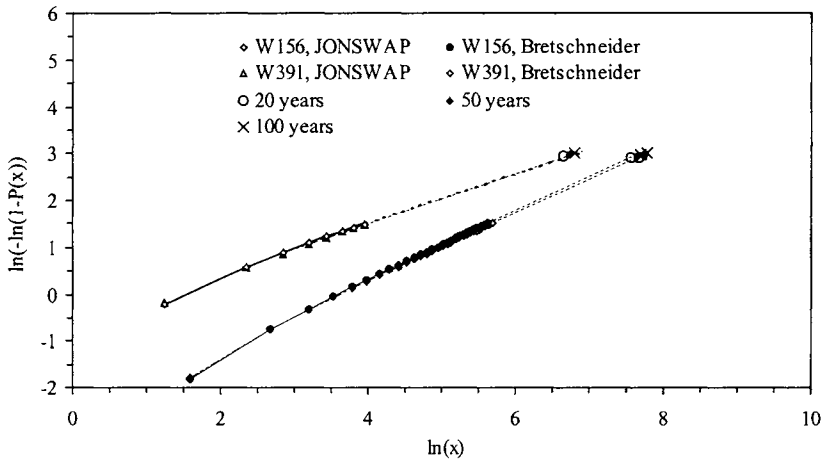
Figure 3.15 Long-term Extremes of Dynamic Stress Responses for Deck Plate (return period = 20, 50, and 100 years) (Zhao, Bai & Shin, 2001)

3.5.4 Prediction of Most Probable Maximum Extreme for Non-Gaussian Process

For a short-term Gaussian process, there are simple equations for estimating extremes. The Most Probable Maximum value (mpm), of a zero-mean narrow-band Gaussian random process may be obtained by Eq. (3.6), for a large number of observations, N. In this Section, we shall discuss the prediction of most probable maximum extreme for non-Gaussian process based on Lu et al (2001, 2002).

Wave and current induced loading is non-linear due to the nonlinear drag force and free surface. Non-linearity in response is also induced by second order effects due to large structural motions and hydrodynamic damping caused by the relative velocity between the structure and water particles. Moreover, the leg-to-hull connection and soil-structure interaction induce structural non-linearity. As a result, although the random wave elevation can be considered as a Gaussian process, the response is nonlinear (e.g., with respect to wave height) and non-Gaussian.

Basically, the prediction procedure is to select a proper class of probabilistic models for the simulation in question and then to fit the probabilistic models to the sample distributions. For the design of jack-ups, the T&R Bulletin 5-5A (SNAME, 1994) recommends four (4) methods to predict the Most Probable Maximum Extreme (MPME) from time-domain simulations and DAFs using statistical calculation.

Drag/Inertia Parameter Method

The drag/inertia parameter method is based on the assumption that the extreme value of a standardized process can be calculated by: splitting the process into drag and inertia two parts, evaluating the extreme values of each and the correlation coefficient between the two, then combining as

$$(mpm_R)^2 = (mpm_{R1})^2 + (mpm_{R2})^2 + 2\rho_{R12}(mpm_{R1}) \cdot (mpm_{R2}) \tag{3.24}$$

The extreme values of the dynamic response can therefore be estimated from extreme values of the quasi-static response and the so-called "inertia" response, which is in fact the difference between the dynamic response and the quasi-static response. The correlation coefficient of the quasi-static and "inertia" responses is calculated as

$$\rho_R = \frac{\sigma_{Rd}^2 - \sigma_{Rs}^2 - \sigma_{Ri}^2}{2\sigma_{Rs}\sigma_{Ri}} \tag{3.25}$$

The Bulletin recommends that the extreme value of the quasi-static response be calculated using one of the three approaches as follows:

Approach 1: Static extreme can be estimated by combing the extreme of quasi-static response to the drag term of Morison's equation and the extreme of quasi-static response to the inertia term of Morison's equation, using Eq. (3.25) as above.

Approach 2: Baar (1992) suggested that static extreme may be estimated by using a non-Gaussian measure. The structural responses are nonlinear and non-Gaussian. The degree of non-linearity and the deviation from a Gaussian process may be measured by the so-called drag-inertia parameter, K, which is a function of the member hydrodynamic properties and sea-state. This parameter is defined as the ratio of the drag force to inertia force acting on a structural member of unit length.

$$K = (2C_D\sigma_V^2)/(\pi C_M D\sigma_A) \tag{3.26}$$

As an engineering postulate, the probability density function of force per unit length may be used to predict other structural responses by obtaining an appropriate value of K from time-domain simulations. K can be estimated from standard deviation of response due to drag force only and inertia force only.

$$K = \sqrt{\frac{\pi}{8}} \frac{\sigma_R(C_M = 0)}{\sigma_R(C_D = 0)} \tag{3.27}$$

Approach 3: Alternatively K can be estimated from the kurtosis of structural response

$$K = \left[\frac{(\kappa - 3) + \left\{ \frac{26(\kappa - 3)}{3} \right\}^{1/2}}{(35 - 3\kappa)} \right]^{1/2} \tag{3.28}$$

The third approach may be unreliable because the estimation is based solely on kurtosis without the consideration of lower order moments. As explained by Hagemeijer (1990), this

approach ignores the effect of free-surface variation. The change in submerged area with time will produce a non-zero skewness in the probability density function of the structural response (say, base shear) which has not been accounted for in the equations for force on a submerged element of unit length. Hagemeijer (1990) also pointed out that the skewness and kurtosis estimated (as is the parameter K) from short simulations (say 1 to 2 hours) are unreliable.

Weibull Fitting

Weibull fitting is based on the assumption that structural response can be fitted to a Weibull distribution:

$$F_R = 1 - \exp\left[-\left(\frac{R-\gamma}{\alpha}\right)^{\beta}\right] \tag{3.29}$$

The extreme value for a specified exceedance probability (say 1/N) can therefore be calculated as:

$$R = \gamma + \alpha\left[-\ln(1 - F_R)\right]^{1/\beta} \tag{3.30}$$

Using a uniform level of exceedance probability of 1/N , Eq.(3.30) leads to

$$R_{MPME} = \gamma + \alpha\left[-\ln(1/N)\right]^{1/\beta} \tag{3.31}$$

The key for using this method is therefore to calculate the parameters α, β and γ, which can be estimated by regression analysis, maximum likelihood estimation, or static moment fitting. For a 3-hour storm simulation, N is approximately 1000. The time series record is first standardized ($R* = \frac{R-\mu}{\sigma}$), and all positive peaks are then sorted in ascending order.

Figure 3.16 shows a Weibull fitting to the static base shear for a jack-up platform.

As recommended in the SNAME Bulletin, only a small fraction (e.g., the top 20%) of the observed cycles is to be used in the curve fitting and least square regression analysis is to be used for estimating Weibull parameters. It is true that for predicting extreme values in order statistics, the upper tail data is far more important than lower tail data. What percentage of the top ranked data should be extracted for regression analysis is, however, very hard to establish.

Gumbel Fitting

Gumbel Fitting is based on the assumption that for a wide class of parent distributions whose tail is of the form:

$$F(X) = 1 - \exp(-g(x)) \tag{3.32}$$

where g(x) is a monotonically increasing function of x, the distribution of extreme values is Gumbel (or Type I, maximum) with the form:

$$F(x_{extreme} \le X_{MPME}) = \exp\left[-\exp(-\frac{1}{\kappa}(X_{MPME} - \psi))\right] \tag{3.33}$$

The MPME typically corresponds to an exceedance probability of 1/1000 in a distribution function of individual peaks or to 0.63 in an extreme distribution function. The MPME of the response can therefore be calculated as:

$$X_{MPME} = \psi - \kappa \cdot \ln(-\ln(F(X_{MPME}))) \tag{3.34}$$

Now the key is to estimate the parameters ψ and κ based on the response signal records obtained from time-domain simulations. The SNAME Bulletin recommends to extract maximum simulated value for each of the ten 3-hour response signal records, and to compute the parameters by maximum likelihood estimation. Similar calculations are also to be performed using the ten 3-hour minimum values. Although it is always possible to apply the maximum likelihood fit numerically, the method of moments (as explained below) may be preferred by designers for computing the Gumbel parameters in light of the analytical difficulty involving the type-I distribution in connection with the maximum likelihood procedure.

For the type-I distribution, the mean and variance are given by

Mean: $\mu = \psi + \gamma \cdot \kappa$, where γ = Euler constant (0.5772...)

Variance: $\sigma^2 = \pi^2 \kappa^2 / 6$

By which means the parameters ψ and κ can be directly obtained using the moment fitting method:

$$\kappa = \frac{\sqrt{6}\sigma}{\pi}, \quad \psi = \mu - 0.57722 \cdot \kappa \tag{3.35}$$

Winterstein/Jensen Method

The basic premise of the analysis according to Winterstein (1988) or Jensen (1994) is that a non-Gaussian process can be expressed as a polynomial (e.g., a power series or an orthogonal polynomial) of a zero mean, narrow-banded Gaussian process (represented here by the symbol U). In particular, the orthogonal polynomial employed by Winterstein is the Hermite polynomial. In both cases, the series is truncated after the cubic terms as follows:

Winterstein:

$$R(U) = \mu_R + \sigma_R \cdot K\left[U + h_3(U^2 - 1) + h_4(U^3 - 3U)\right] \tag{3.36}$$

Jensen:

$$R(U) = C_0 + C_1 U + C_2 U^2 + C_3 U^3 \tag{3.37}$$

Within this framework, the solution is essentially separated into two phases. First, the coefficients of the expansions, i.e., K, h_3, and h_4 in Winterstein's formulation and C_0 to C_3 in

Jensen's formulation are obtained. Subsequently, upon substituting the most probable extreme value of U in Eq.(3.36) or Eq.(3.37), the MPME of the responses will be determined. The procedure of Jensen appears perfectly simple.

Ochi (1973) presented the expression for the most probable value of a random process that satisfies the generalized Rayleigh distribution (i.e. the wide-banded Rayleigh). The bandwidth, ε, of this random variable is determined from the zeroth, 2nd and 4th spectral moments. For ε less than 0.9, the short-term most probable extreme value of U is given by

$$U = \sqrt{2\ln(\frac{2\sqrt{1-\varepsilon^2}}{1+\sqrt{1-\varepsilon^2}}N)} \tag{3.38}$$

For a narrow-banded process, ε approaches zero and the preceding reduces to the more well-known expression:

$$U = \sqrt{2\ln N} \tag{3.39}$$

Comparison of Eq. (3.38) and Eq.(3.39) clearly indicates that the consideration of bandwidth effect for a Gaussian process, U, results in a reduction of the most probable value.

Lu et al (2001, 2002) compared the above four methods recommended in the SNAME Bulletin, investigated the random seed effect on each method, and presented the impact on the dynamic response due to various parameters, e.g. leg-to-hull flexibility, P-delta effect and foundation fixity. The structural models employed in this investigation were constructed to reflect the behavior of two jack-up rigs in service. These rigs were purposely selected to represent two of the most widely used jack-up designs, which are of different leg types, different chord types, and designed for different water depth. Comparison of the four methods was presented in terms of the calculated extreme values and the respective dynamic amplification factors (DAF). Winterstein/Jensen method is considered preferable from the design viewpoint. Gumbel fitting Method is theoretically the most accurate, if enough amount of simulations are generated. Ten simulations are minimum required, which may however, not be sufficient for some cases.

3.6 Concluding Remarks

This chapter gave an overall picture of the environmental conditions and loads for offshore structural design, and detailed the recent developments in the prediction of extreme response. A systematic method for structural analysis of offshore structures has been developed to predict extreme response and fatigue assessment under wave conditions. For the convenience of structural analysis, vibration frequency analysis was also briefly outlined. This Chapter concludes the following:

- Design of offshore structures is highly dependent on wave conditions. Both extreme response and fatigue life can be affected significantly by site-specific wave environments. Collecting accurate wave data is an important part of the design.

- Wave spectral shapes have significant effects on the fatigue life. Choosing the best suitable spectrum based on the associated fetch and duration is required.

- The bandwidth parameter ε of responses is only dependent on the spectral (peak) period. The effect of H_S on ε is negligible.

- The long-term approach is preferred when predicting extreme responses, because it has less uncertainty. However, using the long-term approach is recommended along with the short-term approach for obtaining a conservative result.

- The short-term extreme approach depends on the long-term prediction of extreme wave spectra and proper application of the derived wave spectral family. It is not simpler than the long-term approach.

For more detailed information on environmental conditions and loads for offshore structural analysis, readers may refer to API RP 2T(1997), Sarpkaya and Isaacson (1981), Chakrabarti (1987), Ochi (1990), Faltinsen (1990) and CMPT (1998). On ship wave loads and structural analysis, reference is made to Bhattacharyaa (1978), Beck et al (1989) and Liu et al (1992).

3.7   References

1.   ABS (1992), "Analysis Procedure Manual for the Dynamic Loading Approach (DLA) for Tankers", American Bureau of Shipping.

2.   Almar-Naess, A. (1985), *"Fatigue Handbook – Offshore Steel Structures"*, Tapir Publisher.

3.   API RP 2T (1997), "Recommended Practice for Planning, Designing, and Constructing Tension Leg Platforms", American Petroleum Institute.

4.   Baar, J.J.M. (1992), *"Extreme Values of Morrison-Type Processes"*, Applied Ocean Research, Vol.14, pp. 65-68.

5.   Bai, Y (2001), *"Pipelines and Risers"*, Elsevier Ocean Engineering Book Series, Volume 3.

6.   Bales, S.L., Cumins, W.E. and Comstock, E.N. (1982), "Potential Impact of Twenty Year Hindcast Wind and Wave Climatology in Ship Design", J. of Marine Technology, Vol. 19(2), April.

7.   Beck, R., Cummins, W.E., Dalzell, J.F., Mandel, P. and Webster, W.C. (1989), "Montions in Waves", in *"Principles of Naval Architecture"*, 2nd Edition, SNAME.

8.   Bhattacharyya, R (1978), *"Dynamics of Marine Vehicles"*, John Wiley & Sons, Inc.

9.   Chakrabarti, S.K., (1987), *"Hydrodynamics of Offshore Structures"*, Computational Mechanics Publications.

10. CMPT (1998), *"Floating Structures: A Guide for Design and Analysis"*, Edited by N. Baltrop, Oilfield Publications, Inc.

11. Faltinsen, O.M. (1990), *"Sea Loads on Ships and Offshore Structures"*, Cambridge Ocean Technology Series, Cambridge University Press.

12. Hagemeijer, P. M. (1990), *"Estimation of Drag/Inertia Parameters using Time-domain Simulations and the Prediction of the Extreme Response"*, Applied Ocean Research, Vol.12, pp134-140.

13. Hogben, N. and Lumb, F.E. (1967), *"Ocean Wave Statistics"*, Her Majesty's Stationery Office, London.

14. ISSC (2000), "Specialist Committee V.4: Structural Design of Floating Production Systems", 14th International Ship and Offshore Structures Congress 2000. Nagasaki, Japan, Vol.2.

15. Jensen, J.J. (1994), "Dynamic Amplification of Offshore Steel Platform Response due to Non-Gaussian Wave Loads", Marine Structures, Vol.7, pp.91-105

16. Liu, D, Spencer, J, Itoh, T, Kawachi, S and Shigematsu, K (1992), "Dynamic Load Approach in Tanker Design", SNAME Transactions, Vol. 100.

17. Lu, Y., Chen, Y.N., Tan, P.L. and Bai, Y. (2001), "Prediction of Jack-up Dynamic Response", OMAE, Paper No. 2171.

18. Lu, Y., Chen, Y.N., Tan, P.L. and Bai, Y. (2002), "Prediction of Most Probable Extreme Values for Jack-up Dynamic Analysis", Journal of Marine Structures, Vo. 15, pp.15-34.

19. Ochi, M. K. (1973), *"On Prediction of Extreme Values"*, Journal of Ship Research, Vol.17, No.1.

20. Ochi, MK (1978), "Wave Statistics for the Design of Ships and Ocean Structures" SNAME Transactions, Vol. 86, pp. 47-76.

21. Ochi, MK and Wang, S (1979), "The Probabilistic Approach for the Design of Ocean Platforms", Proc. Conf. Reliability, Amer. Soc. Civil Eng. Pp208-213.

22. Ochi, MK (1981), "Principles of Extreme Value Statistics and their Application" SNAME, Extreme Loads Responses Symposium, Arlington, VA, Oct. 19-20, 1981.

23. Ochi, MK (1990), *"Applied Probability and Stochastic Processes"*, John Wiley and Sons, New York.

24. Pierson, W. J. and Moskowitz, L. (1964), "A Proposed Spectral Form for Fully Developed Wind Seas Based on the Similarity of S. A. Kitaigorodskii", Journal of Geophysical Research, Vol. 69 (24).

25. Sarpkaya, T and Isaacson, M (1981), *"Mechanics of Wave Forces on Offshore Structures"*, Van Nostrand Reinhold Co.

26. SNAME Technical & Research Bulletin 5-5A (1994), "Guideline for Site Specific Assessment of Mobile Jack-up Units", "Recommended Practice for Site Specific Assessment of Mobile Jack-up Units", "Commentaries to Recommended Practice for Site Specific Assessment of Mobile Jack-up Units".

27. Winterstein, S.R. (1988), "Non-linear Vibration Models for Extremes and Fatigue", Journal of Engineering Mechanics, Vol.114, No.10.

28. Yamamoto,Y., Ohtsubo, H., Sumi, Y. and Fujino, M., (1986), "Ship Structural Mechanics", Seisan Tou Publisher (in Japanese).

29. Zhao, CT (1996), "Theoretical Investigation of Springing-ringing Problems in Tension-Leg-Platforms" Dissertation, Texas A&M University.

30. Zhao, CT, Bai, Y and Shin Y. (2001), "Extreme Response and Fatigue Damages for FPSO Structural Analysis", Proc. of ISOPE'2001.

3.8   Appendix A: Elastic Vibrations of Beams

In order to conduct fatigue assessment and the control of vibrations and noises, it is usually necessary to estimate natural frequency and vibration modes of a structure. In this section, basic dynamics is described on the vibration of beams and plates.

3.8.1   Vibration of A Spring/Mass System

Consider a system with a mass m, and spring constant k. When the system does not have damping and external force, the equilibrium condition of the system may be expressed as following,

$$m\ddot{u} + ku = 0 \tag{3.40}$$

where u is the displacement of the mass. The free vibration may be expressed as the solution of Eq.(3.40),

$$u = u_0 \cos(\omega_1 t + \alpha) \tag{3.41}$$

where the natural frequency ω_1 may be expressed as,

$$\omega_1 = \sqrt{\frac{k}{m}} \tag{3.42}$$

and where u_0 and α are determined by the initial condition at time t_0.

Assuming a cyclic force, $F_0 \cos\omega t$, is applied to the mass, the equilibrium condition of the mass may be expressed as following,

$$m\ddot{u} + ku = F_0 \cos\omega t \tag{3.43}$$

and the above equation has a special solution as expressed in the following,

$$u = \frac{F_0/k}{1 - (\omega/\omega_1)^2} \cos(\omega t - \phi) \tag{3.44}$$

where the value of ϕ may be taken as 0 (if $\omega \le \omega_1$) or π (if $\omega > \omega_1$). The general solution is the sum of the special solution and the solution to the free vibration. When $\omega \rightarrow \omega_1$, the value of u will be far larger than that due to F_0 alone that is F_0/k. This phenomenon is called "resonance". In reality, the increase of vibration displacement u may take time, and damping always exists.

Assuming the damping force is proportional to velocity, we may obtain an equilibrium condition of the system as,

$$m\ddot{u} + c\dot{u} + ku = F_0 \cos\omega t \tag{3.45}$$

The general solution to the above equation is

$$u = \frac{F_0/k}{\left(\left(1 - (\omega/\omega_1)^2\right)^2 + 4\zeta^2(\omega/\omega_1)^2\right)^{1/2}} \cos(\omega t - \phi) \tag{3.46}$$

where

$$\zeta = \frac{c}{2m\omega_1} \tag{3.47}$$

$$\tan \phi = \frac{2\zeta(\omega/\omega_1)}{1-(\omega/\omega_1)^2} \tag{3.48}$$

The displacement at resonance ($\omega=\omega_1$) is

$$u = \frac{F_0/k}{2\zeta}\cos(\omega t - \phi) \tag{3.49}$$

3.8.2 Elastic Vibration of Beams

The elastic vibration of a beam is an important subject for fatigue analysis of pipelines, risers and other structures such as global vibration of ships. The natural frequency of the beam may be written as

$$\omega_i = a_i \sqrt{\frac{EI}{ml^4}} \quad (rad/\sec) \tag{3.50}$$

where

EI = bending stiffness of the beam cross-section

L = length of the beam

m = mass per unit length of the beam including added mass

a_i = a coefficient that is a function of the vibration mode, i

The following table gives the coefficient a_i for the determination of natural frequency for alternative boundary conditions.

Table 3.9   Coefficient for Determination of Natural Frequency for Beams

	Clamped-free Beam	Pin-Pin beam	Free-free Beam	Clamped-clamped beam	Clamped-pin beam
1st mode a_1	3.52	π^2=9.87	22	22	15.4
2nd mode a_2	22	$4\pi^2$=39.5	61.7	61.7	50
3rd mode a_3	61.7	$9\pi^2$=88.9	121	121	104
4th mode a_4	121	$16\pi^2$=158	200	200	178
5th mode a_5	200	$25\pi^2$=247	298.2	298.2	272

This Page Intentionally Left Blank

Part I

Structural Design Principles

Chapter 4   Scantling of Ship's Hulls by Rules

4.1   General

In this Chapter, the term "scantling" refers to the determination of geometrical dimensions (such as wall-thickness and sectional modules) for a structural component/system. The initial scantling design is one of the most important and challenging tasks throughout the process of structural design.

After signing the contract, scantling design is the next step and continues throughout the design process until the design is approved by the owner, the shipyard, the classification society, and other maritime authorities. Hull form, design parameters for auxiliary systems, structural scantlings, and final compartmentation are decided on, during the initial design phase. Hull structural scantling itself is a complicated and iterative procedure.

In recent years, the procedure for dimensioning the hull structure is changing rapidly. First, the full benefit of modern information technology is applied to automate the routine scantling calculation based on classification rules. Meanwhile, the application of rational stress analysis and the direct calculation approach using finite element analysis have gained increasing attention in recent years.

In order to develop a satisfactory ship structure, an initial scantling design is generally performed, to establish the dimensions of the various structural components. This will ensure that the structure can resist the hull girder loads in terms of longitudinal and transverse bending, torsion, and shear in still-water and amongst the waves. This process involves combining the component parts effectively. Furthermore, each component part is to be designed to withstand the loads imposed upon it from the weight of cargo or passengers, hydrodynamic pressure, impact forces, and other superimposed local loads such as the deckhouse and heavy machinery.

Generally, this Chapter introduces the design equations for tankers based on IACS (International Association of Classification Societies) requirements and classification rules (e.g. ABS, 2002).

4.2   Basic Concepts of Stability and Strength of Ships

4.2.1   Stability

Two resultant forces act on a free floating body, the force of weight acting downwards and the force of buoyancy acting upwards. The force of weight (W), acts through a point known as the center of gravity (CG), and the force of buoyancy (B) acts through what is known as the center of buoyancy (CB). By Archimedes' Principle, we know that the force of buoyancy equals the

weight of the liquid displaced by the floating body, and thus the center of buoyancy is the center of gravity of the displaced liquid.
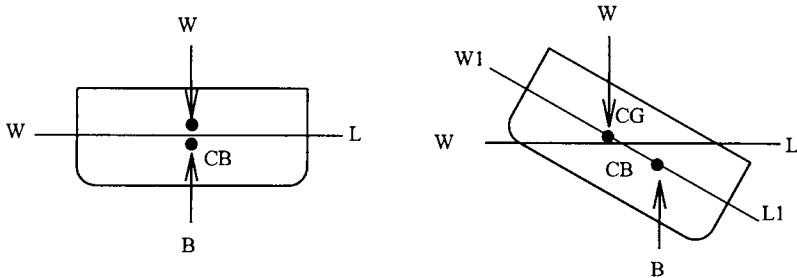
Figure 4.1   Interaction of Weight and Buoyancy

When a floating body is in equilibrium and is displaced slightly from its original position, three conditions may apply. As shown in Figure 4.2 (Pauling, 1988), the body may:

1.   return to its original position, a situation known as positive stability;

2.   remain in its new position, and this is known as neutral stability;

3.   move further from its original position, known as negative stability.

(a)   (b)
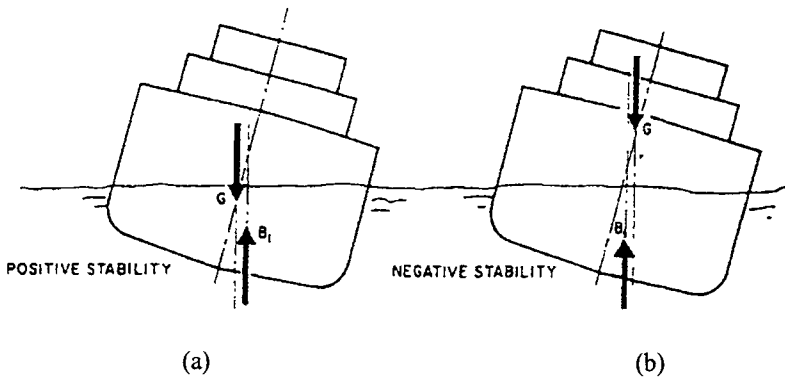
Figure 4.2   Positive and Negative Stability

A ship should be positively stable, so that it can return to its original position without overturning when displaced from its original position, say by a wave.

The stability of a floating body such as a ship is determined by the interaction between the forces of weight, W, and buoyancy, B, as seen in Figure 4.1. When in equilibrium, the two forces acting through the centers of gravity, CG, and buoyancy, CB, are aligned (Figure 4.1(a)). If the body rotates from WL to W1L1, (Figure 4.1(b) and 4.2(a)), a righting moment is created by the interaction of the two forces and the body returns to its original equilibrium state, as shown in Figure 4.1(a). This is a case of positive stability. If the interaction between

the weight and buoyancy forces led to a moment that would have displaced the floating body further from its original position, it would have been a case of negative stability, as shown in Figure 4.2(b). Thus, when designing a ship, it is very important to ensure that the centers of gravity and buoyancy are placed in a position that results in positive stability for the ship.

4.2.2   Strength

Another essential aspect of ship design is the strength of the ship. This refers to the ability of the ship structure to withstand the loads imposed on it. One of the most important strength parameters is the longitudinal strength of the ship, which is estimated by using the maximum longitudinal stress that the hull may withstand. The shear stress is another relevant parameter.

The longitudinal strength of the ship's hull is evaluated based on the bending moments and shear forces acting on the ship. Considering a ship as a beam under distributed load, the shear force at location X, V(X), may be expressed as

$$V(X) = \int_0^X \left(b(x) - w(x) \right) dx \tag{4.1}$$

where b(x) and w(x) denote buoyancy force and weight at location x respectively. The bending moment at location X, M(X) is the integral of the shear curve,

$$M(X) = \int_0^X V(x) dx \tag{4.2}$$

This is further illustrated in Figure 4.3 for a ship in still-water (e.g. in harbors). As may be seen in Figure 4.3(a), an unloaded barge of constant cross-section and density, floating in water would have an equally distributed weight and buoyancy force over the length of the barge. This is represented by the weight and buoyancy curves, seen in Figure 4.3(b). If the barge were loaded in the middle (Figure 4.3(c)), the weight distribution would change and the resulting curve is shown in Figure 4.3(d). This difference between the weight and buoyancy curves results in a bending moment distribution over the length of the ship. This bending moment is known as the still water bending moment, M_S, as seen for a loaded barge in Figure 4.3(e).

For a ship in waves, the bending moment is further separated into two terms:

$$M = M_S + M_W \tag{4.3}$$

where M_S *and* M_W denotes still water and wave bending moment respectively. Figure 4.4 illustrates a ship in a wave equal to its own length. Figure 4.4(a) shows the stillwater condition where the only bending moment acting on the ship is the still water bending moment. Figure 4.4(b) shows the condition when the wave hollow is amidships (i.e. in the middle of the ship). This results in a larger buoyancy distribution near the ends of the ship and thus the ship experiences a sagging condition. In a 'sagging' condition, the deck of the ship is in compression while the bottom is in tension.

Figure 4.4(c) shows a wave crest amidships. In this case, the buoyancy force is more pronounced in the amidships section than at the ends of the ship thus resulting in a hogging condition. 'Hogging' means that the ship is arching up in the middle. Thus, the deck of the ship will be in tension while the bottom will be in compression.

(a) Rectangular barge - unloaded   (c) Barge - half loaded

(b) Weight and buoyancy curves of
    unloaded barge

(d) Weight and buoyancy curves of loaded barge

(e) Still water shear force
    and bending moment curves of loaded barge
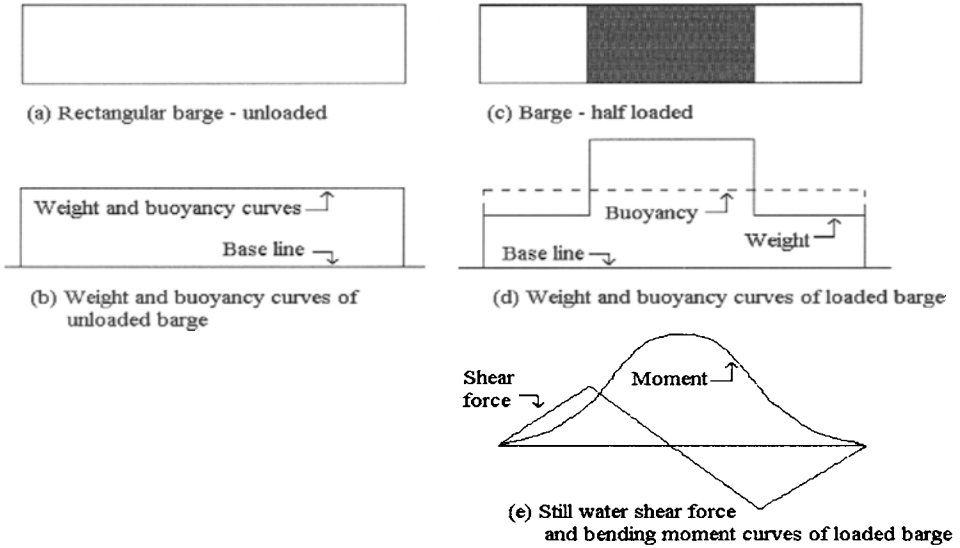
**Figure 4.3   Bending Moment Development of a Rectangular Barge in
Stillwater**

(a) Ship in still water

(b) Ship in sagging condition

(c) Ship in hogging condition
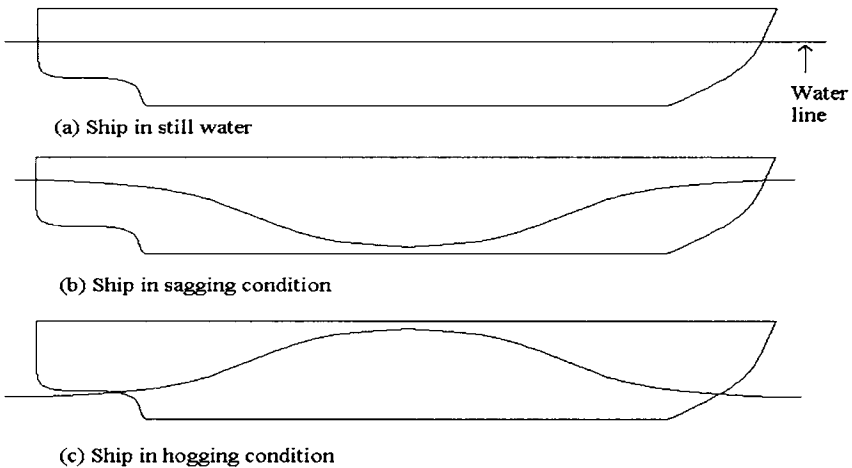
Figure 4.4   Wave Bending Moment in a Regular Wave

In order to compute the primary stress or deflection due to vertical and horizontal bending moments, the elementary Bernoulli-Euler beam theory is used. When assessing the applicability of this beam theory to ship structures, it is useful to restate the following assumptions:

- The beam is prismatic, i.e. all cross sections are uniform.

- Plane cross sections remain plane and merely rotate as the beam deflects.

- Transverse (Poisson) effects on the strain are neglected.

- The material behaves elastically.

- Shear effects can be separated from, and not influence bending stresses or strains.

The derivation of the equations for stress and deflection using the same assumptions as those used for elementary beam theory may be found in textbooks on material strength.

This gives the following well-known formula:

$$\sigma = \frac{M}{SM} = \frac{M_S + M_W}{SM} \qquad (4.4)$$

Where SM, is the section modulus of the ship. The maximum stress obtained from Eq. (4.4) is compared to the maximum allowable stress that is defined in the rules provided by Classification Societies for ship design. If the maximum stress is larger than the maximum allowable stress, the ship's section modulus should be increased, and the drawing changed. The maximum bending moment is usually found in the mid-section of the ship, and thus the longitudinal strength at the mid-section of the ship is usually the most critical.

In general, the maximum shear stress is given by Eq. (4.5):

$$\tau = \frac{F_T S}{tI} \qquad (4.5)$$

where F_T, is the total shear force. t and I denote the web thickness of the hull girder, and the moment of inertia of the hull. S is the first moment of effective longitudinal area above or below the horizontal neutral axis, taken about this axis.

4.2.3 Corrosion Allowance

The strength requirements in ship design rules are based on a "net" ship approach. The nominal design corrosion allowance is to be accounted for, because the scantlings correspond to the minimum strength requirements acceptable for classification regardless of the vessel's design service life. Apart from coating protection for all ballast tanks, minimum corrosion allowance for plating and structural members is to be applied, as shown in Figure 4.5.

For regions of structural members, where the corrosion rates might be higher, additional design margins should be considered for primary and critical structural members. This may minimize repairs and maintenance costs throughout vessel's life cycle.
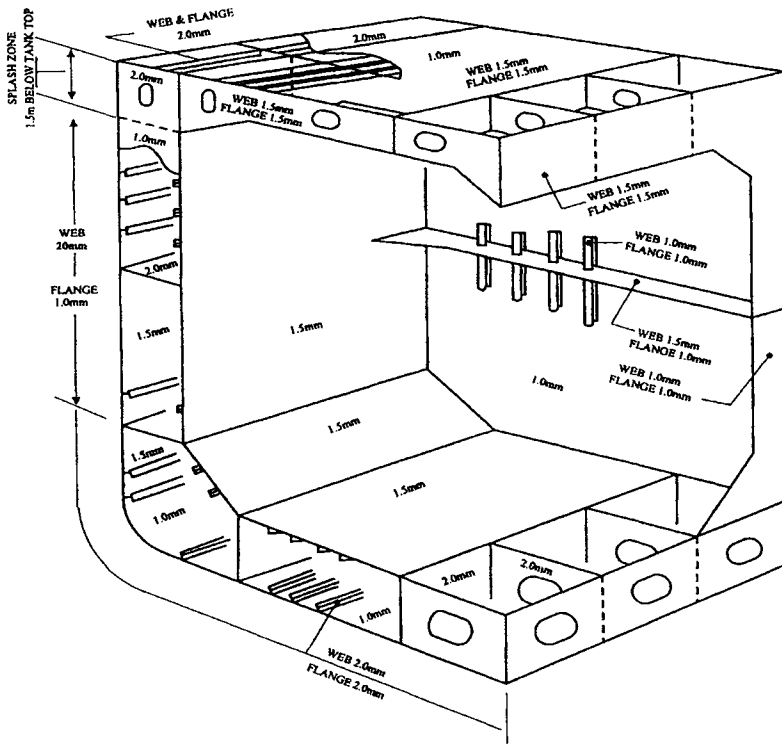
Figure 4.5   Design Corrosion Allowance for Tankers (ABS, 2002)

4.3   Initial Scantling Criteria for Longitudinal Strength

4.3.1   Introduction

In order to assess the structural strength of the ship, the minimum basic scantlings, which depend on the expected loads, must be determined. The load effects acting on a ship may be categorized as primary and secondary stresses. The primary stresses, also termed hull girder stresses, refer to the global response induced by hull girder bending. In contrast, the secondary stresses are termed local stresses and refer to the local response caused by local pressure or concentrated loads. The design rules require that the combined effect of primary and secondary stresses of structural members fall below the allowable strength limits of various failure modes.

Basic scantling is an iterative procedure, as shown in Figure 4.6. The left part of the figure represents the scantling based on function requirements and engineering experience. The right part shows that these basic scantlings have to be evaluated against applicable design rules. Alternatively, the structural strength may be evaluated by means of rational analysis, such as finite element methods, see Chapter 5.
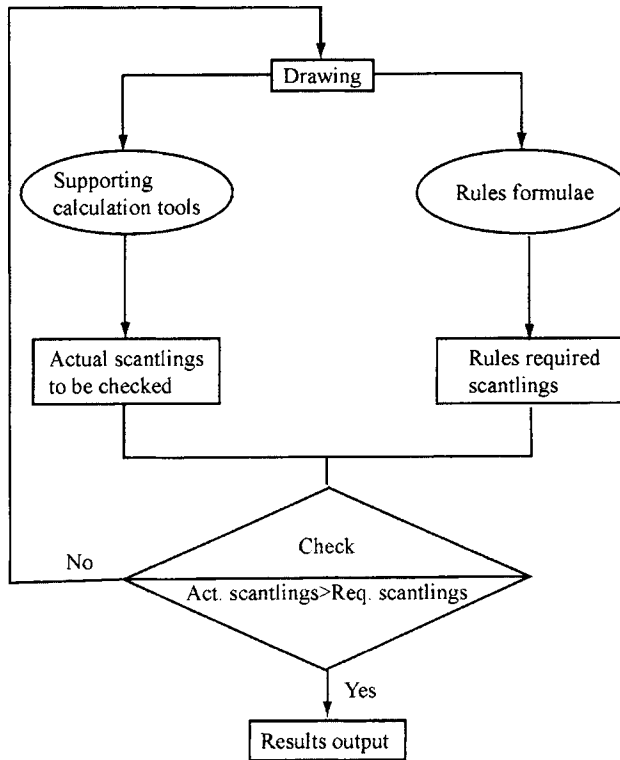
Figure 4.6   Data Flow in the Procedure of Structural Scantling

4.3.2   Hull Girder Strength

The structural members involved in the primary stress calculations are, in most cases, the longitudinally continuous members, such as deck, side, bottom shell, longitudinal bulkheads, and continuous or fully effective longitudinal stiffening members.

Most design rules control hull girder strength by specifying the minimum required section properties of the hull girder cross-sections. The required section properties are calculated based on hull girder loads and maximum allowable hull girder stresses for the mid-ship parallel body (region in which the cross-sections are uniform).

Longitudinal Stress

In order to determine the hull girder section modulus for 0.4L amidships, classification rules require that the greater value of the following equation be chosen:

$$SM = \frac{M_S + M_W}{\sigma_p} \tag{4.6}$$

$$SM = 0.01 C_1 L^2 B (C_b + 0.7) \tag{4.7}$$

σ_p is the nominal permissible bending stress and it may be taken as $17.5 \; KN/cm^2$. The second equation calculates the minimum required section modulus. The constant C_1, depends on the length, and the block coefficient, C_b.

If the top or the bottom flange, or both, consist of higher-strength material, the section modulus calculated above may be reduced by a factor Q, according to the following equation:

$$SM_{hts} = Q \cdot SM \tag{4.8}$$

Q depends on the yield strength and is 0.78 for grade H32 or 0.72 for grade H36 material.

In classification rules, equations and charts are available for calculating still-water bending moment, wave bending moment amidships and wave shear force as well as distribution factor for wave bending moment.

Shear Stress

The distribution of the shear force on the sides and on the bulkheads is very complicated, and hence the required thickness is not easily expressed with a simple formula. Each classification society has its own empirically based formulae for shear force and its distribution along the longitudinal direction.

The general equation for the net thickness is:

$$t = \frac{(F_S + F_W) \cdot S}{I \cdot \sigma_s} \tag{4.9}$$

where F_s is the still-water shear force and F_w is the vertical wave shear force, which is zero for in-port conditions.

The net thickness of the side shell plating is given by:

$$t_s \geq \frac{F_t \cdot D_s \cdot S}{I \cdot \sigma_s} \tag{4.10}$$

and the thickness of the longitudinal bulkhead is given by:

$$t_i \geq \frac{(F_t + R_i) \cdot D_i \cdot S}{I \cdot \sigma_s} \tag{4.11}$$

In these equations, I, is the moment of inertia of the net hull girder section at the position considered. S, is the first moment of the net hull girder section about the neutral axis of the area between the vertical level at which the shear stress is being determined and the vertical extremity of the section, which is being considered. As mentioned above, σ_s is the permissible shear stress, which is defined for either sea or in-port conditions. It is equal to 14.96 divided by Q for sea conditions and 10.87 divided by Q for in-port conditions. Q is the material conversion factor and depends consequently on the material. D is the shear distribution factor, which depends on the design of the longitudinal bulkheads.

4.4   Initial Scantling Criteria for Transverse Strength

4.4.1   Introduction

Ship hull is subjected to static and dynamic hydrostatic pressure in its bottom and two sides, and under loads due to weight of the cargo inside the hull, see Figure 4.7. The transverse loads may cause cross-sectional deformation as shown in dotted lines, and stresses in transverse bulkheads, floors, side frames and deck beams. In general, hulls of the cargo ships are based on transverse system where the transverse strength may be modeled as two-dimensional frames. The two-dimensional frame is subjected to the hydrostatic pressure and loads due to cargo weight as shown in Figure 4.7, as well as the shear forces transferred from the longitudinal members.
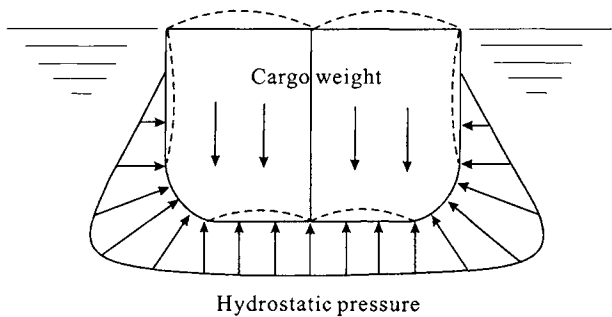
Figure 4.7   Transverse Loads on Ship Hulls

4.4.2   Transverse Strength

Two-dimensional (2D) frame analysis may be applied to calculate transverse strength. The frame analysis may be conducted using analytical equations that are available from typical books on structural analysis, or by the finite element methods.

In some cases, the frame analysis may be based on 2D plane stress analysis. The allowable stress for transverse strength is defined in classification rules with the methods for stress analysis. Typical arrangements for transverse frame may be found in classification rules.

4.5   Initial Scantling Criteria for Local Strength

4.5.1   Local Bending of Beams

The local strength of primary and secondary structural members is evaluated by means of stresses due to local loads, such as lateral pressure or concentrated loads etc. Again, the elementary Bernoulli-Euler beam theory is utilized when computing the stresses or deflections for stiffeners and girders. Plate theory is used for plates. The derivation of the equations for stress and deflection, using the same assumptions as for elementary beam theory or plate theory, may be found in textbooks on material strength, for instance, Timoshenko (1956).

Scantlings of individual structural members, as shown in Figure 4.7, with respect to local bending moments and shear strength are presented in this section.
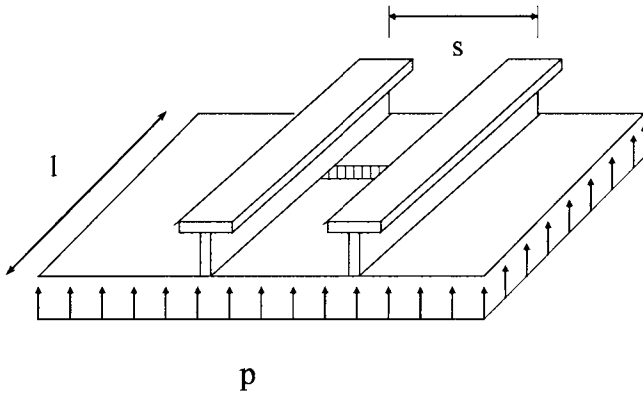
Figure 4.8   Individual Structural Members

Stiffeners

The minimum required stiffener size is specified by the section modulus of the stiffener as a function of stiffener spacing, stiffener span, design pressure, and allowable stress.
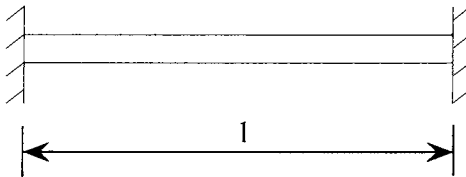
Figure 4.9   Stiffener

From the beam theory, the required section modulus of a stiffener is:

$$SM = \frac{M}{\sigma} \tag{4.12}$$

Considering a stiffener with fixed ends, the maximum bending moment is:

$$M = \frac{ql^2}{12} \tag{4.13}$$

A stiffener is supposed to carry lateral pressure, which acts on the plate attached to the stiffener, with a loading breadth equal to the stiffener spacing. Therefore, the distributed load on the stiffener, q (in N/mm), can be calculated from the following equation:

$$q = p \cdot s \tag{4.14}$$

where, s, is the stiffener spacing, and p, is the design pressure in N / mm^2.

By inserting Eqs. (4.13) and (4.14) into Eq.(4.12), we obtain:

$$SM = \frac{p \cdot s \cdot l^2}{12\sigma} \tag{4.15}$$

The classification rules contain this kind of equations for design of beams under lateral pressure.

Girders

Girders are to comply with the same scantling criteria as stiffeners with respect to the section modulus. In addition, shear force should be considered due to the height of girder. The following equation represents the scantling criterion in terms of the cross sectional area of girders:
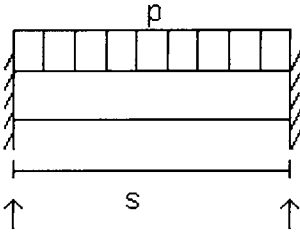
Figure 4.10   Girder

$$\tau = \frac{Q}{A} \tag{4.16}$$

where, τ, is the shear stress at the girder end in N/m^2 and A, is the cross sectional area at the girder end in m^2. If the load is equally distributed, with each end of the girder carrying half the load, Q is defined to be:

$$Q = 0.5 \cdot p \cdot b \cdot S \tag{4.17}$$

where p and b denote the design pressure acting on the girder (in N/m^2), and the loading breadth (in m). The girder span is denoted as S (in m). Substituting Eq.(4.17) into Eq.(4.16), the following equation is obtained:

$$\tau = \frac{Q}{A} = \frac{0.5 \cdot p \cdot b \cdot S}{A} \tag{4.18}$$

From Eq. (4.18), the required sectional area is derived as the following:

$$A \geq \frac{0.5 \cdot p \cdot b \cdot S}{\tau_{all}} \tag{4.19}$$

The allowable shear stress τ_{all}, depends on the girder. In addition, girders are to satisfy the requirements of the web plate thickness, the girder web area, and the ratio of the girder flange thickness to flange width.

4.5.2   Local Bending Strength of Plates

In the design rules, the minimum required plate thickness is defined as a function of stiffener spacing, design pressure, and allowable stress. This criterion may be derived from plate theory: A plate panel between two stiffeners and two girders can be simplified and considered as a rectangular plate under uniform lateral pressure p, with all edges fixed.
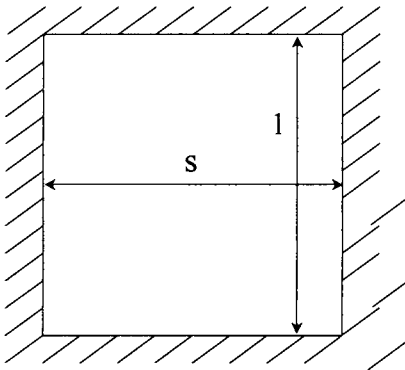
Figure 4.11   Plate

Based on the plate theory, the maximum stresses are given as follows:

$$Max\{\sigma\} = \frac{-\beta_1 p \cdot s^2}{t^2} \text{ (at the center of the long edge)} \qquad (4.20)$$

$$\sigma = \frac{\beta_2 p \cdot s^2}{t^2} \text{ (at the center)} \qquad (4.21)$$

If the aspect ratio of the plate (l/s) is greater than 2, $\beta_1 = 0.5, \beta_2 = 0.25$ are to be used as correction factors for the aspect ratio. For plates with an aspect ratio greater than 2, which are designed against maximum stress at the center, the required minimum thickness is:

$$t = \frac{0.5s\sqrt{p}}{\sqrt{\sigma}} = \frac{s\sqrt{p}}{\sqrt{4\sigma}} \qquad (4.22)$$

where, σ is the allowable local bending stress, p is the design pressure, and s is the spacing. In actual design, a corrosion allowance should be added to the calculated thickness.

Allowable bending stresses should be determined by taking into account the plate location, the stiffening system, and the material strength. Each classification society has its own definition of allowable stresses.

In the classification rules, formulae are available for design of plating under lateral pressure, and for the determination of plate thickness. Between classification rules, there is certain difference in the way corrosion allowance is handled.

4.5.3 Structure Design of Bulkheads, Decks, and Bottom

For each individual longitudinal or vertical/horizontal stiffener on longitudinal and transverse bulkheads, along with the effective plating to which it is attached, the net section modulus is not to be less than that obtained from the following equations:

$$SM = \frac{M}{\sigma_b} \quad (cm^3) \tag{4.23}$$

where

$$M = \frac{1000}{12} c_1 c_2 p s l^2 \quad (Ncm) \tag{4.24}$$

c_1, is different for longitudinal, horizontal, and vertical stiffeners, c_2 depends on the design and loading of the tank. l, is the span of longitudinals or stiffeners between effective supports, p, is defined above, and σ_b, is the permissible bending stress, which depends on the type and position of the stiffener.

4.5.4 Buckling of Platings

General

Buckling is one of the main concerns in structural design. Structural elements, which are exposed to high compressive stress, may experience instability before reaching the yield stress.

Platings should be evaluated to avoid local buckling of plates between stiffeners. This section discusses the scantling of longitudinal members with respect to buckling control by considering the total compressive stresses

Elastic Compressive Buckling Stress

The elastic buckling stress is the highest value of the compressive stress in the plane of the initially flat plate for which a nonzero out-of-plane deflection of the middle portion of the plate can exist. The Bryan Formula gives the theoretical solution for the compressive buckling stress in the elastic range. For a rectangular plate subject to a compressive in-plane stress in one direction, it may be expressed as:

$$\sigma_{el} = k_c \frac{\pi^2 E}{12(1 - \upsilon^2)} \left(\frac{t}{s} \right)^2 \tag{4.25}$$

The plate nomenclature may be obtained from Figure 4.11, and t, is the net thickness, reduced by corrosion addition. The buckling coefficient k_c is a function of the plate aspect ratio $\alpha = l/s$, boundary conditions and loading conditions. If the plate is assumed to have the load applied uniformly to a pair of opposite edges only and if all four edges are simply supported, then k_c is given by the following equation:

$$k_c = \left(\frac{n}{l} + \frac{l}{n} \right)^2 \tag{4.26}$$

Here, n is the number of half-waves of the deflected plate in the longitudinal direction.
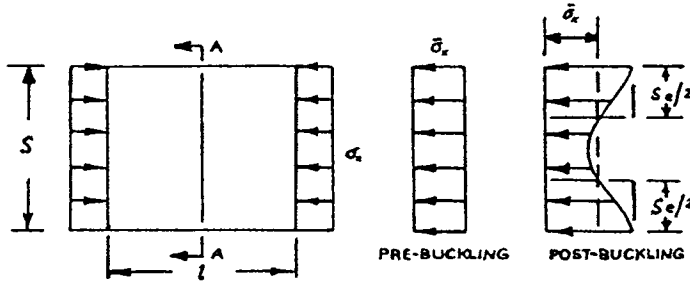
Figure 4.12   Plate Buckling

For a transversely stiffened plate with an aspect ratio of $\alpha < 1$, as shown in Figure 4.12, the critical stress will correspond to n=1, which leads to a more convenient expression for the elastic compressive buckling stress:

$$\sigma_{el} = \frac{\pi^2 E}{12(1-\upsilon^2)}\left(\frac{t}{s}\right)^2 (1+\alpha^2)^2 \tag{4.27}$$
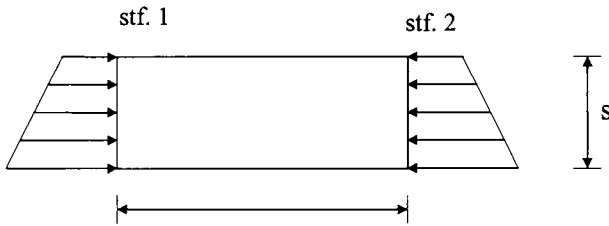
Figure 4.13   Transverse Stiffened Plate
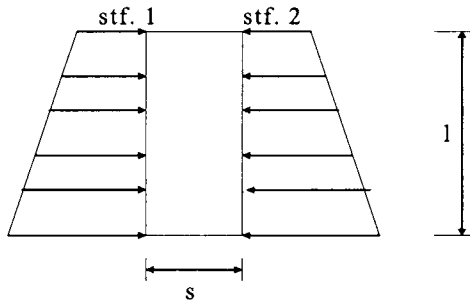
Figure 4.14   Longitudinal Stiffened Plate

Figure 4.13 shows a longitudinal stiffened plate, for which k_c is approximately 4 so that the elastic critical stress is given by:

$$\sigma_{el} = \frac{\pi^2 E}{3(1 - \upsilon^2)} \left(\frac{t}{s}\right)^2 \tag{4.28}$$

The critical compressive buckling stress, σ_c, is given by the equation below:

$$\sigma_c = \sigma_{el} \qquad \text{for } \sigma_{el} < \frac{\sigma_y}{2} \tag{4.29}$$

$$\sigma_c = \sigma_y \left(1 - \frac{\sigma_y}{4\sigma_{el}}\right) \qquad \text{for } \sigma_{el} > \frac{\sigma_y}{2}: \tag{4.30}$$

The elastic shear buckling stress, τ_e, is calculated similarly. The critical buckling shear stress is given by the following equations:

$$\tau_c = \tau_{el} \text{ for } \tau_{el} < \frac{\tau_y}{2} \tag{4.31}$$

$$\tau_c = \left(1 - \frac{\tau_y}{4\tau_{el}}\right) \text{ for } \tau_{el} > \frac{\tau_y}{2} \tag{4.32}$$

where, τ_{el}, is the ideal elastic shear buckling stress and τ_y, is the yield stress in shear of material in N / mm^2, which is given by: $\tau_y = \sigma_y / \sqrt{3}$.

Buckling Evaluation

Design codes with respect to buckling strength are developed based on the above mentioned formulae. The following interaction formula may be used to calculate buckling of plates under combined compression and shear stress (Bannerman and Jan, 1980):

$$\left(\frac{\sigma}{\sigma_c}\right)^2 + \left(\frac{\tau}{\tau_c}\right)^2 \leq 1.0 / S.F. \tag{4.33}$$

where σ *and* τ denote the predicted maximum compressive stress (due to axial compression and bending), and the predicted average shear stress respectively. σ_c *and* τ_c are the critical buckling stress corresponding to axial compression/bending and corresponding to pure shear loading respectively. *S.F.* is the safety factor.

4.5.5 Buckling of Profiles

Axially compressed profiles (longitudinal) should be evaluated to withstand the following buckling modes:

- Lateral buckling mode
- Torsional buckling mode
- Web and flange buckling mode

Transverse stiffeners and girders require special considerations.

The Elastic Buckling Stress will be discussed below.

- Lateral buckling mode:

The elastic buckling stress of lateral buckling may be derived from column buckling theory and is given by:

$$\sigma_{el} = n \cdot E \frac{I_A}{Al^2} (N/mm^2) \tag{4.34}$$

where I_A is the moment of inertia of the longitudinal, including attached plate flange, in cm^4, A is the cross-sectional area of the longitudinal, including the attached plate flange, in cm^2, l is the span of the longitudinal and n is a buckling coefficient, which depends on the end supports (for an ideal case, n=0.001).

It should be noted that the section properties of the longitudinals used in the buckling evaluation should be the deducted net properties with a corrosion allowance.

- Torsional buckling mode:

$$\sigma_{el} = \frac{\pi^2 EI_W}{10^4 I_p l^2} \left(m^2 + \frac{K}{m^2} \right) + 0.385 E \frac{I_T}{I_P} (N/mm^2) \tag{4.35}$$

where

$$K = \frac{Cl^4}{\pi^4 EI_W} 10^6 \tag{4.36}$$

where I_w, is the warping constant of the longitudinal about the connection of the stiffener to the plate, in cm^6, Ip is the polar moment of inertia of the longitudinal about the connection of the stiffener to the plate, in cm^4, l is the span of the longitudinal, in m, I_T is the St. Venant's moment of inertia of the longitudinal (without the attached plate), in cm4, m is the number of half-waves (usually varying from 1 to 4), and C is the spring stiffness exerted by the supporting plate panel.

- Web and flange buckling:

For the web plate of longitudinal, the elastic buckling stress is given by:

$$\sigma_{el} = 3.8E \left(\frac{t_W}{h_W} \right)^2 (N/mm^2) \tag{4.37}$$

where t_W, is the web thickness, in mm, and h_W is the web height, in *mm*.

For flanges on angels and T-beams, the following requirement should be satisfied:

$$\frac{b_f}{t_f} \leq 15 \tag{4.38}$$

where b_f is the flange breadth and t_f is the flange thickness.

Eqs.(4.29) to (4.33) may also be applied to calculate the critical buckling stress for profiles and hence to conduct buckling evaluation. Refer to PART II of this book for further details of buckling evaluation and safety factors.

4.6 References

1. ABS (2002), "Rules for Building and Classing Steel Vessels", American Bureau of Shipping.

2. Bannerman, D.B. and Jan, H.Y. (1980), "Analysis and Design of Principal Hull Structure", in *"Ship Design and Construction"*, SNAME.

3. Paulling, J.R. (1988), "Strength of Ships", in *"Principles of Naval Architecture"*, Vol. I, SNAME.

4. Timoshenko, S., Goodier, J.N. (1956), *"Strength of Materials"*, Vol. I; Vol. II.

This Page Intentionally Left Blank

Part I

Structural Design Principles

Chapter 5   Ship Hull Scantling Design by Analysis

5.1   General

Classification rules have traditionally been the mainstay of ship design practices. These rules are primarily semi-empirical in nature and have been calibrated to ensure successful operational experience. They have obvious advantages - simple in format and familiar to most ship designers. Nevertheless, the ship sizes have increased dramatically and the ship designs have changed remarkably in the past 20 years. The conventional design approach that relied on the "Rule Book", has been seriously challenged with the development of unconventional ship types and complex ship structures such as high speed vessels, large opening container ships with considerably increased capacity, large LNG-carriers, drilling ships, FPSOs, etc. The conventional design rule formulae involve a number of simplification assumptions and can only be used within certain limits. Moreover, scantlings based on rules are not necessarily the most cost efficient designs. Hence, the application of rational stress analysis using FEM has gained increasing attention in the shipbuilding industry. With the rapid growth of information technology, computational complexity is no longer a big issue and numerical efficiency is not the main concern in the design procedure. The actual design approach includes the overall strength analysis by accounting for both static and dynamic loads and evaluation of the fatigue life of all critical structural details. This approach provides a well-designed and uniformly utilized structure, which ensures a higher degree of reliability than past structures.

A rational analysis procedure is presented in this Chapter, starting from design loads, strength criteria, FEM analysis, up to the assessment of the obtained calculation results. FEM analysis is discussed in detail, including modeling, load application, application of boundary conditions, element selection, and post-processing. The summarized procedure of strength analysis can be seen in Figure 5.1.

5.2   Design Loads

The design loads acting on the overall ship structure consist of static and dynamic loads. Static loads include dead and live loads, such as hydrostatic loads, and wind loads. Dynamic loads include wave induced hydrodynamic loads, inertia loads due to vessel motion, and impact loads. The various loading conditions and patterns, which are likely to impose the most onerous local and global regimes, are to be investigated to capture the maximum local and global loads in structural analysis. Sloshing and slamming loads should also be taken into account where applicable. When designing ocean-going ships, environmental loads are usually based on global seastate criteria due to their mobility. While for offshore structures, environmental loads are calculated in accordance with specifically designed routes and/or site data.
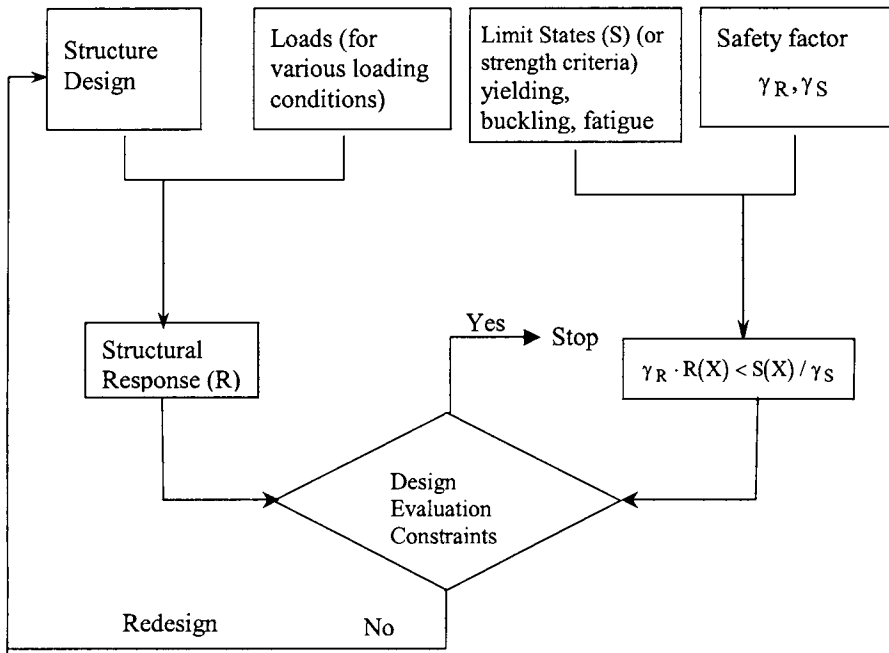
Figure 5.1   Stress Analysis Procedure

Liu et al (1992) developed a Dynamic Load Approach (DLA) for ship design, where the loads experienced by a tanker were calculated, including wave induced loads, ship motions, internal, structural, and cargo inertial loads etc. Three loading conditions are analyzed, namely, full load condition, ballast load condition, and partial load condition.

• Static Loads

The distribution of hull girder shear forces and bending moments is calculated by providing the vessel's hull geometry, lightship (i.e. the weight of the steel structure, outfitting and machinery), and deadweight (i.e. cargoes and consumables such as fuel oil, water and stores), as input for each loading condition. An analysis of a cross-sectional member along the length of the ship is required in order to account for the discontinuities in the weight distribution.

• Hydrodynamic Coefficients

Each loading condition requires hydrodynamic coefficients to determine the ship's motions and dynamic loads. It is important that a significantly broad range of wave frequencies be considered in this calculation.

• Ship Motion and Short-term /Long-term Response

Ship motion analysis should be carried out using a suitable method, e.g. linear seakeeping theory and strip theory. Frequency response functions are to be calculated for each load case.

Short-term response is then obtained by multiplying the frequency response functions by the wave spectra. The long-term response is calculated by using the short-term response and wave statistics, which consist of wave scatter diagrams.

5.3 Strength Analysis using Finite Element Methods

5.3.1 Modeling

In principle, strength analysis by means of finite element methods should be performed with the following model levels:

Global Analysis

A global analysis models the whole structure with a relatively coarse mesh. For a huge structure like ships, the global model mesh must be quite rough; otherwise too many degrees of freedom may consume unnecessary man-hours and cause computational difficulty. The overall stiffness and global stresses of primary members of the hull should be reflected in the main features of the structure. Stiffeners may be lumped, as the mesh size is normally greater than the stiffener spacing. It is important to have a good representation of the overall membrane panel stiffness in the longitudinal and transverse directions. This model should be used to study the global response of the structure under the effects of functional and environmental loads, to calculate global stresses due to hull girder bending, and to provide boundary conditions for local FE models. Design loads should reflect extreme sagging and hogging conditions imposed by relevant operation modes such as transit, operating, storm survival, installation, etc.

Local Structural Models

For instance, cargo hold and ballast tank models for ship shaped structures may be analyzed based on the requirements of classification rules.

Cargo Hold and Ballast Tank Model

The local response of the primary hull's structural members in the cargo and ballast area is analyzed, for relevant internal and external load combinations. The extent of the structural model shall be decided on, by considering structural arrangements and load conditions. Normally, the extent covered is the tank itself, and one half the tank outside each end of the considered structure (Figure 5.2).

The mesh fineness shall be determined based on the method of load application. The model normally includes plating, stiffeners, girders, stringers, web-frames, and major brackets. Additional stiffness may be employed in the structure for units with topsides, and should be considered in the tank modeling.

From the results of the global analysis, the boundary conditions for the cargo hold and ballast model may be defined. The analysis results of the cargo hold/ballast model may be used as the boundary conditions for the frame and girder models.

The following basic loads are to be considered in the model:

- Static and dynamic loading from cargo and ballast,
- Static and dynamic external sea pressure,
- Dead weight, topside loading, and inertia loads
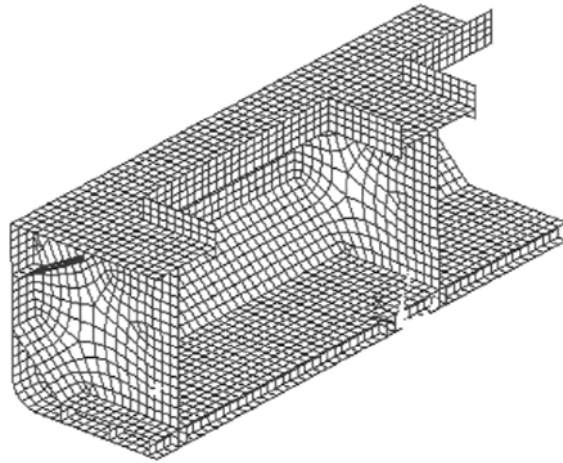
Figure 5.2   Tank model

Frame and Girder Model

The frame and girder analysis is used to analyze the stresses and deformations in the main frame or girder system. The calculations should include the results induced by bending, shear, and torsion. The minimum requirements are a function of the type of vessel being analyzed, but should include at least one transverse web in the forward cargo hold or tank (Figure 5.3)

The model may be included in the cargo hold and ballast tank models or run separately using the boundary conditions from that model analysis.
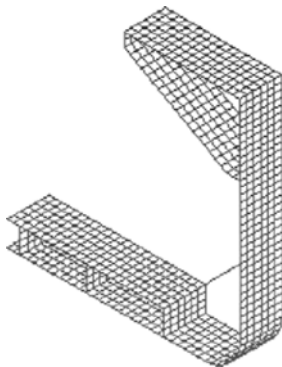
Figure 5.3   Frame model   **Figure 5.4 Stress concentration model**
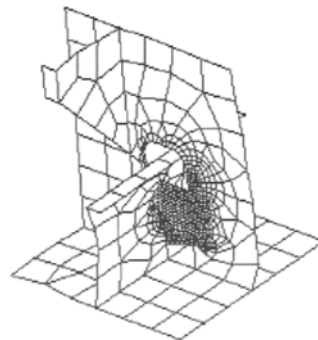
Stress Concentration Area:

In the areas where high stress concentrations may take place, local fine mesh models are to be applied by using forces or forced deformations as boundary conditions based on the results obtained in the global analysis. Alternatively, sub-modeling, super-element techniques or direct mesh refinement may be introduced.

Attention should be paid particularly to the following areas:

- Areas around large openings,

- Longitudinal stiffeners between transverse bulkheads and the first frame at each side of the bulkhead,

- Vertical stiffeners at transverse bulkheads with horizontal stringers in the way of the inner bottom and deck connections,

- Horizontal stiffeners at transverse bulkheads with vertical stringers in the way of the inner side and longitudinal bulkhead connections (Figure 5.4),

- Corrugated bulkhead connections.

Fatigue Model

If fatigue is of concern, analysis of critical structural details should be performed. Fine mesh models shall be completed for critical structural details in the areas such as the following:

- Hopper knuckles in way of web frames,

- Topside support stools,

- Details in way of the moonpool,

- Other large penetrations in longitudinal load bearing elements,

- Longitudinal bulkhead terminations,

- Stiffener terminations,

- Pontoon to column or column to deck connections,

- Other transition areas when large changes in stiffness occur.

The size of the model should be such that the calculated hot spot stresses are not affected significantly by the assumptions made for the boundary conditions. Element sizes for stress concentration analysis should be of the same order of magnitude as the plate thickness. Normally, shell elements may be used for the analysis. Only dynamic loads are to be applied on the model, because only these affect the fatigue life of the structure. The correlation between different loads such as global bending, external and internal pressure, and acceleration of the topside should be considered in the fatigue assessment.

5.3.2 Boundary Conditions

Defining boundary conditions is one of the most important steps in FEM analysis. For local analysis models, the boundary conditions imposed by the surrounding structures should be based on the deformation or forces calculated from the global model.

The boundary conditions, for a global model, have no other purpose than to restrict the rigid body motion. Fixing 6 degrees of freedom (DOF) at both ends (and corners) of the model

should be good enough. The total loading must be balanced so that the reaction forces at the boundaries approach zero.

When modeling, the model length of the ship structure should be sufficient to minimize boundary condition effects over the analyzed area. ABS (2002) requires 3 cargo holds to be covered for models of tankers, bulk carriers, or container ships; LR "Direct calculation - Guidance Notes" (1996) requires that 2 cargo holds be covered for the model of a bulk carrier. All continuous longitudinal elements should be restrained to remain plane under the effects of the hull girder bending and must be rotationally fixed about the vertical axis if the calculated deformations or forces are not available at the free ends of the model. Conditions of symmetry should be applied at each end of the finite element model. Rotation about the two axes in the plane of symmetry is to be constrained where there is symmetry imposed at the centerline or at the ends of the model. The model should be supported vertically by distributed springs with shipsides and longitudinal bulkheads at the intersections of the transverse bulkheads.

5.3.3   Type of Elements

The types of elements are chosen to provide a satisfactory representation of the deflections and stress distributions within the structure. The conventional frame analysis may be carried out with a beam model. It has significant advantages for its modeling simplicity and computational efficiency. However, thanks to the availability of powerful computers, computational efficiency is no longer a concern. More refined and accurate element types can be used.

In a research conducted by the ISSC, Zillottto *et al.* (1991), nine different finite element models were applied to different combinations of beams, trusses, rods, membranes, planes, and shell elements. A considerable scatter was observed in the results. The conclusion was that a detailed analysis of the deformations and stress levels in all the elements of the transverse frames should be performed using a refined finite element model for all the different types of structures and ships.

In "Direct Calculation-Guidance Notes", LR (1996) suggests that all areas of the plating should be modeled by shell elements, secondary stiffeners by line elements (bars or rods), double bottom girders and floors by three or more plate elements over the depth of these members, and side shells by plate or bar elements.

In general, if the structure is not subjected to lateral bending, membrane and rod elements may be applied. Otherwise, plate and beam elements, which have both bending and membrane resistance, should be employed. The selection of element types depends on many aspects, such as the type of structure, the load application approach, the type of analysis performed, the results generated, and the accuracy expected. There is no substitute for engineering judgement.

5.3.4   Post-Processing

The design is a complicated and iterative process in which building and solving a FE model is simply the first step. A more important step is that designers use their knowledge and judgment to analyze the results and, if necessary, redesign or reinforce the structure.

First, the engineer must ensure that the results calculated by the FE program are reasonable, and that the model and the load application are correct. This can be achieved by plotting stress contour, the deformation, the reactions & applied load equilibrium, force & moment diagrams, etc. The next step is to check the strength of the structure against relevant design criteria. Load combinations and stress combinations are not always straightforward. Assumptions are usually

made to certain degrees both in creating the model and in solving the model. The designers must bear this in mind and be familiar with the FE program being used, in order to account for the assumptions adopted, to evaluate the calculated results, and, if necessary, to modify the results.

Yielding Check

The yield check ensures that the stress level on each structural member is below the allowable stress. The allowable stress is defined as the yield limit of the material divided by a safety factor. Stresses calculated from different models are combined to derive the equivalent von Mises stress and evaluated against the yield criterion. Component stresses, such as axial stress, bending stress, normal stress in x-direction, normal stress in y-direction, shear stress, etc. as well as combined stresses, are to be evaluated. The combination of global and local stresses should account for actual stress distributions and phases. If the phase information is limited or uncertain, the maximum design value for each component may be combined as the worst scenario. Possible load offset due to the simplified assumptions made in the FE analysis should be accounted for in the stress combinations.

Buckling Check

Structural members subjected to compressive loads may normally buckle before reaching the yield limit. Various buckling modes should therefore be evaluated. Four different modes of buckling are usually recognized:

- Mode 1: simple buckling of the plate panel between stiffeners and girders.

- Mode 2: flexural buckling of the individual stiffener along with its effective width of plating in a manner analogous to a simple column.

- Mode 3: lateral-torsion or tripping mode. The stiffener is relatively weak in torsion, and failure may be initiated by twisting the stiffener in such a way that the joint between stiffener and plate does not move laterally.

- Mode 4: overall grillage buckling.

See Part II of this book for more information. To ensure that the local bending stress resulting from loads, acting directly on stiffeners, are included in the buckling code check, the lateral pressure should be explicitly included in the capacity check, combined with membrane stresses calculated from the FE analysis. Relevant combinations of buckling load checks should include evaluation of the capacity with relevant lateral pressure applied to either side of the plate. Compressive stresses calculated from global and local models are to be superimposed. Each structural member is to be designed to withstand the maximum combined buckling loads, of which the critical load cases and wave phases may be different to those pertaining to the yield check.

5.4   Fatigue Damage Evaluation

General

The fatigue strength of welded joints (structural details) in highly dynamically stressed areas needs to be assessed to ensure structural integrity and to optimize the inspection effort. The analysis of fatigue strength should be based on the combined effects of loading, material properties, and flaw characteristics. At the global scantling design level, the fatigue strength check for hull-girder members can be conducted for screening purposes. At the final design

level, analysis for structural notches, cutouts, bracket toes, and abrupt changes of structural sections need to be performed.

Stress types commonly used in fatigue analysis based on S-N curves include nominal stress, hot-spot stress, and notch stress. Each of these methods has specific applicable conditions. Although only the nominal stress is used in the examples, the analysis approach is not limited to any stress type.

Spectral Fatigue Analysis (SFA) based on the S-N curve and Palmgren-Miner's cumulative damage hypothesis has been widely applied in the fatigue damage assessment of marine structures, see Part III of this book. Figure 5.4 shows the procedure for spectral fatigue assessment.

```
┌─────────────────────┐        ┌─────────────────────┐
│ Site- and route-    │        │ Structural modeling │
│ specific wave       │        │                     │
│ environment         │        │                     │
└─────────┬───────────┘        └──────────┬──────────┘
          │                               │
┌─────────▼───────────┐        ┌──────────▼──────────┐
│ Long-term wave      │        │ Hydrodynamic        │
│ description (WSD)    │        │ analysis (seakeeping)│
└─────────┬───────────┘        └──────────┬──────────┘
          │                               │
┌─────────▼───────────┐        ┌──────────▼──────────┐
│ Short-term wave     │───────▶│    Stress FRF       │
│ spectrum (Hs,T)(i,j;k,l)│    │                     │
└─────────────────────┘        └──────────┬──────────┘
                                          │
┌─────────────────────┐        ┌──────────▼──────────┐
│ Rainflow correction │───────▶│ (i,j;k,l)-th short- │
│                     │        │ term response spectrum│
└─────────────────────┘        └──────────┬──────────┘
                                          │
                               ┌──────────▼──────────┐
                               │ Closed-form spectral│
                               │ fatigue damge D(i,j;k,l)│
                               └──────────┬──────────┘
                                          │
                               ┌──────────▼──────────┐
                               │ Weighting & summing │
                               │ probability density │
                               │ function            │
                               └──────────┬──────────┘
                                          │
                               ┌──────────▼──────────┐
                               │ Long-term annualized│
                               │ fatigue damage      │
                               └──────────┬──────────┘
                                          │
                               ┌──────────▼──────────┐
                               │ Fatigue Life        │
                               │ (strength)          │
                               └──────────┬──────────┘
                                          │
                               ┌──────────▼──────────┐
                               │ Design rules -      │
                               │ fatigue criteria    │
                               │ check               │
                               └─────────────────────┘
```

Figure 5.4   **Procedure of Spectral Fatigue Analysis (Zhao, Bai & Shin, 2001)**

Fatigue Check

Only cyclic loads are relevant in the fatigue analysis. Static loads should therefore be subtracted from the total design loads. Environmental loads for fatigue analysis may differ from those for the yielding and buckling analysis. Either a stochastic or a simplified fatigue analysis can be performed. When a simplified fatigue analysis is applied, the stress range corresponding to a return period equal to the design life is calculated and the fatigue life is then computed based on S-N curves. If the stochastic fatigue analysis is used, stress ranges corresponding to each sea state in the wave scatter diagram are calculated by FE analysis, and the fatigue life of each stress range is found using S-N curves. The cumulative fatigue damage is then computed using the Miner-Palmgren Hypothesis:

$$D = \sum_i \frac{n_i}{N_i} \tag{5.1}$$

where,

n_i = Number of cycles in the ith stress range interval between stress range $\Delta\sigma_i$ and $\Delta\sigma_{i+1}$

N_i = Number of cycles to failure at stress range $(\Delta\sigma_i + \Delta\sigma_{i+1})/2$ and can be read from S-N curves

D = Allowable cumulative damage varies for different structural members, which should normally be less than 1.

However a significant safety factor is usually employed with the Miner-Palmgren Hypothesis, and D is often less than 0.1, 0.3 or 0.6 depending on the type of structure, the strength significance of the member, availability for inspection, etc. Reference is made to Part III of this book for more information on fatigue assessment.

5.5 References

1. ABS (2002), "Rules for Building and Classing Steel Vessels", American Bureau of Shipping.

2. Liu, D, Spencer, J, Itoh, T, Kawachi, S and Shigematsu, K (1992), "Dynamic Load Approach in Tanker Design", SNAME Transactions, Vol. 100.

3. Lloyd's Register (1996), "Structural Design Assessment Procedure, Direct Calculation-Guidance Notes".

4. Ziliotto, F. et al. (1991), "Comparison of Different Finite Element Analysis of Transverse Frame of a 350,000 TDW Tanker", Marine Structures, Vol. 4, No. 3.

5. Zhao, CT, Bai, Y and Shin Y. (2001), "Extreme Response and Fatigue Damages for FPSO Structural Analysis", Proc. of ISOPE'2001

This Page Intentionally Left Blank

Part I

Structural Design Principles

Chapter 6   Offshore Structural Analysis

6.1   Introduction

6.1.1   General

This chapter describes the primary considerations that the design engineer should bear in mind during the initial design and subsequent structural analysis. In this chapter, the notation 'Structures' refers to all types of marine units ranging from floating ship-shaped vessels to bottom founded platforms. Emphasis has been placed on ship shaped structures. However, consideration is also given to column supported structures (e.g. semi-submersibles, tension leg platforms (TLPs), spars, and mooring buoys) and also to steel bottom founded offshore structures such as fixed steel jackets.

The UK HSE completed a study on offshore structures in the North Sea, which estimated that around 10-15% of failures were related to inadequate design either at the initial design phase or a subsequent upgrade in the design. Inadequacy in design includes lack of operational considerations, failure to evaluate all structural elements and incorrect use of the design formulae.

In the process of design, the primary concerns for the designer are risks to life, the structure, the environment, and project economy. Hence, the relevant design codes and standards employ the appropriate safety factors in order to minimize these risks without being excessively conservative.

Throughout this chapter, emphasis is placed on the design process where the finite element analysis will be employed. Reference is made to the formulae used in the design of marine structures, although these are not reproduced within this Chapter. These formulae may be found from Part II and Part III of this book together with the background information.

6.1.2   Design Codes

The designer is faced with a large number of rules, codes, standards, and specifications describing the general policy for structure systems and the detailed design of structural components. These documents are produced and distributed by:

- National Governments
- Certification Authorities
- Technical Standards Committees
- Companies, Universities, or Individual Expertise

Chapters relating to loads and safety factors, which give a more detailed explanation of the different design methods employed in these codes, should be referenced i.e., the load and resistance factored design method, allowable stress design method, and design by testing or observation.

6.1.3   Government Requirements

Governments set legal requirements for using their ports or territorial waters that must be followed in the design of marine structures. Some of these laws, particularly those relating to vessel movements, are internationally consistent to avoid problems in passing through several national waters during transit. However, most national laws relating to the design, construction, and operation of marine structures will differ from country to country, each reflecting local conditions, health and safety laws, expertise and experience including that learned from previous major incidents and accidents.

The government requirements, such as those published by:

- Norwegian Petroleum Directorate (NPD),

- UK Health and Safety Executive (HSE),

- US Mineral Management Service (MMS).

are the legalities that need to be met rather than specific design methods and criteria to be employed. Such rules are mainly the concern of the project manager and the client representative who should ensure that the relevant pieces of legislation are reflected in the Design Basis (see Section 6.2.2).

6.1.4   Certification/Classification Authorities

Historically, the Certification/Classification Authority (CA) acted as an independent body between the vessel's designer, builder, owner, operator and the insurance company. The government's interest of reducing the risks to life and the environment from marine accidents has increased the need for CA's to also provide their expertise in government policies and legislation.

CAs are companies such as:

- American Bureau of Shipping (ABS),

- Bureau Veritas (BV),

- Det Norske Veritas (DNV),

- Lloyds Register of Shipping (LR),

- ClassNK (NK)

Ships and mobile offshore drilling units (MODU) transit from one location to another worldwide and thus the use of the CA's service may avoid the repetitive approvals from the many national governments concerned. The role of the CA has become questioned in recent years concerning the fixed (bottomed supported) structures, which will generally remain at one location within one nation's territorial waters throughout its life.

CAs perform an independent third party assessment of the structure throughout the design of the structure to ensure that it fits for purpose. This may include review of the design reports and independent structural analyses, particularly with the increasing use of computer aided FEM. The CA's may be chosen based on their office location relative to the sites for structural

design, fabrication or operation, their specialist knowledge in regards to the type of structure, client recommendation, or their ability to meet cost and time budget requirements.

The rules published by CAs emphasize on safety targets and consequently give precedence to safety factors and failure levels, along with general specifications of the design. Consequently, all design engineers should have access to the relevant CA rules to ensure that certification requirements are met.

6.1.5 Codes and Standards

Codes and standards provide details on how structures should be designed, built, and operated.

The difference between a code and a standard is that a code should be followed more rigorously, while a standard sets recommended practices that should be followed. This difference is largely ignored now with, for example, the Eurocode for steel design, which is classified as a national standard.

The range of worldwide codes and Standards is substantial. However, the important aspect of these documents is that they both have national, or in some cases international standing. Examples of the codes and standards for the design of steel marine structures are the following:

- ANSI/AWS D1.1, Structural Welding Code,
- API RP2A (Working Stress Design or Load Resistance Factored Design, Recommended Practice for Planning, Designing and Constructing Fixed Offshore Platforms),
- Eurocode 3 (NS-ENV 1993 1-1 Eurocode 3),
- ISO Codes for Design of Offshore Structures,
- NORSOK Standard N-004, Design of Steel Structures,
- NS3472,
- BS5750.

The design or reassessment of steel marine structures will be based on one or more of the above mentioned documents. The software used, will be an essential program for all members of the design team. However, with regards to the use of the finite element methods during the design, none of these documents give a thorough assessment of the preferred or recommended techniques.

Standards such as NS3472 and BS5750 provide the fundamental equations needed to determine stresses in steel components, regardless of their area of application. Documents such as NORSOK N-004 and API RP2A apply the relevant fundamental equations, along with appropriate factors of safety corresponding to the design limit-states for particular marine structures. NORSOK N-004 (NTS, 1998) gives state of the art specifications for designing floating and fixed marine structures. It is based on NS3472, Eurocode 3, oil company's specifications for the design of steel structures, and many of the best features from technical papers.

API RP 2A (2001) has been widely applied for design and construction fixed platforms, and serve as a basic document for offshore structural design.

API RP 2T (1987) has been mainly used for tension leg platforms. It provides comprehensive guidance on design criteria, environmental forces, global design and analysis, structural design

of hulls and deck, tendon system design, foundation design and analysis, riser systems, facilities design, fabrication, installation and inspection as well as structural materials.

Recently API RP 2FPS (2001) was issued for floating production systems. It gives a high level specification for the design and analysis of floating production systems such as semi-submersibles, spars, FPSO and conversion/reuse of existing structures. The guide defines design environmental criteria, accident loads, fire and blast loads and specifies design requirements with respect to design load cases, structural design of hull and deck, fatigue assessment, weight control, watertight and stability, transit condition and fabrication tolerances. The API RP 2FPS (2001) also provides general guidance on station keeping and anchoring systems, well and production fluid control, transportation system and export system, facilities, fabrication, installation and inspection, material, welding and corrosion protection as well as risk management.

6.1.6   Other Technical Documents

When performing the design or reassessment of steel marine structures, reference may be made to specialized documents. These maybe in the form of:

- Company specifications and procedures that are based on specific expertise or test results developed in-house by the designer, a subcontractor, or the client manuals that give support to finite elements, risk and reliability, or other engineering tools.

- Reports, conference proceedings, or technical journals in the public domain covering a particular design aspect in-depth.

- Books on steel designs that allow fundamental stresses and strains to be estimated.

The above documents will need to be referenced in the Design Basis and made available to the design team members as required.

6.2   Project Planning

6.2.1   General

It is essential that adequate planning be undertaken at the initial stages of the design process in order to achieve a good design within the estimated cost and time schedule.

The main output of the planning process is a 'Design Basis', describing the criteria and a 'Design Brief', describing the procedure to be followed and software to be used. For smaller projects in particular, it may be preferable to gather all the information into one concise document.

Ideally, the Design Basis and Design Brief will be written to and agreed with the Client prior to the design phase. However, in practice this is not always possible. In such cases, it is strongly recommended that these documents be issued in draft format with, as much detail as possible or with relevant items labeled as 'Preliminary'. This will enable the project team to begin developing the design with some understanding of the criteria that will be the most critical throughout the design.

The Design Basis and Design Brief may be updated throughout the project as particular problems arise. It is important that all-relevant team members are aware of such changes.

6.2.2 Design Basis

The Design Basic document lists the basis criteria relevant to the structure and should include the following:

Unit Description and Main Dimensions

A summary describing the structure includes:

- A general description of the structure, including the main dimensions and draught/water depth
- Main structural drawings
- Service and design lives
- Location of the structure, if fixed
- Specification of the system of units employed

Rules, Regulations and Codes

A list of relevant applicable references to the design codes and project related documents include:

- Environmental design criteria, including all relevant conditions, such as wind, wave, current, snow, ice and earthquake description with 10E-1, 10E-2, and 10E-4 annual probability occurrence.
- Soil/foundation criteria for design of fixed structures, mooring/anchoring, pipelines and risers.
- Design temperatures

Stability and Compartmentalization

Stability and compartmentalization design criteria for relevant conditions include:

- External and internal watertight integrity
- Boundary conditions including interfaces with other structures or foundation conditions
- Lightweight breakdown report
- Design load cases and global mass distribution
- Damage condition

Materials and Welding

Design criteria for materials and welding include:

- Yield and ultimate tensile strength
- Corrosion allowances to be taken
- Corrosion Protection (CP) systems or coatings
- Material flexibility and avoidance of brittle fracture
- Crack growth properties
- Weld specification and fatigue classification

- Post weld heat treatment
- Minimum access for welding
- Marine growth type and thickness

Temporary Phases

Design criteria for relevant temporary phases includes:

- Limiting permanent, variable, environmental, and deformation action criteria
- Procedures associated with construction, including major lifting operations
- Essential design parameters associated with the temporary phase
- Relevant Accidental Limit-state (ALS)

Operational Design Criteria

Design criteria for relevant operational phases includes:

- Limiting permanent, variable, environmental, and deformation action criteria
- Deck load description (maximum and minimum)
- Wave motion accelerations on appurtenances
- Mooring actions
- Tank loading criteria
- Fatigue and fracture criteria
- Air gap requirements
- Accidental event criteria

In-service Inspection and Repair

Criteria for inspecting the structure post-fabrication and in-service and criteria for allowing repairs to be efficiently carried out and recorded include:

- Description of the in-service inspection hierarchy and general philosophy
- Access for inspection and repair
- Redundancy and criticality of components

Reassessment

The data needed for re-assessment include:

- Inspection records
- Fabrication and welding records
- Details of cracked and damaged components
- Details of replaced or reinforced components
- Details of on-site measurements
- Details of corrosion protection methods and marine growth state

6.2.3   Design Brief

A Design Brief document lists the procedures to be adopted in the initial stages of the design process as follows:

Analysis Models

A general description of models to be utilized, including the description of:

- Global analysis model(s)
- Local analysis model(s)
- Load cases to be analyzed

Analysis Procedures

A general description of analytical procedures to be utilized including a description of the procedures to be adopted with respect to:

- The evaluation of temporary conditions
- The consideration of accidental events
- The evaluation of fatigue actions
- Air gap evaluation
- The establishment of dynamic responses (including methodology, factors, and relevant parameters)
- The inclusion of 'built-in' stresses
- The consideration of local responses (e.g. those resulting from mooring and riser actions, ballast distribution in tanks as given in the operating manual etc.)
- Consideration of structural redundancy

Structural Evaluation

A general description of the evaluation process including:

- Description of procedures to be completed when considering global and local responses
- Description of fatigue evaluation procedures (including use of design fatigue factors, SN-curves, basis for stress concentration factors (SCFs), etc.)
- Description of procedures to be completed during the code check

6.3   Use of Finite Element Analysis

6.3.1   Introduction

Basic Ideas Behind FEM

The finite element method is a powerful computational tool that has been widely used in the design of complex marine structures over the decades. The basic idea behind the finite element method is to divide the structure, into a large number of finite elements. These elements may be one, two or three-dimensional. The finite element model may be in the form of a truss of members connected at nodal points, or a detailed assembly of elements representing an entire structure, or a particularly complex and critical component of the structure.

Taking a irregularly shaped plate, for example, we may estimate the displacements and consequently the stresses within the plate under a given load for a specified material and boundary conditions. The field variable of interest here is the displacement. Instead of determining the displacement at every point in the plate, the finite element method divides the plate into a finite number of elements, and provides the displacements at the nodal points of each element. Interpolation functions are used within each element to describe the variations of the field variable (e.g. displacement in this example) as a function of the local coordinates. Using nodal displacements and interpolation function, the designer can compute the stress variation within any given region.

Computation Based on FEM

Commercial software has been developed based on finite element theory. As input data for the software, the designer define relevant coordinates of each node, element definitions, material properties, boundary conditions, etc. Generally, the accuracy of the solution improves as the number of elements increase, but the computational time and cost also increase. A high-speed computer is required to perform and solve the large number of element assembly involved.

Different element types (rod, beam, membrane, solid, bending with 3-node, 4-node, 6-node, 8-node, etc) are applied to various types of structures, which yield different accuracy and CPU time. However, there is no substitute of experience when trying to determine the element density and element type in order to achieve the required level of accuracy for the finite element analysis of a particular structure.

The computer program determines the displacements at each node and then the stresses acting through each element. One of the essential tasks in FE analysis is to analyze the results, which is known as post-processing. The designer may view the results in tabular or graphical form. A graphical view may be used initially to identify the regions and nodes of interest and subsequently tabulate the output specified for the chosen areas of interest. If this were not the case, the physical data of the whole structure may otherwise be too large to be structurally assessed.

Marine Applications of FEM

The analyst may then use the results from the finite element analysis to strengthen the structure via an increase in the material strength, via additional reinforcement, or by changing the load path or the boundary conditions.

The critical areas where loads or stresses are concentrated, or where there are complex joint details, will generally need to have a more detailed finite element model or finer element mesh. The finite element analysis output will only be as good as the input data specified. Again, it is particularly important for the designer to consider the limits of the model and consequently the accuracy of analysis results.

Probably the most serious problem affecting ocean-going vessels in recent years has been brittle fracture near bulkheads on very large bulk carriers. Such an effect could be easily missed in a finite element model for such a vessel. Local flexibility/rigidity and material behavior could be overlooked since the design emphasis is placed on increasing the stiffness of local details to meet the requirements of the relevant codes.

In the following stiffness matrices are derived for 2D and 3D beam elements in order to illustrate the finite element methods for offshore structural analysis and to prepare a theoretical basis for Chapter 12 - 15.

6.3.2 Stiffness Matrix for 2D Beam Elements

Figure 6.1 shows a beam element. The neutral axis of beam is defined as x axis, while one of the principal axes of inertia for beam is defined as y axis. In this section, a bending problem is discussed in x-y plane.
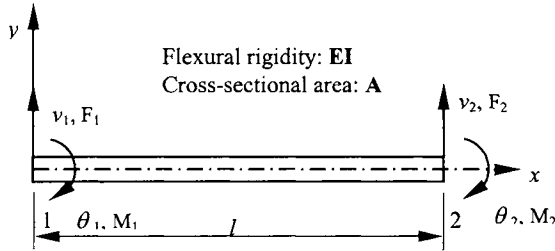
Figure 6.1   Beam Element
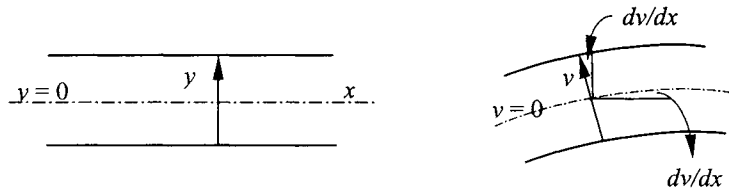
Figure 6.2   Assumption of Bernoulli-Euler

When the depth of bend is very small comparing with length, the assumption of Bernoulli-Euler, the perpendicular cross-section of neutral axis is kept perpendicular to the neutral axis after deformation, is valid. Under this assumption, the angle of clockwise rotation of cross-section θ shown in Figure 6.1 can be expressed as below,

$$\theta = -\frac{dv}{dx} \tag{6.1}$$

If the displacement in y direction of neutral axis is defined as $v(x)$, the point (x, y) before deformation varies in x, y directions as $u(x, y)$, and $v(x, y)$, which is expressed as,

$$u(x, y) = -y \frac{dv(x)}{dx} \tag{6.2}$$

$$v(x, y) = v(x) \tag{6.3}$$

The displacement v may be expressed as the following 3-order polynomial formula,

$$v = a_1 + a_2 x + a_3 x^2 + a_4 x^3 \tag{6.4}$$

When the two nodal points of the element is defined as 1 and 2, and degree of freedom at the nodal point is set as flexure and rotation angle, the displacement vector for the two nodal points of the beam have four degrees of freedom,

$$\{d\}_e = \begin{Bmatrix} v_1 \\ \theta_1 \\ v_2 \\ \theta_2 \end{Bmatrix} \tag{6.5}$$

where the subscript is the number of the nodal points. The undetermined coefficients for v in Eq. (6.4) can be expressed as the four deformations of nodal points, and expressed as

$$\begin{Bmatrix} v_1 \\ \theta_1 \\ v_2 \\ \theta_2 \end{Bmatrix} = \begin{bmatrix} 1 & 0 & 0 & 0 \\ 0 & -1 & 0 & 0 \\ 1 & 0 & l^2 & l^3 \\ 0 & -1 & -2l & -3l^2 \end{bmatrix} \begin{Bmatrix} a_1 \\ a_2 \\ a_3 \\ a_4 \end{Bmatrix} \equiv [A]\{a\} \tag{6.6}$$

By solving Eq. (6.6), we get a solution for $\{a\}$,

$$\{a\} = [A]^{-1}\{d\}_e$$

and the strain is expressed as,

$$\varepsilon_x = \frac{du}{dx} = -y\frac{d^2v}{dx^2} \equiv y\kappa_x \tag{6.7}$$

where κ_x is the curvature and may be expressed as

$$k_x = -\frac{d^2v}{dx^2} = 2a_3 + 6a_4x = \lfloor 0 \ \ 0 \ \ 2 \ \ 6x \rfloor\{a\}$$

$$= \lfloor 0 \ \ 0 \ \ 2 \ \ 6x \rfloor [A]^{-1}\{d\}_e \equiv [B]\{d\}_e$$

The stress σ_x is then given as,

$$\sigma_x = E\varepsilon_x = -Ey\kappa_x$$

The principle of virtual work for this beam element may be expressed as,

$$E\int \int_A \delta\varepsilon_x\sigma_x dAdx = \{\delta \ d\}_e^{\ T}\{f\}_e \tag{6.8}$$

where A is the cross-section area, and $\{f\}_e$ is the nodal force vector corresponding to the nodal displacement,

$$\{f\}_e = \begin{Bmatrix} F_1 \\ M_1 \\ F_2 \\ M_2 \end{Bmatrix} \tag{6.9}$$

where F_α, M_α $(\alpha = 1,2)$ is the shear force and bending moment for nodal point α. Equation (6.8) may be rewritten as,

$$\{\delta \ d\}_e^{\ T}\int_0^l [B]^T EI[B] dx\{d\}_e = \{\delta \ d\}_e^{\ T}\{f\}_e$$

where I is the second order inertia moment for the cross-section, and expressed as,

$$I = \int_A y^2 dA$$

where, $\{\delta\ d\}_e$ is any values, the stiffness matrix equation for an element is

$$\{f\}_e = [K]_e \{d\}_e \tag{6.10}$$

where, $[K_e]$ is a stiffness matrix

$$
\begin{aligned}
[K]_e &= \int_0^l [B]^T EI[B] dx \\
&= \frac{EI}{l^3}
\begin{bmatrix}
12 & 6l & -12 & 6l \\
6l & 4l^2 & -6l & 2l^2 \\
-12 & -6l & 12 & -6l \\
6l & 2l^2 & -6l & 4l^2
\end{bmatrix}
\end{aligned}
\tag{6.11}
$$

6.3.3 Stiffness Matrix for 3D Beam Elements
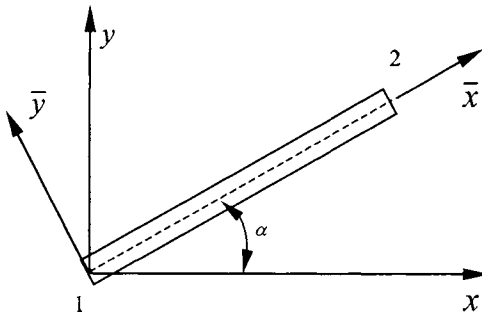
Figure 6.3 Inclined 2D Beam Element

In Figure 6.3, $\bar{x}, \bar{y}$ denote local member axes and x, y denote global system axes. The moments M_1 and M_2 can be considered as vectors normal to the $x - y$ plane, corresponding to angles θ_1 and θ_2. Hence, the transformation equations relating nodal force components in local axes and global axes may be written as,

$$
\begin{aligned}
\{\bar{f}\} &= [T]\{f\} \\
\{f\} &= [T]^T \{\bar{f}\}
\end{aligned}
\tag{6.12}
$$

where nodal force vector in local axes $\{\bar{f}\}$ and nodal force vector in global system $\{f\}$ are defined by

$$
\{\bar{f}\} =
\begin{Bmatrix}
\bar{F}_{1x} \\
\bar{F}_{1y} \\
\bar{M}_1 \\
\bar{F}_{2x} \\
\bar{F}_{2y} \\
\bar{M}_2
\end{Bmatrix}, \qquad
\{f\} =
\begin{Bmatrix}
F_{1x} \\
F_{1y} \\
M_1 \\
F_{2x} \\
F_{2y} \\
M_2
\end{Bmatrix}
$$

and the transformation matrix $[T]$ is given from geometrical consideration as,

$$[T] = \begin{bmatrix} \lambda & \mu & 0 & 0 & 0 & 0 \\ -\mu & \lambda & 0 & 0 & 0 & 0 \\ 0 & 0 & 1 & 0 & 0 & 0 \\ 0 & 0 & 0 & \lambda & \mu & 0 \\ 0 & 0 & 0 & -\mu & \lambda & 0 \\ 0 & 0 & 0 & 0 & 0 & 1 \end{bmatrix} \qquad (6.13)$$

with $\lambda = \cos\alpha, \mu = \sin\alpha$.

Similarly, we have for the nodal displacement components:

$$\{\overline{U}\} = [T]\{U\}$$
$$\{U\} = [T]^T\{\overline{U}\}$$

where $\{\overline{U}\}$ and $\{U\}$ are defined by

$$\{\overline{U}\} = \begin{Bmatrix} \overline{U}_1 \\ \overline{V}_1 \\ \overline{\theta}_1 \\ \overline{U}_2 \\ \overline{V}_2 \\ \overline{\theta}_2 \end{Bmatrix}, \qquad \{U\} = \begin{Bmatrix} U_1 \\ V_1 \\ \theta_1 \\ U_2 \\ V_2 \\ \theta_2 \end{Bmatrix}$$

Based on the element stiffness equation in the local axes,

$$\{\bar{f}\} = [\overline{K}]\{\overline{U}\} \qquad (6.14)$$

we may easily obtain, the element stiffness equation in the global axes,

$$[K] = [T]^T[\overline{K}][T] \qquad (6.15)$$
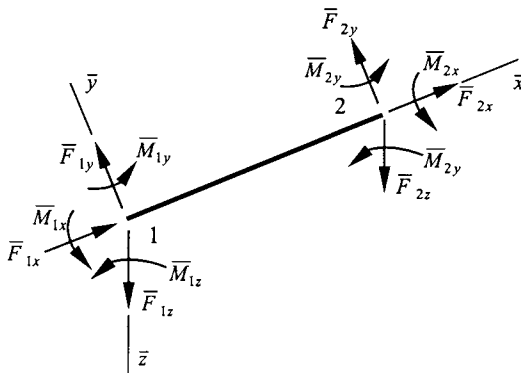
Figure 6.4   Nodal Forces for 3D Beam Element in Local Axes

If we write force and corresponding displacement vectors as

$$
\{\bar{f}\} = \begin{Bmatrix} \overline{F}_{1x} \\ \overline{F}_{1y} \\ \overline{F}_{1z} \\ \overline{M}_{1x} \\ \overline{M}_{1y} \\ \overline{M}_{1z} \\ \overline{F}_{2x} \\ \cdot \\ \cdot \\ \cdot \\ \cdot \end{Bmatrix}, \qquad \{\overline{U}\} = \begin{Bmatrix} \overline{U}_{1} \\ \overline{V}_{1} \\ \overline{W}_{t} \\ \overline{\theta}_{1x} \\ \overline{\theta}_{1y} \\ \overline{\theta}_{1z} \\ \overline{U}_{2x} \\ \cdot \\ \cdot \\ \cdot \\ \cdot \end{Bmatrix}
\tag{6.16}
$$

Having the stiffness matrix $[\overline{K}]$ defined in local axes for each beam element, the stiffness matrix $[K]$ in global axes for the beam element, may be derived using the transformation matrix $[T]$,

$$
[K] = [T]^T [\overline{K}][T]
\tag{6.17}
$$

$$
[\overline{K}] = \begin{bmatrix}
\dfrac{EA}{l} \\
0 & \dfrac{12EI}{l^3} \\
0 & 0 & \dfrac{12EI}{l^3} \\
0 & 0 & 0 & \dfrac{GJ}{l} & & & & \text{Symmetric} \\
0 & 0 & -\dfrac{6EI}{l^2} & 0 & \dfrac{4EI}{l} \\
0 & \dfrac{8EI}{l^2} & 0 & 0 & 0 & \dfrac{4EI}{l} \\
-\dfrac{EA}{l} & 0 & 0 & 0 & 0 & 0 & \dfrac{EA}{l} \\
0 & -\dfrac{12EI}{l^3} & 0 & 0 & 0 & -\dfrac{6EI}{l^2} & 0 & \dfrac{12EI}{l^3} \\
0 & 0 & -\dfrac{12EI}{l^3} & 0 & \dfrac{6EI}{l^2} & 0 & 0 & 0 & \dfrac{12EI}{l^3} \\
0 & 0 & 0 & -\dfrac{GJ}{l} & 0 & 0 & 0 & 0 & 0 & \dfrac{GJ}{l} \\
0 & 0 & -\dfrac{6EI}{l^2} & 0 & \dfrac{2EI}{l} & 0 & 0 & 0 & \dfrac{6EI}{l^2} & 0 & \dfrac{4EI}{l} \\
0 & \dfrac{6EI}{l^2} & 0 & 0 & 0 & \dfrac{2EI}{l} & 0 & -\dfrac{6EI}{l^2} & 0 & 0 & 0 & \dfrac{4EI}{l}
\end{bmatrix}
$$

For a member having circular cross-section, $I, J,$ and A are defined in terms of the external diameter D_e and the internal diameter D_i as,

$$
I = \frac{\pi}{64}\left(D_e^4 - D_i^4\right), \quad J = \frac{\pi}{32}\left(D_e^4 - D_i^4\right), \quad A = \frac{\pi}{4}\left(D_e^2 - D_i^2\right)
$$

where $[T]$ denotes the transformation matrix, which may be expressed in terms of sub-matrices $[L]$ and $[0]$ as,

$$[T] = \begin{bmatrix} [L] & [0] & [0] & [0] \\ [0] & [L] & [0] & [0] \\ [0] & [0] & [L] & [0] \\ [0] & [0] & [0] & [L] \end{bmatrix}$$ (6.18)

with $[L]$ and $[0]$ defined by,

$$[L] = \begin{bmatrix} \lambda_x & \mu_x & v_x \\ \lambda_y & \mu_y & v_y \\ \lambda_z & \mu_z & v_z \end{bmatrix}, \quad [0] = \begin{bmatrix} 0 & 0 & 0 \\ 0 & 0 & 0 \\ 0 & 0 & 0 \end{bmatrix}$$ (6.19)

where λ_x denotes the cosine of the angle between the x and $\bar{x}$ axes, μ_x denotes the cosine of the angle between the y and $\bar{x}$ axes, v_x denotes the cosine of the angle between the z and $\bar{x}$ axes, etc.

The stiffness matrix for the structural system may be established by assembling the stiffness matrices for individual elements of the structural system. Once the system stiffness matrix for the structure is established, boundary conditions can be applied to determine nodal displacements/forces. The element nodal forces in local axes may then be determined and nodal displacements and stresses in local axes estimated. For more information on the finite element methods, reference is made to Zienkiewicz (1977).

6.4   Design Loads and Load Application

Dead Loads

Structural weight can be calculated directly from the structural model based on the material density and volume input. These loads are generated automatically by the FEM program as nodal forces or uniform loads on members. Equipment and miscellaneous loads may be applied by means of surface loads or concentrated nodal forces at their actual location.

Variable Loads

In design of structural members, the variable loads and weights must be analyzed for several cargo distributions in order to capture the extreme values of loads. The variable loads are usually included in the FEM model as surface pressure on relevant decks or tank boundaries.

Static Sea Pressure

Static sea pressure at each design draft is computed and applied in the FEM model as a surface load, which acts like a constant surface pressure on the bottom and as a linearly varying surface pressure on the side plates.

Wave Induced Loads

The wave-induced hydrodynamic loads and inertia loads due to vessel motion are considered to be low-frequency dynamic loads and can be analyzed using a quasi-static approach. The solutions for these ship motions and hydrodynamic loading are most frequently accomplished through the use of strip theory.

For ships: A global extreme sea-state is used and imposed on the structure. Inertia loads are calculated based on a conservatively assumed motion of the vessel.

For offshore structures: A different analysis is carried out and a sufficient number of periods should be analyzed for the following reasons:

- To adequately cover the site-specific wave conditions

- To satisfactorily describe transfer functions at and around the wave cancellation and amplification periods

- To satisfactorily describe transfer functions at and around the heave resonance period of the structure

Global wave frequency: Structural responses should be established by an appropriate methodology, for example:

- A regular wave analysis

- A design wave analysis

- A stochastic wave analysis

Once the extreme waves are selected for a design, wave induced loads may be computed by commercial programs, such as AQUA, WAMIT, etc. The phase angles of waves should be represented properly. The structural members are therefore designed to withstand the maximum stresses resulting from various phases of waves.

Wind Loads

Wind loads are usually considered static loads and are calculated based on the actual area and wind pressure by simply using the following formula:

$$F_{wind} = P_{wind} \cdot A_{wind} \tag{6.20}$$

$$P_{wind} = V^2 \cdot C_h \cdot C_s \tag{6.21}$$

where,

$\quad V \quad$ = Wind velocity

$\quad C_h \quad$ = Height coefficient

$\quad C_s \quad$ = Shape coefficient

$\quad A_{wind}$ = Projected area perpendicular to the wind direction

The height and shape coefficients are specified in classification rules. The quasi-static wind pressure Eq.(6.21) was derived in accordance with Bernoulli's theorem for an idea fluid striking an object which states that the dynamic pressure may be expressed as:

$$P_{wind,dynamic} = \frac{1}{2} \rho V^2 \tag{6.22}$$

where, ρ denotes the mass density of air. Wind loads may be applied as surface loads if the projected areas are modeled. In most cases, they are applied as horizontal concentrated loads at appropriate elevations.

6.5   Structural Modeling

6.5.1   General

This section gives a general overview for the design of marine structures using a finite element modeling technique. Reference is made to recommendations described in NORSOK N-004 (NTS, 1998), which is one of a few codes that provide guidance on the finite element modeling in marine structural design. This section shall address structural modeling defined by industry codes for fixed platforms and floating production installations.

6.5.2   Jacket Structures

A Jacket structure is a welded tubular space frame consisting of vertical or battered legs supported by a lateral bracing system. The function of the jacket is to support the topside facilities, provide supports for conductors, risers, and other appurtenances and serve as a template for the foundation system. Graff (1981) and Dawson (1983) give an introduction to the design and analysis of jacket structures, including basic formulations for environmental loads, modeling of foundation, finite element analysis, dynamic response and stress acceptance criteria. In general the design activities include:

- Identify the project needs

- Evaluate environmental conditions and soil conditions

- Develop preliminary design proposals focusing on the methods of installation

- Evaluate the installation methods in terms of technical and economical feasibility, construction and installation challenge, foundation requirements and cost etc.

- Dimension the structure to resist the in-place load during operating condition, for each mode of operation such as drilling, production, work over, or combinations thereof.

- Evaluate the design to ensure that it can resist actions due to transportation from the fabrication yard to the installation site, including load-out, sea transportation, installation, mating, and hook-up.

- Account for abandonment of the structure after decommissioning

- Meet quality and HSE requirements.

Analysis Models

The global analysis of platforms starts from defining the geometrical and material properties of the structural members, the foundation properties and functional, environmental and accidental loads.

Two types of structural analysis may be conducted:

- A linear analysis to check ultimate strength and fatigue criteria based on industry codes (such as API RP 2A) using internal member forces.

- A non-linear finite element analysis of structural response to accidental loads (such as ship collision, dropped objects, fire, explosion and earthquake) or extreme response to wave load as part of the re-assessment of exiting platforms.

The basic formulation for linear finite element analysis is given in Section 6.3. The nonlinear finite element analysis is detailed in Chapter 12.

The finite element model for analysis of jackets includes:

(1) Loads: The loads include:

- Functional loads such as gravity load

- Environmental loads due to wind, waves, currents, earthquakes, and

- Accidental loads that may occur during its service life.

The increase in hydrodynamic and gravity actions caused by marine growth should be accounted for. The hydrodynamic model of the structure should include appurtenances such as conductors, I-tubes and risers, caisson, ladders and stairs, launch box, boat landing, guides, and anodes. Depending upon the type and number, appurtenances can significantly increase the global wave forces. In addition, forces on some appurtenances may be important for local member design. Appurtenances not welded to the main structure are generally modeled as non-structural members that only contribute as equivalent wave forces.

(2) Foundation: The foundation system for the jacket temporary on-bottom condition prior to installation of the permanent foundation system should be documented to have the required foundation stability for the specified environmental conditions, and for all relevant limit-states. Throughout the analysis, structure-to-ground connections should be selected in order to represent the response of the foundations. They may normally be simulated using linear stiffness matrices. The finite element analysis may model behavior of axial and lateral soil-foundation systems explicitly.

(3) Structures: The stiffness of the deck structure shall be modeled in sufficient detail to ensure compatibility between the deck design and the jacket design. In a linear analysis normally it is sufficient to model one member using only one element. However, in order to account for member buckling and local dynamic response, one or more beam-column elements are required to model each member depending on the element formulation, distribution of actions. Major eccentricities of load carrying members may be modeled as rigid ends in the model.

Modeling for Ultimate Strength Analysis

The load cases include each mode of operation, such as drilling, production, work-over, or a combination thereof. According to NTS (1998), it is necessary to perform analyses to establish:

- maximum base shear of wave and current actions for dimensioning jacket bracing's,

- maximum overturning moments for dimensioning jacket legs and foundation systems.

- maximum local member forces which may occur for wave positions other than that causing the maximum global force.

Modeling for Fatigue Analysis

Fatigue analysis should include all relevant actions contributing to the fatigue damage both in non-operational and in operational design conditions. When calculating fatigue damage, local action effects due to wave slamming and vortex shedding should be included if relevant.

While jackets in shallow water depths are normally insensitive to dynamic effects, non-linearity's associated with wave theory and free-surface effects may be important. A deterministic analysis is normally recommended for such jackets. For deepwater jackets where the dynamic effects are important, a fatigue analysis in the frequency domain (dynamic

stochastic analysis) is recommended. In order to linearize the actual non-linear soil response, the stiffness matrices for structure-soil interaction should be developed based on a wave height, which contributes most significantly to the fatigue damage.

Assessment of Existing Platforms

An existing platform should be re-assessed if the design conditions change such as:

- If the original operating load is significantly exceeded due to the addition of facilities,
- If the structure is altered, degraded due to fatigue and corrosion damages.
- If the structure has an inadequate air gap, is operated under different environmental and operating conditions.
- When the life-safety level becomes more restrictive.

API RP 2A (1997) give a comprehensive recommendation on survey, metocean, seismic and ice load criteria, structural analysis methodologies and evaluation criteria as well as mitigation alternatives.

Fire, Blast and Accidental Loading

API RP 2A (1997) proposed risk-based structural assessment for fire, blast and accidental loading. The assessment includes the following tasks:

- For the selected platform, assign a platform exposure category based on consequence of failure in terms of human life and cost,
- For a given event, assign risk levels Low, Medium and High to the probability (frequency) of the event occurring,
- Determine the appropriate risk level for the selected platform and event based on a risk matrix,
- Conduct further study or analysis to better understand frequency, consequence, and cost of mitigation and set acceptance criteria based on (As Low As Reasonably Practicable) ALARP principle.
- Reassign a platform exposure category and/or mitigate the risk or the consequence of the event.

For those platforms considered as high risk for a defined event, a detailed structural integrity assessment is to be conducted for fire, blast or accidental loading based on nonlinear finite element analyses or experimental tests.

For a comprehensive reference list and guidance on the design against fire and blast loads, reference is made to ISSC (1997). The panel V.2 report for ISSC (1997) summarized design and assessment philosophy, preventive and protective measures for fires, analysis methods for fire loads and load effects, analysis methods for blast loads and load effects, probabilistic analysis and design recommendations.

6.5.3   Floating Production and Offloading Systems (FPSO)

Structural Design General

The design of FPSO should comply with the classification requirements and industry standards, e.g. NORSOK (NTS, 1998) and API RP 2FPS.   In cases where the FPSO is

registered in a specific country, the relevant requirements of the flag state authority shall also be followed.

The main difference between an ocean-going ship and a site-specific FPSO is:

- An FPSO is stationed in a specific site using mooring and anchoring systems, and subjected to site-specific environmental conditions,

- The operating life for an FPSO may be equal to or longer than 20 years,

- Risers are attached to the FPSO hulls through riser porches or I-tubes,

- Topside facilities may impose requirements such as motion/green-water/safety and the standard of living quarter is higher,

- An FPSO may have cyclic offloading offshore with a frequency of approximately once per week,

- An FPSO is designed to have no dry docking imposing stricter requirements for inspection/maintenance and repair.

Design and analysis of an FPSO include the following aspects (Bai et al 2001):

- Vessel hull configuration selection

- Design load case definition

- Stability and compartmentation

- Global performance

- Greenwater

- Intact strength covering transit, temporary conditions, extreme operating conditions, and survival conditions

- Structural strength in damaged condition

- Mooring and riser systems

- Topside consideration

The design load cases include:

- In-place operating condition: environmental loads of up to 100 year return period, quartering/head seas (turret moored) or all headings (spread moored) and various loading conditions from topsides, risers and mooring systems.

- Survival Conditions: 100 years return environment/responses, worst loading conditions from topsides and damaged conditions (for strength and stability)

- Transportation Conditions: 10 years return period or less, ballast loading condition, dry topside and head seas.

- Installation and hoop up: selected weather window(s), ballast tanks, dry topsides and heading of up to quarter seas

In developing the design criteria, consideration should be given to site-specific services, including the following factors that may influence the hull actions:

- Site-specific environmental conditions

- Effect of mooring system

- Long-term service at a fixed location
- Seas approaching predominantly from a narrow sector ahead
- Zero ship speed
- Range of operating loading conditions
- Tank inspection requirements
- Different return period requirements compared with normal trading tankers

For ocean-going vessels, classification Rules specify corrosion control, coating requirements, corrosion prevention equipment/operation and wall-thickness allowance based on 20 years of operating life. For FPSOs, additional wall-thickness allowance may be required considering factors such as,

- An FPSO may have longer operating life,
- An FPSO requires no dry docking inspection and
- The cost for coating repair and reduced production is high.

Analysis Models

Five typical levels of modeling may be developed for the finite element analysis of the hull structure including:

- Global Structural Model (Model level 1),
- Cargo Tank Model & Turret Model for FPSO (Model level 2),
- Frame and Girder Model (Model level 3),
- Local Structural Analysis (Model level 4),
- Stress Concentration Models (Model level 5).

The 3D FEM models are developed for the following:

- Cargo tank area at midship,
- Fore end area including the structure supporting the flare boom,
- Module supports and the supporting structure,
- Main crane pedestals supporting structure,
- Porches for production/injection risers and export risers including the supporting structures, pull-in supports,
- Spread mooring attachments.

The structural design shall give due consideration to the loads imposed by the topsides, risers and mooring connection and this should be reflected in the FEM model. The main stress contributions include:

- Primary stress due to global hull girder bending,
- Secondary stress due to panel bending between bulkheads,
- Tertiary stress due to local plate bending between web frames.

Modeling for Ultimate Strength Analysis

A finite element analysis may be conducted to calculate global longitudinal stresses and global shear stress. For turreted FPSOs, it is necessary to predict the stress distribution around the openings, in particular at the deck and bottom, and at the ends of longitudinal strength elements.

All relevant variations in tank filling should be considered in the analysis and reflected in the Operation Manual. The following stress components can be found from the FEM analysis:

- Local transverse and longitudinal stresses

- Transverse stresses in web frames

- Double shell and double bottom stresses

- Local shear stresses in panels

The combination of global and local stresses should account for actual stress directions and phases. However, if phase information is limited or uncertain, the maximum design value for
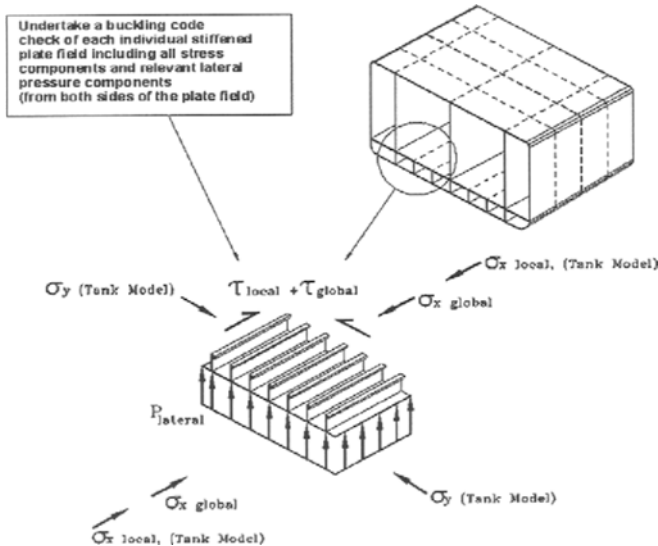
Figure 6.5   Typical Stress Components in the Hull Beam (NTS, 1998)

each component should be combined as a 'worst-case' scenario. A combination of typical stress components is shown in Figure 6.5.

Internal static and dynamic pressures can be calculated using simplified formulas.

In some cases, detailed element mesh models may be necessary in order to check the maximum peak stresses and the possibility of repeated yielding during the ultimate limit-state assessment.

The hull girder strength should be evaluated to withstand relevant combinations of still water and wave induced bending moments and shear forces. The extreme hogging and sagging conditions are considered in the analysis. The appropriate site-specific environmental data should be applied in the analysis.

Transverse strength refers to the hull's ability to resist lateral pressure and racking actions in combination with longitudinal action effects. This resistance is provided by means of transverse bulkheads, web frames, girders, and stringers. Transverse strength should be evaluated using a finite element model of a specific portion of the hull, and the effects of deck equipment actions should be included.

Usually buckling and ultimate strength for plated members and stiffeners are checked based on NTS (1998) or API 2V or classification Rules. Typical criteria for plated members and stiffeners are discussed in Chapter 10. The strength checks are carried out for main structures, secondary structures and structures supporting hull appendages.

In some cases, the FPSO hull is also designed for collision, such that the collision with supply vessels and shuttle tankers does not cause penetration of the side or inner longitudinal bulkhead. Impacts from the bow, stern and side of the supply vessels and shuttle tankers are considered. Fire fighting, explosion protection and heat protection are designed based risk assessment, see PART V.

ABS (2001) gives guidance on SafeHull-Dynamic Loading Approach (DLA) for Floating Production Storage and Offloading Systems (FPSO). The DLA approach provides enhanced structural analysis to assess the capabilities and sufficiency of a structural design. A precondition to use DLA is that the initial scantling for hull structures is based on Rule requirements. The results of a DLA analysis may not be used to reduce the dimension of the hull structures. However, if an increase of basic scantling is identified through the DLA analysis; such an increase is to be accomplished to meet the DLA requirement. The DLA analysis procedure consists of the following (ABS, 2001):

- Create sea-keeping analysis models,
- Assemble hull loading scenarios & create still-water load file,
- Obtain & verify environmental data,
- Conduct analysis of ship motions and predict wave-induced loads & extreme value for each DLP (Dominant Load Parameters, such as vertical hull girder bending moment amidships),
- Derive equivalent wave for each DLP,
- Establish wave-induced load effects,
- Create structural analysis for the defined load cases,
- Conduct global and local structural analysis,
- Check structural analysis results against acceptance criteria.

The benefits from conducting a finite element analysis like DLA analysis is the increased safety (by increasing scantling in the weak areas), reducing possible future renewals and providing structural models that may be used immediately in the events of emergency situations.

Modeling for Compartmentalization and Stability

The relevant detrimental effects in the compartmentalization and stability assessment of an FPSO are:

- Environmental actions

- Relevant damage scenarios

- Rigid body motions

- The effects of free-surface

- Boundary interactions (e.g. mooring and riser systems)

In order to determine the vessel's mass and position of the center of gravity, an inclining test is conducted when the construction is near completion. In the Operational Manual, the vessel's center of gravity is recorded.

The number of openings in watertight structural elements should be kept to a minimum. Arrangements for access, piping, venting, cables, etc., arrangements should be made to ensure that the watertight integrity of the structure is maintained.

The stability of an FPSO should satisfy the requirements stated in relevant Codes. The requirements for stability are given in IMO regulations (resolution A167, A206 and A502, superseded by A749(18)), IMO MODU Code (issued in 1989), and classification Rules. Adequate stability should be established for all relevant in-service and temporary phase conditions. The assessment of stability should consider both the intact and the damaged conditions.

Modeling for Fatigue Analysis

Fatigue sensitive details and the materials selected should be documented to have sufficient fatigue strength for transportation and in-place conditions. Three levels of fatigue analysis may be conducted:

- fatigue check based on simple stress formulae for scantling (primarily aimed at connections between longitudinal stiffeners and transverse web frames in the hull structure), see Section 19.6.

- simplified fatigue assessment to check the allowable stress range assuming the long-term stress range follows the Weibull distribution, see Section 19.3,

- spectral fatigue assessment based on the first principles, see Chapter 20.

The spectral fatigue assessment, makes use of the wave scatter diagrams for the installation sites for in-place conditions and route-specific wave conditions for the transportation phase, see Chapter 3. The wave scatter diagrams define the occurrence probability for various sea-states defined by significant wave height and period. The analysis also takes into account the direction of the sea and swell conditions relative to the vessel heading.

Particular attention should be given to connection details of the following:

- Integration of the mooring system with hull structure,

- Main hull bottom, sides, and decks,

- Main hull longitudinal stiffener connections to transverse frames and bulkheads,

- Main hull attachments, seats, supports, etc,

- Openings in main hull,

- Transverse frames,

- Flare tower,

- Riser porches,

- Major process equipment seats.

Any turret structure will be exposed to high levels of dynamic action. The following actions should be considered throughout the fatigue design of turret structures:

- Dynamic fluctuations of mooring line tension,

- Dynamic actions (tension and bending moment) from risers,

- Local varying hydrodynamic pressure due to wave action and vessel motion,

- Reactions in the bearing structure due to the other effects,

- Inertia actions due to accelerations of vessel motions including variations in internal fluid pressure,

- Fluctuating reactions in pipe supports due to thermal and pressure induced pipe deflections.

Local stress ranges are determined from dynamic pressures acting on panels and accelerations acting on the equipment and topside. Other environmental actions also affect part of the structure as local stresses with a variety of ranges.

The transfer function for the dynamic pressure could either be used directly to calculate local stress transfer functions and combined with the global stress transfer function or a long-term pressure distribution could be calculated. At least, the following dynamic pressure components should be considered:

- Double hull stresses due to bending of double hull sections between bulkheads,

- Panel stresses due to bending of stiffened plate panels,

- Plate bending stresses due to local plate bending.

Global and local stresses should be combined to give the total stress range for the detail in question. The global and the local stress components differ in amplitude, phase, and location. The method of combining these stresses for the fatigue damage calculation will depend on the location of the structural detail.

Local, detailed FE-analysis (e.g. unconventional details with insufficient knowledge about typical stress distribution) should be undertaken in order to identify local stress distributions, appropriate SCFs, and/or extrapolated stresses which will be utilized in the fatigue evaluation. Dynamic stress variations through the plate thickness shall be documented and considered in such evaluations.

During the fatigue assessment, fine element mesh models will be developed for critical stress concentration details that do not comply with the stress concentration factors given in recognized standards. The size of the model should be such that the assumptions made for the boundary conditions do not affect the calculated hot spot stresses significantly. Element sizes for stress concentration analysis should be of the same order of magnitude as the plate thickness. Normally, shell elements may be used for the analysis.

The fatigue hot-spot stresses are obtained by combining stress components from the global hull girder bending, secondary and tertiary bending and locally imposed loading. The stress concentration factors may be obtained using parametric equations or fine mesh finite element analysis of critical regions. Principal stresses are used in the evaluation of fatigue damage. The selection of S-N curves and methodologies for fatigue damage assessment are discussed in detail in PART III.

6.5.4   TLP, Spar and Semi-submersible

A column-stabilized structure (semi-submersible or TLP) is defined as a floating installation consisting of a deck structure with a number of widely spaced, large diameter, supporting columns that are attached to submerged pontoons.

Some special components of column-stabilized structures include:

- Ring (continuous) pontoons,
- Twin pontoons,
- Multi-footing arrangements,
- Tension legs (TLPs).

Such structures may be kept on station by using a passive mooring system (e.g. anchor lines), an active mooring system (e.g. thrusters), or a combination of both.

In recent years Spar structures became a type of popular floating installations for use in the Gulf of Mexico when the water depth is deeper than 1000 m. Production risers are supported by air-filled buoyancy cans in the central moonpool of the hull. For truss spars, the bottom half of the spars consists of tubular truss and heave plate structures.

In the conceptual design phase, the design and analysis for TLP, Spar and semi-submersible include:

- Establish design basis,
- Select facilities and conduct system design,
- Determine layout,
- Size hulls and estimate global performance,
- Design topside and hull structures,
- Design risers and foundations such as piles for mooring/tethering,
- Estimate weight, schedule and costs for fabrication and installation,
- Review HSE compliance and quality assurance.

Successful deepwater development depends on an experienced team using a systems approach to select a concept such for floating installations. Dorgant et al (2001) presented primary drivers for system selection for three major field development projects, and discussed technical/commercial/feasibility/regulatory issues for alternative facility systems (TLP, Spar, FPSO and semi-submersible).

Demirbilek (1989) edited a couple of interesting articles on the various design topics for TLP design and analysis such as environmental criteria, hydrodynamic loads, structural analysis and criteria, foundation design and analysis, riser analysis, tendon analysis, fatigue design and fracture mechanics analysis, material selection, model tests and measurement

A floating installation may be designed to function in a number of modes, e.g. transit, operational, and survival. The limiting design criteria include relevant considerations regarding the following items:

- structural strength in intact condition,
- structural strength in damaged condition,
- air gap,
- compartmentalization and stability.

For novel designs, where limited or no direct experience exists, relevant analysis and model testing should be conducted to demonstrate that an acceptable level of safety is obtained.

The structure should be designed to resist relevant actions associated with conditions that may occur during all stages of the life cycle of the unit, including:

- Fabrication,
- Site moves,
- Mating,
- Sea transportation,
- Installation,
- Decommissioning.

It is generally more practical and efficient to analyze different action effects via a range of models, with the responses superimposed from each model, factored as relevant.
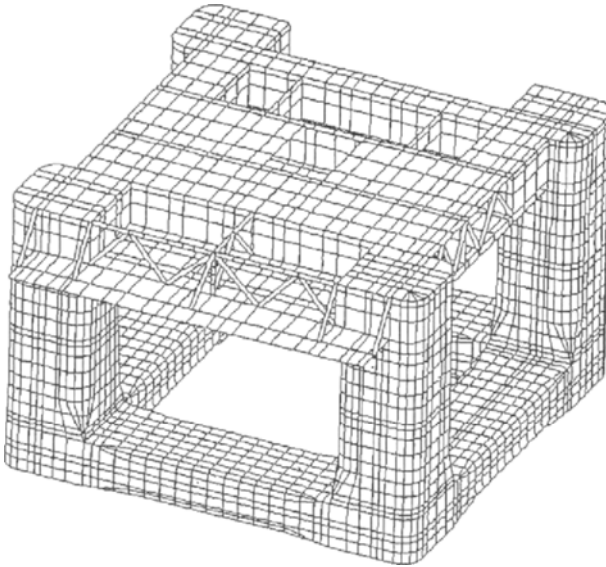
Figure 6.6   Example of Global Analysis Model (NTS, 1998)

A simplified model may be applied for the preliminary design to establish the approximate design responses and to get a feel for how the structure will behave.

The purpose of the global analysis model is to enable the assessment of the responses resulting from the global actions. An example of such a model is given in Figure 6.6. For large, thin-walled structures, 3-dimensional finite element models created in shell (or membrane) finite elements are normally required. For space frame structures consisting of slender members, a 3-dimensional space frame representation of the structure may be adequate.

The stiffness of major structural connections (e.g. pontoon to column or column to deck) should be modeled in detail in order to represent the stiffness of the connection The hydrodynamic loading model may be mapped directly onto the structural model.

Typically, a simplified space-frame model of the structure may be created to obtain the maximum range of stresses in the tank for a range of tank loading conditions. These load conditions will include both full and empty pontoons representing the maximum and minimum sagging and hogging conditions.

The simultaneity of the responses resulting from the global and local analysis models may normally be accounted for by linear superposition with appropriate load factors applied.

In buckling and ultimate strength checks, relevant lateral pressure applied together with in-plane forces. The criteria for plated members, stiffeners and stiffened shells are available from classification rules, industry standards such as NORSOK N-004 (NTS, 1998), API 2U and API 2V, see Chapters 10 and 11.

The ultimate strength criteria for TLP tethers under combined external pressure, tension and bending may govern its design. These strength criteria may be modified using the formulation developed in the 1990s for strength design of deepwater pipelines and risers.

The fatigue assessment of TLP, Spar and semi-submersibles is similar to that described for FPSO, see PART III.

6.6 References

1. ABS (2001), "Guidance Notes on "SafeHull – Dynamic Loading Approach" for Floating Production, Storage and Offloading (FPSO) Systems", American Bureau of Shipping.

2. API (2001), "API RP 2A WSD : Recommended Practice for Planning, Designing and Constructing Fixed Offshore Platforms – Working Stress Design," Latest Edition.

3. API (1993), "API RP 2A LRFD – Recommended Practice for Planning, Designing and Constructing Fixed Offshore Platforms – Load and Resistance Factored Design", First Edition. 1993.

4. API (1997), "Supplement 1 to the API RP 2A LRFD, First Edition.

5. API (1997), "API RP 2T – Recommended Practice for Planning, Designing and Constructing Tension Leg Platforms", Second Edition.

6. API (2001), "API RP 2A WSD, Recommended Practice for Planning, Designing and Constructing Fixed Offshore Platforms - Working Stress Design", American Petroleum Institute, Latest Edition.

7. API (2001), "API RP 2FPS, Recommended Practice for Planning, Designing and Constructing Floating Production Systems", First Edition.

8. Bai, Y., Ayney, C., Huang, E., Maher, J., Parker, G., Song, R. and Wang, M. (2001), *"Design and Construction of Floating Production Systems"*, Course Notes for an

Industry Training Course led by Yong Bai and Organised with Clarion Technical Conferences in Houston and IBC in London.

9.   Dawson, T.H. (1983), "*Offshore Structural Engineering*", Prentice-Hall Inc.

10.   Demirbilek, Z. (1989), "*Tension Leg Platform – A State of the Art Review*", American Society of Civil Engineers.

11.   Dorgant, P.L., Balint, S.W., Rodenbusch, G., Luyties, W.H. and Rainey, R.M. (2001), "System Selection for Deepwater Production Installations", Offshore Technology Conferences, OTC12966.

12.   Graff, W.J., (1981), "*Introduction to Offshore Structures – Design, Fabrication, Installation*", Gulf Publishing Company, Houston, Texas.

13.   ISO Codes for Design of Offshore Structures (being drafted).

14.   ISSC (1997), "Design Against Fire and Blast Loads," The panel V.2 report from International Ship and Offshore Structures Congress, Trondheim, Norway.

15.   NTS (1998), "NORSOK N-004, Design of Steel Structures", Norwegian Technology Standards Institution, (available from: www.nts.no/norsok).

16.   Zienkiewicz, O.C. (1977),"*The Finite Element Method*", McGraw-Hill Book Company.

Part I

Structural Design Principles

Chapter 7   Limit-State Design of Offshore Structures

7.1   Limit State Design

In this Section, the concept of limit state design is introduced to allow an assessment considering the following limit-states:

- ULS - Ultimate Limit States – Ultimate strength behavior
- FLS - Fatigue Limit States – Fatigue and fracture behavior
- SLS- Serviceability Limit States –Displacements and deflections
- ALS- Accidental Limit States – Collision, fire, blast, dropped object, etc.

In general, the structure will need to be checked for all groups of limit states to ensure that there are sufficient safety margins between the maximum likely loads and the minimum resistance of the structure.

The general safety format for limit state design is expressed as:

$$S_d \quad \le \quad R_d \tag{7.1}$$

Where,

$\quad S_d \quad = \Sigma S_k \cdot \gamma_f \quad$ Design action effect

$\quad R_d \quad = \Sigma {R_k}/{\gamma_m} \quad$ Design resistance

$\quad S_k \quad$ = Characteristic action effect

$\quad R_k \quad$ = Characteristic resistance

$\quad \gamma_f \quad$ = Action (Load) factor

$\quad \gamma_m \quad$ = Material factor (= the inverse of the resistance factor)

Both the load and resistance factors may comprise a number of sub-factors reflecting the uncertainties and safety requirements in the load effects and resistance.

Extreme care is required in the finite element analysis to ensure that the correct load and resistance factors have been applied, particularly when several models are being used and the results are linearly superimposed.

In the marine specific finite element programs, the relevant code of practice can be selected by the analyst. This allows the appropriate design formulae to be chosen and the material factor to

be defined by the analyst prior to post-processing the results. The user will generally have to select the load factors prior to the definition of load combinations and ensure the inclusion of the material factors.

When a fine mesh is modeled for a local detailed analysis, the loads and boundary conditions may be taken from a more simplified analysis, which may either include the load factors or may be supplied unfactored. Therefore, it is recommended that all basic loads be tabulated along with the appropriate factors for the limit states considered. In this table, it should be clearly stated whether the load factors are included in the basic loads.

7.2   Ultimate Limit State Design

The codes generally require that the ultimate limit state of the structure complies with two conditions: ULS-A reflecting extreme permanent loads with regular environmental conditions, and ULS-B reflecting large permanent loads with extreme environmental conditions.

The structural analysis may be carried out as linear elastic, simplified rigid-plastic, or elastic-plastic.

7.2.1   Ductility and Brittle Fracture Avoidance

Ductile failure modes will allow the structure to redistribute the forces in accordance to the structural model. However, regardless of the analysis method used, the model will not be able to fully represent the redistribution of forces. The redistribution of forces in the structure will avoid brittle fracture modes or at least verify their excess capacity in relation to the ductile failure modes.

Brittle fracture should be considered in the following areas:

- Unstable fracture caused by a combination of brittle material, high local stresses, and weld defects
- Details where ultimate capacity is reached with only limited plastic deformation thus making the global behavior brittle

Unstable fracture may occur under unfavorable combinations of geometry, fracture toughness, welding defects, and stress levels, with the risk of such failures being the greatest in steels of high thickness (i.e. > 40mm) undergoing a deformation.

In general, the steel structure will meet requirements for adequate ductility when:

- Material toughness requirements are met
- Combinations of high local stresses and undetected weld defects are avoided
- Details are designed to develop plastic deformation
- Components do not exhibit a sudden drop in capacity when deformations continue beyond the maximum capacity
- Local and global buckling interactions are avoided

The maximum allowable defect size can be calculated based on the total stress or strains and the design fracture toughness using a fracture mechanics approach. It should be shown that both the maximum undetected defect following fabrication, and the maximum crack size following fatigue loading over the design life of the structures will be less that the maximum allowable defect size.

7.2.2 Plated Structures

The failure modes to be considered for plate structures are:

- Yielding of the plates
- Buckling of slender plates due to in-plane compressive stresses and lateral pressure
- Buckling of plates due to concentrated patch loads

The plate panel may be part of a box girder, a pontoon, a hull, an integrated plated deck, or merely a web or flange on a simple beam member. An example of a stiffened plate panel is shown in Figure 7.1
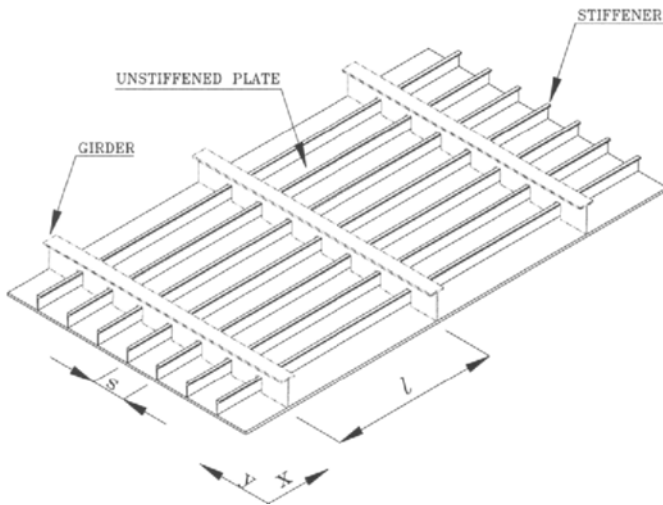
Figure 7.1   Stiffened Panel (NTS, 1998)

Ultimate strength capacity checks shall be performed for all structural components directly to the longitudinal and transverse strength of the structure. The structural components to be checked are all plates and continuous stiffeners including the following structures:

- Main deck, bottom and inner bottom
- Ship side, inner ship side, and longitudinal bulkheads
- Stringers and longitudinal girders
- Foundations of turret and topside structure
- Transverse bulkheads
- Transverse web frames

In finite element analyses, the plated area will generally be formed as one, of simple panel elements. If the panel is stiffened, this strengthening may be ignored in an initial assessment to avoid the need for the inclusion of all structural components, with some or all of the stiffening included in subsequent analyses. While this is a valid approach, the effect of the

plate stiffening upon the ductility of the structure should not be overlooked. Furthermore, if detailed stiffening is added, the analyst should consider the fabrication and inspection consequences of stiffening. For examples, the questions may be given: "Can the welder get sufficient access to the area?", "Will the weld type be limited (e.g. only single sided welding possible)?", "Will the weld detail cause a local stress concentration?", "What are the possibilities for inspection of the weld post fabrication and in-service, if required?" etc.

Plated sections of beams, i.e. web and flange sections or the walls of box sections will be defined as standard sections in the finite element program and will be checked against the appropriate code without the need for additional hand-checks. However, for joints in particular, forces will often need to be taken from the finite element analyses and used in hand or spreadsheet calculations to establish if sufficient strength exists.

The finite element program will generally center both the panel and the stiffeners on the nodal points for stiffened panels. Therefore, a horizontal deck panel's plate will appear to run through the center of the stiffeners rather than being supported on the stiffener ends, see Figure 7.1. There may also be a small inconsistency with the elevation since the nodes may be based on Top Of Steel (TOS) or on the Bottom Of Steel (BOS) coordinates rather than on the centerline of the plate as would be modeled. In both cases, offsets can be modeled to give the correct visual appearance; however, this is generally unnecessary in terms of the calculation of stresses in the model.

NORSOK N-004 gives a useful reference table for buckling checks of plate panels under different loading conditions. The recommended reference for the check is in NORSOK, NS 3472 or Eurocode 3. The most useful are the limiting values in the following section that state where buckling checks are not necessary. These tables are reproduced in Table 7.1.

7.2.3   Shell Structures

Unstiffened and ring-stiffened cylindrical shells subjected to axial forces, bending moments, and hydrostatic pressures may be designed as tubular members, or in a more refined analysis as a shell structure.

A tubular section in air, with a diameter to thickness ratio in excess of 60, is likely to fail by local buckling at an axial stress less than the material yield strength. The capacity of members failing due to local buckling is more sensitive to geometric imperfections than members that can sustain yielding over the thickness, which allows some redistribution of local stress due to yielding. The failure of such members is normally associated with a descending post-critical behavior compared to that of a brittle structure. Structures with this behavior are denoted as shells.

Thin-walled shell structures might not be adequately covered by the formulations for tubular members and joints, which are included in finite element programs that handle truss and beam models. Therefore, in general, shells should not simply be defined as thin-walled tubulars and treated in the same manner. Rather, a more complex finite element mesh should be developed and analyzed, particularly where the shell includes ring and/or longitudinal stiffening, see Figure 7.2.
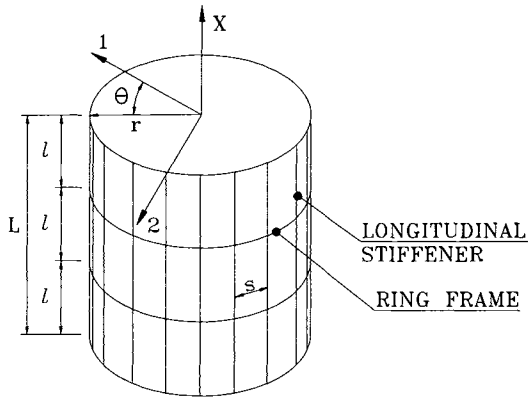
Figure 7.2   Example of a Cylindrical Shell
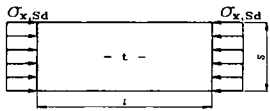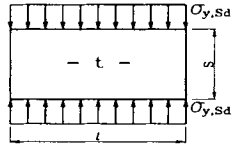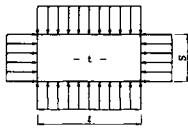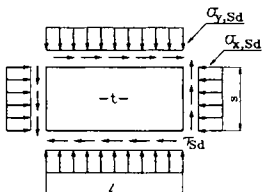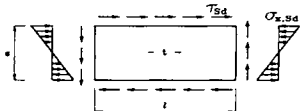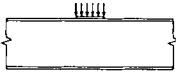
Stiffened cylindrical shells have to be dimensioned against several buckling failure modes. The buckling modes for stiffened cylindrical shells are categorized as:
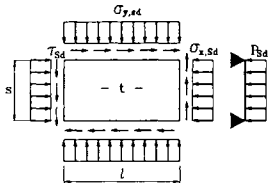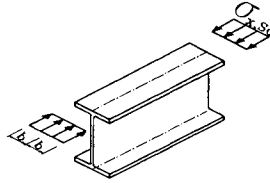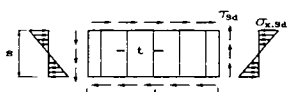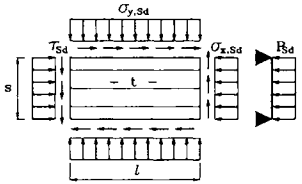
- Shell buckling – buckling of shell plating between rings and longitudinal stiffeners

- Panel stiffener buckling – buckling of shell plating including longitudinal stiffeners, rings are nodal lines

- Panel ring buckling – buckling of shell plating including rings. Longitudinal stiffeners act as nodal lines

- General buckling – buckling of shell plating including longitudinal stiffeners and rings

- Column buckling – buckling of the cylinder as a column

- Local buckling of longitudinal stiffeners and rings

The buckling modes and their relevance for different cylinder geometries are illustrated in Table 7.2 from NORSOK N-004. The strength equations for these failure modes are discussed in Part II Chapter 11 of this book.

Caution should be exercised when performing a finite element analysis of a shell. It has been found by experience that semi-empirical methods give a closer agreement to experimental results than theoretical methods. This is due to the effects of geometric imperfections, residual stresses, and inaccurately defined boundary conditions. Wherever possible, modeling should consider the real boundary conditions, the pre-buckling edge disturbances, the actual geometric imperfections, the non-linear material behavior, the residual welding stresses, and the heat effect zone. Note that relevant strength criteria may also be found from API codes, e.g. those listed in the References.
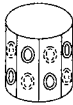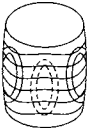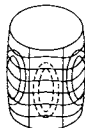
Table 7.1   Reference Table for Buckling Checks of Plate Panels

Description	Load	Sketch	Code Reference	Limiting Value
Unstiffened plate	Longitudinal compression		NORSOK	$s < 1$ Buckling check not necessary if $\dfrac{s}{t} \leq 42\,\varepsilon$
Unstiffened plate	Transverse compression		NORSOK	$s < 1$ Buckling check not necessary if $\dfrac{s}{t} \leq 5.4\epsilon$
Unstiffened plate	Combined longitudinal and transverse compression		NORSOK	$s < 1$ Buckling check not necessary if $\dfrac{s}{t} \leq 5.4\epsilon$
$s < 1$ Buckling check not necessary if $\dfrac{s}{t} \leq 5.4\epsilon$	Combined longitudinal and transverse compression and shear		NORSOK	
Unstiffened plate	Pure bending and shear		NS 3472 or Eurocode 3	
Unstiffened plate	Concentrated loads		NS 3472 or Eurocode 3	

Unstiffened plate	Uniform lateral load and in-plane normal and shear stresses		NORSOK	$s < l$ Buckling check not necessary if $\dfrac{s}{t} \le 5.4\epsilon$

Flange outstand	Longitudinal compression		NS 3472 or Eurocode 3	Buckling check of flange outstand not necessary if $\dfrac{b}{t_f} \le 15\epsilon$
Transverse stiffened plate panel	Bending moment and shear		NS 3472 or Eurocode 3	
Longitudinal stiffened plate panel	Longitudinal and transverse compression combined with shear and lateral load		NORSOK	

$\epsilon = \sqrt{235/\sigma_Y}$ *where* σ_Y *in* (N/mm^2) *unit*

Table 7.2   Buckling Modes for Different Types of Cylinders (NTS, 1998)

Buckling Mode	Type of Structure Geometry		
	Ring Stiffened (unstiffened circular)	Longitudinal Stiffened	Orthogonally Stiffened
Shell buckling			
Panel stiffener buckling			
Panel ring buckling			
General buckling			
Column buckling			

7.3   Fatigue Limit State Design

7.3.1   Introduction

Marine structures are subjected to a wide variety of loads that are cyclic in nature (e.g. storm winds, waves, and currents). These cyclic loadings develop cyclic strains in these structures. If the strains are large enough, then the strength, stiffness, and capacity of the structural elements can be reduced due to fatigue degradation.

Most fatigue problems have been associated with flaws introduced into the structure in the course of its fabrication and construction (e.g. poor welding, misaligned members), or in the course of its operation (e.g. corrosion damage, dropped objects damage). Thus, one of the

primary aspects of design for fatigue reliability includes quality assurance and control throughout the life cycle of the structure (inspection, maintenance, and repair).

In general, the design for fatigue reliability is concentrated on details of elements, and in particular joints. This is the first line of fatigue "defense". It is in the local details and joints that the significant or major stress-strain raisers are developed. However, given the very large uncertainties associated with predictions of the cyclic strain histories and the fatigue strength, high fatigue reliability of elements is rarely achieved.

Structure robustness or the ability of the structure system to tolerate defects without significant reductions in its serviceability or ultimate limit state characteristics is the second line of defense. Effective structure redundancy, ductility, and capacity must be mobilized.

The third line of defense is inspection, maintenance, and repair (IMR). Inspections help disclose unanticipated flaws and defects, and confirm our design objectives. Maintenance is intended to help preserve the structure so that it can fulfill its intended purposes. Repair strategy is intended to draw the engineer's attention to the necessity for restoring the structure's capacity after the future occurrence of damages and defects.

Present experience with the majority of marine structures indicates that although engineers have adequately designed for fatigue failure, there are still notable exceptions, e.g. structures in which certain types of loadings and stress raisers are ignored, high strength steels are used. It should not be expected that the fatigue strength would increase proportionally to the yield strength.

7.3.2 Fatigue Analysis

Fundamentally, the fatigue analysis approaches in engineering applications can be subdivided into the following categories:

- S-N based fatigue analysis approach

- The local stress or strain approach where the calculation includes the local notch effects in addition to the general stress concentration

- The fracture mechanics approach which gives allowance for the effects of cracks in the structure

These approaches have been well implemented in the fatigue design and assessment. However, fatigue limit state design is still one of the most difficult topics in structural design, assessment or reassessment. For marine structures, additional complications arise because of the corrosive environment. The fundamental difficulties associated with fatigue problems are related to:

- Lack of understanding of some of the underlying phenomena at both the microscopic and macroscopic levels

- Lack of accurate information on the parameters affecting the fatigue life of a structure

The general explicit fatigue design by analysis of marine structures involves a complex procedure. The dominant cause of the cyclic stresses within a marine structure is due to the sea environment that it experiences. Therefore, a fatigue assessment requires a description of the sea environment, or sequence of seastates, in which the structure is likely to meet over its planned operational life. Vessel motions, wave pressures, stress transfer functions, and the resulting fatigue stresses (generally expressed in terms of the number of cycles of various stress ranges) at locations of potential crack sites (hotspot) are then calculated. In order to

describe the fatigue durability of joints of marine structures, experimental data based S-N curves are selected or fracture mechanics models are applied. This demand and capability information is then used to calculate fatigue lives via a damage summation process (typically via the Palmgren-Miner hypothesis) or critical crack size. This procedure is summarized as:

- Characterization of the Sea Environment
- Hydrodynamic Response Analysis
- Structural Analysis
- Stress Transfer Function
- Stress Concentration Factor
- Hotspot Stress Transfer Function
- Long-term Stress Range
- Selection of S-N Curves
- Fatigue Analysis and Design
- Fatigue Reliability Analysis
- Inspection, Maintenance, and Repair Plan

Characterization of Sea Environment: The sea environment is represented by the number of occurrences of various sea states, each defined by a set of spectra. A two-parameter (significant wave height, zero up-crossing rate) wave-scatter diagram is used to characterize the sea states. All sea state spectra are defined by e.g. the Pierson-Moskowitz relationship. Wave direction probability is included in the sea environmental characterization.

Hydrodynamic Response Analysis: Once waves with appropriate frequencies, heights, and directions are selected, the hydrodynamic response and the loading of the structure are computed for each wave condition.

Structural Analysis: A global structural analysis is performed to determine the applied loading for the local structure (load transfer function per unit wave amplitude as a function of frequency). The local structural analysis is carried out to determine the stress transfer function per unit load at each hotspot in the structural detail.

Stress Transfer Function: The load transfer function per unit wave amplitude as a function of wave frequency is multiplied by the stress transfer function per unit load.

Stress Concentration Factor: The geometric SCF is considered in the fatigue assessment. For the fatigue screening analysis, an upper bound SCF is assumed 3.0. For the detailed fatigue analysis, the SCF is determined using parametric equations or the fine mesh Finite Element Analysis (FEA).

Hotspot Stress Transfer Function: The stress transfer function is multiplied by the stress concentration factor to determine the hotspot stress transfer function.

Long-term Stress Range: Based on the wave spectrum, wave scatter diagram and hotspot stress response per unit wave amplitude, the long-term stress range is determined. This was done by multiplying the ordinate of the wave amplitude spectrum for each sea state by the ordinate squared of the hotspot stress transfer function to determine the stress spectrum. The stress range distribution is assumed to follow a Rayleigh distribution. The long-term stress

range is then defined through a short-term Rayleigh distribution within each sea state for different wave directions.

Selection of S-N Curve: For each critical location considered in the analysis, S-N curves are assigned based on the structural geometry, applied loading, and welding quality.

Fatigue Analysis and Design: Several levels of fatigue analysis may be performed, including:

- Fatigue screening

- Detailed analysis

- Reanalysis of welding improvements

- Reanalysis of design improvements

- Reanalysis of design and welding improvements

Fatigue Reliability: Each early step involves the considerable uncertainty. There are many sources of complex interrelated uncertainties and variations. It is the primary purpose of a fatigue reliability analysis to logically organize these sources, and then to quantitatively evaluate them to determine what factors-of-safety (alternatively, levels of reliability) should be employed in a given design-analysis framework.

Inspection, Maintenance, and Repair: Given the time dependent fatigue reliability analysis, a rational risk/reliability based inspection, maintenance, and repair plan should be developed to minimize the life-cycle cost at the acceptable fatigue durability.

7.3.3 Fatigue Design

The fatigue resistance of critical structural details (joints) can be expressed in terms of S-N curves. S-N curves are obtained from laboratory testing in which a specimen is subjected to cyclic loading until the occurrence of final fracture.

The spectral method is the most important fatigue design by analysis tool. The Weibull method is a simplified fatigue analysis tool. These methods will be detailed in Part III of this book.

Fatigue durability is a life-cycle problem. The fatigue durability can only be achieved if:

- Minimize stress-strain raisers (stress concentrations) and cyclic straining-stressing through good engineering of the structural system and its details. This requires a high level of engineering quality assurance (QA) at the concept-development-design stage.

- Minimize flaws (misalignments, poor materials, porosity-voids, etc.) through good, practical material and fabrication specifications and practices. This requires a high level of QA during the development of plans and specifications and during construction (involving material selection, fabrication, transportation, and installation). Furthermore, a similar QA program is required during operations to properly maintain the system.

- Minimize degradation at the local element by selecting good materials, fabrication practices, and engineering designs (e.g. crack stoppers, damage localizers, and repairable elements). This requires recognition that when fatigue degradation occurs, all reasonable precautions are taken to restrict its development and effects. Note QA plays an essential role, particularly during operations to disclose the presence of fatigue degradation (early warning).

- Minimize degradation at system level so that when local fatigue degradation occurs, there are no significant effects on the system's ability to perform satisfactorily. Here good fatigue design requires system robustness (redundancy, ductility, capacity) and system QA. Inspections and monitoring to disclose global system degradation are another strategy to minimize potential fatigue effects.

Cyclic strains, material characteristics, engineering design, specifications, and life-cycle QA (inspections, monitoring) are all parts of the fatigue equation. This is the engineering equation of "fail safe design"--fatigue may occur, but the structure can continue to function until the fatigue symptoms are detected and repairs are made.

The alternative is "safe life design" -- no significant degradation will occur and no repairs will be necessary. Safe life designs are difficult to realize in many long-life marine structures or elements of these structures. This is because of the very large uncertainties that pervade in fatigue design and analysis. Safe life design has been the traditional approach used in fatigue design for most ocean systems. The problems that have been experienced with fatigue cracking in marine structures and the extreme difficulties associated with inspections of all types of marine structures, ensure that large factors of safety are needed to truly accomplish safe life designs. For this reason, fail-safe design must be used whenever possible. Because of the extreme difficulties associated with inspections of marine structures and the high likelihood of undetected fatigue damages, it is not normally reasonable to expect that inspections will provide the backup or defenses needed to assure fatigue durability.

7.4   References

1.   NTS (1998), "NORSOK N-004, Design of Steel Structures", Norwegian Technology Standards Institution, (available from: www.nts.no/norsok).

2.   API (2001), "API RP 2A WSD, Recommended Practice for Planning, Designing and Constructing Fixed Offshore Platforms - Working Stress Design", American Petroleum Institute, Latest Edition.

3.   API (1993), "API RP 2A LRFD – Recommended Practice for Planning, Designing and Constructing Fixed Offshore Platforms – Load and Resistance Factor design, First Edition. 1993.

4.   API (2001), "API RP 2FPS, Recommended Practice for Planning, Designing and Constructing Floating Production Systems", First Edition.

5.   API (1997), "API RP 2T – Recommended Practice for Planning, Designing and Constructing Tension Leg Platforms", Second Edition.

6.   ISO Codes for Design of Offshore Structures (being drafted).

Part II: Ultimate Strength

This Page Intentionally Left Blank

Part II

Ultimate Strength

Chapter 8   Buckling/Collapse of Columns and Beam-Columns

8.1   Buckling Behavior and Ultimate Strength of Columns

This Chapter does not intend to repeat the equations and concept that may be found from exiting books on buckling and ultimate strength, e.g. (Timoshenko, 1961 and Galambos, 2000). Instead, some unique formulation and practical engineering applications will be addressed.

8.1.1   Buckling Behavior

For a column subjected to an axial force, the deflection produced by the axial force will be substantially amplified by the initial imperfections.
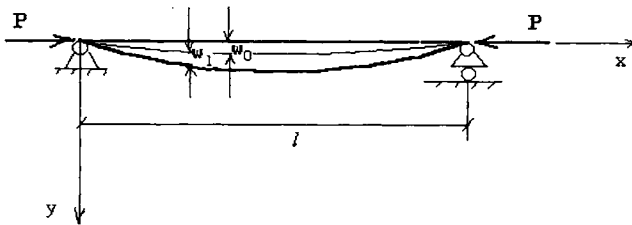
Figure 8.1   Coordinate System and Displacements of a Beam-Column with Sinusoidal Imperfections

Let's consider the case in which the initial shape of the axis of the column is given by the following equation, see Figure 8.1:

$$w_0 = w_{0\,max}\, sin\frac{\pi x}{l} \tag{8.1}$$

Initially, the axis of the beam-column has the form of a sine curve with a maximum value of $w_{0\,max}$ in the middle. If this column is under the action of a longitudinal compressive force P, an additional deflection w_1 will be produced and the final form of the deflection curve is:

$$w = w_0 + w_1 \tag{8.2}$$

The bending moment at any point along the column axis is:

$$M = P(w_0 + w_1) \tag{8.3}$$

Then the deflection w_1 due to the initial deformation is determined from the differential equation:

$$EI\frac{d^2 w_1}{dx^2} = -P(w_0 + w_1)$$

(8.4)

Substituting Eq. (8.1) into Eq. (8.4), we may obtain:

$$\frac{d^2 w_1}{dx^2} + k^2 w_1 = -k^2 w_{0max} \, sin\frac{\pi x}{l}$$

(8.5)

where,

$$k^2 = \frac{P}{EI}$$

The general solution of Eq. (8.5) is:

$$w_1 = A \, sin \, kx + B \, cos \, kx + \frac{1}{\dfrac{\pi^2}{k^2 l^2} - 1} w_{0max} \, sin\frac{\pi x}{l}$$

(8.6)

To satisfy the boundary condition $(w_1 = 0$ for $x = 0$ and $x = l)$ for any value of k, A = B = 0. Also, by using the notation α for the ratio of the longitudinal force to its critical value:

$$\alpha = \frac{P}{P_E}$$

(8.7)

where,

$$P_E = \frac{\pi^2 EI}{l^2}$$

we obtain the following:

$$w_1 = \frac{\alpha}{1-\alpha} w_{0max} \, sin\frac{\pi x}{l}$$

(8.8)

The final form of the deflection curve is:

$$w = w_0 + w_1 = w_{0max} \, sin\frac{\pi x}{l} + \frac{\alpha}{1-\alpha} w_{0max} \, sin\frac{\pi x}{l} = \frac{w_{0max}}{1-\alpha} sin\frac{\pi x}{l}$$

(8.9)

This equation shows that the initial deflection w_{0max} at the middle of the column is magnified at the ratio $\dfrac{\alpha}{1-\alpha}$ by the action of the longitudinal compressive force. When the compressive force P approaches its critical value, α approaches 8.0, the deflection w increases infinitely. Substituting Eq. (8.9) into Eq. (8.3), we obtain:

$$M = \frac{w_{0max} P}{1-\alpha} sin\frac{\pi x}{l} = \frac{w_{0max} P}{1-\dfrac{P}{P_E}} sin\frac{\pi x}{l}$$

(8.10)

From Eq. (8.10), the maximum bending moment at $x = \dfrac{l}{2}$ may be obtained as follows:

$$M_{MAX} = \frac{w_{0\,max}P}{1 - P/P_E} \tag{8.11}$$

The maximum stress in the cross section where $x = \dfrac{l}{2}$ is:

$$\sigma_{MAX} = \frac{P}{A} + \frac{M_{MAX}}{W} \tag{8.12}$$

Eq. (8.12) may be rewritten as follows:

$$\sigma_{MAX} = \frac{P}{A}\left[1 + \frac{w_{0\,max}c}{r^2}\frac{P_E}{P_E - P}\right] \tag{8.13}$$

where,

W	= Section modulus
A	= Area of the cross section
c	= Distance from the neutral axis to the extreme fiber
r	= Radius of gyration of the cross section
s	= Radius of the core: $s = \dfrac{W}{A}$

By taking the first term of the Fourier expansion

$$\frac{P_E}{P - P_E} = 1 + \frac{P}{P_E} + \left(\frac{P}{P_E}\right)^2 + \cdots\cdots$$

we obtain:

$$\frac{P_E}{P - P_E} = 1 + \frac{P}{P_E} \tag{8.14}$$

Combining Eq. (8.14) and Eq. (8.13), the maximum stress is given by:

$$\sigma_{MAX} = \frac{P}{A}\left[\left(1 + \frac{w_{0\,max}}{s}\right) + \frac{w_{0\,max}}{s}\frac{P}{P_E}\right] \tag{8.15}$$

8.1.2 Perry-Robertson Formula

A simple method to derive the ultimate strength of a column is to equate σ_{MAX} in Eq. (8.12) to yield stress σ_Y:

$$\frac{P_{ULT}}{A} + \frac{1}{W}\frac{w_{0\,max}P_{ULT}}{1 - P_{ULT}/P_E} = \sigma_Y \tag{8.16}$$

The above equation may be written as:

$$\sigma_{ULT}^2 - \left[\sigma_y + \left(1 + \frac{w_{0max}A}{W}\right)\sigma_E\right]\sigma_{ULT} + \sigma_E\sigma_Y = 0 \tag{8.17}$$

where,

$$\sigma_E = \frac{P_E}{A} \text{ and } \sigma_{ULT} = \frac{P_{ULT}}{A}$$

Its solution is called the Perry-Robertson Formula and may be expressed as:

$$\frac{\sigma_{ULT}}{\sigma_Y} = \frac{1 + \eta + \gamma - \sqrt{(1 + \eta + \gamma)^2 - 4\gamma}}{2\gamma} \tag{8.18}$$

where,

$$\eta = \frac{w_{0max}A}{W} \qquad \text{and} \qquad \gamma = \frac{\sigma_Y}{\sigma_E}$$

In Perry-Robertson formula, the effect of initial deflection is explicitly included. Comparison with more precise solutions such as finite element results demonstrates that the formula is accurate when the initial deflection is at the range of fabrication tolerance. When the initial deflection is due to in-service damages, which may be up to 1 per cent of the column length, the formula may under-estimate ultimate strength. The formula may be extended to account for the effect of residual stress explicitly. Perry-Robertson Formula has been frequently used in European steel structure codes.

8.1.3   Johnson-Ostenfeld Formula

The effect of plasticity may be accounted for by correcting the Euler buckling stress using the Johnson-Ostenfeld approach (see Galambos, 2000), Figure 8.2:

$$\sigma_{ULT} = \sigma_E \qquad\qquad \text{for } \sigma_E/\sigma_Y \le 0.5 \tag{8.19}$$

$$\sigma_{ULT} = \sigma_Y\left(1 - \frac{1}{4\sigma_E/\sigma_Y}\right) \qquad \text{for } \sigma_E/\sigma_Y \ge 0.5 \tag{8.20}$$
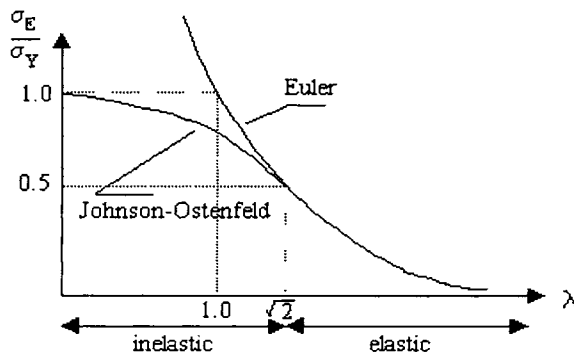
Figure 8.2   Johnson-Ostenfeld Approach Curve

The Johnson-Ostenfeld approach was recommended in the first edition of the book "Guide to Stability Design Criteria for Metal Structures" in 1960 and has been adopted in many North American structural design codes in which a moderate amount of imperfection has been implicitly accounted for. The Johnson-Ostenfeld formula was actually an empirical equation derived from column tests in the 1950s. It has since then been applied to many kinds of structural components and loads, see Part 2 Chapters 10 and 11 of this book.

8.2   Buckling Behavior and Ultimate Strength of Beam-Columns

8.2.1   Beam-Column with Eccentric Load
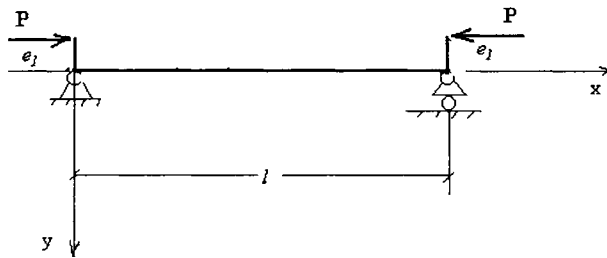
Figure 8.3   Beam-Column Applied Eccentrical Load

Consider a beam-column with an eccentricity e_1 at each end, see Figure 8.3. The equilibrium equation may be written as:

$$EI\frac{d^2w}{dx^2} + P(w + e_1) = 0 \tag{8.21}$$

The general solution of Eq. (8.21) is:

$$w = A\sin kx + b\cos kx - e_1 \tag{8.22}$$

Using boundary conditions

$$w = 0 \qquad at \qquad x = \pm\frac{l}{2}$$

$$EI\frac{d^2w}{dx^2} = -Pe_1 \qquad at \qquad x = \pm\frac{l}{2}$$

the integral constant may be obtained and the solution of Eq. (8.21) is:

$$w = e_1\left(\sec\frac{kl}{2}\cos kx - 1\right) \tag{8.23}$$

The maximum deflection at the middle of the beam-column is given by:

$$w_{MAX} = e_1\sec\frac{kl}{2} \tag{8.24}$$

The maximum moment and stress at the middle of the beam-column are expressed as follows:

$$M_{MAX} = Pe_1 \frac{1}{\cos \dfrac{kl}{2}}$$

(8.25)

$$\sigma_{MAX} = \frac{P}{A} + \frac{Pw_{MAX}}{I} = \frac{P}{A}\left(1 + \frac{e_1 A}{W}\sec\frac{kl}{2}\right)$$

(8.26)

Eq. (8.26) is called the secant formula. Taking the first two terms of the formula expansion:

$$\sec\frac{\pi}{2}\sqrt{\frac{P}{Pe}} \approx 1 + \frac{\pi^2}{8}\frac{P}{P_E}$$

(8.27)

and substituting Eq. (8.27) into Eq. (8.28), we obtain:

$$\sigma_{MAX} = \frac{P}{A}\left[\left(1 + \frac{e_1}{s}\right) + \frac{\pi^2}{8}\frac{e_1}{s}\frac{P}{P_E}\right]$$

(8.28)

8.2.2   Beam-Column with Initial Deflection and Eccentric Load

The deflection for a beam-column in Figure 8.4 may be obtained easily by superposition of Eq. (8.9) and Eq. (8.23), the total deflection is:

$$w = \frac{w_{0max}}{1-\alpha}\sin\frac{\pi x}{l} + \frac{e_1}{\cos\dfrac{kl}{2}}\left[\cos\left(\frac{kl}{2} - kx\right) - \cos\frac{kl}{2}\right]$$

(8.29)

The maximum deflection occurs at the center of the beam-column:

$$w_{MAX} = w\Big|_{x=\frac{l}{2}} = \frac{w_{0max}}{1-\alpha} + e_1\left(\sec\frac{kl}{2} - 1\right)$$

(8.30)

The bending moment at any section x of the beam-column is:

$$M = P(e_1 + w)$$

$$= P\left[\frac{w_{0max}}{1-\alpha}\sin\frac{\pi x}{l} + \frac{e_1}{\cos\dfrac{kl}{2}}\cos\left(\frac{kl}{2} - kx\right)\right]$$

(8.31)

and the maximum moment at the center of the beam-column is:

$$M_{MAX} = P\left(\frac{w_{0max}}{1 - \dfrac{P}{P_E}} + \frac{e_1}{\cos\dfrac{kl}{2}}\right)$$

(8.32)

From Eq. (8.15) and Eq. (8.28), the maximum stress at the center of the beam-column is:

$$\sigma_{MAX} = \frac{P}{A}\left[\left(1 + \frac{w_{0max} + e_1}{s}\right) + \frac{(w_{0max} + 1.234e_1)}{s}\frac{P}{P_E}\right]$$

(8.33)
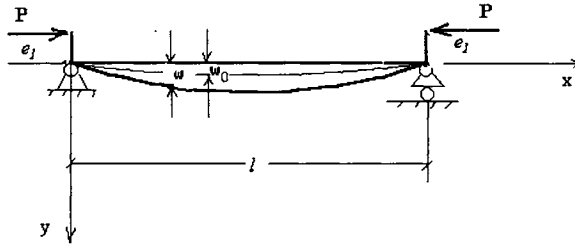
Figure 8.4   An Initially Curved Beam-Column Carrying Eccentrically Applied Loads

8.2.3   Ultimate Strength of Beam-Columns

For practical design, a linear interaction for the ultimate strength of a beam-column under combined axial force and bending is often expressed as:

$$\frac{P}{P_{ULT}} + \frac{M_{MAX}}{M_{ULT}} \leq 1 \tag{8.34}$$

where P_{ULT} and M_{ULT} are the ultimate strength of the beam-column under a single load respectively. Based on Eq. (8.34), the maximum moment in a beam-column under combined axial forces and symmetric bending moments M_0, is given by:

$$M_{MAX} = \frac{M_O}{\cos \frac{\pi}{2}\sqrt{\frac{P}{P_E}}} \approx \frac{M_O}{1 - \frac{P}{P_E}} \tag{8.35}$$

Then, the ultimate strength interaction equation may be expressed as:

$$\frac{P}{P_{ULT}} + \frac{M_O}{\left(1 - \frac{P}{P_{ULT}}\right)M_{ULT}} \leq 1 \tag{8.36}$$

Determining the exact location of the maximum bending moment for beam-columns under non-symmetric bending moments is not straightforward. Instead, M_0 is substituted by an equivalent moment, $M_{EQ} = C_M M_A$.

$$\frac{P}{P_{ULT}} + \frac{C_M M_A}{\left(1 - \frac{P}{P_E}\right)M_{ULT}} \leq 1 \tag{8.37}$$

where (Galambos, 2000)

$$C_M = 0.6 - 0.4\frac{M_B}{M_A} \geq 0.4 \tag{8.38}$$

where M_A and M_B are end moments.

For beam-columns under combined external pressure, compression, and bending moments, the ultimate strength interaction equation may be expressed as:

$$\frac{P}{P_{UQ}} + \frac{C_M M_A}{M_{PQ}\left(1 - P/P_E\right)} = 1 \tag{8.39}$$

where the ultimate axial strength P_{UQ} and the plastic moment capacity M_{PQ} (considering the effects of hydrostatic pressure) are used to replace the parameters in Eq.(8.37) in which the effect of hydrostatic pressure has not been accounted for in calculating P_{ULT} and M_{ULT}.

8.2.4   Alternative Ultimate Strength Equation – Initial Yielding

For a beam-column with initial deflection and eccentric load, as discussed in Section 8.2.2, an ultimate strength equation may be derived by using an initial yielding condition:

$$\sigma_{max} = \sigma_Y \tag{8.40}$$

where, σ_{MAX} is given by Eq. (8.31). Hughes (1988) extended Perry-Robertson Formula to beam-columns under combined axial compression and lateral pressure as follows:

$$\frac{\sigma_{ULT}}{\sigma_Y} = \frac{1}{2\gamma}\left[\left(1 + \eta + \gamma(1-\mu)\right) - \sqrt{\left(1 + \eta + \gamma(1-\mu)\right)^2 - 4\gamma(1-\mu)}\right] \tag{8.41}$$

where

$$\mu = \frac{M_{q\,max}}{\sigma_Y W} \qquad \text{and} \qquad \eta = \frac{\left(w_{o\,max} + w_{q\,max}\right)A}{W} \tag{8.42}$$

In Eq.(8.42), The maximum moment and lateral deflection due to lateral pressure may be obtained as follows,

$$M_{q\,max} = \frac{ql^2}{8} \qquad \text{and} \qquad w_{q\,max} = \frac{5ql^4}{384EI} \tag{8.43}$$

where q is the lateral pressure per unit length of the beam-column. It should be pointed out that the effect of boundary condition on beam-column strength under combined compression and lateral pressure is significant, and may be accounted for using the maximum moment and lateral deflection derived for the boundary conditions of concern. The general solution for elastic deflection of beam-columns under combined axial force, lateral pressure and end moments may be found in Part 2 Chapter 9 of this book.

8.3   Plastic Design of Beam-Columns

8.3.1   Plastic Bending of Beam Cross-section

When a beam cross-section is in fully plastic status due to pure bending, M_p, the plastic neutral axis shall separate the cross-sectional area equally into two parts. Assuming the distance from the plastic neutral axis to the geometrical centers of the upper part and lower part of the cross-section is y_U and y_L, we may derive an expression for M_p as below:

$$M_p = y_U \frac{A}{2}\sigma_Y + y_L \frac{A}{2}\sigma_Y = \frac{A}{2}\sigma_Y(y_U + y_L) \tag{8.44}$$

where A is sectional area and σ_y denotes yield strength of the material. If we define plastic modulus Z as

$$Z = M_p / \sigma_Y \tag{8.45}$$

Substituting Eq.(8.44) into Eq.(8.45), we may get,

$$Z = \frac{A}{2}(y_L + y_U) \tag{8.46}$$

The initial yielding moment M_Y, may be defined using elastic sectional modulus W as.

$$M_Y = \sigma_Y W \tag{8.47}$$

It is then easy to get the ratio of fully plastic moment and initial yielding moment as

$$f = M_P \Big/ M_Y \quad = \quad Z \Big/ W \tag{8.48}$$

Some of the sectional modules for typical cross-sections are given in the following.

Rectangular Cross-Section

$$Z = \frac{A}{2}(y_L + y_U) = \frac{bh^2}{4} \tag{8.49}$$

$$W = \frac{bh^2}{6} \tag{8.50}$$

$$f = \frac{Z}{W} = 1.5 \tag{8.51}$$

Tubular Cross-Section (t<<d)

$$I = \frac{\pi}{8}d^3 t \tag{8.52}$$

$$W = \frac{\pi}{4}d^2 t \tag{8.53}$$

$$f = \frac{Z}{W} = 1.27 \tag{8.54}$$

I-Profile (t<<h)

$$Z = bth + \frac{sh^2}{4} \tag{8.55}$$

$$W = bth + \frac{bh^2}{6} \tag{8.56}$$

For some standard types of hot rolled I-profiles, the ratio of fully plastic moment and initial yielding moment lies in the range of 1.1-1.18.

8.3.2   Plastic Hinge Load

Let's consider a fully clamped beam under laterally uniform pressure p, the work done by external load p may be calculated as,

$$W_e = \int_0^l p\,dy = 2p\int_0^{l/2} \theta x\,dx = \frac{pl^2}{4}\theta \tag{8.57}$$

where l is the beam length and θ denotes the rotational angle at two ends where plastic hinges occurred. The work done by the plastic hinges at two ends and the center is

$$W_i = M_p\theta(1+2+1) = 4M_p\theta \tag{8.58}$$

Equating the work done by lateral pressure and the internal work due to hinging, we may get,

$$M_p = \frac{pl^2}{16} \tag{8.59}$$

The collapse load $P = pl$ may be given as,

$$P = \frac{16}{l}M_p \tag{8.60}$$

For a beam under simply support in its two end, the plastic collapse load P may be derived as,

$$P = \frac{8}{l}M_p \tag{8.61}$$

In design codes, a mean value of the collapse load P for these two extreme conditions of boundary is used to determine the required plastic section module:

$$P = \frac{12}{l}M_p \tag{8.62}$$

The required section module Z is

$$W = \frac{Pl}{12\sigma_Y} \tag{8.63}$$

8.3.3   Plastic Interaction Under Combined Axial Force and Bending

This sub-section derives the plastic interaction equation for a beam-column due to the action of combined moment and axial load, for two most used types of cross-sections.

Rectangular Section

The rectangular section is characterized by its width b and height h. When it is in fully plastic status, the stress in its middle will form the reduced axial load N. The stress in upper and lower parts will contribute to the reduced plastic moment M. Assuming the height of the middle part that forms reduced axial load N is e, we may derive,

$$M = \frac{bh^2}{4}\sigma_Y - \frac{be^2}{4}\sigma_Y = \frac{bh^2}{4}\sigma_Y\left(1-\frac{e^2}{h^2}\right) = M_P\left(1-\frac{e^2}{h^2}\right) \tag{8.64}$$

$$N = be\sigma_Y = bh\frac{e}{h}\sigma_Y = N_P\frac{e}{h} \tag{8.65}$$

Combination of Eqs. (8.64) and (8.65) gives

$$\frac{M}{M_P} + \frac{N^2}{N_P^2} = 1 \tag{8.66}$$

The above equation is the interaction formula for a rectangular cross-section under combined axial load and bending.

Tubular Members

For tubular members, a fully plastic yielding condition for the cross-section may be obtained as:

$$\frac{M}{M_P} = cos\left(\frac{\pi}{2}\frac{P}{P_P}\right) \tag{8.67}$$

where,

$$P_P = \sigma_Y A$$

$$M_P = 2\pi R t \sigma_Y$$

where R is radius of the cross-section.

8.4 Examples

8.4.1 Example 8.1: Elastic Buckling of Columns with Alternative Boundary Conditions

Problem:

Derive elastic buckling strength equation based on the basic differential equation for initially straight columns:

$$\frac{d^4w}{dx^4} + k^2\frac{d^2w}{dx^2} = 0 \tag{8.68}$$

Solution:

The general solution of Eq. (8.68) is:

$$w = A\sin kx + B\cos kx + Cx + D \tag{8.69}$$

(1) Columns with Hinged Ends

The deflection and bending moments are zero at both ends:

$$w = \frac{d^2w}{dx^2} = 0 \quad at \ x = 0 \ and \ x = l \tag{8.70}$$

Applying the boundary conditions to the general solution, we may get:

$$B = C = D = 0 \quad \sin kl = 0 \tag{8.71}$$

Hence,

$$kl = n\pi \quad n = 1 \tag{8.72}$$

Eq.(8.72) yields to

$$P_E = \frac{\pi^2 EI}{l^2} \tag{8.73}$$

(2) Columns with Fixed Ends

The boundary condition is

$$w = \frac{dw}{dx} = 0 \quad at \ x = 0 \ and \ x = l \tag{8.74}$$

Applying the boundary conditions to the general solution, we may get:

$$A = C = 0, \quad B = -D, \quad \sin\frac{kl}{2} = 0 \tag{8.75}$$

Hence,

$$kl = 2n\pi, \quad n = 1 \tag{8.76}$$

Eq.(8.76) yields to

$$P_E = \frac{4\pi^2 EI}{l^2} \tag{8.77}$$

(3) Columns One End Fixed and the Other Free

The boundary condition at the fixed end is:

$$w = \frac{dw}{dx} = 0 \quad at \ x = 0 \tag{8.78}$$

At the free ends, the bending moment and shear force must be equal to zero:

$$\frac{d^2w}{dx^2} = 0 \quad at \ x = l \tag{8.79}$$

$$\frac{d^3w}{dx^3} + k^2\frac{dw}{dx} = 0 \quad at \ x = l \tag{8.80}$$

Applying the boundary conditions to the general solution, the elastic buckling force is then

$$P_E = \frac{\pi^2 EI}{4l^2} \tag{8.81}$$

(4) Columns with One End Fixed and the Other Pinned

Applying the boundary conditions to the general solution, it may be obtained that:

$$P_E = \frac{\pi^2 EI}{(0.7l)^2} \tag{8.82}$$

The results of this example may be summarized in Figure 8.5, showing the end-fixity coefficients and effective length for columns with various boundary conditions. A general buckling strength equation may be obtained as below:

$$P_E = \frac{\pi^2 cEI}{l^2} \tag{8.83}$$

where c is the end-fixity coefficient and

$$P_E = \frac{\pi^2 EI}{l'^2} \tag{8.84}$$

where l' is the effective length.
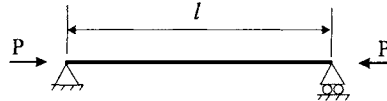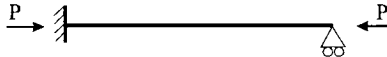
Boundary Conditions	End-Fixity Coefficient c	Effective Length l'
Pinned-Pinned:	1.0	l
Fixed-Guided:	4.0	$0.5l$
Fixed-Pinned:	2.05	$0.7l$
Fixed-Free	0.25	$2l$

Figure 8.5   End-Fixity Coefficients and Effective Length for Column Buckling with Various Boundary Conditions

8.4.2   Example 8.2: Two Types of Ultimate Strength: Buckling vs. Fracture

Problem:

Compare type different types of ultimate strength problems in a table: buckling vs. fracture.

Solution:

Normally ultimate strength analysis is inelastic buckling analysis of beam-columns, plates and shells with initial imperfections. However, it should be pointed out that final fracture is also part of the ultimate strength analysis. The assessment of final fracture has been mainly based on BPD6493 (or BS7910) in Europe and API 579 in the USA, see Chapter 21. In fact there is a similarity between buckling strength analysis and fracture strength analysis, as compared in the table below:

Table 8.1 Comparison of Buckling Strength Analysis and Fracture Strength Analysis

	Buckling Strength	Fracture Strength
Loads	Compression/torsion/shear force	Tensile loads
Imperfection	Geometrical imperfection and residual stress due to welding, impacts etc.	Defects due to fabrication and fatigue loads
Linear Solution	Elastic buckling	Linear fracture mechanics
Design criteria	Curve fitting of theoretical equations (Perry-Robertson, Johnson etc) to test results	Curve fitting of theoretical equations(interaction equation between ductile collapse and brittle fracture) to test results
Analysis Objectives	(1) Determine buckling load, (2) Determine allowable imperfection, (3) Determine dimensions such as stiffness, wall-thickness etc.	(1) Determine fracture load, (2) Determine allowable defect size, (3) Determine dimensions such as wall-thickness etc.

8.5   References

1.   Timoshenko, S. P. and Gere, J. (1961), *"Theory of Elastic Stability"*, McGraw Hill.

2.   Galambos, T.V. (2000), *"Guide to Stability Design Criteria for Metal Structures"*, 4th Edition, John Wiley & Sons.

3.   Hughes, O. (1988), *"Ship Structural Design, A Rationally Based, Computer Aided Optimization Approach"*, SNAME, (previously published by John Wiley & Sons, in 1983).

Part II

Ultimate Strength

Chapter 9   Buckling and Local Buckling of Tubular Members

9.1   Introduction

9.1.1   General

Equations for buckling strength of tubular members may be found from several books (such as Chen and Han, 1985) and offshore design codes (such as AISC (1978) and API RP 2A). This chapter will address the interaction between beam-column buckling mode and local (shell) buckling mode based on Yao *et al* (1986, 1988).

In the past 40 years, many kinds of offshore structures have been built and are in service for drilling and production in the oil and gas industry. Semi-submersible drilling units are one of the most commonly used offshore structures owing to their high operation rate and good performance in rough sea. However, this type of offshore structure has no self-navigating systems, and cannot escape from storms and rough sea conditions. Therefore, the structure must have enough strength to withstand extreme sea conditions (100 years storm). Consequently, no buckling and/or plastic collapse may take place under ordinary, rough sea conditions if the structural members are free of damages.

On the other hand, the bracing members of drilling units are often subjected to accidental loads such as minor supply boat collisions and dropped objects from decks. Furthermore, a fatigue crack may occur after a service period. Such a damage will not only cause a decrease in the load carrying capacity of the damaged member, but will also change the internal forces in undamaged members. Consequently, under rough sea conditions, buckling and/or plastic collapse may take place in the undamaged members as well as in the damaged members. This can cause a loss of integrity of the structure system. From this point of view, the ultimate strength limits and the load carrying capacity of tubular bracing members in semi-submersible drilling units should be assessed carefully.

Many studies have been performed during the last decade regarding the ultimate strength of tubular members. For example, Chen and Han (1985) investigated the influence of initial imperfections such as distortions and welding residual stresses on the ultimate strength of tubular members, and proposed a practical formula to evaluate the ultimate strength. Rashed (1980) and Ueda *et al* (1984) developed the Idealized Structural Unit (element) for a tubular member, which accurately simulates its actual behavior including overall buckling and plastification phenomena. They showed that accurate results are obtained within very short computation time when applying this model.

However, these results can only be applied to tubular members with small diameter to thickness ratios, e.g. D/t less than 30-50, which are typical bracing members in jackets and jack-ups. Local shell buckling need not be considered in these members. On the other hand,

bracing members in semi-submersible drilling units have large D/t ratios, e.g. between 70 and 130. For such tubular members, local buckling may take place before or after the ultimate strength is attained as Smith *et al.* (1979) and Bouwkamp (1975) observed in their experiments. Therefore, the assessment of the load carrying capacity of such bracing members, both ultimate strength and strength reduction due to local buckling, must be considered. However, a systematic study of this phenomenon has not been performed yet.

In this chapter, a series of experiments are first carried out using large scale tubular test specimens, which model a bracing member in an existing semi-submersible drilling unit. Axial compressive loads are applied with eccentricity. Small-scale tubular test specimens are prepared, of which D/t ratios are between 40 and 97, and tested under the same loading conditions. Then, based on experimental results, an analytical model is proposed to simulate the actual behavior of a tubular member considering the influence of local buckling. Furthermore, the Idealized Structural Unit is developed by incorporating this model. The validity and usefulness of the proposed model is demonstrated by comparing the calculated results with the present and previous experimental results.

9.1.2   Safety Factors for Offshore Strength Assessment

The basic safety factors in offshore structural design are defined for two cases:

-   Static loading: 1.67 for axial or bending stress. The static loads include operational gravity loading and weight of the vessel.
-   Combined static and environmental loads: 1.25 for axial or bending stress. The static loads are combined with relevant environmental loads including acceleration and heeling forces.

For members under axial tension or bending, the allowable stress is the yield stress divided by the factor of safety as defined in the above.

9.2   Experiments

9.2.1   Test Specimens

Dimensions of a typical bracing member in an existing semi-submersible drilling unit are shown in Table 9.1. The slenderness ratio is not so different from that of a bracing member in fixed type jackets or jack-up type drilling units.

Table 9.1   Dimensions of Existing Bracing Member and Test Specimen

	Length L (mm)	Outer Diameter D (mm)	Thickness T (mm)	D/t	L/d	R
Existing Bracing Member	27840	1800	14.5	124	15.5	631.3
Test Specimen	8000	508	6.4	78	15.7	177.4

$$r = \sqrt{I/A}, \quad I = \frac{\pi}{64}\left[D^4 - (D-2t)^4\right], \quad A = \frac{\pi}{4}\left[D^2 - (D-2t)^2\right]$$

Taking E and σ_y as 21,000 *kgf / mm*^{2} and 32 *kgf / mm*^{2}, respectively, the critical D/t is 73. If D/t is beyond the critical ratio, local buckling may occur before the plasticity of the cross-section. it is easily known that D/t of 124 for the existing bracing member is far above the critical value.

From this exercise, it may be concluded that local buckling takes place before the fully plastic condition is satisfied at the cross-section where internal forces are most severe. A welded tube on the market is selected as test specimens, whose collapse behavior is expected to be close to the above-mentioned bracing member. The dimensions of the test specimens are shown in Table 9.1. Their diameter is 508 mm, and their length is taken to be 8,000 mm so that their slenderness ratio will close to that of the existing bracing member. The scale factor is 1/3.5, and this specimen is referred to as a large scale test specimen. The D/t is 78, which is small compared to that of the existing one. However, it is still larger enough for local buckling to be a concern.

(a) Test specimen

(b) Detail at G
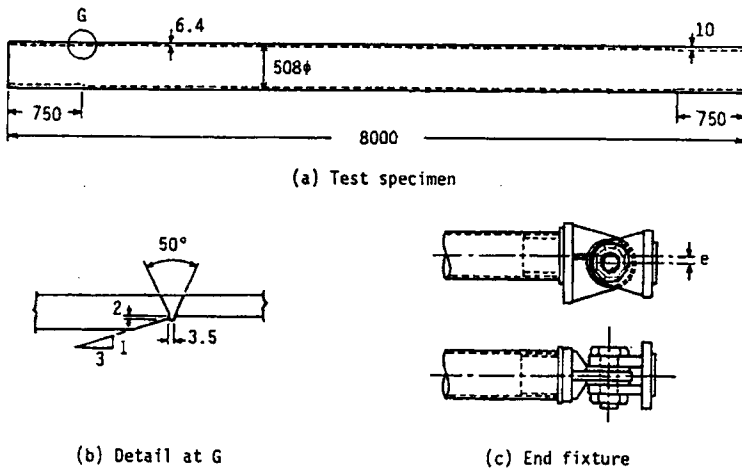
(c) End fixture

Figure 9.1   Large Scale Test Specimen and Its End Fixture

The large-scale test specimen is illustrated in Figure 9.1. The tube's wall thickness is 6.4 mm. However, within 750 mm from both ends, the thickness is increased to 10 mm to avoid the occurrence of local collapse near the ends.

Table 9.2   Dimensions and Test Results for Small Scale Test Specimens

Specimen Number	Outer Diameter D (mm)	Wall Thickness t (mm)	Length L (mm)	Initial Deflection a0 (mm)	Load Eccentricity e/D	Young's Modulus (kgf/mm)	0.2%Yield Stress (kgf/mm)	Ultimate Load (ton)	Buckling Mode
HA0	97.0	1.0	1,430	----	0	19,645	35.25	7.51	DENT
HA2	97.0	1.0	1,635	0.43	¼	19,645	35.25	5.75	DENT
HA3	97.0	1.0	895	0.13	1/16	19,645	35.25	9.78	DENT
HA4	97.0	1.0	605	0.25	1/16	19,645	35.25	10.08	DENT
HB1	97.4	1.2	1,635	0.10	1/32	19,616	37.50	9.90	DENT
HB2	97.4	1.2	1,430	0.61	1/16	19,616	37.50	9.10	DENT
HB3	97.4	1.2	1,430	1.02	1/8	19,616	37.50	7.95	DENT
HC1	98.2	1.6	1,430	0.44	1/32	19,160	37.00	13.76	DENT
HC2	98.2	1.6	1,430	0.64	1/16	19,160	37.00	11.90	DENT
HC3	98.2	1.6	1,430	1.40	1/8	19,160	37.00	9.99	COS
HD1	100.0	2.5	1,430	0.73	1/32	18,109	33.00	19.70	DENT
HD2	100.0	2.5	1,430	0.63	1/16	18,809	33.00	17.95	DENT
HD3	100.0	2.5	1,430	0.87	1/8	18,809	33.00	14.95	DENT
HD4	100.0	2.5	1,635	1.44	1/4	18,809	33.00	13.46	COS
HD5	100.0	2.5	895	0.35	1/32	18,809	33.00	26.85	COS
HD6	100.0	2.5	575	0.35	1/16	18,809	33.00	30.55	COS
BA1	97.0	1.0	650	----	BENDING	19,645	35.25	2.75	DENT
BB1	97.4	1.2	650	----	BENDING	19,616	37.50	3.09	DENT
BB2	97.4	1.2	650	----	BENDING	19,616	37.50	3.05	DENT
BC1	98.2	1.6	650	----	BENDING	19,610	37.00	4.68	DENT
BC2	98.2	1.6	650	----	BENDING	19,610	37.00	4.66	DENT
BD1	100.0	2.5	650	----	BENDING	18,809	33.00	7.84	DENT

Test specimens of alternative sizes are also tested. The inner diameter is kept as 95 mm, and the tube wall thickness varies as 1.0, 1.2, 1.6, and 2.5 mm. The D/t ratios of these test specimens then vary between 40 and 97, and the correspondence with bracing members in existing semi-submersible drilling units is not especially considered. The thickness near both ends is not increased. The dimensions of small-scale test specimens are shown in Table 9.2 along with material properties and experimental results.

9.2.2   Material Tests

The large-scale test specimens were fabricated by welding the circular that has been bent from flat plate. To avoid the effect of residual stress on the measured material properties, 4 pieces of tensile test specimens were cut from the side opposite to the weld line. From the tensile tests, the measured Young's module is E=21180 kgf/ mm^2 . The Poisson's ratio is v = 0.32. The measured yield stress (corresponding to 0.2% offset strain) is: σ_y = 34.55 kgf/ mm ^{2} . The nominal stress-strain relation from the material is shown in Figure 9.2. The small-scale test specimens consist of four different D/t ratios, namely series A. B, C and D. Due to the lack of

availability for the pipe of these sizes, the test specimens were fabricated by cold forming from pipe of 3.2 mm wall-thickness. Due to the Bauschinger's effect introduced in the cold fabrication process, the ultimate tensile stress is much higher than the ultimate compressive stress. Tensile test specimens were fabricated by cutting from the circular pipe along the longitudinal direction. The cross-section of the material test specimens was fabricated to rectangular cross-section, according to the industry standard for material tensile testing. In the 2 sides of the central cross-section, strain gauges were attached for the purpose of measuring the strain. The nominal stress-strain relations for the specimens of A, B, C and D series are shown in Figure 9.3 in solid lines. Due to the cold fabrication process, the ductility of the material was reduced. Tensile failure occurred when the strain was in the order of 6 – 14 %.
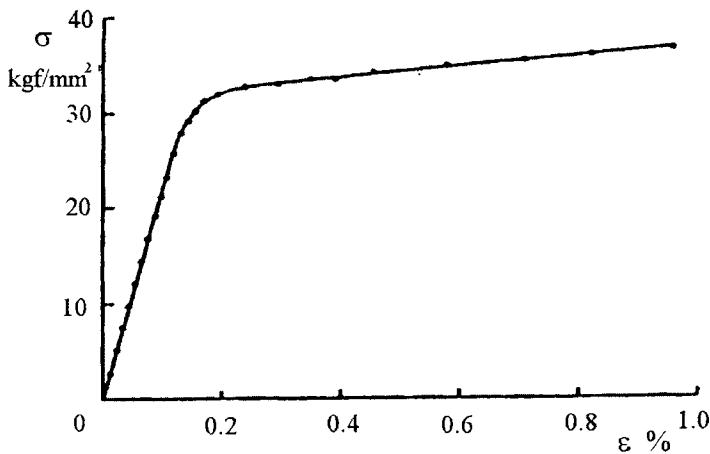
Figure 9.2   Tensile Stress-Strain Curve for Large Scale Test Specimens

The measured cross-section areas for the specimens, the measured Young's modules and yield stress are listed in Table 9.3. Two types yield stresses were defined: yield strength corresponding to 0.2 % offset plastic strain $\sigma_{0.2}$, and yield strength corresponding to 0.5 % total strain $\sigma_{0.5}$.

Table 9.3   Dimensions and Results of Material Tests for Small Scale Test Specimens

Specimen Number	Wall-Thickness t (mm)	D/t ratio (-)	Specimen Cross-Sectional Area A(m²)	Tensile Test Yield Stress $\sigma_{0.2}$ (kgf/mm²)	Tensile Test Yield Force $P_{0.2}$ (kgf)	Compressive Test Yield Stress $\sigma_{0.2}$ (kgf/mm²)	Compressive Test Yield Force $P_{0.2}$ (kgf)	Compressive Test Yield Stress $\sigma_{0.5}$ (kgf/mm²)	Compressive Test Yield Force $P_{0.5}$ (kgf)
A	1.0	97.0	301.59	45.00	13751.55	35.25	10631.05	40.00	12063.60
B	1.2	81.2	362.67	58.00	21034.86	37.50	13600.13	44.50	16138.82
C	1.6	61.4	485.56	54.23	26341.63	37.00	17965.72	42.75	20757.69
D	2.5	40.0	765.76	46.75	35799.28	33.00	25270.08	38.25	29290.32
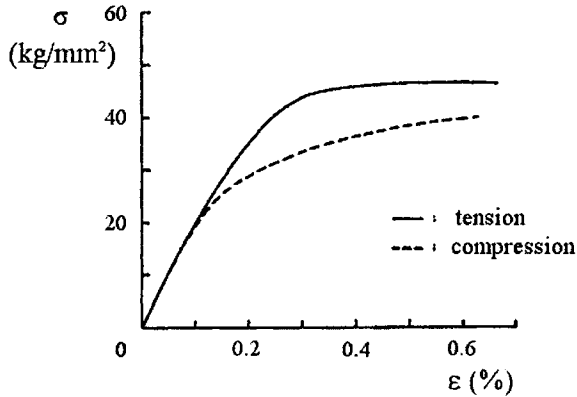
Figure 9.3 **(a) Stress-strain Curves for Small Scale Test Specimens, A Series**

The compressive material tests were conducted using the stub pipe. The length of the test specimen was selected such that column buckling would not be a concern. The selected specimen length is 300 mm for all of the test specimens. 4 pieces of bi-axial strain gauges were put on the central cross-sections of the test specimens. The nominal stress-strain relations are plotted in Figure 9.3 in dotted lines. Because shell mode buckling occurred in the upper or lower edges occurred, strain-strain relation was measured up to the strain level of 1 %. The obtained yield strength was given in Table 9.3.

Due to the tensile expansion applied in manufacturing the specimens along the longitudinal direction, significant Bauschinger's effect was observed. There is little strain hardening effect in the tensile side of the stress-strain relations. On the other hand, significant strain-hardening effect was observed for the compressive side. As shown in the stress-strain curves, there is a significant difference between the material properties in tensile side and in compressive side. This difference in material properties could be one of the main reasons for the difference between the test results and analytical solutions for the load-deflection curves and load-end shortening curves. Heat treatment should probably have been introduced to eliminate the differences in the material properties for tensile and compressive sides, and to reduce the Bauschinger's effect. However, due to the potential of buckling of the thin-walled pipe, such a heat treatment was not applied.
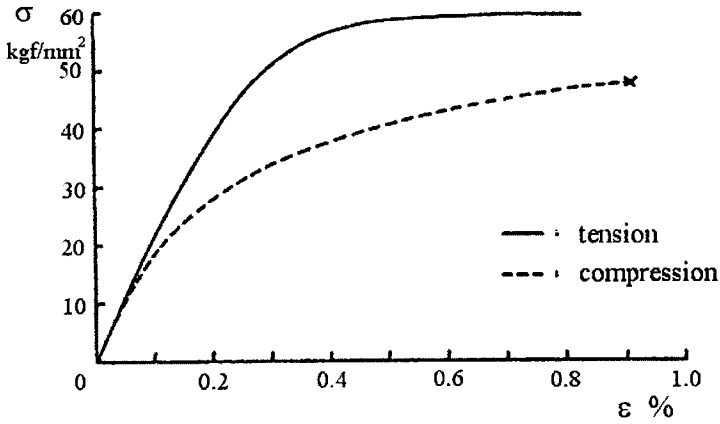
(b) B series
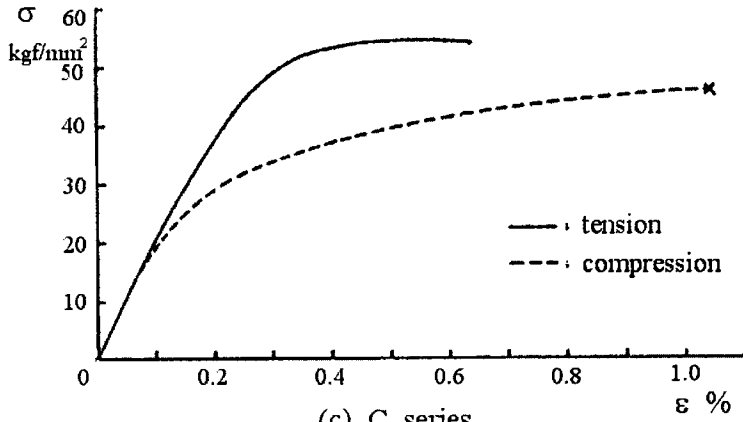
(c) C series
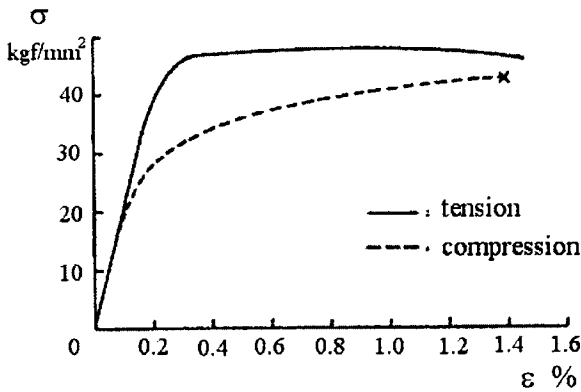
(d) D series

Figiure 9.3   Tensile Stress-Strain Curve for Large Scale Test Specimens (Continued)
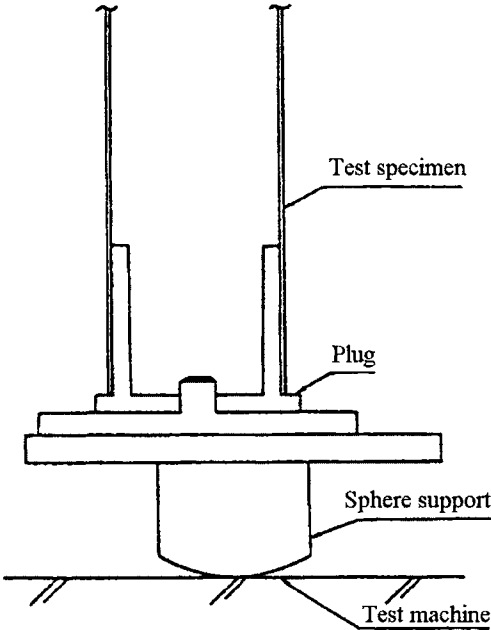
Figure 9.4   End Fixtures for Eccentric Axial Thrust of Small Scale Test Specimens
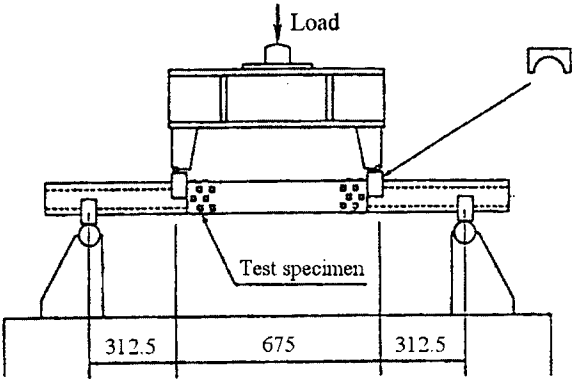
Figure 9.5   Apparatus for Pure Bending Test of Small Scale Test Specimen

9.2.3 Buckling Test Procedures

For large-scale test specimens, axial compressive loads are applied with eccentricity using large-scale model testing machines of 3,000 tons installed at Hiroshima University. Simply supported end conditions are simulated at both ends with pinned joints. Both ends of each test specimen are attached to loading heads through cylindrical plugs as illustrated in Figure 9.1 (c). The eccentricity of the axial load is taken to be 1/8, 1/4, and 3/8 times of the outer diameter. These eccentricities are obtained by changing the position of the plug relative to the loading heads. This testing machine is a horizontal type, and the test specimens are placed horizontally. Therefore, an initial deflection of 0.63 mm is produced due to the specimen's own weight.

For small-scale test specimens, two types of loads are applied, axial compressive loads with eccentricity and pure bending loads. Eccentric axial loads are applied through a plug and a spherical support as illustrated in Figure 9.4. The pure bending is applied using four point bending as illustrated in Figure 9.5. Rigid tubes are inserted into both ends of the specimen so that the specimen does not deform locally at the loading points. A test specimen is connected to rigid tubes with friction bolts.

Unloading and reloading are performed several times during the experiment especially after the occurrence of local buckling. The strain in axial and circumferential directions, lateral deflections, and load-line displacements, are measured during the experiment.

9.2.4 Test Results

Eccentric Axial Compression Tests Using Large Scale Specimens

Axial loads vs. lateral deflection relationships are plotted using solid lines as shown in Figure 9.7. In all cases, no significant deformation of cross-sections is observed until the ultimate strength is attained. After reaching the ultimate strength, the load decreases as lateral deflection increases, local buckling takes place near a mid-span point, and the load carrying capacity suddenly decreases. The local buckling mode in terms of cross-sectional deformation may be approximated by a cosine mode as illustrated in Figure 9.8 (a). The wavelength of this local buckling mode is almost a half circle in the circumferential direction and is very short in the axial direction. With a further increase of lateral deflection, local denting deformation takes place at the foot of the initial cosine-buckling wave as illustrated in Figure 9.8 (b).

The horizontally flattened part grows and folds toward the inside of the cross-section c-c'. At the same time, a similar phenomenon is observed at the cross-section a-a', but with two dents, A-B and A-C. The horizontally flattened part of the cross-section c-c' grows until it becomes nearly equal to a quarter circle, see B'-C' in Figure 9.8 (c). Then, two other dents, A'-B' and C'-D', begin to grow as illustrated in Figure 9.8 (c). At this stage, significant deformation is observed at the cross-section b-b'. A local cosine-buckling wave occurring in the area of maximum compressive strain is followed by the formation of dents at both sides of the wave. Such collapse mode is observed in all large-scale test specimens regardless of the magnitude of eccentricity. It should be noticed that the length of a fully developed buckling wave (B'-C' in Figure 9.8 (c)) is close to that of shell buckling under pure compression.

Eccentric Axial Compression Test Using Small Scale Specimens

The test facilities and instrumentation are illustrated in Figure 9.6.
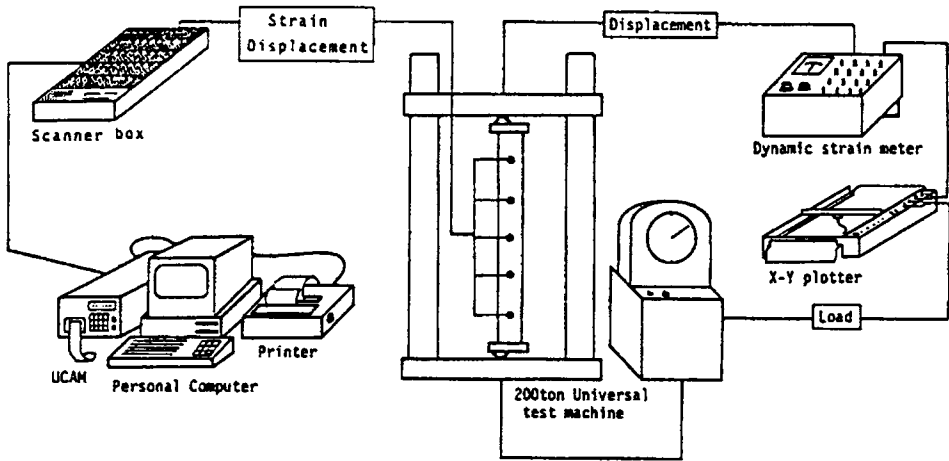
Figure 9.6   Instrumentation Diagram for Buckling/Collapse Tests

Axial loads vs. end shortening relationships are plotted in Figures. 9.9 (a), (b), (c), and (d). Unloading and reloading paths are omitted in these figures. These figures indicate that: As eccentricity increases, the ultimate strength decreases, and a larger displacement is produced before local buckling takes place.

The same tendency is observed as the length increases.

If the length and the D/t ratio are the same, the load-displacement path after local buckling, converges to a certain value.

In the case of large-scale test specimens, local buckling takes place in a cosine mode. However, it is only in three specimens that local buckling of a cosine mode occurred in small scale test specimens. In the other 13 specimens, local buckling takes place in a dent node. The local buckling of a dent type initializes dent growth as the lateral deflection increases until it becomes about the size of a quarter circle. Then, two dents are formed at the cross-section, b-b', adjacent to the initial dent, as illustrated in Figure 9.10 (b). With a further increase of lateral deflection, two other dents begin to grow at the cross-section, a-a', of the initial dent as shown in Figure 9.10 (c). It is not clear which mode of local buckling would take place. However, the buckling mode depends on the diameter to thickness ratio, the combination of axial forces and bending moments at the cross-section, and the material properties.
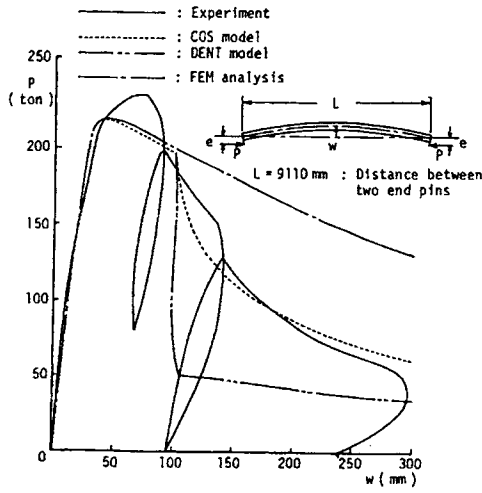
(a) e/D = 1/8
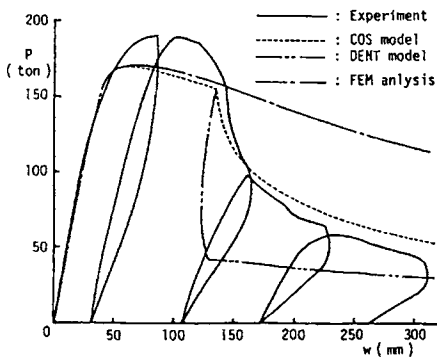
(b) e/D = 1/4
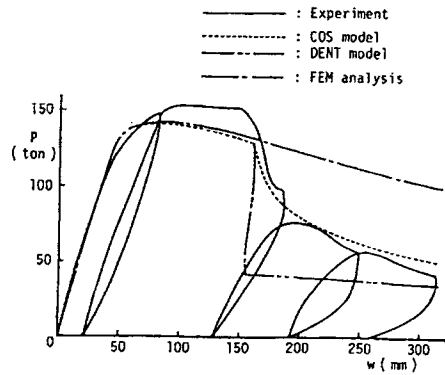
(c) e/D = 3/8

**Figure 9.7   Load-Lateral Deflection Curves of Large Scale Test
Specimens Subjected to Axial Thrust with Eccentricity**
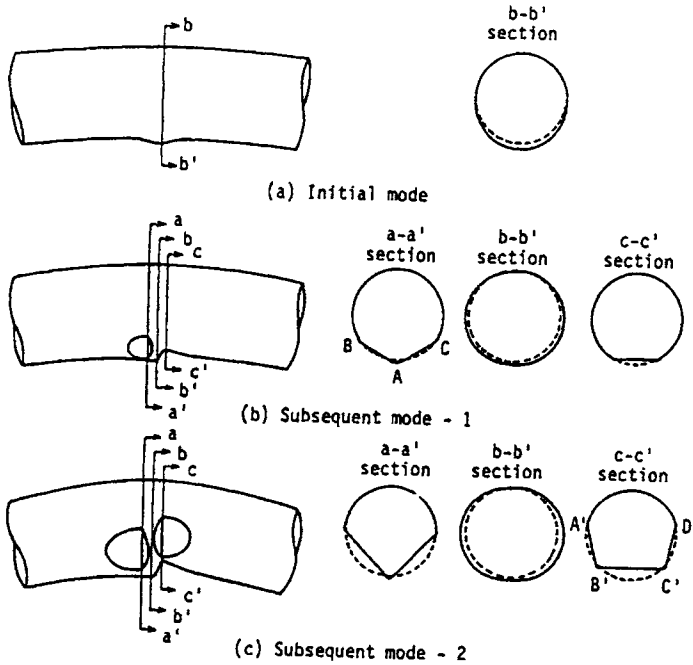
Figure 9.8   Local Buckling in Cosine Mode

Pure Bending Test for Small Scale Specimens

Loads vs. load-line displacement relationships are plotted in Figure 9.11. In the case of BD1 specimen, breaking of a specimen occurred from a bolt-hole near the end before local buckling took place. In all specimens, cross-sectional flattening is observed as the load increases. Furthermore, deformation of a ripple pattern with two or three half waves begins to grow near the ultimate strength. The ultimate strength seems to be attained by the cross-sectional flattening and the formation of ripples. In the case of thin-walled tubes, the bottom of one wave of the ripple suddenly changes to a dent near the ultimate strength, and the load carrying capacity decreases. Contrary to this, the ripple deformation grows after the ultimate strength is attained in the case of thick-walled specimens. Then, the ripple suddenly changes to a local dent.

It is not clear, whether the initiation of local buckling is due to the formation of a ripple pattern or the formation of a dent. However, much attention has to be paid to the formation of a dent, since this causes a sudden drop in the load carrying capacity.

The formation of new dents after the initial dent has formed is almost the same as in the case of eccentric axial compression.
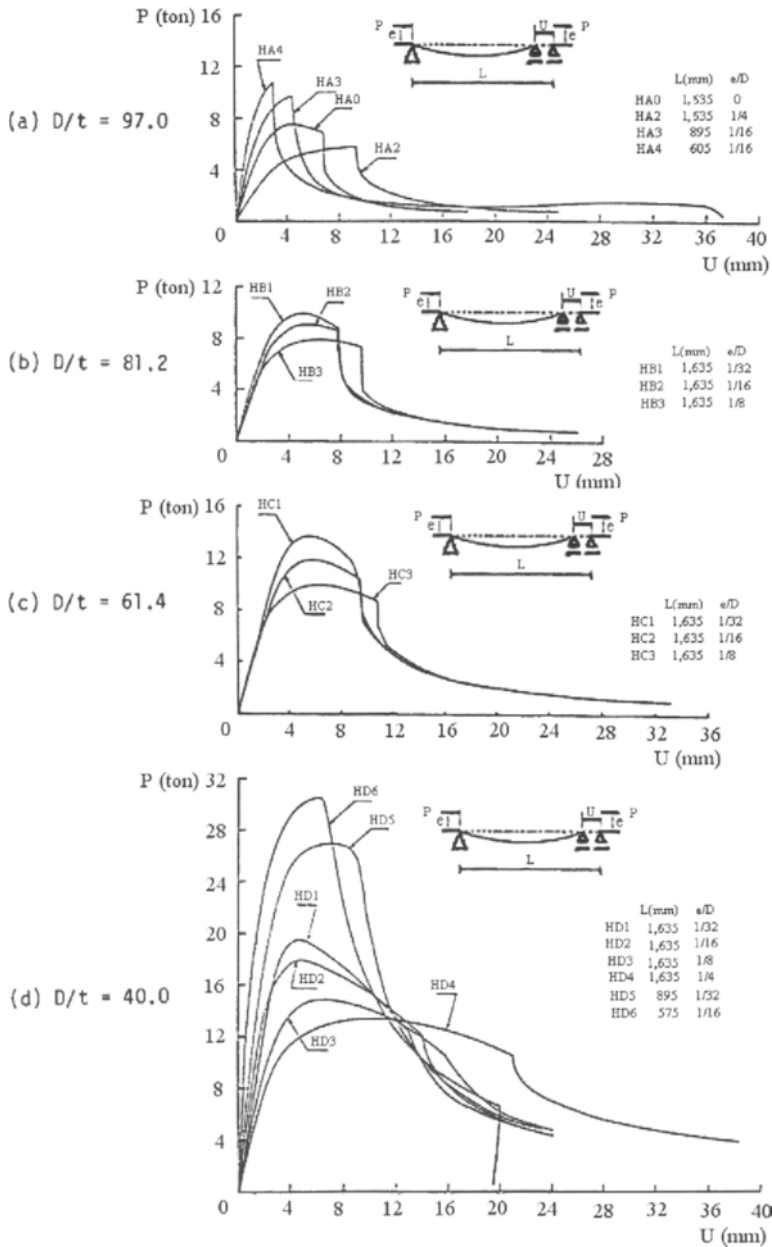
Figure 9.9 **Load-End Shortening Curves for Small Scale Test Specimens Subjected to Axial Thrust With Eccentricity**
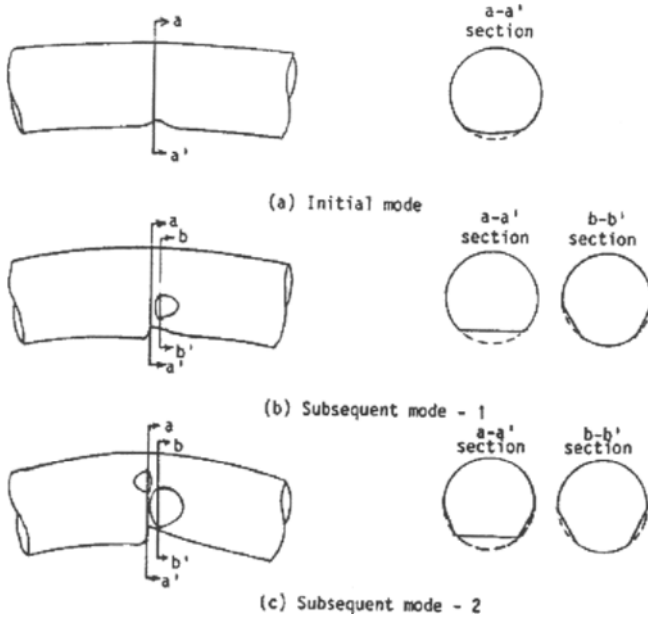
Figure 9.10   Local Buckling in Dent Mode
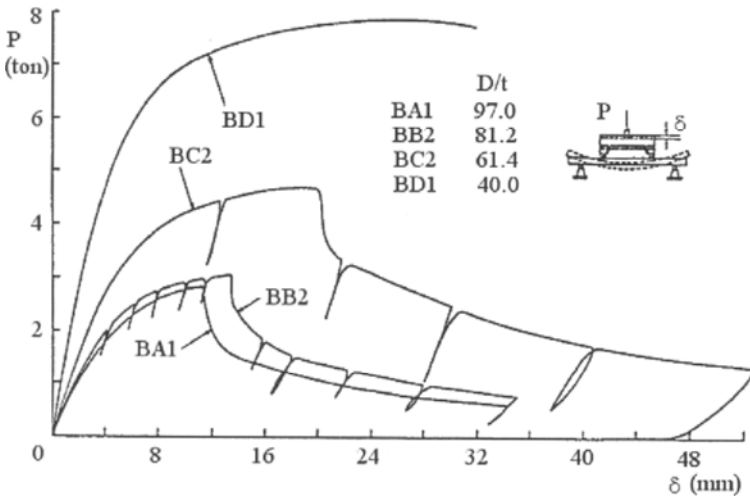
Figure 9.11   Load vs. Load-Line Curves for Small Scale Test Specimens
               Subjected to Pure Bending Loads

9.3 Theory of Analysis

9.3.1 Simplified Elasto-Plastic Large Deflection Analysis

In this section, an analytical model, which simulates the elasto-plastic large deflection behavior of a tubular member, is proposed taking into account the influence of local buckling. The material is assumed elastic-perfectly plastic. It is also assumed that local buckling takes place after plastification occurs.

Pre-Analysis of Local Buckling

A tubular member is assumed to be accompanied by the initial deflection of a sinusoidal form:

$$w_0 = a_0 \, sin \frac{\pi x}{l} \tag{9.1}$$

where, l = Length of a tubular member

   a_0 = Magnitude of initial deflection

The equilibrium equation of a beam-column may be written as:

$$EI \frac{d^4}{dx^4}(w - w_0) + P \frac{d^2 w}{dx^2} = q \tag{9.2}$$

where, w = Total deflection P = Axial force (positive in compressive)

   E = Young's modulus I = Moment of inertia of a cross-section

The general solution of Eq. (9.2) is expressed as follows:

$$w = \alpha_1 \cos kx + \alpha_2 \sin kx + \alpha_3 x + \alpha_4 + Q' \sin \pi x/l + f(q) \tag{9.3}$$

where,

$$k = \sqrt{P/EI} \tag{9.4}$$

$$Q' = a_0 P_E / (P_E - P) \tag{9.5}$$
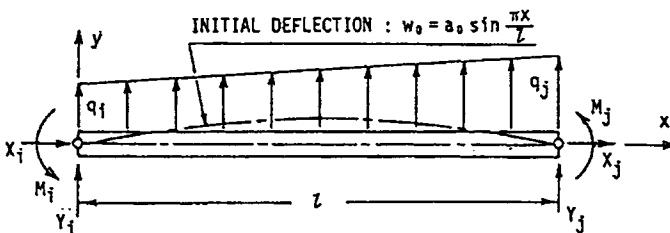
Figure 9.12   Beam-Column Member Under External Loads

$$P_E = \pi^2 \, EI/l^2 \tag{9.6}$$

and f(q) represents the deflection due to lateral load q.

It is assumed that the member is subjected to an axial compression, end moments, and linearly distributed lateral loads as illustrated in Figure 9.12. If both ends are simply supported, Eq. (9.3) reduces to:

$$w_e = \frac{1}{P}\left[\left(M_i + \frac{q_i}{k^2}\right)\left\{\frac{\sin k(l-x)}{\sin kl} + \frac{l-x}{l}\right\} - \left(M_j + \frac{q_j}{k^2}\right)\left(\frac{\sin kx}{\sin kl} + \frac{x}{l}\right)\right]$$
$$+ \frac{a_0 P}{P_E - P} + \frac{1}{P}\left\{-\left[\frac{q_j}{6} + \frac{q_i}{3}\right]lx + \frac{1}{2}q_i x^2 + \frac{1}{6l}(q_j - q_i)x^3\right\} \tag{9.7}$$
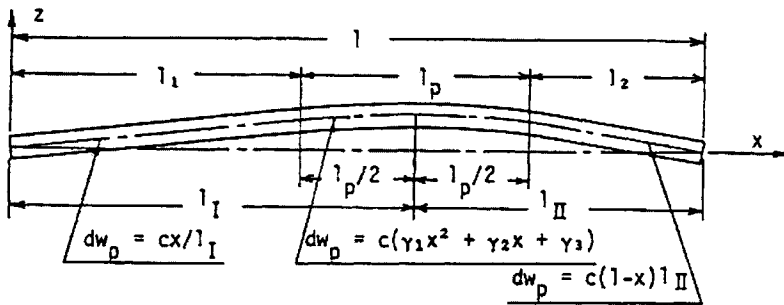
Figure 9.13   Plastic Component of Lateral Deflection

The suffix e in Eq. (9.7) implies the elastic range, and Eq. (9.7) gives the relationship between axial force and lateral deflection until plastification takes place. Using this deflection, the mean compressive axial strain is expressed as follows:

$$\varepsilon = \frac{P}{EA} + \frac{1}{2l}\int_0^l\left[\left(\frac{dw_e}{dx}\right)^2 - \left(\frac{dw_0}{dx}\right)^2\right]dx \tag{9.8}$$

In the inelastic region, the flexural rigidity is not uniform along the length of a member. For this case, the plastic component of deflection w_p is introduced. Then, the total deflection is expressed as the sum of elastic and the plastic components as:

$$w = w_e + w_p \tag{9.9}$$

Here, w_p is evaluated as the cumulative value of the increments of plastic components of deflection which are assumed in the following forms

I $0 \le x \langle l_1$ $dw_p = cx/l_1$ $\tag{9.10}$

II $l_1 \le x \langle l_1 + l_p$ $dw_p = c(\gamma_1 x^2 + \gamma_2 x + \gamma_3)$ $\tag{9.11}$

III $l_1 + l_p \le x \le l$ $dw_p = c(l - x)/l_{11}$ $\tag{9.12}$

where,

$$\gamma_1 = -l/2l_1 l_{11} l_p \tag{9.13}$$

$$\gamma_2 = \left(l_{11}l_p + ll_1\right)/l_1\,l_{11}l_p \tag{9.14}$$

$$\gamma_3 = -l_1^{\,2}\,l/2l_1l_{11}\,l_p \tag{9.15}$$

The deflection mode represented by Eqs. (9.10) thru (9.12) is shown in Figure 9.13. The increment of this plastic deflection component produces a constant plastic curvature in the region, $l_p\left(l_1 \le x \le l_1 + l_p\right)$. The procedure used to estimate l_p will be discussed later.

The inelastic analysis is performed in an incremental form. w_p in Eq.(9.9) at the n-th step of this analysis, is expressed as:

$$w_p(n) = w_p(n-1) + dw_p(n) \tag{9.16}$$

where $w_p(n-1)$ is the cumulative value of the increments of plastic deflection until the (n-1)-th step, and $dw_p(n)$ is the increment at the n-th step.

Two possible stress distributions may exist at a cross-section after initial yielding, depending on the magnitude of the strain at the tension side of the bending; see Figure 9.14. For these stress distributions, the axial force and the bending moment are evaluated as:

$$p = 2\int_0^{\alpha_1} \sigma_y Rtd\theta + 2\int_{\alpha_1}^{\pi-\alpha_2} \frac{\eta + R\cos\theta}{\eta + R\cos\alpha_1}\sigma_y Rtd\theta - 2\int_{\pi-\alpha_2}^{\pi} \sigma_y Rtd\theta \tag{9.17}$$

$$M = 2\int_0^{\alpha_1} \sigma_y R^2 t\cos\theta d\theta + 2\int_{\alpha_1}^{\pi-\alpha_2} \frac{\eta + \cos\theta}{\eta + \cos\alpha_1}\sigma_y R^2 t\cos\theta d\theta - 2\int_{\pi-\alpha_2}^{\pi} \sigma_y R^2 t\cos\theta d\theta \tag{9.18}$$

where σ_y is the yield stress. For Case A stress distribution α_2 is taken as 0.

The equilibrium condition for the bending moment gives the following equation.

$$P\left(w_e + w_p + e_0\right) + Q = M \tag{9.19}$$

where ,

$$e_0 = e_i + l_1\left(e_i - e_j\right)/l, \quad e_i = M_i/P, \quad e_j = -M_j/P \tag{9.20}$$

and Q is the bending moment due to distributed lateral loads, q.

On the other hand, the curvature at a cross-section may be expressed as:

$$\frac{1}{\rho} = -\frac{\sigma_y}{E(\eta + R\cos\alpha_1)} = \frac{d^2}{dx^2}\left(w_e + w_p - w_0\right) \tag{9.21}$$

For case A stress distribution, Eqs. (9.17), (9.19), and (9.21) reduce to the following equations using Eqs. (9.7), (9.10), (9.11), and (9.12):

$$P(\eta + f_1) = f_2 + c_1\eta \tag{9.22}$$

$$P(w + e_0) = f_3 + (f_4 + f_5\eta)/(\eta + f_1) + f_6 \tag{9.23}$$

$$c_2/(\eta + f_1) = \kappa \tag{9.24}$$
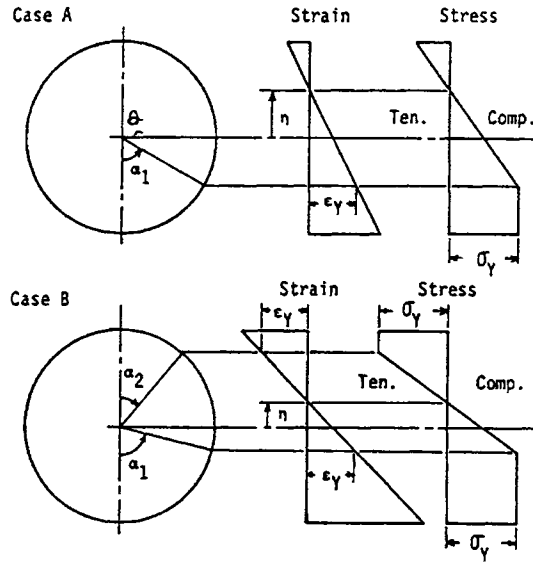
Figure 9.14   Elasto-Plastic Stress Distribution Free from Local Buckling

where,

$$f_1 = R \cos \alpha_1$$

$$f_2 = 2\sigma_y R^2 t \left(\alpha_1 \cos \alpha_1 - \sin \alpha_1 \right)$$

$$f_3 = 2\sigma_y R^2 t \sin \alpha_1$$

$$f_4 = \sigma_y R^3 t \left(\pi - \alpha_1 - \sin \alpha_1 \cos \alpha_1 \right) \tag{9.25}$$

$$f_5 = -2\sigma_y R^2 t \sin \alpha_1$$

$$f_6 = q_j \left(l_1^3 / l - l l_1 \right) / 6 - q_i \left(l_1^3 / 6l - l_1^2 / 2 + l l_1 / 3 \right)$$

$$c_1 = 2\pi \sigma_y R t$$

$$c_2 = l^2 \sigma_y / \pi^2 E \tag{9.26}$$

$$w = \left(w_e + w_p \right) \big|_{x=l_1} \tag{9.27}$$

$$\kappa = \frac{d^2 \left(w_e + w_p - w_0 \right)}{dx^2} \bigg|_{x=l_1}$$

Similarly, the following equations are obtained for the case B stress distribution:

$$P(\eta + f_1) = f_2 + h_1 + (c_2 - h_2)\eta \tag{9.28}$$

$$P(w + e_0) = f_3 + h_4 + \{f_4 - h_3 + (f_5 + h_4)\eta\}/(\eta + f_1) + f_6 \tag{9.29}$$

$$c_2/(\eta + f_1) = \kappa \tag{9.30}$$

$$\eta = R(\cos\alpha_2 - \cos\alpha_1)/2 \tag{9.31}$$

where,

$$h_1 = 2\sigma_y R^2 t(\sin\alpha_2 - \alpha_2 \cos\alpha_1)$$

$$h_2 = 4\sigma_y R t \alpha_2$$

$$h_3 = \sigma_y R^3 t(\alpha_2 + \sin\alpha_2 \cos\alpha_2) \tag{9.32}$$

$$h_4 = 2\sigma_y R^2 t \sin\alpha_2$$

Solving Eqs. (9.22) thru (9.24) for case A and Eqs. (9.28) thru (9.31) for case B, with respect to P, η, and α_1 (and α_2), respectively, the relationship between axial load and lateral deflection may be obtained.

The mean compressive axial strain in the elasto-plastic range may be given as:

$$\varepsilon = \frac{P}{EA}\frac{l-2R}{l} + \frac{2R}{l}\frac{\eta\sigma_y}{E(\eta + R\cos\alpha_1)} + \frac{1}{2l}\int_0^l\left[\left(\frac{dw}{dx}\right)^2 - \left(\frac{dw_0}{dx}\right)^2\right]dx \tag{9.33}$$

The second term in the right-hand side of Eq. (9.33) represents the plastic component of the axial strain. It is assumed that the plastic strain of $\eta\sigma_y/(\eta + R\cos\alpha_1)$ is uniformly distributed within a region 2R.

Critical Condition for Local Buckling

According to the classical theory of elastic stability, critical buckling strain in a cylindrical shell under axial compression is given as follows (Timoshenko and Gere, 1961):

$$\varepsilon_{cr} = \frac{1}{3\sqrt{1-v^2}}\frac{t}{R} = 0.61\frac{t}{R} \tag{9.34}$$

On the other hand, the critical strain for plastic shell buckling is given by Gerard (1962), Batterman (1965) and others. Here, Reddy (1979) concluded that the critical buckling strain of a shell occurs within the limits represented below including the pure bending case:

$$0.2\frac{t}{R} \langle \varepsilon_{cr} \langle 0.4\frac{t}{R} \tag{9.35}$$

In general, axial force and bending moment exist at the cross-section of tubular members. Consequently, the strain at a cross-section is not uniform. This chapter proposes an empirical formula, which represents the critical buckling strain in terms of the ratio of the maximum bending strain to the axial strain $\varepsilon_b/\varepsilon_a$, and the wall thickness to radius ratio t/R, as follows:

$$\varepsilon_{cr} = 0.155\{0.25(\varepsilon_b/\varepsilon_a)^2 + 1.0\}(t/R) \quad \text{for } \varepsilon_b/\varepsilon_a \langle 2.5 \tag{9.36}$$
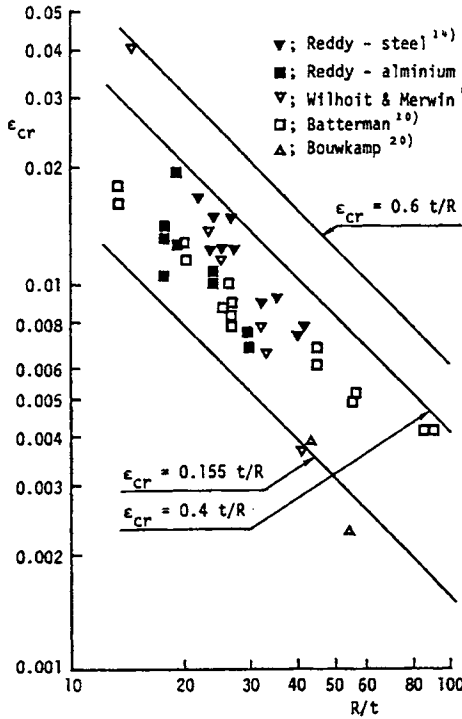
Figure 9.15   Critical Buckling Strain

$$\varepsilon_{cr} = 0.4t/R \qquad\qquad\qquad \text{for } \varepsilon_b/\varepsilon_a \geq 2.5$$

Figure 9.15 shows the experimental critical buckling strains collected and arranged by Reddy (1979). The critical buckling strain evaluated by Eq. (9.36) fall between two lines, 0.115 t/R and 0.4 t/R, depending on the magnitude of $\varepsilon_b/\varepsilon_a$.

Post-Local Buckling Analysis

As described in Chapter 9.2, local buckling takes place in a cosine mode or a dent mode. Accordingly, two kinds of analytical models are proposed, the COS model and the DENT model.

1. COS Model

Within the region where the strain in the axial direction exceeds ε_{cr} , local buckling deformation is assumed to take place. Its mode in the axial direction is approximated as follows (See Figure 9.16 (a)):

$$w_b = (\delta/2)\{1 - cos(2\pi x/s)\} \qquad\qquad (9.37)$$

where s represents the buckling wave length in the axial direction. Here, s is taken as 0.7 times the wavelength of elastic buckling evaluated by the classical theory of elastic stability. That is

$$s = 0.7 \frac{\pi}{\sqrt[4]{12\left(1 - v^2\right)}} \sqrt{Rt} = 1.21\sqrt{Rt} \tag{9.38}$$

The axial strain in a tube wall fiber where local buckling has occurred may be expressed as:

$$\varepsilon = \varepsilon_{cr} + (1/2s)\int_0^\delta \left(dw_b/dx\right)^2 dx = \varepsilon_{cr} + \left(\pi^2/4\right)\left(\delta/s\right)^2 \tag{9.39}$$

On the other hand, considering the equilibrium condition of a bending moment in a strip with its unit width cut out from the tube wall, the following equation is obtained. (See Figure 9.16 (b)):

$$\Delta F_b \delta - 2\Delta M_b = 0 \tag{9.40}$$

The interaction between the strips is not considered when Eq. (9.40) is derived. According to the assumptions previously mentioned, local buckling takes place in the plastic region. Consequently, ΔF_b and ΔM_b should satisfy the fully plastic interaction relationships, which are expressed as:

$$\Delta M_b/M_o = 1 - \left(\Delta F_b/F_0\right)^2 \tag{9.41}$$

where,

$$F_0 = t\sigma_r$$

$$M_0 = t^2\sigma_y / 4 \tag{9.42}$$

Using Eqs. (9.39), (9.40), and (9.41), the stress-strain and local lateral deflection stress relationships may be obtained as follows:

$$\sigma/\sigma_y = \left|\sqrt{4 + \mu^2} - \mu\right|/2 \tag{9.43}$$

$$\delta/t = \left(1 - \sigma/\sigma_y\right)^2 /\left(2\sigma/\sigma_y\right) \tag{9.44}$$

where,

$$\mu = \left(4s/\pi t\right)\sqrt{\varepsilon - \varepsilon_{cr}} \tag{9.45}$$

The stress-strain relationship represented by Eq. (9.43) is schematically illustrated in Figure 9.16 (c). Applying this model, the stress distributions for tube cross-section after the occurrence of local buckling are represented as in Figure 9.17. For a case A' stress distribution, the following relationships are derived in place of Eqs. (9.22) and (9.23).

$$P\left(\eta + f_1\right) = f_2 + f_2' + \left(c + c_1'\right)\eta \tag{9.46}$$

$$P\left(\omega + e_0\right) = f_3 + f_3' + \left(f_4 + f_5\eta\right)/\left(f_1 + \eta\right) + f_6 \tag{9.47}$$

where,

$$f_2' = 2\sigma_y R^2 t\left(g_1 - \alpha\right)\cos\alpha_1 \tag{9.48}$$

$$f_3' = 2\sigma_y Rt\left(g_2 - R\sin\alpha\right)$$

$$g_1 = \int_0^\alpha \left(\sigma/\sigma_y\right)d\theta$$
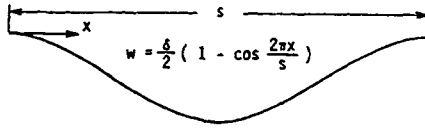
(a) Assumed deflection mode
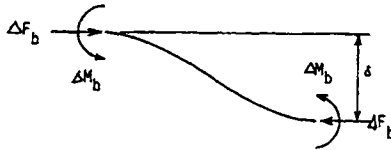
(b) Force and moment acting on cross sections
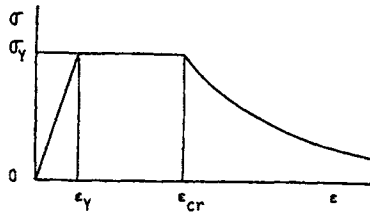
(c) Schematic representation of stress-strain relationship

Figure 9.16   Assumed Local Buckling Mode for COS Model
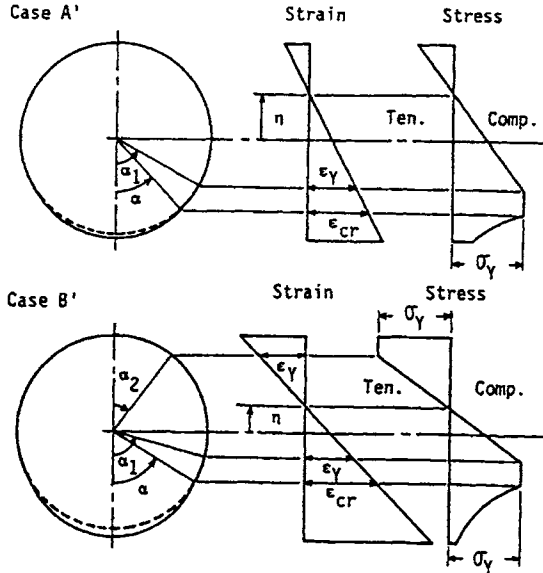
Figure 9.17   Elasto-Plastic Stress Distribution Accompanied by Local Buckling (COS Model)

(a) Assumed dent mode

(b) Force and moment acting
on cross sections
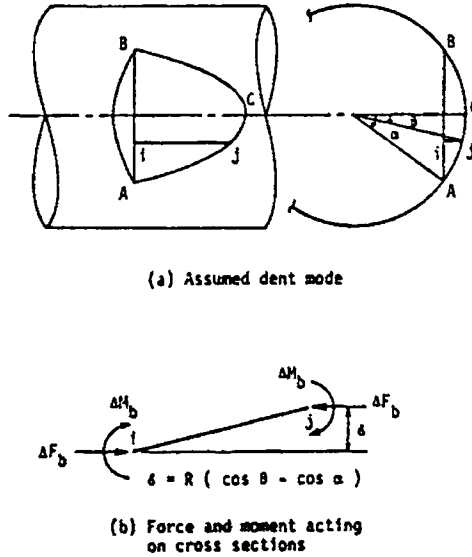
Figure 9.18   Assumed Buckling Mode for Dent Model

$$g_2 = \int_0^\alpha (R + \delta)(\sigma/\sigma_y) \cos\theta d\theta \tag{9.49}$$

$$c_1' = 2\sigma_y Rt(g_1 - \alpha) \tag{9.50}$$

For case B stress distributions, Eqs. (9.28) and (9.29) are replaced by:

$$P(\eta + f_1) = f_2 + f_2' + h_1 + (c + c_1' - h_2)\eta \tag{9.51}$$

$$P(\omega + e_0) = f_3 + f_3' + h_4 + \{f_4 - h_3 + (f_5 + h_4)\eta\}/(\eta + f_1) + f_6 \tag{9.52}$$

2. DENT Model

In this model, the cross-section c-c' in Figure 9.8 is considered. A dent is shown in Figure 9.18, from which, the equilibrium condition of forces and moments acting on a strip ij, with unit width shown in Figure 9.18, the following equation is derived:

$$\Delta F_b R(\cos\theta - \cos\alpha) - 2\Delta M_b = 0 \tag{9.53}$$

Solving Eq. (9.53) and considering the fully plastic condition expressed by Eq. (9.41), ΔF_b, and, ΔM_b are derived from:

$$\Delta F_b = \left[-R(\cos\theta - \cos\alpha) + \sqrt{R^2(\cos\theta - \cos\alpha)^2 + t^2} \right]\sigma_y \tag{9.54}$$

$$\Delta M_b = R(\cos\theta - \cos\alpha)\Delta F_b/2 \tag{9.55}$$

Integrating ΔF_b and ΔM_b respectively, the force F_b and the bending moment M_b acting at the bottom of a dent are obtained as:

$$F_b = 2\int_0^\alpha \Delta F_b d\theta \qquad (9.56)$$

$$M_b = 2\int_0^\alpha \Delta M_b d\theta \qquad (9.57)$$

where α, represents a half dent angle, and has a limiting value, α_L as mentioned in Chapter 9.2. After α_L is attained, two other dents are introduced as illustrated in Figure 9.10 (c). For the specimen tested in this chapter $\alpha_L = \pi/4$, which coincides with the calculated results by Toi et.al. (1983).

Applying this model, the stress distributions after local buckling may be represented as shown in Figure 9.19. In this figure, the case with one dent is indicated as case A" distribution, and that with three dents is a case B" distribution. For a case A" stress distribution, Eqs. (9.22) and (9.23) are replaced with:

$$(P - f_1'')(\eta + f_1) = f_2 + c_1\eta \qquad (9.58)$$

$$P(\omega + e_0) = f_3 + f_3'' + (f_4 + f_5\eta)/(\eta + f_1) + f_6 \qquad (9.59)$$

where,

$$f_1'' = \sum F_{bi} \qquad (9.60)$$

$$f_3'' = \sum M_{bi} + \sum F_{bi} R \cos\beta_i \qquad (9.61)$$

β_i is the angle of the center of the i-th dent measured from the vertical centerline, as shown in Figure 9.19.

For a case B'' stress distribution, Eqs. (9.28) and (9.29) are replaced with:

$$(P - f_1'')(\eta + f_1) = f_2 + h_1 + (c_1 - h_2)\eta \qquad (9.62)$$

$$P(W + e_0) = f_3 + f_3'' + h_4 + \{f_4 - h_3 + (f_5 + h_4)\eta\}/(\eta + f_1) + f_6 \qquad (9.63)$$

Procedure of Numerical Analysis

Until initial yielding is detected, Eq. (9.3) gives the relationship between axial compressive loads and lateral deflection. The mean compressive axial strain is evaluated by Eq. (9.8).

After plastification has started, the analysis is performed in an incremental manner using the plastic component of deflection shown in Figure 9.13. This deflection mode expressed by Eqs. (9.10) thru (9.12) gives a constant plastic curvature increment in the region l_p. If the actual plastic region length l_d in Figure 9.20 (a) is taken as l_p, it reduces to prescribe excess plastic curvature especially near the ends of the plastic region. To avoid this, a bi-linear distribution of plastic curvature increments is assumed in the region l_d, as indicated in Figure 9.20 (b). Then, the change of the plastic slope increment along the plastic region l_d, may be expressed as:

$$d\theta_p = l_d d\kappa_p/2 \qquad (9.64)$$
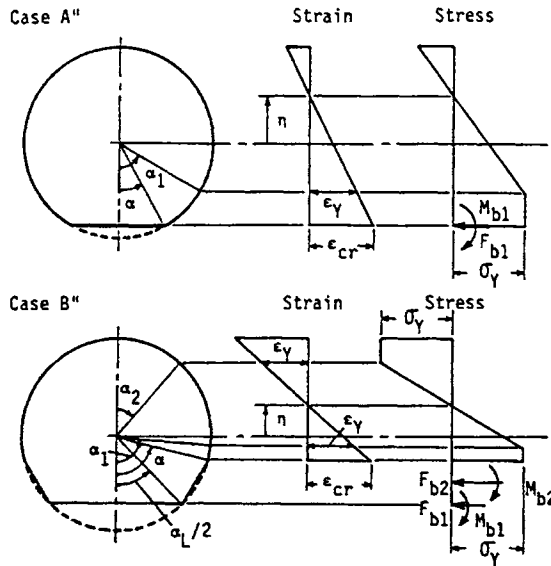
Figure 9.19   Elasto-plastic Stress Distribution Accompanied by Local Buckling (DENT Model)

(a) Actual plastic zone under combined thrust and bending

(b) Distribution of increment of plastic curvature

(c) Disribution of increment of plastic axial strain
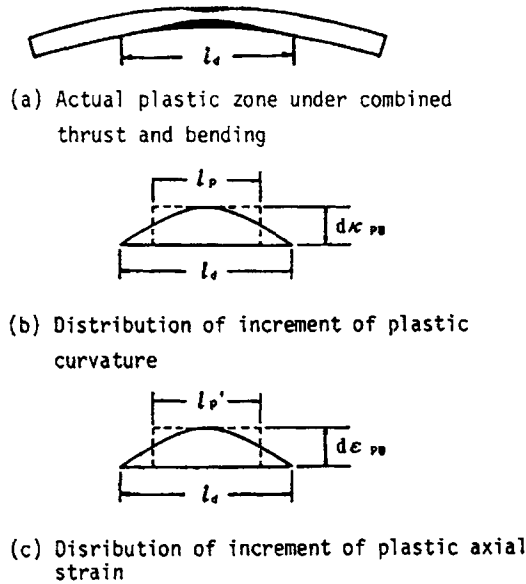
Figure 9.20   Equivalent Length of the Plastic Zone

where $d\kappa_p$, is the increment of plastic curvature at the center of a plastic region.

On the other hand, if $d\kappa_p$ is assumed to be uniformly distributed along the plastic region l_d, as indicated by Eqs. (9.10) thru (9.12), the change of plastic slope increment along the plastic region l_d may be expressed as:

$$d\theta_p^{\cdot} = l_p d\kappa_p \qquad (9.65)$$

Here, l_p is determined so that $d\theta_p^{\cdot} = d\theta_p$. This is equivalent to the condition that the integrated values of plastic curvature in the plastic regions are the same for both cases, which reduces to:

$$l_p = l_d/2 \qquad (9.66)$$

The above-mentioned procedure used to estimate l_p, is only an approximation. In Section 9.3.2, a more accurate procedure is described. To evaluate the actual plastic region size l_d, for the calculated deflection, the stress is analyzed at 100 points along a span, with equal spacing and the bending moment at each point is evaluated. After local buckling has occurred, plastic deformation will be concentrated at the locally buckled part. For this case, l_p is considered equal to the tube's outer diameter, which may approximately be the size of the plastically deformed region after local buckling.

9.3.2 Idealized Structural Unit Analysis

Pre-Ultimate-Strength Analysis

Throughout the analysis of a beam-column using the ordinary Idealized Structural Unit Method, an element is regarded to be elastic until the fully plastic condition and/or the buckling criterion is satisfied. When the axial force is in tension, a relatively accurate ultimate strength may be evaluated with the former condition along with the post-yielding calculation. However, when the axial force is in compression, the ultimate strength evaluated by the latter criterion is not so accurate, since the latter criterion is based on a semi-empirical formula. In the present study, the simplified elasto-plastic large deflection analysis described in 9.3.1 is incorporated in the Idealized Structural Unit (element) in order to accurately evaluate the ultimate strength under the influence of compressive axial forces.

The Idealized Structural Unit Method uses the incremental analyses. The ordinary increment calculation is performed until the initial yielding is detected. The initial yielding is checked by evaluating the bending moment along the span of an element and the deflection expressed by Eq. (9.9). After the yielding has been detected, the simplified method described in 9.3.1 is introduced.

Here, it is assumed that calculation of the (n+1)-th step has ended. Therefore, the following equilibrium equation is derived similar to Eq. (9.19):

$$P(w_e + w_p) + \Delta P(e_m + e_q) + M_i + Q = M \qquad (9.67)$$

where,

P = Axial force given by Eq. (9.17)

ΔP = $P - X_i$ $(\leq \Delta X_i)$

M_i = Bending moment at nodal point i at the end of the n-th step

Q = Bending moment due to distributed lateral load

M = Bending moment given by Eq. (9.18)

X_i = Axial force at the end of the n-th step

ΔX_i = Increment of axial force during the (n+1)-th step

ΔM_i = Increment of bending moment at nodal point i during the (n+1)-th step

ΔQ = Bending moment increment due to distributed lateral load during (n+1)-th

step and

$$e_m = \Delta M_i / \Delta X_i \qquad\qquad e_q = \Delta Q / \Delta X_i \tag{9.68}$$

X_i, ΔX_i, M_i, ΔM_i, Q, and ΔQ are known variables after the (n+1)-th step has ended.

Considering the equilibrium condition of forces in the axial direction, geometrical conditions regarding the slope, and Eq. (9.77), the following equations are obtained:

for Case A Stress Distribution:

$$P(\eta + f_1) = f_2 + c_1\eta \tag{9.69}$$

$$PW + \Delta P(e_m + e_q) = f_3 + (f_4 + f_5\eta)/(\eta + f_1) + f_6 \tag{9.70}$$

$$c_2/(\eta + f_1) = \kappa \tag{9.71}$$

for Case B Stress Distribution:

$$P(\eta + f_1) = f_2 + h_1 + (c_1 - h_2)\eta \tag{9.72}$$

$$PW + \Delta P(e_m + e_q) = f_3 + h_4 + \{f_4 - h_3 + (f_5 + h_4)\eta\}/(\eta + f_1) + f_6 \tag{9.73}$$

$$c_2/(\eta + f_1) = \kappa \tag{9.74}$$

$$\eta = R(cos\,\alpha_2 - cos\,\alpha_1)/2 \tag{9.75}$$

After the initial yielding, elasto-plastic analysis by the simplified method is performed using Eqs. (9.69) thru (9.71) or Eqs. (9.72) thru (9.77) at each step of the Idealized Structural Unit analysis until the ultimate strength is attained at a certain step.

Here, a more accurate method is introduced to determine the length of plastic zone l_p. If the axial force P and bending moment M are given, the parameters η and α_1 (and α_2), which determine the axial strain ε and curvature $\phi(x)$ are obtained from Eqs. (9.17) and (9.18). Then, the increment of the curvature $d\phi(x)$ from the former step is evaluated. With this increment, the length of plastic zone is given as

$$l_p = \int d\phi_p(x)dx/d\phi_{po} \tag{9.76}$$

$$d\phi_p(x) = d\phi(x) - dM(x)/EI \tag{9.77}$$

where $d\phi_{po}$ represents the maximum plastic curvature increment in the plastic region.

System Analysis

The procedure used for the system analysis using the proposed Idealized Structural Unit is as follows:

- At each step of the incremental calculation, moment distributions are evaluated in elements in which axial force is in compression.

- Based on the moment and axial force distribution, the stress is calculated and the yielding of the element is checked.

- If yielding is detected in an element at a certain step, the initial yielding load of this element is evaluated. Then, the elasto-plastic analysis is performed using Eqs. (9.69) thru (9.71) or Eqs. (9.72) thru (9.75) until ΔP becomes ΔX_i.

In the following steps, the same calculation is performed at each element where plastification takes place. If ΔP shows its maximum value ΔP_{max} in a certain element before it reaches ΔX_i at a certain step, this element is regarded to have attained its ultimate strength $P_u (= X_i + \Delta P_{max})$. Then, all the increments at this step are multiplied by $\Delta P_{max} / \Delta X_i$.

For the element that has attained its ultimate strength, its deflection is increased by keeping the axial force constant until the fully plastic condition is satisfied at the cross-section where the bending moment is maximum. Then, this element is divided into two elements and a plastic node is inserted at this cross-section.

The results of such analyses are schematically illustrated in terms of the axial forces and bending moments in Figure 9.21. (O) represents the results of the Idealized Structural Unit Method, and the dashed line represents the results of the simplified method. Up to point 4, no plastification occurs. Between points 4 and 5, yielding takes place, and the analysis using simplified methods starts where the yielding occurs. No decrease is observed in this step. At the next step between points 5 and 6, the ultimate strength is attained. Then, the increment of this step is multiplied by b5/56. While keeping the axial force constant, the bending moment is increased up to point c, and a plastic node is introduced. After this, the Plastic Node Method (Ueda and Yao, 1982) is applied.

Evaluation of Strain at Plastic Node

In the Plastic Node Method (Ueda and Yao, 1982), the yield function is defined in terms of nodal forces or plastic potentials. Therefore, plastic deformation occurs in the form of plastic components of nodal displacements, and only the elastic deformation is produced in an element. Physically, these plastic components of nodal displacements are equivalent to the integrated plastic strain distribution near the nodal point. If the plastic work done by the nodal forces and plastic nodal displacements is equal to those evaluated by distributed stresses and plastic strains, the plastic nodal displacements are equivalent to the plastic strain field in the evaluation of the element stiffness matrix (Ueda and Fujikabo, 1986). However, there is no mathematical relationship between plastic nodal displacements and plastic strains at the nodal point. Therefore, some approximate method is needed to evaluate plastic strain at a nodal points based on the results of Plastic Node Method analysis.

Here, the internal forces move along the fully plastic interaction curve after the plastic node is introduced as indicated by a solid line in Figure 9.22. On the other hand, the result of accurate elasto-plastic analysis using the finite element methods may be represented by a dashed line in

the same Figure. The chain line with one dot represents the results obtained from the simplified method.
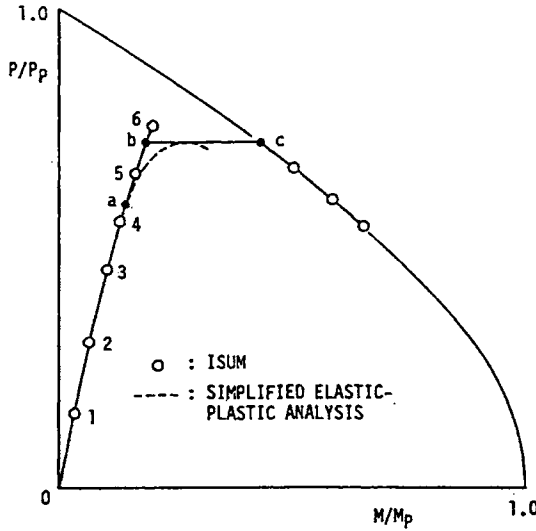
Figure 9.21   Schematic Representation of Internal Forces
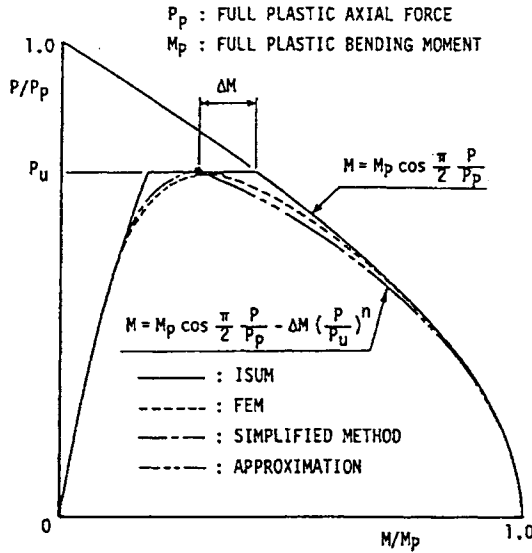
Figure 9.22   Determination of an Approximate Relationship Between Axial Forces and Bending Moments

The bending moment occurring after the ultimate strength is attained, is approximated by the following equation. as

$$M = M_p \cos\frac{\pi}{2}\frac{P}{P_p} - \Delta M\left(\frac{P}{P_u}\right)^n$$

(9.78)

where,

$$M_p = 4\sigma_y R^2 t \qquad\qquad P_p = 2\pi\sigma_y Rt$$

(9.79)

and ΔM is indicated in Figure 9.22. The relationship between this bending moment and the axial force is plotted by a chain line with two dots as shown in Figure 9.22.

Substituting the axial force P and the evaluated bending moment from Eq. (9.79) into Eqs. (9.17) and (9.18), respectively, strain may be evaluated. If the maximum strain (sum of the axial strain and maximum bending strain) reaches the critical strain expressed by Eq. (9.36), the post-local buckling analysis starts.

Post-Local Buckling Analysis

The fully plastic interaction relationship after local buckling takes place may be expressed as

$$\Gamma = M - M_d - M_p \cos\left[\frac{\pi}{2}\left(\frac{P}{P_p} - \frac{F_d}{P_p}\right) + \frac{\alpha}{2}\right] + \frac{1}{2}M_p \sin\alpha$$

(9.80)

where F_d and M_d are given as below:

COS model

$$F_d = 2\int Rt\sigma d\theta$$

(9.81)

$$M_d = 2\int Rt\delta\sigma\cos\theta d\theta$$

(9.82)

DENT model

$$F_d = \sum F_{bi}$$

(9.83)

$$M_d = \sum M_{bi} + \sum F_{bi} R\cos\beta_i$$

(9.84)

In the above expressions, σ and δ are given by Eqs.(9.43) and (9.44), and F_{bi} and M_{bi} are equal to F_b and M_b and given by Eqs. (9.56) and (9.57) of the i-th dent.

Here, the angle α represents the size of a locally buckled part and is a function of the axial strain e and the curvature κ of a cross-section, and is expressed as:

$$\alpha = cos^{-1}\left[(\varepsilon_{cr} - e)/(\kappa R)\right]$$

(9.85)

At the same time, F_d and M_d are functions of e and κ through α. Consequently, the fully plastic interaction relationship is rewritten in the following form:

$$\Gamma(P, M, e, \kappa) = 0$$

(9.86)

As described in 9.3.2.3, there exists no one-to-one correspondence between plastic nodal displacements and plastic strains at a nodal point. However, plastic strains may be concentrated near the cross-section where local buckling occurs. So, the axial strain and curvature at this cross-section are approximated by:

$$e = P/EA + e_{pcr} + \left(u_p - u_{pcr}\right)/l_p \tag{9.87}$$

$$\kappa = M/EI + \kappa_{pcr} + \left(\theta_p - \theta_{pcr}\right)/l_p \tag{9.88}$$

l_p in the above equations represents the length of plastic zone, and is taken to be equal to the diameter $D(=2R)$ as in the case of a simplified method. Considering Eqs. (9.87) and (9.88), the fully plastic interaction relationship reduces to:

$$\Gamma\left(P, M, u_p, \theta_p\right) = 0 \tag{9.89}$$

The elasto-plastic stiffness matrix after local buckling occurs, is derived based on the fully plastic interaction relationship expressed by Eq. (9.89). The condition to maintain the plastic state is written as:

$$d\Gamma = \frac{\partial \Gamma}{\partial P} dP + \frac{\partial \Gamma}{\partial M} dM + \frac{\partial \Gamma}{\partial u_p} du_p + \frac{\partial \Gamma}{\partial \theta_p} d\theta_p = 0 \tag{9.90}$$

or in the matrix form as:

$$\begin{bmatrix} \phi_i^T & 0 \\ 0 & \phi_j^T \end{bmatrix} \begin{Bmatrix} dR_i \\ dR_j \end{Bmatrix} + \begin{bmatrix} \psi_i^T & 0 \\ 0 & \psi_j^T \end{bmatrix} \begin{Bmatrix} dh_{pi} \\ dh_{pj} \end{Bmatrix} = 0 \tag{9.91}$$

where, $\{dR\}$ and $\{dh_p\}$ are the increment of nodal forces and plastic nodal displacements, respectively, see Figure 9.12 and the following Equations:

$$\phi_i = \left\{ \partial\Gamma/\partial X_i, \partial\Gamma/\partial Z_i, \partial\Gamma/\partial M_i \right\}^T$$

$$\phi_j = \left\{ \partial\Gamma/\partial X_j, \partial\Gamma/\partial Z_j, \partial\Gamma/\partial M_j \right\}^T \tag{9.92}$$

$$\psi_i = \left\{ \partial\Gamma/\partial u_{p_i}, \partial\Gamma/\partial w_{p_i}, \partial\Gamma/\partial\theta_{p_i} \right\}^T$$

$$\psi_j = \left\{ \partial\Gamma/\partial u_{p_j}, \partial\Gamma/\partial w_{p_j}, \partial\Gamma/\partial\theta_{p_j} \right\}^T \tag{9.93}$$

Here, considering Γ as a plastic potential, the increments of plastic nodal displacements are given as

$$\begin{Bmatrix} dh_{pi} \\ dh_{pj} \end{Bmatrix} = \begin{bmatrix} d\lambda_i & 0 \\ 0 & d\lambda_j \end{bmatrix} \begin{Bmatrix} \phi_i \\ \phi_j \end{Bmatrix} \tag{9.94}$$

When only nodal point j is plastic, $d\lambda_i = 0$. Contrary to this, $d\lambda_j = 0$ when only node point i is plastic.

On the other hand, the increments of nodal forces are expressed in terms of the elastic stiffness matrix and the elastic components of nodal displacement increments as follows:

$$\begin{Bmatrix} dR_i \\ dR_j \end{Bmatrix} = \begin{bmatrix} K_{ii}^e & K_{ij}^e \\ K_{ji}^e & K_{jj}^e \end{bmatrix} \left(\begin{Bmatrix} dh_i \\ dh_j \end{Bmatrix} - \begin{Bmatrix} dh_{pi} \\ dh_{pj} \end{Bmatrix} \right) \tag{9.95}$$

where $\{dh\}$ represents the increments of nodal displacements.

Substituting Eqs. (9.94) and (9.95) into Eq. (9.92), $d\lambda_i$ and $d\lambda_j$ are expressed in terms of $\{dh\}$. Substituting them into Eq. (9.95), the elasto-plastic stiffness matrix after local buckling is derived as:

$$\begin{Bmatrix} dR_i \\ dR_j \end{Bmatrix} = \begin{bmatrix} K_{ii}^D & K_{ij}^D \\ K_{ji}^D & K_{jj}^D \end{bmatrix} \begin{Bmatrix} dh_i \\ dh_j \end{Bmatrix} \tag{9.96}$$

For the case in which local buckling is not considered, the elasto-plastic stiffness matrix is given in a concrete form in (Ueda et al, 1969). When local buckling is considered, the terms $\phi_i^T K_{ii} \phi_i$ and $\phi_j^T K_{jj} \phi_j$ in the denominators in Ueda and Yao (1982) are replaced by $\phi_i^T K_{ii} \phi_i - \psi_i^T \psi_i$ and $\phi_j^T K_{jj} \phi_j - \psi_j^T \psi_j$, respectively.

9.4 Calculation Results

9.4.1 Simplified Elasto-Plastic Large Deflection Analysis

In order to check the validity of the proposed method of analysis, a series of calculations are performed on test specimens, summarized in Table 9.4, in which a comparison is made between calculated and measured results. Three types of analyses are performed: a simplified elasto-plastic large deflection analysis combined with a COS model and a DENT model, respectively, for all specimens; and an elasto-plastic large deflection analysis without considering local buckling by the finite element method. The calculated results applying COS model and DENT model are plotted in the following figures, along with those analyzed using the finite element method. The experimental results are plotted by the solid lines.

H series

This series is newly tested. The measured and calculated load -deflection curves are plotted in Figure 9.7. First, the results from the simplified method have a very good correlation with those obtained from the finite element method until the ultimate strength is attained. However, they begin to show a little difference as lateral deflection increases. This may be attributed to the overestimation of the plastic region size at this stage.

The calculated ultimate strengths are 7-10% lower than the experimental ones. This may be due to a poor simulation of the simply supported end condition and the strain hardening effect of the material. Contrary to this, the onset points of local buckling calculated using Eq. (9.33) agree quite well with the measured ones. The post - local buckling behavior is also well simulated by the COS model, but not so well simulated by the DENT model. Such difference between the measured and the calculated behaviors applying DENT model is observed in all analyzed test specimens except for the D series. This may be due to the underestimation of forces and moments acting at the bottom of a dent, and further consideration may be necessary for the DENT model.

C Series

C series experiments are carried out by Smith et al. (1979). Specimens C1 and C2 which are not accompanied by a denting damage are analyzed. The calculated results for Specimen C2 are plotted together with the measured result in Figure 9.23. Smith wrote in his paper that local buckling took place when the end-shortening strain reached 2.5 times the yield strain ε_y, while it occurred in the analysis when the strain reached 1.4 ε_y. However, the behavior up to the onset of local buckling is well simulated by the proposed method of simplified elasto-plastic large deflection analysis. On the other hand, in the case of Specimen C1, local buckling takes place just after the ultimate strength is attained both in the experiment and in the analysis. However, the calculated ultimate strength is far below the measured one as indicated in Table 9.4. This may be attributed to some trouble in the experiment, since the measured ultimate strength is 1.1 times the fully plastic strength.

D Series

This series is also tested by Smith et al. (1979). The analysis is performed on Specimens D1 and D2. Here, the results for Specimen D1 are plotted in Figure 9.24. It may be said that a good correlation is observed between the calculated and measured results in the ultimate strength and in the onset of local buckling. However, the behavior occurring just after the local buckling is somewhat different between the experiment and the analysis. This may be because the experimental behavior at this stage is a dynamic one, which is a kind of a snap-through phenomenon as Smith mentioned. As for the load carrying capacity after the dynamic behavior, the DENT model gives a better estimate than the COS model.

A similar result is observed in Specimen D2. However, in this case, the predicted onset of local buckling is later than the measured one.

S Series

This series is a part of the experiments carried out by Bouwkamp (1975). The calculated and measured results for Specimen S3 are shown in Figure 9.25. First, the measured ultimate strength is far above the elastic Eulerian buckling strength. This must be due to a difficulty in simulating the simply supported end condition. Consequently, instability took place just after the ultimate strength was attained, and a dynamic unloading behavior may occur. After this, a stable equilibrium path was obtained, which coincides well with the calculated results.

Table 9.4   Specimen size, material properties and results of experiment and calculation

Specimen Number	Mean Diameter D (mm)	Thickness t (mm)	Length L (mm)	Initial deflection a (mm)	Load eccentricity e (mm)	Young's modulus E (kg/mm)	Yield Stress σ_y (kg/mm)	Ultimate strength σ_u/σ_y Measured	Calculated	Ref. No.
H1	501.6	6.40	8000	0.63	63.50	21180.0	34.55	0.68	0.63	Present
H2	501.6	6.40	8000	0.63	127.00	21180.0	34.55	0.55	0.49	Present
H3	501.6	6.40	8000	0.63	190.50	21180.0	34.55	0.44	0.41	Preaent
A1	61.5	2.11	2150	0.0	0.00	20496.3	23.25	0.84	0.76	11
A2	61.5	2.12	2150	0.0	9.84	21210.1	23.25	0.49	0.43	11
B1	77.8	1.74	2150	0.0	0.00	20802.2	19.88	1.00	0.94	11
B2	77.8	1.71	2150	0.0	10.11	23351.5	20.29	0.60	0.59	11
C1	100.0	1.66	2150	0.0	0.00	20496.3	21.52	1.10	0.95	11
C2	99.9	1.73	2150	0.0	9.99	21006.2	28.95	0.58	0.63	11
D1	89.0	1.02	2150	0.0	0.00	22535.7	49.46	0.75	0.83	11
D2	89.0	1.01	2150	0.0	15.13	26002.8	47.52	0.50	0.47	11
S1	213.5	5.56	4572	0.0	0.00	20256.1	41.69	0.84	0.82	5
S2	213.5	5.56	6096	0.0	0.00	20256.1	41.69	0.72	0.59	5
S3	213.5	5.56	7620	0.0	0.00	20256.1	41.69	0.54	0.41	5
S4	213.5	5.56	9144	0.0	0.00	20256.1	41.69	0.32	0.29	5
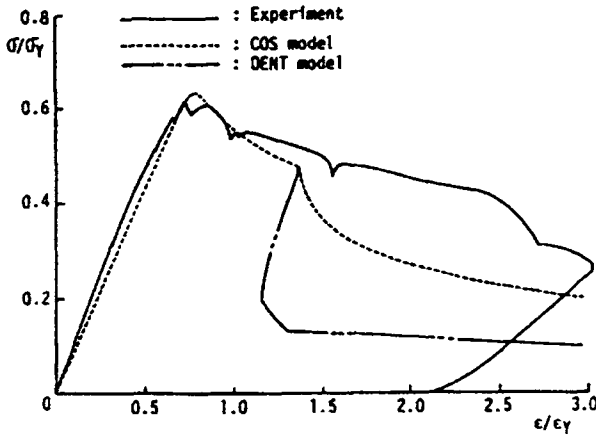
Figure 9.23   Comparison of Measured and Calculated Results (C2)
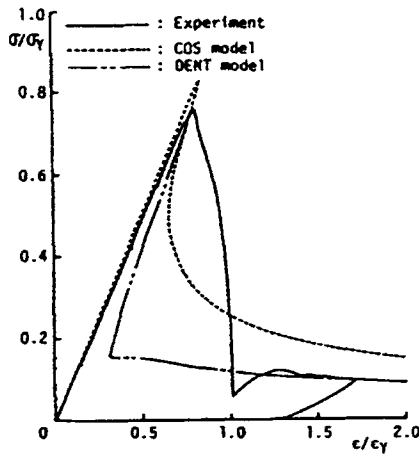
Figure 9.24   Comparison of Calculated and Measured Results (D1)

The same features are observed in Specimens S1, S2, and S3. Bouwkamp wrote in his paper that local buckling took place after the ultimate strength was attained. However, no local buckling occurred for this series analysis.

A Series and B Series

A and B series by Smith et al. (1979), show no local buckling in either one of the experiments and analyses. The calculated ultimate strengths show good agreement with the measured ones, with the exception of Specimen A1.
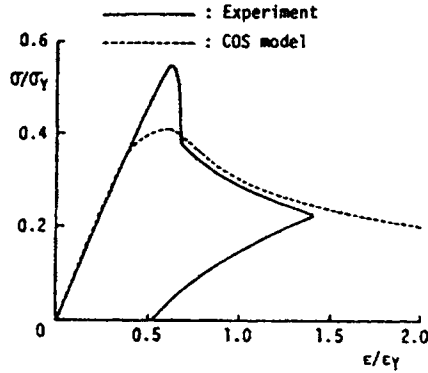
Figure 9.25   Comparison of Calculated and Measured Results (S3)

9.4.2   Idealized Structural Unit Method Analysis

Members with Constraints against Rotation at Both Ends

An end rotation of a structural member in a structural system is constrained by other members. This effect of constraint may be equivalent to placing springs, which resist rotation at both ends of a member when one member is isolated from the system. For such a member with springs at both ends, a series of analyses are performed by changing the spring constant between 0 and ∞. The wall thickness and outer diameter are taken as 20 mm and 2,000 mm, respectively. The initial deflection of magnitude $1/500$ times the length is imposed to know the characteristics of the proposed Idealized Structural Unit model. The yield stress of the material is chosen as 30 kgf/mm2, and the magnitudes of springs at both ends are the same. Local buckling is not considered in this analysis. The calculation results for $l/\sqrt{I/A} = 100$ are shown in Figures 9.26 and 9.27. Figure 9.26 represents the load vs. lateral deflection relationships, and Figure 9.27 represents the change of internal forces at a mid-span point and end. In these figures, the solid lines and chain lines represent the results obtained by using the present method and the finite element method, respectively. On the other hand, the dashed lines represent the analytical solutions expressed as follows:

Perfectly elastic solution

$$w = 2M\left[1/(2\cos kl/2) - 1\right] + a_0\, P_E/(P_E - P) \qquad (9.97)$$

where,

$$M = -\left[\pi a_0 P \Big/ l(P_e - P)\right] \Big/ \left[k(1 - \cos kl)\Big/(P\sin kl) + \frac{1}{k}\right] \qquad (9.98)$$

and k represents the magnitude of springs placed at both ends, and P_E is given in Eq. (9.6).

Rigid plastic solution

$$w = M_p\left[\cos(\pi P/2P_p)\right]/P \qquad \text{for } k=0 \qquad (9.99)$$

$$w = 2M_p\left[\cos(\pi P/2P_p)\right]/P \qquad \text{for } k=\infty \qquad (9.100)$$

where k/k_0 is taken as 0. 0, 0. 1, 1. 0 and ∞, where $k_0 = 4EI/l$.

The ultimate strength evaluated by the proposed method is slightly lower than the ultimate strength proposed by the finite element method when the constraint is weak, but it becomes higher proportionally, as the constraint is increased. However, the proposed method gives a very accurate ultimate strength.

In the case of $K = \infty$, the axial load still increases after a plastic node is introduced at a mid-span point where the ultimate strength is attained according to a simplified method. It begins to decrease after the fully plastic condition is satisfied at both ends. However, the load increment after a plastic node has been introduced at a mid-span point is very small. Therefore, an alternative analysis is performed, in which three plastic nodes are simultaneously introduced at a mid-span and both ends when the ultimate strength is attained by a simplified method. The curves for K $= \infty$ in Figures 9.26 and 9.27 are the results of the latter analysis. Further considerations should be taken when regarding this procedure.
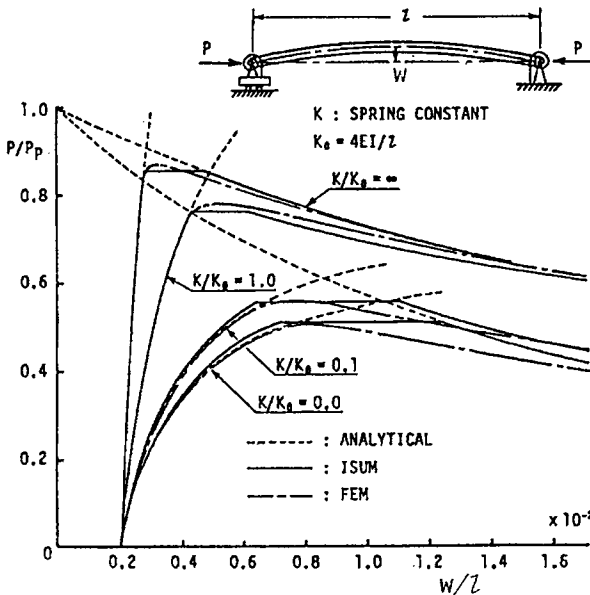
Figure 9.26   Load - lateral Deflection Curves of Simply Supported Tube with End Constraint Against Rotation

H Series

A series of analyses are performed on H series specimens in order to check the accuracy of post - local buckling behavior predicted by the present method. The coefficient, n, in Eq. (9.78) is interchanged between 8 and 16 when using the COS model.

The load vs. lateral deflection relationships and the interaction relationships of internal forces are plotted in Figures 9.28 and 9.29, respectively. The solid and dashed lines represent the results obtained from the present method and experiment, respectively, and the chain lines

represent the results obtained from the finite element method without considering local buckling.

Until local buckling takes place, both results obtained from the present method and the finite element method, show good correlation's including the ultimate strength. The comparison of these results using the FEM to the results of other experiments shows little differences among them, which may be attributed to the reasons described in 9.4.1. However, judging from the interaction relationships shown in Figure 9.29, these differences may be attributed to the material properties of the actual material and assumed material used for the analysis. The yield stress used in the analysis is determined, based on the results of the tensile test, and may be very accurate as long as the stress is in tension. It is not completely clear, but there may be some differences in the material properties in a tensile and a compressive range.
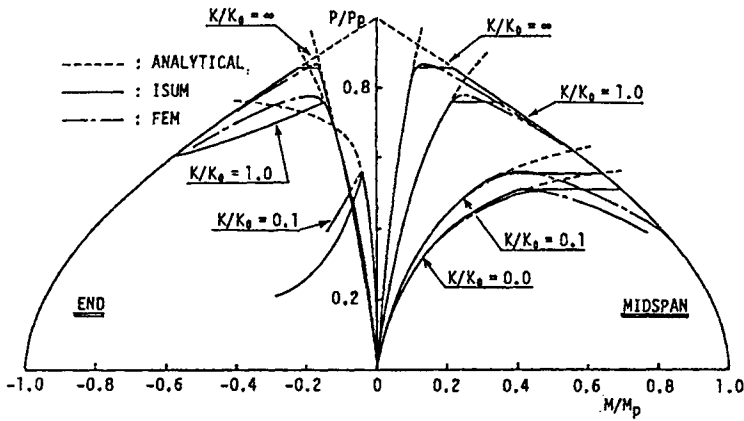
Figure 9.27   Axial Force Bending Moment Relationships

Post-local buckling behavior is simulated quite well although the calculated starting points of local buckling are a little different from the measured ones. The difference in the onset point of local buckling may be due to inaccuracies of the critical buckling strain evaluated by Eq.(9.31) and the estimated strain using Eq.(9.67). At present, the value to be employed as n remains unknown. Although larger values may give good results as indicated in Figures 9.28 and 9.29.

The curves changing the value of n may be regarded as the results of the numerical experiment, changing the onset point of local buckling. A greater reduction is observed in the load carrying capacity (axial load) as the critical load for buckling increases.

The same analysis is performed on small-scale test specimens. Relatively good correlation's are observed between the calculated and experimental results for the ultimate strength in all specimens. However, the calculated post-ultimate strength behavior is slightly different from the observed behavior. This may be attributed to a difference in the assumed stress-strain relationship used during the analysis and the actual one. An elastic-perfectly plastic stress-strain relationship is assumed in the analysis. Contrary to this, the actual material showed relatively high strain hardening. In order to analyze such cases, the influence of strain hardening must be taken into account. The strain hardening effect may be easily incorporated

in the simplified analysis. Applying the Plastic Node Method for the post-ultimate strength analysis is a basic idea that is presented in Ueda and Fujikubo (1986). These remain as ideas in progress.
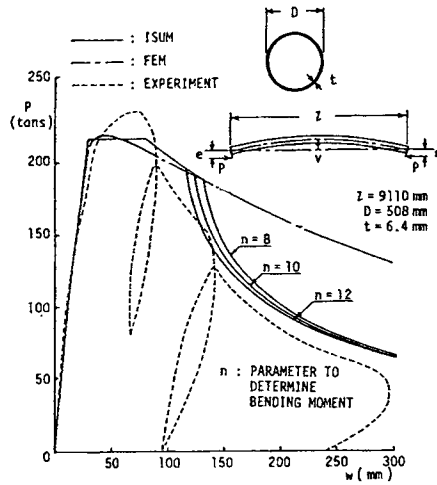
(a) e/D = 1/8
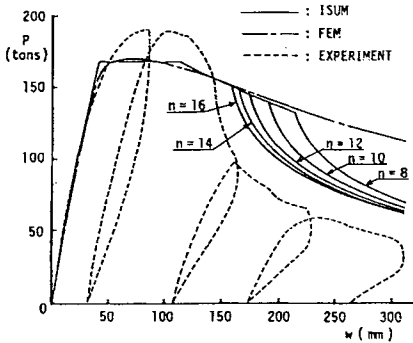
(b) e/D = 1/4
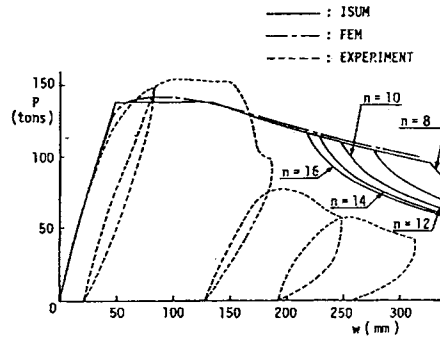
(c) e/D = 3/8

Figure 9.28   Load Lateral Deflection Curves of H Series Specimens
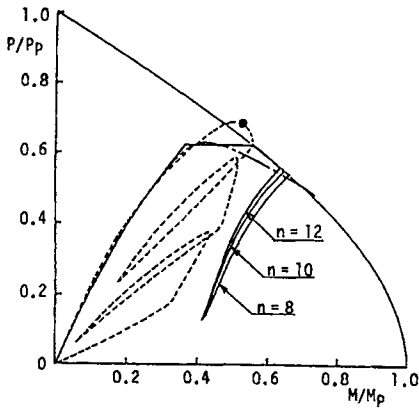
(a) e/D = 1/8
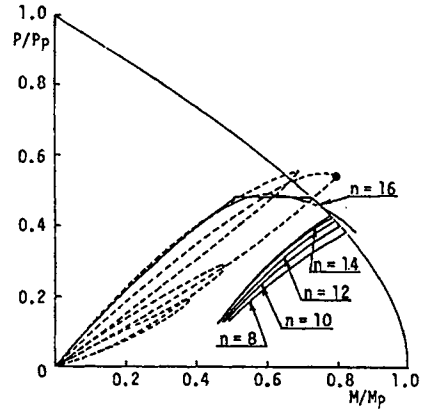
(b) e/D = 1/4
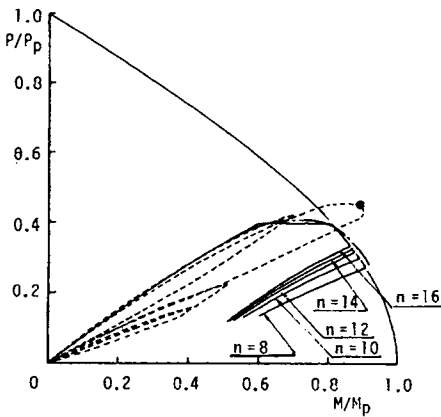
(c) e/D = 3/8

n : PARAMETER TO DETERMINE BENDING
    MOMENT

———— : ISUM

—— · —— : FEM

— — — — : EXPERIMENT

● : ONSET OF
    LOCAL BUCKLING
    IN EXPERIMENT

**Figure 9.29   Measured and Calculated Relationship Between Axial Force
and Bending Moment**

If pure bending is obtained, the axial force is zero and the proposed method does not need to be applied. In this case, the fully plastic condition will give an accurate ultimate strength. Furthermore, this method is not necessary when the axial force is in tension.

9.5   Conclusions

Local buckling of tubular members is investigated in this chapter both theoretically and experimentally. First, a series of experiments are carried out on large and small-scale tubular specimens. Large-scale test specimens are 1/3.5 scale model of a bracing member in an

existing semi-submersible drilling unit, and their diameter to thickness ratio, D/t, is 78. The D/t ratio of small-scale specimens varies between 40 and 97. Axial compression tests with load eccentricity are carried out on both specimens, and pure bending tests on small-scale specimens only. These experiments have shown that after the ultimate strength has been attained, local buckling takes place at the area of maximum compressive strain. Two types of buckling mode are observed, which are denoted as a cosine mode and a dent mode. The buckling wave of a cosine mode spreads about a half circle in the circumferential direction, and that of a dent mode about a quarter circle in the circumferential direction. Nevertheless, it has a short wavelength in the axial direction in both modes.

The load carrying capacity suddenly decreases due to the initiation of local buckling.

In the case of a cosine mode, the formation of local denting deformation follows at the foot of the initial cosine-buckling wave. Other local denting deformations are formed adjacent to the initial dent and in the case of dent mode buckling.

A simplified method is proposed to analyze the elasto-plastic behavior of a tubular member subjected to axial compression, end moments, and distributed lateral loads. Two models are proposed which simulate the post-local buckling behavior of a tubular member based on the observed results of experiments. They are the COS and the DENT model.

Combining these models with the simplified method, a series of analyses have been performed on the newly tested specimens and on those previously reported. The analyses results are compared with experimental results, and the validity and usefulness of the proposed simplified methods of analysis are demonstrated.

Furthermore, the Idealized Structural Unit model (element) is developed by incorporating the proposed simplified method. Using this model, the ultimate strength is automatically evaluated under axial compression. After the local buckling has started, its influence is reflected upon the fully plastic strength interaction relationship through plastic nodal displacements of the element. Some example calculations are performed by applying the newly developed element. The calculated results are compared with those obtained using the finite element method and the validity and usefulness of this element is demonstrated.

Research remaining for future work is:

- Accurate estimates of plastic strain and curvature at a plastic node
- Accurate evaluation of critical buckling strain
- System analysis using the proposed Idealized Structural Unit model

9.6   Example

Example 9.1: Comparison of the Idealized Structural Unit Method and the Plastic Node Methods

Problem:

Describe the differences and similarities between the Idealized Structural Unit Methods and the Plastic Node Methods.

Solution:

The Plastic Node Methods, as described in Part II Chapter 12, is a generalization of the plastic hinge methods that have been popular for plastic analysis of beams and framed structures. The

generalization makes it possible to effectively conduct analysis of plated structures and shell structures (see Ueda and Yao, 1982). It is also possible to include the effect of strain hardening in the formulation, see Ueda and Fujikubo (1986). However, geometrical nonlinearity is not a subject discussed in the plastic node methods.

The Idealized Structural Unit Methods (Ueda and Rashed, 1984) make use of the Plastic Node Methods to deal with the plasticity, and utilize empirical formulae (such as those in design codes) for ultimate strength analysis of individual components. In this Chapter, however, an attempt has been made to predict the ultimate strength of the components using simplified inelastic analysis instead of empirical formulae. The advantage of using the simplified inelastic analysis is its ability to account for more complex imperfection and boundary conditions that are not covered in the empirical formulae. However, the disadvantage is its demand for computing effort and its complexity that may lead to loss of convergence in a complex engineering analysis.

9.7   References

1.   AISC (1978), "Specification for the Design, Fabrication and Erection of Structural Steel for Buildings, with Commentary", American Institute of Steel Construction.

2.   API RP 2A, (2001), "Recommended Practice for Planning, Designing and Constructing Fixed Offshore Platforms – Working Stress Design (WSD), or – Load Resistance Factored Design (LRFD)", (latest revision), American Petroleum Institute.

3.   Bai, Y. (1989), "Load Carrying Capacity of Tubular Members in Offshore Structures", Ph.D. Thesis, Hiroshima University, Jan. 1989.

4.   Batterman, C.S. (1965), "Plastic Buckling of Axially Compressed Cylindrical Shells", AIAA J., Vol.3 (1965), pp.316-325.

5.   Bouwkamp, J.G. (1975), "Buckling and Post-Suckling Strength of Circular Tubular Section", OTC, No-2204, PP.583-592.

6.   Chen, W.F. and Han, D.J. (1985),"*Tubular Members in Offshore Structures*", Pitman Publishing Ltd, (1985).

7.   Det norske Veritas (1981), Rules for Classification of Mobile Offshore Units (1981).

8.   Gerard, G. (1962), "*Introduction to Structural Stability Theory*", McGraw-Hill International Book Company, New York.

9.   Rashed, S.M.H (1980), "Behaviour to Ultimate Strength of Tubular Offshore Structures by the Idealized Structural Unit Method", Report SK/R 51, Division of Marine Structure, Norwegian Institute of Technology, Trondheim, Norway.

10.   Reddy, B.D. (1979), "An Experimental Study of the Plastic Buckling of Circular Cylinder in Pure Bending", Int. J. Solid and Structures, Vol. 15, PP. 669-683.

11.   Smith, C.S., Somerville, W.L. and Swan, J.W. (1979), "Buckling Strength and Post-Collapse Behaviour of Tubular Bracing Members Including Damage Effects", BOSS, PP.303-325.

12.   Toi, Y. and Kawai, T. (1983), "Discrete Limit Analysis of Thin-Walled Structures (Part 5) - Non-axisymmetric Plastic Buckling Mode of Axially Compressed Circular Shells", J. Society of Naval Arch. of Japan, Na.154, pp.337-247 (in Japanese).

13. Ueda, Y., Akamatsu, T. and Ohmi, Y. (1969), "Elastic-Plastic Analysis of Framed Structures Using Matrix Method (2nd Rep.)", J. Society of Naval Arch. of Japan, Vol.126, pp.253- 262 (in Japanese).

14. Ueda, Y. and Fujikubo, M. (1986), "Plastic Collocation Method Considering Strain-Hardening Effects", J. Society of Naval Arch. of Japan, Val.160, pp.306-317 (in Japanese).

15. Ueda, Y., Rashed, S.M.H. and Nakacho, K. (1984), "New Efficient and Accurate Method of Nonlinear Analysis of Offshore Structures", Proceeding of OMAE, PP.528-536.

16. Ueda, Y. and Yao, T. (1982), "The Plastic Node Method: A New Method of Plastic Analysis", Computer Methods in Appl. Mech. and Eng., Val.34, pp.1089-1104.

17. Yao, T., Fujikubo, M., Bai, Y., Nawata, T. and Tamehiro, M. (1986), "Local Buckling of Bracing Members (1st Report)", Journal of Society of Naval Architects of Japan, Vol. 160.

18. Yao, T., Fujikubo, M. and Bai, Y., Nawata, T. and Tamehiro, M. (1988), "Local Buckling of Bracing Members (2nd Report)", Journal of Society of Naval Architects of Japan, Vol. 164.

This Page Intentionally Left Blank

Part II

Ultimate Strength

Chapter 10   Ultimate Strength of Plates and Stiffened Plates

10.1 Introduction

10.1.1 General

Stiffened plates are frequently used as load-bearing components in marine structures. Typical example uses are the hull girder of a ship, the pontoons of a semi-submersible, and the deck of offshore platforms. The main type of framing system in hull girders consists of relatively closely spaced longitudinal stiffeners with more widely spaced heavier girders in the transverse direction. This is illustrated in Figure 10.1 for a bottom/side structure. The hydrostatic load, that is the difference between external and internal pressure, is transfer from plates to stiffeners, which again, through beam action, transfer the loads to the transverse girders.
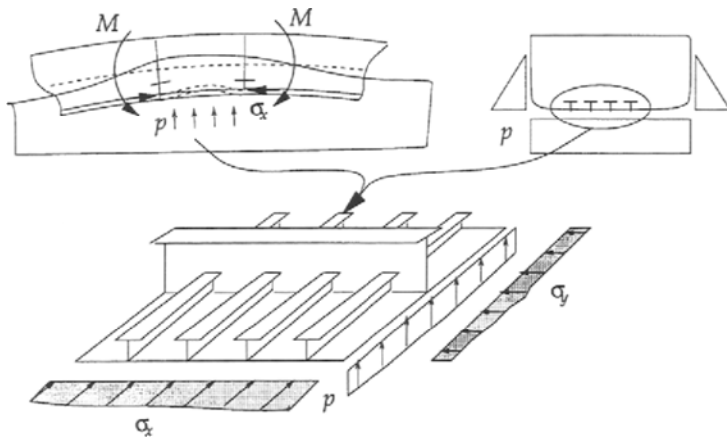
Figure 10.1   Stiffened Panels in a Ship Bottom Structure

As illustrated in Figure 10.1, the bottom plates will, in addition to the hydrostatic pressure, be subjected to bi-axial in-plane loads caused by the longitudinal bending of the hull girder and by the hydrostatic pressure applied on the sides.

Factors affecting the behavior of stiffened plates are e.g. stiffener slenderness and spacing, plate geometry and material yield stress. In addition, residual stresses, initial deformation, boundary conditions and types of loading will also affect the behavior of stiffened plates.

The potential failure modes for plates (or stiffened plates) under combined loads may be classified as:

- Buckling and collapse of plates - Lateral deflection develops in post-buckling region and ultimate strength is reached due to yielding, see Sections 10.3 and 10.4.

- Collapse of stiffeners with associated plates – Beam-column mode buckling in which attaching plates are accounted for as effective plates, see Section 10.5.1.

- Tripping of stiffeners – Tripping due to buckling of stiffeners and loss of the rotational restraint provided by the plating, see Section 10.5.2.

- Grillage buckling - Involves bending of transverse girders and longitudinal stiffeners, see Section 10.6.

As a book for graduate courses, the objective of this Chapter is to give an introduction to buckling strength analysis, while more details for mathematical theory may be found from the books listed in the references. Some equations from design codes are used for illustration and educational purpose only and engineering projects should directly use the relevant codes without any deviations from them.

10.1.2 Solution of Differential Equation

The procedure for calculating the elastic buckling load is illustrated for an initially plane plate subjected to an in-plane uniform compression. The equilibrium equation for a plate is given by:

$$\nabla^4 w = \frac{1}{D}\left(q + N_x \frac{\partial^2 w}{\partial x^2} + 2N_{xy}\frac{\partial^2 w}{\partial x \partial y} + N_y \frac{\partial^2 w}{\partial y^2}\right) \tag{10.1}$$

where the plate stiffness is given by:

$$D = \frac{Et^3}{12(1-v^2)} \tag{10.2}$$

and,

$$\nabla^4 = \left(\nabla^2\right)^2 = \left(\frac{\partial^2}{\partial x^2} + \frac{\partial^2}{\partial y^2}\right)^2 \tag{10.3}$$

The quantities,

$$\left.\begin{array}{l} N_x = \sigma_x t \\ N_y = \sigma_y t \\ N_{xy} = \sigma_{xy} t \end{array}\right\} \tag{10.4}$$

are the membrane stress resultants.

For simply supported plates under pure compression (see Figure 10.2), Eq. (10.1) takes the form:

$$\nabla^4 w = \frac{N_x}{D} \frac{\partial^2 w}{\partial x^2} \tag{10.5}$$

Based on the boundary conditions, the following displacement function are assumed and submitted to Eq. (10.5):

$$w = C_{mn} sin\frac{m\pi x}{a} sin\frac{n\pi y}{b} \tag{10.6}$$

where m and n are number of half waves in the x- and y-directions. The solution gives elastic buckling stress as given by the expression:

$$\sigma_\varepsilon = \frac{\pi^2 E}{12(1-v^2)}\left(\frac{t}{b}\right)^2 \cdot c = \frac{\pi^2 D}{tb^2} \cdot c \tag{10.7}$$

where c is a factor depending on the plate aspect ratio a/b, (see Figure 10.3).
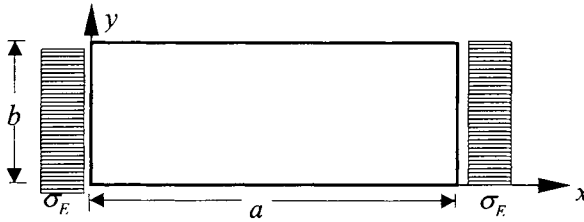
Figure 10.2   Simply Supported Plate Subjected to Uniform Compression.
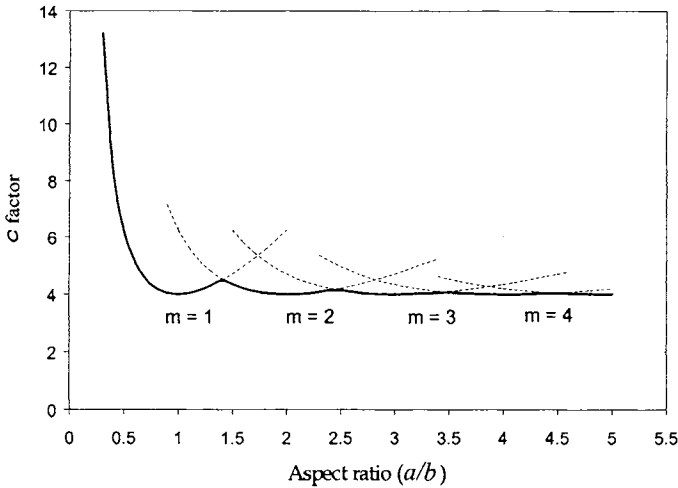
Figure 10.3   Buckling Coefficient Versus Plate Aspect Ratio.

In Figure 10.3, the buckling coefficient c has been plotted against the aspect ratio for a simply supported plate subjected to uniform compression. It appears that the minimum buckling stress occurs when the length is a multiple of the width. For intermediate values, the number of waves is incompatible with the plate's length, hence raising the buckling load. In practice, however, this additional strength is not taken into account.

10.1.3 Boundary Conditions

The actual boundary conditions will differ from the idealized cases. The major influence stems from the conditions at the unloaded edges. With reference to Figure 10.4, plate F can be considered as restrained, plate B as constrained, and plate A as unrestrained. In the restrained case, the edges remain undistorted while in the constrained case, lateral deflection is allowed but the edges are forced to remain straight. In the unrestrained case, the edges are completely free with respect to lateral deflection. The difference in boundary conditions, between plates B and F, is caused by the aspect ratio. The closeness of the transverse girders at F does not allow lateral deflection, while that may easily occur at the mid-section of plate B.
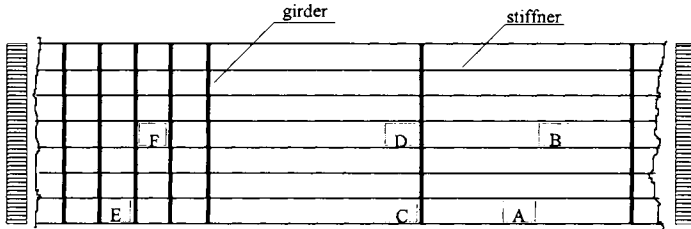
Figure 10.4   Various Boundary Conditions for Plate Elements in a Stiffened Panel.

In general the boundary conditions of the loaded edges do not have a significant influence on the ultimate strength. In this Chapter, the strength criteria are based on the assumption that, at the ultimate load condition:

- All boundary conditions may be taken as simply supported (due to yielding)

- Boundary edges are kept straight by the supporting structures

These two approximations will lead to slightly pessimistic, but adequate results.

10.1.4 Fabrication Related Imperfections and In-Service Structural Degradation

Several sources of structural deterioration affecting the buckling and ultimate strength may exist in the actual structure, such as:

- Residual stresses due to welding

- Initial deflection due to welding and other fabrication related processes

- Plate perforations such as e.g. manholes and cut-outs

- Corrosion damages and fatigue cracks of structures in-service

Usually residual stresses and initial deflection are implicitly included in the strength formulations as long as these do not exceed the fabrication tolerance criteria. If other types of

structural deterioration are present, it is recommended that additional strength analyses by more refined methods be performed to derive reduction factors.

The welding induced residual stress pattern in a stiffened panel is shown in Figure 10.5, including a tension block in yield at the stiffener attachment, which is balanced by a zone of uniform compressive residual stresses in the center of the plate. The magnitude of the compressive residual stresses may be obtained from equilibrium considerations:

$$\frac{\sigma_r}{\sigma_Y} = \frac{2\eta}{\dfrac{b}{t} - 2\eta} \tag{10.8}$$

The value of η tends to be high for as-welded structures. However, if the member is subject to alternating in-service loads, the residual stresses will be reduced due to shakeout by occasional tensile loads. Faulkner (1975) has suggested that design values of η may be taken between 3 and 4.5.
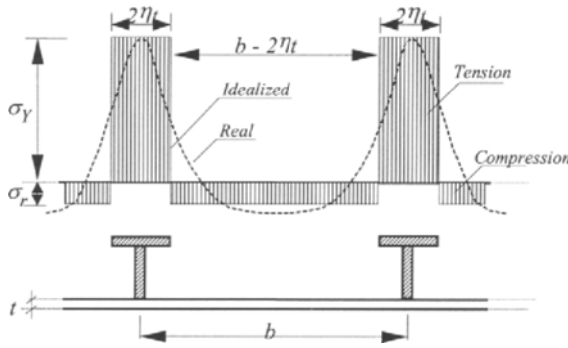
Figure 10.5   Welding Stress Pattern in Plates

The effect of residual stresses may cause a loss of compressive plate stiffness because of premature yielding in the compression zone. A reduction factor R_r may be introduced for strength analysis as below.

$$R_r = 1 - \frac{\sigma_r}{\sigma_Y}\frac{E_t}{E} = 1 - \frac{2\eta}{\dfrac{b}{t} - 2\eta}\frac{2(\beta-1)}{\beta}, \quad 1 < \beta < 2.5 \tag{10.9}$$

where E_t is the tangent modulus of the plate.

The levels and distributions of residual stresses in plates and stiffeners are illustrated in Figure 10.5. They vary depending on the plate's material properties and on the fabrication methods used, such as, rolling, welding, mechanical straightening, and heat treatment. Special high strength steels allow large heat affected zones with considerable residual stresses to form. High residual stresses may be a considerable source to structural strength loss.

The welding induced residual tensile stresses along welded edges are assumed to not exceed the plate's yield stress. For mild steels, the compressive residual stresses in any direction may

be taken as 5 to 10 percent of the plate's yield stress. For high strength steels, a higher value for the compressive residual stresses should be considered.

For the stiffener web, the residual compressive stresses may be taken as 3 to 5 percent of the stiffener yield stress for mild steels and a little higher for high strength steels.

Initial structural imperfections may be induced by welding, manufacturing, heat treatment, transportation, and storage. The effect of imperfections on the ultimate strength of plates depends strongly on their shape. In most theoretical studies, initial deflections have been assumed to have the same shape as the buckling mode, because initial deflection has the most significant influence on the ultimate strength when its shape coincides with the buckling mode. Statistical analysis of measured plate distortions shows that the amplitude of the buckling component is about half of the maximum distortions.

Various formulas are available for predicting the maximum distortion. However, the following relation has been frequently used:

$$\frac{\delta_o}{t} = C_2 \frac{b}{t} - C_3, \frac{b}{t} > 40 \tag{10.10}$$

where, typically, $C_2 = 0.016$ and $C_3 = 0.36$.

The fabrication tolerance criteria are usually defined in design codes for the strength criteria defined. If the fabrication tolerance criteria are violated, the imperfections will have to be repaired. Alternatively the effects of imperfections are to be explicitly accounted for using advanced formulae or numerical/mechanical tests.

10.1.5 Correction for Plasticity

For plates with a low width to thickness ratio, Eq. (10.7) may theoretically predict a critical stress if an excess of the yield stress occurs, but physically it cannot. Various methods exist to account for plasticity effects. A convenient technique for modifying the elastic critical stress caused by plasticity is the ϕ-method, where the elastic-plastic buckling stress is given by:

$$\sigma_{cr} = \phi \cdot \sigma_Y \tag{10.11}$$

where ϕ is an empirical function of the structural slenderness, as defined below:

$$\bar{\lambda} = \sqrt{\frac{\sigma_Y}{\sigma_E}} \tag{10.12}$$

Various expressions for ϕ exist. One method for plasticity correction is to use an elliptical interaction equation (Odland, 1988):

$$\left(\frac{\sigma_{cr}}{\sigma_Y}\right)^2 + \left(\frac{\sigma_{cr}}{\sigma_E}\right)^2 = 1$$

It is seen that:

$$\sigma_{cr} \rightarrow \sigma_Y \text{ when } \sigma_E \rightarrow \infty$$
$$\sigma_{cr} \rightarrow \sigma_E \text{ when } \sigma_E \ll \sigma_Y$$

Hence, the formula converges to the correct solution for both of stocky members and slender members. Solving for σ_{cr}, we obtain:

$$\sigma_{cr} = \frac{\sigma_Y}{\sqrt{1+\bar{\lambda}^4}} \quad \Rightarrow \quad \phi = \frac{1}{\sqrt{1+\bar{\lambda}^4}} \tag{10.13}$$

Another well-known solution is the so-called Johnson-Ostenfeld formula that is adopted by several North American Design Codes:

$$\phi = \begin{cases} 1 - \dfrac{\bar{\lambda}^2}{4}, & \bar{\lambda}^2 \leq 2 \\ \dfrac{1}{\bar{\lambda}^2}, & \bar{\lambda}^2 \geq 2 \end{cases} \tag{10.14}$$

10.2 Combined Loads

In limit state design, buckling criteria and ultimate strength criteria are also termed Serviceability Limit State (SLS) and Ultimate Limit State (ULS).

10.2.1 Buckling – Serviceability Limit State

In the case of a combined loading, as shown in Figure 10.6, the above procedure may be applied if an equivalent stress and an equivalent elastic buckling stress are defined. This is conveniently expressed by the following interaction formula:

$$\left(\frac{\sigma_e}{\sigma_{Ee}}\right)^c = \left(\frac{\sigma_x}{\sigma_{Ex}}\right)^c + \left(\frac{\sigma_y}{\sigma_{Ey}}\right)^c + \left(\frac{\tau}{\tau_E}\right)^c \tag{10.15}$$

where σ_{Ex}, σ_{Ey} and τ_E are the elastic buckling stresses when the corresponding stress component acts alone and σ_{Ee} is the equivalent elastic buckling stress corresponding to the equivalent stress $\sigma_e = \sqrt{\sigma_x^2 + \sigma_y^2 - \sigma_x \sigma_y + 3\tau^2}$.
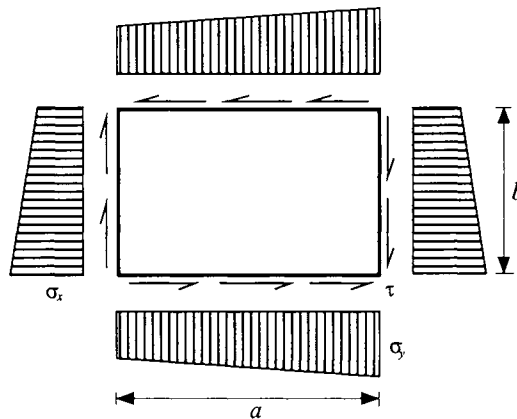
Figure 10.6   Combined Loading.

The equivalent reduced slenderness ratio to be used in the above plasticity correction may then be expressed as (DNV, CN 30.1, 1995):

$$\bar{\lambda}_e^2 = \frac{\sigma_Y}{\sigma_{Ee}} = \frac{\sigma_Y}{\sigma_e}\left[\left(\frac{\sigma_x}{\sigma_{Ex}}\right)^c + \left(\frac{\sigma_y}{\sigma_{Ey}}\right)^c + \left(\frac{\tau}{\tau_E}\right)^c\right]^{\frac{1}{c}}$$

(10.16)

The exponent c depends on the plate aspect ratio. Square plates tend to be more sensitive to combined loading than long plates, because the two buckling modes coincide for bi-axial compression. Therefore, a linear interaction is often used for square plates and an elliptic interaction for long plates. DNV CN 30.1 (1995) propose the following equation for the buckling strength of the plate under combined loads:

$$\sigma_{cr} = \frac{\sigma_Y}{\sqrt{1 + \bar{\lambda}_e^4}}$$

(10.17)

10.2.2 Ultimate Strength – Ultimate Limit State

The ultimate strength of the plate may be estimated as (DNV, CN 30.1, 1995):

$$\sigma_{ult} = \frac{\sigma_Y}{\sqrt{1 + \bar{\lambda}_e^4}} \quad , \; \bar{\lambda}_e \le 1$$

(10.18)

$$\sigma_{ult} = \frac{\sigma_Y}{\bar{\lambda}_e \sqrt{2}} \quad , \; 1.0 < \bar{\lambda}_e \le 5.0$$

(10.19)

The Serviceability Limit State (SLS) and Ultimate Limit State (ULS) are compared in Figure 10.7. For very slender plates, the ultimate strength is significantly larger than buckling strength.
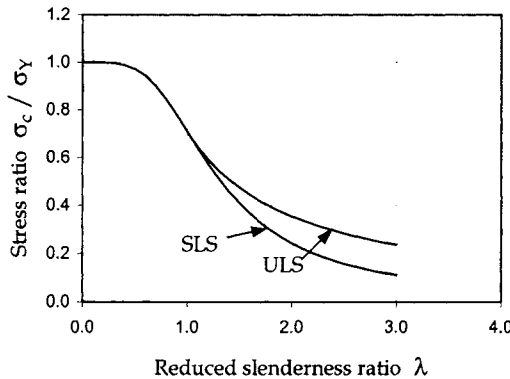
Figure 10.7   Ultimate Strength versus Buckling Strength of Plates.

Balint et al (2002) proposed the following equation for ultimate strength of plates under combined loads:

$$\left(\frac{\sigma_1}{\sigma_{L1}}\right)^4 - \alpha\left(\frac{\sigma_1}{\sigma_{L1}}\right)\left(\frac{\sigma_2}{\sigma_{L2}}\right) + \left(\frac{\sigma_2}{\sigma_{L2}}\right)^2 + \left(\frac{\tau}{\tau_L}\right)^2 = 1 \tag{10.20}$$

where,

σ_1 = Axial stress in direction 1

σ_2 = Axial stress in direction 2

τ = Shear stress

σ_{L1} = Limiting axial stress for σ_1

σ_{L2} = Limiting axial stress for σ_2

τ_L = Limiting shear stress

Following Bai (2001), the following strength criteria may also be applicable for ultimate strength (of plates or stiffened plates) under combined loads:

$$\left(\frac{\sigma_1}{\sigma_{L1}}\right)^2 - \alpha\left(\frac{\sigma_1}{\sigma_{L1}}\right)\left(\frac{\sigma_2}{\sigma_{L2}}\right) + \left(\frac{\sigma_2}{\sigma_{L2}}\right)^2 + \left(\frac{\tau}{\tau_L}\right)^2 + \left(\frac{p}{p_L}\right)^2 = 1 \tag{10.21}$$

where,

p = Lateral pressure

p_L = Limiting lateral pressure

Eq.(10.21) has been proposed because it approaches to von Mises yield conditions for inelastic buckling cases and may lead to linear interaction for elastic buckling cases. According to API 2V (1987), the coefficient α may be taken as 0 when both stresses σ_1 and σ_2 are compressive, and as 1 when either σ_1, σ_2 or both are tensile. To be accurate, the coefficient α should be derived based on finite element analysis and mechanical test.

10.3 Buckling Strength of Plates

Johnson-Ostenfeld formula (or Odland, 1988) may be applied for plasticity correction. To calculate elastic buckling stress under combined loads, the equations in Section 10.2 may be used. The elastic buckling strength for plates under compressive stress and in-plane bending may be expressed as

$$\sigma_E = k_s \frac{\pi^2 E}{12(1-\upsilon^2)}\left(\frac{t}{b}\right)^2 \tag{10.22}$$

An expression giving good accuracy with the exact elastic buckling solution for a simple supported plate exposed to pure shear stress is given in Timoshenko and Gear (1961),

$$\tau_{EI} = k_s \frac{\pi^2 E}{12(1-\upsilon^2)}\left(\frac{t}{b}\right)^2 \tag{10.23}$$

where

$$k_s = 4.0\left(\frac{b}{a}\right)^2 + 5.34 \tag{10.24}$$

υ =Poisson's ratio

Yield stress in shear may be estimated as $\dfrac{\sigma_o}{\sqrt{3}}$ where σ_0 =yield stress of the plate .

10.4 Ultimate Strength of Un-Stiffened Plates

10.4.1 Long Plates and Wide Plates

Slender plates can carry loads larger than what is predicted by elastic theory if their unloaded edges are constrained to remain straight. Because of large lateral deflections, membrane stresses develop in the transverse direction, which tend to stabilize the plates. At this stage, the distribution of stresses along the unloaded edges is no longer uniform but rather, it increases towards the stiffeners. According to the effective width method, the ultimate strength is obtained when the edge stress, σ_e, in Figure 10.8, approaches the yield stress. The following formula has been widely used for simply supported plates where the unloaded edges are constrained to remain straight (Faulkner, 1975).

$$\frac{b_e}{b} = \frac{\sigma_{xm}}{\sigma_y} = \begin{cases} \dfrac{2}{\beta} - \dfrac{1}{\beta^2} & \beta \geq 1 \\ 1 & \beta \leq 1 \end{cases} \tag{10.25}$$

where the plate slenderness ratio is given by,

$$\beta = \frac{b}{t}\sqrt{\frac{\sigma_Y}{E}} \tag{10.26}$$
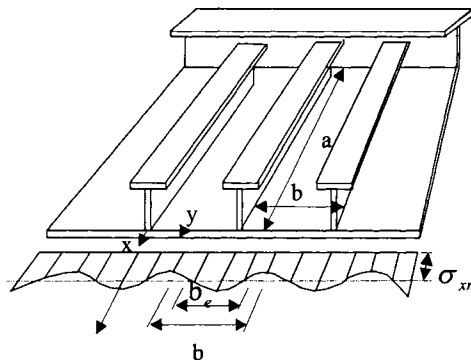
Figure 10.8   Actual Stress Distribution in a Compressed Stiffened Plate

Eq. (10.35) accounts for a reasonable degree of initial deflection in the buckling mode, but does not account for residual stresses.

The following effective width formula may be used for compressive loads acting on the long edge, a/b≥1.0 and short edge, a/b<1.0 (Mansour, 1997).

$$b_e = \begin{cases} C_b & \text{for} \quad \dfrac{a}{b} \geq 1.0 \\ \dfrac{a}{b} C_b + 0.08 \left(1 - \dfrac{a}{b}\right)\left(1 - \dfrac{1}{\beta^2}\right)^2 \leq 1.0 & \text{for} \quad \dfrac{a}{b} < 1.0 \end{cases} \tag{10.27}$$

$$C_b = \begin{cases} 1 & \text{for} \quad \beta < 1.25 \\ \dfrac{2.25}{\beta} - \dfrac{1.25}{\beta^2} & \text{for} \quad 1.25 \leq \beta < 3.5 \\ \sqrt{\dfrac{4\pi^2}{12(1 - \upsilon^2)} \dfrac{1}{\beta^2}} & \text{for} \quad \beta \geq 3.5 \end{cases} \tag{10.28}$$

10.4.2 Plates Under Lateral Pressure

Ultimate strength of plates in shear may be assumed to be shear yield stress.

10.4.3 Shear Strength

Ultimate strength of plates in shear may be assumed to be shear yield stress.

10.4.4 Combined Loads

The equations for plates under combined loads may be found from Section 10.2.2.

10.5 Ultimate Strength of Stiffened Panels

10.5.1 Beam-Column Buckling

When a stiffened panel is subjected combined axial stress σ and bending moment M (induced by lateral load), the ultimate strength may be predicted using Mansour (1997):

$$\frac{\sigma}{\sigma_{column}} + C_M \frac{M}{\sigma_{beam}} = 1 \tag{10.29}$$

where the column buckling strength for stiffened plates, σ_{column}, may be predicted using Johnson-Ostenfeld formula or Perry-Robertson formula based on elastic buckling stress:

$$\sigma_E = \frac{\pi^2 E I_s}{l_s^2 A_s} \tag{10.30}$$

where

    E =Elasticity modulus

    I_s =Moment of inertia of the stiffened plate

l_s =Stiffener length

A_s =Cross sectional area of the stiffened plate

While Johnson-Ostenfeld formula for column buckling is very simple, it does not account for the effect of initial imperfection. An alternative equation is Perry-Robertson formula, see Part II Chapter 8 of this book. The coefficient C_M is a function of the ratio of the bending moment acting at the two ends of the beam M_A / M_B:

$$C_m = \frac{0.6 + 0.4 M_A / M_B}{1 - \sigma / \sigma_E}$$ (10.31)

The ultimate bending stress for the stiffened plates under pure bending may be taken as fully plastic bending moment.

10.5.2 Tripping of Stiffeners

When the web height to thickness ratio is large combined with a flange that is inadequate to remain straight under the combined uniaxial compressive load and lateral pressure, the stiffener may twist sideways in the tripping failure mode. The tripping strength may be predicted Johnson-Ostenfeld formula and elastic buckling stress equation (see Eq.(4.30) in Part I Chapter 4 and e.g. Ma (1994)).

10.6 Gross Buckling of Stiffened Panels (Overall Grillage Buckling)

Using orthotropic plate theory, Mansour (1977) derived the following buckling equation that may be used in the number of stiffeners in each direction exceeds 3,

$$\sigma_E = k \frac{\pi^2 \sqrt{D_x D_y}}{h_x B^2}$$ (10.32)

where B is gross panel width, h_x is effective thickness. For simply supported gross panel, k may be taken as

$$k = \frac{m^2}{\rho^2} + 2\mu + \frac{\rho^2}{m^2}$$ (10.33)

where m is number of half-waves of buckled plate, μ and ρ are torsion coefficient and virtual aspect ration respectively.

10.7 References

1.   ABS (2001), "Rules for Building and Classing Steel Vessels", American Bureau of Shipping.

2.   API 2V (1987), "Bulletin on Design of Flat Plate Structures", 1st Edition, 1987 (ANSI/API Bull 2V-1992).

3.   Amdhal, J. (1997), *"Buckling and Collapse of Structures"*, Lecture Notes, NTNU.

4.   Bai, Y. (2001), *"Pipelines and Risers"*, Elsevier Ocean Engineering Book Series, Vol. 3.

5.   Balint, S.W., Serrahn, C.S. and Chang, B.C. (2002), "Background to New Edition of API Bulletin 2V: Design of Flat Plate Structures", Proceedings of Offshore Technology Conferences, OTC 14187.

6.   DNV CN 30.1 (1995), "Buckling Strength Analysis", Det Norske Veritas.

7.   Ellinas, C.P., Supple, W.J., and Walker, A.C. (1984), *"Buckling of Offshore Structures"*, Granada.

8.   Faulkner, D. (1975), "A Review of Effective Plating for Use in the Analysis of Stiffened Plating in Bending and Compression", Journal of Ship Research, Vol. 19.

9.   Faulkner, D. (1979), "Design Against Collapse for Marine Structures", International Symposium on Advances in Marine Technology, Trondheim.

10.   Galambos, T.V. (2000), *"Guide to Stability Design Criteria for Metal Structures"*, 5th Edition, John Wiley & Sons.

11.   Hughes, O. (1983), *"Ship Structural Design – A Rationally-based Computer-Aided, Optimization Approach"*, SNAME, Society of Naval Architects and Marine Engineers.

12.   Jones, N. (1976), "Plastic Behavior of Ship Structures", Transactions of SNAME, Vol. 84, pp. 115-139.

13.   Ma, M. (1994), "Elastic and Inelastic Analysis of Panel Collapse by Stiffener Buckling", Ph.D. Thesis, Virginia Polytechnic Institute and State University.

14.   Mansour, A. (1977), "Gross Panel Strength under Combined Loading", Ship Structures Committee Report, SSC-270.

15.   Mansour, A. E. (1997): "Assessment of Reliability of Ship Structures", SSC Report, SSC-398.

16.   Odland, J.(1988), "Improvement in Design Methodology for Stiffened and Unstiffened Cylindrical Structures", BOSS-1988, Edited by T. Moan, Tapir Publisher, June 1988.

17.   Timoshenko S. and Gere, J.M. (1961), *"Theory of Elastic Stability"*, McGraw-Hill Book Company, Inc.

This Page Intentionally Left Blank

Part II

Ultimate Strength

Chapter 11 Ultimate Strength of Cylindrical Shells

11.1 Introduction

11.1.1 General

Cylindrical shells are important structural elements in offshore structures, submarines and airspace crafts. They are very often subjected to combined compressive stress and external pressure, and must be designed to meet the strength requirements. A theoretical load end-shortening curve representing unstiffened cylindrical shells under axial compression is shown in Figure 11.1. For a perfect shell, the stress-strain relation is linear until the bifurcation point, B, where buckling occurs and load-carrying capacity decreases sharply. For an imperfect shell, the stress-strain relation starts is non-linear from an early stage of loading, buckling occurs at point L without showing obvious bifurcation phenomenon.
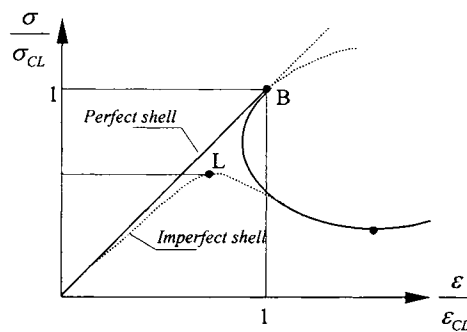
Figure 11.1   Stress Strain Relations for Perfect and Imperfect Shells

Strength of imperfect cylindrical shell may be significantly lower than the bifurcation load. The design of cylindrical shells is based on the modification of the theoretical predictions using a knockdown factor for imperfection effect.

11.1.2 Buckling Failure Modes

The characteristic geometric parameters of a stiffened cylindrical shell are defined in Figure 11.2.
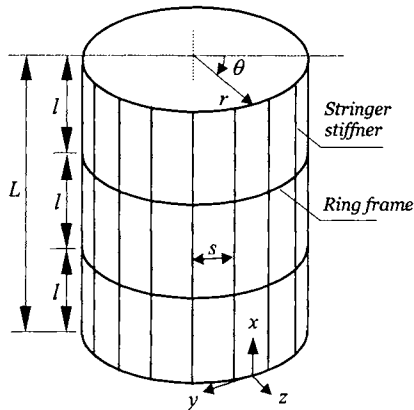
Figure 11.2   Geometrical Parameters of a Stiffened Cylindrical Shell

The boundary conditions are assumed simply supported and constrained. The design loads are:

- Compressive stress due to longitudinal force and bending moment
- External overpressure
- Combined compressive stress and external pressure

Major factors affecting strength of cylindrical shells include:

- Residual stresses and geometrical imperfections
- Dents
- Corrosion defects

The effects of residual stresses and geometric imperfections have been implicitly accounted for in the criteria discussed in this Chapter. However, if the fabrication tolerance is violated, or dents and significant corrosion defects are found in in-service structures, repair and additional strength analysis are necessary. For pressure vessels, pipelines and risers, criteria for pressurized cylinders under combined external/internal pressure, axial force and bending are given in Bai (2001), among other references.

11.2 Elastic Buckling of Unstiffened Cylindrical Shells

11.2.1 Equilibrium Equations for Cylindrical Shells

Figure 11.3 shows an infinitesimal element of a shell with its associated stress resultants from the membrane and bending actions. Considering equilibrium in the axial, circumferential, and radial directions, the following equations may be obtained:
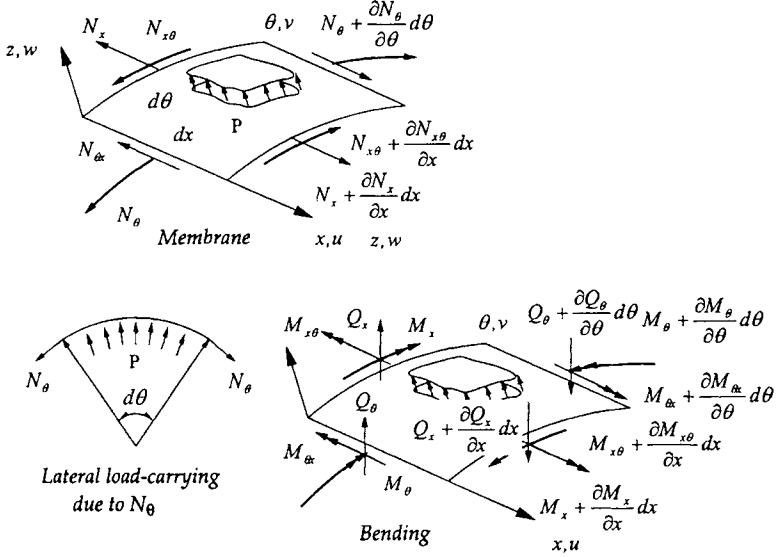
Figure 11.3   Shell Stress Resultants

$$r\frac{\partial N_x}{\partial x} + \frac{\partial N_{\theta x}}{\partial \theta} = 0 \tag{11.1}$$

$$r\frac{\partial N_{x\theta}}{\partial x} + \frac{\partial N_\theta}{\partial \theta} = 0 \tag{11.2}$$

$$\nabla^4 w = \frac{1}{D}\left(p + N_x\frac{\partial^2 w}{\partial x^2} + \frac{2}{r}N_{x\theta}\frac{\partial^2 w}{\partial x\partial\theta} + \frac{1}{r^2}N_\theta\frac{\partial^2 w}{\partial \theta^2} - \frac{1}{r}N_\theta\right) \tag{11.3}$$

where,

$$\begin{aligned}
N_x &= \sigma_x t \\
N_{x\theta} &= N_{\theta x} = \sigma_{x\theta} t \\
N_\theta &= \sigma_\theta t
\end{aligned} \tag{11.4}$$

$$\nabla^4 = \left(\nabla^2\right)^2 = \left(\frac{\partial^2}{\partial x^2} + \frac{1}{r^2}\frac{\partial^2}{\partial \theta^2}\right)^2$$

The plate stiffness, D, is given by:

$$D = \frac{Et^3}{12(1-v^2)} \tag{11.5}$$

The pressure, p, is positive outwards. Note the similarity between Eq. (11.3) and the corresponding expression for plate equilibrium by substituting:

$$\frac{\partial}{\partial y} = \frac{1}{r}\frac{\partial}{\partial \theta}, \frac{\partial^2}{\partial y^2} = \frac{1}{r^2}\frac{\partial^2}{\partial^2 \theta} \tag{11.6}$$

The only new term is N_θ/r, which represents the lateral component of the circumferential stress. Thus, unlike plates, cylindrical shells can carry lateral loads by pure membrane action and no bending. This is a very efficient property, but at the same time, this makes shells sensitive to buckling.

Eqs. (11.1) thru (11.3) form a coupled set of three non-linear equations with four variables-- N_x, $N_{x\theta}$, N_θ, and w. By introducing the kinematic and constitutive relationships, and applying the operator ∇, Eq. (11.3) may also be written as,

$$\nabla^8 w = \frac{\nabla^4}{D}\left(N_x \frac{\partial^2 w}{\partial x^2} + \frac{2}{r} N_{x\theta}\frac{\partial^2 w}{\partial x \partial \theta} + \frac{1}{r^2}N_\theta \frac{\partial^2 w}{\partial \theta^2}\right) - \frac{Et}{Dr^2}\frac{\partial^4 w}{\partial x^4} \tag{11.7}$$

which is also known as Donnel's equation.

11.2.2 Axial Compression

Consider a cylinder subjected to an axial compressive load, P. If the end effects are neglected, the following assumptions apply:

$$N_x = \frac{P}{2\pi r}, \quad N_{x\theta} = N_\theta = 0 \tag{11.8}$$

Introduction of these values into Eq. (11.7) gives:

$$D\nabla^8 w + \frac{Et}{r^2}\frac{\partial^4 w}{\partial x^4} + \frac{P}{2\pi r}\nabla^4\left(\frac{\partial^2 w}{\partial x^2}\right) = 0 \tag{11.9}$$

The solution to this differential equation takes the form:

$$w = \delta\left(\sin\frac{m\pi x}{l}\right)\sin n\theta \tag{11.10}$$

where m is the number of half waves in the longitudinal direction and n is the number of entire waves in the circumferential direction, which gives:

$$\sigma_{xE} = \frac{\pi^2 E}{12(1-v^2)}\left(\frac{t}{l}\right)^2\left[\frac{\left(m^2 + \bar{n}^2\right)^2}{m^2} + \frac{12 Z^2}{\pi^4}\frac{m^2}{\left(m^2 + \bar{n}^2\right)^2}\right] \tag{11.11}$$

where Z is the Batdorf parameter,

$$Z = \frac{l^2}{rt}\sqrt{(1-v^2)} \tag{11.12}$$

and

$$\bar{n} = \frac{nl}{\pi r} \tag{11.13}$$

The solution to Eq. (11.11) may be expressed as:

$$\sigma_{xE} = k_c \frac{\pi^2 E}{12(1-\nu^2)}\left(\frac{t}{l}\right)^2 \tag{11.14}$$

For cylinders of intermediate length, a close estimate of the smallest critical load may be obtained by analytically minimizing Eq. (11.11) with respect to the following quantity:

$$\left(\frac{m^2 + \bar{n}^2}{m}\right)^2$$

Then, the minimum is found to be:

$$\left(\frac{m^2 + \bar{n}^2}{m}\right)^2 = \frac{2\sqrt{3}}{\pi^2} Z \tag{11.15}$$

which gives the following critical load,

$$\sigma_{xE} = \frac{\pi^2 E}{12(1-\nu^2)}\left(\frac{t}{l}\right)^2 \cdot \frac{4\sqrt{3}}{\pi^2} Z = 0.605 \frac{Et}{r} = \sigma_{cl} \tag{11.16}$$

This is the classical solution for an axially compressed cylinder. It should be noted that m and $\bar{n}$ are treated as continuous variables (for diamond-shaped bulges) in the minimization process while they are actually discrete quantities. The correct values can be found by trial and error.

For short cylinders, the buckling mode will be asymmetric with m=1 and n=0, which is plate-like buckling. The following buckling coefficient may be obtained:

$$k_c = 1 + \frac{12 Z^2}{\pi^4} \tag{11.17}$$

is valid for:

$$Z < \frac{\pi^2}{2\sqrt{3}} = 2.85 \tag{11.18}$$

For long cylinders, column buckling is a potential collapse mode, and the buckling stress is expressed by:

$$\sigma_E = \frac{\pi^2 EI}{Al^2} \approx \frac{\pi^2 E}{2}\left(\frac{r}{l}\right)^2 \tag{11.19}$$

11.2.3 Bending

In elastic region, studies carried out in this field indicate that the buckling stress in bending is close to that for buckling in axial compression for all practical purposes, see Timoshenko and Gere (1961). It is more complicated to analyze cylinders subjected to bending because,

- The initial stress distribution is no longer constant around the circumference.

- The pre-buckling deformations of cylinders are highly non-linear due to ovalization of the cross-section.

Brazier (1927) was the first researcher who derived elastic bending moment and cross-sectional ovalization as a function of curvature in elasticity. He found that the maximum moment is reached when critical stress is

$$\sigma_{xE} = 0.33 \frac{Et}{r} \tag{11.20}$$

However, in plastic region, the buckling strain for cylinders in pure bending may be substantially higher than that given by plastic buckling theory for cylinders in pure compression. Many researchers have been trying to derive mathematical solutions for inelastic cylinders in pure bending (see Ades, 1957 and Gellin, 1980). Unfortunately no one has been successful so far.

The effect of boundary conditions may also play an important role affecting buckling strength of un-stiffened short shells under bending. The shorter the cylinder, the higher the buckling strength is. This is because pre-buckling deformation, which is less for shorter cylinder, may reduce shell buckling strength. When the length of the cylinder is long enough, the bending strength may be close to those given by Beazier (1927), Ades (1957) and Gellin (1980).

11.2.4 External Lateral Pressure

In the pre-buckling state, the external pressure sets up compressive membrane stresses in the meridian direction. Retaining only the linear terms in Eq. (11.3):

$$N_\theta = -pr \tag{11.21}$$

Introducing Eq.(11.21) into Eq. (11.8) yields the following stability equation:

$$D\nabla^8 w + \frac{Et}{r^2} \frac{\partial^4 w}{\partial x^4} + \frac{1}{r} p\nabla^4 \left(w \frac{\partial^2 w}{\partial \theta^2} \right) = 0 \tag{11.22}$$

The displacement function is of the same form as the axial compression. Introducing Eq. (11.22) yields:

$$\sigma_{\theta E} = -\frac{pr}{t} = \frac{\pi^2 E}{12(1-v^2)} \left(\frac{t}{l}\right)^2 \left[\frac{\left(1+\bar{n}^2\right)^2}{\bar{n}^2} + \frac{12Z^2}{\pi^4 \bar{n}^2 \left(1+\bar{n}^2\right)^2} \right] \tag{11.23}$$

where one axial wave (m = 1) gives the lowest buckling load. The last term is interpreted to be the buckling coefficient, k_θ. The smallest value of k_θ may be determined by trial. If $\bar{n}$ is assumed large (>>1), analytically minimizing Eq. (11.23) gives:

$$k_\theta = \frac{4\sqrt{6}}{3\pi} \cdot \sqrt{Z} \tag{11.24}$$

The approximate buckling coefficient valid for small and medium values of Z now reads:

$$k_\theta = 4\sqrt{1 + \frac{2Z}{3\pi^2}} \tag{11.25}$$

The first term is identical to the buckling coefficient of a long plane plate. When l/r approaches infinity, Eq. (11.23) reduces to:

$$\sigma_{\theta E} = \frac{n^2 E}{12(1-v^2)} \left(\frac{t}{r}\right)^2 = 0.275E(\frac{t}{r})^2 \tag{11.26}$$

Long cylinders fail by ovalization for which n = 2 and the above equation yield to elastic buckling stress for pipelines and risers under external pressure.

11.3 Buckling of Ring Stiffened Shells

This section discusses the ultimate strength of cylindrical shells strengthened by ring frames, which are subjected to axial compression, external pressure and their combinations. The formulation deals with shell failure. For the stiffener design, separate consideration should be given against general stability and torsional instability, see Ellinas (1984).

11.3.1 Axial Compression

The potential failure modes for ring stiffened shell under compression are:

- Un-stiffened cylinder or inter-ring shell failure (axi-symmetric collapse & diamond shape collapse)

- General instability

- Ring stiffener failure

- Combination of the above

Due to the catastrophic consequence, the failure mode of general instability failure is avoided by placing requirements on stiffener geometry (such as moment of inertia) in design codes. Design codes require that the buckling stress for general instability be 2.5 times of that for local panel buckling.

Once general instability failure is suppressed, ring stiffener failure is unlikely to occur in ring-stiffened cylinders. However, tripping of the ring stiffeners may possibly occur in conjunction with general instability, weakening the strength against general instability. Therefore, geometric requirements are applied to ring stiffeners to avoid the interaction of tripping and general instability.

In the following, formulation is given for the 1st failure mode listed in the above: un-stiffend cylinder failure. Balint et al (2002) proposed to use the format of Batdorf for elastic buckling of perfect cylinders:

$$\sigma_{crx} = k_{xL} \frac{\pi^2 E}{12(1-\upsilon^2)} \left(\frac{t}{L_r}\right)^2 \tag{11.27}$$

where the buckling coefficient k_{xL} is a function of geometric parameter M_{xL} (Capanoglu and Balint, 2002):

$$k_{xL} = \sqrt{1 + \frac{150}{D/t}(\alpha_{xL})^2 (M_x)^4} \tag{11.28}$$

and where

$$M_x = \frac{L_r}{\sqrt{Rt}} \tag{11.29}$$

and where L_r is the ring spacing. The coefficient α_{xL} may be expressed as (Capanoglu and Balint, 2002):

$$\alpha_{xL} = \frac{9}{[300 + D/t]^{0.4}}$$ (11.30)

Eq.(11.27) will yield to buckling stress for flat plate when the plate curvature is small. This is an advantage over the critical buckling stress equation for long cylinders used in API Bulletin 2U and API RP 2A.

Inelastic buckling strength may be estimated using plasticity correction factor presented in Part II Chapter 10.

11.3.2 Hydrostatic Pressure

General

Three failure modes may possibly occur for ring stiffened cylinders under external pressure:

- Local inter-ring shell failure
- General instability
- Ring stiffener failure

For ring-framed cylinders subject to external hydrostatic pressure, BS5500 (1976) and Faulkner et al (1983) combined elastic buckling stress with Johnson-Ostenfeld plasticity correction factor, that was presented in Part II Chapter 10. It is noted that about 700 model tests, with geometries in the range of $6 \leq R/t \leq 250$ and $0.04 \leq L/R \leq 50$, lie above the so-called 'guaranteed' shell collapse pressure predicted by this formulation. The bias of the mean strength for this lower bound curve is estimated to be 1.17 and in the usual design range the COV is estimated to be 5% (Faulkner et al, 1983).

Local Inter-Ring Shell Failure

The best known solution for elastic buckling of the unsupported cylinder is that due to Von Mises which is given by (see Timoshenko and Gere, 1961)

$$p_E = \frac{\frac{Et}{R}}{n^2 - 1 + \frac{1}{2}\left(\frac{\pi R}{L}\right)^2} \left\{ \frac{1}{\left[\left[n^2\left(\frac{L}{\pi R}\right)^2 + 1\right]\right]^2} + \frac{t^2}{12R^2(1-\mu^2)}\left[n^2 - 1 + \left(\frac{\pi R}{L}\right)^2\right]^2 \right\}$$ (11.31)

minimized with respect to n (circumferential mode number).

Windenburg (1934) minimized the expression with respect to n, the number of complete circumferential waves or lobes. By making further approximations he obtained the following expression for the minimum buckling pressure:

$$p_E = \frac{0.919\,E(t/R)^2}{L/(Rt)^{\frac{1}{2}} - 0.636}$$ (11.32)

Eq.(11.32) is invalid for very small or very large values of $L/(Rt)^{\frac{1}{2}}$, but in the design range its accuracy is sufficient. The analysis assumes the cylinder is pinned at non-deflecting

cylindrical supports. More refined analyses are now available which, for example, consider the influence of the ring frames on the deformations before and during buckling. These analyses show that p_E becomes inaccurate for closely spaced frames. Nevertheless, the Von Mises expression is still widely used because it can be represented in a relatively simple form and it is in most cases only slightly conservative.

General Instability

Due to the catastrophic post-collapse characteristics associated with this failure mode, design codes require the effective moment of inertia for the ring stiffeners with associated shell plating to be sufficiently high so that the ratio of general and local elastic buckling stresses is 1.2 (e.g. ASME (1980) Boiler and Pressure Vessel Code).

Ring Stiffener Failure

Ring stiffener failure may occur as torsional buckling or tripping of the stiffeners, seriously weakening the resistance of the shell to general instability. Therefore, design codes specify requirements on the ring stiffener geometry to prevent this type of failure from occurring. Imperfections in the form of lateral deformations of the ring stiffeners may have a strong detrimental effect in reducing the stiffener's resistance to torsional buckling. Similar to tripping of stiffened plates, fabrication tolerance has been established on such imperfections.

11.3.3 Combined Axial Compression and Pressure

The strength of ringer stiffened cylinders under combined axial compression and external pressure may be expressed as:

$$\left(\frac{\sigma}{\sigma_c}\right)^m + \left(\frac{p}{p_{hc}}\right)^n \leq 1 \tag{11.33}$$

Recommendations by various codes are found differing widely, ranging from the linear interaction (m = n = 1) recommended by ECCS (1976) to a circular one (m = n = 2) required by DNV (2000). The ASME Code Case N-284 suggests a combination of straight lines and parabolas that appears to agree quite well with test data. Das et al (2001) suggested that the parabola (m = 1, n = 2) offers the best fit to available data and is very close to the ASME recommendations.

11.4 Buckling of Stringer and Ring Stiffened Shells

11.4.1 Axial Compression

General

This section is based on simplifications to Faulkner et al (1983), Ellinas (1984), Das et al (1992) and Das et al (2001). Stinger-stiffened cylinder buckling is usually the governing failure mode. Other failure modes such as local panel buckling, local stiffener tripping and general instability may also occur, see Ellinas (1984). In many practical design situations, buckling of stringer and ring stiffened shells is assessed as buckling of stiffened plates using formulation presented in Part II Chapter10.

Local Panel Buckling

Similar to Eq. (10.19) in Section 10.3, the elastic buckling strength of axially compressed cylindrical panels may be expressed as

$$\sigma_E = k_s \frac{\pi^2 E}{12(1-v^2)}\left(\frac{t}{L_S}\right)^2 \tag{11.34}$$

where L_s is distance between adjacent stringer stiffeners. Buckling coefficient k_s is a function of the geometrical parameter $M_s = L_s / \sqrt{Rt}$, and may be taken as 4 when $M_s < 1.73$. Capanoglu and Balint (2002) proposed to use the following equation for the geometric parameter k_s:

$$k_s = 4\alpha_{xL}\left[1 + 0.038(M_s - 2)^3\right] \tag{11.35}$$

The plasticity correction factor ϕ in Section 10.1.6 may then be used to derive inelastic buckling strength.

Stinger-Stiffened Cylinder Buckling

The elastic stress for column shell combinations may be estimated as:

$$\sigma_E = \sigma_{col} + \rho_s \sigma_s$$

where ρ_s is Shell Knockdown factor, to be taken as 0.75.

The elastic stress for column:

$$\sigma_{col} = \frac{\pi^2 E I_e'}{L^2(A_s + s_{ew}t)} \tag{11.36}$$

where S_{ew} is the effective width of shell plating and I_e' is effective moment of inertia. The elastic critical stress for unstiffened shell:

$$\sigma_s = \frac{0.605 E \dfrac{t}{R}}{1 + \dfrac{A_s}{s_{ew}t}} \tag{11.37}$$

The inelastic buckling stress σ_c may be calculated using plasticity correction factor ϕ in Section 10.1.6.

Local Stiffener Tripping

When the torsional stiffness of the stiffeners is low and the shell skin D/t ratio is relatively high, the stiffeners can experience torsional instability at a stress lower than that required for local or orthotropic buckling. When the stiffener buckles, it loses a large portion of its effectiveness in maintaining the initial shape of the shell. This reduction in lateral support will eventually lead to overall shell failure. Much of the load carried by the stiffener will then be shifted to the shell skin. Therefore, restrictions on the geometry of the stiffeners are applied in the design codes to avoid this failure mode. The restrictions on the geometry of the stiffeners are similar to those used for stiffened plates. Out of straightness of the stiffeners can result in a

reduction of the load carrying capacity, as effect of initial deflection on column buckling. Therefore fabrication tolerance is applied to the stiffeners.

General Instability

General instability involves buckling of both the stringer and ring stiffeners together with the shell plating. Due to the catastrophic consequences this failure mode may result in, restrictions are applied in the design codes on the second moment of inertia for the ring stiffeners. Such restrictions are to assure that the buckling strength for general instability mode is 1 to 4 times of that for stringer-stiffened cylinder buckling.

11.4.2 Radial Pressure

External pressure may be applied either purely radially, known as "external lateral pressure loading", or all around the shell (both radially and axially), known as "external hydrostatic pressure loading". Potential failure modes include:

- Local buckling of the panels between stringer stiffeners,

- Stringer buckling,

- General instability,

- Local stiffener tripping,

- Interaction of the above failure modes.

The formulation for collapse pressure p_{hc} may be found from API Bulletin 2U (1987) and Das et al (1992, 2001).

Balint et al (2002) modified the formulae in API Bulletin 2U (1987) and suggested the following elastic buckling equation:

$$\sigma_E = k_\theta \frac{\pi^2 E}{12(1 - v^2)} \left(\frac{t}{L_r} \right)^2$$

(11.38)

Capanoglu and Balint (2002) proposed to use the following equation for the geometric parameter k_θ:

$$k_\theta = \alpha_{\theta L} \left[\frac{1 + (L_r / L_s)^2}{L_r / L_s} \right]^2 \left[1 + \frac{0.011 M_x^2}{0.5 \left[1 + (L_r / L_s)^2 \right]^2} \right]$$

(11.39)

where the imperfection parameter $\alpha_{\theta L}$ may be taken as 0.8. The plasticity correction factor ϕ in Section 10.1.6 may then be used to derive inelastic buckling strength.

11.4.3 Axial Compression and Radial Pressure

A simple interaction equation for the strength of stringer and ringer stiffened cylinders under combined axial compression and external pressure may be expressed as:

$$\left(\frac{\sigma}{\sigma_c} \right)^m + \left(\frac{p}{p_{hc}} \right)^n \leq 1$$

(11.40)

where σ and p are applied axial compressive stress and radial pressure respectively. Ellinas et al (1984) recommended that m=n=2. A more refined interaction equation for the combined axial compression and radial pressure may be found in Das et al (1992, 2001). The accuracy of the above equations, as compared to mechanical tests and other design codes is given in Das et al (2001).

11.5 References

1. Ades, C.S. (1957), "Buckling Strength of Tubing in Plastic Region", J. of Aeronautical Science, Vol. 24, pp.605-610.

2. Amdhal, J. (1997), *"Buckling and Collapse of Structures"*, Lecture notes, NTNU.

3. API 2U (1987), "Bulletin on Stability Design of Cylindrical Shells", 1st Edition, 1987 (ANSI/API Bull 2U-1992).

4. ASME (1980), "Boiler and Pressure Vessel Code Case N-284".

5. Bai, Y. (2001), *"Pipelines and Risers"*, Elsevier Ocean Engineering Book Series, Vol. 3.

6. Balint, S.W., Capanoglu, C. and Kamal, R. (2002), "Background to New Edition of API Bulletin 2U: Stability Design of Cylindrical Shells", Proceedings of Offshore Technology Conferences, OTC 14188.

7. Brazier, L/G. (1927), "On the Flexure of Thin Cylindrical Shells and Other Thin Sections", Proc. Of Royal Society, Series A, Vol. 116, pp.104-114.

8. BS 5500 (1976), "Specification for Unfired Fusion Welded Pressure Vessels", B.S.I., Section 3.

9. Capanoglu, C. and Balint, S.W. (2002), "Comparative Assessment of Design Based on Revised API Bullitin 2U and Other Recommendations", Proceedings of ISOPE Conf.

10. Das, P.K., Faulkner, D. and Zimmer, R.A. (1992), "Selection of Robust Strength Models for Efficient Design and Ring and Stringer Stiffened Cylinders under Combined Loads", 1992 OMAE, Vol. II – Safety and Reliability.

11. Das P.K., Thavalingam, A., Hauch, S. and Bai, Y. (2001), "A New Look into Buckling and Ultimate Strength Criteria of Stiffened Shells for Reliability Analysis", OMAE 01-2131.

12. DNV (2000) RP-C202, "Buckling Strength of Shells", Det Norske Veritas. (also in DNV CN 30.1).

13. ECCS: (1981), "European Recommendations for Steel Construction", Section 4.6, Buckling of Shells.

14. Ellinas, C.P., Supple, W.J., and Walker, A.C. (1984), *"Buckling of Offshore Structures"*, Granada.

15. Faulkner, D., Chen, Y.N., de Oliveira (1983), "Limit State Design Criteria for Stiffened Cylinders of Offshore Structures", ASME 83-PVP-8, Presented in Portland, Oregon, June 1983.

16. Galambos, T.V. (2000), *"Guide to Stability Design Criteria for Metal Structures"*, 5th Edition, John Wiley & Sons.

17. Gellen, S. (1980), "The Plastic Buckling of Long Cylindrical Shells under Pure Bending", Int. J. of Solids and Structures, Vol. 10, pp. 394-407.

18. Odland, J. (1988), "Improvement in Design Methodology for Stiffened and Unstiffened Cylindrical Structures", BOSS-1998, Edited by T. Moan, Tapir Publisher, June 1988.

19. Timoshenko S. and Gere, J.M. (1961), *"Theory of Elastic Stability"*, McGraw-Hill Book Company, Inc.

20. Von Sanden, K. and Gunther, K. (1920), "Uber das Festigkeits Problem Quersteifter Hohlzylinder Unter Allseitig Gleichmassigen Aussendruck", Werft and Reederei, Vol. 1, Nos. 8, 9, 10 (1920) and Vol. 2, No. 17 (1921) - Also DTMB translation No. 38, March 1952.

21. Wilson, L.B. (1966), "The Elastic Deformation of a Circular Cylindrical Shell Supported by Equally Spaced Ring Frames under Uniform External Pressure", Trans. RINA, Vol. 108.

22. Windenburg, D.F. and Trilling, C. (1934), "Collapse of Instability of Thin Cylindrical Shells under External Pressure", Trans. ASME, Vol. 56, 1934, p 819.

This Page Intentionally Left Blank

Part II

Ultimate Strength

Chapter 12   A Theory of Nonlinear Finite Element Analysis

12.1 General

A variety of situations exist, in which a structure may be subjected to large dynamic loads, which can cause permanent deformation or damage to the structure. Therefore, structural dynamics and impact mechanics have an important role in the engineering design.

Earlier investigations on structural impacts have been well described by Jones (1989). The development of theoretical methods for impact mechanics has been aided by an idealization of real complex material behavior as a rigid perfectly plastic material behavior. These methods are classified as rigid-plastic analysis methods. Theoretical predictions based on rigid-plastic analyses may give some important information about the impact plastic behavior in a simple form. The results are often in good agreement with the corresponding experimental results. However, it is difficult to make a more realistic modeling of the plastic deformations because they are interspersed with elastic deformation. Plastic flow causes a change in shape and size, and the plastic regions may disappear and re-appear. The structure may invoke strain hardening as well as strain-rate hardening when it is yielded due to time dependent loading.

General solutions for arbitrary types of structures subjected to arbitrary impacts can be obtained by numerical methods such as finite element methods. Considerable progress has been made in both the theoretical aspects as well as in the development of general purpose computer programs for dynamic plastic analysis. Unfortunately, there is insufficient theoretical knowledge on the effect of strain-rate on material properties and on consistent constitutive modeling of plasticity. Bench mark tests using a number of well known computer programs require substantial computer speed and capacity and show that only a few programs can give reliable solutions (Symonds and Yu, 1985). In addition, such programs are not particularly well-suited and convenient to use for analysis of complex structures. Therefore, there is a demand for numerical analysis procedures, which can be used to simulate impact behavior of frame structures with large displacements and strain hardening as well as strain-rate hardening.

This chapter presents a simple and efficient procedure for large displacement plastic analysis of beam-column elements. The elastic stiffness matrix is established by combining a linear stiffness matrix (Przemienicki 1968), a geometrical stiffness matrix (Archer 1965), and a deformation stiffness matrix (Nedergaard and Pedersen, 1986). Furthermore, the effect of plastic deformation is taken into account in an efficient and accurate way by the plastic node method (Ueda and Yao, 1982, Ueda and Fujikubo, 1986, and Fujikubo et al, 1991). In the plastic node method, the distributed plastic deformation of the element is concentrated to the nodes using plastic hinge mechanism. The elastic-plastic stiffness matrices of the elements are derived without requiring numerical integration.

The objective of this chapter is to present a theoretical formulation for the modeling of strain-rate hardening effects, and show how these effects can be implemented into three-dimensional finite beam-column elements. The finite beam-column element is ideally suited for the impact analysis of frames with large displacements, strain hardening, and strain-rate hardening. The accuracy and efficiency of the element is examined by comparing the present results with those obtained from experiments by others, rigid-plastic analyses, and from existing finite element analysis results, see Part II Chapters 13 to 15. For the fundamental theory of finite element analysis, the readers may refer to Przemieniecki (1968), Zienkiewicz (1977), Bathe (1987), among many other books. To understand plasticity used in the section on the plastic node method, some basic books such as Save and Massonnet (1972), Yagawa and Miyazaki (1985), Chen and Han (1987), Chakrabarty (1987) may be helpful. To aid the understanding of the plastic node method, a basic theory of plasticity is presented for finite element analysis of solids, based on Yagawa and Miyazaki (1985).

Part of the formulation presented in this Chapter appeared in Bai and Pedersen (1991) and Fujikubo et al (1991). The new extension is to account for the effect of strain-rate hardening for dynamic analysis.

12.2 Elastic Beam-Column With Large Displacements

The element has three translational displacements u_x, u_y, and u_z and three rotational displacements θ_x, θ_y, and θ_z, see Figure 12.1.
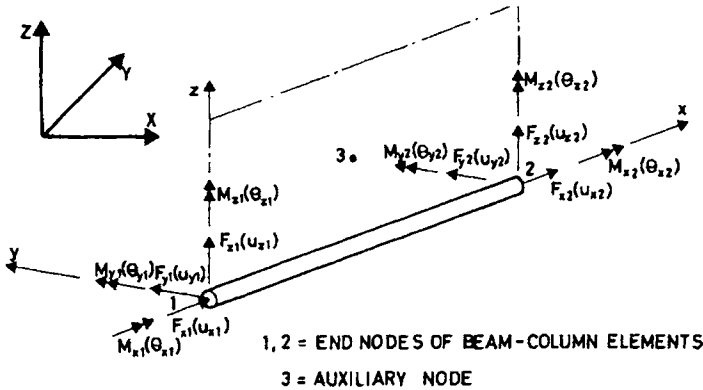
Figure 12.1   Three-Dimensional Beam Elements with Nodal Forces

These displacements are interpolated by using a polynomial interpolation of functions, which are associated with the Timoshenko beam theory. A generalized strain vector is subsequently established in the form:

$$\{\varepsilon\} = \begin{Bmatrix} e_x \\ e_y \\ e_z \\ \kappa_x \\ \kappa_y \\ \kappa_z \end{Bmatrix} = \begin{Bmatrix} u'_x + \dfrac{1}{2}\left[(u'_x)^2 + (u'_y)^2 + (u'_z)^2\right] \\ u'_y - \theta_z \\ u'_z + \theta_y \\ \theta'_x \\ \theta'_y \\ \theta'_z \end{Bmatrix} \tag{12.1}$$

where $(\ )' \equiv d/ds$ and s denotes the axial coordinate of the element.

A generalized elastic stress vector $\{\sigma\}$ is expressed as:

$$\{d\sigma\} = [D_E]\{d\varepsilon\}$$

$$\{\sigma\} = \{F_x \ F_y \ F_z \ M_x \ M_y \ M_z\}^T \tag{12.2}$$

$$[D_E] = \lfloor EA_x \ GA_y \ GA_z \ GI_x \ GI_y \ GI_z \rfloor$$

where E is Yong's modulus ,G the shear modulus, A_x denotes the area of the cross-section, A_y, and A_z denote the effective shear areas, I_y and I_z are moments of inertia, and I_x denotes the torsional moment of inertia.

Applying a virtual work principle, we obtain:

$$\{\delta du^e\}^T \left(\{f\} + \{df\}\right) = \int_L \{\delta d\varepsilon\}\left(\{\sigma\} + \{d\sigma\}\right)ds \tag{12.3}$$

where L is the length of the element, $\{u^e\}$ is the elastic nodal displacement vector, and the external load vector is $\{f\}$. Substituting the strains and stresses defined in Eqs. (12.1) and (12.2) into Eq.(12.3), and omitting the second order terms of the displacements, we get (Bai and Pedersen, 1991):

$$[k_E]\{du^e\} = \{dx\} \tag{12.4}$$

where,

$$[k_E] = [k_L] + [k_G] + [k_D] \tag{12.5}$$

and

$$\{dx\} = \{f\} + \{df\} - ([k_L] + [k_G])\{u^e\} \tag{12.6}$$

The matrix $[k_L]$ is a standard linear stiffness matrix (Przemieniecki, 1968), $[k_G]$ is a geometrical stiffness matrix (Ancher, 1965), and $[k_D]$ is a deformation stiffness matrix (Nedergaard and Pedersen, 1986).

12.3 The Plastic Node Method

12.3.1 History of the Plastic Node Method

The Plastic Node Method was named by Ueda *et al* (1979). It is a generalization of the Plastic Hinge Method developed by Ueda *et al* (1967) and others. Ueda and Yao (1980) published

the plastic node method in an international journal, and Fujikubo (1987) published his Ph.D. thesis on this simplified plastic analysis method.

Fujikubo (1991) further extended the theory of plastic node method to account for the effect of strain hardening. In the following sections, the existing theory is further extended to account for the effects of strain-rate hardening.

12.3.2 Consistency Condition and Hardening Rates for Beam Cross-Sections

For a beam-column element with strain hardening and strain-rate hardening, the yield condition of its cross-section is expressed as:

$$f = Y(\{\sigma - .\alpha\}) - \sigma_0\left(\bar{\varepsilon}^P, \dot{\bar{\varepsilon}}^P\right) = 0 \tag{12.7}$$

where Y is the yield (full plastic) function, $\{\alpha\}$ represents the translation of the yield surface due to kinematic hardening, and σ_0 is a parameter expressing the size of the yield surface. The vector $\{\alpha\}$ has the same dimension as the generalized stress and is expressed as:

$$\{\alpha\} = \left\{\alpha_{fx} \ \alpha_{fy} \ \alpha_{fz} \ \alpha_{mx} \ \alpha_{my} \ \alpha_{mz}\right\}^T \tag{12.8}$$

Due to isotropic hardening, the yield surface is expanding as the plastic deformations increase. This expansion of the yield surface is expressed by the stress parameter σ_0, which is a function of the generalized equivalent plastic strain $\bar{\varepsilon}^P$ and of the plastic strain-rate $\dot{\bar{\varepsilon}}^P$. The equivalent strain $\bar{\varepsilon}^P$ is evaluated as a summation of its increments, which are defined as:

$$\sigma_0 d\bar{\varepsilon}^P = \{\sigma - \alpha\}^T\left\{d\varepsilon^P\right\} \tag{12.9}$$

where the increments of the generalized plastic strain are taken to be:

$$\left\{d\varepsilon^P\right\} = \left\{de_x^P \ de_y^P \ de_z^P \ d\kappa_x^P \ d\kappa_y^P \ d\kappa_z^P\right\}^T \tag{12.10}$$

The equivalent plastic strain-rate, $\dot{\bar{\varepsilon}}^P$ is defined as:

$$\dot{\bar{\varepsilon}}^P = \frac{d\bar{\varepsilon}^P}{dt} \tag{12.11}$$

where dt is an increment of time t.

The increment of the parameter σ_0 due to isotropic strain hardening and that due to strain-rate hardening are de-coupled to the simplest form.

$$d\sigma_0 = dg_1\left(\bar{\varepsilon}^P\right) + dg_2\left(\dot{\bar{\varepsilon}}^P\right) \tag{12.12}$$

where $dg_1\left(\bar{\varepsilon}^P\right)$ expresses the increment of the parameter σ_0 for a beam cross-section due to isotropic strain hardening and $dg_2\left(\dot{\bar{\varepsilon}}^P\right)$ denotes the increment of the parameter σ_0 due to strain-rate hardening. Similar equations were used by Yoshimura *et al* (1987), and Mosquera *et al*, (1985).

The consistency condition for a yielded cross-section satisfying the yield condition Eq.(12.7) is expressed as:

$$df = \left\{\frac{\partial f}{\partial \sigma}\right\}^T \{d\sigma\} - \left\{\frac{\partial f}{\partial \alpha}\right\}^T \{d\alpha\} - \frac{dg_1}{d\bar{\varepsilon}^P}d\bar{\varepsilon}^P - \frac{dg_2}{d\dot{\bar{\varepsilon}}^P}d\dot{\bar{\varepsilon}}^P = 0 \tag{12.13}$$

Here, we introduce a kinematic hardening rate H'_{sk} and an isotropic hardening rate H'_{si} for the full plastic cross-sections, which are defined by:

$$H'_{sk} = \{\partial f / \partial \sigma\}^{\mathrm{T}} \{d\alpha\} / d\bar{\varepsilon}^P \tag{12.14}$$

and

$$H'_{si} = dg_1 / d\bar{\varepsilon}^P \tag{12.15}$$

Similarly, a strain-rate hardening rate H'_{sr} for the full plastic cross-section is defined as:

$$H'_{sr} = dg_2 / d\dot{\bar{\varepsilon}}^P \tag{12.16}$$

With these definitions, the consistency condition Eq. (12.13) may be rewritten as:

$$df = \left\{\frac{\partial f}{\partial \sigma}\right\}^T \{d\sigma\} - \left(H'_{sk} + H'_{si}\right)d\bar{\varepsilon}^P - H'_{sr}d\dot{\bar{\varepsilon}}^P = 0 \tag{12.17}$$

The subscript "s" in Eqs. (12.14) thru (12.17) indicates generalized values related to the full beam cross-section. To avoid confusion, the kinematic and isotropic material-hardening rate obtained from uni-axial tests is denoted by H'_k and H'_i, respectively.

Introducing a linear interpolation for $d\bar{\varepsilon}^P$, we obtain:

$$d\bar{\varepsilon}^P = \dot{\bar{\varepsilon}}^P_{(t+dt)}\theta dt + \dot{\bar{\varepsilon}}^P_{(t)}(1-\theta)dt \tag{12.18}$$

where θ is a parameter, which will be taken as $1/2$ in the numerical examples.

From Eq. (12.18), we find:

$$\dot{\bar{\varepsilon}}^P_{(t+dt)} = \left[d\bar{\varepsilon}^P - (1-\theta)\dot{\bar{\varepsilon}}^P_{(t)}dt\right] / (\theta dt) \tag{12.19}$$

Then the increment of the equivalent plastic strain-rate $d\dot{\bar{\varepsilon}}^P$ may be estimated as:

$$d\dot{\bar{\varepsilon}}^P = \dot{\bar{\varepsilon}}^P_{(t+dt)} - \dot{\bar{\varepsilon}}^P_{(t)} = \left[d\bar{\varepsilon}^P - \dot{\bar{\varepsilon}}^P_{(t)}dt\right] / (\theta dt) \tag{12.20}$$

For simplicity, in the following equations, the subscript "t" will be omitted.

Considering Eq. (12.20), the consistency condition Eq. (12.17) is rewritten in the form:

$$df = \{\partial f / \partial \sigma\}^{\mathrm{T}} \{d\sigma\} - (H'_{sk} + H'_{si} + H'_{sr} / (\theta dt))d\bar{\varepsilon}^P + [H'_{sr} / \theta]\dot{\bar{\varepsilon}}^P = 0 \tag{12.21}$$

in the following, the hardening rates H'_{si}, H'_{sk} and H'_{sr} in Eq. (12.21) will be discussed.

The isotropic hardening rate for the cross-section is evaluated as follows. Following Ueda and Fujikubo, (1986) and Fujikubo *et al*, (1991), the increments of the generalized stress due to isotropic hardening are estimated to be:

$$\{d\sigma\} = [H'_{si}]\{d\varepsilon^P\} \tag{12.22}$$

and the matrix $[H'_{si}]$ is obtained by first deriving a relationship between the stress increments and the plastic strain increments for points and after integrating those stresses over the cross-section. If we use the Von Mises yield criteria and neglect the interaction between shear stress and axial stresses Eq. (12.23) is obtained:

$$[H'_{si}] = [H'_i A_x \quad H'_i A_y /3 \quad H'_i A_z /3 \quad H'_i I_x /3 \quad H_i I_y \quad H'_i I_z]$$ (12.23)

Considering f in Eq. (12.7) as a plastic potential and applying the flow theory of plasticity, we may obtain:

$$\{d\varepsilon_P\} = cd\bar{\varepsilon}_P \left\{ \frac{\partial f}{\partial \sigma} \right\}$$ (12.24)

where

$$c = \sigma_0 / \left(\{\sigma - \alpha\}^T \{\partial f / \partial \sigma\} \right)$$ (12.25)

The increment of the parameter σ_0 due to isotropic strain hardening is defined as:

$$dg_1 = \{\partial f / \partial \sigma\}^T \{d\sigma\}$$ (12.26)

Substituting Eqs. (12.24) and (12.22) into Eq. (12.26), the isotropic cross-sectional strain hardening rate defined in Eq. (12.15) is given as:

$$H'_{si} = c \left\{ \frac{\partial f}{\partial \sigma} \right\}^T [H'_{si}] \left\{ \frac{\partial f}{\partial \sigma} \right\}$$ (12.27)

The kinematic hardening rate for the cross-section will be derived using a similar approach. The yield surface translation increment $\{d\alpha\}$ can be obtained by using Ziegler's rule and the Mises yield criteria (Fulikubo *et al*, 1991):

$$\{d\alpha\} = [H'_{sk}]\{d\varepsilon^p\}$$ (12.28)

where $[H'_{sk}]$ used in the present chapter is taken as:

$$[H'_{sk}] = [H'_k A_x \quad H'_k A_y /3 \quad H'_k A_z /3 \quad H'_k I_x /3 \quad H'_k I_y \quad H'_k I_z]$$ (12.29)

Substituting Eqs. (12.24) and (12.28) into Eq. (12.14), we obtained:

$$H'_{sk} = c \left\{ \frac{\partial f}{\partial \sigma} \right\}^T [H'_{sk}] \left\{ \frac{\partial f}{\partial \sigma} \right\}$$ (12.30)

Finally, we shall determine the strain-rate hardening rate for the cross-sections. The increment of the parameter σ_0, due to strain-rate hardening is estimated by use of a constitutive equation that expresses the relationship between g_2 and the equivalent plastic strain. For instance, the Cowper-Symonds constitutive equation is expressed as (Jones, 1989):

$$\sigma_{0x} = \sigma_y \left[1 + \left(\dot{\bar{\varepsilon}}_x^p / D \right)^{1/q} \right]$$ (12.31)

where σ_y is the yield stress and $\bar{\varepsilon}_x^p$ denotes the plastic strain-rate for a point. Values of D and q that are often used are the following:

for mild steel   D=40.4 *sec*$^{-1}$ q=5

and for aluminum alloy   D= 6500 *sec*$^{-1}$ q=4

Eq. (12.31) was obtained for uni-axial stress tests. It is assumed that this equation is still a valid approximation when it is applied to multi-axially loaded beam cross-sections. Eq. (12.31) becomes:

$$g_2(\dot{\bar{\varepsilon}}^p) = N_Y \left[1 + (\dot{\bar{\varepsilon}}^p/D)^{1/q} \right]$$ (12.32)

where $N_Y = A_x \sigma_y$

Using Eq. (12.32), the strain-rate hardening rate defined in Eq. (12.16) may be given as:

$$H'_{sr} = N_Y (\dot{\bar{\varepsilon}}^p/D)^{\left(\frac{1}{q}-1\right)} / q$$ (12.33)

12.3.3 Plastic Displacement and Strain at Nodes

The plastic deformations of the element are concentrated at the node in a mechanism similar to the plastic hinge. Referring to Eq. (12.7), the yield condition at the node is expressed as:

$$F_i = Y_i(\{\sigma_{,} - \alpha_i\}) - \sigma_{0i}(\bar{\varepsilon}_i^p, \dot{\bar{\varepsilon}}_i^p) = 0$$ (12.34)

where the subscript "i", denotes values at the node No. i. From Eq. (12.21), the consistency condition for node i is expressed as:

$$dF_i \{\phi_i\}^T \{dx\} - \left[H'_{sk} + H'_{si} + H'_{sr}/(\theta dt) \right]_i d\bar{\varepsilon}_i^p + a_i = 0$$ (12.35)

where,

$$\{\phi_i\} = \{\partial F_i/\partial x\}$$ (12.36)

$$a_i = \left[H'_{sr}/\theta \right]_i \dot{\bar{\varepsilon}}_i^p$$ (12.37)

where $\{x\}$ is the nodal force vector.

Applying the plastic flow theory, the increments of plastic nodal displacement of the element due to plasticity at node i, are estimated as (Ueda and Yao, 1982):

$$\{du_i^p\} = d\lambda_i \{\phi_i\}$$ (12.38)

where $d\lambda_i$ is a measure of the magnitude of plastic deformation.

In the following paragraphs, we shall establish a relationship between $d\bar{\varepsilon}_i^p$ and $d\lambda_i$ using a plastic work procedure (Ueda and Fujikubo, 1986 and Fujikubo et al, 1991). The increment of the plastic work done at the plastic node "i" is expressed as:

$$dw_i^p = \{x\}^T \{du_i^p\} = \{x\}^T \{\phi_i\} d\lambda_i$$ (12.39)

The increment of the plastic work done in the actual plastic region around node i is evaluated as:

$$dw_i^{p^*} = \int_{L_i^p} \{\sigma\}^T \{d\varepsilon^p\} ds = \int_{L_i^p} c\{\sigma\}^T \left\{ \frac{\partial f}{\partial \sigma} \right\} d\bar{\varepsilon}^p ds$$ (12.40)

From Eq. (12.21) the increment of the equivalent plastic strain at a coordinate s, can be expressed as a function of the value at node i in the form:

$$d\bar{\varepsilon}^p = g(s) d\bar{\varepsilon}_i^p$$ (12.41)

where,

$$g(s) = \frac{\left[H'_{sk} + H'_{si} + H'_{sr}/(\theta dt)\right]_i}{H'_{sk} + H'_{si} + H'_{sr}/(\theta dt)} \frac{\{\partial f/\partial\sigma\}^T\{d\sigma\} + (H'_{sr}/\theta)\dot{\bar{\varepsilon}}^p}{\{\partial f_i/\partial\sigma_i\}^T\{d\sigma_i\} + (H'_{sr}/\theta)_i\dot{\bar{\varepsilon}}^p_i}$$

substituting Eq. (12.41) into Eqs. (12.40) and (12.42) is obtained:

$$dw_i^{p^{\bullet}} = d\bar{\varepsilon}_i^p \int_{L_i^p} c\{\sigma\}^T \left\{\frac{\partial f}{\partial\sigma}\right\}g(s)ds \tag{12.42}$$

Equating the plastic work increments dw_i^p in Eq. (12.39) and $dw_i^{p^{\bullet}}$ in Eq. (12.42), Eq. (12.43) is obtained:

$$d\bar{\varepsilon}_i^p = h_i d\lambda_i \tag{12.43}$$

where,

$$h_i = \{x\}^T\{\phi_i\}/ \int_{L_i^p} c\{\sigma\}^T \left\{\frac{\partial f}{\partial\sigma}\right\}g(s)ds \tag{12.44}$$

A simpler alternative approach for determining the strain-hardening rate at a plastic node is to establish relationships between the plastic nodal displacements and the generalized plastic strain vector at the node in the form of:

$$\{d\bar{\varepsilon}_i^p\} = \{du_i^p\}/L_{di} = \{\phi_i\}d\lambda_i/L_{di} \tag{12.45}$$

where L_{di} denotes an equivalent length of the plastic region.

The increment of the equivalent plastic strain at the node can be evaluated by substituting Eq. (12.45) into Eq. (12.9) and obtain Eq. (12.43):

$$h_i = \{\sigma_i - \alpha_i\}^T\{\phi_i\}/(L_{di}\sigma_{0i}) \tag{12.46}$$

Integration along the axial axis of the element becomes unnecessary when Eq. (12.46) is applied to calculate $d\varepsilon_i^p$ instead of Eq. (12.44). This results in an extremely simple numerical procedure. Unfortunately, the actual regions where the plastic flow occurs, causes a change in shape, size, and may disappear/re-appear. Evidently, the equivalent length of the plastic region for each stress component should be different and considered to be a function of time. However, for simplicity, we would like to find a constant value that will provide adequate approximations. Then length L_{di} can simply be approximated as:

$$L_{di} = \alpha_D H \tag{12.47}$$

or

$$L_{di} = \alpha_L L \tag{12.48}$$

where α_D and α_L are coefficients, H is the diameter for a circular cross-section or a width (or height) for a rectangular cross-section, etc. This approach will be used in the case where a structural member is modeled by only one element. Substitution of Eq. (12.43) into Eq. (12.35) gives:

$$dF_i = \{\phi_i\}^T\{dx\} - H'_{ni}d\lambda_i + a_i = 0 \tag{12.49}$$

where,

$$H_{ni} = \left[H'_{sk} + H'_{si} + H'_{sr} / (\theta dt) \right]_i h_i \qquad (12.50)$$

12.3.4 Elastic-Plastic Stiffness Equation for Elements

When both nodes 1 and 2 are plastic, the following matrix equation may be established from Eq. (12.49):

$$[\varPhi]^T \{dx\} - [H'] \{d\lambda\} + \{A\} = 0 \qquad (12.51)$$

where,

$$[\varPhi] = [\{\phi_1\} \{\phi_2\}]$$

$$[H'] = [H'_{n1} \; H'_{n2}] \quad (2 \times 2 \text{ diagonal matrix})$$

$$\{d\lambda\} = \{d\lambda_1 \; d\lambda_2\}^T$$

and

$$\{A\} = \{a_1 \; a_2\}^T$$

From Eq. (12.38), the increments of the plastic nodal displacement $\{du^p\}$ are given as:

$$\{du^p\} = [\varPhi]\{d\lambda\} \qquad (12.52)$$

The increments of the total nodal displacement $\{du\}$ are expressed by the summation of the elastic and plastic components as:

$$\{du\} = \{du^e\} + \{du^p\} \qquad (12.53)$$

Substitution of Eqs. (12.52) and (12.53) into Eq. (12.4) gives:

$$[k_E]\left(\{du\} - [\varPhi]\{d\lambda\}\right) = \{dx\} \qquad (12.54)$$

Solving Eqs. (12.51) and (12.54) with respect to $\{d\lambda\}$ we obtain:

$$\{d\lambda\} = \left([H'] + [\varPhi]^T [k_E][\varPhi]\right)^{-1} \left([\varPhi]^T [k_E]\{du\} + \{A\}\right) \qquad (12.55)$$

substituting $\{d\lambda\}$ into Eq. (12.54) gives the elastic plastic stiffness equation:

$$[k_p]\{du\} = \{dx\} + \{dx'\} \qquad (12.56)$$

where,

$$[k_P] = [k_E] - [k_E][\varPhi]\left([H'] + [\varPhi]^T [k_E][\varPhi]\right)^{-1} [\varPhi]^T [k_E] \qquad (12.57)$$

$$\{dx'\} = [k_E][\varPhi][H'] + [\varPhi]^T [k_E][\varPhi]\big]^{-1} \{A\} \qquad (12.58)$$

If the sign of $\{d\lambda_1\}$ or $\{d\lambda_2\}$ is found to be negative, unloading occurs at the plastic node and the node should then be treated as elastic. It is noted that the effects of large displacements and strain hardening as well as strain-rate hardening have been taken into account in the derived elastic-plastic stiffness equation.

12.4 Transformation Matrix

In this section, a new transformation matrix $[T_t]$ is described, which transfers element displacements measured in the global coordinate system XYZ to element displacements measured in the local coordinate xyz, at time t. The transformation matrix is evaluated as

$$[T_t] = [\Delta T][T_t - dt] \qquad (12.59)$$

where $[T_t - da]$ is a matrix, which transfers the element displacements to the local coordinate system at time t-dt. $[\Delta T]$ is a matrix that transfers the element displacements measured in the local coordinate system at the time t-dt to the local coordinate system at time t.
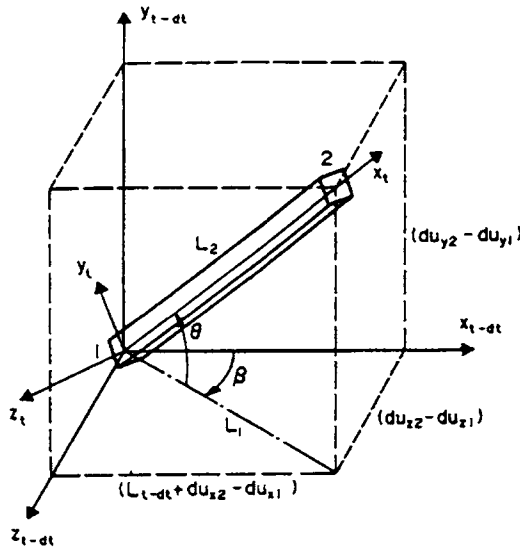
Figure 12.2   Transformation Matrix

The transformation matrix $[\Delta T]$ is composed of submatrices $[tt]$ which transform the displacement vectors. The submatrix $[tt]$ is evaluated as:

$$[tt] = [t_a] + [t_b] \qquad (12.60)$$

where,

$$[t_a] = \begin{bmatrix} 1 & 0 & 0 \\ 0 & \cos\alpha & \sin\alpha \\ 0 & -\sin\alpha & \cos\alpha \end{bmatrix}$$

$$ \qquad (12.61)$$

$$[t_b] = \begin{bmatrix} \cos\beta\cos\theta & \sin\theta & \sin\beta\cos\theta \\ -\cos\beta\sin\theta & \cos\theta & -\sin\beta\sin\theta \\ -\sin\beta & 0 & \cos\beta \end{bmatrix}$$

By considering the increments of nodal displacement from time *t-dt* to time *t*, measured in the local coordinate system at time *t-dt*, we obtain:

$$\sin \beta = \left(du_{z2} - du_{z1}\right)/L_1$$
$$\cos \beta = \left(L_{t-dt} + du_{x2} - du_{x1}\right)/L_1$$
$$\sin \theta = \left(du_{y2} - du_{y1}\right)/L_2 \tag{12.62}$$
$$\cos \theta = L_1/L_2$$

where,

$$L_1 = \left[\left(L_{t-dt} + du_{x2} - du_{x1}\right)^2 + \left(du_{z2} - du_{z1}\right)^2\right]^{\frac{1}{2}}$$
$$L_2 = \left[L_1^2 + \left(du_{y2} - du_{y1}\right)^2\right]^{\frac{1}{2}} \tag{12.63}$$

L_{t-dt} is the distance between nodes 1 and 2 at time *t-dt*. Furthermore, the angle α is calculated as:

$$\alpha = \frac{1}{2}\left[t_{b11}\left(d\theta_{x1} + d\theta_{x2}\right) + t_{b12}\left(d\theta_{y1} + d\theta_{y2}\right) + t_{b13}\left(d\theta_{z1} + d\theta_{z2}\right)\right] \tag{12.64}$$

12.5 Appendix A: Stress-Based Plasticity Constitutive Equations

12.5.1 General

This appendix is written based on a Japanese book authored by Yagawa and Miyazaki (1985). When the formulation presented in this chapter was made, the author had been inspired by this book and Yamada (1968). The objective of this Appendix is to describe the basics of plasticity that may be useful to help understand the mathematical formulation presented in the main body of this chapter.

In the uni-axial tensile test, when the stress is small, the material behavior is elastic. The proportional constant E is Young's modulus. If the load is released, the stress will become 0, and the material will return to its original condition. On the other hand, when the stress exceeds a limit, permanent deformation may occur. The permanent deformation is called plastic deformation.

Figure A.1 shows a typical stress-strain diagram of metallic materials. The material is in elastic behavior range until the yield point A, and the stress σ and strain ε are in proportion. This proportion relationship is called Hook's law. After going over point A, the gradient of the stress-strain curve decreases, and the gradient, H'_0 is called tangent modulus. If unloading occurs at point B, the stress will decrease along with $B \to C$, which is parallel to OA. The residual strain is called plastic strain, ε^P. On the other hand, the recovered strain corresponding with CB' is called elastic strain, ε^e. The total strain is the sum of the elastic strain and plastic strain.

$$\varepsilon = \varepsilon^e + \varepsilon^P \tag{A.1}$$

Figure A.2 shows the relationship between stress and plastic strain. The gradient H' in this stress - plastic strain curve is called strain-hardening rate. Referring to Figs. A.1, A.2, the following relationship may be obtained.

$$d\varepsilon = \frac{d\sigma}{H_0^{'}} = d\varepsilon^e + d\varepsilon^p = \frac{d\sigma}{E} + \frac{d\sigma}{H'} \qquad (A.2)$$

where $H_0{'}$ and H' can be expressed as follow,

$$H' = \frac{EH_0^{'}}{E - H_0^{'}}, \qquad H_0^{'} = \frac{EH'}{E + H'} \qquad (A.3)$$

As shown in Figure A.3, when the stress is beyond the yield point of material, plastic strain occurs; if the load is released after point B, and a compressive load is applied, the relationship between stress and strain will follow curve BCD, and the material yields at a compressive stress (point C) that is lower than its initial yield stress. This phenomenon is called Bauschinger's effect.
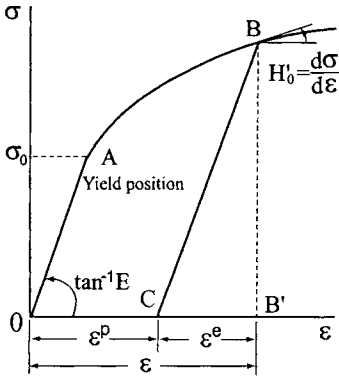
Figure A.1   Stress and Strain Diagram
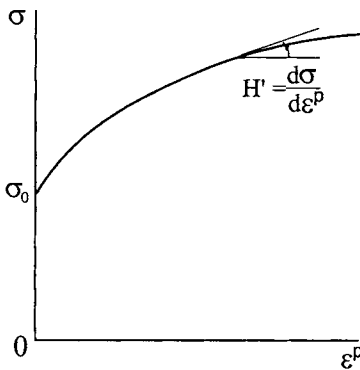
Figure A.2   Curve of Strain Hardening

Although there is a one-to-one correspondence between stress and strain in the elastic region as described by Hook's law, this correlation does not exist in the plastic region. This means

that if the strain is above a certain level, it is dependent on the deformation history along with the stress. For an elasto-plastic solid, the incremental theory (or flow theory) is widely used to account for the deformation history. However, for the simplification of calculation, the total strain theory (or deformation theory) is also used when the finite element method is not applied.
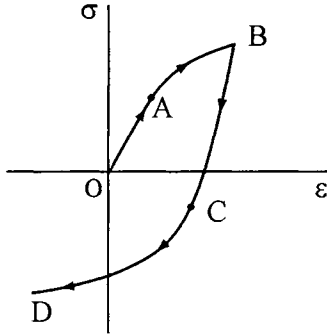
Figure A.3   Bauschinger's Effect

12.5.2 Relationship Between Stress and Strain in Elastic Region

The relationship between stress and strain in the elastic region can be repressed in a matrix form as follows,

$$\left.\begin{array}{ll} \{\sigma\} = [D^e]\{\varepsilon\} & or \quad \{\varepsilon\} = [C^e]\{\sigma\} \\ [D^e] = [C^e]^{-1} \end{array}\right\} \tag{A.4}$$

where,

$$\{\sigma\} = \left\{\begin{array}{c} \sigma_x \\ \sigma_y \\ \sigma_z \\ \tau_{xy} \\ \tau_{yz} \\ \tau_{zx} \end{array}\right\}, \quad \{\varepsilon\} = \left\{\begin{array}{c} \varepsilon_x \\ \varepsilon_y \\ \varepsilon_z \\ \gamma_{xy} \\ \gamma_{yz} \\ \gamma_{zx} \end{array}\right\} \tag{A.5}$$

For an isotropic material, $[D^e]$, $[C^e]$ are formulated with the Young's modulus, E, and Poisson's ratio in the form,

$$[D^e] = \frac{E(1-v)}{(1+v)(1-2v)} \begin{bmatrix} 1 & \dfrac{v}{1-v} & \dfrac{v}{1-v} & 0 & 0 & 0 \\ & 1 & \dfrac{v}{1-v} & 0 & 0 & 0 \\ & & 1 & 0 & 0 & 0 \\ & & & \dfrac{1-2v}{2(1-v)} & 0 & 0 \\ & & & & \dfrac{1-2v}{2(1-v)} & 0 \\ & & & & & \dfrac{1-2v}{2(1-v)} \end{bmatrix} \tag{A.6}$$

$$[C^e] = \frac{1}{E} \begin{bmatrix} 1 & -v & -v & 0 & 0 & 0 \\ & 1 & -v & 0 & 0 & 0 \\ & & 1 & 0 & 0 & 0 \\ & & & 2(1+v) & 0 & 0 \\ & & & & 2(1+v) & 0 \\ & & & & & 2(1+v) \end{bmatrix} \tag{A.7}$$

In the elastic region, the relationship between stress increment and strain increment may be written based on Eq.(A.4) as follow.

$$\{\varDelta\sigma\} = [D^e]\{\varDelta\varepsilon\} \qquad or \qquad \{\varDelta\varepsilon\} = [C^e]\{\varDelta\sigma\} \tag{A.8}$$

where, $\varDelta$ is an increment.

12.5.3 Yield Criterion

The stress condition for the initiation of plastic deformation is called yield criterion and is generally written as a yield function f.

$$f(J_1, J_2, J_3) = 0 \tag{A.9}$$

where, J_1, J_2, J_3 are the invariants and expressed as,

$$\left. \begin{array}{l} J_1 = \sigma_x + \sigma_y + \sigma_z \\ J_2 = -(\sigma_x\sigma_y + \sigma_y\sigma_z + \sigma_z\sigma_x) + \tau_{xy}^2 + \tau_{yz}^2 + \tau_{zx}^2 \\ J_3 = \sigma_x\sigma_y\sigma_z - \sigma_x\tau_{yz}^2 - \sigma_y\tau_{zx}^2 - \sigma_z\tau_{xy}^2 + 2\tau_{yz}\tau_{zx}\tau_{xy} \end{array} \right\} \tag{A.10}$$

The geometrical surface for the yield criterion in a stress space is called yield surface. Because the first approximation of the yield function has no relation with the hydrostatic pressure for the metallic materials, the yield criterion can be expressed as,

$$f(J_2', J_3') = 0, \qquad J_1' = 0 \tag{A.11}$$

where, J'_1, J'_2, J'_3 are called the invariants of deviatoric stress as shown below,

$$\left.\begin{array}{l} \sigma_x^{'} = \sigma_x - \sigma_m, \qquad \sigma_y^{'} = \sigma_y - \sigma_m, \qquad \sigma_z^{'} = \sigma_z - \sigma_m, \\[2mm] \sigma_m = \dfrac{\sigma_x + \sigma_y + \sigma_z}{3}, \\[2mm] \tau_{xy}^{'} = \tau_{xy}, \qquad \tau_{yz}^{'} = \tau_{yz}, \qquad \tau_{zx}^{'} = \tau_{zx} \end{array}\right\} \qquad (A.12)$$

The most widely used yield criterion for metallic materials is Mises's yield criterion, in which the function f in Eq.(A.11) is only expressed as a function of the secondary invariant of deviatoric stress, J'_2.

$$f = \sqrt{3J_2^{'}} - \sigma_0 \qquad (A.13)$$

where, σ_0 is the yield stress for the uniaxial loading. Here, J'_2 is ,

$$\begin{aligned} J_2^{'} &= -\left(\sigma_x^{'}\sigma_y^{'} + \sigma_y^{'}\sigma_z^{'} + \sigma_z^{'}\sigma_x^{'}\right) + \tau_{xy}^{'2} + \tau_{yz}^{'2} + \tau_{zx}^{'2} \\[2mm] &= \frac{1}{2}\left[\sigma_x^{'2} + \sigma_y^{'2} + \sigma_z^{'2} + 2\left(\tau_{xy}^{'2} + \tau_{yz}^{'2} + \tau_{zx}^{'2}\right)\right]^{\frac{1}{2}} \\[2mm] &= \frac{1}{6}\left[\left(\sigma_x - \sigma_y\right)^2 + \left(\sigma_y - \sigma_z\right)^2 + \left(\sigma_z - \sigma_x\right)^2 + 6\left(\tau_{xy}^2 + \tau_{yz}^2 + \tau_{zx}^2\right)\right] \end{aligned} \qquad (A.14)$$

If the equivalent stress $\overline{\sigma}$ is defined as,

$$\begin{aligned} \overline{\sigma} &= \sqrt{3J_2^{'}} = \sqrt{\frac{3}{2}}\left[\sigma_x^{'2} + \sigma_y^{'2} + \sigma_z^{'2} + 2\left(\tau_{xy}^{'2} + \tau_{yz}^{'2} + \tau_{zx}^{'2}\right)\right]^{\frac{1}{2}} \\[2mm] &= \frac{1}{\sqrt{2}}\left[\left(\sigma_x - \sigma_y\right)^2 + \left(\sigma_y - \sigma_z\right)^2 + \left(\sigma_z - \sigma_x\right)^2 + 6\left(\tau_{xy}^2 + \tau_{yz}^2 + \tau_{zx}^2\right)\right]^{\frac{1}{2}} \end{aligned} \qquad (A.15)$$
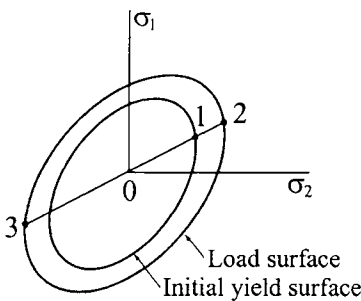
Figure A.4   Isotropic Hardening Rule.
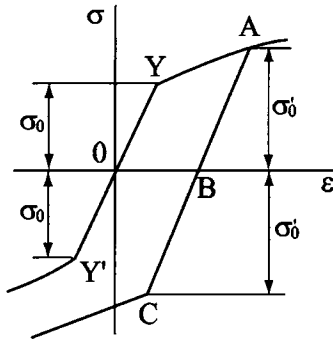
Figure A.5   Uniaxial Stress and Strain Relation Based on Isotropic Hardening Rule.

the yield criterion becomes,

$$\overline{\sigma} = \sigma_0 \tag{A.16}$$

the multi-axial stress condition can then be corresponded to the uniaxial stress condition.

When the stress is larger than the yield criterion of the material, the hardening and plastic deformation occur, and the yield function $f = 0$ must be satisfied. However, if $f < 0$, unloading occurs, the material is in elastic region.

12.5.4 Plastic Strain Increment

When plastic deformation occurs, the shape of yield surface may change following the hardening rule. Here, the isotropic hardening rule and the kinematic hardening rule are described in below.

Isotropic Hardening Rule

As shown in Figure A.4, in the hardening process, the size of the yield surface may increase but no change to the position and shape of the yield surface. Figure A.5 shows the relationship between uniaxial stress and strain. After loading along with the curve OYA, and unloading to point B, and then continue in reverse direction to point C, $\overline{AB} = \overline{BC}$, $\overline{BC} > \overline{OY}$. If the strain hardening is considered, the yield function in Eq. (A.13) becomes,

$$f = \sqrt{3J_2'} - \sigma_0 = \overline{\sigma} - \sigma_0\left(\overline{\varepsilon}^p\right) \tag{A.17}$$

where, $\overline{\varepsilon}^p$ is the equivalent plastic strain, and may be expressed as,

$$\overline{\varepsilon}^p = \int d\overline{\varepsilon}^p \tag{A.18}$$

$d\overline{\varepsilon}^p$ in the above equation may be estimated as below,

$$d\bar{\varepsilon}^p = \varDelta\bar{\varepsilon}^p = \sqrt{\frac{2}{3}\left[\varDelta\varepsilon_x^{p2} + \varDelta\varepsilon_y^{p2} + \varDelta\varepsilon_z^{p2} + \frac{1}{2}\left(\varDelta\gamma_{xy}^{p2} + \varDelta\gamma_{yz}^{p2} + \varDelta\gamma_{zx}^{p2}\right)\right]}$$

$$= \frac{\sqrt{2}}{3}\left[\left(\varDelta\varepsilon_x^p - \varDelta\varepsilon_y^p\right)^2 + \left(\varDelta\varepsilon_y^p - \varDelta\varepsilon_z^p\right)^2 + \left(\varDelta\varepsilon_z^p - \varDelta\varepsilon_x^p\right)^2 \right. \tag{A.19}$$

$$\left. + \frac{3}{2}\left(\varDelta\gamma_{xy}^{p2} + \varDelta\gamma_{yz}^{p2} + \varDelta\gamma_{zx}^{p2}\right)\right]^{1/2}$$

If the plastic strain increment in uniaxial loading in x direction is defined as $\varDelta\varepsilon_x^p$, and the condition for incompressibility of plastic strain

$$\varDelta\varepsilon_x^p + \varDelta\varepsilon_y^p + \varDelta\varepsilon_z^p = 0 \tag{A.20}$$

is used, the following equation may be obtained.

$$\varDelta\varepsilon_y^p = \varDelta\varepsilon_z^p = -\frac{\varDelta\varepsilon_x^p}{2}, \qquad \varDelta\gamma_{xy}^p = \varDelta\gamma_{yz}^p = \varDelta\gamma_{zx}^p = 0 \tag{A.21}$$

Substituting Eq.(A.21) into Eq. (A.19), we obtain,

$$\varDelta\bar{\varepsilon}^p = \varDelta\varepsilon_x^p \tag{A.22}$$

This means that the increment of equivalent plastic strain is a conversion of the plastic strain increment in multi-axial stress condition to that of the uniaxial stress condition.

The plastic strain increment may be obtained from the flow rule. If the plastic potential is defined as yield function f, the plastic strain increment is expressed as,

$$\{\varDelta\varepsilon^p\} = \varDelta\lambda\left\{\frac{\partial f}{\partial\sigma}\right\} = \varDelta\lambda\frac{3}{2\bar{\sigma}}\{\sigma'\} \tag{A.23}$$

where, yield function f is expressed in Eq. (A.17). $\varDelta\lambda$ $(:>0)$ is a undetermined scalar constant, and $\{\sigma'\}$ is a vector of deviatoric stress as below,

$$\{\sigma'\} = \begin{Bmatrix} \sigma_x' \\ \sigma_y' \\ \sigma_z' \\ 2\tau_{xy} \\ 2\tau_{yz} \\ 2\tau_{zx} \end{Bmatrix} \tag{A.24}$$

Eq. (A.24) means that the plastic strain increment is in the perpendicular direction of yield surface, $f=0$ as shown in Figure A.6.
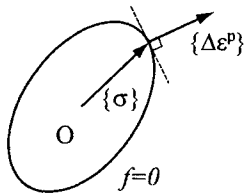
Figure A.6   Flow Rule
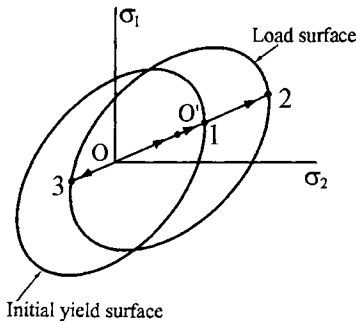
Figure A.7   Kinematic Hardening Rule
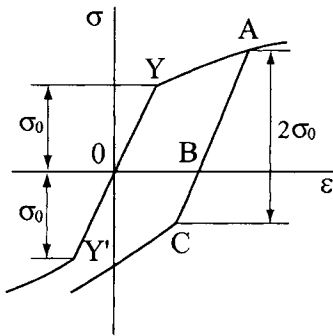
**Figure A.8   Uni-Axial Stress and Strain Relation Based on Kinematic
                        Hardening Rule.**

Kinematic Hardening Rule

In the kinematic hardening rule, although the size of yield surface does not change due to the hardening process, the position of its center moves as shown in Figure A.7. The relationship between stress and strain for a uniaxial stress case is shown in Figure A.8. From the relation of $\overline{YY'} = \overline{AC}, \overline{BC} < \overline{OY}$, the Bauschinger's effect may be qualitatively expressed in the figure.
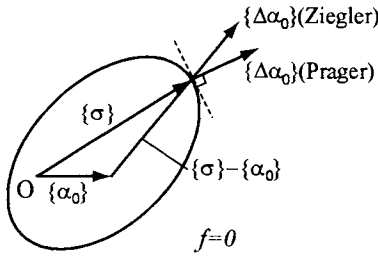
Figure A.9   Move Direction of Center for Yield Surface

The yield function for kinematic hardening rule is defined as,

$$f = f(\{\sigma\} - \{\alpha_0\})$$ (A.25)

where, $\{\alpha_0\}$ is the center of yield surface, and may be expressed as,

$$\{\alpha_0\} = \begin{Bmatrix} \alpha_x \\ \alpha_y \\ \alpha_z \\ \alpha_{xy} \\ \alpha_{yz} \\ \alpha_{zx} \end{Bmatrix}$$ (A.26)

There are two ways to determine $\{\alpha_0\}$: Prager kinematic hardening rule and Ziegler kinematic hardening rule.

$$\{\Delta\alpha_0\} = C\{\Delta\varepsilon^p\} \qquad \text{: Prager}$$ (A.27)

$$\{\Delta\alpha_0\} = \Delta\mu(\{\sigma\} - \{\alpha_0\}) \qquad \text{: Ziegler}$$ (A.28)

As shown in Figure A.9, Prager kinematic hardening rule moves in the direction perpendicular to the yield surface; Ziegler kinematic hardening rule moves along the direction from the center of yield surface $\{\alpha_0\}$ to the stress point $\{\sigma\}$.

From Eq. (A.25), the yield condition becomes,

$$f(\{\sigma_\alpha\}) = \overline{\sigma}_\alpha - \sigma_0 = 0$$ (A.29)

where,

$$\{\sigma_\alpha\} = \{\sigma\} - \{\alpha_0\}$$ (A.30)

$\overline{\sigma}_\alpha$ is the equivalent stress which considers the movement of yield surface, and is expressed as below,

$$\bar{\sigma}_\alpha = \frac{1}{\sqrt{2}}\left[\left\{\left(\sigma_x - \alpha_x\right) - \left(\sigma_y - \alpha_y\right)\right\}^2 + \left\{\left(\sigma_y - \alpha_y\right) - \left(\sigma_z - \alpha_z\right)\right\}^2 \right.$$
$$+ \left\{\left(\sigma_z - \alpha_z\right) - \left(\sigma_x - \alpha_x\right)\right\}^2$$
$$\left. + 6\left\{\left(\tau_{xy} - \alpha_{xy}\right)^2 + \left(\tau_{yz} - \alpha_{yz}\right)^2 + \left(\tau_{zx} - \alpha_{zx}\right)^2\right\}\right]^{1/2} \qquad (A.31)$$

By setting yield function f as the plastic potential, plastic strain increment may be expressed as,

$$\{\Delta\varepsilon^p\} = \Delta\lambda\left\{\frac{\partial f}{\partial\sigma}\right\} = \Delta\lambda\frac{3}{2\bar{\sigma}_\alpha}\{\sigma_\alpha'\} \qquad (A.32)$$

where,

$$\{\sigma_\alpha'\} = \{\sigma'\} - \{\alpha_0'\} \qquad (A.33)$$

12.5.5 Stress Increment – Strain Increment Relation in Plastic Region

Total strain increment is the sum of elastic strain increment and plastic strain increment,

$$\{\Delta\varepsilon\} = \{\Delta\varepsilon^e\} + \{\Delta\varepsilon^p\} \qquad (A.34)$$

On the other hand, the relationship between stress increment and elastic strain increment may be expressed as below,

$$\{\Delta\sigma\} = \left[D^e\right]\{\Delta\varepsilon^e\} \qquad (A.35)$$

Substituting this equation into Eq. (A.34), we obtain,

$$\{\Delta\sigma\} = \left[D^e\right]\left(\{\Delta\varepsilon\} - \{\Delta\varepsilon^p\}\right) \qquad (A.36)$$

If the associated flow rule according with the yield function and plastic potential are used, the plastic strain increment $\{\Delta\varepsilon^p\}$ can be expressed as,

$$\{\Delta\varepsilon^p\} = \Delta\lambda\left\{\frac{\partial f}{\partial\sigma}\right\} \qquad (A.37)$$

In general, the yield function f is a function of stress and plastic strain, and may be written as,

$$f = f\left(\{\sigma\}, \{\varepsilon^p\}\right) \qquad (A.38)$$

when plastic deformation occurs, the following equation may be obtained.

$$\Delta f = \left\{\frac{\partial f}{\partial\sigma}\right\}^T \{\Delta\sigma\} + \left\{\frac{\partial f}{\partial\varepsilon^p}\right\}^T \{\Delta\varepsilon^p\} = 0 \qquad (A.39)$$

Substituting Eq. (A.37) into Eqs. (A.36), (A.39), we obtain,

$$\{\Delta\sigma\} = \left[D^e\right]\left(\{\Delta\varepsilon\} - \Delta\lambda\left\{\frac{\partial f}{\partial\sigma}\right\}\right) \qquad (A.40)$$

$$\left\{\frac{\partial f}{\partial\sigma}\right\}^T \{\Delta\sigma\} + \left\{\frac{\partial f}{\partial\varepsilon^p}\right\}^T \left\{\frac{\partial f}{\partial\sigma}\right\}\Delta\lambda = 0 \qquad (A.41)$$

Eliminating $\{\Delta\sigma\}$ from Eqs. (A.40), (A.41), $\Delta\lambda$ is obtained from the following equation,

$$\Delta\lambda = \frac{\left\{\dfrac{\partial f}{\partial\sigma}\right\}^{T}[D^{e}]\{\Delta\varepsilon\}}{-\left\{\dfrac{\partial f}{\partial\varepsilon^{p}}\right\}^{T}\left\{\dfrac{\partial f}{\partial\sigma}\right\}+\left\{\dfrac{\partial f}{\partial\sigma}\right\}^{T}[D^{e}]\left\{\dfrac{\partial f}{\partial\sigma}\right\}}$$
(A.42)

Substituting Eq. (A.42) into Eq. (A.40), we obtain,

$$\{\Delta\sigma\} = \left([D^{e}] - \frac{[D^{e}]\left\{\dfrac{\partial f}{\partial\sigma}\right\}\left\{\dfrac{\partial f}{\partial\sigma}\right\}^{T}[D^{e}]}{-\left\{\dfrac{\partial f}{\partial\varepsilon^{p}}\right\}^{T}\left\{\dfrac{\partial f}{\partial\sigma}\right\}+\left\{\dfrac{\partial f}{\partial\sigma}\right\}^{T}[D^{e}]\left\{\dfrac{\partial f}{\partial\sigma}\right\}}\right)\{\Delta\varepsilon\}$$
(A.43)

$$= \left([D^{e}] + [D^{p}]\right)\{\Delta\varepsilon\}$$

here, $[D^{p}]$ is expressed as,

$$[D^{p}] = -\frac{[D^{e}]\left\{\dfrac{\partial f}{\partial\sigma}\right\}\left\{\dfrac{\partial f}{\partial\sigma}\right\}^{T}[D^{e}]}{-\left\{\dfrac{\partial f}{\partial\varepsilon^{p}}\right\}^{T}\left\{\dfrac{\partial f}{\partial\sigma}\right\}+\left\{\dfrac{\partial f}{\partial\sigma}\right\}^{T}[D^{e}]\left\{\dfrac{\partial f}{\partial\sigma}\right\}}$$
(A.44)

and this must be considered when the material is in the plastic condition.

Substituting Eq. (A.42) into Eq. (A.37), the plastic strain increment is expressed in the following equation.

$$\{\Delta\varepsilon^{p}\} = \frac{\left\{\dfrac{\partial f}{\partial\sigma}\right\}\left\{\dfrac{\partial f}{\partial\sigma}\right\}^{T}[D^{e}]\{\Delta\varepsilon\}}{-\left\{\dfrac{\partial f}{\partial\varepsilon^{p}}\right\}^{T}\left\{\dfrac{\partial f}{\partial\sigma}\right\}+\left\{\dfrac{\partial f}{\partial\sigma}\right\}^{T}[D^{e}]\left\{\dfrac{\partial f}{\partial\sigma}\right\}}$$
(A.45)

In the process of plastic deformation, $\Delta\lambda$ in Eq. (A37) must have a positive value. Therefore, by checking the sign of $\Delta\lambda$ in Eq. (A.42), the unloading condition can be detected.

12.6 Appendix B: Deformation Matrix

The deformation matrix $[k_{D}]$ is symmetric, nonzero terms are given below:

$$k_{D}(1,2) = k_{D}(7,8) = -k_{D}(1,8) = -k_{D}(2,7) = -\rho_{z}^{2}(EA/L)(\theta_{z1}+\theta_{z2})/10$$
(B.1)

$$k_{D}(1,3) = k_{D}(7,9) = -k_{D}(1,9) = -k_{D}(3,7) = \rho_{y}^{2}(EA/L)(\theta_{y1}+\theta_{y2})/10$$
(B.2)

$$k_{D}(1,5) = -k_{D}(5,7) = -\alpha_{y} + \rho_{y}^{2}EA(-4\theta_{z1}+\theta_{z2})/30$$
(B.3)

$$k_{D}(1,6) = -k_{D}(6,7) = -\alpha_{z} + \rho_{z}^{2}EA(-4\theta_{z1}+\theta_{z2})/30$$
(B.4)

$$k_{D}(1,11) = -k_{D}(7,11) = \alpha_{y} + \rho_{y}^{2}EA(\theta_{y1}-4\theta_{y2})/30$$
(B.5)

Part II Ultimate Strength

$$k_D(1,12) = -k_D(7,12) = -\alpha_z + \rho_z^2 EA(\theta_{z1} - 4\theta_{z2})/30 \qquad \text{(B.6)}$$

where,

$$\eta_y = EI_y/(GA_zL^2) \qquad \eta_z = EI_z/(GA_yL^2) \qquad \text{(B.7)}$$

$$\rho_y = 1/(1 + 12\eta_y) \qquad \rho_z = 1/(1 + 12\eta_z) \qquad \text{(B.8)}$$

$$\alpha_y = 2\rho_y^2 EA\eta_y(1 + 6\eta_y)(\theta_{y1} - \theta_{y2}) \qquad \text{(B.9)}$$

$$\alpha_z = 2\rho_z^2 EA\eta_z(1 + 6\eta_z)(\theta_{z1} - \theta_{z2}) \qquad \text{(B.10)}$$

12.7 References

1. Archer, J.S. (1965), "Consistent Matrix Formulations for Structural Analysis Using Finite Element Techniques", AIAA Journal, 3, 1910 - 1918.

2. Bai Y. and Pedersen, P.T. (1991), "Earthquake Response of Offshore Structures", Proc. of the 10th Int. Conference on Offshore Mechanics and Arctic Engineering, OMAE '91, Stavanger.

3. Bai,Y. and Pedersen, P.T. (1991), "Collision Response of Offshore Structures and Bridges", International Symposium on Marine Structures, ISMS '91, Shanghai.

4. Bai,Y. (1991), "SANDY - A Structural Analysis Program for Static and Dynamic Response of Nonlinear System", User's Manual, Version 2, Department of Ocean Engineering, The Technical University of Denmark, March 1991.

5. Bathe, K.J. (1986), *"Finite Element Methods"*, Springer.

6. Chakrabarty, J. (1987), *"Theory of Plasticity"*, McGraw-Hill Book Company.

7. Chen, W.F. and Han, D.J. (1987), *"Plasticity for Structural Engineers"*, Springer.

8. Fujikubo, M., Bai, Y., and Ueda, Y., (1991), "Dynamic Elastic-Plastic Analysis of Offshore Framed Structures by Plastic Node Method Considering Strain-Hardening Effects", Int. J. Offshore Polar Engng Conf. 1 (3), 220-227.

9. Hill, R. (1950), *"The Mathematical Theory of Plasticity"*, Oxford Univ. Publisher.

10. Jones, N. (1989), *"Structural Impacts"*, Cambridge University Press.

11. Liu, J.H. and Jones, N. (1987), "Experimental Investigation of Clamped Beams Struck Transversely by a Mass", Int. J. Impact Engng. 6(4), 303 - 335.

12. Liu, J.H. and Jones, N. (1988), "Dynamic Response of a Rigid Plastic Clamped Beam Struck by a Mass at Any Point on the Span", Int. J. Solids Struct, 24(3), 251- 270.

13. Messmer, S. and Sayir, M. (1988), "Dynamic Elastic-Plastic Behavior of a Frame", Engineering Computation, 5, 231 - 240.

14. Mosquera, J.M., Symonds, P.S. and Kolsky, H. (1985), "On Elastic-Plastic Rigid-Plastic Dynamic Response with Strain Rate Sensitivity", Int. J. Mech. Sci., 27, 741 - 749.

15. Mosquera, J.M., Symonds, P.S. and Kolsky, H. (1985), "Impact Tests on Frames and Elastic-Plastic Solutions", J. of Eng. Mech., ASCE, 111(11), 1380 - 1401.

16. Nedergaard H. and Pedersen, P.T. (1986), "Analysis Procedure for Space Frame with Material and Geometrical Nonlinearities", Europe-US Symposium - Finite Element Methods for Nonlinear Problems, Edited by Bergan, Bathe and Wunderlich, Springer, 211 - 230.

17. Przemieniecki, J.S. (1968), *"Theory of Matrix Structural Analysis"*, McGraw-Hill Inc.

18. Save, M.A. and Massonnet, C.E. (1972), *"Plastic Analysis and Design of Plates, Shells and Disks"*, North-Holland Publishing Company.

19. Symonds, P.S. and Yu, T.X. (1985), "Counter-Intuitive Behavior in a Problem of Elastic-Plastic Beam Dynamics", J. Appl. Mech. 52, 517-522.

20. Ueda,Y. and Fujikubo, M. (1986), "Plastic Collocation Method Considering Strain Hardening Effects", Journal of the Society of Naval Architects of Japan, Vol. 160, 306 - 317(in Japanese).

21. Ueda,Y. and Yao, T. (1982), "The Plastic Node Method: A New Method of Plastic Analysis", Comp. Meths. Appl. Mech. Engrg., 34, 1089 - 1104.

22. Yamada, Y., Yoshimura, N., and Sakurai, T. (1968), "Plastic Stress-Strain Matrix and its Application for the Solution of Elastic-Plastic Problems by the Finite Element Method", Int. J. Mech. Sci., Vol. 10, pp. 343-354.

23. Yagawa, G. and Miyazaki, N. (1985), *"Heat Induced Stress, Creep and Heat Transfer Analysis Based on the Finite Element Analysis"*, Science Publisher (in Japanese).

24. Yoshimura,S., Chen, K.L. and Atluri, S.N. (1987), "A Study of Two Alternate Tangent Modulus Formulations and Attendant Implicit Algorithms for Creep as well as High-Strain-Rate Plasticity", Int. J .Plasticity , 3, 391 - 413.

25. Zienkiewicz, O.C. (1977), *"The Finite Element Method"*, McGraw-Hill Book Company.

This Page Intentionally Left Blank

Part II

Ultimate Strength

Chapter 13   Collapse Analysis of Ship Hulls

13.1 Introduction

In carrying out the limit state design of ship hulls, it is necessary to estimate the ultimate longitudinal strength of hull girders. Furthermore, in order to estimate oil spills due to tanker collisions and grounding, an investigation of the global dynamic behavior as well as the local plastic response of the individual ship hulls is required.

The collapse strength of the ship hull is governed by buckling, yielding, tension tearing rupture, and brittle failure of materials. Moreover, the strength against each failure mode is influenced by initial deformations, residual stresses, corrosion damages, and fatigue cracks. The complexity of these problems requires that the collapse response of ship hulls be investigated by means of numerical procedures such as finite element methods (FEM). However, traditional FEM requires a considerable amount of computer CPU and manpower to prepare input data and to interpret output data. Consequently, their applications to hull strength and collision problems are limited. Besides, the accuracy of these FEM methods is not always guaranteed (Valsgård & Steen, 1991).

During the last 35 years, several mathematical models have been applied to longitudinal strength analysis of ship hulls. First, Caldwell (1965) introduced a plastic design method for ships. He estimated the longitudinal strength of a ship hull based on the full plastic moment of a cross-section. The effect of buckling is accounted for by reducing the load-carrying capacity of compressed members. Mansour & Thayamballi (1980) considered torsional buckling of stiffeners in their analysis.

Caldwell's method was further modified by Smith (1977) who proposed that the progressive collapse of stiffened plates due to buckling and yielding can be included as stress-strain relationships of fibers of the hull cross-section, while also considering post-buckling behavior. In the Smith method, the hull section is discretized into stiffened panels and corner elements. The prediction of load-shortening behavior of stiffened panels up to the post collapse region is very important. Several algorithms for the modified Smith method have been applied based on different formulas for plating effective width and beam-column.

The above mentioned methods are simple and accurate for prismatic ship hulls subjected to pure bending. However, they are less accurate when other sectional forces and lateral pressure present, because plane sections of hull girders are assumed to remain plane in the modeling.

Chen *et al* (1983) presented a general finite element approach for the collapse analysis of ship hulls. Their approach is applicable to any type of loading and any type of structure, but it is costly with respect to both computer CPU and manpower. Ueda *et al* (1986) presented a finite element procedure based on the Idealized Structural Unit Method (ISUM), which has been

used, for the ultimate strength analysis of ship hulls by Paik (1991). This method leads to a considerable reduction in the size of the mathematical model. Furthermore, Valsgård & Pettersen (1982) and Valsgård & Steen (1991) developed a non-linear super-element procedure, which can also model a complicated structure using only a few elements. So far the ISUM method has not been applied to dynamic response analysis because geometrical nonlinearities have been accounted for using empirical equations. It is difficult to derive empirical equations for dynamic geometrically nonlinear analysis.

With regards to collision damages to ship hulls, there is an increasing international concern for oil pollution from tankers due to different degrees of collision damage. Very little research has been done on minor ship collisions, as opposed to the extensive investigations in the seventies, which related to major collisions involving nuclear vessels. McDermott *et al* (1974) and Kinkead (1980) presented simplified methods for analyzing local deformations of the struck ships in minor collisions. Van Mater *et al* (1979) reviewed low-energy ship collision damage theories and design methodologies. Ito *et al* (1984) conducted systematic large-scale static tests and presented an excellent simplified method, which was used to analyze the strength of double-hulled structures in collision.

The purpose of this chapter is to develop a procedure to enable the calculation of the ultimate hull girder strength, which is as accurate as Smith's method (1977) is for pure bending. It is based on a FEM approach, and the procedure may save manpower and computer CPU as much as the ISUM and the super-element approach can do. Combining the plastic node method (PNM) with the general FEM approach for geometrically nonlinear problems, the present PNM approach may be applied to dynamic geometrical and material nonlinear analysis that is useful for both ultimate strength and impact response analysis.

This Chapter first presents an accurate and efficient finite element procedure for the static and dynamic collapse analyses of ship hulls. This procedure accounts for geometric and material nonlinearities by combining elastic, large displacement analysis theories with a plastic hinge model. A set of finite elements such as beam-column, stiffened plate, and shear panel are developed. Secondly, mathematical equations for the estimation of ultimate moment and moments interaction are then presented and discussed. Thirdly, the Smith method for hull girder analysis is modified to account for the effect of corrosion defects and fatigue cracks. These equations and analysis methods are then compared through ultimate strength analysis of a couple of ship hull girders. Finally, practical applications to the ultimate longitudinal strength analysis of ship hulls and response analysis of tankers involved in collisions are also demonstrated.

This Chapter is based on Bai, Bendiksen and Pedersen (1993) and Sun and Bai (2001).

13.2 Hull Structural Analysis Based on the Plastic Node Method

The finite element formulation for the collapse analysis of ship hulls is described in the following sections. The analysis is based on a standard beam-column analysis. This involves formulations for the collapse of plates and stiffened plates, shear panel elements, and non-linear spring elements.

13.2.1 Beam-Column Element

Figure 13.1 shows a three-dimensional beam-column element. It is a prismatic Timoshenko beam, which has an arbitrary cross-sectional shape. An updated Lagrangian approach has been

adopted for large displacement analyses. Arbitrarily large rotations but small strains are assumed. Using the virtual work principle, we obtain (Bai & Pedersen, 1991):

$$[k_E]\{du^e\} = \{dx\} \tag{13.1}$$

where,

$$[k_E] = [k_L] + [k_G] + [k_D] \tag{13.2}$$

and where $\{d_u^e\}$ and $\{dx\}$ are the increments of the elastic nodal displacements and nodal forces. The elastic stiffness matrix $[K_E]$ is composed of a linear stiffness matrix $[K_L]$, a geometric stiffness matrix $[K_G]$, and a deformation stiffness matrix $[K_D]$. The deformation stiffness matrix $[K_D]$, makes it possible to model a beam-column member using a minimum number of elements, since it accounts for the coupling between axial and lateral deformations.

The elastic-plastic stiffness matrix $[K_P]$ is obtained by applying the plastic node method (Ueda & Yao, 1982):

$$[k_P]\{du\} = \{dx\} \tag{13.3}$$

where,

$$[k_P] = [k_E] - [k_E][\Phi] \left([\Phi]^T [k_E][\Phi] \right)^{-1} [\Phi]^T [k_E] \tag{13.4}$$

$$[\Phi] = \begin{bmatrix} \{\Phi_1\} & \{0\} \\ \{0\} & \{\Phi_2\} \end{bmatrix} \tag{13.5}$$

and where $\{du\}$ denotes the increment of nodal displacements

$$\{\Phi_i\} = \begin{cases} \{0\} & \text{for elastic node} \\ \{\partial\Gamma_i/\partial x_i\} & \text{for plastic node} \end{cases} \quad (i = 1, 2) \tag{13.6}$$

where Γ_i is a fully plastic yield function and $\{x_i\}$ denotes the nodal forces at node "i".
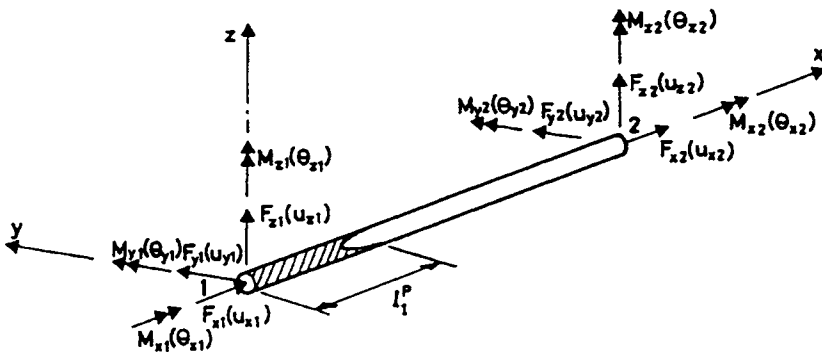
Figure 13.1   Beam-column Element l_1^p and Plastic Region Length near Node 1

In order to apply the fracture mechanics criteria, the increment of plastic strain $\{d_\varepsilon^P\}$ at every node is evaluated as:

$$\{d\varepsilon^P\} = \frac{1}{l_d}\{du_P\} \tag{13.7}$$

where l_d is the equivalent length of the plastic region. The value of l_d is evaluated to be half the partial-yielded region l_p as show in Figure 13.1.

Before the local stiffness matrix is added to the global stiffness matrix, several transformations are necessary. It may be convenient that the local axes do not coincide with the neutral axes. Furthermore, the neutral axis moves when the effective width of the plating changes during loading. Finally, the shear center may differ from the neutral axis of bending. A transformation matrix [S] that accounts for this can be found in standard textbooks (Pedersen, P. Terndrup & Jensen, J. Juncher 1983). This matrix transforms the stiffness matrix to:

$$[k^*] = [S]^T[k_P][S] \tag{13.8}$$

where $[k_P]$ is the local stiffness matrix with respect to the neutral axes, and [k*] is the local stiffness matrix with respect to the nodal axis. This matrix is transformed to obtain the global coordinate:

$$[k_{\text{glob}}] = [T]^T[k^*][T] = [T]^T[S]^T[k_P][S][T] \tag{13.9}$$

where $[k_{\text{glob}}]$ is the stiffness matrix in global coordinates:

$$[S] = \begin{bmatrix} [S_1] & [0] \\ [0] & [S_2] \end{bmatrix} \tag{13.10}$$

and

$$[S_i] = \begin{bmatrix} 1 & 0 & 0 & 0 & E_{zi} & -E_{yi} \\ 0 & 1 & 0 & -e_{zi} & 0 & E_{xi} \\ 0 & 0 & 1 & e_{yi} & E_{xi} & 0 \\ 0 & 0 & 0 & 1 & 0 & 0 \\ 0 & 0 & 0 & 0 & 1 & 0 \\ 0 & 0 & 0 & 0 & 0 & 1 \end{bmatrix} \tag{13.11}$$

where (e_{yi}, e_{zi}) are the coordinates of the shear-center and (E_{yi}, E_{zi}) are the coordinates of the neutral-axis in the local system to the beam end for node "i". This transformation for a neutral axis offset is extremely convenient when only part of the hull is analyzed.

13.2.2 Attached Plating Element

The stiffened plate element is an extension of the beam-column in which an effective width is added to the beam. For a long plate, see Figure 13.2, the effective width is obtained by assuming that Carlsen's ultimate stress equation (Carlsen, 1977) is valid for the region up to, and beyond, the ultimate state:

$$\frac{b_e}{b} = \left(\frac{2.1}{\beta_e} - \frac{0.9}{\beta_e^2}\right)\left(1 - \frac{0.75w_{0max}}{\beta t}\right)\left(1 + \frac{\sigma_r}{\sigma_y}\right)^{-1} R_2 R_\tau \tag{13.12}$$

where $\beta_e = \frac{b}{t}\sqrt{\frac{\sigma_x}{E}}$ and $\beta = \frac{b}{t}\sqrt{\frac{\sigma_y}{E}}$ and where b and t are plate width and thickness, respectively. The maximum initial deflection w_0 max and the residual stress σ_r can be determined by following Faulkner (1975). The reduction coefficient R_2 for the transverse stress σ_2 can be determined from:

$$R_2 = \begin{cases} 1 - (\sigma_2/\sigma_{2u})^2 & \text{for compressive } \sigma_2 \\ 1 & \text{for tensile } \sigma_2 \end{cases} \tag{13.13}$$

where σ_{2u} is the ultimate stress of the plate subjected to uniaxial transverse compression. The reduction coefficient R_τ for shear stress τ is determined by:

$$R_\tau = \left[1 - (\tau/\tau_u)^2\right]^{1/2} \tag{13.14}$$

where,

$$\tau_u = \sigma_y / \sqrt{3}. \tag{13.15}$$
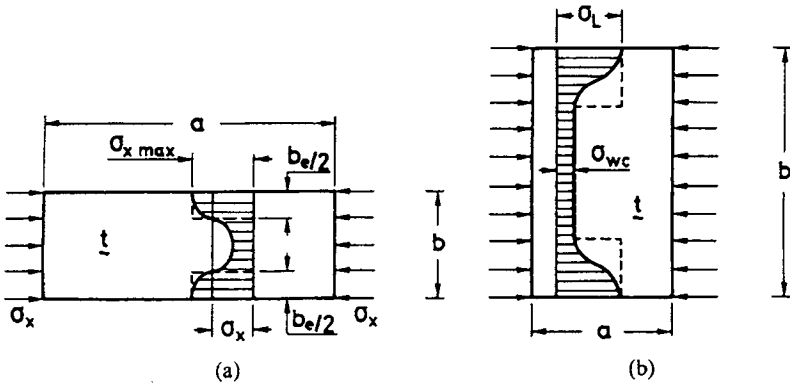
Figure 13.2   Stress Distribution after Buckling in Long and Wide Plate.
(a) Long Plate; (b) Wide Plate

To calculate the stiffness of the plate part, a reduced effective width $\tilde{b}_e$ is introduced as:

$$\tilde{b}_e = b \cdot \frac{d(b_e \sigma_x)}{d\sigma_x} \tag{13.16}$$

For a wide plate (Figure 13.2), the ultimate effective width b_{eu} is determined by following Hughes (1983):

$$\frac{b_{eu}}{b} = \frac{\sigma_L}{\sigma_Y}\frac{a}{b} + \left(1 - \frac{a}{b}\right)\frac{\sigma_{WC}}{\sigma_Y} \tag{13.17}$$

where the ultimate stress at two sides of the plate, σ_L, is equal to the ultimate stress of a square plate of width a, evaluated according to Carlsen (Eq. (13.9)). Finally, σ_{WC} is the ultimate strength of a wide column. According to Smith (1981) it may be approximated by:

$$\sigma_{WC} = \frac{0.63}{1 + 3.27\dfrac{W_{0max}}{\beta_L^2 t}} \tag{13.18}$$

where $\beta_L = \dfrac{a}{t}\sqrt{\dfrac{\sigma_Y}{t}}$ and W_{0max} denotes the maximum initial deflection of the wide column. In the present study, the effective width of the plate is assumed to change until it reaches the ultimate state in a similar manner to the effective width of a long plate:

$$\frac{b_e}{b} = \begin{cases} R_2 R_r & \text{for } \sigma_x\langle\sigma_{WC} \\ \left(\dfrac{c_1}{\sqrt{\sigma_x}} - \dfrac{c_2}{\sigma_x}\right)R_2 R_r & \text{for } \sigma_{WC} \le \sigma_x\langle\sigma_y \\ \dfrac{b_{eu}}{b} & \text{for } \sigma_x = \sigma_y \end{cases} \tag{13.19}$$

where the coefficients c_1 and c_2 can be determined from two points A and B in Figure 13.3.
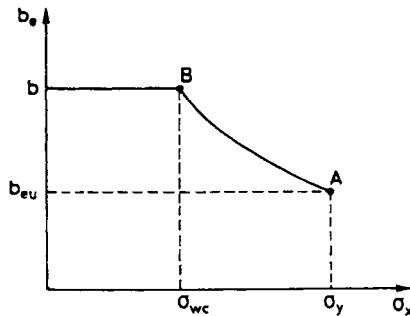
Figure 13.3   Effective Width for a Wide Plate

The contribution of the plate to the beam-column's stiffness is updated every time a load is added. The generalized ultimate plastic forces in compression, tension, and bending are calculated using the corresponding ultimate reduction factors. A yield surface in the form of a sphere is constructed based on these reduction factors. After yielding, the surface is kept constant and the nodal forces will move along the surface following the plastic node method (Ueda & Yao, 1982).

13.2.3 Shear Panel Element

The shear stiffness is lost when a stiffened plate structure is modeled as a grillage. Considering this, an additional element that only has shear stiffness is used. The increment of the shear strain $d\gamma$ in the local coordinate system is related to the increments of nodal displacements $\{du_s\}$ as follows (Bathe, 1982):

$$d\gamma = [B_s]\{du_s\} \tag{13.20}$$

where $[B_s]$ denotes the strain-displacement matrix.

The tangent stress-strain relationship is taken as:

$$d\tau = G_T d\gamma \tag{13.21}$$

where,

$$G_T = \begin{cases} G & \text{for } \gamma \le \gamma_y \\ 0 & \text{for } \gamma \rangle \gamma_y \end{cases} \tag{13.22}$$

where γ_y denotes the shear strain for yielding.

Finally, the element stiffness matrix is obtained:

$$[k_s] = \int_V [B_s]^T G_T [B_s] \, dv \tag{13.23}$$

where V is the volume of the element. The local coordinate system of the element is updated and a coordinate transformation is carried out at each time step.

The element and their interaction are best understood in Figure 13.4.

13.2.4 Non-Linear Spring Element

In addition to the three element types, a spring with non-linear stiffness may also be employed. Any node may be connected, in any of the six degrees of freedom, by non-linear springs. The stiffness is given by points on the force-displacement curve. Stiffness as a function of displacement is the slope of the force displacement curve (see Figure 13.5). In addition to the points on this curve, the unloading stiffness must be defined.

13.2.5 Tension Tearing Rupture

Fatigue cracks and/or welding defects may initiate cleavage, ductile tearing, plastic collapse, or a combination of these events during the collapse. This paper determines the capacity of cracked members by either the CTOD design curve approach (Burdekin, & Dawes, 1971), or the level-3 CTOD method (Andersen, 1988).

In terms of the applied strain ε, the CTOD design curve is expressed as:

$$\Phi = \frac{\delta_{cr}}{2\pi \, a\sigma_y} = \begin{cases} (\varepsilon_{max} / \varepsilon_y)^2 & \text{for } \varepsilon_{max} / \varepsilon_y \le 0.5 \\ \varepsilon_{max} / \varepsilon_y & \text{for } \varepsilon_{max} / \varepsilon_y \rangle 0.5 \end{cases} \tag{13.24}$$

where, δ_{cr} and $\bar{a}$ are a critical CTOD and an equivalent crack length, respectively. E, σ_y, and ε_y are Young's modulus, yield stress, and yield strain, respectively. It is noted that the applied strain εmax is evaluated by disregarding the effects of the crack.

To achieve a more accurate CTOD prediction, we may used the level-3 CTOD method:

$$\frac{\delta_{cr}E}{\pi \bar{a}\sigma_y} = \left[\left(\frac{\sigma_{max}}{\sigma_y}\right)\left\{\frac{\sigma_{max}^2}{2\sigma_y^2\left(1+\sigma_{max}/\sigma_y\right)} + \frac{E\varepsilon_{max}}{\sigma_{max}}\right\}^{1/2} + \frac{\sigma_r}{\sigma_y}\right]^2 \qquad (13.25)$$

where σ_{max} and ε_{max} are the maximum stress and strain respectively, and σ_r denotes the residual welding stress.

Failure is assumed to take place and the cracked member is removed from the structural system when the specified equivalent strain satisfies the selected fracture mechanics criterion. The element forces are applied as unbalanced forces to the system. This fracture mechanics criteria are used for all of the elements presented in this paper.

After collision, the area where tension-tearing rupture has taken place is considered as the "hole". This data is important for the simulation of oil spills resulting from collisions and groundings.
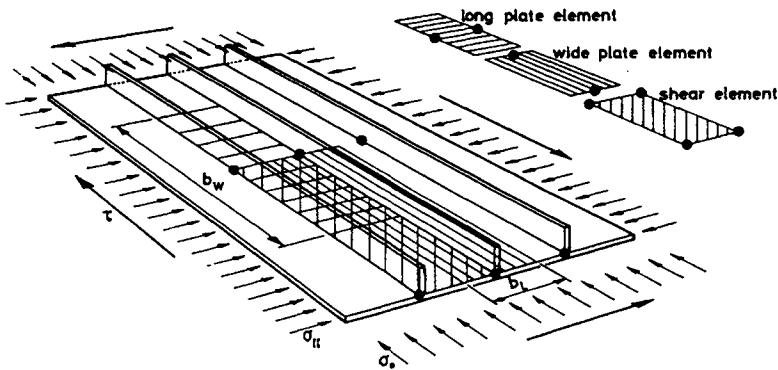
Figure 13.4   Element Type
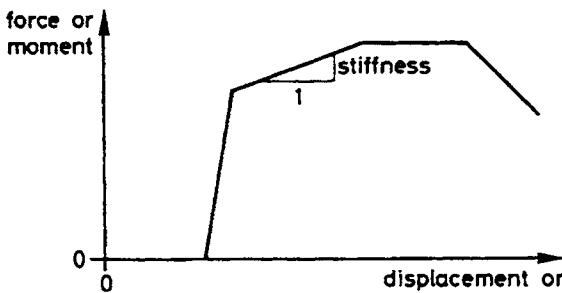
Figure 13.5   Force-displacement Curve for a Non-linear Spring

13.2.6 Computational Procedures

This chapter outlines the computer program SANDY and the computational procedure implemented in the program. Further information can be found in the program manuals (Bai, Y. 1991) and in publications (Bai & Pedersen, 1991, 1993, Bendiksen 1992).

Computer Program SANDY

The theory presented in this paper has been implemented in the general-purpose computer program SANDY (Bai, 1991). Depending on the problem, the following solution procedures can be applied:

- Quasi-static analysis using:

- Load increment

- Displacement, or

- Automatic loading, by using the current stiffness parameter method (Bergan & Søreide, 1978).

- Dynamic analysis (time integration method):

1. Applying dynamic loads as time histories of nodal and element forces

2. Modeling the problem as a structure struck by a deformable mass

3. Applying dynamic loads as initial nodal velocities

4. Earthquake response analysis

Computational Procedure

The non-linear calculation procedure is as follows:

- The size of the increment is determined, this is often determined in the input data

- The increment of the load vector is assembled

The stiffness matrix is calculated for each element. Shear elements Gt, and stiffness matrices are dependent on the current load. For non-linear spring elements, the stiffness factor is calculated as a function of the displacement and of the direction of the increment. For plate elements, the effective width and the linear stiffness plus the eccentricity are calculated. Subsequently, the element is treated in the same way as any other beam-column element. The two geometric matrices are calculated and added to the linear matrix. If the element is in the plastic range, the plastic stiffness matrix is calculated.

If a standard stiffened plate section is used, the program may first recalculate the yield surface, by taking the new reduction factors caused by transverse and shear stress into account. If the element is already plastic, these reduction factors are kept constant; otherwise, they would influence the compatibility equations.

The transformation equation for each element is updated and the stiffness matrices are transformed and added into the global matrix.

In the first step of a dynamic simulation, the global mass matrix is calculated. The system of equations is modified according to a time-integration scheme, e.g. Newmark-β method. Finally, the system of equations is solved. Here we use LDL decomposition and a back substitution.

Each plastified node is checked for unloading. For nodes in non-linear spring elements as well as for shear panel elements, unloading is detected when the load increment and the load have different signs. For all elements with unloading nodes, the stiffness is changed and the procedure is continued from point (f).

When no further unloading is detected, the increments of displacement are obtained. Then the internal forces for each element are calculated. For each elastic element, a check may be made to determine whether yielding occurs during the step. If this is the case, the increment for that element is divided into a part that is treated elastically and a part that is treated like plastic. The increment in the internal force for the element is calculated from:

$$\{dx\} = factor \cdot [K_E]\{du\} + (1 - factor)[K_P]\{du\} \tag{13.26}$$

where *factor* is the elastic fraction of the increment.

Unloading is again checked.

If either loading or unloading takes place, and no kind of iteration is carried out, the change of state gives rise to unbalanced forces, which should be added to the load in the next step. This unbalanced force is calculated to be the difference in internal forces due to changes in the elastic-plastic state. This gives place to yielding $\{dx\} = (1 - factor)([K_E] - [K_P])\{du\}$ and to unloading $\{df\} = ([K_P] - [K_E])\{du\}$.

Note that the global set of equations remains unchanged due to plastification in elements, this means that the influence on the global situation from one node changing state, is disregarded.

A revision is made to determine whether any elements have torn. If this is the case, these elements are removed and their internal forces are added as unbalanced loads in the next step.

When the step is accepted, a new increment begins at point (a).

13.3 Analytical Equations for Hull Girder Ultimate Strength

Buckling and collapse strength of hull girders under bending may be predicted as the fully plastic moment, the initial yield moment, and the progressive collapse moment. The last includes buckling and post-buckling strength of individual components of the hull girder. The fully plastic mode provides an upper bound of the ultimate strength, which is never attained in a hull of normal configurations. The initial yield mode assumes that buckling does not occur prior to yielding. The initial yield strength is a function of the elastic section modulus of the hull girder and yield strength of the material.

In this section, an ultimate strength equation is proposed to account for the effects of lateral pressures, bi-axial loading, and shear stress using analytical solutions. The ultimate strength equation is then compared to the sophisticated approach described in Section 13.4. The ultimate strength equation may be applied for the quantification of structural risks of aging ships with corrosion and fatigue defects, see Parts IV and I of this book.

13.3.1 Ultimate Moment Capacity Based on Elastic Section Modulus

In the initial yield moment approach, it is assumed that the ultimate strength of the hull girder is reached when the deck (alone) has yielded. Premature buckling is assumed not to occur. In this approach, the elastic section modulus is the primary factor for measuring the longitudinal bending strength of the hull. With these assumptions, the initial yield moment can be written as:

$$M_I = (SM)_e \sigma_y \tag{13.27}$$

Here $(SM)_e$ is the elastic section modulus. Due to the use of greater slenderness ratios for stiffeners and plate panels, and high yield steels, the possibility of buckling failure has increased. The initial yield moment may not always be the lower bound to hull girder strength, since the buckling of the individual structural elements has not been accounted for.

Due to the simplicity of the initial yield moment equation, it may be frequently used in practical engineering. Vasta (1958) suggested that the ship hull would reach its ultimate strength when the compression flange in the upper deck (in the sagging condition) or the bottom plating (in the hogging condition) collapses, and that the yield stress in the initial yield moment Eq. (13.24) may be replaced by the ultimate strength σu of the upper deck or bottom plating.

Mansour and Faulkner (1973) suggested the Vasta formula may be modified to account for the shift of the neutral axis location after buckling of the compression flange.

$$M_u = (1+k) \ (SM)_e \sigma_u \tag{13.28}$$

where k is a function of the ratio of the areas of one side shell to the compression flange. For a frigate, they calculated the value of k to be approximately 0.1.

Viner (1986) suggested that hull girder collapses immediately after the longitudinals on the compression flange reach its ultimate strength, and suggested the following ultimate moment equation,

$$M_u = a \ (SM)_e \sigma_u \tag{13.29}$$

where a is normal in the range of 0.92 – 1.05 (mean 0.985).

The findings of Mansour and Faulkner (1973) and Viner (1986) are very useful because of their simplicity – ultimate moment capacity is approximately the product of the elastic section modulus and the ultimate strength of compression flange.

Valsgaard and Steen (1991) pointed out that hull sections have strength reserve beyond the onset of collapse of hull section strength margin, and suggested that a is 1.127 for the single-hull VLCC Energy Concentration, which collapsed in 1980.

A further modification was made by Faulkner and Sadden (1979) as:

$$M_I = 1.15(SM)_e \sigma_y [-0.1 + 1.4465 \sigma_u / \sigma_y - 0.3465(\sigma_u / \sigma_y)^2] \tag{13.30}$$

where σ_U is the ultimate strength of the most critical stiffened panels.

13.3.2 Ultimate Moment Capacity Based on Fully Plastic Moment

Caldwell (1965) assumed that the ultimate collapse condition is reached when the entire cross-section of the hull including side shell has reached the yield state. The material is assumed to be elastic-perfectly-plastic, e.g. strain-hardening effect is ignored. Also, the effect of buckling, and the effects of axial and shear forces are neglected. With these assumptions, the fully plastic collapse moment, M_p can be estimated as:

$$M_p = (SM)_p \sigma_y \tag{13.31}$$

where M_p is the fully-plastic moment, σ_y is the yield strength of the material and $(SM)_p$ is the plastic section modulus.

Frieze and Lin (1991) derived ultimate moment capacity as a function of normalized ultimate strength of the compression flange using quadratic equation,

$$M_u / M_p = d_1 + d_2 \frac{\sigma_u}{\sigma_y} + d_3 \left(\frac{\sigma_u}{\sigma_y}\right)^2 \tag{13.32}$$

where

$d_1 = -0.172, \quad d_2 = 1.548, \quad d_3 = -0.368,$ \qquad for sagging

$d_1 = 0.003, \quad d_2 = 1.459, \quad d_3 = -0.461,$ \qquad for sagging

Mansour (1997) reviewed the above mentioned empirical moment capacity equations and compared them with test results.

Based on fully plastic moment interaction, Mansour and Thayamballi (1980) derived the following ultimate strength relation between vertical and horizontal moments,

$$m_x + k m_y^2 = 1 \quad if \quad \left|m_y\right| \le \left|m_x\right| \tag{13.33}$$

$$m_y + k m_x^2 = 1 \quad if \quad \left|m_y\right| \ge \left|m_x\right| \tag{13.34}$$

where

$$m_x = \frac{M_x}{M_{xu}} \quad , \quad m_y = \frac{M_y}{M_{yu}} \tag{13.35}$$

$$k = \frac{(A + 2A_S)^2}{16 A_S (A - A_S) - 4(A_D - A_B)^2} \tag{13.36}$$

$$A = A_D + A_B + 2A_S \tag{13.37}$$

and where

$\quad M_x$ \qquad = bending moment in vertical direction

$\quad M_y$ \qquad = bending moment in horizontal direction

$\quad M_{xu}$ \qquad = vertical ultimate collapse bending moment

$\quad M_{yu}$ \qquad = horizontal ultimate collapse bending moment

$\quad A_D$ \qquad = cross-sectional area of the deck including stiffeners

$\quad A_B$ \qquad = cross-sectional area of the bottom including stiffeners

$\quad A_S$ \qquad = cross-sectional area of one side including stiffeners

Mansour (1997) demonstrated the above equations fit well with finite element analysis results for ultimate strength of hull girders under combined vertical and horizontal moments.

13.3.3 Proposed Ultimate Strength Equations

The ultimate moment capacity obtained from the modified Smith is the maximum value on the bending moment-curvature curve. Therefore, it is time consuming when reliability analysis relative to the ultimate strength failure mode is carried out by means of the modified Smith method. Some ultimate strength equations have been proposed based on various assumptions of stress distribution over the cross-section. For instance, a moment capacity equation may be derived based on the assumption that the midship section is fully plastic (elastic-perfectly plastic) for the tensile side and is in ultimate strength condition for the compressive side. This assumption gives generally good agreement with more exact predictions by correctly estimating the position of the neutral axis. Successful experience using this approach has been described in a study involving the ultimate strength of corroded pipes under combined (internal/external) pressure, axial force and bending. See Bai, (2001).

Several other assumed stress distributions are available in the literature, including a stress distribution that assumes the middle of the hull depth is elastic while the rest of the hull depth is plastic/ultimate strength. Xu and Cui (2000) assumed a stress distribution in which the middle 1/3 of the hull depth is elastic while the rest of the hull depth is plastic/ultimate strength. The present authors suggest that the ultimate moment capacity M_u can be predicted by the following equation:

$$M_u = \sum_i \sigma_{u_i}^c A_{ps_i} z_i + \sum_j \sigma_{u_j}^t A_{ps_j} z_j + \sum_k \sigma_k^e A_{ps_k} z_k \tag{13.38}$$

where A_{ps} is the area of stiffened panels/hard corners and z is the distance to the neutral axis. Figure 13.6 shows a schematic diagram of stress distribution under sagging condition. The stress distribution used in Eq.(13.38) does account for the ultimate strength of individual stiffened panels and hard corners, e.g. it is not uniformly distributed in Figure 13.6.

In Eq.(13.38), the compressive ultimate strength region, tensile ultimate strength region and elastic region are denoted by i, j, k respectively. σ_u^C is the ultimate compressive strength for stiffened panels or yield stress for hard corners. σ_u^T is the ultimate tensile strength (yield stress). Elastic stress σ^e has a linear distribution around the neutral axis. Based on observations of stress distribution from more comprehensive numerical analysis, it is suggested by the present authors that the total height of the elastic region may be taken as half of the hull depth, e.g. $g_1 + g_2 = D/2$ The height of the compressive region g_1, and the height of the tensile region g_2, may be estimated based on beam theory, which assumes plane remains plane after bending.

Based on Eq.(13.38), the ultimate moment capacity of a hull girder may be estimated by the following steps:

- Subdivide the cross-section into stiffened panels and hard corners;

- Estimate the ultimate strength of each stiffened panel using recognized formulas;

- Calculate the distance "H" from the bottom of the ship to the neutral axis by assuming the total force from the stress integration over the cross-section is zero;

- Calculate the ultimate moment capacity of the hull girder using Eq.(13.38).
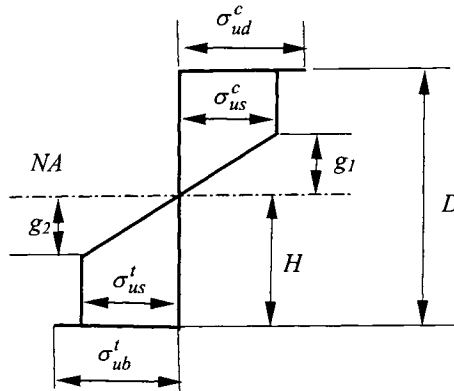
**Figure 13.6   Illustration of the Assumed Stress Distribution for Hull
Girder Collapse - Deck in comprossion**

In addition, it is necessary to check vertical shear strength Fu using

$$F_u = \sum \tau_{u_i} A_{p_i} \tag{13.39}$$

where A_{p_i} is the area of the panel in the shear element (plate area only) and τ_u is the characteristic ultimate shear stress in the panel. Here, i includes all panels in the longitudinal shear element.

13.4 Modified Smith Method Accounting for Corrosion and Fatigue Defects

Considering a hull girder as a beam section under bending, Smith (1975, 1977) proposed a simple procedure to calculate the moment – curvature relationship and ultimate strength of a hull girder. The basic assumptions of the Smith method are summarized as follows:

(1)   The hull cross-section is subdivided into a number of subdivisions such as stiffeners with associated plating and the corner elements, which are considered to act and behave independently.

(2)   For each such panel the load-shortening curve is constructed. This can be accomplished by any of a number of methods, including experimental results, nonlinear finite element analysis and simplified elastic-plastic buckling analysis. The Smith method can also account for the manufacturing residual imperfections including deflections and stresses of plating and columns.

(3)   The hull is then subjected to an incrementally increasing curvature in which it is assumed that the cross-sections that is initially plane remains plane after bending, and experience only rotation about an assumed neutral axis. The overall grillage collapse of the deck and bottom structures is avoided by using sufficiently strong transverse frames.

(4)   The total axial force and bending moment acting on the cross-section are obtained through an integration of the stress over all of the components that making up the cross-section. Through iteration, the location of the neutral axis is obtained by equating the total axial force to the longitudinal force that is zero.

This Section presents a modified Smith method (Smith, 1975, 1977 and Yao, 1991, 1992 Rahman and Chow, 1996) in which the effect of corrosion defects, fatigue crack and lateral pressure are accounted for.

As demonstrated by previous researchers, the advantages of the modified Smith method include (1) efficiency, (2) flexibility to account for the effects of corrosion defects, fatigue cracks, and other factors and (3) accuracy.

The stress-strain relationships for the elements are given below.

13.4.1 Tensile and Corner Elements

The stress-strain relationship for tensile and corner elements is assumed linear elastic and elastic-perfectly plastic:

$$\sigma_x = \begin{cases} \varepsilon_x E & \varepsilon \le \varepsilon_y \\ \sigma_y & \varepsilon \ge \varepsilon_y \end{cases} \tag{13.40}$$

where E, σ_y, and ε_y are the elastic modulus, yield stress and, yield strain of the material, respectively.

13.4.2 Compressive Stiffened Panels

A stiffened panel is composed of a longitudinal stiffener with its attached plating. Following the approach of Rahman and Chowdhury (1996), three distinct zones in the whole range of the loading-shortening behavior are considered: stable zone, no-load-shedding zone and load-shedding zone, as shown in Fig 13.7. The stable zone is in the pre-ultimate strength region. The no-load-shedding zone does not require any load-shedding to maintain equilibrium. When the strain increases, the final zone is characterized by a drop-off.

More information on compressive stiffened panels may be found from Smith (1975).
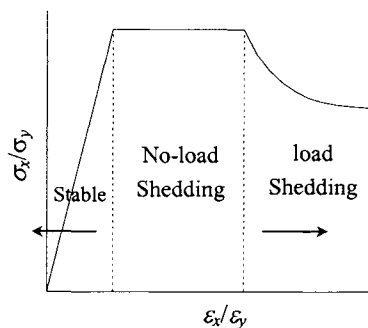
Figure 13.7   Typical Stress-Strain Relation of a Stiffened Panel

A stiffened panel is composed of a longitudinal stiffener with its attached plating. Following the approach of Rahman and Chowdhury (1996), three distinct zones in the whole range of the stiffened panel's loading-shortening behavior are considered. The ultimate strength of a stiffened panel is given by

$$\sigma_{pu} = min(\sigma_{uf}, \sigma_{up})$$ (13.41)

where σ_{uf} and σ_{up} are the ultimate beam-column failure values of the panel when lateral pressure causes compression of stiffener flange and plating respectively. According to Hughes (1983), a solution may be obtained by solving the following equations for stiffener failure,

$$\sigma_y = \sigma_{uf} + \frac{M_0 y_f}{I} + \frac{\sigma_{uf} A(\delta_0 + \Delta) y_f}{I} \Phi$$ (13.42)

and for plate failure,

$$\sigma_y = \sigma_{up} + \frac{M_0 y_p}{I_e} + \frac{\sigma_{up} A_e (\delta_0 + \Delta + \Delta_p / \Phi) y_p}{I_e} \Phi$$ (13.43)

where Δ is the initial eccentricity, δ_0 and M_0 are the maximum deflection and bending moment due to lateral load alone; Δ_P is the eccentricity caused by reduced stiffness of compressed plating; I and A are respectively the second moment and the sectional area of the panel, considering b_P (panel width) is fully effective where as I_e and A_e are the similar properties but for transformed section replacing b_P by b_{Pe} (effective width); y_f is the distance from the panel neural axis to the stiffener flange and y_P to the plating of the transformed section; Φ is the magnification factor for combined loading.

13.4.3 Crack Propagation Prediction

To predict the crack propagation and fatigue life, the Paris-Erdogan equation is used

$$\frac{da}{dN} = C \Delta K^m$$ (13.44)

where a is the crack size, N is the number of cycles, ΔK is the stress range intensity factor and C and m are material parameters. The stress intensity factor is given by:

$$\Delta K = \Delta \sigma Y(a) \sqrt{\pi a}$$ (13.45)

where $\Delta \sigma$ is the stress range and $Y(a)$ is the geometry function.

If $Y(a)=Y$ is a constant and $m \neq 2$, then integration of Eq.(13.44) gives

$$a(t) = [a_0^{(1-m/2)} + (1 - \frac{m}{2}) C (\Delta \sigma Y \sqrt{\pi})^m v_0 t]^{\frac{1}{1-m/2}}$$ (13.46)

where a_0 is the initial crack size, and the complete fatigue life T_f is equal to the sum of the time to crack propagation T_p and the time to crack initiation T_i

$$T_i = k T_p$$ (13.47)

where k can vary from 0.1 to 0.15. The crack size is assumed to have a normal distribution with the mean and variance, see Guedes Soares and Garbatov (1996, 1999).

Two types of cracks are considered in the stiffened panel, one propagating away from the stiffener in a transverse direction decreasing the width of attached plating, and the other across the web of stiffener decreasing the web height.

13.4.4 Corrosion Rate Model

Corrosion rates depend on many factors including coating properties, cargo composition, inert gas properties, temperature of cargo, and maintenance systems and practices. For this reason, the corrosion rate model should be appropriately based on the statistics of measurement data.

Practically, the time-variant corrosion rate model may be divided into three phases. In the first one, there is no corrosion because of the protection of coatings, and corrosion rate is zero. The second phase is initiated when the corrosion protection is damaged and corrosion occurs, which reduces the plate thickness. The third phase corresponds to a constant corrosion rate. The present authors suggested a model as

$$r(t) = r_s \left(1 - e^{-\frac{t - \tau_i}{\tau_t}} \right) \tag{13.48}$$

where τ_i is the coating lifetime, τ_t is the transition time and r_s is the steady corrosion rate. Figure 13.8 shows the corrosion rate model.
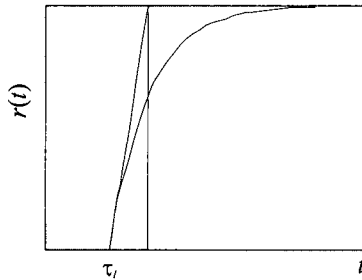
Figure 13.8   Model of Corrosion Rate
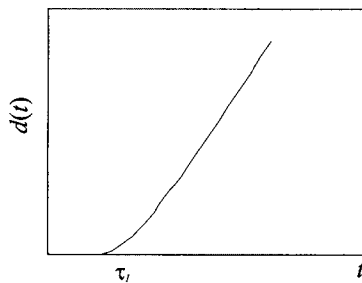
Figure 13.9   Loss of Plating Thickness from Corrosion as Time Function.

By integrating Eq.(13.36), the corrosion depth can be obtained by:

$$d(t) = r_s \left[t - (\tau_i + \tau_t) + \tau_t e^{-\frac{t - \tau_i}{\tau_t}} \right] \tag{13.49}$$

where the parameters τ_i, τ_t and r_s should be fitted to inspection results. Figure 13.10 shows the corrosion depth as a time function. The coating lifetime τ_i can be assumed to be fitted by a Weibull distribution,

$$f(\tau_i) = \frac{\alpha}{\beta}\left(\frac{\tau_i}{\beta}\right)^{\alpha-1} exp\left[-\left(\frac{\tau_i}{\beta}\right)^{\alpha}\right] \tag{13.50}$$

and r_s, to be fitted by a normal distribution. Figures 13.8 and 13.9 illustrate the corrosion depth reproduced by the present model based on the net measurement data of Yamamoto (1998). There exists some variability of the data along the regression curve.
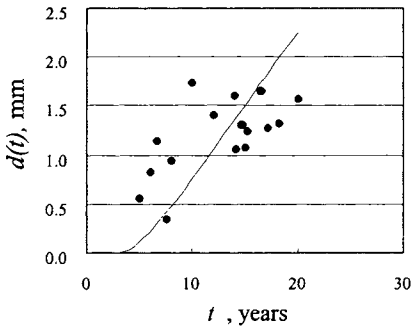
Figure 13.10 Loss of Plating Thickness from Corrosion for Inner Bottom Plates of Bulk-Carriers.
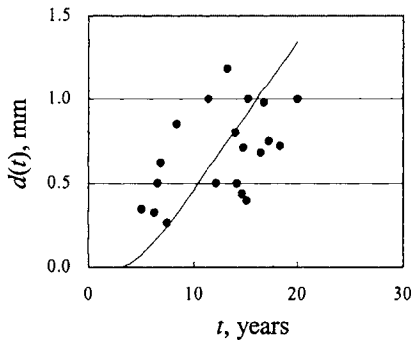
Figure 13.11 Loss of Plating Thickness from Corrosion for Side Shells of Bulk Carriers.

The net area $A_i(t)$ of the stiffened panel available to carry longitudinal stress is dependent on the crack size $a_i(t)$ and the corrosion depth $d_i(t)$,

$$A_i(t) = [b_p - 2a_i(t)][h_p - d_i(t)] + [h_s - a_i(t)t][b_s - d_i(t)]$$ (13.51)

where b_p and hp are the width and thickness of the attached plating, and h_s and b_s are the web height and thickness of the stiffener.

From an engineering viewpoint, a stiffened panel is considered ineffective when the crack size exceeds the critical crack size determined by the Crack Tip Opening Displacement (CTOD) method (Ghose, 1995) or when the corrosion induced thickness reduction exceeds 25% of the original plate thickness.

13.5 Comparisons of Hull Girder Strength Equations and Smith Method

Many examples of progressive collapse analysis for box girders and ship primary hulls have been calculated to verify the efficiency and accuracy of the present modified Smith method. The examples used in the International Ship and Offshore Structures Congress (ISSC) benchmark calculations by Yao *et al* (2000) are given in Table 13.1 together with the results of the modified Smith method described in Section 13.4, and the equation described in Section 13.3.

Table 13.1   Ultimate Strength Calculations

Ship Type	Load Cond.	ISSC*		Modified Smith Method (MNm)	Proposed Equation (MNm)
		Mean	Cov		
Bulk Carrier	Sagging	1.52×10^4	0.07	1.53×10^4	1.53×10^4
	Hogging	1.86×10^4	0.04	1.72×10^4	1.70×10^4
Container Ship	Sagging	6.51×103	0.14	5.84×10^3	6.25×10^3
	Hogging	7.43×103	0.08	6.93×10^3	6.80×10^3
DH VLCC	Sagging	2.24×10^4	0.11	1.98×10^4	2.23×10^4
	Hogging	2.91×10^4	0.04	2.76×10^4	2.68×10^4
SH VLCC	Sagging	1.72×10^4	0.02	$1.46 \times 10^{4}**$	1.70×10^4
	Hogging	1.82×10^4	0.02	$1.79 \times 10^{4}**$	1.81×10^4
Frigate Model	Sagging	10.39	0.07	9.61	9.73
	Hogging	12.38	0.08	12.10	12.26
FPSO	Sagging	-	-	3.58×10^3	3.61×10^3
	Hogging	-	-	5.14×10^3	4.90×10^3

* The results are obtained by averaging the values of all participants in ISSC VI.2.(Yao, 2000)

**The external pressure is applied consistent with the analysis by Rutherford and Caldwell(1990).
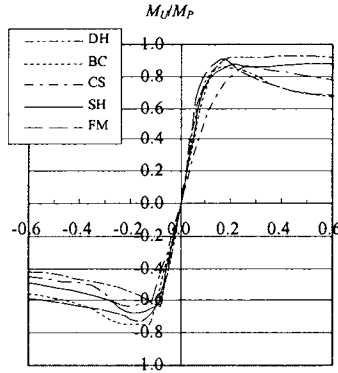
**Figure 13.12   Bending Moment vs. Curvature Response for the Hull
Girders used in ISSC Benchmark.**

The results from the simplified method and ultimate strength equation presented by the authors agree well with the results reported by Yao *et al* (2000). Figure 13.12 shows the moment-curvature response for the five hull girders. In Figure 13.12, the positive value of M_U / M_P is hogging.

The mean moment-curvature responses of the FPSO hull girder are shown in Figure 13.13 for different service years considering the degradation effects of fatigue and corrosion, where the number on the curve represents the service year.
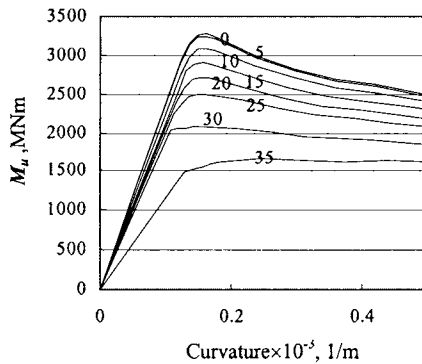
Figure 13.13   Mean Moment-Curvature Responses

From Figure 13.13 it is easy to appreciate the importance of conducting inspection and repair. When inspection and repair are not conducted the load-carrying capacity decreases with time.

The mean maximum values of the ultimate strength are plotted in Figure 13.14 as a time function where four cases of degradation effects are considered based on the corrosion rates in Table 2 of Sun and Bai (2001), i.e.

Case (1): no corrosion;

Case (2): half-mean steady corrosion rates;

Case (3): mean steady corrosion rates;

Case (4): double mean steady corrosion rates.
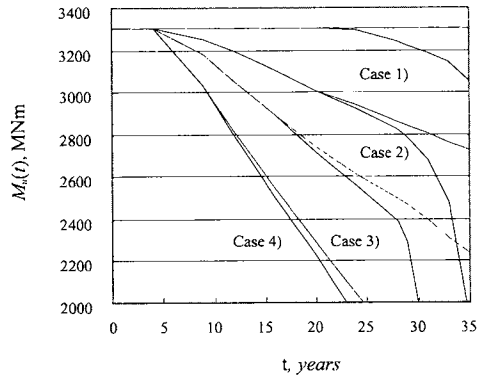
Figure 13.14   Mean Ultimate Strength for Four Cases of Mean Steady Corrosion Rates.

The solid lines in Figure 13.14 denote when both corrosion and fatigue degradation effects are taken into account, while the dotted lines indicate only the corrosion effect is considered. The mean maximum ultimate strength of the hull girder has been observed to be reduced significantly, mainly as a result of the corrosion defects. If additional effects of fatigue are relatively small although residual strength is dictated primarily by corrosion rates. The degradation rates are different from those of Ghose et al (1995), because only fatigue effects were considered therein.

13.6   Numerical Examples Using the Proposed Plastic Node Method

In this chapter, five typical application examples of ship collapse analysis are presented. The first three examples have been chosen to validate the proposed analysis procedure. The complexity of the analyzed structures has changed from a single structural component to a structural system. After validating the analysis procedure, examples of ultimate longitudinal strength and collision analyses of hull scale ships are presented. The analysis is described in more detail by Bendiksen, (1992).

13.6.1   Collapse of a Stiffened Plate

This procedure has been compared to a model of an experimental investigation of the ultimate load carrying capacity of longitudinally stiffened plates (Faulkner, D. 1976). The plate is compressed in the longitudinal direction (see Figure 13.15) and has residual stresses from

welding and an initial deflection $\left(w_0 = 0.12\beta^2 t\right)$ In addition, the stiffener has an initial deflection (of magnitude *L/1000*). The load-end-shortening curve shown in Figure 13.16 was obtained by the present method by using two elements. The obtained buckling load agrees with the experimental result within 2%. In conclusion, the position of the loading plane is a decisive parameter.
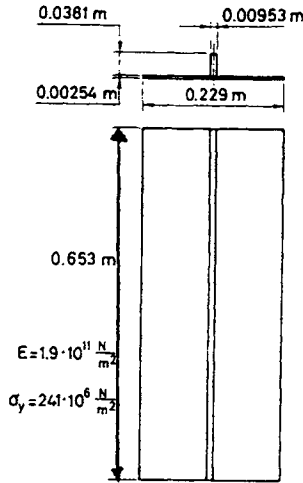
Figure 13.15   Stiffened Plate
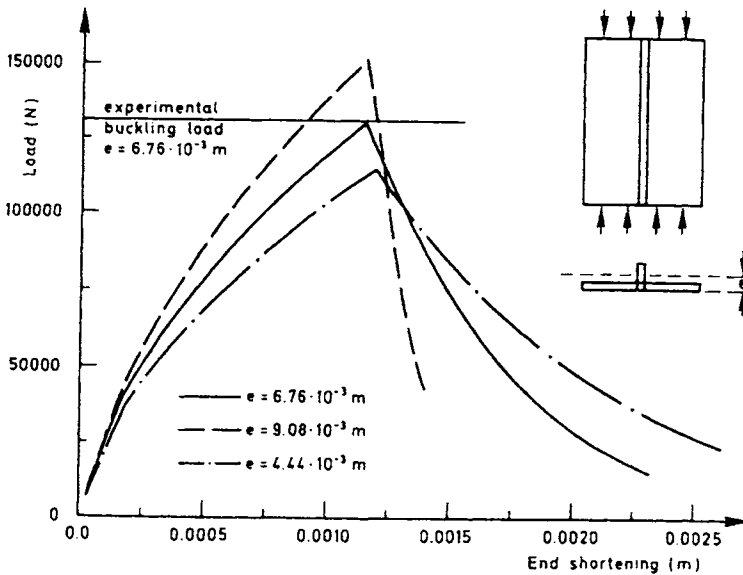
Figure 13.16   Load End-Shortening Curve for Stiffend Plates

13.6.2 Collapse of an Upper Deck Structure

The next example, shown in Figure 13.17, is a longitudinally- and transversely stiffened plate. The plate is analyzed by means of four nodal plate elements in an ISUM procedure by Ueda *et al* (1986). The plate has an average initial deflection of $w_0/t = 0.25$ and a welding residual stress of $\sigma_r / \sigma_y = 0.2$. The shifting of the neutral axis is not considered in this example. The result of the analysis, as shown in Figure 13.18, provides a very good agreement between the FOUR-NODE ISUM procedure and the present procedure. Both were evaluated with respect to buckling loads and end shortening loads by using only 24 nodes.
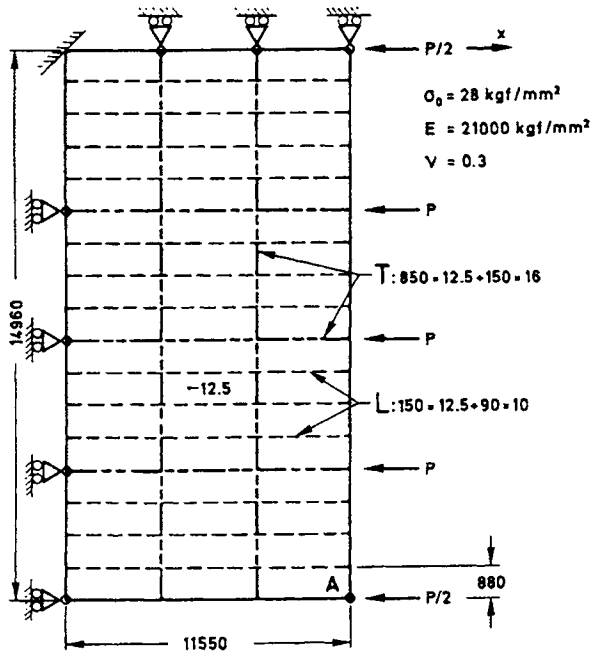
Figure 13.17 Upper Deck Structure in Compression
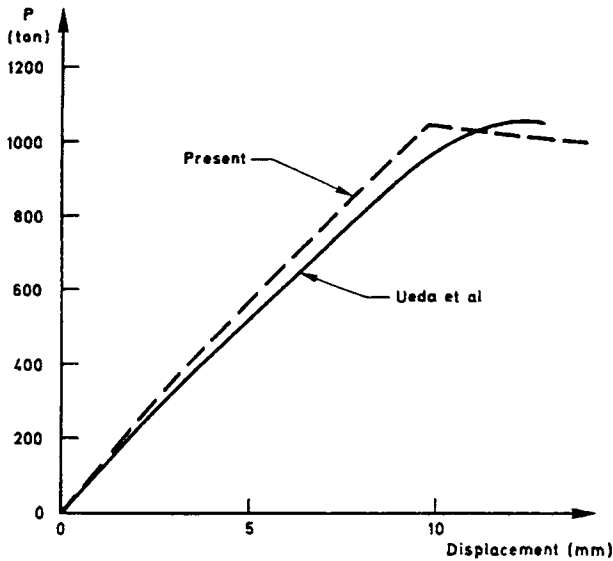
Figure 13.18   Load –Diaplacement Curves for Deck Structure

13.6.3 Collapse of Stiffened Box Girders

This procedure has been compared to experimental results based on the ultimate longitudinal strength of ship hull models (Nishihara, 1984). The experiments consisted of a ship hull model being exposed to a four point bending load. The present numerical analysis connected a detailed model of the middle section of the hull to simple beams modeling the less stressed ends of the hull. This was done by using a transformation for the nodes placed outside the neutral axis. This allows a number of longitudinal plate elements in the cross section to be connected to one node at each end of the analyzed model.

If the initial plate and overall deflections are of magnitude $0.12\beta^2 t$ and $L/1000$, respectively and the residual stress level is $\sigma_r/\sigma_y = 0.1$, then the result for a tanker-like section, (spectrum MST-3) Figure 13.19, is compared with the experimental result in Figure 13.19. Figure 13.19 shows the analysis is in good agreement with the experiment and the initial imperfections reduce the ultimate moment approximately by 14%. Furthermore, the analytical fully plastic moment $M_p = 787kNm$ is a well-predicted value by the present method.

In Figure 13.20, the collapsed shape of the hull is indicated and the buckling of the bottom is evident. Figure 13.21 shows how the nodes are connected using the transformation matrix $\underline{S}$.
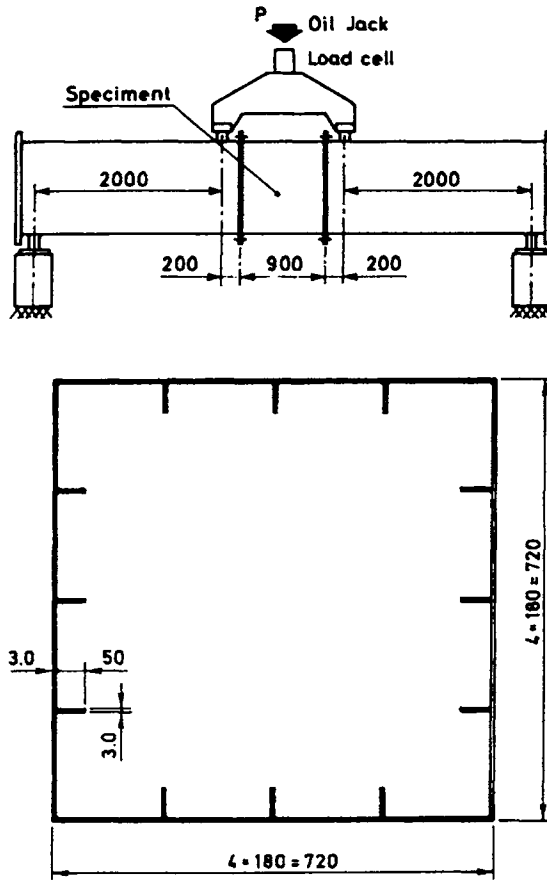
Figure 13.19   Model of a Tanker Measured in Millimeters
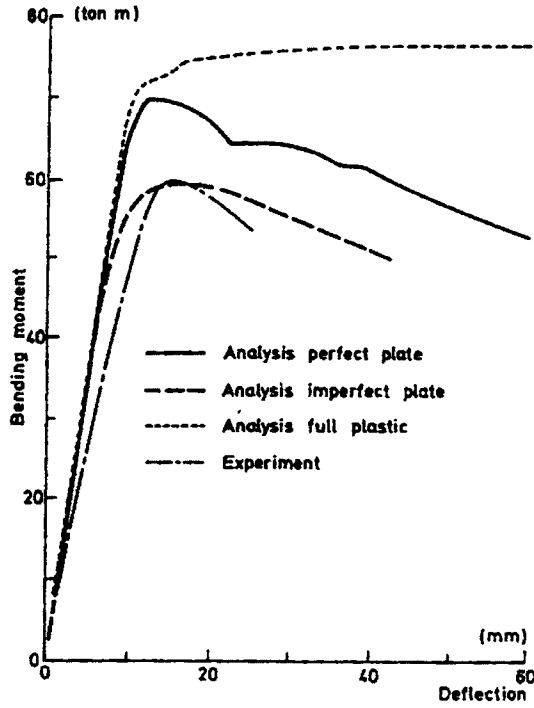
Figure 13.20   Ultimate Behavior for the Tanker Model

13.6.4 Ultimate Longitudinal Strength of Hull Girders

The ultimate longitudinal strength is calculated for a 60 000 dwt double hull, double bottom product tanker. Because of symmetry, only a quarter of the center tank is modeled (see Figure 13.22). Boundary conditions are specified in the planes of symmetry.
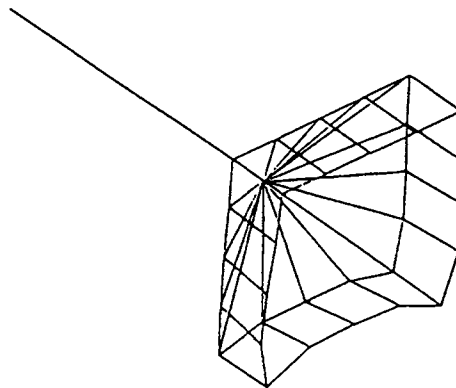
Figure 13.21   Bondary Condition Model for Ship's Mid-section
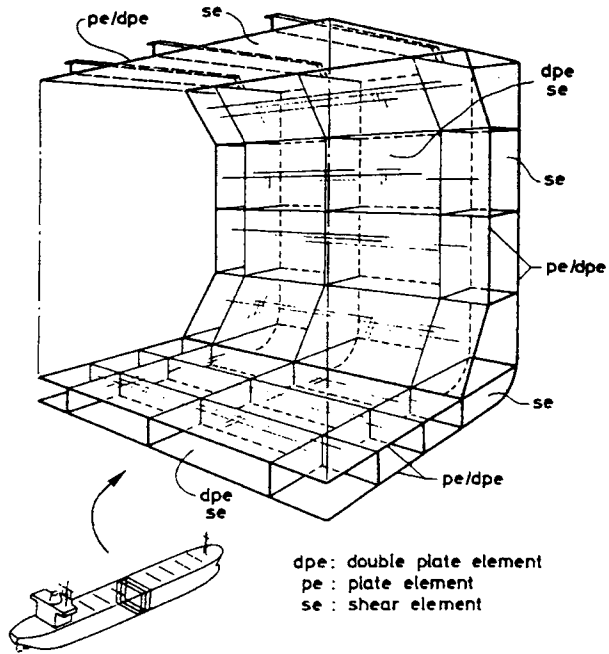
Figure 13.22 Quarter of the Tank which is the Extent of the Detailed Model
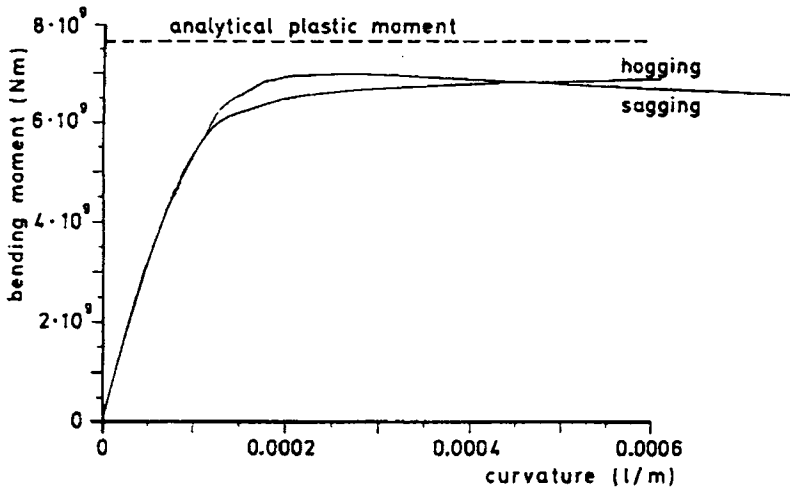
Figure 13.23 Moment and Curvature Relation of the Ship
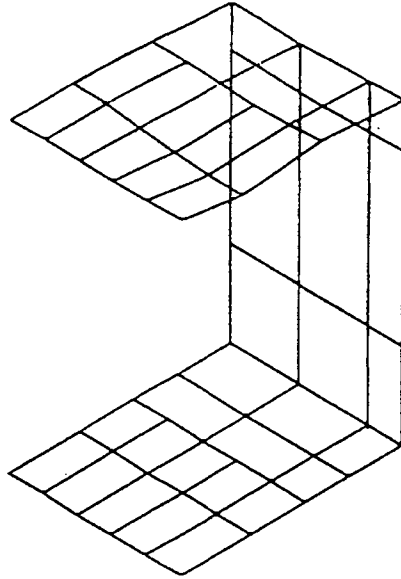
Figure 13.24   Deflected Shape in Sagging

Since pure bending is applied, it is valid to assume that plane boundaries remain plane. Therefore, only one nodal point is used in the fore end of the tank. Again, this is possible with the transformation for node points out of the neutral axis. The end of the section is loaded with a vertical bending moment that is controlled by the current stiffness parameter method. It is possible to load the hull in pure bending throughout the calculation without knowing the new position of the neutral axis for the hull. Note that in this procedure, plane sections are not restricted to remain plane, except for the end section described by only one node. The curvature-moment relationship for the hull is shown in Figure 13.23 and is compared to the full plastic moment.

The formulae relating the ultimate moment to the fully plastic moment, imply that the ultimate moment under the influence of a sagging load is 0.86 M_p and under the influence of a hogging type load is 0.89 M_p (Frieze and Lin, 1991). The present analysis gives results of 0.89 M_p and 0.88 M_p, respectively. The failure mode in sagging causes overall buckling of the deck as shown in Figure 13.24. The failure mode in hogging causes plate buckling combined with plasticity in the bottom and lower part of the side and limits the load carrying capacity.

13.6.5 Quasi-Static Analysis of a Side Collision

The next example is a side collision. To be more precise, an infinitely stiff object is forced into the side of a ship hull in a quasi-static analysis. The ship hull is the same as the one used in the hull-bending example; therefore, the finite element model used in this example has minor modifications. Shear elements have been added in the deck and at the bottom.

A concentrated load is applied at the middle of the side. The Current Stiffness Parameter method is employed to control the load. The force-indentation curve for this example can be seen in Figure 13.25.
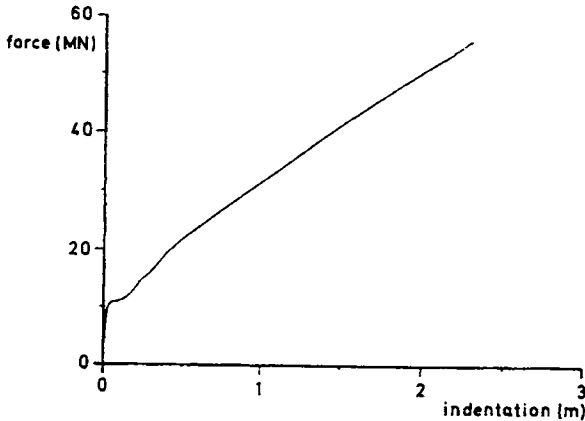
Figure 13.25 Force/Indentation Curve for the Hull Loaded Quasi-static by A Concentrated Force

The results may be compared with simplified analyses (Søreide, 1981). The maximum force in the first phase can be calculated as the load that makes the longitudinal beam, which represents the side, collapse as if it were a plastic mechanism. Assuming it is clamped when Mp is calculated for a beam breadth of 5m, its collapse load becomes 6.65MNm and the load at the end of phase one becomes:

$$P_0 = \frac{46.65\,MNm}{2.5\,m} = 10.6\,MN$$

This is extremely close to what is seen Figure 13.25.

In phase two, the membrane forces in the two side shells carry the load. Simplified calculations can be used to verify the numerical results.

In this example, tearing is assumed to take place at an equivalent strain of 5%. The calculation shows that the vertical elements near the collision point begin to tear at an indentation of 1.5m. The calculation ends when the longitudinal elements, at the collision point and at an indentation of 2.3 m, begin to tear.

13.7 Conclusions

The progressive collapse of ship hulls subjected to bending and collision loads has been studied using the Plastic Node Method(PNM). A new element for modeling stiffened plates has been derived. A transformation between the nodal axis and the neutral axis is used when parts of the modeled structure in different finite element meshes are connected. No

assumptions about the position of the neutral axis for the hull beam are made when progressive collapse is analyzed. By using this transformation, the shifting of the neutral axis in the plate elements is also taken into account.

The results obtained from this PNM method have been compared with experimental results and other numerical solutions, which have experienced problems with plate and overall buckling. The comparison appears to be in good agreement with these simple examples.

The present PNM method has been compared with experiments that deal with the ultimate longitudinal strength of a tanker. Calculations have been performed with and without initial plate imperfections. When disregarding the plate imperfections, the ultimate load is 16% higher.

The calculation of the ultimate longitudinal strength of an existing double hull product tanker is shown. The ratio between the ultimate moment and the plastic moment was compared with an empirical prediction and the results showed to be in good agreement. The result of the analysis is not only the ultimate bending moment, but is also the ultimate failure mode. A failure in sagging would be the most dramatic.

Finally, the PNM method was used to derive the force-indentation curve for a double-hulled product tanker subjected to a concentrated force in the middle of the side. The force-indentation curve derived by a quasi-static analysis is in agreement with the approximate method.

This work has shown that the Plastic Node Method, along with the new element, is in agreement with existing approximate methods for hull collapse loads and moreover, provides much more information about the progressive failure. In this respect, the Plastic Node Method approaches the general finite element method while using a much simpler element mesh, which is considered to be more efficient.

A modified Smith method to compute the ultimate value of the longitudinal bending moment at the midship section was introduced using an effective width formula for the plating. The modified Smith method accounts for the manufacturing imperfections, including initial eccentricity of stiffeners, the plating's initial residual stress, and deflection. The corrosion defect was considered as an exponential time function with a random steady corrosion rate, which is assumed to uniformly reduce the plate thickness. Crack propagation was predicted based on the Paris-Erdogen equation. Crack initiation time and coating lifetime were also taken into account.

An equation for estimating ultimate strength of hull girders was suggested. The hull girders used in the ISSC benchmark calculations by Yao *et al* (2000), were used to examine the accuracy of this equation. It has been demonstrated that the equation provides quite reasonable results and may be useful in estimating the bending moment strength.

13.8 References

1.   Andersen, T. L., (1988), "Ductile and Brittle Fracture Analysis of Surface Flows Using CTOD", Experimental Mechanics, pp. 188-193.

2.   Bai, Y., Bendiksen, E. and Pedersen, P. Terndrup (1993) "Collapse Analysis of Ship Hull", J. of Marine Structures, Vol.6, pp. 485-507.

3. Bai, Y. & Pedersen, P. Terndrup, (1991), "Earthquake Response of Offshore Structures", Proceedings of the 10th Offshore Mechanics and Arctic Engineering Conference, OMAE'91, Vol. 1, Part B, Stavanger, pp. 571-578.

4. Bai, Y. & Pedersen, P. Terndrup, (1993), "Elastic-Plastic Behaviour of Offshore Steel Structures Under Impact Loads", Internat. J. Impact Engng, 13(1) pp.99-115.

5. Bai, Y., (1991), "SANDY - A Structural Analysis Program for Static and Dynamic Response of Nonlinear Systems. Theoretical Manual and Demonstration Problem Manual", Version 2. Department of Ocean Engineering, The Technical University of Denmark, August 1991.

6. Bai, Y. (2001), *"Pipelines and Risers"*, Elsevier Science Ocean Engineering Book Series.

7. Bathe, L, (1982), *"Finite Element Procedures in Engineering Analysis"*, Prentice-Hall, Englewood Cliffs, NJ, pp. 200-210.

8. Bendiksen, E., (1992), "Hull Girder Collapse", Ph.D. Dissertation, Department of Naval Architecture and Offshore Engineering, The Technical University of Denmark.

9. Bergan, P. G. & Sorelde, T. H., (1978), "Solution of Large Displacement and Instability Problems Using the Current Stiffness Parameter", In *"Finite Elements in Nonlinear Mechanics"*, ed. P. G. Bergan, et al. Tapir, pp. 647-699.

10. Burdekin, F. M. & Dawes, M. G., (1971), "Practical Use of Linear Elastic and Yielding Fracture Mechanics With Particular Reference to Pressure Vessels", In Proceedings of the Institute of Mechanical Engineers Conference, London, May 1971.

11. Caldwell, J. B., (1965), "Ultimate Longitudinal Strength", Trans. Royal Inst. Nav. Arch., 107, (1965) 411-430.

12. Carlsen, C. A., (1977), "Simplified Collapse Analysis of Stiffened Plates", Norwegian Maritime Research, 5(4) pp. 20-36.

13. Chen, Y. K., Kutt, L. M., Plaszczyk, C. M. & Bieniek, M. P., (1983), "Ultimate Strength of Ship Structures", Trans. Soc. Nav. Arch. and Marine Engrs., 91 pp. 149-168.

14. Evans, J.H., (1974), *"Ship Structural Design Concepts"*, Cornell Maritime Press.

15. Faulkner, D., (1975), "A Review of Effective Plating for Use in the Analysis of Stiffened Plating in Bending and Compression", J. Ship Research, 19(1) pp. 1-17.

16. Faulkner, D., (1976), "Compression Test on Welded Eccentrically Stiffened Plate Panels", In *"Steel Plated Structures"*, ed. P.J. Dowling, J.E. Harding & P.A. Frieze. Crosby Lockwood Staples, London.

17. Faulkner, D. and Sadden, J.A. (1979), "Toward a Unified Approach to Ship Structural Safety", Trans. RINA, Vol.121, pp. 1- 38.

18. Frieze, P.A. and Lin, Y.T. (1991), "Ship Longitudinal Strength Modeling for Reliability Analysis", Proc. of the Marine Structural Inspection, Maintenance, and Monitoring Symposium, SSC/SNAME, pp.III.C.

19. Ghose, DJ et al. (1995), "Residual Strength of Marine Structures", Ship Structure Committee, SSC-381.

20. Guedes Soares, C and Garbatov, Y. (1996), "Fatigue Reliability of the Ship Hull Girders", Marine Structures, 9: 495-516.

21. Guedes Soares, C and Garbatov, Y. (1999), "Reliability of Corrosion Protected and Maintained Ship Hulls Subjected to Corrosion and Fatigue", Journal of Ship Research, 43:2 65-78.

22. Hughes, O. (1983), *"Ship Structural Design", A Rationally Based, Computer Aided, Optimization Approach"*, John Wiley & Sons, New York, pp. 432-436.

23. Ito, H., Kondo, K., Yoshimura, N., Kawashima, M. & Yamamoto, S. (1984), "A Simplified Method to Analyse the Strength of Double Hulled Structures in Collision", J. Soc. Nav. Arch. Japan, 156 pp. 283-296.

24. Kinkead, A. N. (1980), "A Method for Analysing Cargo Protection Afforded by Ship Structures in Collision and Its Application to an LNG Carrier", Trans. Royal Inst. Nav. Arch., 122 pp. 299-323.

25. Mansour, A. and Faulkner, D. (1973), "On Applying the Statistical Approach to Extreme Sea Loads and Ship Hull Strength", RINA Trans, Vol. 115, pp. 277-313.

26. Mansour, A. E. & Thayamballi, A. (1980), "Ultimate Strength of a Ship's Hull Girder Plastic and Buckling modes", SSC Report-299, Ship Structure Committee.

27. Mansour, A. (1997), "Assessment of Reliability of Ship Structures", SSC-398, Ship Structures Committee.

28. MeDermott, J. F., Kline, R. G., Jones, E. J., Maniar, N. M. & Chang, W. P., (1974), "Tanker Structural Analysis for Minor Collisions", Trans. Soc. Nav. Arch. and Marine Engrs, 82, 382-416.

29. Nishihara, S., (1984), "Ultimate Longitudinal Strength Modeling", Naval Architecture and Ocean Engineering (SNAJ Publication), 22, pp. 200-216.

30. Paik, J. K., (1990, 1991) "Ultimate Longitudinal Strength-Based Safety and Reliability Assessment of Ship's Hull Girder", J. Soc. Nav. Arch. Japan, 168 (1990) 395-407 and 169 (1991) 403-416.

31. Pedersen, P. Terndrup & Jensen, J. Juncher, (1983), "Strength Analysis of Maritime Structures, Part 2 Numerical Methods", Den Private Ingeniorfond, Copenhagen, 1983 (in Danish).

32. Rahman, M K and Chowdhury, M. (1996), "Estimation of Ultimate Longitudinal Strength of Ships and Box Girders", Journal of Ship Research, 40: pp.244-257.

33. Rutherford, S E and Caldwell, J B. (1990), "Ultimate Longitudinal Strength of A Ship's Hull", Trans. SNAME, pp.441-471 (Vol. 98).

34. Smith, C S, (1975), "Compressive Strength of Welded Steel Ship Grillages", Trans. RINA, 117(1975), pp. 325-359.

35. Smith, C. S., (1977), "Influence of Local Compressive Failure on Ultimate Longitudinal Strength of a Ship's Hull", Proc. of International Symposium on Practical Design in Shipbuilding (PRADS). Society of Naval Architects of Japan, Tokyo, Oct. 1977, pp. 73-79.

36. Smith, C. S., (1981), "Imperfection Effects and Design Tolerances in Ships and Offshore Structures", Trans. Inst. Engrs, Shipbuilder Scotland, 124 (1981) 37-46.

37. Sun, H.H. and Bai, Y. (2001), "Time-Variant Reliability of FPSO Hulls", Trans. Soc. Nav. Arch. and Marine Engrs., Vol. 109.

38. Søreide, T.H., (1981), "Ultimate load analysis of marine structures", Tapir, Trondheim, 1981.

39. Ueda, Y., Rashed, S. M. H. & Paik, J. K., (1984, 1986), "Plates and stiffened plate units of the Idealized Structural Unit Method", J. Soc. Nav. Arch. Japan 156 (1984) 366-377 and 160 (1.986) 318-36 (in Japanese).

40. Ueda, Y. & Yao, T., (1982), "The Plastic Node Method: A new method of plastic analysis", Comput. Meths. Appl. Mech. Engng, 34 1089-106.

41. Valsgård, S. & Pettersen, E., (1982), "Simplified nonlinear analysis of ship/ship collisions", Norwegian Maritime Research, 10(3) pp. 2-17.

42. Valsgård, S. & Steen, E., (1991), "Ultimate hull girder strength margins in present class requirements", The Marine Structural Inspection, Maintenance and Monitoring Symposium, III B-1-19, Society of Naval Architects and Marine Engineers, Arlington, VA, 1991.

43. Vasta, J. (1958), "Lessons Learned From Full-Scale Structural Tests", Trans SNAME, Vol. 66, pp. 165-243.

44. Van Mater, P. R., Glannotti, J. G., Jones, N. & Genalls, P., (1979), "Critical Evaluation of Low Energy Ship Collision-Damage Theories and Design Methodologies", Vol. 11 SSC Report-285, Ship Structure Committee, Washington, April 1979.

45. Viner, A.C. (1986), "Development of Ship Strength Formulation", Proc. of Int, Conf. On Advanced in Marine Structures, Elsevier, pp. 152-173.

46. Xu, X D., Cui, W. et al. (2000), "An Experimental and Theoretical Study on Ultimate Strength of A Box Girder", Journal of Ship Mechanics, 4:5: pp.36-43.

47. Yao, T and Nikolov, P I. (1991, 1992), "Progressive Collapse Analysis of a Ship's Hull under Longitudinal Bending (1st and 2nd Reports)", J. SNAJ , 171(1991): 449-461 and 172(1992): 437-446.

48. Yao T et al.(2000), "Ultimate Hull Girder Strength", ISSC Special Task Committee, VI.II. Proc.14th, Nagasaki, Japan.

49. Yamamoto, N. (1998), "Reliability Based Criteria for Measures to Corrosion", Proc.17th OMAE'98, New York, USA: ASME.

This Page Intentionally Left Blank

Part II

Ultimate Strength

Chapter 14 Offshore Structures Under Impact Loads

14.1 General

Large plastic deformation may develop in offshore structures due to severe ship-platform collisions. Such collisions are considered to be a dynamic phenomenon that has costly consequences in material, environmental, and human terms. The dynamic collision response of platforms should be analyzed at the design stage. This precaution ensures that the structure has sufficient strength to withstand impact and therefore has a low probability of severe collision damage.

Petersen and Pedersen (1981) and Pedersen and Jensen (1991) pointed out that after a minor collision, a considerable amount of the available kinematic energy could be stored as elastic vibration energy in the affected structure. In such cases, the global dynamic load effects can be significant and the equations of motion of the structural system, for the striking and the struck structures, should be established and solved. The elastic-plastic deformation modes of the structural system in a collision may be classified as (1) indentation of the striking ship, (2) local indentation of the hit member, and (3) overall deformation of the affected structure. In earlier studies, the response of the affected structure, excluding the hit member, was treated linearly. This analysis approach overlooked the possibility of analyzing and treating the plastic deformation behavior of the affected structure.

Based on Bai and Pedersen (1993), this Chapter deals with the dynamic response of the steel offshore structure. A system of equations is derived which describes the local as well as the global elastic-plastic behavior of the structural system. These highly nonlinear equations are then solved in the given time domain. In order to derive these equations, a nonlinear force-deformation relation that can model the local indentation of a hit tubular member is calculated. This derivation is based on a linear elastic solution, numerical results from Ueda et al (1989) and experimental results from Smith (1983) and Ellinas and Walker (1983). Thereafter, a three-dimensional beam-column element is developed which is used to model the global behavior of the affected structure. A large displacement analysis of the beam-column elements is established by combining a linear stiffness matrix, a geometrical stiffness matrix, and a deformation stiffness matrix (Bai & Pedersen, 1991). Furthermore, the effects of plasticity and strain hardening of beam-column elements are taken into account by the plastic node method.

Some basic numerical examples are presented in order to demonstrate the accuracy and efficiency of the developed beam-column element. Calculated results are compared with numerical results obtained from general-purpose finite element programs, reported experimental results and rigid-plastic analysis results. In addition, the dynamic plastic responses of two offshore platforms in typical ship-platform collision situations are analyzed.

14.2 Finite Element Formulation

14.2.1 Equations of Motion

The striking and the affected structure are considered one structural system connected by spring elements.

The equations of motion for the structural system are established under the following assumptions:

- The striking ship is treated as a rigid body without volume, and all the deformations in the ship are assumed to take place in a zone around an impact point.

- The deformations in the ship and the local indentation in the affected member of the offshore structure are simulated by using nonlinear spring elements in which only compression forces act. The force deformation curves for those spring elements are functions of the strain-rate.

- The deformation of the affected structure, except for the local indentation in the hit member, is taken into account by using a model of the structure, which is composed of three-dimensional beam-column elements.

- The hydrodynamic forces acting on the ship are accounted for, by introducing an added mass concept. Morison's Equation is applied with the purpose of including the fluid-structure interaction to the affected structure's analysis.

When considering the dynamic equilibrium of the structural system, the equations of motion may be written in an incremental form as:

$$[M]\{d\ddot{u}\} + [C]\{d\dot{u}\} + [K_T]\{du\} = \{dF_d\} \tag{14.1}$$

where $\{du\}$, $\{d\dot{u}\}$, and $\{d\ddot{u}\}$ are the increments of nodal displacements, velocities, and accelerations, respectively. $[M]$ is a structural mass matrix, $[C]$ is a structural damping matrix, and $[K_T]$ denotes the structural tangent stiffness matrix. The external load vector $\{dF_d\}$ is due to the drag force term in Morison's equation, which is evaluated using an approach described by Bai and Pedersen (1991). The added mass term in Morison's equation is included in the structural mass matrix $[M]$.

The equation of motion, Eq. (14.1) is solved by using the Newmark-β method.

14.2.2 Load-Displacement Relationship of the Hit Member

In this section, a derivation of a nonlinear spring element will be used to model the local indentation in the hit/affected member. The spring element will be used for steel platforms and the hit/affected members are therefore assumed circular thin-walled tubes.

The linear elastic displacement of the load point for a pinch loaded tubular member can be determined by:

$$\delta_E = 0.1116 \left(\frac{D}{T}\right)^3 \frac{P}{EL_c} \tag{14.2}$$

where P is the force and δ_E denotes the elastic displacement, E is Young's modulus, and T is the thickness of the tube wall. D denotes the outer diameter of the tube while L_c is the characteristic length of the contact area along the axial direction of the tube.

The characteristic length L_c, is a function of the outer diameter, the length of the tube, and the shape of indenture. In order to get an empirical equation, linear finite shell element analysis results from Ueda et al (1989) and indentation tests conducted by Smith (1983) are analyzed. A mean value is found to be:

$$L_c = 1.9D \tag{14.3}$$

More experimental or numerical data are necessary to get a more rational value of the characteristic length L_c.

When the load P is larger than the critical value P_0. A permanent indentation will take place, and the critical value can be determined using a rigid-plastic analysis for a pinch loaded ring with length L_c. The result obtained is:

$$P_0 = 2\sigma_y T^2 L_c / D \tag{14.4}$$

where σ_y is the yield stress of the material.

The permanent indentation δ_P can be calculated using a semi-empirical equation. Through energy considerations and curve fitting of experimental data, Ellinas and Walker, 1983 obtained:

$$\delta_P = D \left(\frac{P}{37.5 \sigma_y T^2} \right)^2 \tag{14.5}$$

The unloading linear deformation δ_E' can be obtained by multiplying the linear elastic solution by a coefficient α:

$$\delta_E' = 0.1116\alpha \left(\frac{D}{T} \right)^3 \frac{P}{EL_c} \tag{14.6}$$

The coefficient α will be less than or equal to 1.0 depending on the deformation at the unloading point.

Finally, the local displacement at the load point for a load larger than the P_0 is calculated as:

$$\delta = \delta_E' + \delta_P \tag{14.7}$$

14.2.3 Beam-Column Element for Modeling of the Struck Structure

A finite beam-column element as described in Chapter 12 of this Part is adopted to model the affected structure.

14.2.4 Computational Procedure

The procedure described above has been implemented into the computer program SANDY (Bai, 1991), three types of loads can be applied, to the simulated model, to obtain a collision analysis of the affected structure.

Impact loads are applied at the node points and/or spatially distributed over the finite elements. The time variation of these loads is given as input data before initiating a calculation. This type of loading is used in Examples 14.1-14.3.

Dynamic loads applied as initial velocities of a colliding structure initiate the calculation with the simulation of the dynamic motion of the colliding structure. The impact loads between the structures are obtained as the results of the simulation. Once an impact force in a certain direction is detected to be in tension during the simulation the contact is released. Thereafter, the striker is assumed to move as a free body in that direction with a given constant velocity. The criterion for re-establishing a contact is that the displacement of the striker will exceed the displacement of the corresponding point on the affected structure. This type of loading is used in Examples 14.5-14.7.

Dynamic loads applied as initial velocities of the struck/affected structure are usually used only in high-speed impacts. In such cases, the time history of the applied loading is not of interest. The response of the struck/affected structure depends on the time integration of the loads (the momentum of pulse), in other words, initial velocities of the affected structure.

For large displacement analyses, an updated Lagrangian approach is adopted. At each load step, the element stiffness matrices are reformed in the local coordinate systems and then transformed to the global coordinate system. Here, the global stiffness matrix is assembled and the increments of nodal displacements, measured in the global coordinate system, are evaluated. Using the element transformation matrix, the increments of element displacements can be calculated and the element displacements and forces are updated. The new transformation matrices can then be evaluated and the updated element displacements and forces transformed to the new local coordinate system and used in the following calculation of new element forces and displacements for the next load step.

During the elastic-plastic analysis, the loading and unloading of nodes are checked carefully. Once loading takes place in a node, a Newton-Raphson iteration is carried out in order to find the exact load increments at which the element nodal forces may come to and thereafter move along the yield surface. At each time step, the structural stiffness matrix is evaluated based on the elastic-plastic status of the element nodes, at the end of the previous load increment. However, as soon as the equations of motion are solved, a check is performed to analyze whether unloading of the plastic nodes takes place. If this is the case, the structural stiffness matrix is updated until no further unloading of plastic nodes is detected. Finally, the nodal displacement increments are the solution to the equations of motion after the last iteration. The nodal forces and the elastic-plastic status of elements are updated and unloading is re-evaluated. In addition, when the elastic-plastic status of a node has changed, the unbalanced forces are evaluated and transformed to the global coordinate system. The transformed unbalanced forces are added to the load increments for the next time step.

For further cross-sections, there are two corners on the yield surface. The corners are at the points where there are only axial forces acting on the beam element. When the forces at an element node are at such a corner or close to a corner, then the element is treated as a truss element, which is only subjected to an axial force. For such truss elements, unloading is checked based on the axial forces and the axial displacement increments. The elements are treated as normal three-dimensional beam-column elements once unloading is detected for them.

14.3 Collision Mechanics

14.3.1 Fundamental Principles

The analysis of collision mechanics is generally based upon the solution of the differential equations of dynamic equilibrium. The collision force is a function of the relative indentation of the ship and platform. Thus, an incremental solution procedure is required.

The problem is greatly simplified if the collision duration is considerably smaller than the natural period of the governing motion. This assumption is often valid for relevant rigid body motions of floating and articulated platforms. In this case, the solution can be based upon a quasi-static solution using the principles of:

- Conservation of momentum
- Conservation of energy

This way, the determination of impact kinematics and energy transfer during collisions can be decoupled from the analysis of strain energy dissipation in colliding objects.

A static solution applies for collisions lasting significantly longer than the natural period of the governing motion.

For jackets at medium water depths, the ratio between the collision duration and the natural period of vibration for leg impacts may be such that significant dynamic effects are involved. This has been investigated to a very small extent. Normally, a static analysis is considered appropriate, but possible dynamic magnification should also be evaluated.

14.3.2 Conservation of Momentum

In the following sections, the energy to be dissipated as strain energy is determined by considering translational motions only. More accuracy may be obtained by considering more motion components (platform and vessel rotations), and therefore formulating a complex derivation. It is always conservative to use the formulas given in Section 14.3.3.

The conservation of momentum for a central collision between a ship and a platform moving in the same direction is expressed by:

$$m_s v_s + m_p v_p = (m_s + m_p) v_c \tag{14.8}$$

where,

v_c = Common velocity after impact

v_s = Velocity of ship $v_s > v_p$

v_p = Wave induced velocity of platform

m_s = Mass of ship including added mass

m_p = Mass of platform including added mass

The common velocity is thus defined by:

$$v_c = \frac{m_s v_s + m_p v_p}{m_s + m_p} \tag{14.9}$$
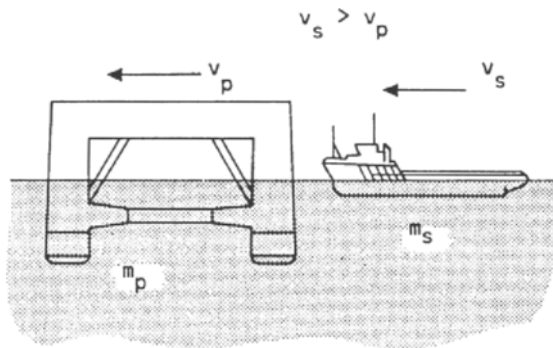
Figure 14.1   Collision between Supply Vessel and Semi-submersible Platform

14.3.3 Conservation of Energy

In a central collision, all the kinematic energy dissipates as strain energy (elastic or plastic) in the ship (E_s) and in the platform (E_p).

In the case of an eccentric collision, some of the kinematic energy will remain as rotational energy of the vessel or of the platform after the collision.

The equation of conservation of energy assuming central collision reads:

$$\frac{1}{2}m_s v_s^2 + \frac{1}{2}m_p v_p^2 = \frac{1}{2}(m_s + m_p)v_c^2 + E_s + E_p \tag{14.10}$$

where,

E_s = Strain energy dissipated by the ship

E_p = Strain energy dissipated by the platform

Combining this equation with the equation for the common velocity, v_c the following expression for the dissipated strain energy emerges:

$$E_s + E_p = \frac{1}{2}m_s v_s^2 \frac{\left(1 - \dfrac{v_p}{v_s}\right)^2}{\left(1 + \dfrac{m_s}{m_p}\right)} \tag{14.11}$$

The wave induced platform motion is often small compared to the ship velocity and can be neglected. Otherwise, the characteristic velocity should be based upon a stochastic evaluation of the relative collision velocity between the ship and the platform $(v_s - v_p)$ accounting for the phase lag between the respective motions.

Table 14.1   Total Strain Energy Dissipation

Platform Types			
Fixed	Floating	Articulated Column	Jackup*
$\dfrac{1}{2} m_s v_s^2$	$\dfrac{1}{2} m_s v_s^2 \dfrac{\left(1 - \dfrac{v_p}{v_s}\right)^2}{1 + \dfrac{m_s}{m_p}}$	$\dfrac{1}{2} m_s v_s^2 \dfrac{\left(1 - \dfrac{v_p}{v_s}\right)^2}{1 + \dfrac{m_s \cdot z^2}{J}}$	$\dfrac{1}{2} m_s v_s^2 \dfrac{1}{1 + \dfrac{m_s}{m_p}}$

* If the duration of the collision is significantly smaller than the fundamental period of vibration.

where,

J = Mass moment of inertia of the column (including added mass) with respect to the effective pivot point.

Z = Distance from the effective pivot point to the point of contact.

14.4 Examples

14.4.1 Mathematical Equations for Impact Forces and Energies in Ship/Platform Collisions

Problem:

Derive equations for calculating maximum impact force, impact energy during a collision between ship and fixed platform (Soreide, 1985). The force-deformation relations for the ship and platform may be modeled as linear springs of k_s and k_p respectively. The ship is assumed to have weight of m (including added mass) and move at speed of v immediately prior to the collision. In deriving the formulation, it is further assumed that the damping effect may be ignored, and the impact mechanics may be expressed as free vibration a mass-spring system.

Solution:

The ship/platform system may be considered as a mass-spring system. The deformations in the ship and platform are denoted as x_s and x_p respectively. Denoting total deformation as $x = x_s + x_p$, we may derive the following from the force equilibrium:

$$F = kx = k_s x_s = k_p x_p \tag{14.12}$$

where,

$$k = \frac{k_s k_p}{k_s + k_p} = \text{the equivalent spring stiffness for the system}$$

The motion of the mass-spring system may then be expressed as

$$m\frac{d^2x}{dt^2} + kx = 0 \tag{14.13}$$

Considering the initial condition (mass move at velocity v, x=0 when t=0, the solution to the above differential equation is,

$$x = v\sqrt{\frac{m}{k}}\sin\omega\, t \tag{14.14}$$

where the natural frequency is

$$\omega = \sqrt{\frac{k}{m}} \quad (rad\,/\sec) \tag{14.15}$$

From Eq.(14.14), the maximum impact force is obtained as,

$$F_{\max} = kx_{\max} = v\sqrt{mk} \tag{14.16}$$

and impact duration (the time from the initiation of the impact to the peak impact force) is

$$T_0 = \frac{\pi}{2}\sqrt{\frac{m}{k}} \tag{14.17}$$

The impact duration T_0 is typically 1-2 seconds, (see also Figures 14.16 and 14.17), and it is much longer than the natural frequency of the main hit member and structure system. Hence, ship impact is usually handled in a quasi-static way. The time history of the impact force is further illustrated in Figure 14.16 (e) and Figure 14.17 (b). When the impact force is the maximum, the velocity of the motions for the ship and platform is zero and the deformation energies in the ship and platform are as follows:

$$E_s = \frac{1}{2}k_s x_s^2 = \frac{F_{\max}^2}{2k_s} \tag{14.18}$$

$$E_p = \frac{1}{2}k_p x_p^2 = \frac{F_{\max}^2}{2k_p} \tag{14.19}$$

The maximum impact force expressed in Eq.(14.16) may also be obtained from the following,.

$$E_s + E_p = \frac{1}{2}mv^2 \tag{14.20}$$

14.4.2 Basic Numerical Examples

In the following section, a number of simple numerical examples, which serve to demonstrate the accuracy and the efficiency of the developed three-dimensional beam-column elements, will be presented (Bai and Pedersen, 1993).

The first three examples are problems that can be solved assuming small displacements, but the material has kinematic strain hardening. The last example is a clamped beam struck by a mass, which involves both large displacements and strain hardening.

EXAMPLE 14.1: Fixed Beam Under a Central Lateral Impact Load

The dynamic elastic-plastic behavior of a rectangular beam, clamped at both ends, as shown in Figure 14.2 (a) is analyzed.

The beam is subjected to a concentrated step load at the midspan, as shown in Figure 14.2 (b). Symmetry allows only half of the beam to be modeled. In an analysis using the MARC FEM program, five elements of element type 5 are used as illustrated in Figure 14.2 (c). The element is a two-dimensional rectangular section of a beam-column element. In the evaluation of the element stiffness, three Gaussian integration points are chosen along the axial direction of the element. At each Gauss point, the cross-section is divided in to 11 Simpson integration points. Only normal stresses are considered in the elastic-plastic analysis. Since this is a small displacement problem, the axial sectional force will always be zero. Therefore, the plastic yield condition used in the present analysis is taken to be:

$$M_z / M_{zp} - 1 = 0 \tag{14.21}$$
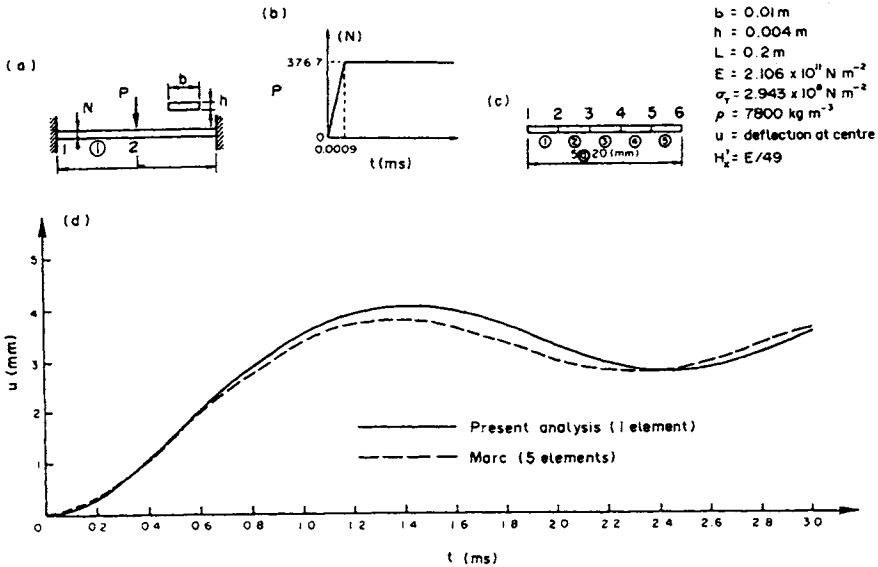
Figure 14.2 Dynamic Elastic-plastic Behavior of a Clamped Beam under Central Lateral Impact Load

  a. Calculation model
  b. Applied load-time relationship
  c. FE model in MARC analysis
  d. Time history of displacement at impact point

where m_z is a bending moment and the subscript "p" indicates the fully plastic value for the corresponding force component. The time history of the displacement at the impact point is shown in Figure 14.2 (d). The results obtained, by using only one element, are depicted by the solid line. It is easily observed that even one element is sufficient to obtain reasonably accurate results.

EXAMPLE 14.2: Rectangular Portal Frame Subjected to Impact Loads

The rectangular portal frame shown in Figure 14.3(a) is subjected to concentrated pulse loads as shown in Figure 14.3(b).

In a MARC FEM analysis, the frame is modeled using 32 elements (element type 16) as shown in Figure 14.3(c). The element is a curved, two-dimensional, rectangular, cross-section beam-column element. Integration points for the evaluation of element stiffness are the same as in EXAMPLE 14.1. Only normal stresses due to axial forces and bending moments are considered in the plastic analysis.

The plastic yield condition used in the present analysis is taken as:

$$\left(M_z/M_{zp}\right)^2 + F_x/F_{xp} - 1 = 0 \tag{14.22}$$

where f_x is an axial force.

The time history of displacements located at the impact points along the load direction is plotted in Figure 14.3(d). Again, it is observed that the present method is quite accurate when using only one element for each structural member.
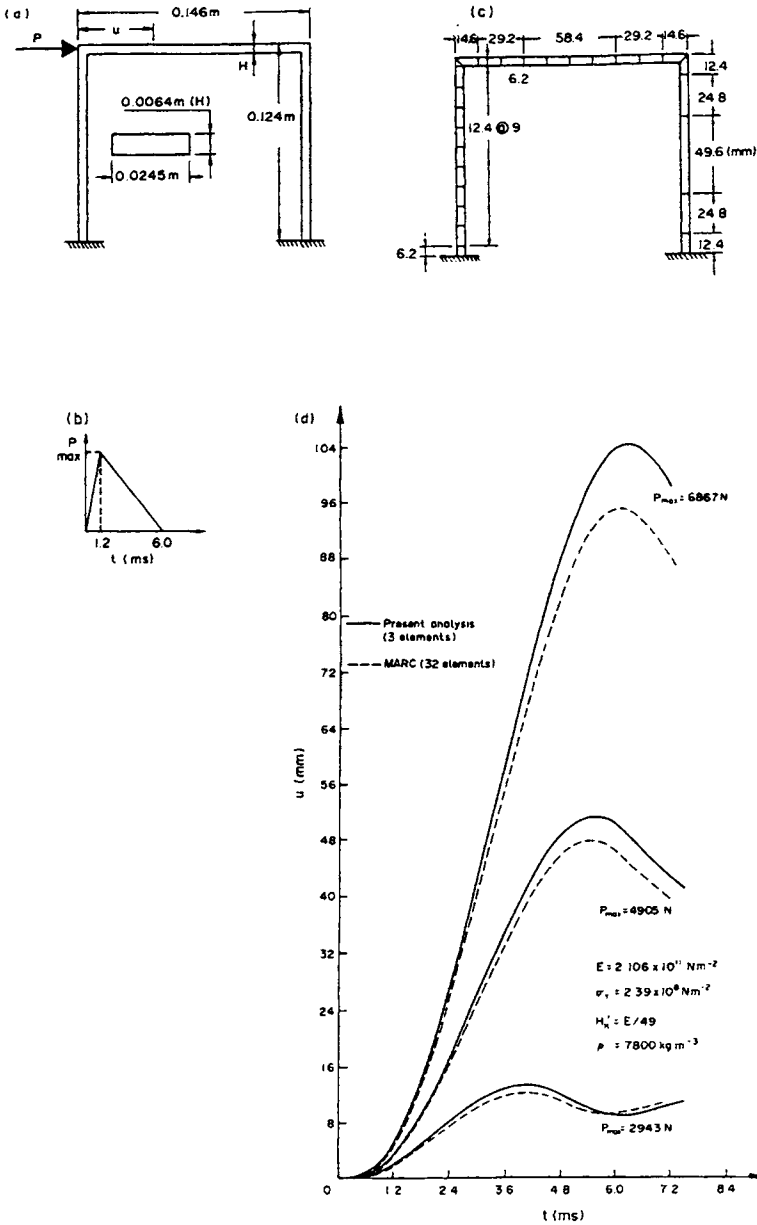
Figure 14.3 **Dynamic Elastic-plastic Behavior of Portal Frame Subjected to Impact Loads**

a. A2D frame
b. Applied impact load
c. FE model in MARC analysis
d. Time history of displacement at impact point

EXAMPLE 14.3: Tubular Space Frame Under Impact Load

The tubular space frame shown in Figure 14.4 (a) is subjected to a step load as illustrated in Figure 14.4 (b).

In a MARC FEM analysis, element type 14 is used and each structural member is discretized by 10 elements as shown in Figure 14.4 (c). The element is a three-dimensional thin-walled tubular beam- column. There are three Gaussian points, which are further divided into 16 Simpson integration points along the circumferential direction. Plasticity is taken into account at these integration points by applying the Von Mises's yield condition and taking the stresses due to axial forces, two bending moments, and torsional moments into account. Therefore, the plastic yield condition used in the present analysis is taken to be:

$$\left(M_x/M_{xp}\right)^2 + \left(M_y/M_{yp}\right)^2 + \left(M_z/M_{zp}\right)^2 + sin\left(\frac{\pi}{2}\left(F_x/F_{xp}\right)\right) - 1 = 0 \tag{14.23}$$

where M_x is the sectional torsional moment and M_y and M_z are the bending moments.

The time history of the impact displacement is presented in Figure 14.4(d).
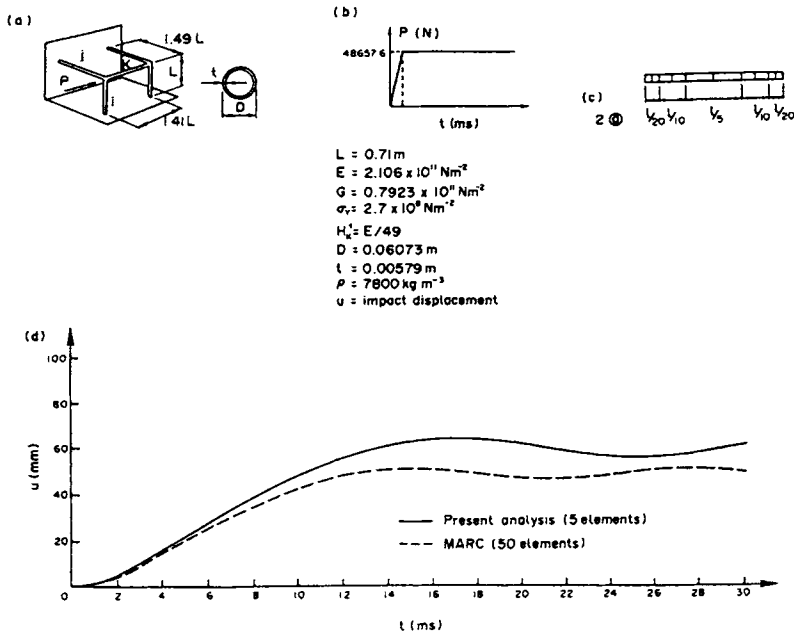
Figure 14.4   Dynamic Elastic-plastic Behavior of Space Frame under Impact Load
    a. Calculation model
    b. Applied load-time relationship
    c. FE model in MARC analysis
    d. Time history of displacement at impact point

EXAMPLE 14.4: Clamped Aluminum Alloy Beam Struck Transversely by a Mass

The clamped beam shown in Figure 14.5 (a) was studied by Yu and Jones 1989, using the ABAQUS FEM program. In their analysis, eight-node isoparametric plane stress elements were used. The finite element mesh consists of 75 elements and 279 nodes. The mesh near the impact point and the supports was made finer in order to obtain detailed information. A true stress/true strain relationship of the material is shown in Figure 14.5(b). The time variations of the maximum transverse deflection are shown in Figure 14.5 (c). The experimental results conducted by Liu and Jones as described by Yu and Jones, 1989 are also plotted. The associated time histories of the dimensionless bending moment

M_z/M_{zp} and axial force F_x/F_p are shown in Figures 14.5 (d) and (e).
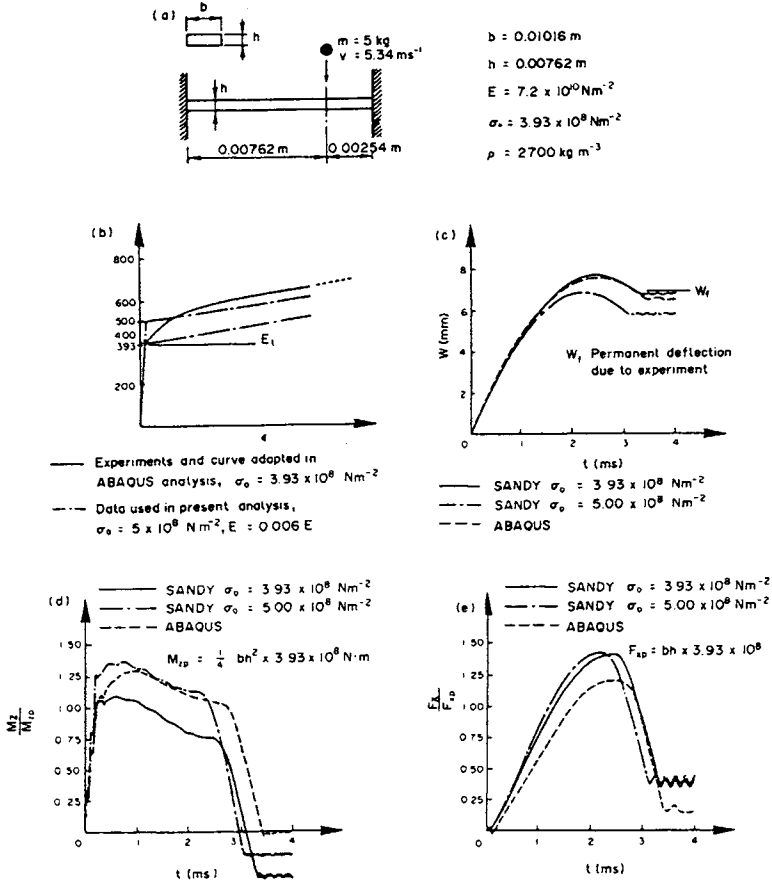
Figure 14.5   Dynamic Elastic-plastic Behavior of a Clamped Beam Struck by Mass

    a. A clamped beam struck by a mass
    b. True stress-true strain relationship
    c. Time histories of deflection at the impact point
    d. Time histories of bending moment at impact point
    e. Time histories of axial force at the impact point

The plastic yield condition used in this example is the same as in EXAMPLE 14.2.

The ABAQUS FEM analysis employs the true stress/true strain curve, shown in Figure 14.5 (b). This analysis assumes the material has linear kinematic strain hardening and each side of the beam is modeled as one element. Figures 14.5 (c-e) show that the structural response is sensitive to the yield stress. However, the agreement between the results predicted by both programs is good.

The examples presented in this section demonstrated that the nodal displacements and forces predicted by the actual beam-column element agree with those obtained by experiments and by general finite element program analyses. Reasonable results can be obtained by the beam-column element even when the structural member is discretized by the absolute minimum number of elements (normally one element per member).

14.4.3 Application to Practical Collision Problems

The procedure implemented in the SANDY program can be used to simulate many different ship collision problems, such as side central collisions, bow collisions, and stern collisions against structures like offshore platforms and ridges. The simulation results include: motion (displacements), velocities/accelerations of the striking and the struck structures, indentation in the striking ship and the hit member, impact forces, member forces, base shear and overturning moments for the affected structures, kinetic energy, and elastic/plastic deformation energy of the striking and the affected structures.

In this section three typical ship collision problems are selected. These are ship-unmanned, platform, and ship-jacket platform collisions.

EXAMPLE 14.5: Unmanned Platform Struck by a Supply Ship

The small unmanned platform, shown in Figure 14.6 (a), which is struck by a 5000 ton supply vessel, is considered first. The dominant design criterion for this platform type is often ship collisions, while it is normally wave loading for traditional platforms. The supply ship is supported to drift sideways with a speed 2.0 ms-1 under calm sea conditions. The added mass for the sideways ship sway motion is taken to be 0.5 times the ship mass. The force-indentation relationship for the ship is taken as is shown in Figure 14.6 (b). The added mass is included following Morison's equation and the added mass and drag coefficients are taken to be 1.0. The tubes under the water surface are assumed to be filled with water. Therefore, the mass due to the entrapped water is also included. The force-indentation relationship is established by following Eqs. (14.2) and (14.7) by following further approximations such as multi-linear lines, as illustrated in Figure 14.6 (c). The soil-structure interaction is taken into account using linear springs.

First, a linear analysis was carried out by using a load vector given by the gravity loading on the structures. Then, a dynamic analysis considering large displacements, plasticity, and hardening effects followed. The plastic yield condition was taken to be:

$$\left(M_z/M_{zp}\right)^2 + sin^2\left[\frac{\pi}{2}\left(F_x/F_{xp}\right)\right] - 1 = 0 \tag{14.24}$$

It is noted that the indentation in the hit tube will reduce the load carrying capacity of the tube greatly. This effect has not been taken into account in the present analysis. However, a

possible procedure to account for the indentation effect is to reduce the plastic yield capacity of the element nodes at the impact point using the procedure suggested by Yao *et al* (1986).

The numerical results are shown in Figures 14.6 (d-e). The effect of strain hardening in these figures is indicated; when the strain hardening is included, the structure becomes stiffer and more energy will be absorbed by the ship. Therefore, the deck displacement is smaller, and the collision force and overturning moment increase.
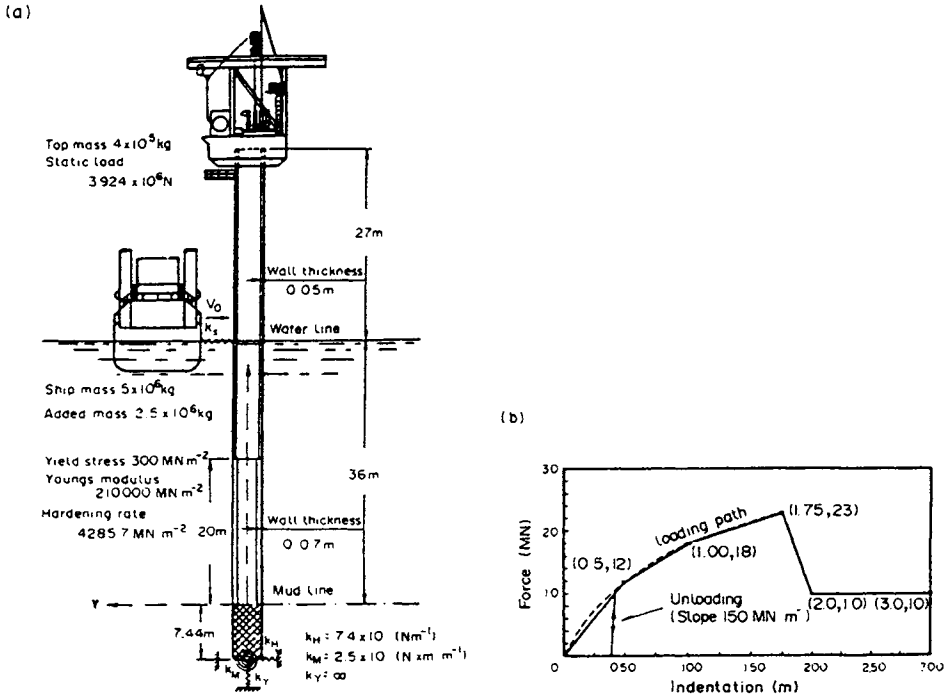
Figure 14.6   Response Caused by Collision between Supply Ship and Unmanned Platform

a. Ship-platform collision
b. Local load-indentation relationship for the ship side

(Continued overleaf)

(c)

(d)

(e)

(f)
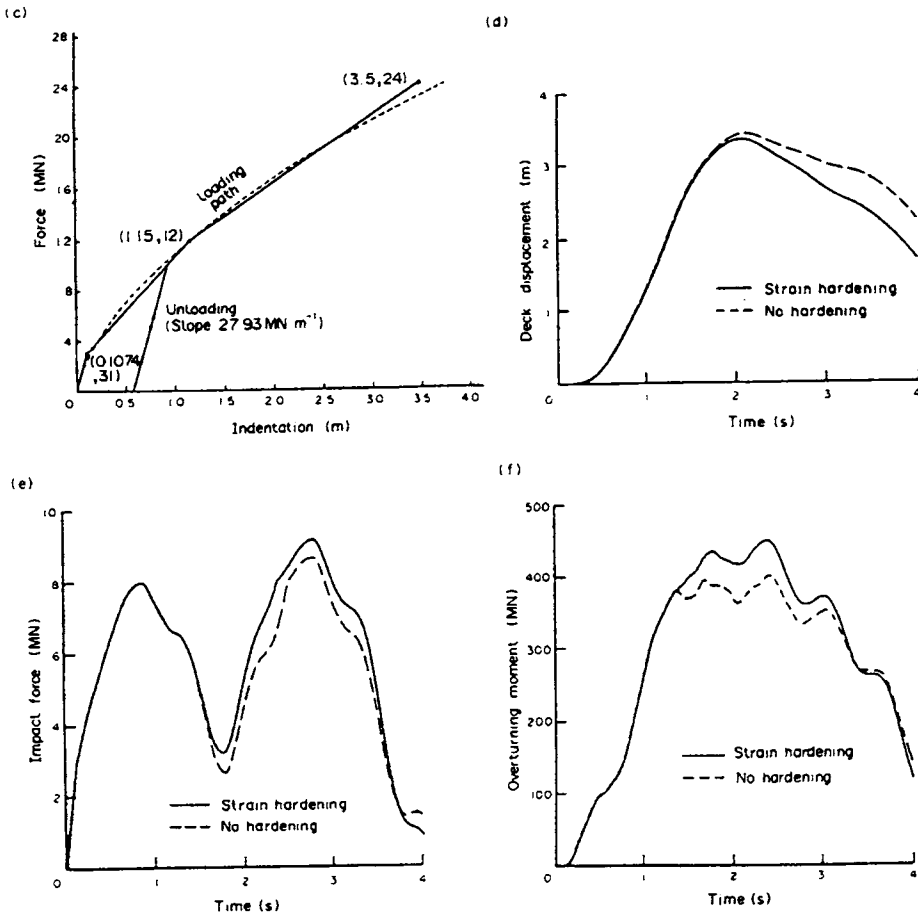
Figure 14.6 (continued).

    c. Local force-indentation relati nship for the hit tube
    d. Deck displacement time history of the platform
    e. Impact force time history
    f. Overturning moment time history of the platform

EXAMPLE 14.6: Jacket Platform Struck by a Supply Ship

The four-legged steel jacket platform shown in Figure 14.7 (a) is struck by a 4590-ton supply ship. Both the platform and the ship are existent structures. The ship is supposed to surge into the platform with the velocities 0.5, 2, and 6 ms-1 corresponding to operation impact, accidental impact, and passing vessel collision, respectively. The force-indentation relationship for the ship bow is obtained using axial crushing elements in which a mean crushing force applied by a rigid-plastic theory has been adopted. The local indentation curve for the hit tubular member in the jacket platform is established following Eqs. (14.2) and

(14.7). Both indentation curves are further approximated as multi-linear curves. First, a linear static analysis is carried out for the gravity loading and after, a nonlinear dynamic analysis is performed which includes fluid-structure interaction, soil-structure interaction, large displacements, and plasticity and kinematic strain-hardening effects for the affected platform.

The time history of the impact deflections is shown in Figure 14.7 (b). Figures 14.7 (c-e) show how the energy is shifted between the ship and the platform and between kinetic energy, elastic deformation energy, and plastic deformation energy.

Using the present procedure, impact forces, dent in ship, and local dent depth of the hit member, can be obtained, provided the impact velocity and indentation curve of the ship are known. The main results of the example are listed in Table 14.2.

Finally, the distribution of the plastic nodes for an impact velocity of 5ms-1 at time 1.45s is shown in Figure 14.7(a).

Table 14.2 Main Results of Ship-Jacket Platform Collisions

Impact Velocity (ms-1)	Impact Energy (MJ)	Impact Force (MN)	Dent in Ship (m)	Local dent In platform (m)
0.5	0.631	2.116	0.437	0
2.0	10.1	8.194	1.69	0.083
5.0	63.1	18.88	3.40	0.616
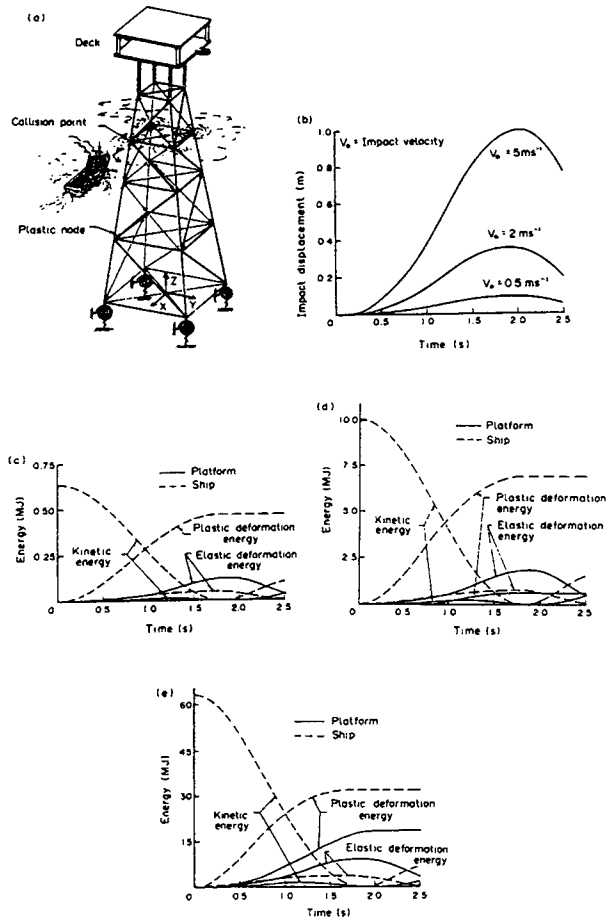
Figure 14.7 **Response caused by Collision between Supply Ship and Jacket Platform**

a. Jacket platform struck by supply ship showing distribution of plastic nodes (Ship velocity, $v_0 = 5ms^{-1}$ time 1.45s)

b. Impact displacement time histories of the platform

c. Time history of energies during ship impact on jacket platform   (Impact velocity, $V_0 = 0.5ms^{-1}$)

d. Time history of energies during ship impact on jacket platform (Impact velocity, $V_0 = 2ms^{-1}$)

e. Time history of energies during ship impact on jacket platform (Impact velocity, $V_0 = 5ms^{-1}$)

14.5 Conclusions

A consistent procedure has been presented for collision analysis. A nonlinear force-displacement relationship has been derived for the determination of the local indentation of the hit member and a three-dimensional beam-column element has been developed for the modeling of the damaged structure. The elastic large displacement analysis theory and the plastic node method have been combined in order to describe the effects of large deformation, plasticity, and strain hardening of the beam-column members.

The accuracy and efficiency of the beam-column elements have been examined through simple numerical examples by comparing the present results with those obtained by experiments and finite element program analyses using the MARC and ABAQUS programs. It is shown that the present beam-column elements enable accurate modeling of the dynamic plastic behavior of frame structures by using the absolute minimum number of elements per structural member.

In addition, examples, where the dynamic elastic-plastic behavior of offshore platforms and bridges in typical collision situations is calculated, have been presented.

All examples show that strain-hardening plays an important role in the impact response of the struck or affected structure. The strain-hardening results in smaller deformations and more energy will be absorbed by the striking structure. Therefore, the impact force is bigger. Thus, a rational collision analysis should take the strain hardening effect into account.

14.6 References

1. Bai, Y., (1991), "SANDY-A Structural Analysis Program for Static and Dynamic Response of Nonlinear Systems", User's Manual, Version 2, Department of Ocean Engineering, The Technical University of Denmark.

2. Bai, Y. and Pedersen, P. Terndrup, (1991), "Earthquake Response of Offshore Structure", Proc. 10th int. Conf. on Offshore Mechanics arctic Engineering, OMAE'91, June.

3. Bai Y. and Pedersen, P. Terndrup, (1993), "Elastic-Plastic Behavior of Offshore Steel Structures Under Impact Loads", Internat. J. Impact Engng, 13 (1) pp.99-117.

4. Ellinas, C.P. and Walker, A.C. (1983), "Damage of Offshore Tubular Bracing Members", Proc. IABSE Colloquium on Ship Collision with Bridges and Offshore Structures, Copenhagen, pp. 253-261.

5. Fujikubo, M., Bai, Y., and Ueda, Y., (1991), "Dynamic Elastic-Plastic Analysis of Offshore Framed Structures by Plastic Node Method Considering Strain-Hardening Effects", Int. J. Offshore Polar Engng Conf. 1 (3), 220-227.

6. Fujikubo, M., Bai, Y., and Ueda, Y., (1991), "Application of the Plastic Node Method to Elastic-Plastic Analysis of Framed Structures Under Cyclic Loads", Int. Conf. on Computing in Engineering science, ICES'91, August.

7. Petersen, M.J., and Pedersen, P. Terndrup, (1981), "Collisions Between Ships and Offshore Platforms", Proc. 13th Annual offshore Technology Conference, OTC 4134.

8. Pedersen P. Terndrup and Jensen, J. Juncher, (1991), "Ship Impact Analysis for Bottom Supported Offshore Structures", Second Int. Conf. on advances in Marine

structures, Dunfermline, Scotland, May 1991 (edited by Smith and Dow), pp. 276-297. Elsevier, Amsterdam.

9.   Smith, C.S. (1983), "Assessment of Damage in Offshore Steel Platform", Proc. Int. Conf. on Marine Safety, Paper 15.

10.   Søreide, T.H., (1985), "Ultimate Load Analysis of Marine Structures", Tapir, Trondheim, Norway.

11.   Ueda, Y. Murakawa, H., and Xiang, D. (1989), "Classification of Dynamic Response of a Tubular Beam Under Collision", Proc. 8th Int. Conf. on Offshore Mechanics and Arctic Engineering, Vol. 2, pp. 645-652.

12.   Ueda, Y. and Fujikubo, M., (1986), "Plastic Node Method Considering Strain-Hardening Effects", J. Soc. Naval Arch. Japan 160, 306-317 (in Japanese).

13.   Yao, T., Taby, J. and Moan, T. (1988), "Ultimate Strength and Post-Ultimate Strength Behaviour of Damaged Tubular Members in Offshore Structures", J. Offshore Mech. Arctic Engng, ASMA 110, 254-262.

14.   Yu, J. and Jones, N. (1989), "Numerical Simulation of a Clamped Beam Under Impact Loading", Comp. Struct. 32(2), 281-293.

This Page Intentionally Left Blank

Part II

Ultimate Strength

Chapter 15   Offshore Structures Under Earthquake Loads

15.1 General

Bottom supported offshore structures in seismic areas may be subjected to intensive ground shaking causing the structures to undergo large deformations well into the plastic range. Previous research in this area has mainly resulted in procedures where the solutions have been sought in the frequency plane (Penzien, 1976). The present chapter is devoted to time domain solutions such that the development of plastic deformations can be examined in detail.

The basic dynamics of earthquake action on structures has been discussed in Clough and Penzien (1975) and Chopra (1995). There have been extensive investigations on earthquake response of building structures in the time domain (Powell, 1973). Unfortunately, most of works have been limited to plane frames. Furthermore, for offshore structures hydrodynamic loads have to be taken into account and the geometrical nonliearities become more important than in building structures. Therefore, there is a need for a procedure to predict earthquake response of offshore structures including both geometrical and material nonlinearities.

Methods for analysis of frame structures including geometrical nonlinearities have been based on either the finite element approach (Nedergaard and Pedersen, 1986) or on the beam-column approach (Yao et al, 1986). Nedergaard and Pedersen, (1986) derived a deformation stiffness matrix for beam-column elements. this matrix is a function of element deformations and incorporates coupling between axial and lateral deformations. It is used together with the linear and geometrical stiffness matrices.

Material nonlinearity can be taken into account in an efficient and accurate way by use of the plastic node method (Ueda and Yao, 1982). Using ordinary finite elements, the plastic deformation of the elements is concentrated to the nodes in a mechanism similar to plastic hinges. Applying the plastic flow theory, the elastic-plastic stiffness matrices are derived without numerical integration.

In this Chapter, a procedure based on the finite element and the plastic node method is proposed for earthquake response analysis of three-dimensional frames with geometrical and material nonlinearities. Using the proposed procedure, earthquake response of a jacket platform is investigated. Part of this Chapter appeared in Bai and Pedersen (1991). The new extension is to outline earthquake design of fixed platforms based on API RP2A.

15.2 Earthquake Design as per API RP2A

API RP2A (1991) applies in general to all fixed platform types. Most of the recommendations are, however, typical for pile steel jacket platforms. The principles and procedures given in

API (1991) are summarized below. The design philosophy for earthquake leads in API (1991) is illustrated in Table 15.1.

Table 15.1   Earthquake Design Philosophy, API RP2A

	Strength Level Earthquake (SLE)	Ductility Level Earthquake (DLE)
Philosophy	Prevent interruption of normal platform operations.	Prevent loss of life and maintain well control.
Design	Ground shaking which has a reasonable likelihood of not being exceeded during the platform life.	Rare intense ground shaking that unlikely to occur during the platform life.
Performance	No significant structural damage, essentially elastic response.	No collapse, although structural damage is allowed; inelastic response.

The API's seismic design recommendation are based upon a two level design approach, these are

- Strength Requirements

    The platform is designed for a severe earthquake which has reasonable likelihood of not being exceeded during the platform life (typical return period hundreds of years, Strength Level Earthquake SLE).

- Ductility Requirements.

    The platform is then checked for a rare earthquake with a very low probability of occurrence (typical return period thousands of years, Ductility Level Earthquake DLE).

The objective of the strength requirements is to prevent significant interruption of normal platform operations after exposure to a relatively severe earthquake. Response spectrum method of time history approach is normally applied.

The objective of the ductility requirements is to ensure that the platform has adequate capacity to prevent total collapse under a rare intense earthquake. Member damage such as in-elastic member yielding and member buckling are allowed to occur, but the structure foundation system should be ductile under severe earthquakes, such that it absorbs the imposed energy. The energy absorbed by the foundation is expected to be mostly dissipated through non-linear behaviour of the soil.

For some typical jacket structures, both strength and ductility requirements are by API considered satisfied if the below listed previsions are implemented in the strength design of these platforms:

- Strength requirements for strength level earthquake loads (SLE) are in general documented.
- Strength requirements are documented for jacket legs, including enclosed piles, using 2 times the strength level earthquake loads (i.e. 2*SLE).
- Rare, intense earthquake ground motion is less than 2 times the earthquake ground motions applied for documentation of strength level requirements (i.e. DLE < 2*SLE).

- Geometrical and ultimate strength requirements for primary members and their connections as given in API are satisfied. These requirements concern number of legs, jacket foundation system, diagonal bracing configuration in vertical frames, horizontal members, slenderness and diameter/thickness ratio of diagonal bracing, and tubular joint capacities.

15.3 Equations and Motion

15.3.1 Equation of Motion

The equations of motion for a nonlinear offshore structure subjected to a earthquake loading can be expressed as

$$[M]\{d\ddot{U}\} + [C]\{d\dot{U}\} + [K_T]\{dU\} = -[M]\{d\ddot{U}_g\} + \{dX_e\}$$ (15.1)

where $\{dU\}$, $\{d\dot{U}\}$ and $\{d\ddot{U}\}$ are the increments of nodal displacement, velocity and acceleration relative to the ground respectively. [M] is the structural mass matrix, while [C] is the structural damping matrix. $[K_T]$ denotes the structural tangent stiffness matrix. $\{dX_e\}$ are the increments of the hydrodynamic load. The ground acceleration vector $\{\ddot{U}_g\}$ is formed as an assembly of three-dimensional ground motions.

We shall here assume that at the time of the earthquake there is no wind, wave or current loading on the structure. According to the Morison equation (Sarpkaya and Isaacson, 1981), the hydrodynamic load per unit length along a tubular beam member can be evaluated as

$$\{f_M\} = -\rho C_A A\{\ddot{u}_n\} - \frac{1}{2}\rho C_D D|\{\dot{u}_n\}|\{\dot{u}_n\}$$ (15.2)

where ρ is the mass density of the surrounding water, D is the beam diameter, C_A is an added mass coefficient, C_D the drag coefficient, $A=\pi D^2/4$, and $\{\dot{u}_n\}$ denotes the normal components of the absolute velocity vector. The absolute velocity vector is

$$\{\dot{u}_a\} = \{\dot{u}\} + \{\dot{u}_g\}$$ (15.3)

Using a standard lumping technique, Eq. (15.1) can be rewritten as

$$([M] + [M_a])\{d\ddot{U}\} + [C]\{d\dot{U}\} + [K_T]\{dU\} = -([M] + [M_a])\{d\ddot{U}_g\} + \{dF_D\}$$ (15.4)

where $[M_a]$ is an added mass matrix containing the added mass terms of Eq. (15.2). The increments of drag force terms from time (t) to (t+dt) are evaluated as

$$\{dF_D\} = \sum [T_{t+dt}]^T \{f_D\}_{(t+dt)} - \sum [T_t]^T \{f_D\}_{(t)}$$ (15.5)

where $\sum$ denotes summation along all members in the water, while $\{f_D\}$ are results of integration of the drag force terms of Eq. (15.2) along the member. $[T_t]$ is the transformation matrix. the equations of motion Eq. (15.4) are solved by the Newmark-β method (Newmark, 1959).

15.3.2 Nonlinear Finite Element Model

The finite element model was given in Part II Chapter 12.

15.3.3 Analysis Procedure

Design of offshore structure for earthquake resistance should consider operational and safety requirements of critical piping, equipment and other important components. This dual criteria is usually provided for by designing a structure where the deformations are within acceptable levels and satisfy a set of yield or buckling criteria for the maximum expected level of the earthquake ground motion. Therefore, a nonlinear dynamic analysis is necessary.

Some of the features of the present analysis procedure are:

- A acceleration record, such as EL CENTRO N-S, is scaled by a scale factor to match the probable earthquake in the areas where the structure will be installed.

- A frame model is established by three-dimensional finite elements. Soil structure interaction is taken into account by used of spring elements.

- Fluid-structure interaction is induced. The contribution form the added mass in taken into accounted by an increase of the mass of the beam-column element s. the drag forces are treated as external loads.

- A linear static analysis is performed for the structure subjected gravity loading. The results are used as an initial condition for the subsequent dynamic analysis.

- The structure mass matrix may consist of both masses applied directly at the nodes, and element masses which are evaluated using either a lumped mass method or a consistent mass method.

Geometrical and material nonlinearities are taken in account by use of the theory described in the proceeding chapters.

Time history, and maximum and minimum values of displacements, and forces are presented as calculation results. From these results, the structural integrity against the earthquake is assessed.

The procedure has been implemented in the computer program SANDY (Bai, 1990), and used in several analyses.

15.4 Numerical Examples

EXAMPLE 15.1: Clamped Beam Under Lateral Load

This example (see Figure 15.1) is chosen to show the efficiency of the present procedure. In the present analysis, only one beam-column element is used to model half of the beam. The linear and geometrical stiffness matrices as well as the deformation matrix are used. The plastic yield condition used for rectangular cross-section is taken as

$$M_z/M_{zp} + \left(F_x/F_{xp}\right)^2 - 1 = 0 \tag{15.6}$$

where the subscript "p" indicates fully-plastic values for each stress components.

Figure 15.1 shows that the present results agree with the experimental results and the limit load theory results (Haythornthwaite, 1957). The limit load is P_y when the geometrical nonlinearity is not taken into account.
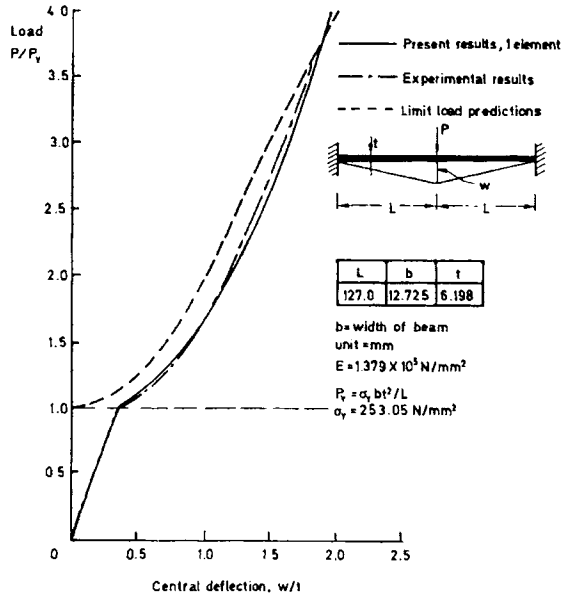
Figure 15.1   Elastic-Plastic Large Displacement Analysis of a Clamped Beam Under Central load

Figure 15.2   Two-Dimensional Frame Subjected to Earthquake Loading

(a) Roof   27.318 N/mm   29.244 N/mm

(b) All floors
      64496 N   49.558 N/mm   64496 N
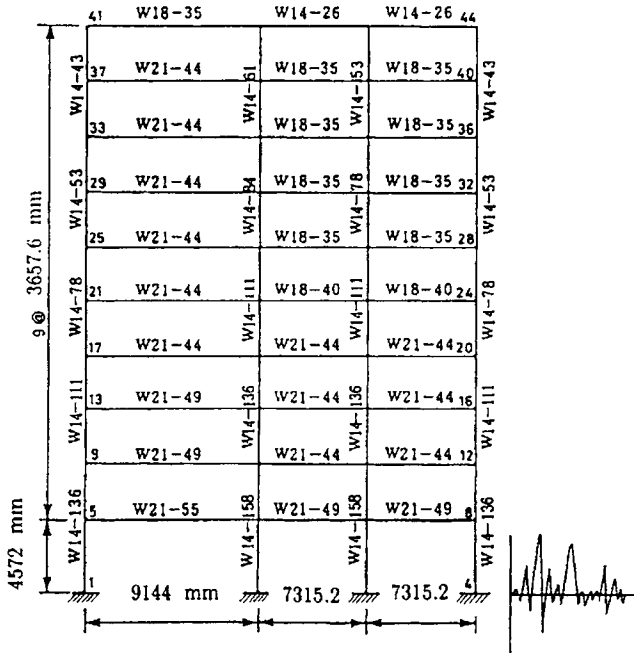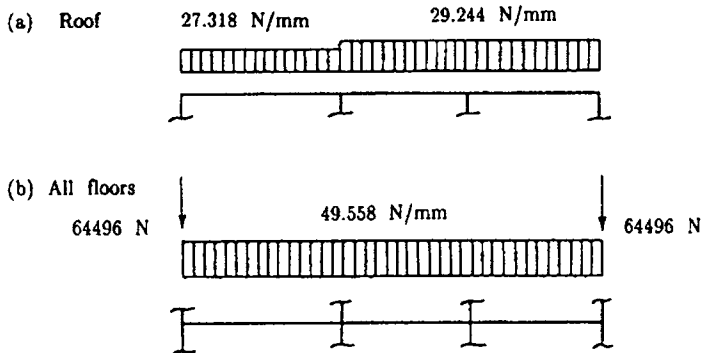
Figure 15.3   Lumped Masses and Static Loads Applied on the 2-D Frame

EXAMPLE 15.2: Two-Dimensional Frame Subjected to Earthquake Loading

The ten story, three bay frame shown in Figure 15.2 has been taken from the user's guide of DRAIN-2D, which is a well known nonlinear earthquake response analysis program for plane structures (Kannan and Powell, 1973). Using the static load shown in Figure 15.3, a linear static analysis is performed. The results are used as the initial conditions for the dynamic analysis. The frame has been analyzed for the first 7seconds of the EL CENTRO, 1940, N-S record, scaled by a factor of 1.57, to give a peak ground acceleration of 0.5 g. the mass lumped at the nodes are based on the dead load of the structure. The damping matrix is determined as [C] = 0.3 [M]. The frame is modeled by using one element per physical member. Horizontal nodal displacements at each floor are constrained to be identical. In the analysis, the geometrical nonlinearity is not taken into account. The plastic yield condition for the i steel beam is assumed as:

$$M_z/M_{zp} + 1.66(F_x/F_{xp})^2 - 1 = 0 \tag{15.7}$$

Typical results are shown in Figure 15.4, together with those predicted by DRAIN-2D. The agreement between the two programs is good.

EXAMPLE 15.3: Offshore Jacket Platform Subjected to Earthquake Loading

The four-legged steel jacket platform shown in Figure 15.5 is an existing structure. It is subjected to a horizontal earthquake loading. The applied ground acceleration time history is again the first 7 seconds of EL CENTRO N-S, with amplification factors. A linear static analysis is carried out using dead load applied on the deck. Fluid-structure interaction, soil-structure interaction, and geometrical and material nonlinearities are taken into account. Each structural member is modelled as only one beam-column element. The plastic yield condition used for thin-walled circular tubs is expressed as

$$(M_x/M_{xp})^2 + (M_y/M_{yp})^2 + (M_z/M_{zp})^2 +$$

$$\sin^2\left\{\frac{\pi}{2}[(F_x/F_{xp})^2 + (F_y/F_{yp})^2 + (F_z/F_{zp})^2]^{1/2}\right\} - 1 = 0 \tag{15.8}$$

The effects of earthquake acceleration amplification factors have been shown in Figure 15.8. Plastic nodes have been observed when the amplification is bigger than 2.25. the distribution of plastic nodes at time 3.00 second for a scale factor 4.5 has been shown in Figure 15.5. The

structure undergoes large deformations as well as plasticity when it is subjected to intensive ground shaking.
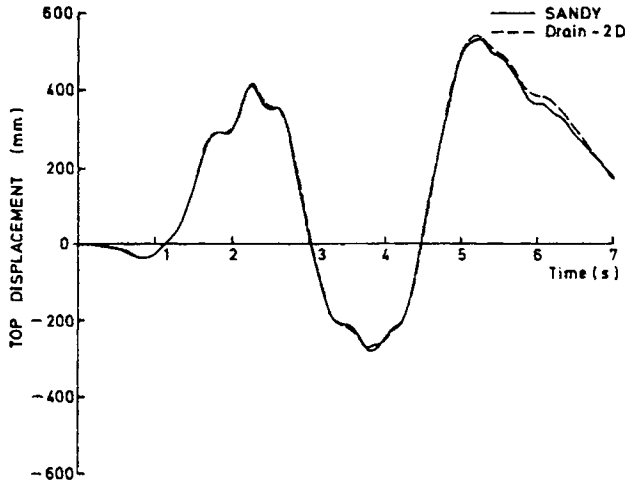
Figure 15.4   Time History of Roof Displacement for the 2-D Frame
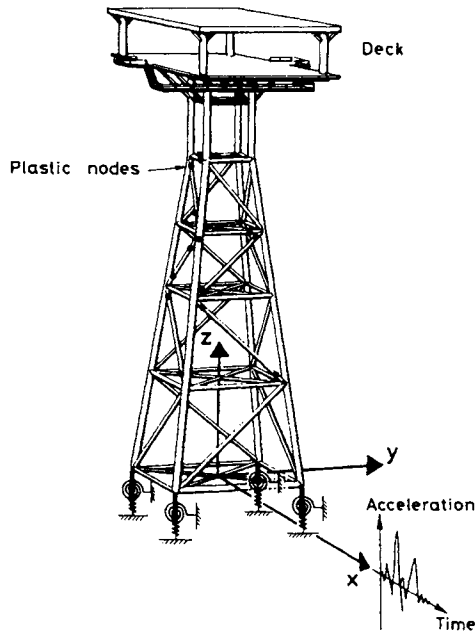
Figure 15.5   Offshore Jacket Platform Subjected to Earthquake Loading Showing Distribution of Plastic Nodes (Earthquake Scale Factor 4.5, Time 3.0 Second)
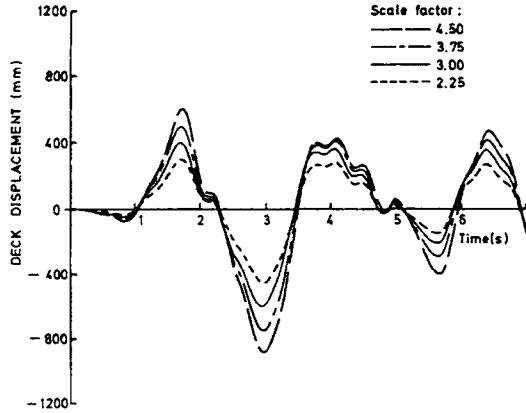
Figure 15.6   Effects of Earthquake Acceleration Scale Factors
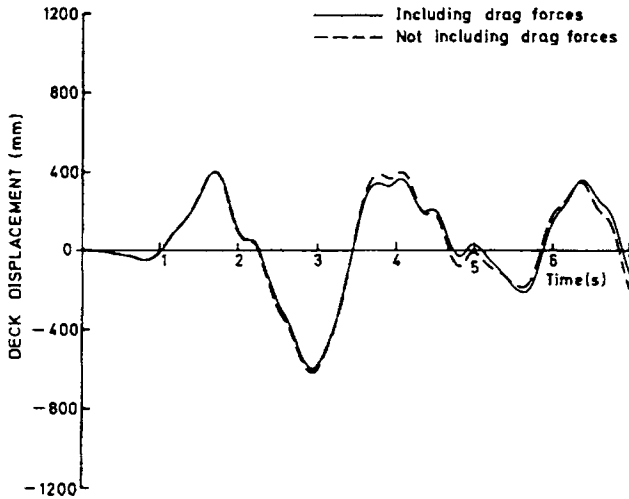
**Figure 15.7   Hydrodynamic Damping Effect Associated With Drag Forces
(Earthquake Acceleration Scale Factor 3.0)**

Figure 15.7 shows time histories of the lateral displacements at the deck of the platform in X-direction for a scale factor 3.0. It is observed that in this example the hydrodynamic damping effect associated with drag forces can be ignored.

Figure15.8. Presents foundation stiffness effects on the time histories of the lateral displacements. The vibration period and maximum displacement increase greatly as the soil stiffness decrease. No plastic node has been observed when soil stiffness has been scaled by a factor 0.1. This figure also shows the importance of modelling soil-structure interaction reasonably accurate. The maximum value of the lateral displacement will be very large and it will cause problems for the piping system and equipment on the deck.
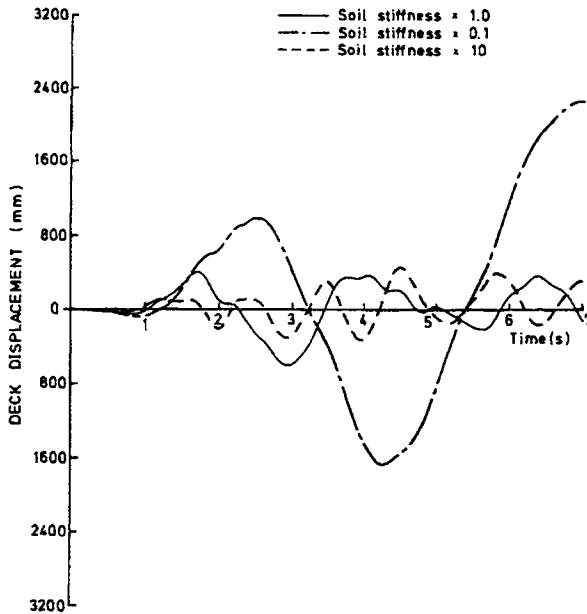
Figure 15.8   Foundation Stiffness Effects (Earthquake Acceleration Scale Factor 3.0)

15.5 Conclusions

A procedure for earthquake response analysis of three dimensional frames with geometrical and material nonlinearities has been presented. A deformation stiffness matrix $[k_D]$ and an internal force vector $\{r\}$ have been derived. This matrix incorporates the coupling between axial and lateral deformations of the elements. In conjunction with the plastic node method, the proposed approach enables accurate modeling of frames using only one element per physical member. The element stiffness matrices are evaluated without numerical integration which is usually required by the traditional finite element methods.

The numerical examples show that the procedure is efficient and accurate. In addition time to prepare input data is low. It can also be applied to nonlinear dynamic response analysis of offshore structures under collision loads.

From Example 15.3, the following results have been observed:

• In an analysis of a structure subjected to strong earthquake loading, It is important to take both geometrical and material nonlinearities into account.

• The hydrodynamic damping effects associated with drag forces are small.

• The foundation stiffness effects are very significant and it is important to accurately model soil-structure interaction.

15.6 References

1. API (1991), "Recommendations for Planning, Designing and Constructing Fixed Offshore Platforms", API Recommended Practice 2A (RP 2A), 19th Edition, August 1, American Petroleum Institute.

2. Archer, J.S., (1965), "Consistent Matrix Formulations for Structural Analysis using Finite Element Techniques", AIAA journal, Vol. 3, pp. 1910-1918.

3. Bai, Y., (1990), "SANDY-A Structural Analysis Program for Static and Dynamic Response of Nonlinear Systems", Theoretical Manual. User's Manual and Demonstration Problem Manual, Century Research Center Corporation, Japan.

4. Bai, Y and Terndrup Pedersen, P. (1991), "Earthquake Response of Offshore Structures", Proc. 10th int. Conf. on Offshore Mechanics Arctic Engineering, OMAE '91, June.

5. Chopra, A.K. (1995), *"Dynamics of Structures, Theory and Applications to Earthquake Engineering"*, Prentice-Hall, Inc.

6. Clough, R.W. and Penzien, J. (1975), *"Dynamics of Structures"*, MsGrwa-Hill.

7. Haythornthwaite, R.M., (1957), "Beams with Full End Fixity", Engineering, Vol. 183 pp. 110-112.

8. Kannan, A.E. and Powell, G.H., (1973), "DRAIN-2D – A General Purpose Computer Program for Dynamic Response of Inelastic Plane Structures", *User's Guide*, Report No. EERC 73-6 University of California, Berkeley.

9. Nedergaard, H. and Pedersen, P.T., (1986), "Analysis Procedure for Space Frames with Material and Geometrical Nonlinearities", Europe-US Symposium – Finte Element Methods for Nonlinear Problems, Edited by Bergan, Bathe and Wunderlich, Springer, pp. 211-230.

10. Newmark, N.M., (1959), "A Method of Computation for Structural Dynamics", Journal of Engineering Mechanics Division, ASCE, Vol. 85, pp. 67-94.

11. Penzien, J., (1976), "Seismic Analysis of Gravity Platforms Including Soil-sttructure Interaction Effects", Offshore Technology Conference (OTC), Paper No. 2674.

12. Przemieniecki, J.S., (1968), *"Theory of Matrix Structural Analysis"*, McGraw-Hill, Inc.

13. Sarpkaya, T. and Isaacson, M., (1981), *"Mechanics of Wave Forces on Offshore Structures"*, Van Nostrand Reinhold Company.

14. Ueda, Y. and Yao, T., (1982), "The Plastic Node Method: A New Method of Plastic Analysis", Computer Methods in Applied Mechanics and Engineering, Vol. 34, pp. 1089-1104.

15. Yao, T., Fujikubo, M., Bai, Y.; Nawata. T. and Tamehiro, M., (1986), "Local Buckling of Bracing Members in Semi-Submersible Drilling Unit (1st Report)", Journal of the Society of Naval Architects of Japan, Vol. 160, pp. 359-371 (in Japanese).

Part III: Fatigue and Fracture

This Page Intentionally Left Blank

Part III

Fatigue and Fracture

Chapter 16   Mechanism of Fatigue and Fracture

16.1 Introduction

Fatigue is the cumulative material damage caused by cyclic loading.   Many structural members must withstand numerous stress reversals during their service life. Examples of this type of loading in marine structures include alternating stresses associated with the wave induced loading, vortex-induced-vibration (VIV) and load fluctuations due to the wind and other environmental effects. In the following Sections, the basic fatigue mechanism will be reviewed. A detailed theoretical background for fatigue analysis is given by Almar-Naess (1985), Gurney (1979), Maddox (1991), Suresh (1991), Dover and Madhav Rao (1996). An extensive list of recently published papers may be found from the proceedings of ISSC (1988, 1991, 1994, 1997, 2000). AWS (1985) can be considered as a representative code for fatigue strength design. Recent developments in ship fatigue research may be found in Xu (1997) and Xu and Bea (1997).

As part of the limit-state design criteria, Part III of this book covers the following aspects:

Chapter 16   Basic mechanism of fatigue and fracture

Chapter 17   Fatigue criteria such as S-N curves, stress concentration factors

Chapter 18   Fatigue loads and stresses determined based on deterministic methods, stochastical methods and Weibull distribution.

Chapter 19   Simplified fatigue assessment based on a Weibull distribution of long-term stress range

Chapter 20   Spectral fatigue analysis and time-domain fatigue analysis and their applications to structural design

Chapter 21   Fracture mechanics and its applications to the assessment of crack propagation, final fracture and calibration of fatigue design S-N curves.

Chapter 22   Material selection and damage tolerance criteria

16.2 Fatigue Overview

Generally, the load amplitude of each cycle is not large enough to cause the structural failure by itself. But failure could occur when the accumulated damage experienced by the structure reaches a critical level. The fatigue life of a structural detail is directly linked to the fatigue process, which can be grouped into the following three stages:

- Crack initiation

- Crack propagation
- Final fracture failure

Crack Initiation: This is tied to the microscopic material behavior. To a certain degree weld defects always exist both internally and on the weld surface. These weld defects may trigger the cracks to grow, which usually from the weld surface.

Crack Propagation: Compared to the crack initiation, the crack propagation stage is better understood and different theories exist to model the crack growth, e.g. fracture mechanics. The major parameter governing crack propagation is the stress range to which the structural detail is subject to. Besides, the welding geometry and initial crack size have a large impact on the fatigue life of the structural detail. In welded structures, fatigue cracks almost always start at a weld defect and the propagation period accounts for more than 90% of the fatigue life.

Fracture Failure: Fracture failure of the structural details will occur eventually when the crack size propagates to a critical size. The final fracture depends upon a couple of parameters, such as stress level, crack size and material toughness. Similar to crack initiation, the fatigue life during the final fracture is a small part and is usually negligible compared to the crack propagation stage.

Fatigue can be classified as:

- High-cycle (low stress) fatigue
- Low-cycle (high stress) fatigue

Typically, a fatigue failure is called "low-cycle fatigue" if the number of cycles to failure is less than 10^4. The number of cycles in a high-cycle fatigue is usually several millions. For marine structures, the latter has been of real concern.

Methods for Fatigue Analysis: In general, there are two methods for fatigue analysis, namely S-N approach (based on fatigue tests, see Chapters 17) and fracture mechanics approach (see Chapter 21). For fatigue design purpose, the S-N curve approach is widely used and is the most suitable one. Fracture mechanics method is used to determine acceptable flaw size; assessing the fatigue crack growth; planning inspection and repair strategy, etc. For the S-N curve approach, there are three methodologies for fatigue damage calculations, depending on the methods of determining fatigue loads (see Chapter 18):

- Simplified Fatigue Analysis (see Chapter 19)
- Spectral Fatigue Analysis (see Chapter 20)
- Time Domain Fatigue Analysis (see Chapter 20)

In order to study the fatigue and fracture damage mechanism, numerous experiments have been conducted to investigate the material characteristics. These experiments can be divided into two categories: stress-controlled fatigue and strain-controlled fatigue.

16.3 Stress-Controlled Fatigue

Stress-controlled fatigue is generally related to high cycle (low stress) fatigue, in which a major part of the material behaves elastically. Even though the material immediately adjacent to the notch may become plastic, both the extent of plastic zone, and the stress in it are limited. Since stress is directly proportional to strains, conventionally, the fatigue strength is expressed in terms of stress.
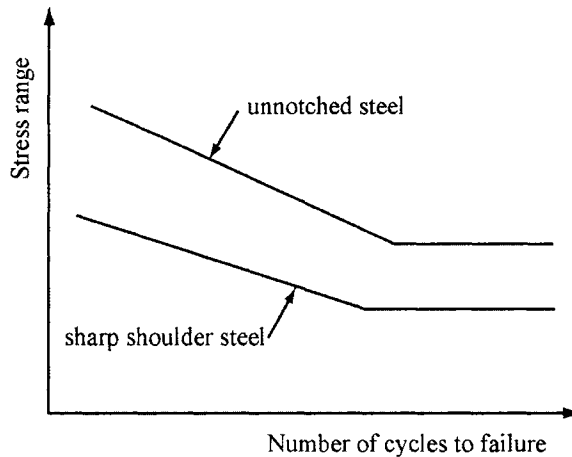
Figure 16.1   Wohler's S-N Curves for Krupp Axle Steel

One of the earliest investigations of stress-controlled cyclic loading effects on fatigue life was performed by Wohler in 1893 who studied railroad wheel axle failure. Several important facts were revealed from this investigation as can be seen in the plot of stress range vs. the number of cycles to failure, see Figure 16.1. First, the number of cycles to failure increases with decreasing stress range. Below a certain stress range, which is referred to as fatigue endurance limit, the fatigue life is infinite. Second, the fatigue life is reduced dramatically by the presence of a notch. These observations indicate that fatigue is a three-stage process involving initiation, propagation, and a final failure stage (Figure 16.2).

The S-N curves established by stress controlled fatigue tests are generally expressed as:

$$N = K \cdot S^{-m} \tag{16.1}$$

where:

N = Number of cycles to failure

S = Stress range

m, K = Material constants depending on the environment, test conditions, etc.

In most cases, the Y-axis of the S-N diagrams is stress amplitude which is half of the total stress range. It should be noted that considerable scatter exists in the S-N Curves. The scatter is due to the factors affecting S-N curves such as:

- wall-thickness

- corrosion

- type and condition of the material including a number of metallurgical variables.

- test environment, specimen surface, alignment of the test machine etc.

- residual stress, mean stress or stress ratio

- local stress peaks (notch effects)
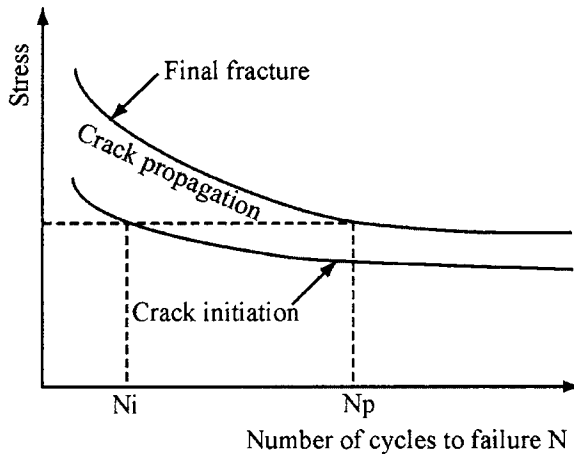
Figure 16.2   **Illustration of Fatigue Life(Initiation and Propagation Stages)**

The first two factors in the above list are explicitly accounted for in fatigue design codes.

16.4 Cumulative Damage for Variable Amplitude Loading

Much of the fatigue data discussed so far was generated from constant amplitude and constant frequency tests. However, these results are not realistic in actual field service conditions. Many structures are subjected to a range of load fluctuations and frequencies. In order to predict the fatigue life of a structural detail subjected to a variable load history based on constant amplitude test data, a number of cumulative damage theories have been proposed. For instance, the Palmgren-Miner cumulative damage law (Miner, 1945) states that.

$$\sum_{i=1}^{k} \frac{n_i}{N_i} = 1 \tag{16.2}$$

where,

k = Number of stress range levels in the block of load spectrum

S_i = ith stress range level

n_i = Number of stress cycles applied at S_i

N_i = Fatigue life at S_i

The hypothesis of Miner was originally based on several assumptions (Fricke et al, 1997):

- sinusoidal load cycles
- purely alternating load
- crack initiation as the failure mode
- No contribution to damage by load cycles below the endurance limit
- Sequence of load cycles not considered

In the literature, several modifications to the Palmgren-Miners law have been suggested related to the damage ratio, endurance limits, etc. The Palmgren-Miner law has still been widely applied in engineering due to its simplicity.

16.5 Strain-Controlled Fatigue

The fatigue of a specimen subjected to strain controlled loading is generally related to low cycle high stress fatigue. The stress associated with low cycle fatigue will usually be high enough to cause a considerable amount of plastic deformation in the region of the stress concentration. Thus, the relation between stress and strain will no longer be linear. This relation is often characterized by a hysteresis loop (Figure 16.3) which may change from cycle to cycle. In Figure 16.3, $\Delta\varepsilon_p$ is the plastic strain range and $\Delta\varepsilon_t$ is the total strain range. $\Delta\varepsilon_e = \Delta\varepsilon_t - \Delta\varepsilon_p$ is the elastic strain range.

In engineering applications, much of the basic testing related to low cycle fatigue has been carried out under constant strain range conditions. The test results have indicated that there is a relation between the fatigue life (N) and a strain parameter. Based on his test data, Manson (1964) suggested that the relationship between the strain and the fatigue life may be expressed as:

$$(\Delta\varepsilon_p)^m N = cons\tan t \tag{16.3}$$

The above equation implies a straight line relation between $\log(\Delta\varepsilon_p)$ and $\log N$ with the slope of -m. The value of the index m is a variable depending on material and environmental conditions, and is approximately 0.5.

In order to derive $\Delta\varepsilon$ –N curves, it is convenient to consider the elastic and plastic strains separately. The elastic strain range is often described in terms of a relationship between the stress amplitude and the number of load reversals (S-N diagram).
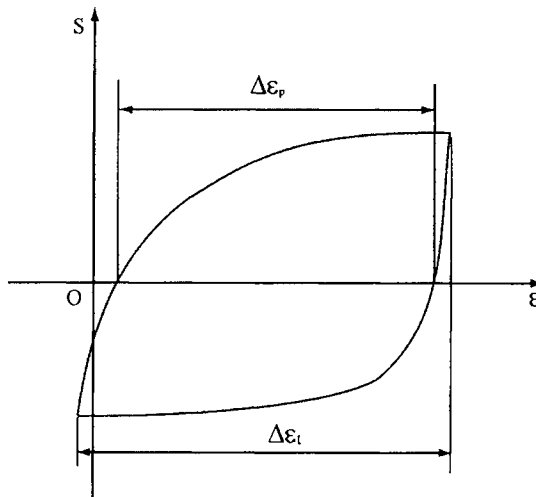
Figure 16.3   Cyclic Stress-strain Loop

$$\frac{\Delta\varepsilon_e E}{2} = S_a = S_f'(2N_f)^b \tag{16.4}$$

where,

$\dfrac{\Delta\varepsilon_e}{2}$ = Elastic strain amplitude

E = Modulus of elasticity

S_a = Stress amplitude

S_f' = Fatigue strength coefficient, defined by the stress intercept at one load reversal $(2N_f = 1)$

N_f = Cycles to failure

$2N_f$ = Number of load reversals to failure

b = Fatigue strength exponent

The plastic component of strain is described by the Manson-Coffin relation (Manson, 1964 and Coffin, 1959):

$$\frac{\Delta\varepsilon_p}{2} = \varepsilon_f'(2N_f)^c \tag{16.5}$$

where,

$\dfrac{\Delta\varepsilon_p}{2}$ = Plastic strain amplitude

ε_f' = Fatigue ductility coefficient defined by the strain intercept at one load reversal $(2N_f = 1)$

$2N_f$ = Total strain reversals to failure

c = Fatigue ductility exponent, a material property in the range of -0.5 to -0.7

Manson suggested that the fatigue resistance of a material subjected to a given strain range could be estimated by superposition of the elastic and plastic strain components. Therefore, by combining Eqs. (16.4) and (16.5), the total strain amplitude may be given by

$$\frac{\Delta\varepsilon_T}{2} = \frac{\Delta\varepsilon_e}{2} + \frac{\Delta\varepsilon_p}{2} = \frac{S_f'}{E}(2N_f)^b + \varepsilon_f'(2N_f)^c \tag{16.6}$$
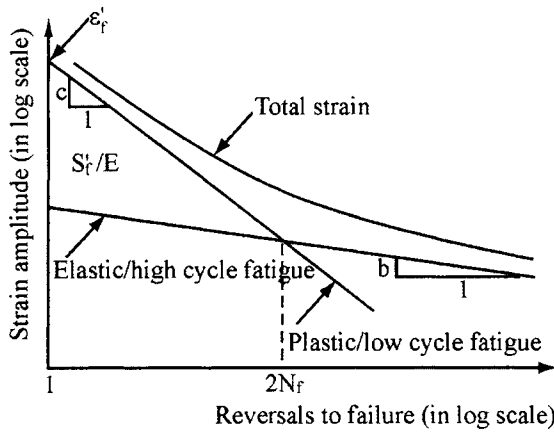
Figure 16.4   Superposition of Stress (High Cycle) Life Curve and Strain (Low Cycle) Life Curve

Figure 16.4 illustrates the combination of the high cycle fatigue and low cycle fatigue. The total strain life curve approaches the plastic strain life curve in the low cycle region, and the stress life curve in the high cycle region. The parameters used in Eq.(16.6) for the determination of the strain-life curves have been given by Boller and Seeger (1987) for various materials.

According to the American Welding Society (AWS), a $\Delta\varepsilon$-N curve is expressed as below (Marshall, 1992):

$$\Delta\varepsilon = 0.055N^{-0.4} \qquad for\ \Delta\varepsilon \geq 0.002 \tag{16.7}$$

and

$$\Delta\varepsilon = 0.016N^{-0.25} \qquad for\ \Delta\varepsilon \leq 0.002 \tag{16.8}$$

The strain range $\Delta\varepsilon$ is the maximum strain less the minimum strain near the weld during steady cyclic bending loads.

Test data for design of the Asgard flowlines (Bai et al, 1999) confirmed that the above AWS curves were applicable to flowlines and risers although they were originally developed for tubular joints. Original test data for pipes under low-cycle fatigue are also given in Bai et al (1999). A study of low-cycle fatigue conducted as part of the DEEPIPE JIP was summarized by Igland et al. (2000).

16.6 Fracture Mechanics in Fatigue Analysis

For a plate under uniform stress, the stress intensity factor K may be estimated as:

$$K = \sigma\sqrt{\pi a}\ F \tag{16.9}$$

where a is the crack width and geometrical correction factor F is the product of a couple of factors such as back crack shape factors, front face factor, finite thickness factor, finite width factor and stress gradient factor.

For fatigue crack growth, the zone of inelasticity is often small enough for the small scale yielding assumption to be valid. Linear fracture mechanics can thus be applied in the fatigue crack growth analysis.

Paris and Erdogan (1963) suggested that the most relevant parameter to describe the fatigue crack growth was the range of the stress intensity factor ΔK. In Figure 16.5, a schematic crack growth rate curve is shown. Three distinct regions are indicated: 1) the well-known threshold region, 2) intermediate region, and 3) the failure region.

At a sufficiently low-stress intensity range in the threshold region, there is no crack growth. The corresponding value of the stress intensity factor is called the threshold stress intensity factor range (ΔK_{th}).

At intermediate values of K, there is an approximate linear relationship between the crack growth rate and ΔK on a log-log scale. This is generally characterized by the Paris equation:

$$\frac{da}{dN} = C(\Delta K)^m \tag{16.10}$$

where

$$\Delta K = K_{max} - K_{min} \tag{16.11}$$

K_{max} and K_{min} are the maximum and minimum values of the stress intensity factor, at the upper and lower limit stresses during a cyclic loading. References on fracture assessment are e.g. Broek (1989), Rolfe and Barsom (1999), see Part III Chapter 21 for more details.
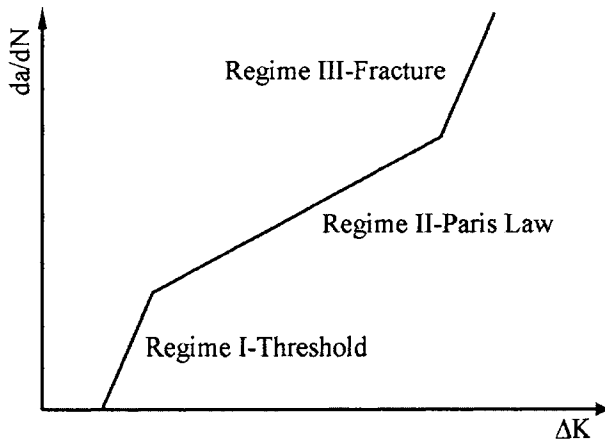
Figure 16.5   Schematic Crack Growth Rate Curve Showing the Relation of Crack Propagation Rate (da/dN) and Stress Intensity Factors

16.7 Examples

Example 16.1: Fatigue Life Cycle Calculation

Problem:

A pipe of 30mm wall thickness is subjected to a long-term stress distribution as shown in the figure below. What is the fatigue life of this pipe that is welded from one side?

Solution:

The welded component falls in class F2 joint classification. By including thickness effect, the S-N curve can be formulated as

$$log\ N = 11.63 - \frac{3}{4}log\left(\frac{t}{22}\right) - 3\,log\ S = 11.53 - 3.0\,log\ S$$

According to the damage calculation tabulated below, the total damage ratio is 0.3523. The number of cycles to failure is then

$$N = \frac{n_0}{D} = \frac{411110}{0.3523} = 1.1669 \cdot 10^6$$
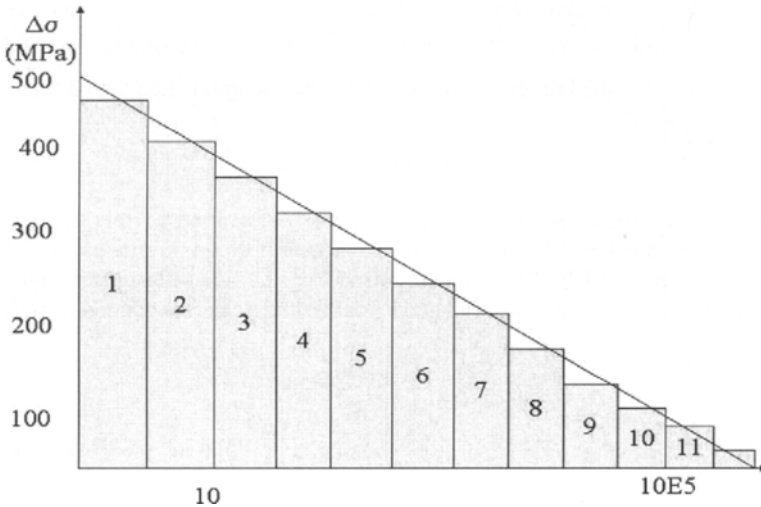
Figure 16.6   Stress Cycles for Fatigue Life Calculation

Block	n_i	S_i	N_i	n_i / N_i
1	3	450	3718	0.0008
2	7	400	4941	0.0014
3	30	350	7903	0.0038
4	70	300	12550	0.0056
5	300	250	21686	0.1353
6	700	210	36588	0.0191
7	3000	170	68969	0.0435
8	7000	130	154230	0.0454
9	30000	90	464807	0.0645
10	70000	50	2710753	0.0258
11	300000	20	4235552	0.0071
$n_0 = 411110$		D=0.3523		

Example 16.2: Fracture Mechanics Based Crack Growth Life Integration

Problem: Assuming that a very wide plate is subjected to a contact amplitude uniaxial cyclic loading that produces nominal varying stresses between 200 MPa and -100 MPa, Critical stress intensity factor is $K_{CR} = 104$ MPa $\sqrt{m}$. Material constants m=3, C=7.1E-12 $m/(MPa\sqrt{m})^3$. What is the fatigue life if the initial crack length is less than 2.5 mm?

Solution:

Crack growth can be predicted using Paris Equation. Integration of this equation involves numerical methods unless F is independent of crack length. In an infinite plate under uniform tension, F is constant (16.12). The compressive stress of -100 MPa may be ignored in the fracture calculation. The critical crack length at final fracture can be obtained from Eq.(16.9),

$$a_{CR} = \frac{1}{\pi}\left(\frac{K_{CR}}{F \cdot \sigma_{max}}\right)^2 = \pi^{-1}\left(\frac{104}{1.12 \cdot 200}\right)^2 = 0.068m$$

Integrating the Paris equation Eq.(16.10), the constant amplitude fatigue life can be estimated as

$$N_p = \frac{\int_{a_0}^{a_{CR}} \dfrac{da}{a^{m/2} \cdot F^m}}{C \cdot S^m \pi^{m/2}} = \frac{0.068^{-0.5} - 0.0025^{-0.5}}{-0.5 \cdot \left(7.1 \cdot 10^{-12}\right) \cdot 200^3 \cdot \pi^{1.5} \cdot 1.12^3} = 72887 cycles$$

16.8 References

1.   Almar-Naess, A. (1985), *"Fatigue Handbook, Offshore Steel Structures"*, Tapir, Norway.

2. AWS (1985), "Structural Welding Code – Steel", ANSI/AWS D1-85, American Welding Society, Miami, U. S. A. (now updated to AWS D1-92-14th Edition).

3. Bai, Y., Damsleth, P.A. and Dretvik, S. (1999), "The Asgard Flowlines Project – Limit State Design Experience", IBC Conference on Risk-Based & Limit-State Design & Operation of Pipelines, Oslo, Oct. 1999.

4. Boller, C. and Seeger, T. (1987), *"Materials Data for Cyclic Loading, Part A-E"*, Elsevier, Amsterdam.

5. Broek, D. (1989), *"The Practical Use of Fracture Mechanics"*, Kluwer Academic Publisher.

6. Coffin, L.F. and Tavernelli, J.F. (1959), "The Cyclic Straining and Fatigue of Metals", Trans. Of the Metallurgical Society of AIME, Vol. 215, p.794.

7. Dover, W.D. and Madhav Rao, A.G. (1996), "Fatigue in Offshore Structures", A.A. Balkema.

8. Fricke, W., Petershagen, H. and Paetzold, H., *"Fatigue Strength of Ship Structures, Part I: Basic Pronciples, Part 2: Examples"*, GL Technology.

9. Gurney, T.R. (1979), *"Fatigue of Welded Structures"*, 2nd Edition, Cambridge University Press.

10. Igland, R.T., Saevik, S., Bai, Y., Berge, S., Collberg, L., Gotoh, K., Mainuon, P. and Thaulow, C. (2000), "Deepwater Pipelines and Flowlines", Proc. of OTC'2000 Conference.

11. ISSC (1988, 1991, 1994, 1997, 2000), "Fatigue and Fracture, Report of technical Committee III.2", Proceedings of the International Ship ad Offshore Structures Congress.

12. Maddox, S.J. (1992), *"Fatigue Strength of Welded Structures"*, Abington Publishing.

13. Manson, S.S. and Hirschberg, M.H. (1964), *"Fatigue: An Interdisciplinary Approach"*, Sycracuse University Press, N.Y., pp.133.

14. Marshall P. W. (1992), *"Design of Welded Tubular Connections"*, Elsevier Press, Amsterdam.

15. Miner, M.A. (1945), "Cumulative Damage in Fatigue", Journal of Applied Mechanics, ASME, Vol. 12(3), pp.159-164.

16. Paris, P. and Erdogan., F. (1963), "A Critical Analysis of Crack Propagation Laws", Journal of Basic Engineering.

17. Rolf, S.T. and Barsom, J.T. (1999), *"Fracture and Fatigue Control in Structures"*, 3rd Edition, Prentice-Hall, Englewood Cliffs, N.J.

18. Suresh, S. (1991), *"Fatigue of Materials"*, Cambridge Press.

19. Xu, T. (1997), "Fatigue of Ship Structural Details – Technical Development and Problems", Journal of Ship Research.

20. Xu, T. and Bea, R.G. (1997), "Fatigue of Ship Critical Structural Details", Journal of Offshore Mechanics and Arctic Engineering, ASME, Vol. 199(2), May, pp. 96-107.

Part III

Fatigue and Fracture

Chapter 17   Fatigue Capacity

17.1   S-N Curves

17.1.1   General

In Part III Chapter 16, it is stated that the relationship between the stress range and the number of cycles to failure is a function of the type of joint, the environment, and the plate thickness. In this Chapter, factors affecting S-N curves will be discussed in Section 17.1, while the determination of the stress range at the critical location (hot spot) of the joint will be discussed in Section 17.2. Methods for determining stress concentration factors will be presented in Section 17.3. In Part III, tubular joints and plated connections are also termed "critical details", or "details".

For fatigue analysis based on the nominal stress approach, welded joints are divided into several classes. Each class has a designated S-N curve. The classification of S-N curves depends on the geometry of the detail, the direction of the fluctuating stress relative to the detail, and the method of fabrication and inspection of the detail. The types of joint, including plate-to-plate, tube-to-plate, and tube-to-tube connections have alphabetical classification types, where each type relates to a particular S-N relationship as determined by experimental fatigue tests. The design S-N curves are based on the mean-minus-two-standard-deviation curves for relevant experimental data. The S-N curves are thus associated with a 97.6% probability of survival.

For example, Norwegian and British codes reference the D curve for simple plate connections with the load transverse to the direction of the weld and the T curve for tubular brace to chord connections, see Figure 17.1.

In the American codes (e.g. API RP2A), fatigue has been relatively less of concern. Consequently, the number of joint classifications is less than that recommended in Europe.

Each construction detail, at which fatigue cracks may potentially develop, should be placed in its relevant joint class in accordance with criteria given in the codes. Fatigue cracks may develop in several locations, e.g. at the weld toe in each of the parts joined, at the weld ends, and in the weld itself. Each location should be classified separately.

The basic design S-N curve is given as:

$$\log N = \log K - m \log S \tag{17.1}$$

where,

$\quad\quad S \quad\quad$ = Stress range

N = Predicted number of cycles to failure for stress range S

m = Negative inverse slope of S-N curve (typically m=3)

$log\,K$ = Intercept of log N-axis by S-N curve = log a − 2std

where, a and std are constant relating to mean S-N curve and standard deviation of log N, respectively.

Examples of S-N curves in-air are given in Figure 17.1. These S-N curves have a bi-linear relationship between Log(S) and Log(N), and the change in slope from a gradient (of 1/3) to a gradient (of 1/5) occurs at 10E7 cycles. The lower right side of the S-N curves reflects the considerably longer life associated with tests of joints at low stress ranges.

The second part of the design S-N curve is given as (NTS, 1998):

$$log\,N = log\,C - r\,log\,S \qquad\qquad (17.2)$$

where,

r = Negative inverse slope of the second S-N curve (typically r=5)

$log\,C$ = Intercept of log N-axis by the second S-N curve

The relationship between the stress range and the number of cycles to failure indicates that a relatively small change in the estimated stress range has a significant effect on the fatigue life. For example, the life of a joint will be halved for an increase of 26% in stress. Estimates of stresses in joints are considered to be within 20% from mechanical tests or refined FE analyses and within 25% from the well-calibrated empirical formulae for stress concentration factors. Thus, accurate estimates of stress ranges at the critical areas on joints are essential when determining fatigue lives. Methods for estimating stress ranges will be discussed further in Section 17.2.
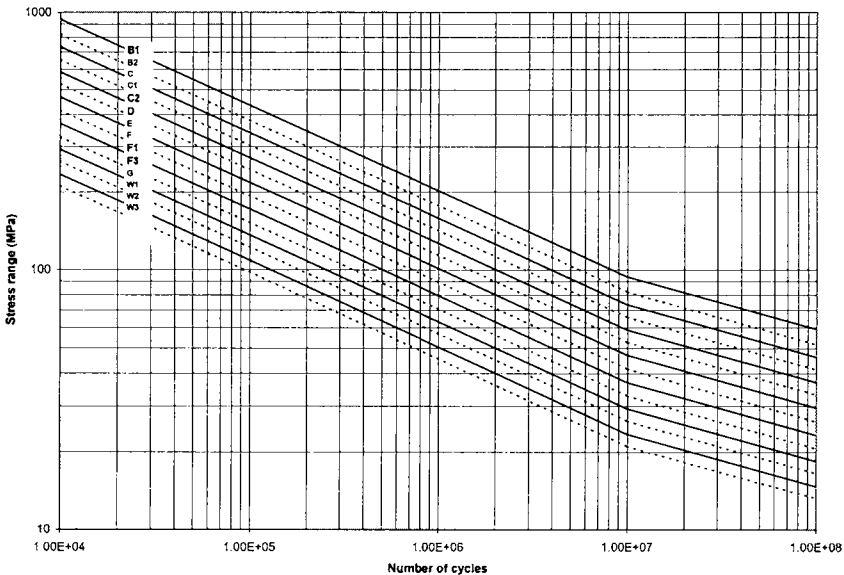
Figure 17.1   Examples of S-N Curves in Air (NTS, 1998)

In some of the design codes, there is a cut-off limit, and low fatigue damage is assumed when the stress range is below the cut-off limit.

For the sake of consistency, discussions of the fatigue criteria in this chapter will be mainly based on NORSOK (NTS, 1998). However, readers are recommended to refer the codes relevant to their projects such as IIW (Hobbacher, A. (1996), Eurocode 3 (1992), IACS (1999), ABS (1992) and DNV (2000), among of others.

17.1.2 Effect of Plate Thickness

The thickness effect is due to the local geometry of the weld toe in relation to the thickness of the adjoining plates and to the stress gradient over the thickness. It may be accounted for by:

$$\log N = \log K - m \log \left(S \left(\frac{t}{t_{ref}} \right)^k \right) \tag{17.3}$$

where, t_{ref} = Reference thickness which in some design codes is 32 mm and 25 mm for tubular joints and other types of welded connections respectively (NTS, 1998).

   t = Thickness through which a crack will most likely grow.

   k = Thickness exponent on fatigue strength in the range 0.00 to 0.25 depending on the code employed, the S-N curves selected etc (NTS, 1998).

In other words, the thickness effect may be accounted for by multiplying a factor of $(t/t_{ref})^k$ to the stress range. In HSE (1995), the value of k and reference thickness t_{ref} is 0.25 and 22 mm, respectively. In general, the thickness correction to the design equation for the S-N curve is required when the plate thickness is thicker than the reference thickness. To some extent, the thickness correction also accounts for the size of the weld and its attachments. However, it does not account for the weld length or the length of component different from the tested component.

17.1.3 Effect of Seawater and Corrosion Protection

In Figure 17.2, three types of S-N curve are compared for the tubular T S-N curves in air, seawater with CP, and seawater under free corrosion. The relationship between in-air and in-seawater with cathodic protection (CP) varies between codes. Using NORSOK (NTS, 1998), the fatigue life at high stress ranges (when N is less than 10^6 cycles) in seawater with CP is considered to be 40% of that in-air. However, there is no difference between the S-N curves at lower stress ranges (when N is in excess of 10^7 cycles).

In general, the fatigue life in seawater under free corrosion is 33% of the life in air at high stress ranges (when N is less than 10^7 cycles). There is no change in slope for the free corrosion S-N curve and hence the fatigue lives are around 10%, of the equivalent lives for in-air S-N curve when N is more than 10^7 cycles.

17.1.4 Effect of Mean Stress

Compressive mean stress has a beneficial effect on fatigue capacity. Normally it is not required to account for the effect of mean stress. However, in some special cases, it is necessary to take into account the mean stress effect to modify the selected S-N curves, e.g. for the fatigue assessment of TLP tethers and mooring lines whose non-linear response is

important. In the literature, several models are available to correct the S-N curves for the mean stress effect. The most popular model is the so-called Modified Goodman relation that my be expressed as (Almar-Naess, 1985):

$$S_{a,N} = \frac{S_a}{1 - \sigma_m / \sigma_u} \qquad (17.4)$$

where, $S_{a,N}$ = the stress at a given fatigue life under reversed loading (mean stress is 0) and where S_a and are the alternative stress applied and σ_m and σ_u are the mean stress and ultimate stress respectively. $S_{a,N}$ defined in Eq.(17.4) should be used as the stress range in the corrected S-N curve.

17.1.5 Comparisons of S-N Curves in Design Standards

There are various kinds of fatigue design codes in the literature, e.g.:

- General steel codes: BS 7608, BS 7910, Eurocode 3, NS 3472
- Offshore industry: NORSOK, UK HSE (UK Den), API, etc.
- Ship industry: classification Rules, IACS requirements
- IIW (International Institute of Welding), AWS (American Welding Society).
- Automobile industry, aerospace & aircraft industries, etc.
- Bridges industry: BS5400 (BSI, 1979), AASHTO (1989)
- ASME Pressure Vessels Codes
- Welded Aluminum Codes: BS8118 (BSI, 1991), ECCS (1992)
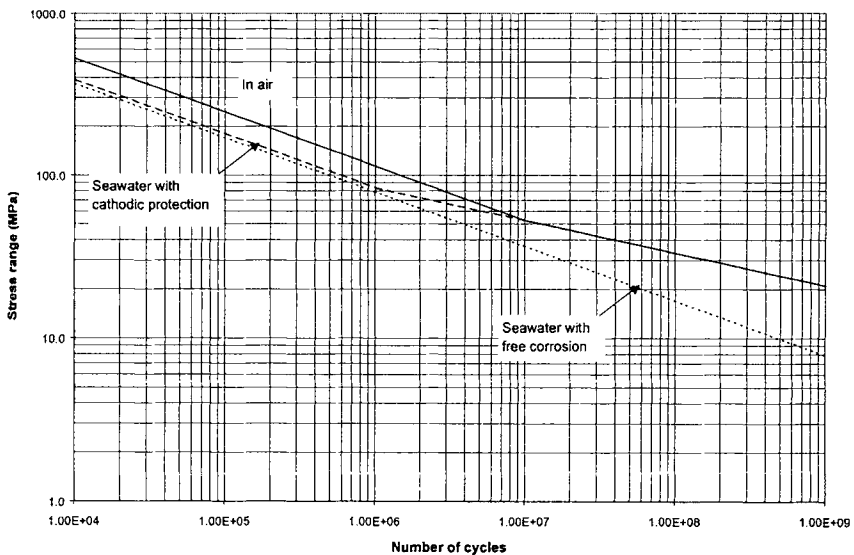
Figure 17.2   Comparison of S-N Curves for Tubular Joints (NTS, 1998)

**Table 17.1   Comparison of European Standards for Fatigue S-N Curves for Air
Environments (Fricke et al, 2000)**

Euro Code 3 Notation (FAT)	NORSOK/ NS 3472/ HSE Notation	Log K For N≤10E7 (m=3)	Log C For N>10E7 (r=5)	Stress Amplitude at transition (MPa)	Thickness Exponent k	SCF as Derived by the Hot-Spot Stress
160	B1	12.913	16.856	93.57	0	
140	B2	12.739	16.566	81.87	0	
125	C	12.592	16.320	73.10	0.15	
112	C1	12.449	16.081	65.50	0.15	
100	C2	12.301	15.835	58/48	015	
90	D	12.164	15.606	52.63	0.25	1
80	E	12.010	15.350	46.78	0.25	1.13
71	F	11.855	15.091	41.52	0.25	1.27
63	F1	11.699	14.832	36.84	0.25	1.43
56	F3	11.546	14.576	32.75	0.25	1.61
50	G	11.398	14.330	29.24	0.25	1.80
45	W1	11.261	14.101	26.32	0.25	2.00
40	W2	11.107	13.845	23.39	0.25	2.25
36	W3	10.970	13.617	21.05	0.25	2.50
	T	Same as D	Same as D	Same as D	Same as D	Same as D

Note: For thickness correction, the reference thickness is 32 mm and 25 mm for welded connections for tubular joints and non- tubular joints, respectively.

In Europe, the UK HSE (1995) replaced the UK DEn (1990). The main change is that m and r become independent of the S-N curves selected. A weld classification factor f (to be multiplied to the stress range) has been introduced in UK HSE (1995) so that various S-N curves in UK Den (1990) may be expressed in one S-N equation. In other word, the S-N curves in UK HSE (1995) are unified to a single equation by defining stress range as:

$$S = f * S_g \left(\frac{t}{t_{ref}} \right)^k \qquad (17.5)$$

where, S_g = stress range which includes weld macro-geometry but excludes the peak stress due to local defects that have been implicitly accounted for in the weld classification factor f.

The relationship between the weld class (B, C, D, ...) and the weld classification factor f is B(f=0.64), C(f=0.76), D(f=1), E(f=1.14), F(f=1.34), F2 (f=1.52), G (f=1.83) and W (f=2.13).

Since 1948 the Norwegian standard NS3472 has been used for design of land and offshore steel structures in Norway. In 1998, NS3472 was revised and in the same time, NORSOK N-004 (NTS, 1998) was developed for design of offshore steel structures. NORSOK is a Norwegian initiative by the industry to develop a design standard for more cost effective offshore development. Eurocode 3 is a European standard for design of building structures. Table 17.1 lists the S-N curves used in Europe for air environments.

In the USA, fatigue design is based on API RP 2A WSD and AWS D1.1. A detailed background of the AWS code Provisions is given by Marshall (1992) and outlined by Marshall (1993). Geyer and Stahl (1986) presented a simplified fatigue design procedure for offshore

structures. The latest developments in the research on S-N curves may be found from Maddox (2001).

In the API RP 2A, the X' curve is used for welded connections without profile control, thickness correction applies if wall-thickness is greater than 0.625 inches (16 mm). In API RP2A, thickness correction exponent k is taken as 0.25. The X curve is used for welded connections with profile control, and wall-thickness correction factor applies when the wall-thickness is greater than 1 inch (25 mm). However, after thickness correction, the X-curve shall not be reduced to be lower than the X' curve.

API S-N curves are single (not bi-linear) and have an endurance limit. The endurance limit for the X curve and X' curve is 35 MPa and 23 MPa respectively. K and m for the X curve are 1.15E15 and 4.38 respectively. For the X' curve, K and m are 2.50E13 and 3.74 respectively.

The classification societies define fatigue criteria in their Rules and guidance/guidelines. IACS requirements for fatigue assessment have been developed by unifying the requirements of individual classification societies for ship structural assessment. The fatigue S- curves for ship structures are mainly based on UK Den basic S-N curves and IIW S-N curves.

The IIW S-N curves assume that the slope of al S-N curves is m=3 and the change in slope (m-5) occurs for N=5x10E6 cycles (Hobbacher, A. (1996). These S-N curves are based on nominal stress range and correspond to non-corrosive conditions, are given for mean minus two standard deviations. Their fatigue class is characterized by the fatigue strength at 2x10E6 cycles, e.g. the stress range corresponding to 2x10E6 cycles (FAT) are 160, 140, 125, 112, 100, 90, 80, 71, 63, 56, 50, 45, 40, 36, see Table 17.1.

BV (1998) proposed corrections of the design S-N curves to account for the various factors such as:

- **Influence of static and residual stresses**: Tensile residual stress of the magnitude of yield stress will reduce fatigue life, and in such cases the maximum stress should be assumed to be yield stress irrespective of the amount of actual maximum stress. Post-weld treatment may improve the weld geometry and fatigue capacity.

- **Influence of compressive stresses**: To account for the less damaging effect of compressive stresses while the stress range is greater than the yield stress, the calculated local stress range S_{local} may be corrected using the British Standard 5400: defining stress range as:

$$S = \sigma_Y + 0.6(S_{local} - \sigma_Y) \quad for \quad \sigma_Y \leq S_{local} \leq 2\sigma_Y \tag{17.6}$$

$$S = 0.8 S_{local} \quad for \quad S_{local} > 2\sigma_Y \tag{17.7}$$

- **Influence of plate thickness**

- **Influence of the material**: the fatigue strength of welded joints is nearly independent on the material properties such as material grades. However, for machined plates the effect of yield strength is large.

- **Influence of the environment**

- **Workmaship**: S-N curves have been derived for standard workmanship and welding procedures. In some instances, the effect of imperfection and misalignment should be taking into account when determining the hot spot stresses.

While the influences of the environment and plate-thickness are explicitly account for in most of the design codes, other items listed in the above may or may not be required to be considered by some design codes.

17.1.6 Fatigue Strength Improvement

When the theoretically calculated fatigue life is less than the required, methods of justifying the fatigue design include:

- By improving the design of structural details (e.g. to reduce stress concentration, residual stress and misalignment, and locally increase the wall-thickness)

- By using improved analysis methods: Spectral fatigue analysis is usually more accurate that simplified fatigue assessment. Time-domain analysis may be better than the spectral fatigue analysis. The selection of sea states and loading conditions and quality of the environmental data all will influence the fatigue analysis results.

From capacity point of view, the three most important factors that affect fatigue are: stress concentration due to weld geometry, defect shape and distribution and residual stress. Hence, methods for improving fatigue capacity through fabrication and repair include (BV, 1998):

- Modification of the weld geometry by grinding or weld toe remelting

- Improvement of the welding procedures and workmanship

- Introduction of compressive stresses, for example by hammer or shot peening

- Post-weld heat treatment

However, the most efficient methods re possible improvement of the design such as reducing the geometric stress concentration factors (BV, 1998):

- Improvement of the shape of cut-outs

- Softening of brackets toes

- Local increase in thickness

More detailed discussions on improvement of weld details and fatigue design are given in Part III Chapter 22.

17.1.7 Experimental S-N Curves

Most of the S-N curves are determined in laboratories where test specimens are subjected to constant amplitude until failure. The S-N curves are derived by their mean fatigue life and standard deviation of log N. The mean S-N curve is defined as 50 percent of the specimens will fail. The basic design S-N curve is given as:

$$\log N = \log K_{50} - m \log S \tag{17.8}$$

where K_{50} is obtained from the mean value of $\log K_{50}$. To derive the S-N curves, a large number of tests are required. However, when the coefficient m is known, 10 tests may be sufficient to accurately derive the S-N curve (BV, 1998):

- 5 at stress level corresponding to $N = 10^4$

- 5 at stress level corresponding to $N = 5 \bullet 10^5$

If p is the per cent of the test specimens that fall below the design S-N curve, the design S-N curve may be defined as follows: en as:

$$\log N = \log K_{50} - \lambda_p S_d - m \log S \qquad (17.9)$$

where S_d is the standard deviation of $\log K_{50}$. The relationship between the value of λ_p and the failure probability is (BV, 1998):

- fail safe design: p=2.5%, $\lambda_p = 2$ (normally used to derived design S-N curves)

- safe life design: p=0.1%, $\lambda_p = 3$ (for special welded specimens that represent structural details which can not be easily inspected and repaired.)

17.2 Estimation of the Stress Range

The fatigue analysis procedure is based on the ranges of cyclic principal stresses.

To determine the stress range, two approaches have been developed. The "nominal stress" approach has been applied to plated structures and the "hotspot stress" approach has been developed for tubular joints. Note that a "notch stress" approach is also suggested by some design codes. In recent years, attempts are being made to apply the hot spot stress approach to plated structures.

17.2.1 Nominal Stress Approach

In the nominal stress approach, the stress concentrations caused by the weld profile have been included in the S-N curves.

The determination of stresses applied to fatigue analysis of structural details, is generally undertaken by a global-local finite element analysis of the pertinent stress in accordance with the chosen S-N curves. In other words, the calculated stress for the considered local hot spot area of structural details should resemble the nominal stress of the test specimens from which the S-N curves were established. Unfortunately, in most cases, structural details are more complex than the test specimens, both in geometry and in applied loading. Consequently, a relationship between the S-N data stress and calculated stress may not be easily established.

Another problem associated with the nominal stress approach is the classification of structural details. The primary difference between UK DEn curves and recent European S-N curves is that UK DEn curves do not have fatigue endurance limit. The fatigue endurance limit, which is found in the constant cyclic loading test, usually does not exist for marine structural details due to a variety of causes such as welding, corrosion, and load sequence effects of the random loading.

The relevant fatigue stress for fatigue design would be the tensile stress σ, for example, for the weld shown in Figure 17.3a. For the weld shown in Figure 17.3b, the stress concentration factor for the global geometry must be accounted for, using the relevant fatigue stress of SCF·σ, where SCF is the stress concentration factor due to the hole.

If a corner detail with zero radii is modeled, the calculated stress will approach infinity as the element size is decreased to zero. The modeling of a relevant radius requires a very fine element mesh, increasing the size of the finite element model. In addition, selection of the proper radius to be used for the analysis will be a matter for discussion.
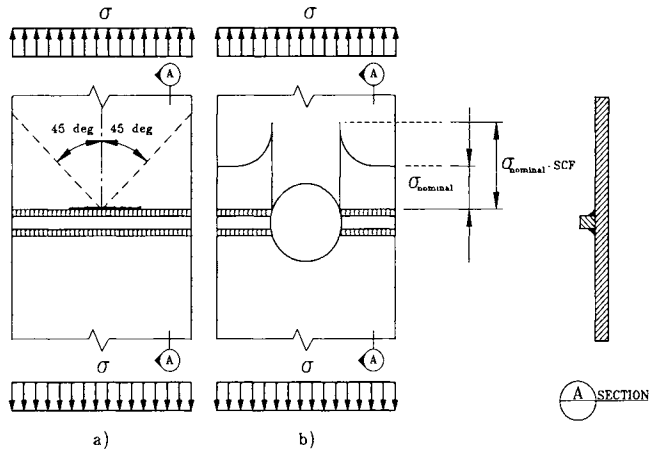
Figure 17.3   Description of Stress in Two Plated Sections (NTS, 1998)

17.2.2 Hotspot Stress Approach

The nominal stress approach has two disadvantages for tubular joints. First, it is not possible to define a reasonable nominal stress due to the complex geometry and applied loading. Second, suitable fatigue test data are often not available for large complex tubular joints. Therefore, a hot spot stress approach has been developed in order to overcome these difficulties (Kung, 1975 and Lalani, 1992).

The hot spot stress reduces the various S-N design curves of the nominal stress approach to two base line curves. One is the curve for non-welded structures (e.g. cutout, plate edges), and the other is the curve for welded structures. This is accomplished by using the stress nearest to the weld, which is defined as the hot spot fatigue stress.

The hot spot stress approach was developed based on an observation that the experimentally derived S-N curves are nearly parallel. This implies that all the S-N curves can be related to each other by some factors. For example, in the UK DEn Curves, the E curve, and the F curve are correlated by a factor of 1.2 or 1.3, assuming the following:

- This correlated factor represents the difference of structural configurations between different details.

- The local fatigue failure is independent of the detail type. The difference in fatigue resistance between details is due to different structural configurations.

- The structural stress concentration factor (SCFstruct) can represent the effects of structural configurations entirely.

The stress range at tubular joint's hot spots should be combined with the S-N curve T. The stress range at the hot spot of plated structures should be combined with UK S-N curve D. The C-curve may be used if machining of the weld surface to the base material is performed. Then,

the machining has to be performed such that the local stress concentration due to the weld is removed.

The hot spot stress concept assumes that the effect of the local stress factor, which is due to the weld profile, should be included in the S-N curves. The stress concentration due to gross geometry change and local geometry change should be included in the hot spot stress. The problem with the hot spot stress approach is that the stress gradients are very high in the vicinity of the weld and plate intersections. Because of the high gradients, the stresses computed in FEA are extremely sensitive to the finite element mesh size. This mesh sensitivity results in an inaccurate definition of the hot spot stress in application.

In order to define the hotspot stress, stresses from a finite element analysis or a mechanical test may be linearly extrapolated, see Figure 17.4. The dotted straight line is based on the stresses at a distance t/2 and 3t/2 from the weld toe (this distance may depend on the codes used).

The hot spot stress approach is preferred in cases where:

- There is no defined nominal stress due to complicated geometry effects

- The structural discontinuity is not comparable with any classified details

- The fatigue test is performed together with strain gauge measurements to determine the hot spot stress.

- The offset or angular misalignments exceed the fabrication tolerance used for the of nominal stress approach.
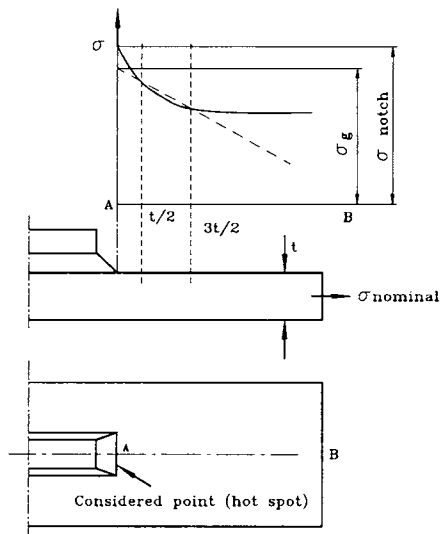
Figure 17.4   Stress Distribution at an Attachment and Extrapolation of Stresses (NTS, 1998)

17.2.3 Notch Stress Approach

The notch stress approach is based on the determination of peak stress that account for the weld profile. The notch stress is therefore estimated as the product of the hot-spot stress and rhe stress concentratio factor for weld profile (so-called weld concentration facyor). The weld concentratio factor may be estimated from diagrams, parametrci equations, experimental measurements and finite element analysis. The presence of the welds should be given due consideration in the notch stress approach.

The IIW (Hobbacher, 1996) recommended the following procedure for the calculation of notch stresses:

- An effective weld root radius of r=1mm is to be considerd,

- The method is restricted to weld joints which are expected to fail from weld toe or weld root.

- Flank angle of 30 degrees for butt welds and 45 degrees for filler welds may be considerd,

- The method is limited to thickness of larger than 5 mm.

17.3 Stress Concentration Factors

17.3.1 Definition of Stress Concentration Factors

The aim of the stress analysis is to calculate the stress at the weld toe (hot spot), $\sigma_{hot\ spot}$. The stress concentration factor due to the geometry effect is defined as,

$$SCF = \frac{\sigma_{hot\ spot}}{\sigma_{nominal}} \qquad (17.10)$$

There are three approaches to determining the SCF:

- Experimental Data,
- Finite Element Analysis, and
- Parametric equations based on experimental data or finite element analysis.

The above approaches will be detailed in the following sub-sections.

Structural Detail

Model with 20-node solid elements

Model with 8-node shell elements (size: t x t)
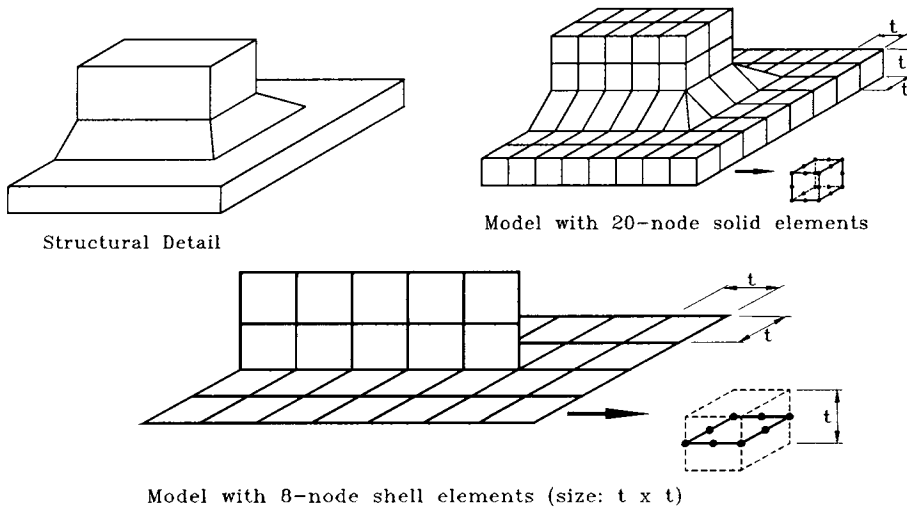
Figure 17.5   Examples of Modelling (NTS, 1998)

17.3.2 Determination of SCF by Experimental Measurement

Determination of the SCF by using strain measurements in fatigue tests is the most reliable method. However, it is important to decide exactly where to locate strain gauges to ensure that the value obtained is compatible with the chosen design S-N curve. If this is not achieved, gross error may occur.

The existing method of defining SCF for use in the S-N curves is established based on the extrapolation to the weld toe from an area of linear stress data, which would include varying proportions of the notch SCF depending on the weld detail and the geometric stress concentration. This is basically due to the fundamental assumption in hotspot stress concept since the structural geometry effects may not be completely separated from the local weld geometry effects. Size effects, weld profiles, residual stresses, and stress distributions are usually the sources of this variation. The weld profile effect in tubular joints, is not primarily due to the weld shape itself, it is due to the position of the weld toe on the chord, which significantly affects the hot spot stress at the weld toe. Therefore, a consistent stress recovery procedure should be developed in SCF measurement.

17.3.3 Parametric Equations for Stress Concentration Factors

Given that a variety of SCFs need to be estimated on any given tubular joint, SCF determinations have to rely more on sets of parametric equations, which account for the joint geometry configurations and applied loading.

A stress concentration factor may be defined as the ratio of the hot spot stress range over the nominal stress range. All stress risers have to be considered when evaluating the stress concentration factors (SCF). The resulting SCF is derived as:

$$SCF = SCF_g \cdot SCF_w \cdot SCF_{te} \cdot SCF_{ta} \cdot SCF_n \qquad (17.11)$$

where,

SCF_g = Stress concentration factor due to the gross geometry of the detail considered

SCF_w = Stress concentration factor due to the weld geometry

SCF_{te} = Additional stress concentration factor due to eccentricity tolerance (nominally used for plate connections only)

SCF_{ta} = Additional stress concentration factor due to angular mismatch (normally used for plate connection only)

SCF_n = Additional stress concentration factor for un-symmetrical stiffeners on laterally loaded panels, applicable when the nominal stress is derived from simple beam analysis.

The best-known SCF formulae for the fatigue assessment of offshore structures are those of Efthymious (1988). There are various parametric equations in the literature for the determination of SCFs, for instance:

- SCF equations for tubular connections: API RP2A-WSD, NORSOK N-004 (NTS 1998) and Efthymiou (1988). In addition, Smedley and Fisher (1990) gave SCFs for ring-stiffened tubular joints under axial loads, in-plane and out-of-plane bending. For rectangular hollow sections, reference is made to Van Wingerde, Packer, Wardenier, Dutta and Marshall (1993) and Soh and Soh (1993).

- SCF equations for Tube to Plate Connections: NORSOK N-004 and Pilkey (1997).

- SCF for girth welds: NORSOK N-004 (NTS, 1998).

The SCF equations from the references mentioned in the above have been summarized in DNV (2000).

It should be indicated that the parametric equations are valid only for the applicability range defined in terms of geometry and loads. A general approach for the determination of SCFs is to use the finite element analysis, see the sub-section below.

17.3.4 Hot-Spot Stress Calculation Based on Finite Element Analysis

The aim of the finite element analysis is to calculate the geometric stress distribution in the hot spot region so that these stresses can be used to derive stress concentration factors. The result of finite element analysis of SCFs largely depends on the modeling techniques and the computer program used. The use of different elements and meshes, modeling of the welds, and definition of the chord's length substantially influence the computed SCF (Healy and Bultrago, 1994).

By decreasing the element size, the FEM stresses at discontinuities may approach infinity. In order to have a uniform basis for comparison of results from different computer programs and users, it is necessary to set a lower bound for the element size and use an extrapolation procedure to the hot spot.

Stresses in finite element analysis are normally derived at the Gaussian integration points. Depending on the element type it may be necessary to perform several extrapolations in order to determine the stress at the weld toe. In order to preserve the information of the direction of principal stresses at the hot spot, component stresses are to be used for the extrapolation.

The analysis method should be tested against a well-known detail, prior to using it for fatigue assessment. There are numerous types of elements that can be used, and the SCF obtained, depends on the elements chosen. Therefore, a consistent stress recovery procedure must be calibrated when assessing data from finite element analysis.

Finite element analysis programs, such as NASTRAN, ABAQUS and ANSYS, use structural elements such as thin, thick plate, or shell element. When modeling fabricated tubular joints, the welds may not be properly modeled by thin plate or shell elements. Consequently, the model does not account for any notch effects due to the presence of the weld and micro effects due to the weld shape.

The stresses in thin shell plates are calculated from a membrane stress and a moment at the mid-surface of element. The total free surface stresses are determined by superposition. At a plate intersection, the peak stresses will be predicted at positions that lie inside the actual joint. Comparisons between these values and experimental measurements have indicated that thin shell analysis overestimates the actual surface stresses or SCF present in the real structure.

Most finite element elements are based on a displacement formulation. This means that displacements or deformation will be continuous throughout the mesh, but stresses will be discontinuous between elements. Thus, the nodal average stresses may be recommended. However, limited comparison between these values and experimental measurements indicate that this will generally over-predict hotspot stress or SCF especially on the brace side.

As opposed to shell elements, a model using solid elements may include the welded region, see Figure 17.5. In such models, the SCFs may be derived by extrapolating stress components to relevant weld toes. The extrapolation direction should be normal to the weld toes. However, there is still considerable uncertainty associated with the modeling of weld region and weld shape.

Fricke (2002) recommended hot-spot analysis procedures for structural details of ships and FPSOs based on round-robin FE analysis. Some of his findings are:

- If hot-spot stress is evaluated by linear extrapolation from stresses at 0.5t and 1.5t, the fatigue strength may be assessed using a usual design S-N curve based on hot-spot stress (e.g. Hobbacher, 1996 and Maddox, 2001).

- If hot-spot stress is defined at 0.5t without stress extrapolation, the design S-N curve should be downgraded by 1 fatigue class.

- If the hot-spot stress is evaluated from strain measurements or from refined models with improved finite elements, a stress extrapolation over reference points at distance 0.4t and 1.0t or a quadratic extrapolation is recommended (Hobbacher, 1996).

It should be pointed out the determination of hot spot stress based on finite element analysis is still a very active field of on-going research since the accuracy and efficiency of the stress determination are of importance. Other known research work includes Niemi (1993, 1994).

17.4 Examples

17.4.1 Example 17.1: Fatigue Damage Calculation

Problem:

Two plates A and B are doubled sided butt welded, another plate C is welded to plate A by fillet welds, as shown in Fig. 17.6. The thickness of the plate is 20 mm. The plate is subjected to cyclic loading with a constant stress range of S=200 MPa and a total number of cycles $n_0 = 10^5$. It is assumed that the maximum misalignment of the weld is 4mm. What is the fatigue damage at these welds?
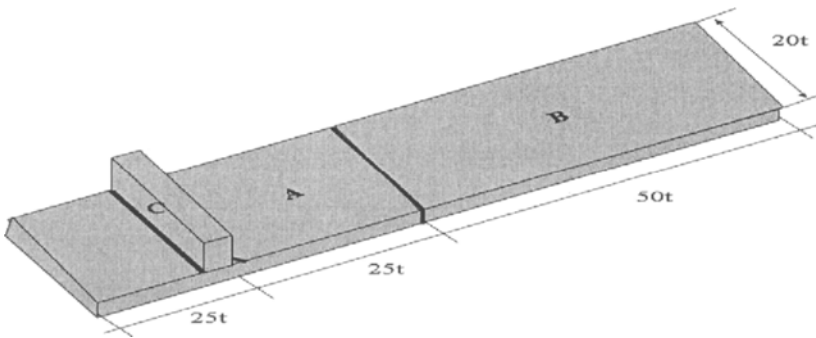
Figure 17.6   Fatigue of Welded Plates

Solution:

Misalignment introduces the bending moment in the plates. The corresponding bending stress range at the butt weld is:

$$S_b = \frac{\Delta M}{W} = \frac{S \cdot t \cdot \dfrac{e}{2}}{\dfrac{t^2}{6}} = \frac{S \cdot 3e}{t}$$

The maximum stress range at butt weld is:

$$S_{local} = \left(1 + \frac{3e}{t}\right) \cdot S = SCF_{global} \cdot S = 120 MPa$$

S-N curve C should be used for butt weld with m=3.5, $\log \overline{a} = 13.63$. This gives the following damage ratio:

$$D = \frac{\Delta \sigma_{local}^m}{\overline{a}} \cdot n_0 = \frac{120^{3.5}}{10^{13.63}} \cdot 10^5 = 0.044$$

The local stress range at the fillet weld is:

$$S_{local} = 0.5\left[S + S\left(1 + \frac{3e}{t}\right)\right] = 160 MPa$$

Since the fillet weld is going out of the edge of the plate, S-N curve G should be used with
$m=3.0$, $\log \bar{a} = 11.39$, this gives the following damage ratio:

$$D = \frac{\Delta \sigma_{local}^{m}}{\bar{a}} \cdot n_0 = \frac{160^{3.0}}{10^{11.39}} \cdot 10^5 = 1.669$$

17.5 References

1.   AASHTO (1989), "*Standard Specification for Highway Bridges, 14th Ed.*", American Association of State Highway Transportation Officials, Washington D.C.

2.   ABS (1992), "Guide for the Fatigue Strength Assessment of Tankers". In ABS Steel Vessel Rules (latest revision), American Bureau of Shipping.

3.   Almar-Naess, A. (1985), "*Fatigue Handbook, Offshore Steel Structures*", Tapir, Norway.

4.   API RP2A-WSD (2001), "Planning, Designing and Constructing Fixed Offshore Platforms – Working Stress Design".

5.   AWS D 1.1 (1992), "Structural Welding Code – Steel", American Welding Society.

6.   BS 5400 (1979), "*Steel, Concrete and Composite Bridges, Part 10, Codes of Practice for Fatigue*", British Standard Institute.

7.   BS 8118 (1991), "*Structural Use of Aluminum*", British Standard Institute.

8.   BS 7608 (1993), "*Code of Practice for Fatigue Design and Assessment of Steel Structures*", British Standard Institute.

9.   BS 7910 (2001), "*Guide on Methods for Assessing the Acceptability of Flaws in Structures*", British Standard Institute.

10.   BV (1998), "*Fatigue Strength of Welded Ship Structures*", Bureau Veritas.

11.   DNV (2000), "RP-C203, Fatigue Strength Analysis of Offshore Steel Structures", Det Norske Veritas.

12.   ECCS (1992), "*European Recommendations for Aluminum Alloy Structures: Fatigue Design* ", ECCS Report No. 68, Brussels, Belgium, European Convention for Structural Steelwork.

13.   Eurocode 3 (1993), "Design of Steel Structures", European Standards.

14.   Efthymiou, M. (1988), "Development of SCF Formulae and Generalized Influence Functions for Use in Fatigue Analysis", Offshore Tubular Joints Conference OTJ, Egham, Surrey, U. K.

15.   Fricke, W. (2002), "Recommended Hot-Spot Analysis Procedures for Structural Details of Ships and FPSOs Based on Round-Robin FE Analysis", Journal of ISOPE, Vol. 12(1), pp. 40-47.

16.   Fricke, W., Berge, S., Brennan, F., Cui, W., Josefson, L., Kierkegaard, H., Kihl, D., Koval, M., Mikkola, T.P., Parmentier, G., Toyosada, M., Yoon, J.H., (2000), "Fatigue and Fracture", Committee report of ISSC (Int. Ship and Offshore Structures Congress), Nagasaki, Japan.

17. Geyer, J.F. and Stahl, B. (1986), "Simplified Fatigue Design Procedure for Offshore Structures", Offshore Technology Conference, OTC Paper 5331, Houston, Texas, May 5-8.

18. Healy B.E. and Bultrago, J. (1994), "Extrapolation Procedures for Determining SCFs in Mid-surface Tubular Joint Models", 6th Int. Symposium on Tubular Joint Structures, Monash University, Melbourne, Australia.

19. Hobbacher, A. (1996), *"Fatigue Design of Welded Joints and Components"*, International Institute of Welding (IIW), XIII-1539-96/XV-845-96, Abington Pub., Cambridge, UK.

20. HSE (1995), "Offshore Installation, Guidance on Design, Construction and Certification", UK Health and Safety Executives, 4th Edition, Section 21.

21. IACS (1999), "Recom. 56.1: Fatigue Assessment of Ship Structures", International Association of Classification Societies, July 1999.

22. ISO/CD 19902 "Petroleum and natural Gas Industries - Offshore Structures - Fixed Steel Structures", Chapter 16, Fatigue Strength of Connections, International Standard Organization.

23. Kung J.G., Potvin A et al (1975), "Stress Concentrations in Tubular Joints", Paper OTC 2205, Offshore Technology Conference.

24. Lalani, M. (1992), "Developments in Tubular Joint Technology for Offshore Structures", Proceedings of the International Conference on Offshore and Polar Engineering, San Francisco, CA.

25. Maddox, S. (2001), "Recommended Design S-N Curves for Fatigue Assessment of FPSOs," ISOPE-2001, Stavanger.

26. Marshall P. W. (1992), *"Design of Welded Tubular Connections"*, Elsevier Press, Amsterdam.

27. Marshall, P.W. (1993), "API Provisions for SCF, SN and Size-Profile Effects," Offshore Technology Conference, Houston, TX.

28. Niemi, E. (1993), *"Stress Determination for Fatigue Analysis of Welded Components"*, International Institute of Welding (IIW), Technical Report IIS/IIW-1221-93.

29. Niemi, E. (1994), *"On the Determination of Hot Spot Stress in the Vacinity of Edge Gussets"*, International Institute of Welding (IIW), Technical Report IIS/IIW-1555-94.

30. NS 3472 (1984), "Design of Steel Structures", Norwegian Standards.

31. NTS (1998), "Design of Offshore Structures, Annex C, Fatigue Strength Analysis", NORSOK Standard N-004.

32. Pilkey, W. (1997), *"Petersen's Stress Concentration Factors"*, 2nd Edition, John Wiley and Sons, Inc.

33. Radaj, D. (1990), *"Design and Analysis of Fatigue Resistant Structures"*, Abington Pub., Cambridge, UK.

34. Smedley, P. and Fisher, P. (1990), "Stress Concentration Factors for Ring-Stiffened Tubular Joints", International Symposium on Tubular Structures, Delft, June 1990.

35. Soh, A.K. and Soh, C.K. (1992), "Stress Concentrations in T/Y nd K Spare-to-Spare and Sqare-to-Round Tubular Joints", Journal of OMAE, Vol. 114.

36. UK DEn (1990), "Offshore Installations: Guidance on Design, Construction, and Certification," 3rd Edition, UK Department of Energy (Now UK Health and Safety Executives).

37. Van Wingerde, A.M., Packer, J.A., Wardenier, J., Dutta, D. and Marchall, P. (1993), "Proposed Revisions for fatigue Design of Planar Welded Connections made of Hollow Structural Sections", paper 65 in "Tubular Structures", Edited by Coutie et al.

Part III

Fatigue and Fracture

Chapter 18 Fatigue Loading and Stresses

18.1 Introduction

Marine structures may be exposed to a variety of loads during their life cycle. The loads are commonly classified as follows

- Functional loads
- Dead loads
- Live Loads
- Environmental Loads
- Sea Loads (waves and currents)
- Wind Loads
- Seismic Loads
- Accidental loads

All loads that vary in magnitude and/or direction will cause stress variations in the structure, which may lead to fatigue damage. Live loads and environmental loads are especially important in this aspect. The environmental loads are dominating for the main part of marine structures. The waves and currents are considered the most important sources of environmental loads acting on marine structures. Moored floating structures are also sensitive to wind loads.

Fatigue loading is one of the key parameters in the fatigue analysis. It is the long-term loading during the fatigue damage process. Various studies have been conducted on fatigue loading on marine structures, to characterize the sea environment, the structural response, and a statistical description. The sea environment is generally characterized by the wave spectrum. The structural response is determined using hydrodynamic theory and finite element analysis.

The objective of this Chapter is to present a general procedure for long-term fatigue stress described using Weibull distribution function. Other methods of fatigue loading include design wave approach and wave scatter diagram approach. The Weibull stress distribution function has been used in the simplified fatigue assessment (see Chapter 19), while the wave scatter diagram approach is applied in frequency-domain fatigue analysis and time-domain fatigue analysis (See Chapter 20).

Some of the earlier research on fatigue loads has been summarized by Almar-Naess (1985). Recent developments in this field may be found in Baltrop (1998) and papers such as Chen and Shin (1995) and ISSC committee reports.

18.2 Fatigue Loading for Ocean-Going Ships

For ocean-going ships, two basic sea states are to be considered in the determination of global bending loads and local pressure: the head sea condition and oblique sea condition. The cumulative fatigue damages should be calculated for full laden condition and ballast condition respectively. The probability for each of these conditions is defined by classification rules according to the type of vessels as below:

Table 18.1 Percentages of Fatigue Loading Conditions (IACS, 1999)

	Full laden load, α	Ballast, β
Oil tankers, liquefied gas carriers	50 %	50 %
Bulk carriers	60 %	40 %
Container ship, cargo ships	75 %	25 %

Two basic sea states are to be considered in the determination of global bending loads and local pressure: the head sea condition and oblique sea condition. These basic sea states combine the various dynamic effect of environment on the hull structure. The load components for these sea states depend on the ship classification rules applied. For instance, BV (1998) further defines the hull girder loads and local loads (pressure & internal loads) for four cases as Table 18.2.

Table 18.2 Load Cases for Ocean Going Ships (BV, 1998)

	Head-Sea Condition, α	Oblique-Sea Condition, β
Static sea pressure associated to maximum and minimum inertia cargo or blast loads	**Case 11,** Amax=-0.45, Amin=0.45, B=0	**Case 21,** Amax=-0.30, Amin=0.30, B=0.45
Maximum (ship on crest of wave) and minimum (ship on tough of wave) wave-induced sea pressure associated to static internal cargo or ballast loads	**Case 12,** Amax=0.625, Amin=-0.625, B=0.45	**Case 22,** Amax=-0.30sgn(z-N), Amin=0.30sgn(z-N), B=-0.625

The global loads include still water bending moment M_{sw} for the load condition considered, and vertical wave bending moment. The vertical bending stress σ_L is further defined:

• In sagging condition for maximum internal cargo or ballast loads:

$$\sigma_L = \left(M_{SW} + A_{max}(M_{WV})_S\right)\frac{z-N}{I_V} + B \ M_{WH} \frac{y}{I_H} \tag{18.1}$$

- In hogging condition for minimum internal cargo or ballast loads

$$\sigma_L = \left(M_{SW} + A_{min}(M_{WV})_H\right)\frac{z-N}{I_V} + B \ M_{WH} \frac{y}{I_H} \tag{18.2}$$

where

I_V and I_H: moment of inertia of a cross-section about the horizontal neutral axis, and vertical neutral axis respectively,

N and z: vertical distance from the keel line to the neutral axis, and from the keel line to the load point, respectively.

y: horizontal distance from the load point to the centerline,

$(M_{WV})_S$ and $(M_{WV})_H$: vertical wave bending moment for sagging and hogging conditions respectively, according to IACS requirements.

A_{max}, A_{min} and B: Coefficients are defined in Table 18.2.

The local loads include the static sea pressure and internal cargo or ballast loads. The stress ranges for full laden load conditions may be estimated as:

$$S_{ij} = \left|\left(\sigma_{ij}\right)_{max} - \left(\sigma_{ij}\right)_{min}\right| \tag{18.3}$$

Similarly, the stress ranges for ballast load conditions may be estimated as:

$$S_{ij}' = \left|\left(\sigma_{ij}'\right)_{max} - \left(\sigma_{ij}'\right)_{min}\right| \tag{18.4}$$

The long-term distribution of the hull girder stress range may be represented by a two-parameter Weibull distribution. When a long-term analysis of the ship behavior at sea is performed enabling to determine the long-term distribution of hull girder bending stress, the shape parameter ξ may be determined as follows (BV, 1998):

$$\xi = 0.47 / \ln\left(\frac{\sigma_{10^{-8}}}{\sigma_{10^{-5}}}\right) \tag{18.5}$$

where $\sigma_{10^{-8}}$ and $\sigma_{10^{-5}}$ are extreme hull girder bending stress for a probability of exceedance probability of 10^{-8} and 10^{-5} respectively.

If no direct analysis of the ship behavior at sea is performed, a first approximation of the shape parameter ξ for ocean-going steel vessels, may be taken from IACS (1999) as:

$$\xi = 1.1 - 0.35\frac{L-100}{300} \quad \textit{where L is ship length in m} \tag{18.6}$$

18.3 Fatigue Stresses

18.3.1 General

As a preparation for Chapter 19, this Section presents three approaches for the estimation of long-term fatigue stresses that will be used respectively by the subsequent chapters. They are:

- Long-term fatigue stress based on Weibull distribution
- Long-term fatigue stress based on deterministic approach
- Long-term fatigue stress based on stochastic approach

18.3.2 Long Term Fatigue Stress Based on Weibull Distribution

The Weibull probability density function for long-term fatigue stress, S, may be described as:

$$f(S) = \frac{\xi}{A}\left(\frac{S}{A}\right)^{\xi-1} exp\left[-\left(\frac{S}{A}\right)^{\xi}\right] \qquad (18.7)$$

where A is a scale parameter, and ξ is the shape parameter which is a function of the type of structure and its location, see Table 18.1 for typical values for the shape parameter ξ.

Table 18.3 Typical Weibull Shape Parameter Values for Simplified Fatigue Assessment

	Typical Values for shape parameter ξ
Fast cargo ships	$\xi>1$, maybe as high as 1.3 or a little more
Slower ships in equatorial waters	$\xi<1$, and perhaps as low as 0.7
Gulf of Mexico fixed platforms	$\xi\cong0.7$
North Sea fixed platforms	$\xi>1$, maybe as high as 1.4 if the platform is slender and dynamically active

The Weibull shape parameter is generally dependent on the load categories contributing to the occurrence of cyclic stress.

The Webull distribution function is then:

$$F(S) = \int_0^S f(S)dS = 1 - exp\left[-\left(\frac{S}{A}\right)^{\xi}\right] \qquad (18.8)$$

The stress exceedance probability may then be expressed as:

$$p = 1 - \int_0^S f(S)dS = exp\left[-\left(\frac{S}{A}\right)^{\xi}\right] \qquad (18.9)$$

If S_0 is the expected extreme stress occurring once in a lifetime of N_0 wave encounters (or stress reversals), Eq.(18.9) becomes

$$p(S_0) = exp\left[-\left(\frac{S_0}{A}\right)^{\xi}\right] = \frac{1}{N_0} \tag{18.10}$$

From the above equation, we may get (Almar-Naess, 1985):

$$A = S_0(\ln N_0)^{-\frac{1}{\xi}} \tag{18.11}$$

The special case of $\xi=1$ is the well-known exponential distribution in which the log (n) plot of stress exceedance is a straight line. Substituting Eq.(18.10) into Eq.(18.7), we may obtain:

$$p = exp\left[-(\ln N_0)\left(\frac{S}{S_0}\right)^{\xi}\right] = \frac{1}{N} \tag{18.12}$$

From Eq.(18.11), it may be obtained that

$$S = S_0\left[\frac{\log N}{\log N_0}\right]^{1/\xi} \tag{18.13}$$

18.3.3 Long Term Stress Distribution Based on Deterministic Approach

This method is based on the deterministic calculation of wave force and it involves the following steps (Almar-Naess, 1985):

1. Selection of major wave directions

   4 to 8 major wave directions are selected for analysis. The selection of major wave directions shall consider the directions that cause high stresses to key structural members. All of the waves are distributed between these major directions.

2. Establishment of long-term distributions of waves

   For each wave direction selected, a long-term distribution of wave height is established by a set of regular waves, which adequately describes the directional long-term wave distributions. The range of wave heights, that give the highest contribution to the fatigue damage, should be given special attention. The most probable period may be taken as the wave period.

3. Prediction of stress ranges

   For each wave identified (direction, height, period), the stress range is predicted using a deterministic method for hydrodynamic loads and structural response.

4. Selection of stress distribution

   The long-term stress exceedance diagram from a wave exceedance diagram is as illustrated in Figure 18.1, where $\Delta\sigma_i$ and H_i denote the stress range and wave height.

A simplified fatigue analysis has been coded in API 2A-WSD(2001) assuming a relation between the stress range S and wave height H obtained based on the deterministic approach described in the above:

$$\Delta\sigma = CH^g \tag{18.14}$$

where C is a calibrated constant and g is a calibrated exponent. The long-term wave height distribution is represented by the sum of two Weibull distribution: one for normal condition H_0, the other for hurricane condition H_1: :

$$\Delta\sigma = CH_0{}^g \text{ for normal condition} \tag{18.15}$$

$$\Delta\sigma = CH_1{}^g \text{ for hurricane condition} \tag{18.16}$$

Based on the methodology described in Chapter 19, the cumulative fatigue damage may be easily derived for normal condition and hurricane condition respectively. The formulae for the cumulative fatigue damage based on the deterministic method may be found form the commentary on fatigue in API RP 2A – WSD.
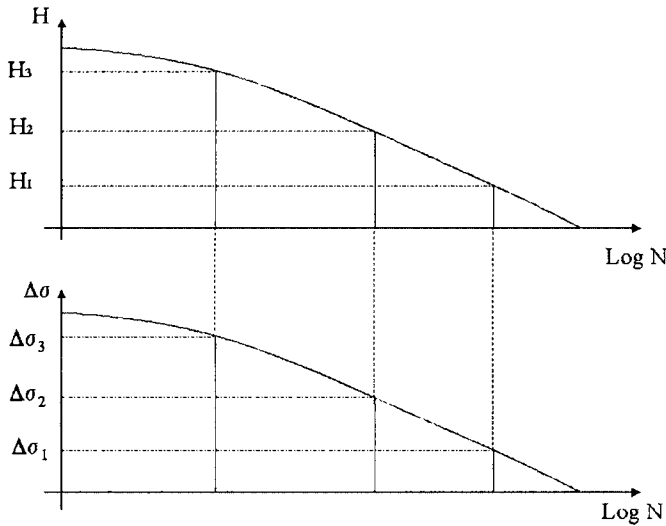
Figure 18.1   Stress Distribution Illustration

18.3.4 Long Term Stress Distribution – Spectral Approach

A spectral approach requires a more comprehensive description of the environmental data and loads, and a more detailed knowledge of these phenomena. Using the spectral approach, the dynamic effects and irregularity of the waves may be more properly accounted for.

This approach involves the following steps:

- Selection of major wave directions. The same considerations as discussed for the deterministic approach apply,

- For each wave direction, select a number of sea states and the associated duration, which adequately describe the long-term distribution of the wave,

- For each sea state, calculate the short-term distribution of stress ranges using a spectral method,

Combine the results for all sea states in order to derive the long-term distribution of stress range. In the following, a formulation is used to further illustrate the spectral approach (DNV, 1998).

A wave scatter diagram may be used to describe the wave climate for fatigue damaged assessment. The wave scatter diagram is represented by the distribution of H_s and T_z. The environmental wave spectrum $S_\eta(\omega)$ for the different sea states can be defined, e.g. applying the Pierson-Moskowitz wave spectrum (see Chapter 2).

When the relationship between unit wave height and stresses, "the transfer function $H_\sigma(\omega|\theta)$", is established, the stress spectrum $S_\sigma(\omega)$ may be obtained as:

$$S_\sigma(\omega) = |H_\sigma(\omega)|^2 \cdot S_\eta(\omega) \tag{18.17}$$

The nth spectral moment of the stress response may be described as:

$$m_n = \int_0^\infty \omega^n \cdot S_\sigma(\omega) d\omega \tag{18.18}$$

A spreading function may be used to include wave spreading,

$$f(\theta) = k \cos^n(\theta) \tag{18.19}$$

where k is selected such that $\sum_{\theta-90^0}^{\theta+90^0} f(\theta) = 1$. Normally n=2. The spectral moment may then be expressed as:

$$m_{ni} = \int_0^\infty \sum_{\theta-90}^{\theta+90} f_S(\theta) \omega^n \cdot S_\sigma(\omega) d\omega \tag{18.20}$$

where m_0 is the 0th spectral moment. The average stress cycle period is thus

$$T_{02i} = \frac{1}{v_{0i}} = 2\pi \sqrt{\frac{m_{0i}}{m_{2i}}} \tag{18.21}$$

and the number of cycles within the sea state of period T_i is

$$n_i = \frac{T_i}{T_{02i}} \tag{18.22}$$

Nonlinear effects due to large amplitude motions and large waves can be neglected in the fatigue assessment since the stress ranges at lower load levels contribute relatively more to the cumulative fatigue damage. In cases where linearization is required, it is recommended that the linearization is performed at a load level representative of the stress ranges that contribute the most to fatigue damage, i.e. stresses at probability levels of exceedance between 10^{-2} to 10^{-4}. The stress range response may be assumed to be Rayleigh distributed within each sea state as

$$F_i(S) = 1 - exp\left(-\frac{S^2}{8m_{0i}}\right) \tag{18.23}$$

The long-term distribution of the stress range may be estimated by a weighted sum over all sea states as

$$F(S) = \sum_{i=1}^{AllSeasates} r_i p_i F_i(S) \tag{18.24}$$

where p_i is the probability of occurrence of the ith sea state and the weighted coefficient is

$$r_i = \frac{v_{0i}}{\sum v_{0i} p_i} \tag{18.25}$$

The obtained long-term distribution of the stress range may be described using a probability function, e.g. Weibull distribution function in which the Weibull parameters are determined through curve fitting.

18.4 Fatigue Loading Defined Using Scatter Diagrams

18.4.1 General

A "short-term" description of the sea (or sea state) means the significant wave height and the mean wave period are assumed to be constant during the time period considered. To construct a "long-term" description of the sea, we need scatter diagrams. The scatter diagrams are used for spectral fatigue analysis and time-domain fatigue analysis, where waves and currents are defined using wave scatter diagram and current scatter diagrams respectively. The environmental criteria are defined as combinations of directional sea, swell, winds and currents as well as their combinations that the structure will be subject to through its life cycle.

Unless the mean stress is very large (e.g. for TLP tethers), the effect of mean stress is ignored. Hence, steady current is normally not given attention except its effect on nonlinear dynamic response. The current scatter diagram is mainly used for the prediction of vortex-induced vibrations.

The joint frequency of significant wave height H_s and spectral wave period T_z are defined using the wave scatter diagram. Each cell of the diagram represents a particular combination of H_s, T_z and its probability of occurrence. The fatigue analysis involves a random sea analysis for each sea state in the scatter diagram and then summing the calculated fatigue damages based on the probability of occurrence for the corresponding sea-state. From motion analysis, the stress amplitude operator (RAO) is obtained for a particular reference sea state.

Long-term directionality effects are also accounted for using wave scatter diagrams in which the probability of each direction is defined. For each set of the significant wave height H_s and spectral wave period T_z, the total probability for all directions should then be equal to 1.0.

18.4.2 Mooring and Riser Induced Damping in Fatigue Seastates

Viscous damping due to drag on mooring lines and risers may significantly affect the motion of deepwater floating structures. Traditionally, the motion response of moored floating structures has been evaluated by modeling the mooring lines and risers as massless springs. In this un-coupled approach, the inertia, damping and stiffness of the mooring lines and risers have not been properly included in the prediction of the vessel motions.

The dynamic interaction between the floating structure, mooring lines and risers should be evaluated using a coupled analysis that provides a consistent modeling of the drag-induced damping from mooring lines and risers. The coupled analysis may be based on a frequency domain approach (Garret, et al , 2002) or a time-domain approach. In the coupled approaches, the mooring lines and risers are included in the model together with the floating structure.

In return, the vessel motions impact fatigue of TLP tethers, mooring lines and risers. For fatigue analysis of the tethers, mooring lines and risers, it is necessary to calculate vessel motions such as:

- Linear wave-induced motions and loads

- Second-order non-linear motions

The motion-induced fatigue is a key factor for selecting riser departure angle that's riser dynamic response.

18.5 Fatigue Load Combinations

18.5.1 General

One of the fields that need research effort is perhaps load combinations for fatigue design. Earlier research in this field has been summarized by Wen (1990) and Chakrabarti (1991). In the determination of extreme loads for ultimate strength analysis, the aim is to select the maximum anticipated load effect when the structure is subject to one of the design load sets. However, for fatigue design, it is necessary to estimate the governing design load set and the shape of the long-term stress range distribution at any structural location.

18.5.2 Fatigue Load Combinations for Ship Structures

One of the fields that need research effort is perhaps load combination. For ship structural design, Munse et al (1983) identified the following cyclic fatigue load sources:

- Low frequency wave-induced loads: $10^7 - 10^8$ reversals during ship's life

- High frequency wave-induced loads: 10^6 reversals during ship's life

- Still water loading: 300 - 500 cycles

- Thermal loads: 7000 cycles

The amplitude of the fatigue loads is influenced by the wave statistics, change in the sourse, speed and deadweight condition. Mansour and Thayamballi (1993) suggested to consider the following loads and their combinations:

- Fatigue loads resulting from hull girder bending

- Fatigue loads resulting from local pressure oscillations

- Cargo loading and unloading (low cycle effects)

- Still water bending (mean level) effects

Of the loads listed in the above, the hull girder bending and local pressure fluctuation give far more contribution to total fatigue damage. Depending on the location, one of these two loads

will typically dominate. For instance, the vertical bending moment related stress fluctuation at ship deck is predominant, while the stress range on the side shell near waterline is nearly entirely due to local (internal/external) pressure. Structural details in the ship bottom is under a combination of bending and local pressure effects.

Pressure variations near the waterline are the main cause of fatigue damages on side shell (Friis-Hansen and Winterstein, 1995).

For spectral fatigue analysis of ships for unrestricted service, the nominal North Atlantic wave environment is usually used. For a site-specific assessment (of FPSO) or for a trade route known to be more severe than the North Atlantic, the more stringent wave scatter diagram should be applied. When motion and loads are highly frequency dependent, it is necessary to include wave-period variation.

The fatigue loading conditions for ships is fully laden and ballast. According to classification Rules (e.g. BV, 1998), for each relevant loading condition, two basic sea states should be considered: head sea conditions and oblique sea condition. The total cumulative damage may be estimated as:

$$D = \alpha \ D_0 + \beta \ D_0^{'}$$
(18.26)

where the coefficients α and β are given in Table 18.1. D_0 *and* $D_0^{'}$ are cumulative damage due to full laden load conditions and ballast load conditions respectively.

$$D_0 = (D_1 + D_2)$$
(18.27)

$$D_0^{'} = (D_1^{'} + D_2^{'})$$
(18.28)

where .

$$D_i = \max(D_{i1}, D_{i2}), \ i = 1,2 \ \text{for full laden load condition}$$
(18.29)

$$D_i^{'} = \max(D_{i1}^{'}, D_{i2}^{'}), \ i = 1,2 \ \text{for ballast load condition}$$
(18.30)

where D_{11}, D_{12} or $D_{11}^{'}, D_{12}^{'}$ are cumulative damage for static sea pressure associated to maximum and minimum inertia cargo or blast loads, respectively. D_{21}, D_{22} or $D_{21}^{'}, D_{22}^{'}$ are cumulative damage for maximum (ship on crest of wave) and minimum (ship on tough of wave) wave-induced sea pressure associated to static internal cargo or ballast loads, respectively.

18.5.3 Fatigue Load Combinations for Offshore Structures

In defining the environmental conditions for offshore structural design, it is necessary to derive combinations of directional sea, swell, wind and current that the offshore structure will encounter during its life. The fatigue of hull structures, mooring lines and risers will largely dependent on the sea and swell conditions, while the current may cause vortex-induced vibrations of risers, mooring lines and TLP tethers. It is therefore required to define a directional scatter diagrams for sea states, swells and sometimes for currents. Swells will only be considered properly (typically by adding a separate swell spectrum into the analysis and so obtaining a multi peaked sea plus swell spectrum) if it is of particular importance as, for instance, offshore west Africa and Australia (Baltrop, 1998). An alternative approach to properly account for swells is to use two separated scatter diagrams for directional sea and swell respectively. In this case, the probability of individual bins (sea-states, cells) should be properly defined, and each bin (cell) is represented by a single peak spectrum defined by

significant wave height H_s and spectral wave period T_z. Swell may in some instance come from a single direction without much variation of the direction. However, in general, the directionality should be explicitly considered in defining the scatter diagrams. The selection of sea states for combined sea, swell, current and wind is a complex subject, and requires certain engineering judgement based on the understanding of the environmental data and structural dynamic response.

Another critical issue to be taken into account is load cases and the loading conditions. To estimate fatigue damage during operating conditions, the vessel motions and RAO data should be generated for the normal operating condition. Similar statement may be valid for estimation of fatigue damage during transportation and installation phases. The total accumulated damage is then obtained by adding the damage for each phase of the design fatigue life and the period/probability of the respective phase. For fatigue analysis of TLP tethers, mooring lines and risers, it is necessary to define the vessel motions and the RAO at the point where the tethers, mooring lines and risers are attached to the vessel.

Francois et al (2000) compared fatigue analysis results from classification societies nd full-scale field data.

An example analysis was conducted by Nordstrom et al (2002) to demonstrate the heading methodology and assess its efficiency for project use for an FPSO. Their proposed heading and fatigue analysis procedure may lead to more effective fatigue design for FPSOs in non-collinear environment.

18.6 Examples

Example 18.1: Long-term Stress Range Distribution – Deterministic Approach

Problem:

Determine the long-term stress range distribution of the spanned riser clamped to a jacket platform, as shown in Figure 18.2 below. This example is chosen to illustrate the deterministic approach in sub-section 18.3.3 (Almar-Næss, 1985). It may be assumed that the riser span length is l=10m, outer diameter OD=0.27m, wall thickness WT=0.0015m, moment of inertia I=$9.8*10^{-5} m^4$ and water depth is 100m. All waves are assumed to approach from the same direction.

Solution:

The first natural period of the span, f_N, can be calculated from:

$$f_N = \frac{1}{2\pi} \cdot a_N \cdot \sqrt{\frac{EI}{m \cdot l^4}} = 0.17s$$

where,

EI	= Bending stiffness
l	= Span length
m	= Mass per unit length
a_N	= Numerical constant, for a beam fixed at both ends, a_N =22 for the first mode.
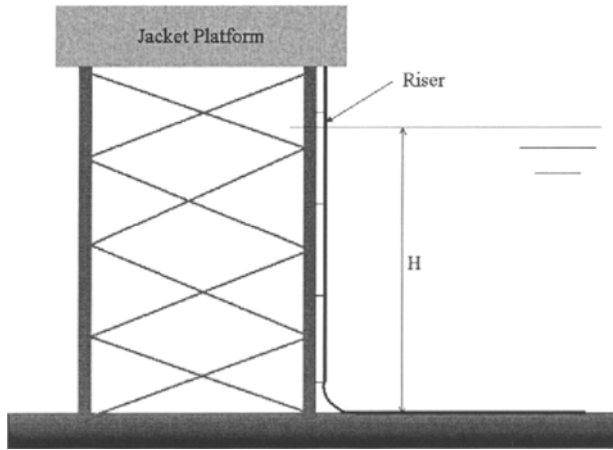
Figure 18.2   Spanned Riser Attached to Platform

The wave force intensity is denoted as F(x). The moment at the span center is given by:

$$M = \int_{-25}^{-15} [x - (-20)] \cdot F(x) \cdot dx$$

The long-term distribution of individual wave heights is given by:

$$P_L(H) = 1 - exp\left[1 - \left(\frac{H}{C * H_C}\right)^D\right]$$

where, H_c =2.7, C=0.462, D=0.928.

The number of waves exceeding a wave height H per year is given by

$$N = N_0 [1 - P_L(H)]$$

where N_0 is the total number of wave in one year, N_0=106.72. The wave force is calculated based on Morison's equation,

$$F = \frac{1}{2}\rho C_D D \cdot v^2 + \rho C_M \frac{\pi D^2}{4} a$$

where C_D =1.0, C_M =2.0

Considering the wave: H=11.0m, T=11.7sec, the angular frequency is:

$$\omega = \frac{2\pi}{T} = 0.537 s^{-1}$$

Applying linear wave theory, the wave number k is given by:

$$\frac{\omega^2}{g} = k \cdot tanh(kd)$$

where d is the water depth. Numerically solve this equation, it gives k=0.0296 m^{-1}

Setting x=0 at the riser center, the horizontal wave induced water particle velocity is given by:

$$v(x) = \omega \frac{H}{2} \cdot \frac{cosh(k*(x+d))}{sinh(k*d)} * sin(\omega t)$$

and the horizontal wave-induced acceleration is

$$a(x) = \omega^2 \cdot \frac{H}{2} \cdot \frac{cosh(k*(x+d))}{sinh(k*d)} cos(\omega t)$$

When the linear wave theory is used, one can simplify the calculations by separating drag and inertia forces:

$$M(\omega t) = M_D(\omega t) + M_I(\omega t)$$

where the moment due to the drag forces and inertia forces are given below.

$$M_D(\omega t) = M_{D,max} * sin^2(\omega t) = 4596 * sin^2(\omega t)(Nm)$$

$$M_I(\omega t) = M_{I,max} * cos(\omega t) = 1306 * cos(\omega t)(Nm)$$

Maximizing M(ωt) gives:

$$cos(\omega t) = \frac{M_{I,max}}{2 * M_{D,max}} = 0.142, \omega t = 81.8^0$$

The maximum moment is then given by:

M_{max}=4689 Nm

And the resulting stress range is,

$$S = 2\sigma_{max} = \frac{MD}{I} = 12.9 MPa$$

The procedure above is repeated for all waves and the analysis results are summarized in Table 18.4 below for the establishment of a stress range exceedance diagram.

Table 18.4   Long-Term Distribution of Wave Height and Stress Range

H (m)	T (sec)	F_{max} (N/m)	S (Mpa)	Log N
0		0	0	6.72
3.0	7.2	28	1.0	5.74
5.0	8.7	66	2.3	5.14
7.0	9.8	140	4.8	4.57
9.0	10.8	250	8.6	4.00
11.0	11.7	384	13.2	3.45
15.0	13.1	738	25.4	2.35
20.0	14.6	1326	46.7	1.00

Note that N is the number of cycles exceeding a given wave height, forces and stress range in one year. A stress range exceedance diagram may be plotted based on the S – Log N relation in the table.

Example 18.2: Long-term Stress Range Distribution – Spectral Approach

Problem:

Determine the long-term stress range distribution of the spanned riser considered in Example 18.1 using spectral approach. This example is chosen to illustrate the spectral approach for the determination of long-term stress range described in Section 18.3.4 (Almar-Næss, 1985).

Solution:

The long-term stress range distribution is obtaining using Eq. (18.21) summing up the short-term distribution for a number of sea states. In the following, the procedure used to derive short-term stress distribution as per Eq.(18.20) is illustrated. The most probable wave period for a given wave height is:

$$T = \frac{2\pi}{\omega} = 0.7 + 4.2H^{0.4}$$

The transfer function may be expressed as

$$H_\sigma(\omega) = \frac{\sigma_{max}(\omega)}{H/2}$$

where $\sigma_{max}(\omega)$ is the maximum stress cased by wave frequency ω.

Consider again the wave height H=11m, T=11.7 sec and ω =0.539. From deterministic analysis, we may find that

$$M_{max}(\omega = 0.539) = 4698Nm, \quad \sigma_{max}(\omega = 0.539) = 6.9MPa$$

The transfer function may then be calculated using the above value of $\sigma_{max}(\omega)$ and H. This calculation is repeated for a set of wave periods between 3 and 25 to derive the relationship between $H_\sigma(\omega)$ and ω.

When the relationship between unit wave height and stresses, "the transfer function $H_\sigma(\omega|\theta)$", is established, the stress spectrum may be given as:

$$S_\sigma(\omega) = |H_\sigma(\omega)|^2 \cdot S_\eta(\omega)$$

The nth spectral moment of the stress response may be described for the ith sea state as:

$$m_{0i} = \int_0^\infty S_\sigma(\omega)d\omega = 115.6MPa^2$$

$$m_{2i} = \int_0^\infty \omega^2 S_\sigma(\omega)d\omega = 35.74(MPa/\sec)^2$$

The average stress cycle period is thus

$$T_{02i} = 2\pi\sqrt{\frac{m_{0i}}{m_{2i}}} = 11.3\sec$$

and the number of cycles within the sea state of period T_i is

$$n_i = \frac{T_i}{T_{02i}} = \frac{3 \times 3600}{11.3} = 956$$

The stress range response may be assumed to be Rayleigh distributed within each sea state as

$$F_i(S) = 1 - exp\left(-\frac{S^2}{8m_{0i}}\right)$$

18.7 Concluding Remarks

In this Chapter, fatigue loads for ship and offshore structures have been discussed for simplified fatigue assessment and spectral fatigue assessment.

For ship structures, key fatigue loads are the global wave loads local pressure and internal loads. These fatigue loads are applied to a structural response model. The fatigue loads may be applied using simplified fatigue assessment and spectral fatigue assessment, see Section 18.3 and Section 18.4. Areas that required future research include (Chen and Shin, 1995):

- Calculation of the loads accounting for nonlinearities

- Development of a theoretical method to combine high frequency and low frequency response (e.g. ordinary wave-induced loads plus slam-induced whipping).

- Development of hull-stress monitoring system that may link ship's service experience with anticipated fatigue failure

- Quantification of uncertainty in load predictions including load combinations.

For offshore structures, key issues are the definition of scatter diagrams for random sea, swell, wind and current loads for specific site offshore, and the estimation of vessel motions and RAO based on the structural model, environmental conditions and loads. Areas that required more research include:

- Collection of reliable environmental data for specific sites

- Fatigue load combinations for random sea, swell, wind and currents

- Evaluation of vessel motion, RAO and low-frequency motions

18.8 References

1. Almar-Næss, A. (ed.) (1985), *"Fatigue Handbook - Offshore Steel Structures"*, Tapir Press, Norway.

2. API RP2A – WSD (2001), *"Frecommended Practice for Planning, Designing and Constructing Fixed Offshore Platforms – Working Stress Design"*, American Petrileum Institute.

3. Baltrop, N. (1998) (editor), *"Floating Structures: A Guide for Design and Analysis"* Oilfield Publications, Inc., Vol. 1.

4. BV, (1998), *"Fatigue Strength of Welded Ship Structures*□, Bureau Veritas, July 1998

5.   Chakrabarti, S.K. (1987), *"Hydrodynamics of Offshore Structures"*, Computational Mechanics Publications.

6.   Chakrabarti, S.K. (1991), *"Strategies for Nonlinear Analysis of marine Structures"*, Report No. SSC-347, Ship Structure Committee.

7.   Chen, Y.N. and Shin, Y.S, (1995), "Consideration of Loads for Fatigue Assessment of Ship Structures", Proc. Symposium and Workshop on the Prevention of Fracture in Ship Structures, Washington, DC.

8.   DNV (1998), *"Fatigue Assessment of Ship Structures"*, Det Norske Veritas, Classification Notes No.30.7.

9.   Faltinsen, O.M. (1990), *"Sea Loads on Ships and Offshore Structures"*, Cambridge Ocean Technology Series, Cambridge University Press.

10.   Francois, M., Mo, O., Fricke, W., Mitchell, K. and Healy, B. (2000), *"FPSO Integrity: Comparative Study of Fatigue Analysis Methods"*, OTC 12148.

11.   Friis-Hansen, P. and Winterstein, S.R. (1995), *"Fatigue Damage in the Side Shell of Ships"*, Journal of Marine Structures, Vol.8(6), pp. 631-655.

12.   Garrett, D.L., Gordon, R.B. and Chappell, J.F. (2002), *"Mooring and Riser Induced Damping in Fatigue Seastate"*, OMAE2002-28550.

13.   Hogben, N. (1985), *"Global Wave Statistics"*, British Maritime Technology.

14.   IACS (1999), *"Fatigue Assessment of Ship Structures"*, International Association of Classification Societies, Recommendation 56.1.

15.   Mansour, A. and Thayamballi, A. (1993), *"Probability-Based Ship Design Loads and Load Combinations"*, Report No. SSC-373, Ship Structure Committee.

16.   Munse, W.H., Wibur, T.W., Telalian, M.L., Nicol, K., and Wilson, K. (1983), *"Fatigue Characetrization of Fabricated Ship Details for Design"*, Report No. SSC-318, Ship Structure Committee.

17.   Nordstrom, C.D., Lacey, P.B., Grant, R. and Hee, D.D. (2002), *"Impact of FPSO Heading on Fatigue Design in Non-Collinear Environments"*, OMAE2002-28133.

18.   Wen, Y.K. (1990), *"Structural Load Modeling and Combination for Performance and Safety Evaluation"*, Elsevier.

Part III

Fatigue and Fracture

Chapter 19   Simplified Fatigue Assessment

19.1 Introduction

Fatigue assessment of structural connections (tubular joints, plated connections, pipe welds etc.) is one of the most critical issues in the design of marine structures such as ships, fixed platforms, floating structures, pipelines, risers and mooring lines. The results of fatigue assessment will influence costs and safety from several aspects:

- Quality of the connection material

- Quality of welding fabrication (such as welding, heat treatment, etc.)

- Frequency of inspection and repairs

- Consequence of potential fatigue failure and

- Residual strength of partially damaged structural system

There are four key methodologies for the estimation of accumulated fatigue damages:

1. Deterministic Fatigue Analysis

2. Simplified Fatigue Assessment - assuming that the stress range follows a Weibull distribution (discussed in this Chapter)

3. Spectral Fatigue Analysis (Chapter 20)

4. Time-Domain Fatigue Analysis (Chapter 20)

5. Fracture Mechanics-based Assessment of Fatigue Damages (Chapter 21)

The first four methodologies estimate fatigue damages using the S-N curve, while the last methodology is based on fracture mechanics (FM) approach.

Fatigue criteria in classifications rules (such as ABS (2002) Steel Vessel Rules) use a simplified fatigue assessment based on empirical values for the Weibull shape parameters. The simplified fatigue assessment is also supported by API RP 2A (2001) for some cases.

This Chapter describes a simplified procedure for fatigue assessment based on a two parameter Weibull distribution. The Weibull shape parameter depends on the wave climate and the character of the structural response, especially the possible influence of structural dynamics. The fatigue evaluation result is very sensitive to the Weibull shape parameter. The advantage of the simplified fatigue assessment is that closed form expression for fatigue damage may be derived, and that the Webull shape parameter may be calibrated based on historical data of fatigue cracks.

19.2 Deterministic Fatigue Analysis

In the deterministic fatigue analysis of marine structures, "blocks" of periodic single waves of specified wave height H_i and period T_i are used, where $i = 1,2,3,...I$. Considering the fatigue damage for a reference time period T_R, the analysis procedures are illustrated in Figure 19.1 and as below:

- Calculate the number of occurrence for the i-th wave block: $n_i = T_R \cdot P_i / T_i$ where P_i is the probability (relative frequency) of the wave height H_i.

- Calculate the stress range $s_i(H_i)$ based on static analysis of the structural response to wave height H_i and period T_i. The stress concentration factor SCF (which is denoted as K in Figure 19.1) is obtained using parametric equations or experimental/numerical analysis. The dynamic amplification factor D represents the ratio of the dynamic stress range to the quasi-static stress range.

- Calculate the number of cycles to failure N_i for the stress range $D \cdot SCF \cdot s_i(H_i)$ based on the design S-N curve.

- Calculate the fatigue damage for each wave block: n_i / N_i.

- Calculate the cumulative fatigue damage based on Miner's law.

$$D_{fat} = \sum_{i=1}^{I} \frac{n_i}{N_i} \tag{19.1}$$
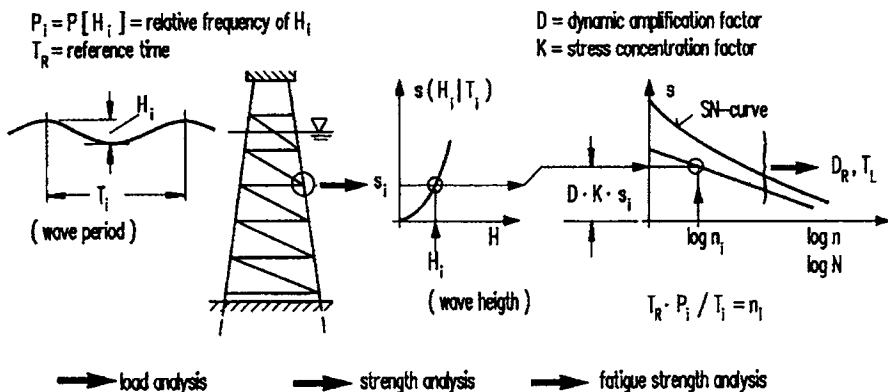
Figure 19.1   Deterministic Fatigue Analysis (Clauss et al, 1994)

19.3 Simplified Fatigue Assessment

19.3.1 Calculation of Accumulated Damage

It is assumed that the linear cumulative Palmgren-Miner Law is applicable, and may be written as:

$$D_{fat} = \int_0^\infty \frac{N_0 f(S)}{N(S)} dS \tag{19.2}$$

where,

N_0 = Total number of cycles in the long-term period considered

$f(S)$ = probability density function for the stress range (which means that the number of cycles for the stress range S is $N_0 f(S) dS$)

As discussed in Chapter 16, S-N curves may be expressed as $N = KS^{-m}$. Substituting this equation into Eq.(19.2), we may get:

$$D_{fat} = \frac{N_0}{K} \int_0^\infty S^m f(S) dS \tag{19.3}$$

For marine structures, the probability density function of stress range may be represented by a two-parameter Weibull distribution.

$$f(S) = \frac{\xi}{A} \left(\frac{S}{A}\right)^{\xi-1} exp\left(-\frac{S}{A}\right)^\xi \tag{19.4}$$

where A and ξ denote a scale parameter and a shape parameter respectively. Combining Eq.(19.3) and Eq.(19.4), we may get:

$$D_{fat} = \frac{N_0}{K} \int_0^\infty S^m \frac{\xi}{A} \left(\frac{S}{A}\right)^{\xi-1} exp\left(-\frac{S}{A}\right)^\xi dS \tag{19.5}$$

Introducing

$$x = \left(\frac{S}{A}\right)^\xi \tag{19.6}$$

we may get

$$D_{fat} = \frac{N_0}{K} A^m \int_0^\infty x^{1+m/\xi} exp(-x) dx \tag{19.7}$$

The Gamma function is defined as:

$$\Gamma(k) = \int_0^\infty e^{-x} x^{k-1} dx \tag{19.8}$$

Combining Eq.(19.7) and Eq.(19.8), the long-term cumulative damage may be written as:

$$D_{fat} = \frac{N_0}{K} A^m \Gamma\left(1 + \frac{m}{\xi}\right) \tag{19.9}$$

In Part III Chapter 18, it has been derived that:

$$A = \left[\frac{S_0^\xi}{\ln N_0}\right]^{1/\xi} \tag{19.10}$$

Hence, it is obtained that the long-term cumulative damage may be written as (Almar-Naess, 1985):

$$D_{fat} = \frac{N_0}{K}\left[\frac{S_0^\xi}{\ln N_0}\right]^{m/\xi} \Gamma\left(1 + \frac{m}{\xi}\right) \tag{19.11}$$

where,

> N_0 = Total number of cycles in the long-term period (e.g. service life) considered
>
> S_0 = Expected maximum stress range in N_0 cycles,
>
> $P(S > S_0) = \dfrac{1}{N_0}$ (fatigue stress range S exceeds S_0 once every N_0 cycles)
>
> ξ = Shape parameter of the Weibull distribution for the stress cycles
>
> K, m   = Material parameters of the S-N curve

19.3.2 Weibull Stress Distribution Parameters

When the shape parameter, ξ, equals to 1, the Weibull distribution yield to the Exponential distribution. The value of ξ can be larger or smaller than 1. The higher the ξ values, the more severe cyclic loading conditions are. The shape parameter is a function of the cyclic loading environment in which the system exists, and how the system responds to this environment (e.g. local loading effects, dynamic loading effects). A suitable value for the shape parameter should be chosen based on fatigue analysis of similar structures in the same site. In order to evaluate the accuracy of the selected shape parameters, the predicted fatigue damage corresponding to given shape parameters shall be compared with the measured data or more refined analysis (e.g. spectral fatigue analysis). Typical values for the Weibull shape parameter ξ are given in Table 18.1 for some commercial ships and offshore structures.

The spectral fatigue analysis and extensive fatigue damage data may be used to calibrate the Weibull parameters for various types of ship and offshore structures. Luyties and Stoebner (1998) presented a procedure to calibrate the API simplified fatigue design method using spectral fatigue analysis.

19.4 Simplified Fatigue Assessment for Bilinear S-N Curves

When the S-N curves are expressed as bilinear curves (see Part III Chapter 17), the fatigue damage may be predicted using

$$D_{fat} = \frac{N_0}{K}\left[\frac{S_0^\xi}{\ln N_0}\right]^{m/\xi}\Gamma\left(1+\frac{m}{\xi},\ z\right) + \frac{N_0}{C}\left[\frac{S_0^\xi}{\ln N_0}\right]^{r/\xi}\Gamma_0\left(1+\frac{r}{\xi},\ z\right) \quad (19.12)$$

where the incomplete Gamma functions are defined as:

$$\Gamma(k,z) = \int_z^\infty e^{-x}x^{k-1}dx \quad (19.13)$$

$$\Gamma_0(k,z) = \int_0^z e^{-x}x^{k-1}dx \quad (19.14)$$

and

$$z = \left(\frac{S_1}{S_0}\right)^\xi \quad (19.15)$$

where S_1 is the stress range at the crossing of two S-N curves (e.g. corresponding to fatigue life of 10^7).

The formulation for simplified fatigue assessment based on bi-linear S-N curves was derived by Wirsching and Chen (1987), and appeared in DNV Classification Note 30.7 for ship structures and DNV (2000) for steel offshore structures.

Tables of Gamma function and incomplete Gamma function are given in BV (1998) fr convenience of fatigue damage estimation.

19.5 Allowable Stress Range

A fatigue check format based on the simplified fatigue assessment is:

$$S_0 \le S_{o\ allowable} \quad (19.16)$$

where the design stress range S_0 is the local stress range related to a given probability of occurrence during the design life. The allowable extreme stress range $S_{0\ allowable}$ is determined by solving Eq.(19.12) using the appropriate S-N curve, allowable cumulative damage ratio and knowledge about stress distribution.

For prompt fatigue assessment, usually allowable extreme stress ranges have been pre-calculated and listed in fatigue guidance documents as functions of the types of S-N curves, Weibull shape parameter and the environment.

Reference is made to Zhao et al (2001) for formulations for the strength and fatigue assessment of converted FPSOs.

19.6 Design Criteria for Connections Around Cutout Openings

19.6.1 General

Cracks around cutout openings (also known as slots) are often seen in many types of ship structures, see Figure 19.2. Past studies (Bea, et al., 1995) have concluded that single-hull tankers experienced most of these cracking in the side shell and bottom shell areas due to

cyclic wave pressure. In double-hull tankers, however, the double bottom seems to be the main problem area due to a very high differential pressure between laden and ballast conditions. A large number of cracks have been observed in inner bottom structures of several double-hull tankers (Cheung & Slaughter, 1998). Many cracks occur along the flat-bar weld, between frame vertical stiffeners and inner bottom longitudinals.

Similarly, many survey reports show that cracks also occur in way of connection of longitudinals with transverse floors inside double bottom and hopper of bulk carriers (IACS, 1994).

The flat bar appears to be the weakest link in the connections. Some survey reports list up to hundreds of flat bar failures in a single vessel (Ma, 1998, Bea, et al., 1995). This subject was investigated by Glasfeld et al (1977) which concluded that approximately 75% of the total number of cracks found around slots are at flat bars.

Cracking around end connection typically follows a sequence. The first crack normally appears along the footprint of flat bar on the flange of longitudinal (type B crack in Figure 19.2). Extensive corrosion, commonly observed at these cracks, indicates that crack growth rate is slow. As the flat bar cracks grow slowly with time, stresses redistribute to the web frame through collar plates. Once the flat bar has cracked through, it loses its load-carrying capability completely and the additional load transfers to the remaining one or two collar connections. If this defect is not found and rectified, a second crack will start at the radius of cutout (type D in Figure 19.2) and a third crack eventually occurs at the fillet weld on shell plate (type C or C1 in Figure 19.2). This crack sequence has been confirmed by many survey reports and field observations. These show that a cutout radius crack is only found when flat bar has completely cracked through.

19.6.2 Stress Criteria for Collar Plate Design

In Ma et al (2000), simple criteria have been developed for ship designers to perform a quick check of their designs of end connections. The criteria require two checks be performed for each design of end connection. First, the calculated mean normal stress in flat bar, σ_{fb}, should be less than an allowable value (see Eq. (19.17)). Second, the calculated mean shear stress at collar plate, τ_{dc}, should also be less than its allowable value (see Eq. (19.18)).

$$\sigma_{fb} = \frac{ps(l - 0.7s)}{A_1 + 0.33c_s\left(A_2 + A_3\right)} < 140 \ N/mm^2 \tag{19.17}$$

$$\tau_{dc} = \frac{ps(l - 0.7s)}{\dfrac{3.0}{c_s}A_1 + \left(A_2 + A_3\right)} < 70 \ N/mm^2 \tag{19.18}$$

Here p, s and l represent static design pressure, panel width and panel length (see Figure 19.3), respectively. A_1, A_2 and A_3 are flat bar footprint area, direct connection area, and collar connection area (see Figure 19.4), respectively. Units are in millimeters, Newtons or their combinations.

A: Longitudinal Cracked
B: Flat Bar Cracked
C: Shell Plate to Web/Floor Weld Cracked
C1: Type C Crack Extending into Shell Plate
D: Web Frame (Cutout) Cracked
E: Bracket Cracked
F: Lug Cracked
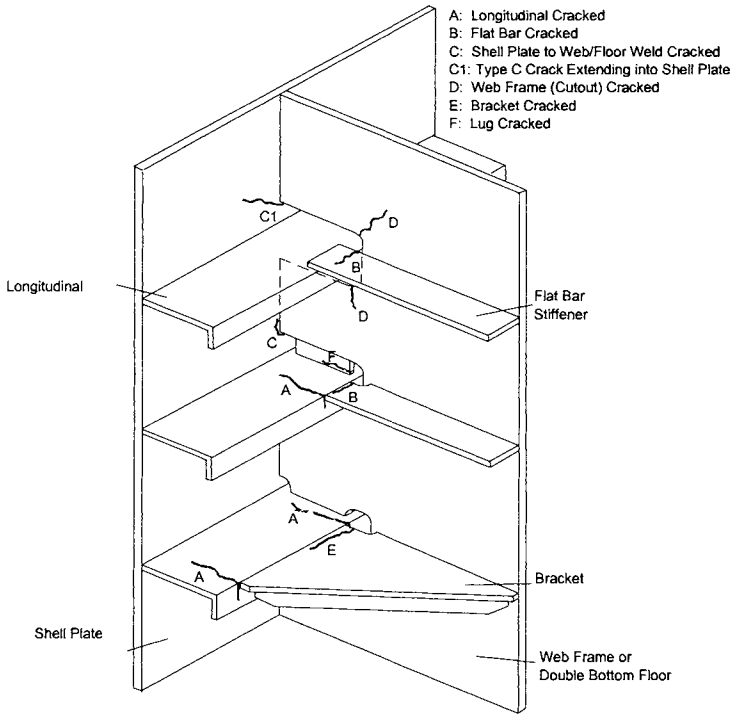
Figure 19.2   Different Types of Cracks around Cutout Openings

The coefficient, c_s, can be easily determined as following:

c_s = 1.0 for symmetrical longitudinal stiffeners;

c_s = 1.41 for unsymmetrical longitudinal stiffeners with one-sided support.

c_s = 1.12 for unsymmetrical longitudinal stiffeners with two-sided supports.
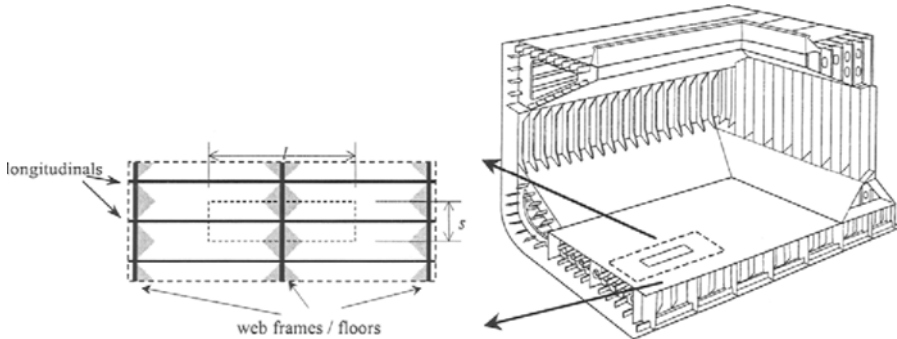
**Figure 19.3   Pressure on Shaded Area Goes into Web Frame/floor
Different (Ma et al 2000)**
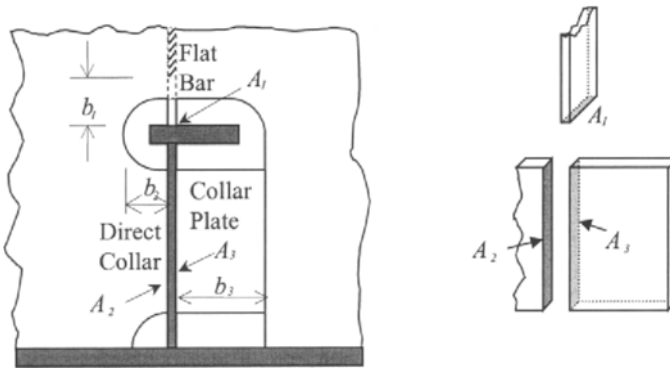
Figure 19.4   Definitions of Geometry Parameters (Ma et al 2000)

19.7 Examples

Example 19.1: Fatigue Design of a Semi-submersible

Problem:

Calculate the maximum allowable stress range for a semi-submersible with a long-term stress range distribution as:

$$S = S_0 \left[1 - \frac{\log N}{\log N_0} \right]^{1/\xi}$$

and the Weibull distribution parameter $\xi=1.1$. Total number of stress cycles $N_0 =108$, allowable damage ratio $\eta=0.20$, class F weld (m=3, K=10E11.8).

Solution:

The maximum allowable stress range can be derived as:

$$S_{0allowable} = \left(\frac{\eta K}{N_0} \right)^{1/m} \cdot \frac{(ln\,N_0)^{1/\xi}}{\sqrt[m]{\Gamma\left(1+\frac{m}{\xi}\right)}} = 93.6 MPa$$

If the maximum allowable stress range is scaled by a factor of $\eta^{1/3}$. For instance, for $\eta=0.1$, the maximum allowable stress range becomes:

$$S_{0allowable} = 93.6 \cdot (0.1/0.2)^{1/3} = 74.2 MPa$$

19.8 References

1. ABS (2000), "Guide for Building and Classing Floating Production Installations", American Bureau of Shipping.

2. ABS (2002), "Rule for Building and Classing Steel Vessels", American Bureau of Shipping.

3. Almar-Naess, A. (1985), *"Fatigue Handbook, Offshore Steel Structures"*, Tapir, Norway.

4. API (2001), "Recommendations for Planning, Designing and Constructing Fixed Offshore Platforms", API Recommended Practice 2A (RP 2A), 21st Edition, American Petroleum Institute.

5. Bea, R. G., Cramer, E., Schulte-Strauthaus, R., Mayoss, R., Gallion, K., Ma, K.T., Holzman, R. and Demsetz, L. (1995), "Ship's Maintenance Project", Conducted at University of California, Berkeley for U.S. Coast Guard/Ship Structure Committee (SSC), SSC-386.

6. BV (1998), "*Fatigue Strength of Welded Ship Structures* ", Bureau Veritas.

7. Cheung, M.C. & Slaughter, S.B. (1998), "Inner Bottom Design Problems in Double-Hull Tankers", Marine Technology, April.

8. Clauss, G., Lehmann, E. and Ostergaard, C. (1994), *"Offshore Structures, Vol. II - Strength and Safety for Structural Design"*, Springer-Verlag.

9. DNV (2000), "RP-C203, Fatigue Strength Analysis of Offshore Steel Structures", Det Norske Veritas.

10. Glasfeld, R., Jordan, D., Kerr, M., and Zoller, D. (1977), "Review of Ship Structural Details", Ship Structure Committee Report SSC-226.

11. IACS (1994): "Bulk Carriers – Guidelines for Surveys, Assessment and Repair of Hull Structure", International Association of Classification Societies.

12. Luyties, W.H. and Stoebner, A.M. (1998), "The Use of API Simplified Fatigue Design Methodology for Gulf of Mexico Structures", OTC 8823.

13. Ma, K.T. (1998), "Tanker Inspection and a Risk-Based Approach", Proceedings of ISOPE98, International Offshore and Polar Engineering Conference, Montreal.

14. Ma, K.T., Srinivasan, S., Zhang, H., Healy, B. and Peng, H. (2000), "Developing Design Criteria for Connections around Cutout (Slot) Openings", SNAME Transactions, pp. 227-248.

15. Munse, W.H., Wibur, T.W., Telalian, M.L., Nicol, K., and Wilson, K. (1983), "Fatigue Characetrization of Fabricated Ship Details for Design", Ship Structure Committee Report SSC-318.

16. Yoneya, T., Kumano, A., Yamamoto, N. and Shigemi, T. (1993), "Hull Cracking of Very Large Ship Structures", Integrity of Offshore Structures - 5.

17. Zhao, CT, Bai, Y and Shin Y. (2001), "Extreme Response and Fatigue Damages for FPSO Structural Analysis", Proc. of ISOPE'2001.

18. Wirsching, P.H. and Chen Y.N. (1987), "Fatigue Design Criteria for TLP Tendons", J. Structural Engineering, ASCE, Vol. 113 (7).

This Page Intentionally Left Blank

Part III

Fatigue and Fracture

Chapter 20   Spectral Fatigue Analysis and Design

20.1   Introduction

20.1.1   General

Recent offshore field development based on Tension Leg Platforms (TLP), semi-submersibles, SPARs, FPSOs and other types of floating structures has clearly demonstrated that operators are confident in deepwater technology and will continue the development of fields in ever increasing water depths. Therefore, cost-effective floating structures will continue to be developed for deepwater field development.

In the simplified fatigue assessment, the fatigue damage is estimated assuming that the stress follows a Weibull distribution for long-term response. The simplified fatigue assessment has been successfully applied to the ship fatigue design in which allowable stresses are pre-calculated for different locations in a ship. Due to the excessive sensitivity of the estimated fatigue damage to the Weibull parameters, a spectral fatigue assessment becomes more popular for offshore structural analysis (Chen and Mavrakis, 1988).

Fatigue analysis and design include several steps of analysis:

- Fatigue screening
- Detailed structural analysis
- Reanalysis of welding improvements
- Reanalysis of design improvements
- Reanalysis of design and welding improvements

This chapter describes a fatigue analysis of floating structures, such as:

- Spectral fatigue analysis, including computer modeling, load conditions, structural analysis and validation, loading combinations, and fatigue damage assessment
- Time-domain fatigue analysis
- Fatigue design of local structural details

The spectral fatigue analysis may also be applied to ship structures provided that the wave scatter diagram is adequately defined because the ships are designed for un-restricted services.

The frequently used codes and standards for fatigue analysis of the floating structures are API RP 2T (1997), API 2FPS (2001), AWS (1997) and UK DEn (1990) and guidance from classification societies.

20.1.2 Terminology

Some terms, applied in fatigue analysis, have specific meanings as defined below:

Mean Zero-Crossing Period: The mean zero-crossing period is the average time between successive crossings with a positive slope (up crossings) of the zero axis in a time history.

Random Waves: represent the irregular-surface elevations and associated water particle kinematics of the marine environment. Random waves can be represented analytically by a summation of sinusoidal waves of different heights.

Regular Waves: are un-directional waves having cyclic water particle kinematics and surface elevation.

Sea state: is an oceanographic wave condition, which can be characterized for a specified time period as a stationary random process.

Significant Wave Height: is the average height of the highest 1/3 of all the individual waves presented in a seastate.

Transfer Function: is defined to be the ratio of a structural response quantity to the wave-height as a frequency function.

S-N curves: empirically represent relationships between stress range and number of cycles to failure.

Nominal Stress: is the stress determined from member section properties and the resultant forces and moments at the members end. The section properties must account for the existence of thickened or flared stub ends.

Hot Spot Stress: is the stress located at the weld toe of a structural detail.

20.2 Spectral Fatigue Analysis

20.2.1 Fatigue Damage Acceptance Criteria

The fatigue damage assessment is based on Miner's rule:

$$D_{fat} = \sum \frac{n_i}{N_i} \le \eta \tag{20.1}$$

where D_{fat} is the accumulated life time fatigue damage, η is the allowable damage ratio and N_i is the number of cycles to failure at stress S_i as defined by the S-N curve of the form:

$$N = K \cdot S^{-m} \tag{20.2}$$

20.2.2 Fatigue Damage Calculated Using Frequency Domain Solution

Fatigue Damage for the *i*-th Sea-State

For narrow banded response, the accumulated damage of a sea-state may be expressed in the continuous form:

$$D_{fat} = \int_0^\infty \frac{n(S)}{N(S)} dS \tag{20.3}$$

where $n(S)dS$ represents the number of stress ranges between S and S+dS. If a stationary response process of duration T_{life} is assumed, the total number of stress cycles will be:

$$n(S)dS = v_{0i}T_{life}p(S)dS \tag{20.4}$$

where the zero-up crossing frequency v_{0i} is

$$v_{0i} = \frac{1}{2\pi}\sqrt{\frac{m_{2i}}{m_{0i}}} \tag{20.5}$$

where,

m_{0i} = Spectral zero moment of the hotspot stress spectrum

$m_{2i,}$ = Spectral second moment of the hotspot stress spectrum

The Rayleigh probability density function for stress range S is:

$$p(S) = \frac{S}{4\sigma_i^2}exp\left(-\frac{S^2}{8\sigma_i^2}\right) \tag{20.6}$$

where the root mean square stress σ_i is

$$\sigma_i = \sqrt{m_{0i}} \tag{20.7}$$

Then, one can obtain:

$$D_{fat} = v_{0i}T_{life}\int_0^\infty \frac{p(S)}{N(S)}ds = \frac{v_{0i}T_{life}}{K}\int \frac{S^{m+1}}{4\sigma_i^2}exp\left(-\frac{S^2}{8\sigma_i^2}\right)ds \tag{20.8}$$

Using the following notation,

$$x = \frac{S^2}{8\sigma_i^2} \tag{20.9}$$

and Gamma function:

$$\Gamma\left(1+\frac{m}{2}\right) = \int_0^\infty e^{-x}x^{\frac{m}{2}}dx \tag{20.10}$$

We may get:

$$D_{fat} = \frac{v_{0i}T_{life}}{K} \cdot (8m_{0i})^{\frac{m}{2}} \cdot \Gamma\left(1+\frac{m}{2}\right) \tag{20.11}$$

Fatigue Damage for All Sea-States

From the damage equation for one sea-state, one may easily calculate the damage accumulated for all sea-states.

$$D_{fat} = \sum_{i}^{all\,sea-states} p_i \frac{\upsilon_{0i} T_{life}}{K} \cdot (8m_{0i})^{\frac{m}{2}} \cdot \Gamma\left(1+\frac{m}{2}\right) \tag{20.12}$$

where, p_i = Probability of occurrence of the ith seastate

Based on Eq. (20.12), the transformation of a stress range spectrum to fatigue damage is straightforward. Applying a spectral fatigue analysis, analytical expressions may be derived as transfer functions from wave spectra to response amplitude spectra and finally to stress range spectrum. Using the root mean square stress σ_i, the accumulated damage equation (Eq.(20.12) may be re-expressed as,

$$D_{fat} = \sum_{i} p_i \frac{\upsilon_{0i} T_{life}}{K} \cdot (2\sqrt{2}\sigma_i)^m \cdot \Gamma\left(1+\frac{m}{2}\right) \tag{20.13}$$

When wave direction is also accounted for in defining the sea states, the probability of each sea state may be expressed as p_{ij} where j denotes the jth direction.

$$D_{fat} = \sum_{i} \sum_{j} p_{ij} \frac{\upsilon_{0ij} T_{life}}{K} \cdot (8m_{0ij})^{\frac{m}{2}} \cdot \Gamma\left(1+\frac{m}{2}\right) \tag{20.14}$$

When the S-N curves are defined using bi-linear curves, the accumulated fatigue damage may be determined as:

$$D_{fat} = \sum_{i}^{all\,sea-states} p_i \frac{\upsilon_{0i} T_{life}}{K} \cdot (8m_{0i})^{\frac{m}{2}} \cdot \Gamma\left(1+\frac{m}{2},\ z\right)$$
$$+ \sum_{i}^{all\,sea-states} p_i \frac{\upsilon_{0i} T_{life}}{C} \cdot (8m_{0i})^{\frac{r}{2}} \cdot \Gamma_0\left(1+\frac{r}{2},\ z\right) \tag{20.15}$$

where the incomplete Gamma functions are defined as:

$$\Gamma(k,z) = \int_{z}^{\infty} e^{-x} x^{k-1} dx \tag{20.16}$$

$$\Gamma_0(k,z) = \int_{0}^{z} e^{-x} x^{k-1} dx \tag{20.17}$$

and

$$z = \left(\frac{S_1}{2\sqrt{2m_{0i}}}\right)^2 \tag{20.18}$$

where S_1 is the stress range at the crossing of two S-N curves (e.g. corresponding to fatigue life of 10^7).

The formulation for spectral fatigue assessment based on bi-linear S-N curves appeared in DNV Classification Note 30.7 for ship structures and DNV (2000) for steel offshore structures.

20.3 Time-Domain Fatigue Assessment

20.3.1 Application

- Similarity between Time-Domain Fatigue Analysis (TFA) and Spectral Fatigue Analysis (SFA): Both procedures are based on wave-scatter diagram.

- Difference between Time-Domain Fatigue Analysis and Spectral Fatigue Analysis: TFA is a deterministic analysis, and includes the effect of non-linearity. SFA is a stochastic approach based on linear analysis.

Time-domain fatigue assessment is mainly applied to the following scenarios:

- Fatigue of pipelines and risers due to wave-induced forces (Bai, 2001)

- Fatigue of TLP tethers (Fylling and Larsen, 1989)

- Fatigue of Spar structures due to low frequency motions (Luo, 2001)

20.3.2 Analysis Methodology for Time-Domain Fatigue of Pipelines

In the following, a fatigue damage equation will be derived for fatigue of pipelines and risers due to wave forces. The number of cycles n_i corresponding to the stress range block S_i is given by

$$n_i = P(\cdot)f_v T_{life} \tag{20.19}$$

$P(\cdot)$ is the probability of a combined wave and current induced flow event. f_v is the dominating vibration frequency of the considered pipe response and T_{life} is the time of exposure to fatigue load effects. Using Miner's law and a S-N curve, Eq.(20.3), the fatigue damage may be evaluated for each sea-state of the scatter diagram in terms of H_s, T_p and θ_w as below.

$$D_{fat} = \frac{T_{life}}{K} \sum_{H_S T_p \theta_w} P(\cdot) \int_0^\infty \max\left[f_v S^m \right] dF_{Uc} \tag{20.20}$$

where:

$P(\cdot)$ is the joint probability of occurrence for the given sea state in terms of significant wave height H_s, wave peak period T_p, mean wave direction.

dF_{U_c} denotes the long term distribution function for the current velocity. The notation "max" denotes that the mode associated with the largest fatigue damage must be applied when several potential modes may exist at a given current velocity.

In the time domain analysis, the long-term irregular wave condition is divided into representative sea-states. For each sea-state, a time history of the wave kinematics is generated from the wave spectrum. Hydrodynamic loads are then predicted using the wave kinematics and applied to the structures. Stress ranges are calculated through structural analysis. Fatigue damage is then calculated using Miner's law.

In Bai (2001), the stress range is calculated in the time domain model for each sea-state with a constant value of wave-induced velocity but for a range of current velocities, from zero to a

maximum value with nearly zero probability of occurrence. The calculated stress ranges are used to evaluate the integral in Eq. (20.20). For each sea-state, the fatigue damage associated with each current velocity is multiplied by the probability of occurrence of the current velocity. When stress ranges for all sea-states are obtained through the wave force model, the fatigue damage is calculated using Eq. (20.20). The advantage of using the time-domain fatigue for pipeline ad riser assessment is to account for the non-linearity in the drag forces and structural dynamic response. The other benefit is to reduce the conservatism introduced in the boundary condition for spectral fatigue analysis. An engineering practice is to derive the ratio of the predicted fatigue life from these two approaches for a few well-selected and performed analyses, and then to apply this ratio to similar fatigue scenarios.

20.3.3 Analysis Methodology for Time-Domain Fatigue of Risers

In time-domain analysis, a time domain dynamic analysis is performed for all sea states in the wave scatter diagram, and for each direction with a non-zero probability of occurrence. In frequency-domain fatigue analysis of risers, the touch-down point is fixed. The time-domain analysis is applied when the soil-pipe interaction needs to be accounted for in order to remove the conservatism introduced in the frequency-domain analysis. Besides, the second order (drift) motions of the vessel may significantly affect the result of fatigue analysis. It is difficult to include the second-order motions using stress RAOs to transfer wave spectra into stress spectra. Based on the stress time histories from the time-domain dynamic analysis, the fatigue damage may be estimated as follows:

- The fatigue damage is estimated based on the moments of spectra (as those used in the frequency-domain analysis), and the stress-spectra are calculated using the Fast Fourier Transform algorithm.

- The fatigue damage is calculated directly from the stress time-history using a rainflow counting techniques.

The dynamic simulation should be long enough because the dominant period of second order motions is of the order of 100 seconds.

20.3.4 Analysis Methodology for Time-Domain Fatigue of Nonlinear Ship Response

Jha and Winterstein (1998) proposed a "Nonlinear Transfer Function (NTF)" method for efficient prediction of the stochastic accumulation of fatigue damage due to nonlinear ship loads in random seas. Nonlinear time-domain ship-load analysis may reveal asymmetry in sag and hog moment at mid-ship. The goal of the NTF method is derive accurate prediction using only a limited amount of nonlinear analysis based on regular waves. The analysis cost is reduced because expensive time-domain analysis over many cycles of ir-regular sea is replaced by a limited number of regular-wave analysis.

The NTF is the generally nonlinear transformation from wave amplitude and period to the load amplitude measure of interest (e.g., total load range for rainflow-counting). Stochastic process theory is applied to

- Identify a minimal set of regular waves (i.e., wave heights and associated periods) to be applied based on a discretized version of the Foristall (1978) wave height distribution and Longuet-Higgins (1983) model for wave period selection.

- Assign an appropriate set of "side-waves" to be spatially distributed along the ship based on probability theory.

- Determine how these results should be weighted in predicting statistics of the loads produced in random seas.

The prediction of the time-domain fatigue analysis was compared with frequency-domain stochastic fatigue analysis that assumes linear model of ship behavior. It was revealed that the nonlinear effect is significant. The NTF method may also be applied to any offshore structures.

20.4 Structural Analysis

20.4.1 Overall Structural Analysis

Overall structural analyses are usually performed using space frame models and fine FEA models. The space frame analyses define the boundary loads for local structural models. To get the stress transfer functions for the fatigue damage assessment, these boundary loads are used to factor the results of fine, FEA unit load analysis results.

This section presents aspects of modeling, load evaluation, and structural analysis applicable to the overall structural analysis.

Space Frame Model

The space frame model includes all the important characteristics of the stiffness, mass, damping, and loading properties of the structure and the foundation for the structural system. It consists primarily of beam elements. The accuracy of the calculated member end forces is influenced by the modeling techniques used.

Figure 20.1 shows a space frame model for TLP hull primary structures and deck primary structures. Although not shown in this figure, tendons are included in the model as supporting structure to provide the proper vertical stiffness. Tubular beam elements are used to model the tendons. Applied load cases are, in general, self-balancing and should result in zero net load at the tops of the tendons. Thus, relatively flexible lateral springs are provided at the tops of all tendons in order to stabilize the analysis model against small net lateral loads.

The hull's column and pontoon structures are modeled using beam-column elements. Joint and member definitions are interfaced from the global analysis model because interfaced loads from this analysis must be consistent with the model. Member properties are determined based on the member cross-sectional properties and material properties. Yield stresses of plate and stiffener components are input, along with the maximum bracket spacing for ring stiffener frames.

Additional joints and members are included to ensure that the tendons and deck structure are structurally stable and as additional load collectors where appropriate. Deck members are modeled using the tubular or AISC (American Institute of Steel Constructions) elements. Deck equipment mass locations are determined for each major deck area and specifically included in the model so that proper inertial load magnitudes and centers of action are generated in the analysis.
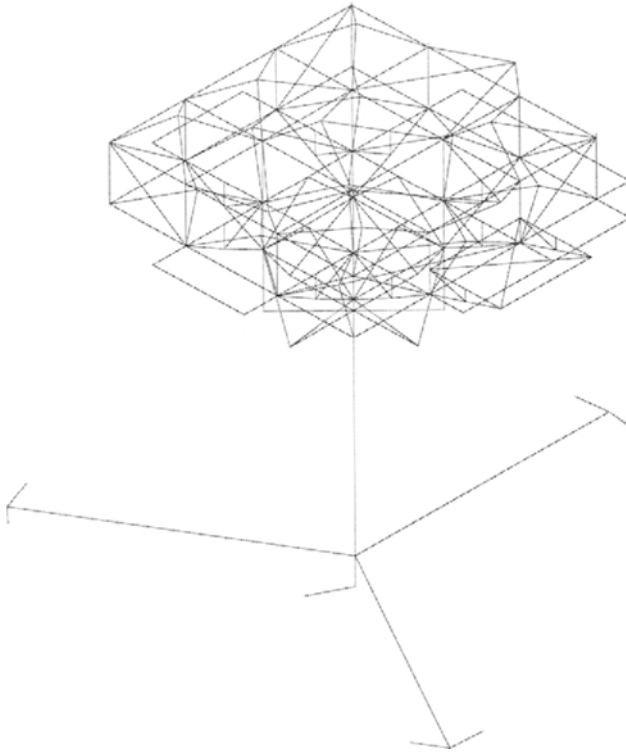
Figure 20.1   Space Frame Model for a TLP

Fine FEA Model

A fine FEA model may be used to analyse the hull structure or a part of the hull structure in detail. All relevant structural components shall be included in the model. In the fine FEA model, major primary structural components are fully modeled using three- and four-node plate/shell elements and solid elements. Some secondary structural components may be modeled as two-node beam elements.

Design Loading Conditions

To adequately cover the fatigue environment, fatigue design loading conditions consist of cyclic environmental load components at a sufficient number of wave frequencies. These loading conditions include:

- Hydrodynamic loads due to waves, including dynamic pressure
- Inertial loads due to motions
- Other cyclic loading

The loading components are either explicitly generated or interfaced from the global motion analysis. Load summaries are made for each design loading condition and checked for accuracy and load imbalance.

The global motion analysis serves as a basis for dynamic load development. The actual interface from the global analysis to the structural analysis consists of several loading components for each analyzed wave period and direction: the real and imaginary applied unit amplitude, wave diffraction and radiation loads, the associated inertial loads and other cyclic loading such as tendon dynamic reactions. The successful interface of these load components is dependent on a consistent geometric and mass model between the motion and the structural analyses and is also dependent on a consistent generation of the loading components in the motion analysis. Consistent modeling is obtained by interfacing the model geometry directly from the motion analysis wherever possible. Consistent mass is obtained by interfacing with the same weight control database for both the motions and structural analyses, when available.

Load combinations are formed for each wave period and direction. These combinations consist of the applied wave load, the generated inertial load, and the associated cyclic loadings such as tendon dynamic reactions for both real and imaginary loadings of the floating structures. These combinations form the total cyclic load condition for each wave period and direction to be used in the spectral fatigue analysis.

Analysis and Validation

Hull structural analyses are performed using linear finite element methods. The reaction forces include total force and moment reactions and the analysis results are verified. Symmetrical or asymmetrical load conditions are checked to confirm symmetrical or asymmetrical analysis results.

20.4.2 Local Structural Analysis

Local structural details are included as a part of the analyses for the entire hull structure.

The analysis of the structural details may be performed using the finite element program such as ABAQUS (HKS, 2002) and other software. The FEM model is three-dimensional and linear stress analysis is performed. The results from the FEA model are interfaced into the fatigue model for additional model validation and subsequent spectral fatigue analysis of the local structural details. The entire model is plotted and revised for accuracy both from the FEA model and after interface to the fatigue model.

Loading conditions for finite element analysis of local structural details should be based on the hull's structural analysis since it includes all cyclic loadings of the structure.

The unit loading conditions are frequently applied. The resulting stresses for each unit load condition are interfaced to the fatigue model for subsequent combination into fatigue design loads.

20.5 Fatigue Analysis and Design

20.5.1 Overall Design

A spectral fatigue assessment should be carried out for each individual structural detail. It should be noted that every structural detail, every welded joint and attachment or any other form of stress concentration is potentially a source of fatigue cracking and should be considered individually.

The UK DEn procedure or its modified versions are recommended in Europe for the fatigue analysis and design of floating structures since it is the most widely accepted code. Design

standards such as AWS (1997) are used in the USA. However, it should be noted that different design standards provide different procedures in the fatigue stress determination and S-N classification, which result in large discrepancies in the predicted fatigue damages. Therefore, a consistent procedure based on one design standard shall be used.

The safety factors for fatigue design of floating structures are given by the design standards listed in Section 20.2 based on:

• Criticality of the joint

• Inspectability and repairability

The criticality of a join is determined based on its structural redundancy. A joint is critical if its failure will potentially lead to the failure of the structure.

20.5.2 Stress Range Analysis

A stress range analysis is performed using the fatigue software as a precursor to the fatigue damage calculation. The FEA unit load, model geometry and element stress results are interfaced into the fatigue calculation model. Loading combinations will then be defined for each fatigue wave load based on the applied boundary loads.

Geometry and element properties from the space frame model are plotted and revised for accuracy. Any detected errors are corrected in the FEA input file and the FE analysis repeated.

The finite element model of the specific hotspot region shall be developed based on the procedures, finite element size requirement defined by the design standards.

In the FEA model, unit load results will be interfaced into the space frame model database. These unit loads are then appropriately combined based on the applied boundary loads.

20.5.3 Spectral Fatigue Parameters

Wave Environment

The wave environment consists of wave scatter diagram data and wave directional probabilities.

The scatter diagram data consists of annual probabilities of occurrence as functions of significant wave heights and peak periods in the structure installation site. For spectral fatigue analysis, a wave spectrum (e.g. Pierson-Moskowitz) is associated with each cell of the scatter diagram.

Directional probabilities for fatigue waves are also included in the fatigue assessment. It is usually unconservative to ignore any non-uniform distribution in directional probabilities. However, in lieu of such information, the wind directional probability may be used to account for the non-uniformity in the wave approaching direction and to provide conservatism in the fatigue damage calculation.

Stress Concentration Factors

The determination of the appropriate SCF in the fatigue analysis is a complex task. It is also dependent on the S-N classification and stress analysis methods. The general rule of thumb is that the stress used in the fatigue analysis should resemble the fatigue stress obtained from the specimen tested when deriving the S-N curves. The fatigue stress does not mean the most accurate stress determined by the high-resolution fine mesh FEA. It is the pertinent stress, in

accordance with the chosen S-N curves. A discussion of the SCF and S-N classification is given in later Sections.

The SCF can be determined based on parametric equations and finite element analysis.

S-N Curves

In the United States, the AWS (1997) S-N curves are used to analyze structural details of floating structures. Where variations of stress are applied to conventional weld details identified in Figure 9.1 of AWS (1997), the associated S-N curves in Figures 9.2 or 9.3, should be used, depending on the degree of criticality. Where such variations of stress are applied to situations identified in AWS (1997) Table 10.3. The associated S-N curves are provided in AWS D1.1, Figure 10.6. For referenced S-N curves in AWS (1997), Figures 9.2, 9.3 and 10.6, are Class Curves. For such curves the nominal stress range in the vicinity of the detail should be used.

In Europe, UK DEn (1990) S-N curves are used for structural details in floating structures. The S-N classification is determined based on the structural configurations, applied loading and welding quality.

As discussed earlier, the UK DEn procedure is recommended in this chapter. Therefore, the S-N classification based on UK DEn curves will be discussed in detail, see Table 20.1.

Table 20.1   Comparison between European Standards and US Standards

Subject	Europe Standards (refers to e.g. UK DEn, 1990)	US Standards (refers to e.g. AWS D1.1, 1997)
S-N Curves	Mean-minus-two-standard deviation curves.	Lower bound
S-N Classifications	Full penetration welds - T curve Partial penetration welds – W curve One of 8 classes: B, C, D, E, F, F2, G and W, depending on geometry, stress direction, and method of fabrication and inspection.	X curve is sufficiently devalued to account for thickness/size effect Smooth weld metal merging with parent metal - X curve, otherwise, X' curve
Fatigue Damage Assessment	Simplified Fatigue - The long-term wave height distribution can be represented by the Weibull distribution Or Spectral Fatigue Analysis	Simplified Fatigue - The long-term wave height distribution may be represented by the sum of two Weibull distributions one for normal and the other for hurricane conditions Or Spectral Fatigue Analysis
Cathodic Protection	Cathodically protected joints in Seawater equivalent to joints in air. Unprotected joints in Seawater require S-N curve to be reduced by a factor of 2 on life.	S-N curves (X' and X) presume effective cathodic protection. Fatigue provisions of AWS D1.1 apply to members and joints in atmospheric service. Does not recommend further reduction of S-N curve for free corrosion.
Welding Improvement	Included	Not covered Use X curve rather than X' curve

Joint Classification

Guidelines on joint classification may be found from the UK DEn (1990). Note that the S-N curves in the UK DEn (1990) was modified by HSE(1995).

The UK DEn (1990) guidelines apply only to welded joints that are free from serious defects or discontinuities. Factors such as undercut at the toe, internal or surface breaking defects or cracks, and geometric irregularities may cause a reduction in fatigue strength and should be evaluated separately.

The UK DEn (1990) guidelines allocate various types of welded joints into one of nine joint classes. To determine the correct classification for a particular weld detail, it is necessary to identify the weld type, the direction of the applied loading, and to consider all potential cracking locations. For most types of joint, the weld toes, weld ends, and weld roots are considered the most important locations.

The joints with the highest classifications are those that are stressed in a direction parallel to the weld. Fillet or butt weld joints fall into Class C or B in the UK DEn (1990) guidelines depending on whether the manufacturing process is manual or automatic. Such joints seldom govern the fatigue strength of a welded details since other joints are likely to fall into lower joint classes.

The classification of transverse butt welds is more complex. They can fall into Class D or E, depending upon the details of the manufacturing process, position, and location, all of which may influence the weld profile. Class C may be justified if the weld overfill is removed by grinding or the weld is shown to be free from significant defects by using non-destructive testing. However, if access is limited and the weld must be made from one side only, a lower fatigue strength should be assumed.

The UK DEn (1990) guidelines downgrade butt welds, made onto a permanent backing strip, to Class F. The guidelines also warn against the use of tack welds within small distances of the plates edge, in which case, the classification is lowered to Class G.

Tack welds are a controversial topic. A number of studies have been conducted for different methods of attaching the backing to the plates prior to making the butt weld. Tacking the backing strip to the root preparation, and incorporating this into the final weld, gives small improvement in fatigue strength over joints in which the backing strip is fillet welded to one of the plates. However, the increase is not sufficient to warrant a higher joint classification. In both cases, failure may initiate at the root of the butt weld.

Currently butt welds made onto temporary backing such as glass or ceramic backing strips are not classified and require further research. The availability of electrodes designed specifically for root runs has resulted in an improvement in the quality of single-sided welds made without backing. In recognition of this welding quality improvement, such joints can be considered as Class F2 if full penetration is achieved. This classification should be used with caution, because fatigue strength in some areas may be much lower due to lack of penetration at the root.

The fatigue strength is seldom governed by butt welded joints, because these joints in general posses a superior strength over fillet welded joints. Fillet welds fall into Class F, F2, or G depending on their size, orientation, and location in relation to a free plate edge. However, recent studies have shown that fillet welds posses a fatigue strength lower than that predicted by Class G, if the weld is continued over the corner of the plate.

In addition to the weld toe, which is the most usual site for fatigue cracking to occur, all load carrying fillet welds and partial penetration butt welds must be evaluated to assess possible weld throat failure. To avoid this type of failure, it is necessary to ensure that these joints are adequately dimensioned. This may be achieved using the Class W design S-N curve. One should note that the maximum shear stress range is associated with the class W design S-N curve.

Structural Details

The UK DEn fatigue design and assessment guidelines provide sketches, which provide assistance in the S-N classification of structural details. According to UK DEn (1990) guidelines, joints are subdivided into the following types:

- Metal free from welding
- Continuous welds essentially parallel to the direction of applied stress
- Transverse butt welds
- Weld attachments on the surface of a stressed member
- Load-carrying fillet and T butt welds
- Details in welded girders

The UK DEn Curves were developed based on small test specimens. In the S-N classification of structural details, the users first carefully relate the fatigue stress in tests with the stress of structural details under consideration. For example, the fatigue stress in the test for the weld shown in Figure 20.2a, would be the tensile stress, S, on the cross-section, but for the weld shown in Figure 20.2b, it would be $SCF \cdot S$, where SCF is the stress concentration factor caused by the hole. This is due to the fact that at point x, the stress near the weld is $SCF \cdot S$. However, for a small cutout in Figure 20.4c, the stress concentration due to the small hole shall not be included since micro-structural effects have been included in the S-N curves.
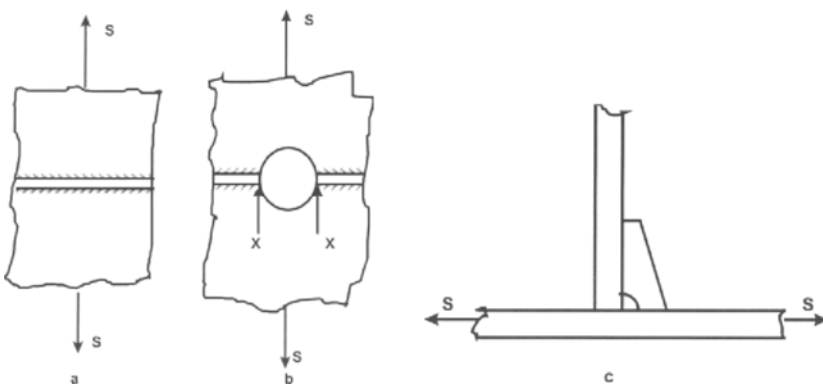
Figure 20.2   Explanation of Fatigue Stress When Weld is Situated in Region of Stress Concentration Resulting from Structure's Gross Shape

Theoretically, structural details should be classified and considered for each loading step throughout the fatigue analysis since different loading steps result in different applied loading

directions. This approach is generally prohibitively complex. Therefore, simplified S-N classification is used based on the rule of thumb in engineering applications.

When classifying the weld's structural details in large, complex structural systems from a series of design drawings, it is important to:

- Consider each weld individually
- Consider each direction of applied stress
- Evaluate all possible cracking locations, because each may yield a different classification
- Consider any possible stress concentration effects

Figures 20.3 and 20.4 show two typical examples of details found in a floating structure. In the section shown in Figure 20.3, the classifications range from C to F2 and W, depending upon the direction of the applied stress. In these examples, stresses in the three principal directions S_x, S_y and S_z, are not equal. Thus the design stress range for each class will differ. However, for simple design purposes, the maximum principal stress and F2 classification are assigned for the overall structural details.

It is particularly difficult to classify the details that have a hole and to identify potential crack locations. Holes in a continuous longitudinal weld are covered in the UK DEn fatigue design guidelines as Class F, without requirement for an additional stress concentration factor. However, a web should be incorporated to this detail. The end of a web butt weld at the hole is a more severe detail that should be ground. For the ground detail, Class E or D is recommended. Due to the presence of the hole, a stress concentration factor of 2.2 or 2.4 should be included. If the end of the butt weld is not ground, a Class F or F2 curve, together with the geometrical stress concentration factor (2.2-2.4), is recommended.
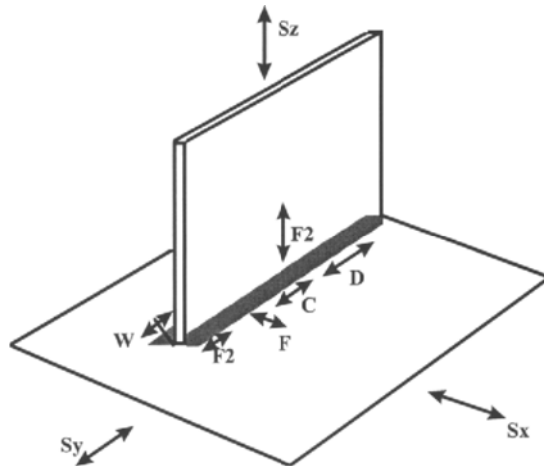
Figure 20.3   S-N Classification of Structural Details Subjected to Triaxial Loading
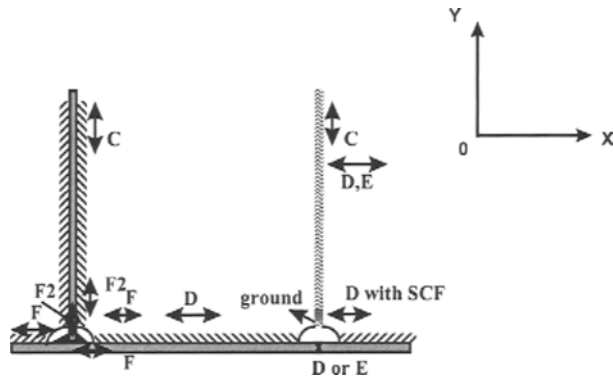
Figure 20.4   S-N Classification of Structural Details

If concerns remain about the use of a cope hole, it is possible to improve its fatigue strength by cutting back and grinding the weld end as shown in Figure 20.3. In such cases, the weld between the flange and web should be full penetration over the regions on either side of the cope hole in order to avoid failure through the weld throat (W class).

Figure 20.4 illustrates the third example of S-N classification of structural details. It's the small bracket between the pontoon and the base node in a TLP structure. Based on the UK DEn (1990) Guidelines and published fatigue test data, the hotspot areas can be classified as F or F2.

S-N classification of the structural details in floating structures is a challenging task. During the design process, there are many structural details, which cannot be classified based on the UK DEn (1990) guidelines. In this case, other design standards such as AWS (1997) or published fatigue test data may be used to justify the classification.

20.5.4 Fatigue Damage Assessment

The fatigue life of structural details is calculated based on the S-N curve approach assuming linear cumulative damage (Palmgren-Miner rule). A spectral fatigue analysis is used where the long term stress range distribution is defined through a short term Rayleigh distribution within each short-term period for different wave directions. A one-slope or bi-linear S-N curve may be assumed.

Fatigue lives are determined by the service life and safety factors. Additional margin is desirable due to the uncertainties associated with fatigue assessment procedures.

Initial Hotspot Screening

The objective of the initial screening is to identify the fatigue critical areas based on the experience and the in-service data. Fatigue damage is calculated for each element in the group assuming a conservative S-N curve and upper-bound SCF for each element. The calculated damages are reviewed and all elements with fatigue lives less than the minimum required, are analyzed in further detail in the specific hotspot analysis.

Specific Hotspot Analysis

Elements that do not pass the initial hotspot screening need to be reanalyzed using SCFs and the associated S-N curves that are more appropriate for the actual structural detail and welding procedure to be used. The calculated damages are reviewed and, at least, all elements with fatigue lives less than the minimum required are summarized for further review and potential redesign and/or modification of welding procedures, and reanalysis.

Specific Hotspot Design

Structural details that do not pass the specific hotspot analysis are redesigned to improve their fatigue strength. SCFs and associated S-N curves that are appropriate for the redesigned structural details and welding procedures will be used in the fatigue reanalysis. All structural details must meet the minimum fatigue requirements after their re-design and welding procedures are finalized.

Detail Improvement

It is clear that the best time to improve the fatigue strength of welded structural details is during the design stage. There are two factors, which need to be specially considered when improving the fatigue strength of a structural detail:

- Nominal stress level

The most efficient approach to improving fatigue strength is to increase the local scantling and to configure the additional load path within the structure. This approach may reduce the nominal stress level and hence the hotspot stress for a given structural detail.

- Geometrical stress concentration

Adopting a good design of detail configuration by providing softer connections reduces the geometrical stress concentration factor originally caused by the geometric discontinuity. It is the most effective technique to improve fatigue strength. However, this technique usually requires good workmanship since a soft toe/heel is used.

20.5.5 Fatigue Analysis and Design Checklist

Each item in the following checklist should be checked prior to the completion of fatigue analysis:

- Computer model topology - the model is plotted in sufficient views to validate model connectivity.

- Loading conditions - each applied loading condition is checked for accuracy.

- Analysis and validation - Analysis results are checked step-by-step; discrepancies between expected and obtained analysis results should be documented and explained.

- Loading combinations - each applied loading combination should be summarized and checked for accuracy.

- Environmental conditions - wave scatter diagram and directional probability input should be checked.

- SCFs - SCFs used in the analysis should be confirmed for validity and applicability.

- S-N curves - S-N curves used in the analysis should be confirmed for validity and applicability.

20.5.6 Drawing Verification

Design drawings corresponding to this design task should be verified according to design results, for correctness and acceptability. Non-conforming drawings are to be revised and/or documented depending on their acceptability in the task technical report.

20.6 Classification Society Interface

20.6.1 Submittal and Approval of Design Brief

The design brief is submitted to the classification society for review, comments, and approval. The classification society's comments are to be incorporated into the design brief and the revised design brief will be reissued. If necessary, the analysis should be repeated to verify and validate the analysis results and design brief revisions.

20.6.2 Submittal and Approval of Task Report

A technical task report is issued after the analysis is completed to document the analysis and design results. This report should follow the analysis methodology documented in the design brief and discuss any variations from the design brief. The task report includes supporting information, hand calculations and computer output.

This task report and supplemental calculations are submitted to the classification society for review, comment, and approval and will be available to the post-design personnel for reference during fabrication.

20.6.3 Incorporation of Comments from Classification Society

Comments on the design brief and the task report should be incorporated into the applicable revised document. The revised document is issued for record and final approval, if required.

20.7 References

1.   ABS (2002), "Rule for Building and Classing Steel Vessels", American Bureau of Shipping.

2.   API (1997), "Recommended Practice for Planning, Designing, and Constructing Tension Leg Platforms", API Recommended Practice 2T (RP 2T), First Edition, American Petroleum Institute.

3.   API (2001), "API RP 2FPS, Recommended Practice for Planning, Designing and Constructing Floating Production Systems", First Edition.

4.   AWS (1997), "AWS Structural Welding Code - Steel, AWS D1.1-96", American Welding Society.

5.   Bai, Y. (2001), *"Pipelines and Risers"*, Elsevier Ocean Engineering Book Series, Vol. 3.

6.   BSI (1993), "BSI 7608-Code for Practice for Fatigue Design and Assessment of Steel Structures", British Institute of Standards.

7.   DNV (2000), "RP-C203, Fatigue Strength Analysis of Offshore Steel Structures", Det Norske Veritas.

8.   Forristall, G.Z. (1978), "On the Statistical Distribution of Wave Heights in A Storm", J. of Geophysical Research, 83(C5), pp.2353-2358.

9.   Fylling, I.J. And Larsen, C.M. (1989), "TLP Tendon Analysis", in an ASCE book entitled *"Tension Leg Platforms – A State of the Art Review"* Edited by Demirbilek, Z.

10. HKS (2002), "ABAQUS/Standard User's Manual, Version 5.6", Hibbitt, Karlsson & Sorensen, Inc.

11. HSE (1995), "Offshore Installation, Guidance on Design, Construction and Certification", UK Health and Safety Executives, 4th Edition, Section 21.

12. Jha, A.K. and Winterstein, S.R. (1998), "Stochastic Fatigue Damages Accumulated Due to Nonlinear Ship Loads", Proceedings of OMAE, Lisbon.

13. Longuest-Higgins, M.S. (1983), "On the Joint Distribution of Wave Periods and Amplitude in a Random Wave Field", Proc. of Royal Society of London, pp. 241-258.

14. Luo, Y.H., Lu, R., Wang, J. and Berg, S. (2001), "Time-Domain Analysis for Critical Connections of Truss Spar", Proceedings of ISOPE, Stavanger.

15. MCS, "Flexcom 3D User's Manual", Marine Computational Services.

16. UK DEn (1990), "Offshore Installations: Guidance on Design, Construction, and Certification", 3rd Edition, UK Department of Energy (Now UK Health and Safety Executives).

Part III

Fatigue and Fracture

Chapter 21   Application of Fracture Mechanics

21.1 Introduction

21.1.1 General

Applications of the fracture mechanics in marine structural design include:

- Assessment of final fracture,

- Determination of crack propagation to plan in-service inspection and determine remaining life of an existing structure,

- Fatigue assessment in case S-N based fatigue assessment is inappropriate,

- Calibration of fatigue design S-N Curves

In this Chapter, three levels of fracture assessment are outlined, Paris equation is applied to predict crack propagation and the comparison is made between S-N curve based fatigue assessment and fracture mechanics-based fatigue assessment.

21.1.2 Fracture Mechanics Design Check

The Fracture Mechanics Design Check of Ultimate Limit-State can be applied in three alternative ways. These are evaluation of:

- Maximum allowable stress

- Minimum required fracture toughness

- Maximum tolerable defect size

Maximum Allowable Stress

The fracture mechanics strength criteria can be applied to the derivation of the maximum allowable stress at a given cross section. This value is obtained when the material fracture toughness and the defect size are specified. If the actual local stress exceeds the maximum allowable stress derived through this procedure, a different local design should be undertaken in order to reduce the local stress level and fulfill the fracture mechanics criteria.

Minimum Required Fracture Toughness

The minimum required fracture toughness should be derived through the fracture mechanics design check when the design geometry is established and a defect tolerance parameter is specified. The derived fracture toughness then allows designers to select a suitable material for any particular structure of concern.

Maximum Tolerable Defect Size

A maximum tolerable defect size can be derived when the geometry and the fracture toughness of the selected material are known. For statically loaded structures, the maximum tolerable defect size must satisfy the fracture mechanics criteria. For dynamically loaded structures, the maximum tolerable defect size represents the critical crack size in a fatigue failure event. It may be used to minimise the risk of unstable fracture throughout the operating life of the structure. The result also gives direct input to the calculation of fatigue crack growth period.

There are three levels of procedure that are applied in fracture assessment (Reemsnyder, 1997):

Level 1.   Utilisation of the Crack-Tip Opening Displacement (CTOD) Design Curve (explained in Section 21.2)

Level 2.   The Normal Assessment or Design Safety Format that makes use of the Failure
 to   Assessment Diagram (described in Section 21.3). No practical safety factors need be applied here.

Level 3.   Utilisation of the Failure Assessment Diagram based on detailed information of stress-strain curves of materials. Partial safety factors are applied to the defect size, stress level, etc., see Section 21.4.

More information may be found from API 579 (2001), Andersen (1991) and BSI (1999).

21.2 Level 1: The CTOD Design Curve

21.2.1 The Empirical Equations

The CTOD Design Curve may be used to evaluate the resistance against fracture of a wide range of structures such as pipelines, pressure vessels, ship and offshore structures, buildings and bridges. One of the most commonly used CTOD Design Curves is the one developed by the British Welding Institute (TWI) that relates the CTOD at some critical event, the yield strength σ_Y, nominal strain at a notch ε, and flaw size a (Burdekin and Dawes, 1971; Dawes, 1974). This Design Curve was initially included in the first edition of the BSI fitness for purpose guidance (BSI PD 6493, 1980). The BSI (1980) CTOD design curve may be expressed as:

$$\Phi = \left(\frac{\varepsilon}{\varepsilon_Y}\right)^2 \quad for \quad \frac{\varepsilon}{\varepsilon_Y} \leq 0.5 \tag{21.1}$$

and

$$\Phi = \left(\frac{\varepsilon}{\varepsilon_Y}\right) - 0.25 \quad for \quad \frac{\varepsilon}{\varepsilon_Y} \rangle 0.5 \tag{21.2}$$

where the non-dimensionalised CTOD is Φ,

$$\Phi = \frac{CTOD}{2\pi\varepsilon_Y a} \tag{21.3}$$

with the yield strain ε_Y

$$\varepsilon_Y = \frac{\sigma_Y}{E} \tag{21.4}$$

where a is the length of a through-crack in an infinite plate equivalent in severity to that of the crack in the element under investigation, and E is Young's Modulus.

21.2.2 The British Welding Institute (CTOD Design Curve)

The BSI (1980) CTOD Design Curve shown in Figure 21.1 was constructed relative to the wide-plate test results with a safety factor of 2 on flaw size a.

There are three alternative applications for the CTOD Design Curve:

* **Maximum Allowable Strain**: Solving Eqs (21.1) and (21.2) for $\varepsilon / \varepsilon_Y$, we may define the maximum allowable strain for the given values of material fracture toughness CTOD and crack size a.

* **Minimum Required Fracture Toughness**: A material with an adequate toughness CTOD can be selected for the critical region, given the maximum possible flaw size a and strain level of $\varepsilon / \varepsilon_Y$.

* **Maximum Allowable Flaw Size**: This design curve may be used in the following manner: Given $\varepsilon / \varepsilon_Y$ in a critical region from a stress analysis of the structure, Φ is determined from the diagram. From this value of Φ, the maximum allowable flaw size, a, in the critical region may be established given the toughness CTOD of the material.

The TWI CTOD Design Curve was also adopted by the American Petroleum Institute in its API 1104 (1983) as a basis for its fitness-for-purpose criteria.
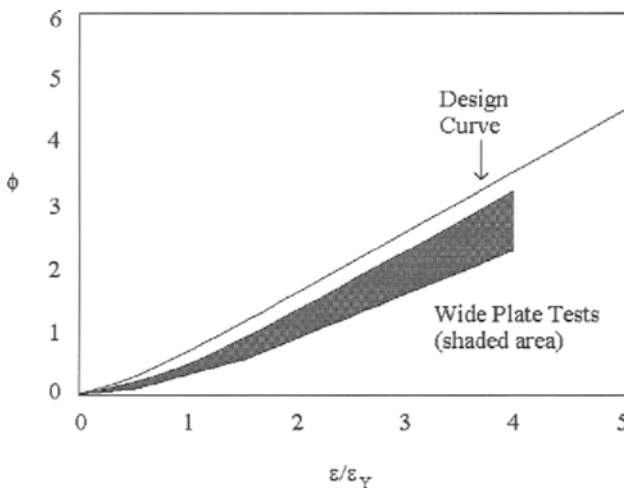
Figure 21.1   The British Welding Institute CTOD Design Curve

21.3 Level 2: The CEGB R6 Diagram

This Level 2 Assessment provides a simplified method of checking whether particular flaws present in the structure may lead to fracture failure, or whether the flaws can be considered safe without having to go through more complex assessment procedures. The approach adopted in this preliminary assessment uses a variable safety factor on flaw size averaging about 2. No additional partial safety factors should be used in Level 2 Assessment.

Two normalised parameters are specified and given as follows:

$$K_R = \frac{K}{K_{MAT}} \tag{21.5}$$

and

$$S_R = \frac{\sigma_N}{\sigma_{FLOW}} \tag{21.6}$$

where K_R is the fracture ratio,

K = Stress-intensity factor (a function of net section stress σ_N, crack size a, and geometry) at fracture of the component.,

K_{MAT} = Linear elastic fracture toughness of the component,

S_R = Collapse ratio,

σ_N = Net section stress in the component at fracture, and

σ_{FLOW} = Flow stress that is defined as the average of yield stress and tensile stress in BS 7910 (1997).
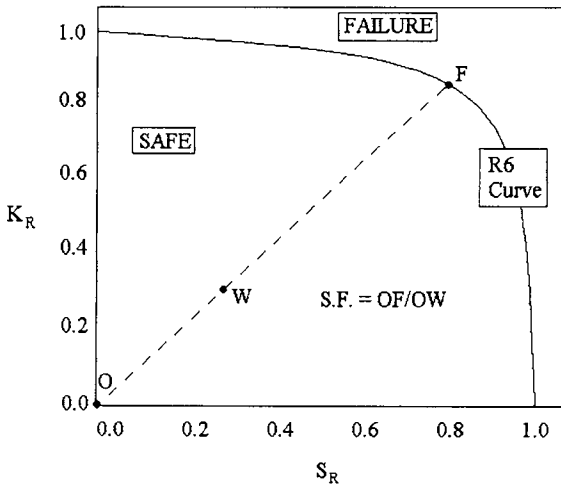
Figure 21.2 CEGB R6 Curve

The original failure assessment diagram (FAD) was developed by the U.K. Central Electricity Generating Board (CEGB). This FAD is shown in Figure 21.2. The CEGB approach (Milne et al., 1986, 1988; Kanninen and Popelar, 1985) addressed post-yield fracture by an interpolation formula between two limiting cases: linear elastic fracture and plastic collapse. The interpolation formula, called the failure assessment or R6 curve (see Fig. 21.2) is:

$$K_R = \frac{S_R}{\sqrt{\frac{8}{\pi^2} \ln[\sec(0.5\pi S_R)]}} \tag{21.7}$$

The right-hand side of Eq. (21.7) is the plastic correction to the small-scale yielding prediction. The CEGB R6 curve in Figure 21.2 may be interpreted as follows: A structural component is safe if the point W describing its state falls inside of the R6 curve. The component fails if the point W is on or above the R6 curve. The utilisation factor on load is OW/OF, where point F is on the R6 curve and point O is in the origin.

21.4 Level 3: The Failure Assessment Diagram (FAD)

The FAD utilised in Level 3 Assessment is as depicted schematically in Figure 21.3:

- The collapse ratio, L_R, is the ratio of the net section stress at fracture to the flow stress.
- The fracture ratio, K_R, is the ratio of the crack driving force (including residual stresses) to the material toughness (which could be K_{MAT} or CTOD).

The failure assessment curve defines the critical combination of service loads, material stress-strain properties, and geometry of the cracked member at which failure might be expected. Applications of the FAD to design codes include:

- CEGB R6 – Revision 3
- BSI (1999) PD 6493
- Electric Power Research Institute/General Electric (EPRI/GE) model
- ASME Section XI Code Case (DPFAD) for ferritic piping
- API 579 (2001)
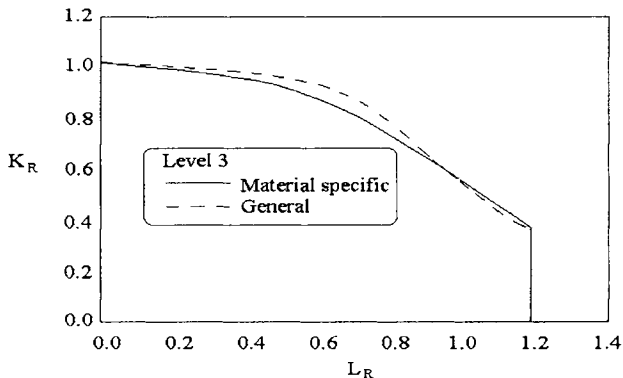
Figure 21.3   The Failure Assessment Diagram

Level 3 is the most sophisticated one among of the three levels and will normally be used in the assessment of high strain-hardening materials and/or stable tearing where the Level 2 approach would prove too conservative. In PD 6493 (now BS 7910), Level 3 FAD consists of two alternative criteria: 1) a general FAD and 2) a material specific FAD in which material stress-strain curves are also input data to the FAD assessment.

CTOD is popular in the UK nd European countries, while J-integral is used in the USA, e.g. by the nuclear engineering industry.

21.5 Fatigue Damage Estimation Based on Fracture Mechanics

21.5.1 Crack Growth Due to Constant Amplitude Loading

The total number of cycle to final fracture is the sum of the number of cycles for the crack initiation phase and crack propagation phase. The number of cycles for crack propagation phase, N_p, my be estimated using,

$$N_p = \int_{a0}^{a_{CR}} \frac{da}{da/dN} \tag{21.8}$$

where a_o and a_{CR} are crack depth (or length) at crack initiation and final fracture respectively. The value of a_{CR} may be determined using methods for the assessment of final fracture, as discussed in Section 21.1 thru Section 21.4. The crack propagation may be predicted using Paris Law. Substituting the Paris Law into the above equation, we may obtain that

$$N_p = \int_{a0_i}^{a_{CR}} \frac{da}{C(\Delta K)^m} = \int_{a0}^{a_{CR}} \frac{da}{C\left(S\sqrt{\pi a}\ F\right)^m} \tag{21.9}$$

where F is so-called crack shape factor and S denotes the stress range. When the stress range S is of constant amplitude, the above equation may be re-written as:

$$N_p = \frac{1}{C\left(S\sqrt{\pi}\ \right)^m} \int_{a0}^{a_{CR}} \frac{da}{\left(\sqrt{a}\ F\right)^m} \tag{21.10}$$

If F does not dependent on a, the above equation may lead to (Almar-Naess, 1985):

$$N_p = \frac{a_{CR}^{1-m/2} - a_0^{1-m/2}}{C\left(S\sqrt{\pi}\ F\right)^m (1-m/2)} \quad for\ m \neq 2 \tag{21.11}$$

The Paris parameters C and m may be found from Gurney (1979), IIW(1996), BS 7910 (1999) and API 579 (2001). The values of C and m depend on the material, service environment and stress ratio. The value of C may also be determined by mechanical tests and the chosen value is to be the mean value plus two standard deviation of log da/dN.

The size of initial crack a_0, should be determined considering the accuracy of the non-destructive testing which is used to inspect the defects during fabrication.

21.5.2 Crack Growth due to Variable Amplitude Loading

The equations presented in Section 21.5.1 may be applied to risk-based inspection in which the crack growth is predicted using Paris Law. Predicting the number of cycles for the crack propagation phase for variable amplitude loading is complex and needs a computer program to do numerical integration of Eq.(21.9). The number of occurrence n_i in a block for stress range S_i for crack depth from a_i to a_{i+1} may be estimated as (Almar-Naess, 1985),

$$n_I = \frac{1}{C\left(S_I \sqrt{\pi}\right)^m} \int_{a_I}^{a_{I+1}} \frac{da}{\left(\sqrt{a}\ F\right)^m} \tag{21.12}$$

and the fatigue life N_i at a constant amplitude stress S_i is given by

$$N_I = \frac{1}{C\left(S_I \sqrt{\pi}\right)^m} \int_{a_0}^{a_{CR}} \frac{da}{\left(\sqrt{a}\ F\right)^m} \tag{21.13}$$

Hence, the accumulated fatigue damage may then be estimated using the Miners Law, which is:

$$D = \sum_{I=1}^{K} \frac{n_I}{N_I} \tag{21.14}$$

21.6 Comparison of Fracture Mechanics & S-N Curve Approaches for Fatigue Assessment

As compared in Table 21.1, the Paris Equation may be transformed to the equation of an S-N curve. Eq.(21.10) may be written as

$$N_p = \frac{I}{C_I (S)^m} \tag{21.15}$$

where I in Eq.(21.15) is an integral. The total number of cycles N is close to N_p because the number of cycles to the initiation of crack propagation is small. Hence the above equation may be further written to:

$$N = \frac{I}{C_I} (S)^{-m} \tag{21.16}$$

Table 21.1   Comparison of Fracture Mechanics and S-N Curve for Fatigue

Fracture Mechanics	S-N Curve
Region I: Threshold Region (no crack growth)	Fatigue Endurance Limit (infinite life)
Region II: Paris Equation	S-N Curve (high cycle fatigue)
Region III: Final Fracture (yielding)	Low-cycle fatigue, failure region

21.7   Fracture Mechanics Applied in Aerospace, Power Generation Industries

Fracture control in the aerospace industry is based on the fracture mechanics analysis of the growth of assumed preexisting cracks of a size related to inspection detection capabilities (Harris, 1997). For space structures, the NASA (1988) requirements are applied to all pay loads in space shuttle, as well as life/mission-control items in space applications, such as space station. A fracture mechanics analysis of the component is conducted using an initial flaw size that is referred to as the nondestructive examination (NDE) size. Smaller size can be assumed in the analysis if a better detection capability can be demonstrated for the particular examination method applied. Median material properties are used in the crack growth calculations. Commercial software is available to calculate crack-growth based on fracture mechanics. The requirement is that the flaw size should demonstrate to survive four lifetimes.

Fracture mechanics has been applied to aircraft structures because of the high-required reliability and severe weight penalties for overly conservative design. Probabilistic methods have been applied to deal with the randomness of initial flaws and load spectra. Provan (1987) described the military aircraft approach known as "damage tolerance" and "fail safe", see Part III Section 22.4. The purpose of a damage tolerance analysis is to ensure structural safety throughout the life of a structure. The analysis evaluates the effects of accidental damage that might occur during the service life and verify that the structure can withstand this damage until the next inspection or until the current mission is completed with a safety factors of two.

Harris (1997) also reviewed applications of fracture mechanics in the electric power generation industry, such as nuclear pressure vessels, steam turbine rotors, and the like. The requirement for extreme reliability and the prohibitive cost of full-scale testing (as used in the aircraft industry) led to extensive use of fracture mechanics to predict behavior of defected components. The ASME (1989) Boiler and Pressure Vessel Code Section XI was developed for in-service nondestructive inspection intended to detect cracks before they grow to lead a failure. The code defined locations to be inspected, procedures to be used, and procedures for analyzing its future behavior if a crack is found. As the codes used in airspace and aircraft industries, the ASME code also gives procedures for defining initial crack size, material (fatigue crack-growth) properties, and stress intensity factors to be used in the fracture mechanics analysis. Tables of crack size are also given to define the crack sizes that need not be further analyzed if the detected size is smaller. Cracks larger than these tabulated values can still be left in service if a more detailed analysis shows them not to grow beyond a specified fraction of the critical crack size in the remaining desired lifetime. The ASME (1991, 1992, 1994) provides guidelines for risk-based inspection of the most risk-prone locations, and consequently provide a greater risk reduction for given number of inspections or the same risk reduction for fewer inspections.

The probabilistic fracture mechanics developed in these industries have been applied and further developed by the shipping, bridge and oil/gas industries for the design and operation of marine structures. In particular, the defect control criteria for pipeline installation, the damage/defect tolerance criteria and inspection planning methods applied in operation of tubular joints and pipelines have been benefiting the research efforts of the airspace and aircraft industries.

Fracture mechanics also plays a major role in the analysis nd control of failure in the chemical and petroleum industries, where the "fitness-for-service" is employed.

21.8 Examples

Example 21.1: Maximum Tolerable Defect Size in Butt Weld

Problem: A butt-welded plat thickness of 150mm, yield stress of 500MPa. There is a surface crack with an aspect ratio c/a=1. Its minimum critical CTOD is 0.00036m. The weld is loaded in uniaxial tension perpendicular to the crack plane, and the stress in the weldment is less than or equal to 0.60 of the yield stress. What is maximum allowable crack width?

Solution:

$$\frac{\varepsilon}{\varepsilon_y} = 0.60$$

$$\Phi = \frac{\delta_c}{2\pi\varepsilon_y a_{max}} = \frac{0.00036}{2\pi \frac{500}{2.0E5} a_{max}} = \frac{0.0259}{a_{max}}$$

The following relation exists:

$$\Phi = \frac{\varepsilon}{\varepsilon_y} - 0.25 = \frac{0.0259}{a_{max}}$$

and therefore, the maximum half-width is a_{max} =0.074m

21.9 References

1.   Almar-Naess, A. (1985), "*Fatigue Handbook, Offshore Steel Structures*", Tapir, Norway.

1.   API 1104 (1994), "Alternate Standards for Acceptability for Girth Welds. Appendix A, Standards for Welding Pipelines and Related Facilities", 18th edition, American Petroleum Institute.

2.   API 579 (2001), "Recommended Practice for Fitness for Service", American Petroleum Institute.

3.   ASME (1989), "*ASME Boiler and Pressure Vessel Code, Section XI, Rules for In-service Inspection of Nuclear Plant Components*", American Society of Mechanical Engineers.

4.   ASME (1991, 1992, 1994) "*Risk-Based Inspection - Development of Guidelines, Vol. 20.1 (1991): General Guidelines, Vol.20.2 (1992): Light Water Reactor Nuclear Power Plant Components, Vol.20.3 (1994): Fossil Fuel-Fired Electric Power Generating Station Applications* ", American Society of Mechanical Engineers.

5.   Andersen, T.L., (1991), "*Fracture Mechanics – Fundamentals and Application*", CRC Press.

6.   BSI. (1980), "PD 6493 - Guidance on Some Methods for the Derivation of Acceptance Levels for Defects in Fusion Welded Joints", London: BSI.

7.   BSI (1999) "BS7910-Guidance on Methods for Assessing the Acceptability of Flows in Fusion Welded Structures".

8.   Burdekin, F.M., and Dawes, M.G. (1971), "Practical Use of Linear Elastic and Yielding Fracture Mechanics with Particular Reference to Pressure Vessels", pp. 28-37 in

Practical Application of Fracture Mechanics to Pressure Vessel Technology. London: The Institution of Mechanical Engineers.

9.   Dawes, M.G. (1974), "Fracture Control in High Strength Weldments", Welding Journal 53:369-s-379-s.

10. Gurney, T.R. (1979), *"Fatigue of Welded Structures"*, 2nd Edition, Cambridge University Press.

11. Harris, D.O. (1995), "Fatigue and Fracture Control in the Aerospace and Power Generation Industries from the book entitled *"Prevention of Fracture in Ship Structures"* by the Committee on Marine Structures, Marine Board, National Research Council. Washington, D.C.

12. Hertzberg, R. W. (1989), "Deformation and Fracture Mechanics of Engineering Materials", 3rd Edition, John Wiley & Sons.

13. IIW (1996), "Fatigue Design of Welded Joints and Components", Report XIII-1539-96/XV/845-96, The International Institute of Welding, Abington Publishing, Cambridge, England.

14. Kanninen, M.F., and Popelar, C.H. (1985), "Advanced Fracture Mechanics", New York: Oxford University Press.

15. Milne, I., Ainsworth, R.A., Dowling, A.R., and Stewart, A.T. (1986) "Assessment of the Integrity of Structures Containing Defects. R/H/R6", Revision 3. Leatherhead, Surrey, England: Central Electricity Generating Board.

16. Milne, I., Ainsworth, R.A., Dowling, A.R., and Stewart, A.T. (1988), "Assessment of the Integrity of Structures Containing Defects", International Journal of Pressure Vessels and Piping 32:3-104.

17. NASA (1988), *"Fracture Control Requirements for Payloads using the National Space Transportation System, NASA NHB 8071.1"*, National Aeronautics and Space Administration.

18. Newman J.C., and Raju., I.C. (1981), "An Empirical Stress Intensity Factor Equation for the Surface Crack", Engineering Fracture Mechanics, Vol. 51, pp185-192.

19. Provan, J.W. (1987), *"Probabilistic Fracture Mechanics and Reliability"*, Boston, Massachusetts, Martinus Nijhoff Publishers.

20. Reemsnyder, H.S. (1997), "Fatigue and Fracture of Ship Structures", from the book entitled *"Prevention of Fracture in Ship Structures"* by the Committee on Marine Structures, Marine Board, National Research Council. Washington, D.C.

Part III

Fatigue and Fracture

Chapter 22 Material Selections and Damage Tolerance Criteria

22.1 Introduction

Engineering applications of the fatigue and fracture technologies will be discussed in this Chapter, including:

- Material Selections and Fracture Prevention
- Weld Improvement and Repair
- Damage Assessment and Damage Tolerance Criteria
- Non-Destructive Inspection

22.2 Material Selections and Fracture Prevention

22.2.1 Material Selection

Tensile strength is the key mechanical properties for strength design of structures. The materials used are required to have satisfactory weldability and fracture toughness that is satisfactory for the intended application environment (temperature). Fatigue and corrosion characteristics are also important material properties. In the design codes, requirements for materials and welding are defined for the construction of the hull and machinery, see e.g. ABS (2002). The material requirements in Rules are defined for mild steel, higher strength steel and low temperature materials, including:

- process of manufacture
- chemical composition
- condition of supply
- tensile properties
- impact properties
- marking
- surface finish

To certificate compliance with the above material requirements, the test specimens and number of tests are defined by the Rules along with the requirements for approval of welding procedures and qualification of welders.

22.2.2 Higher Strength Steel

For ship structures, the yield strength for mild steel is 24 (kgf/mm^2)(or 235 N/mm^2). The higher strength steel is HT32 (yield strength of 32 kgf/mm^2) and HT36 (Yamamoto et al 1986). The allowable stress for hull girder strength is defined for the individual grades of material. The use of higher strength steel may lead to reduction of plate wall-thickness. However, corrosion resistance for higher strength steel is equivalent to that for the mild steel. Therefore corrosion allowance should also be taken as 2.5 to 3.5 mm. Elastic buckling strength is only determined by geometrical dimensions, and it is not influenced by the yield strength. Therefore, Elastic buckling strength my decreased due to the wall-thickness deduction for higher strength steel. To avoid the reduction of buckling strength, it may be necessary to reduce the spacing of stiffeners. The post-yielding behaviour for higher strength steel is different from that for mild steel in that the ratio between linear stress limit and yield strength is higher for higher strength steel. For instance, the proportional limit for steel of yield strength between 50 and 60 kgf/mm^2 is 0.7 to 0.8, while the proportional limit for mild steel is 0.6. Hence there is less tensile strain (at tensile failure) for higher strength steel and the strength redundancy in the post-yield region is less. In the heat affected zone (HAZ), Charpy V-notch energy for high strength steel may be significantly low. It may be necessary to control the heat energy in welding process and increase the number of passes in single sided welding.

The weldability of a steel is a measure of the ease of producing a crack-free and sound structural joint. The carbon equivalent (C_{eq}) for evaluating the weldability may be calculated from the ladle analysis in accordance with the following equation:

$$C_{eq} = C + \frac{M_n}{6} + \frac{C_r + M_0 + V}{5} + \frac{N_i + C_u}{15} \% \qquad (22.1)$$

Selection of C_{eq} and its maximum value is a matter to be agreed between the fabricator and the steel mill because its value represents the tensile strength and weldability. The higher the C_{eq}, the higher the tensile strength and the worse the weldability.

Welding procedures should be based on a steel's chemistry instead of the published maximum alloy content, since most mill runs are usually below the maximum alloy limits set by its specification. When a mill produces a run of steel, chemical content is also recorded in a Mill Test Report. If there is any variation in chemical content above the maximum allowable limits, special welding procedures should be developed to ensure a properly welded joint.

For higher strength steel, the fatigue resistance may not increase as much as the increase of the stress in the stress concentration areas of the weld details. It is therefore necessary to reduce stress concentration and improve the fatigue resistance for the weld details.

22.2.3 Prevention of Fracture

During the 2nd world war, accidents occurred due to brittle fracture in welded ships. In the USA, a throughout investigation was carried out on the temperature dependency of brittle fracture. It is now known that the toughness is higher if the Mn/C ratio is higher. With the development of fracture mechanics, it became clear that brittle fracture is due to the reduction of the fracture toughness K_{IC} in lower temperature (below 0 ^{0}C). In order to determine fracture toughness, it is necessary to conduct accurate measurement using large test specimens. For practical purpose, the result of Charpy V-notch impact tests has been correlated with the fracture toughness K_{IC} and used in the specification for steels used in lower temperature. In ship design Rules, Charpy V-notch impact tests are not required in production for A-grades, B,

D, and E grades are to be tested at 0^0C, -10^0C and –40^0C respectively. The energy average for standard Charpy test specimens is required to be higher than 27 J (or 2.8 kgf-m). As steels for hull structures, the E grades have the highest toughness, and may be used as crack arrestor to stop the propagation of brittle fracture. They are used in location for primary members that are critical for longitudinal strength. In many cases, the toughness criteria for secondary members may be relaxed.

In order to present fatigue cracks in welded details, allowable stress criteria have been defined in ship design Rules based on simplified fatigue analysis (see Part III Chapter 19) and an assumed design life of 20 years. The allowable stress criteria shall be satisfied in the determination of net wall-thickness.

For quality control purpose, the materials are inspected when the steel is delivered from the steel makers. The inspection requirements are given in classification Rules. For ships in operation, surveys are conducted by classification societies, the reduction of wall-thickness due to corrosion is measured, fatigue cracks and dent damages are also given due attention in the survey process. The causes for damages are investigated, and damages are repaired or weld details are modified when necessary. The damage tolerance criteria are discussed in Section 22.4 of this Chapter. The feedback from the process of inspection, causes investigation, repair and modification is given to design through Rule changes and development of design guidance, such as fatigue resistant details, see Sub-section 22.3.2 of this Chapter.

22.3 Weld Improvement and Repair

22.3.1 General

In many cases, the fatigue performance of severely loaded details can be design to be fatigue resistant details, and improved by upgrading the welded detail class to one having higher fatigue strength. In some cases, procedures that reduce the severity of the stress concentration at the weld, remove imperfections, and/or introduce local compressive stresses at the weld can be used for improvement of the fatigue life. Similarly these fatigue improvement techniques can be applied as remedial measures to extend the fatigue life of critical weld details that have cracked.

In the following sub-sections, discussions will be made to the welding improvements through modification of weld toe profile and modification of residual stress distribution (Almar-Naess, 1985, Kirkhope, 1997).

22.3.2 Fatigue-Resistant Details

Fatigue strength of weld details is based on "good" fabrication practice in terms of

- design: to minimize the restraint and geometrical discontinuity in the design of cruciform joint misalignment, lap connection and fillet welds.

- welding practice: fillet weld fit up, weld shape and continuity

- residual stress

- weld toe dressing treatments

Based on classification Rules, Glenn et al (1999) catalogued fatigue resistant details in tanker structures, bulk carrier structures, container ships and warships. These catalogued details may

be used for designers as guidance, while the criteria made by Ma et al (2000) may be used to assess the acceptability of a particular design (see Part III Section 19.6).

22.3.3 Weld Improvement

Both contour grinding of the weld profile and the local grinding of the weld toe area, are recommended to modify the weld profile and improve fatigue strength. When modifying the weld toe profile, the essential objectives are:

- Remove defects at the weld toe

- Develop a smooth transition between weld material and parent plate

The fatigue life can be increased by applying local grinding or re-melting techniques to remove defects and discontinuities.

Grinding

Full-profile burr grinding, toe burr grinding or localized disc grinding are widely used grinding methods. Considering the time required for grinding, local weld toe grinding has become one of the best grinding methods. Careful and controlled local grinding of the weld toe improves the fatigue strength of a specimen in air by at least 30%, this is equivalent to an increase in fatigue life by a factor greater than 2. However, in order to obtain such a benefit the grinding should extend about 0.04 inch (1 mm) beneath the plate surface.

Controlled Erosion

An alternative weld toe modification technique uses a high-pressure water jet. Under carefully controlled conditions, the weld toe area can be eroded as if it were ground. Early research indicates that fatigue life improvement due to Abrasive Water Jetting (AWJ) erosion and toe grinding are comparable. The advantage of controlled erosion is that it does not require heat input and it can be carried out quickly.

Re-melting Techniques

Re-melting weld material to a shallow depth along the weld toe results in removal of inclusions and helps achieve a smooth transition between the weld and the plate material. Tungsten-Inert-Gas (TIG) and plasma welding are not practical techniques for routine use, but TIG and plasma dressing can be used to improve the fatigue strength of selected hotspot areas.

TIG welding is based on a stringer bead process. TIG dressing is performed on welds made by other processes where the toe region is melted to a shallow depth without the use of filler material. Slag particles in the re-melted zone are brought to the surface, leaving the weld toe area practically defect free. High heat input should be maintained to obtain a good profile and a low hardness. A low hardness in the heat-affected zone (HAZ) may also be achieved by a second TIG application.

Plasma dressing requires re-melting the weld toe using the plasma arc welding technique. It is very similar to TIG dressing, but plasma dressing uses a wider weld pool and higher heat input. This technique is relatively insensitive to the electrode position, because fatigue strength improvements using plasma dressing, are better than those obtained when using TIG.

Although overall weld profiling is considered desirable for fatigue strength improvement, rules and recommendations, other than API (2001), do not allow improvement in fatigue strength due to weld profiling unless weld profiling is accompanied by weld toe grinding. It should also be noted that the data associated with weld profiling and weld toe grinding is limited. Therefore,

expert judgement should be used to quantify the fatigue strength improvement due to the modification of the weld profile.

22.3.4 Modification of Residual Stress Distribution

By using the following methods, the undesirable tensile residual stresses found at the weld can be modified to obtain desirable compressive stresses at the weld toe:

Stress Relief

Various fatigue tests on simple small plate specimens indicate that improved fatigue strength can be obtained by stress relief due to post-weld heat treatment (PWHT). However, plate and stiffening elements of continuous systems rarely require stress relief. It is also doubtful that a complex structural detail with built in constraints can be effectively stress relieved.

Compressive Overstressing

Compressive overstressing is a technique in which compressive residual stresses are introduced at the weld toe. Experimental results and analytical work demonstrate the effectiveness of pre-overstressing, but the procedure to be implemented does not appear to be practical for most marine structures.

Peening

Peening is a cold working process intended to produce surface deformations with the purpose of developing residual compressive stresses. When impact loads on the material surface would cause the surface layer to expand laterally, the layer underneath prevents such surface layer expansion, creating the compressive residual stresses at the surface. Typical peening methods are hammer peening, shot peening, and needle peening.

22.3.5 Discussions

Fatigue strength improvement techniques are time consuming and costly and they should be applied selectively. Comparison of different techniques allows assessment of their effectiveness and cost. The recommended improvement strategies depend on the characteristics of the (global and local) structure and the preference for one technique over others is based on effectiveness, cost and fabrication yard characteristics.

Some of the comparisons of various approaches available, which improve fatigue strength of welded details, are the following:

- Full profile burr grinding is preferable to toe burr grinding or disc grinding only, because it results in higher fatigue strength even at a substantial cost penalty.

- Disc grinding requires the least time and cost. However, it produces score marks perpendicular to the principal stress direction, making this technique less effective than others.

- Using a high-pressure abrasive water jet (AWJ) process for controlled erosion of the weld toe area can be as effective as grinding. Its simplicity, speed and non-utilization of heat make controlled erosion very promising.

- A wider weld pool makes plasma dressing less sensitive to the position of the electrode relative to the weld toe, compared with TIG dressing. Therefore, the fatigue strength improvement obtained from plasma dressing is better than that obtained from TIG dressing.

- Review of grinding, re-melting and peening techniques indicate substantial scatter of fatigue strength improvements. Typically, the best fatigue strength improvements are achieved when using TIG dressing and hammer peening. Toe disc grinding is the least effective technique.

22.4 Damage Tolerance Criteria

22.4.1 General

Marine structures are subjected to various sources of cyclic loading that may cause fatigue cracks to propagate at welded details. The propagation of these cracks may eventually threaten the structural strength and stability. Therefore, severe fabrication flaws and cracks detected in service are to be repaired. Similarly corrosion defects and dent damages also need to be inspected and repaired. In order to optimize the life-cycle inspection and maintenance costs, there is a need for a rational criterion to determine the acceptability of damages.

Damage tolerance is the ability of structure to sustain anticipated loads in the presence of fatigue cracks, corrosion defects, or damages induced by accidental loads until such damage is detected through inspection or malfunctions and repaired. In this Section, focus will be devoted to fatigue cracks. A damage tolerance analysis for fatigue cracks makes use of fracture mechanics to quantitatively assess the residual strength and residual life of a cracked weld detail.

Yee et al (1997) and Reemsnyder (1998) presented detailed guidance on the application of damage tolerance analysis to marine structures. The damage tolerance analysis consists of the following essential elements:

- the use of Failure Assessment Diagrams to assess the local residual strength of a cracked structural detail,
- the use of linear elastic fracture mechanics models for fatigue crack growth to predict the residual life of a cracked structural member,
- the estimation of peak stress and cyclic loads over the assessment interval of interest, and
- the inspection to detect damages and its accuracy.

Some of the above items will be discussed in the following sub-sections.

22.4.2 Residual Strength Assessment Using Failure Assessment Diagram

The failure assessment diagram (FAD) may be used to predict residual strength of a cracked member for a given set of fracture toughness and defect size, see Part III Section 21.1.2. If the peak stress exceeds the residual strength derived through FAD, failure may occur. For the accurate prediction of residual strength, it is important to properly

- assess the maximum defect size, considering damage detachability for the inspection programs,
- determine the material toughness and the applied/residual stresses
- select an appropriate failure assessment diagram and define its net-section stress and stress intensity factor

While the residual strength represents the "capacity" of the damaged member, the "load" is the peak stress that may be applied to the cracked member over the assessment interval of interest.

The calculation of stresses and crack driving forces may also significant influence the result of the safety check for the cracked weld detail.

22.4.3 Residual Life Prediction Using Paris Law

The Paris Law may be used to calculate the crack growth due to cyclic loads of constant amplitude or variable amplitude, see Part III Section 21.5. For the reliable prediction of crack growth, it is important to accurately

- predict the Paris parameters (C and m) used in the Paris equation
- assess the initial crack size to be used in the Paris equation
- calculate cyclic stresses and the stress intensity range

The outcome of integrating the Paris equation is the number of cycles from the time the crack is inspected to the final fracture. The damage tolerance criterion requires that this predicted fatigue life be longer than the sum of the time to the next inspection and the time required for repair or replacement. If no damage is detected in the inspection, the minimum inspectable size for cracks shall be used as the initial crack size.

22.4.4 Discussions

A damage tolerance analysis may be conducted during the design and fabrication stage, while performing an in-service inspection or in the course of extending the design life of a structure. BS 7608 (BSI, 1993) may be used for the damage tolerance analysis. It recommends to select materials and to reduce stresses so that the crack growth rate is low and critical crack size is large. Providing readily inspectable details and crack arresting details may also help.

The above discussions are made using fatigue and fracture as an example. Similar discussions may be made on corrosion defects and wear out. In the evaluation of the tolerance criterion for corrosion defects, it is necessary to predict

- the initial corrosion defect size,
- the residual strength of corroded member,
- the future growth of corrosion defects using an adequate corrosion rate model,
- the maximum loads that may occur for the period of interests or until the end of design life.

The dent damage caused by accidental loads will not grow and therefore its tolerance criterion may be simply determined by comparing the residual strength with the maximum load expected for the interval of interests.

22.5 Non-Destructive Inspection

Almar-Naess (1985) and Marshall (1992) outlined several methods for the inspection of cracks in weld details, such as:

- liquid penetrant (to reveal surface flaws, require a clean surface)
- magnetic particles (to reveal surface flaws, dos not require a clean surface)
- eddy currents (primarily for detecting surface flaws, magnetic field based)
- radiography (for detecting internal cracks, using x or γ radiation recorded in film)

- ultrasonic testing (UT) (sizing internal defects using ultrasonic signals)

Radiography is most sensitive to volumetric defects, such as porosity and slag. Any detectable crack is rejected because of the difficulty to detect and size crack-like defects.

Among of the above inspection methods, the ultrasonic inspection is the most reliable way of detecting and sizing internal defects. UT works very much like radar. Probes can be moved over the surface in the region to be inspected, in which piezo-electric crystals generate ultrasonic signals. The waves are reflected by the surface of the examined body, and also by any defects that might come in their way. The probe that generates the signal also detects these echoes. By measuring the time delay between the emission signal and the reception of each reflection, the source of reflection can be located and the position of defects identified. The basic features of UT are:

- UT is more sensitive to the more serious types of defects because it depends on the signals reflected. In decreasing order, the severity of defects is: cracks, incomplete fusion, inadequate penetration, slag and porosity.

- UT can locate defects in three dimension.

- UT can be conducted quickly and simply, without radiation hazards.

- UT can handle complex geometry of welded connections though use of the transducer.

Over 70% of the defects may be detected by UT, and the false alarm is less than 30%.

Where radiographic or ultrasonic inspection is required, the extent and location of inspection and choice of inspection methods are to be in accordance with AWS (1997) and ABS (1986), the materials and welding procedures involved, the quality control procedures employed and the results of visual inspection. In AWS (1997) and ABS (1986), criteria are defined to determine whether the inspection results (signals) are to be non-conforming or to be disregarded or to be evaluated against defect acceptance criteria.

22.6 References

1.   ABS (1986), "Rules for Non-destructive Inspection of Hull Welds", American Bureau of Shipping.

2.   ABS (2002), "Rule Requirement for Materials and Welding", American Bureau of Shipping.

3.   Almar-Naess, A. (1985), "*Fatigue Handbook, Offshore Steel Structures*", Tapir, Norway.

4.   API 1104 (1994), "Alternate Standards for Acceptability for Girth Welds. Appendix A, Standards for Welding Pipelines and Related Facilities", 18th edition, American Petroleum Institute.

5.   AWS (1997), "AWS Structural Welding Code - Steel, AWS D1.1-96", American Welding Society.

6.   Bai, Y. (2001), "*Pipelines and Risers*", Elsevier Science Ocean Engineering Book Series.

7.   BSI (1993) "BS 7608 - Code of Practice for Fatigue Design and Assessment of Steel Structures".

8.   BSI (1999) "BS7910 - Guidance on Methods for Assessing the Acceptability of Flows in Fusion Welded Structures".

9. Glenn, I.F., Paterson, R.B., Luznik, L., Dinovitzer, A. and Bayley, C. (1999), "Fatigue Resistant Detail Design Guide for Ship Structures", Ship Structures Committee Report SSC-405.

10. Kirkhope, K.J., Bell, R., Caron, L. and Basu, R. (1997), "Weld Detail Fatigue Life Improvement Techniques", Ship Structures Committee Report SSC-400.

11. Ma, K.T., Srinivasan, S., Zhang, H., Healy, B. and Peng, H. (2000), "Developing Design Criteria for Connections Around Cutout (Slot) Openings", SNAME Transactions, pp. 227-248.

12. Marshall, P.W. (1992), *"Design of Welded Tubular Connections"*, Elsevier Press, Amsterdam.

13. Reemsnyder, H.S. (1998), "Guide to Damage Tolerance Analysis", in Course Notes "Fatigue and Fracture Analysis of Ship Structures", SSC.

14. Yamamoto, Y., Ohtsubo, H., Sumi, Y. and Fujino, M. (1986), "Ship Structural Mechanics", Nariyamatou Book, (in Japanese).

15. Yee, R.D., Malik, L., Basu, R. and Kikhope, K. (1997), "Guide to Damage Tolerance Analysis of Marine Structures", Ship Structures Committee Report SSC-402.

This Page Intentionally Left Blank

Part IV: Structural Reliability

This Page Intentionally Left Blank

Part IV

Structural Reliability

Chapter 23   Basics of Structural Reliability

23.1 Introduction

Part IV describes structural reliability methods for the design of marine structures with emphasis on their practical application, e.g. to ship structures. Focuses are given to basic concept, methodology and application. Examples are given to demonstrate the application of the methodology.

Details of the structural reliability theory can be referred to, e.g. Ang and Tang (1975, 1984), Thoft-Christensen and Baker (1982), Madsen (1986), Schnerder (1997), Melchers (1999). Discussions are given on simple analytical equations that are based on lognormal assumptions. The papers on numerical approaches, e.g. Song and Moan (1998) are also mentioned briefly.

The following subjects are addressed in detail:

- Reliability of marine structures
- Reliability based design and code calibration
- Fatigue reliability
- Probability and risk based inspection planning

23.2 Uncertainty and Uncertainty Modeling

23.2.1 General

In general, a marine structural analysis deals with the load effects (demand) and the structural strength (capacity). In design, the dimensions of the structural members are determined based on the requirement that there is a sufficient safety margin between the demand and the capacity.

Uncertainties are always involved in all the steps of structural analysis and in strength evaluation. These uncertainties are due to the random character of the environment, geometric and material properties, as well as inaccuracy in prediction of loads, response and strength.

Rational design and analysis of marine structures require consideration of all the uncertainties involved in predicting load effects and structural modeling. Uncertainty analysis is the key in any reliability evaluation such as reliability-based design and re-qualification for marine structures.

The development of probabilistic analysis methods and design codes increased the importance of quantifying uncertainties. The results of the studies on uncertainty modeling can be used to

assess the relative importance of the various types of uncertainties. For example, one of the conclusions drawn from a study on offshore structures was that the uncertainty in the lifetime extreme wave height is the most significant one. The error in predicting the most severe sea condition over the design lifetime is one of the major ingredients of the uncertainty.

The reliability of a structural system depends on load and strength variables. Each variable can be calculated with different degree of accuracy. For example, for most of the cases, the response of an offshore platform to dead loads can be evaluated with high accuracy, while wave induced response may not be predicted with the same confidence. Therefore, when assessing structural safety and making design decisions, we must take into account the differences in the confidence levels associated with each load and strength variable. For example, in a reliability based design code for offshore structures, the load factor for wave loads is larger than that for dead loads, because the modeling uncertainty associated with the former is larger.

23.2.2 Natural vs. Modeling Uncertainties

Uncertainties in analysis of marine structures can be categorized into natural (random) and modeling types. The former is due to the statistical nature of the environment and the resulting loads. The latter are due to the imperfect knowledge of various phenomena, and idealizations and simplifications in analysis models. These uncertainties introduce bias and scatter. An example of a natural uncertainty is that associated with the wave elevation at a given position in the ocean. An example of a modeling uncertainty is the error in calculating the stresses and strength in a structure, when the applied loads are known. For this case, the error is only due to the assumptions and simplifications in structural analysis.

Modeling uncertainties can be reduced as the mathematical models representing them become more accurate. This is not the case with random uncertainties that do not decrease as we gather more information. Both random and modeling uncertainties must be quantified and accounted for in reliability analysis and development of reliability based design codes.

Let X be the actual value of some quantity of interest and X_0 the corresponding value specified by a design code. According to Ang and Cornell (1974),

$$X = B_I B_{II} X_0 \tag{23.1}$$

where $B_I = X_P / X_0$ and where X_P is the theoretically predicted value for this quantity, and $B_{II} = X / X_P$. B_I is a measure of natural (random) variability and B_{II} is a measure of modeling uncertainty.

The mean values of random variables B_I and B_{II}, $E(B_I)$ and $E(B_{II})$, are the biases corresponding to natural and modeling uncertainties, respectively. Assuming that the random and modeling uncertainties are statistically independent, and by using a linear expansion of the expression for B about the mean value of the random variables, we can quantify the total uncertainty in X as follows:

$$E(B) = E(B_I)E(B_{II}) \text{ and } COV_B = (COV_{BI}^2 + COV_{BII}^2)^{1/2} \tag{23.2}$$

where $B = B_I B_{II}$ and COV stands for the coefficient of variation of the quantity specified by the subscript.

Equation (23.2) is valid for small coefficients of variation (less than 0.10) only. However, the above approximations are frequently used.

23.3 Basic Concepts

23.3.1 General

Structural engineering deals with load (S) and strength (R) in terms of forces, displacements and stresses acting on the structures. Structural design codes commonly specify loads, strength and appropriate safety factors to be used. Structural reliability theory is about the evaluation of the failure probability taking into account the uncertainties in loads and strength. During the last two decades, many efforts have been given on structural reliability and their application to practical structural engineering.

23.3.2 Limit State and Failure Mode

A structural component can fall into safe or failure state. The border line (or surface) between the safe and failure states is named as limit state, and expressed as $g(Z) = R - S$. The following conditions describe the possible states of a structural component.

$g(Z)<0$ represents a failure state where loads S exceeds the strength R.

$g(Z)>0$ represents a safe state since strength R is larger than loads S.

$g(Z)=0$ represents the limit state line (or surface).

The figure below shows the concept of limit state sketchily

For marine structures, the limit states are defined in accordance with the different requirements, such as serviceability, ultimate strength, etc.

23.3.3 Calculation of Structural Reliability

By quantifying the uncertainties using probabilistic methods, structural reliability can be measured by means of failure probability.

For a structure described by a set of random variables Z with joint distribution $f_Z(z)$, it must be possible for each set of values of z to state whether or not the structure has failed. This leads to a unique division of Z space into two sets, called the safe set and the failure set respectively. These two sets are separated by the failure surface (limit state).
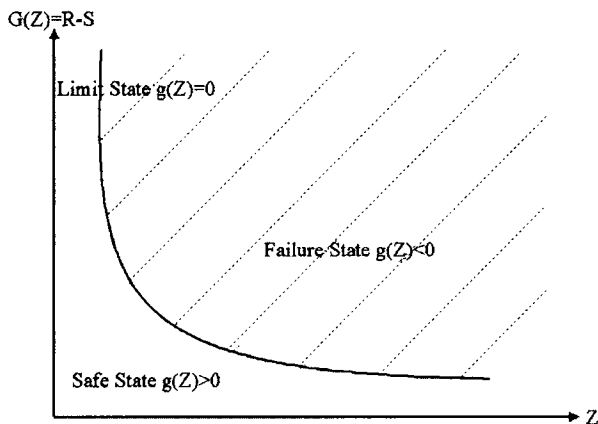
Figure 23.1   Limit State Concept

The structural failure probability P_f can then be calculated as

$$P_f = P(g(Z) \le 0) = \int_{g(z)\le 0} f_z(z) dz \tag{23.3}$$

and the reliability R is

$$R = 1 - P_f = P(g(Z) > 0) \tag{23.4}$$

The exact numerical integration is only practical for a very limited class of simple problems. A variety of procedures representing different levels of sophistication may be used to calculate the failure probabilities, namely safety index method, analytical approach and numerical approach.

Cornell Safety Index Method

Assuming that the limit state function is given below

$$g(Z) = R - S \tag{23.5}$$

where R and S are random variables representing the strength and load respectively. Cornell (1969) proposed to estimate the safety index using

$$\beta = \frac{\overline{g(Z)}}{\sigma_g} = \frac{\overline{R} - \overline{S}}{\sqrt{\sigma_R^2 + \sigma_S^2}} \tag{23.6}$$

where, $\overline{R}$ and $\overline{S}$ are the mean values of R and S; σ_R and σ_S are standard deviations of R and S respectively. The safety index is uniquely related to the failure probability by

$$P_f = \Phi(-\beta) \tag{23.7}$$

where Φ is the standard normal distribution function, see the table below.

Table 23.1   Relation between β and Φ(-β)

Standard Normal Distribution Table									
β	0.0	0.1	0.2	0.3	0.4	0.5	0.6	0.7	0.8	0.9
Φ(−β)	0.5	0.46017	0.42074	0.38209	0.34458	0.30854	0.27425	0.24196	0.21186	0.18406
β	1.0	1.1	1.2	1.3	1.4	1.5	1.6	1.7	1.8	1.9
Φ(−β)	0.15866	0.13567	0.11507	0.09680	0.08076	0.06681	0.0548	0.04457	0.03593	0.02872
β	2.0	2.1	2.2	2.3	2.4	2.5	2.6	2.7	2.8	2.9
Φ(−β)	0.02275	0.01786	0.0139	0.01072	0.0082	0.00621	0.00466	0.00347	0.002555	0.001866
β	3	3.1	3.2	3.3	3.4	3.5	3.6	3.7	3.8	3.9
Φ(−β)	0.001499	0.000968	0.000687	0.000483	0.000337	0.000233	0.0001591	0.0001078	0.0000723	0.0000483
β	4	4.1	4.2	4.3	4.4	4.5	4.6	4.7	4.8	4.9
Φ(−β)	3.170E-05	2.070E-05	1.330E-05	8.500E-06	5.400E-06	3.400E-06	2.100E-06	1.300E-06	8.000E-07	5.000E-07

The reliability index β is related approximately to the failure probability as

$$P_f \approx 0.475 \exp\left(-\beta^{1.6}\right) \tag{23.8}$$

or

$$P_f \approx 10^{-\beta} \tag{23.9}$$

The Hasofer-Lind Safety Index Method

An important step to calculation of failure probability was made by Hasofer and Lind (1974), who transformed the limit state function into the so-called standard space. This transformation is shown here for the two variables R and S only.

The random variables R and S are transformed and standardized into U_1 and U_2 respectively:

$$U_1 = \frac{R - \mu_R}{\sigma_R} \tag{23.10}$$

$$U_2 = \frac{S - \mu_S}{\sigma_S} \tag{23.11}$$

Hence, the random variables R and S can be expressed as

$$R = U_1 \sigma_R + \mu_R \tag{23.12}$$

$$S = U_2 \sigma_S + \mu_S \tag{23.13}$$

Thus, the new variables have a mean value of 0 and a standard deviation of 1. In the new coordinate system, the straight line is expressed as the following:

$$g(Z) = R - S = \left(\mu_R - \mu_S\right) + \left(U_1 \sigma_R - U_2 \sigma_S\right) \tag{23.14}$$

The distance from the design point to the origin is equal to the distance marked with β, the so-called β safety index (or β index, or Hasofer/Lind index), as shown in the figure below.
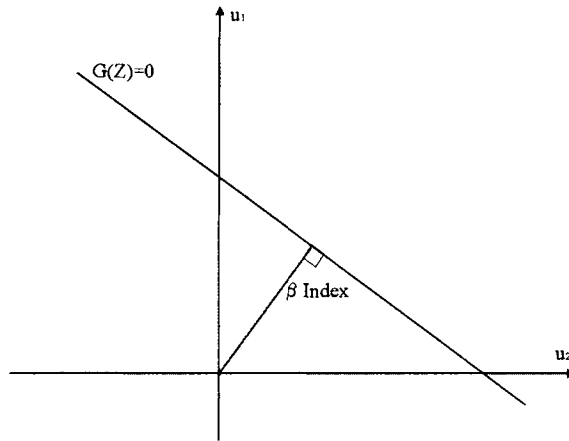
Figure 23.2   β Index Method

Example 23.1 is given in Section 23.11 to demonstrate the β index method.

Analytical Approach

As an approximate method to compute the failure probability, the first order reliability method (FORM) is the most widely accepted one. FORM also provides the sensitivity of the failure probability with respect to different input parameters, which is essential to optimize the reliability of the structure in design, construction and maintenance.

The second order reliability method (SORM) is to approximate the limit-state surface by a second order surface fitted at the design point. The most common approximation is the parabolic surface.

FORM and SORM usually give good approximation for small probabilities, but their accuracy and feasibility decrease with increasing non-linearity for the limit state and number of non-normal random variables. In such cases, the failure probability may be estimated by simulation methods.

Simulation Approach

Instead of using analytical solution, Monte Carlo Simulation (MCS) is a numerical technique based on experiments on a digital computer. The failure probability is interpreted as relative frequency. MCS involves randomly sampling a large number of realization of the failure function, $g(Z)$, and observe the results, i.e, whether the failure function is less or equal to zero. If the experiment is repeated N times and failure occurs n times, the failure probability is estimated as $P_f = n/N$.

There are two main classes of the simulation methods applied for reliability analysis, 1) the zero-one indicator methods and 2) the semi-analytical conditional expectation methods.

23.3.4 Calculation by FORM

In the First Order Reliability Method (FORM) the failure set is approximated by first transforming the limit state surface into U space and then replacing it by its tangent hyperplane at the design point $\mathbf{u}^*$.

The Rosenblatt transformation is used,

$$U_i = \Phi^{-1}\left(F_i\left(Z_i | Z_1, \cdots, Z_{i-1}\right)\right) \quad i = 1,2, \ldots, n \tag{23.15}$$

If the random variables Z are mutually independent, the transformation is simply

$$U_i = \Phi^{-1}\left(F_i\left(Z_i\right)\right) \quad i = 1,2, \ldots, n \tag{23.16}$$

The limit state surface $g(Z)=0$ in Z space is transformed into a corresponding limit state surface $g(u)=0$ in U space. In a next step, the design point has to be determined in U space. This points lies on $g(u)=0$, and is the point in the failure set with the largest probability density, that is, the closest point on the failure surface to the origin of the U space. An interactive procedure is applied to find the design point $\mathbf{u}^*$, which is expressed as

$$\mathbf{u}^* = \beta\boldsymbol{\alpha}^* \tag{23.17}$$

in which β is the first order reliability index, or the distance between the design point and the origin. The unit normal vector $\boldsymbol{\alpha}^*$ to the failure surface at $\mathbf{u}^*$ are calculated by

$$\boldsymbol{\alpha}^* = -\frac{\nabla g(\mathbf{u}^*)}{\left|\nabla g(\mathbf{u}^*)\right|} \tag{23.18}$$

where $\nabla g(u)$ is the gradient vector. The actual limit state surface $g(u)=0$ is then approximated by its tangent hyperplane, which has the equation at the design point $\mathbf{u}^*$ as

$$g(\mathbf{u}) = \beta + \boldsymbol{\alpha}^T \mathbf{u} = 0 \tag{23.19}$$

The first order safety margin M is defined as

$$M = g(U) = \beta + \boldsymbol{\alpha}^T U \tag{23.20}$$

The corresponding approximation to the failure probability is

$$P_f \approx \Phi(-\beta) \tag{23.21}$$

From the above descriptions of FORM, it is seen that FORM is to approximate the failure set through replacement of the limit state surface in u-space by its tangent hyperplane at the design point, as defined by Eq. (23.19). Figure 23.3 illustrates this method.

This is the first order approximation to the failure probability P_f, and β is the corresponding first order approximation to the reliability index. The accuracy of the estimate depends upon how well the true failure surface is represented by the linear approximation, and may usually be improved by SORM, which described in the following sub-section. The problem which affects the accuracy most is that FORM may not be able to find the global design point in cases of multiple design points.
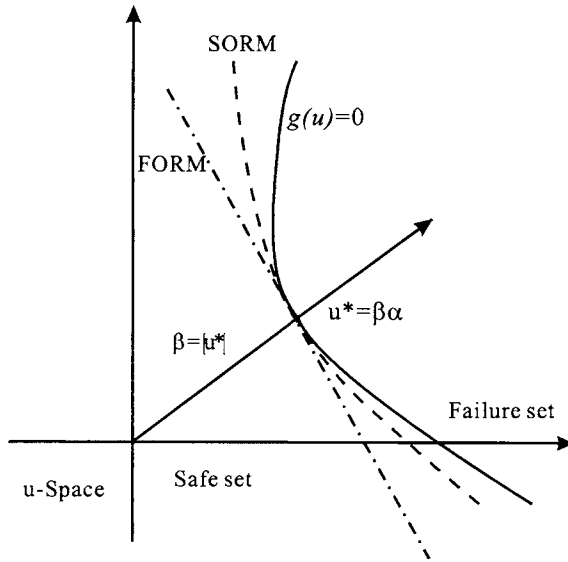
Figure 23.3   Illustration of FORM and SORM

23.3.5 Calculation by SORM

In the second order reliability method (SORM), the limit state surface is approximated by a hyperparaboloid with the same tangent hyperplane and the main curvatures at the design point. An approximation to the failure probability is then

$$
P_{f,SORM} \approx \Phi(-\beta)\prod_{j=1}^{n-1}\left(1-\beta_{k_j}\right)^{-1/2} +\left[\beta\Phi(-\beta)-\phi(\beta)\right]\left\{\prod_{j=1}^{n-1}\left(1-\beta_{k_j}\right)^{-1/2} - \prod_{j=1}^{n-1}\left(1-(\beta+1)_{k_j}\right)^{-1/2}\right\} +
$$
$$
(\beta+1)\left[\beta\Phi(-\beta)-\phi(\beta)\right]\left\{\prod_{j=1}^{n-1}\left(1-\beta_{k_j}\right)^{-1/2} - \mathrm{Re}\left\{\prod_{j=1}^{n-1}\left(1-(\beta+i)_{k_j}\right)^{-1/2}\right\}\right\}
$$

(23.22)

where i in the third term is the imaginary unit, Re() denotes the real part, and k_j (j=1,2,...,n-1) are the principal curvatures at the design point. The first term is the asymptotic result for $\beta\to\infty$

Using SORM, an equivalent hyperplane can be defined as a linear approximation to the true failure surface with a reliability index

$$
\beta_{SORM} = -\Phi^{-1}\left(P_{f,SORM}\right)
$$

(23.23)

The unit normal vector α_{SORM} is, in practice, approximately set equal to that obtained by FORM.

In SORM, the limit state surface is approximated by a curvature fitted hyperparaboloid at the design point u^*, as sketched in Figure 23.3 above. Compared SORM with FORM, the estimate accuracy has been improved by second order approximation.

23.4 Component Reliability

The concepts introduced in Section 23.3 are mainly for the reliability evaluation at component level, which means that the concern is on the failure probability for problems modeled by a single limit state function. A component reliability is the basis for structural reliability analysis since all marine structures are composed of components.

23.5 System Reliability Analysis

23.5.1 General

This section deals with the formulation and evaluation of the failure probability in the problems where more than one limit state function must be considered, i.e. system reliability analysis.

A system is generally composed of many elements where each element may have one or more failure modes described by their individual limit state functions. Moreover, a system may have many failure modes, where each system failure mode may be due to the failure of one element only or due to the failure of several elements jointly.

Series and parallel systems are the two fundamental types of systems from which any system can be built.

23.5.2 Series System Reliability

A system is called series system if the system is in a state of failure whenever any of its elements fails. Such systems are often referred to as weakest-link systems. A typical example of this is the marine pipeline or risers.

The failure probability of a series system can be formulated as the probability of union of failure events. For a system with m failure elements defined by their safety margins M_l, the probability of failure can be formulated as

$$
\begin{aligned}
P_{f,sys} &= P\left[\bigcup_{i=1}^{m}(M_i \leq 0)\right] = P\left[\bigcup_{i=1}^{m}(\beta_i - \alpha_i^T u)\right] \\
&= 1 - \Phi_m(\beta, \rho)
\end{aligned}
\tag{23.24}
$$

where, Φ_m is the m-dimensional standard normal distribution function, $\beta=[\beta_1, \beta_2 \ldots]$ is the vector of reliability indices for the m failure elements, and ρ is the corresponding correlation matrix.

To demonstrate the reliability calculation of series system, an example is given in Section 23.11.

23.5.3 Parallel System Reliability

A parallel system fails when all elements in the system fail. For a parallel system all elements have to fail for system failure to occur. The failure probability can be formulated as the intersection of the element failure events

$$P_{f,sys} = P\left[\bigcap_{i=1}^{m} (M_i \leq 0)\right] = P\left[\bigcap_{i=1}^{m} (\beta_i - \alpha_i^T u)\right]$$
$$= \Phi_m(-\beta, \rho) \tag{23.25}$$

It is seen from the above tow equations that the evaluation of the failure probability of series and parallel systems amounts to evaluation of the standard multi-normal integral. This is however a difficult task for problems of large dimensions.

To demonstrate the reliability calculation of a simple parallel system, an example is given in Section 23.11.

23.6 Combination of Statistical Loads

23.6.1 General

In general, loads can be grouped into the following three classes based on statistical characteristics of their form and history

- Time-invariant loads: e.g. dead loads
- Random loads: e.g. wave loads
- Transient random loads: e.g. earthquake loads

When two or more random loads acting on the structures, the combination of statistical loads must be considered based on the statistical characteristics of individual loads.

For instance, the primary types of load combinations for ship structures are:

- Hull girder loads
- Hull girder loads and local pressure
- Hull girder loads and transient loads

A simple load combination problem can be expressed as, e.g. for hull girder collapse

$$M_t(t) = M_s(t) + M_w(t) \tag{23.26}$$

where,

   $M_t(t)$ = total bending moment acting ship hull girder;

   $M_s(t)$ = still water bending moment;

   $M_w(t)$ = vertical wave bending moment;

In most of the current ship design Rules, the peak coincidence method for the combination of still water bending moment and vertical wave bending moment is applied as follows

$$M_{t,max}(t) = M_{s,max}(t) + M_{w,max}(t) \tag{23.27}$$

This is based on the very conservative assumptions that the maximum values of the two bending moments occur simultaneously.

However, the combination of statistical loads is fairly complex and a number of methods have been derived to solve this problem. Here, only the application of Turkstra's rule (Turkstra, 1972) and the Ferry Borges-Castanheta (1971) model are presented.

23.6.2 Turkstra's Rule

The loading processes may be searched for some defined maximum in a systematic manner. A procedure proposed by Turkstra (1972) has found its way into practice. It is based on a combination model for stationary random process. Its principle is that when one random load achieves its maximum value in time T, the transient values of other loads can be used to form the maximum load combination value. Assuming the random loads are represented by $S_i(t)$, the load combination is S(t), i.e.

$$S(t) = \sum_i S_i(t) \tag{23.28}$$

Then, the maximum value of S(t) can be expressed as

$$S_M = \max_{t \in T} S(t) = \max_{t \in T} \left[\max_{t \in T} S_i(t) + \sum_{j=1}^{n} S_j(t) \right] \tag{23.29}$$

Where, max $S_i(t)$ is the maximum value of $S_i(t)$ in time T and $S_j(t)$ is the transient value of other random loads.

It should be noted that different load combinations shall be performed for Eq. (23.29) to derive the maximum value.

23.6.3 Ferry Borges-Castanheta Model

Ferry Borges-Castanheta (FBC) model (Ferry-Borges, 1971) represents each individual stochastic process in the form of a series of rectangular pulses as shown in Figure 23.4 below. The value of such a pulse represents the intensity of the load. The duration of the pulse remains constant within the series. This time interval is chosen such that the pulses can be considered as independent repetitions of the respective actions.
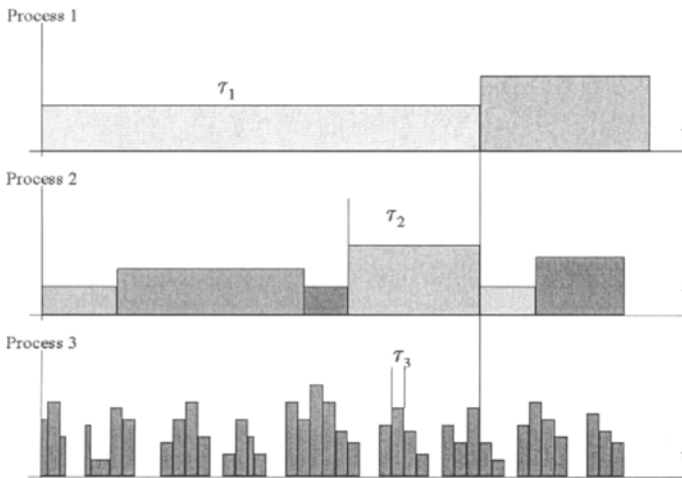
Figure 23.4   Illustration of FBC Model

Time intervals of different processes are chosen such that the longer interval is an integer multiple of the next shorter one, valid for all processes involved. This is a prerequisite for easy calculation of the maximum value distribution of the combination of two processes because pulse of the shorter step process are repeated exactly n-times within the pulse duration of the longer step one.

Consider the case where three load processes X_1, X_2, and X_3 are acting on a marine structure. The FBC load model then considers a new variable of the maximum of X_3 within an interval τ_2 together with X_2. This variable, in turn, is searched for its maximum during an interval τ_1 and added to X_1. From this, finally, the maximum during the life time T is considered as the variable representing all three processes together.

The variable Y representing the maximum combined loads of the three processes thus may be written as follows

$$Y = \max_{T}\left\{ X_1 + \max_{\tau_1}\left(X_2 + \max_{\tau_2} X_3 \right)\right\} \tag{23.30}$$

Herein, the X_I represents the load distribution. The terms max X_I represents the maximum values of the random variable X_I within the period τ_I or T, respectively.

23.7 Time-Variant Reliability

Marine structures can be subjected to time-varying loads, e.g. wind loads. Structural strength may also present a time-varying behavior, e.g. deterioration of component strength due to corrosion attacks. The basic variables that are related to these time-dependent values are stochastic processes. The reliability problem becomes time-variant, as defined by,

Set of basic stochastic processes: $X(t) = \{X_1(t), X_2(t), \cdots, X_n(t)\}$

Joint distribution function of X(t): $F_{X(t)}(X(t),t)$

Limit state surface: $g(x(t))=0$

The main interests in time-variant reliability problem lies in the time t of the first passage from the safe domain, g(x(t))>0, to the failure domain, $g(x(t)) \le 0$, during the life of the structure, $t \in [0,T]$, as illustrated in Figure 23.5 below. T is the design life of the marine structure or the reference period for the reliability analysis. The time t for the first excursion $g(x(t)) \le 0$ is called time to failure and it is also a random variable.

The probability of occurrence of $g(x(t)) \le 0$ during the design life of the marine structures, T, is called first-passage probability. This probability may be considered equivalent to the failure probability $p_f(t)$ during a given period [0,t], defined by (Melchers, 1999).
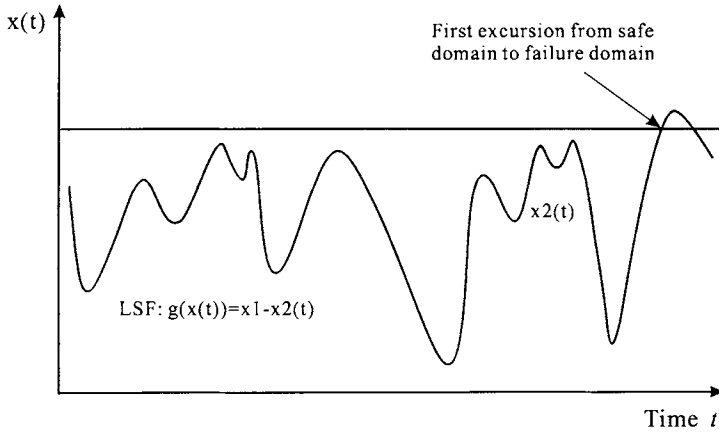
Figure 23.5   Time Variant Reliability

$$p_f(t) = 1 - P[N(t) = 0 \cap g(x(0)) > 0] \tag{23.31}$$

or

$$p_f(t) = 1 - P[N(t) = 0 | g(x(0)) > 0] \cdot P[g(x(0)) > 0] \tag{23.32}$$

where, N(t) is the number of out-crossing in the interval [0,t]. Out crossings are the excursions from safe domain to failure domain.

For marine structural analysis, stochastic load processes are often replaced by time-invariant random variables to represent the lifetime loads. This also applies to cases of simultaneous random loads. The combined extreme load needs to be determined appropriately since the respective maximum values of different load processes do not necessarily occur simultaneously. This depends upon the application of methods of load combination as described in the above subsection.

23.8 Reliability Updating

Reliability methodology can be used as a tool to reassess structural integrity. Such reassessment is required, e.g. when the inspection results are available or design conditions are changed. New measures of structural reliability are achieved based on new information. The information can be grouped in two classes

- Sampling of quantities
- Observations

To demonstrate the reliability updating, a component with load S and strength R is taken as an example. The failure probability is

$$P_f = P[R - S \le 0] = \int_{-\infty}^{\infty} F_R(s) f_s(s) ds \tag{23.33}$$

Assuming that the component is subject to proof load, q^* and that it survives the load. This implies that the strength r≥q*.

The updating of P_f can be formed as follows

$$P_{f,up} = P\left[R - S \le 0 \middle| R \ge q^*\right]$$
$$= P\left[R - S \le 0 \middle| H \ge 0\right] \tag{23.34}$$
$$= \frac{P\left[R - S \le 0 \cap H \ge 0\right]}{P\left[H \ge 0\right]} = \frac{P\left[R - S \le 0 \cap -H \le 0\right]}{P\left[-H \le 0\right]}$$

where, $H = R - q^*$

In general, different methods are available to update the structural reliability based on the new information. Song and Moan (1998), Moan and Song (1998) presented the methods of reliability updating for ships and jackets, which will be detailed in Part IV Chapter 27.

23.9 Target Probability

23.9.1 General

Guidelines are provided for structural designers on acceptable failure probability associated with each failure mode, i.e. minimum acceptable reliability index β_0, frequently referred to as target probability. When carrying out structural reliability analysis, an appropriate safety level should be selected based on factors like consequence of failure, relevant design codes, accessibility to inspection and repair, etc. Target probability levels have to be met in design in order to ensure that certain safety levels are achieved.

23.9.2 Target Probability

A design is safe if

$$\beta > \beta_0 \tag{23.35}$$

where β_0 = target safety index

   β = safety index as estimated from analyses

The regulatory bodies or classification societies and/or professions agree upon a reasonable value. This may be used for novel structures where there is no prior history.

Code calibration is to calibrate reliability levels that are implied in currently used codes. The level of risk is estimated for each provision of a successful code. Safety margins are adjusted to eliminate inconsistencies in the requirements. This method has been commonly used for rules development.

Target probabilities are chosen to minimize total expected costs over the service life of the structure. A cost-benefit analysis approach may be used effectively to define target probability for design in which failures result in only economic losses and consequences. Although this method is logical on an economic basis, a major shortcoming is its need to measure the value of human live.

The target probabilities, for a reliability based design, are based calibrated values of implied safety levels in the currently used design practice, as shown, e.g. by Bai et al (1997). The argument behind this approach is that a code represents a documentation of an accepted

practice. Therefore, it can be used as a launching point for code revision and calibration. Any adjustments in the implied safety levels should be for the purpose of creating consistency in reliability among the resulting designs according to the reliability-based code.

23.9.3 Recommended Target Safety Indices for Ship Structures

Recommended target safety levels for hull girder (primary), stiffened panel (secondary) and unstiffened plate (tertiary) modes of failure and the corresponding notional probabilities of failure are summarized in the table below (Mansour, 1997). It should be pointed out the values of the target safety index are also dependent on the methods used to calibrate the reliability levels.

Table 23.2   Recommend Target Safety Indices for Ship Structures

Failure Mode	Commercial Ships	Naval Ships
Primary (initial yield)	5.0 (2.97E-7)	6.0 (1.0E-9)
Primary (ultimate)	3.5 (2.3E-4)	4.0 (3.2E-5)
Secondary	2.5 (6.2E-3)	3.0 (1.4E-3)
Tertiary	2.0 (2.3E-2)	2.5 (6.2E-3)

23.10 Software for Reliability Calculations

The following is a few selected computer programs for the calculation of structural reliability,

PROBAN: A probabilistic analysis tools for general structures developed by DNV. It is part of the SESAM packages.

STRUREL: A general structural reliability analysis software including component reliability calculation (COMREL), system reliability calculation (SYSREL), statistical analysis of reliability data (STAREL), etc., developed by RCP consulting group in Germany.

ISPUD: Specially designed for structural reliability calculation by use of Monte Carlo Simulation.

CALREL: A general structural reliability software developed by U.C. Berkeley. Its capabilities include: a) failure probability estimate for components; b) failure probability estimate for systems; c) FORM and SORM analysis; d) direct MCS analysis and e) sensitivity analysis.

23.11 Numerical Examples

23.11.1 Example 23.1: Safety Index Calculation of a Ship Hull

Problem

The sketch in Figure 23.6 shows the probability density functions (PDF) of the load and strength of ship hull girder in terms of applied bending moment and ultimate moment capacity of the hull, respectively. Both the load S and the strength R are

assumed to follow normal probability distribution with mean value μ_S=20,000 ft-ton and μ_Z=30,000 ft-ton, respectively, and standard deviations of σ_Z=2,500 ft-ton and σ_S=3,000 ft-ton, respectively. What is failure probability for the hull?

Solution

The reliability index, β, may be estimated using Cornell safety index method:

$$\beta = \frac{\mu_R - \mu_S}{\sqrt{\sigma_R^2 + \sigma_S^2}}$$

Substituting in the numerical values for μ_R, μ_S, σ_R and σ_S, we may get

$$\beta = \frac{30000 - 20000}{\sqrt{2500^2 + 3000^2}} = 2.56$$

The corresponding failure probability is

$$P_f \quad = \quad 5.23*E\text{-}3$$
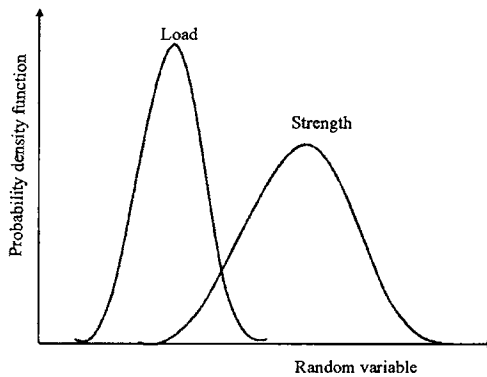
Figure 23.6   Load and Strength Probability Density Functions

23.11.2 Example 23.2: β Safety Index Method

Problem

Assuming the random variables R and S are corresponding to the bending moments of a ship hull girder with normal distributions. The mean value and standard deviations of R and S are μ_R=150, σ_R=20 and μ_S=90, σ_S=30 respectively. What is the β index value and P_f using Hasofer Lind method?

Solution

The limit state function can be formed as

g(Z)=R-S

Based on Eqs. (23.12) and (23.13), the random variables R and S can be expressed using variables in standard normal space as

R=20*U_1+150

S=30*U_2+90

Then, the limit state function can be reformed as

G(Z)=20U_1-30U_2+60

The distance of the straight line from the origin of coordinates can be quickly calculated as

$$\beta = \frac{60}{\sqrt{20^2 + (-30)^2}} = 1.664$$

Using the standard normal distribution table (Table 23.1), the probability of failure can be estimated as

$$P_f = \Phi(-\beta) = \Phi(-1.664) = 4.9\%$$

23.11.3 Example 23.3: Reliability Calculation of Series System

Problem

Considering a simple structure as shown in the figure. Assuming the capacity of component 1 and 2 are R_1=1.5R and R_2=R respectively, the acting load, P, and resistance, R, following independent normal distributions with the following characteristics

μ_P=4 kN, σ_P =0.8 kN

μ_R=4 kN, σ_R =0.4 kN
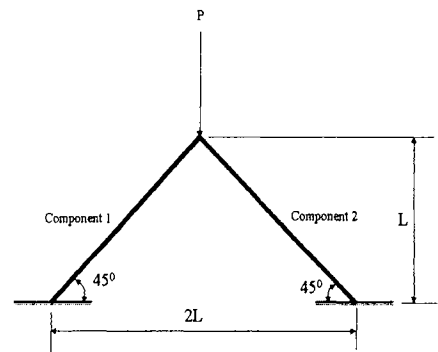
Figure 23.7 Reliability of Series System

What is the probability of failure for this system?

Solution

The LSFs of component 1 and 2 can be formulated as

$$g_1(Z) = \frac{3}{2}R - \frac{\sqrt{2}}{2}P$$

$$g_2(Z) = R - \frac{\sqrt{2}}{2}P$$

To normalize the random variables in above equations, the followings can be formed

$$x_1 = \frac{R-4}{0.4}$$

$$x_2 = \frac{P-4}{0.8}$$

Based on the β index method described in section 23.3.3 and Example 23.2, the followings can be obtained,

$$Z_1 = 0.728x_1 - 0.686x_2 + 3.846$$
$$Z_2 = 0.577x_1 - 0.816x_2 + 1.691$$

Accordingly, the reliability index of component 1 and 2 are estimated as

β_1=3.846

β_2=1.691

The corresponding probabilities of failure are obtained as

$$P_{f,1} = \Phi(-\beta_1) = 0.00006$$

$$P_{f,2} = \Phi(-\beta_2) = 0.04794$$

The failure probability of the system is approximated by

$$\max P_{f,i} \le P_{f,sys} \le \sum P_{f,i}$$

Hence,

$$0.04794 \le P_{f,sys} \le 0.04800$$

Besides, the correlation coefficient of Z_1 and Z_2 is obtained as

$$\rho = \sum a_i b_i = 0.728 \times 0.577 + 0.686 \times 0.861 = 0.98$$

For this system, the correlation coefficient is nearly equal to 1. Accordingly, the failure probability of the system $P_{f,sys}$ is equal to the lower bound approximately, i.e.

$P_{f,sys}$=0.04794

23.11.4 Example 23.4: Reliability Calculation of Parallel System

Problem

Assume that a structure is composed of 4 parallel components, their corresponding reliability index are, β_1=3.57, β_2=3.41, β_3=4.24 and β_4=5.48 respectively. What are the bounds of the failure probably of the parallel system?

Solution

The failure probability of each component can be estimated as

$$P_{f,1} = \Phi(-\beta_1) = 1.7849 \times 10^{-4}$$

$$P_{f,2} = \Phi(-\beta_2) = 3.2481 \times 10^{-4}$$

$$P_{f,3} = \Phi(-\beta_3) = 1.1176 \times 10^{-5}$$

$$P_{f,4} = \Phi(-\beta_4) = 2.1266 \times 10^{-8}$$

For a parallel system, the following bounds exist

$$\prod P(Q_i) \le P_{f,sys} \le \min P(Q_i)$$

Hence, the simple bounds of this parallel system can be estimated as

$$1.3779 \times 10^{-20} \le P_{f,sys} \le 2.1266 \times 10^{-8}$$

and corresponding bounds of the reliability index can be obtained as

$$5.48 \le \beta_{sys} \le 9.23$$

It should be noted that in general, the bound values given by the equation above for parallel system is too wide.

23.12 References

1. Ang, S.H. and Cornell, C.A. (1974), "Reliability Bases of Structural Safety and Design", Journal of Structural Engineering, ASCE, Vol. 100, No. 9, pp. 1755-1769.

2. Ang, A.H.-S and Tang, W. (1975, 1984), "*Probability Concepts in Engineering Planning and Design*, Volume I & II", John Wiley and Sons, New York.

3. Bai, Y., Xu, T. and Bea, R. (1997), "Reliability-Based Design and Requalification Criteria for Longitudinally Corroded Pipes", ISOPE-1997.

4. Cornell, C.A. (1969), "A Probability-Based Structural Code", ACI-Journal, Vol. 66, pp. 974-985.

5. Ferry-Borges, J and Castrnheta, M. (1971), "Structural Safety", Laboratoria Nacional de Engenhera Civil, Lisbon

6. Hasofer, A.M. and Lind, N.C. (1974), "An Exact and Invariant First Order reliability Format", ASCE J. Eng. Mech. Div., pp.111-121.

7. Madsen, H.O., et al (1986), "*Methods of Structural Safety*, Prentice-Hall, Inc., Englewood Cliffs

8. Mansour, A. E., et al (1997), "Assessment of Reliability of Ship Structures", SSC-398. Ship Structures Committee.

9. Melchers, R.E. (1999), "*Structural Reliability Analysis and Prediction*", 2nd Edition, John Wiley & Sons Ltd.

10. Moan, T. and Song, R. (1998), "Implication of Inspection Updating on System Fatigue Reliability of Offshore Structures", the *Proc. 17th OMAE*, Lisbon, Portugal, 1998

11. RCP Consult (1996), "STRUREL - *A Structural Reliability Analysis Program System,*" Munchen, Germany.

12. Schnerder, J. (1997), *"Introduction to Safety and Reliability of Structures"*, Structural Engineering Documents Vol. 5, International Association for Bridge and Structural Engineering (IABSE).

13. Song, R. and Moan, T. (1998), "Fatigue Reliability of Large Catamaran Considering Inspection Updating", Proceeding of the 8th International Offshore and Polar Engineering Conference (ISOPE'98), Montreal, Canada, May, 1998.

14. Thoft-Christensen, P. and Baker, M.J., (1982), *"Structural Reliability, Theory and Its Applications"*, Springer-Verlag.

15. Turkstra, C.J. (1972), "Theory of Structural Design Decisions", Study No. 2, Solid Mechanics Division, University of Waterloo, Canada.

Part IV

Structural Reliability

Chapter 24   Random Variables and Uncertainty Analysis

24.1 Introduction

Strictly speaking, all the variables in the engineering structures are stochastic to a certain degree. Structural reliability analysis deals with the rational treatment of random variables and uncertainties in the structural engineering design, inspection, maintenance and decision making.

This Chapter presents the basics of statistical description of random variables that are the foundation for reliability analysis. Measures of uncertainties are discussed, loads and capacity of ship structures are used to illustrate the uncertainty analysis. Further reading is referred to Ang and Tang (1975), Benjamin and Cornell (1970), Thoft-Christensen and Baker (1982), Mansour (1997) and Melchers (1999).

24.2 Random Variables

24.2.1 General

Marine structures are subjected to loads that are random in nature, such as wave, current and wind actions. It is not possible to forecast deterministically, e.g. the height and direction of the next single wave that will act on the structures. Neither it is possible to predict deterministically the structural response to those actions for a certain coming instant.

Random variables may be used to describe the uncertainties in the basic variables such as spatial and time variation of external loads, material properties, dimensions, etc. In practice, these variables are basic in the sense that they are the most fundamental quantities used by engineers and analysts in structural analysis and design. For instance, the yield stress of steel can be considered as a basic random variable for the purposes of structural reliability analysis. It should be mentioned that it is generally impracticable to obtain sufficient statistical data to model the variations in the loads and strength for structures. Reliance must be placed on the ability of the analyst to synthesize this higher level information when required.

24.2.2 Statistical Descriptions

A random variable X is a real function defined on a sample space. For every real number x there exists a probability $P[X \leq x]$. A realization x of the random variable X is any outcome of the random phenomenon X. In this Section, the random variables are denoted by capital letters and the corresponding small letters denote their realizations.

A random variable is characterized by its probability density function p*(x)* and its cumulative distribution function $F_X(x) = P[X \leq x]$. The random variable is often described by its statistical description, namely mean (or expected) value and variance (or standard deviation), that are defined below

The *n-th moment*:

$$\mu_n = E[X^n], \quad n = 1,2,3,...$$
(24.1)

The *n-th central moment*:

$$\varsigma_n = E[(X - \mu_1)^n]$$
(24.2)

where,

μ_1 = mean (or expected) value of X

$\varsigma_2 = Var[X] =$ variance of X

$\sigma_X = \sqrt{\varsigma_2}$ = standard deviation of X

The mean value is the center of gravity of the probability density function. The standard deviation is a measure of the dispersion around the mean value. The coefficient of variation (CoV) is an uncertainty measure for the random variable X, which is defined by

The following non-dimensional values of the central moments may be defined.

Coefficient of variance: $CoV = \dfrac{\sqrt{\varsigma_2}}{\mu_1}$
(24.3)

Skewness: $\gamma_1 = \dfrac{\varsigma_3}{\varsigma_2^{3/2}}$
(24.4)

Kurtosis: $\gamma_2 = \dfrac{\varsigma_4}{\varsigma_2^2}$
(24.5)

24.2.3 Probabilistic Distributions

A random variable may be described by its cumulative distribution function. Some distributions models are of special interests for stochastic and reliability analysis of marine structures. These models are normal distribution, the lognormal distribution, the Rayleigh distribution and the Weibull distribution, which are detailed below. Melchers (1999) also defined other types of distribution function such as Poison, gamma, Beta, extreme value distribution type I, II, III etc.

Normal (or Gaussian) Distribution

The probability density function and its cumulative distribution function for the normal distribution are defined by

$$p(x) = \frac{1}{\sqrt{2\pi}\sigma_X} \exp\left[-\frac{1}{2}\left(\frac{x - \mu_X}{\sigma_X}\right)^2 \right] \qquad \text{for} \quad -\infty \leq x \leq \infty$$
(24.6)

$$F_X(x) = \frac{1}{\sqrt{2\pi} \int_{-\infty}^{s} \exp\left(-\frac{1}{2}v^2\right) dv} \qquad \text{for} \quad -\infty \le x \le \infty \qquad (24.7)$$

where $s = (x-\mu_X)/\sigma_x$. When $\mu_X = 0$, $\sigma_X = 1$, the normal distribution is called Standard Normal Distribution.

Lognormal Distribution

The probability density function and its cumulative distribution function for the lognormal distribution are defined by

$$p(x) = \frac{1}{\sqrt{2\pi} x \sigma_{\ln X}} \exp\left[-\frac{1}{2}\left(\frac{\ln(x) - \mu_{\ln X}}{\sigma_{\ln X}}\right)^2\right] \qquad \text{for} \quad x \ge 0 \qquad (24.8)$$

$$F_X(x) = \Phi\left(\frac{\ln(x) - \mu_{\ln X}}{\sigma_{\ln X}}\right) \qquad \text{for} \quad x \ge 0 \qquad (24.9)$$

where the mean value and standard deviation are given by

$$\mu_X = \exp\left(\mu_{\ln X} + \frac{\sigma_{\ln X}^2}{2}\right) \qquad (24.10)$$

$$\sigma_X = \sqrt{\mu_X^2 \left[\exp\left(\sigma_{\ln X}^2\right) - 1\right]} \qquad (24.11)$$

Rayleigh Distribution

The Rayleigh distribution is defined by

$$p(x) = \frac{(x-u)}{\alpha^2} \exp\left[-\frac{1}{2}\left(\frac{x-u}{\alpha}\right)^2\right] \qquad \text{for} \quad x \ge u \qquad (24.12)$$

$$F_X(x) = 1 - \exp\left[-\frac{1}{2}\left(\frac{x-u}{\alpha}\right)^2\right] \qquad \text{for} \quad x \ge u \qquad (24.13)$$

where

u = location parameter

α = scale parameter

The mean value and standard deviation are given by

$$\mu_X = u + \alpha\sqrt{\frac{\pi}{2}} \qquad (24.14)$$

$$\sigma_X = \alpha\sqrt{\frac{4-\pi}{2}} \qquad (24.15)$$

Weibull Distribution

The Weibull distribution is defined by

$$p(x) = \frac{(x-u)^{\lambda-1}}{\alpha^{\lambda}} \lambda \exp\left[-\left(\frac{x-u}{\alpha}\right)^{\lambda}\right] \qquad \text{for } x \geq u \qquad (24.16)$$

$$F_X(x) = 1 - \exp\left[-\left(\frac{x-u}{\alpha}\right)^{\lambda}\right] \qquad \text{for } x \geq u \qquad (24.17)$$

where

u = location parameter

α = scale parameter

λ = shape parameter

The mean value and standard deviation for the Weibull distribution are defined by

$$\mu_X = u + \alpha\Gamma\left(1 + \frac{1}{\lambda}\right) \qquad (24.18)$$

$$\sigma_X = \alpha\sqrt{\Gamma\left(1 + \frac{2}{\lambda}\right) - \Gamma^2\left(1 + \frac{1}{\lambda}\right)} \qquad (24.19)$$

24.3 Uncertainty Analysis

24.3.1 Uncertainty Classification

For the purpose of reliability analysis, the uncertainties may be classified as

- Inherent uncertainty
- Measurement uncertainty
- Statistical uncertainty
- Model uncertainty

Inherent Uncertainty

Inherent uncertainty is also known as fundamental or physical uncertainty. It is a natural randomness of a quantity, such as the variability in wave and wind loading. The uncertainty source cannot be reduced by more information. These uncertainties are the results of natural variability inherent in physical wave and wind processes, or man-made processes. For instance, the variability of wave height for a sea state with a given significant wave height and period, is fundamentally random. Also, the occurrence of sea states, characterized by Hs and Ts is fundamentally random. Examples of man-made phenomena that are fundamentally random are functional loads on structures and structural resistance. Contrary to natural processes, man-made processes can be influenced by human intervention, by QA/QC of human activities and the fabricated structure itself.

Measurement Uncertainty

This uncertainty is caused by imperfect instruments and sample disturbance when observing a quantity by some equipment. This uncertainty source can be reduced by more information.

Statistical Uncertainty

Statistical uncertainty is due to limited information such as a limited number of observations of a quantity. Clearly, this uncertainty can be reduced by obtaining more information.

The statistical uncertainty associated with limited data is represented by applying statistical methods. Data may be collected for the selection of an appropriate probability distribution type, and determination of numerical values for its parameters. In practice very large samples are required to select the distribution type, and to reliably estimate the numerical values for its parameters. For a given set of data, therefore, the distribution parameters may themselves be considered to be random variables, whose uncertainty is dependent on the amount of sample data and any prior knowledge.

Model Uncertainty

Model uncertainty is the uncertainty due to imperfections and idealizations made in physical model formulations for load and resistance as well as in choices of probability distribution types for representation of uncertainties.

With very few exceptions, it is rarely possible to make highly accurate predictions about the magnitude of the response of typical structures to loading even when the governing input quantities are known exactly. In other words, the structural response contains a component of uncertainty in addition to those arising from uncertainties in the basic loading and strength variables. This additional source of uncertainty is termed model uncertainty and occurs as a result of simplifying assumptions, unknown boundary conditions and as a result of the unknown effects of other variables and their interactions which are not included in the model.

Model uncertainties can be assessed by comparisons with other more refined methods, or test results and in-service experiences. Assuming that the true value X_{true} is observed in service or in a laboratory test and the predicted value is X_{pred}, the model uncertainty B is then defined by

$$B = \frac{X_{true}}{X_{pred}} \qquad (24.20)$$

By making many observations and corresponding predictions, B can be characterized probabilistically. A mean value not equal to 1.0 expresses a bias in the model. The standard deviation expresses the variability of the predictions by the model. In many cases the model uncertainties have a large effect on structural reliability and should not be neglected.

24.3.2 Uncertainty Modeling

Variables whose uncertainties are judged to be important, e.g. by experience or by sensitivity study, shall be represented as random variables. The corresponding probability distributions can be defined based on statistical analyses of available observations of the individual variables, providing information on their mean values, standard deviations, correlation with other variables and in some cases also their distribution types, as presented in Section 24.2 in this Chapter. In some cases, the correlation between variables exists, e.g. the two parameters used to describe Weibull long-term stress distribution.

24.4 Selection of Distribution Functions

The probability distribution function for a random variable is most conveniently given in terms of a standard distribution type with some distribution parameters. Regressions of available observations of a quantity will not always given enough information to allow for interpretation of the distribution type for the uncertain quantity and a choice of the distribution type has to be made. The results of a reliability analysis may be vary sensitive to the tail of the probability distribution, so a proper choice of the distribution type will often be crucial. Mean and standard deviations are normally obtained from recognized data sources.

Normal or lognormal distributions are normally used when no detailed information is available. The lognormal distribution is used to describe load variables, whereas the normal distribution is used to describe resistance variables. However, a variable that is known never to take on negative values is normally assigned a log-normal distribution rather than a normal distribution. The following procedure may be applied for determination of the distribution type and estimation of the associated distribution parameters:

1. Based on experience from similar types of problems, physical knowledge or analytical results, choose a set of possible distribution.

2. Estimate the parameters in these distributions by statistical analysis of available observations of the uncertainty quantities. Regressions may be based on

    *   Moment estimators

    *   Least square fit methods

    *   Maximum likelihood methods

    *   Visual inspections of data plotted on probability paper

3. If there are several possible choices, the following technique can be used for acceptance or rejection of the selection of distribution functions.

    *   Visual identification by plot of data on probability paper or by comparison of moments

    *   Statistical tests e.g. Chi-square

    *   Asymptotic behavior for extreme value distributions

4. If two types of distributions given equally good fits, it is recommended, particularly for load variables, to choose the distribution that fits possible data observations in the tail better than the other.

When distributions are chosen using the above methods, it is important that such choices, including the steps leading to the choices, are satisfactorily documented.

24.5 Uncertainty in Ship Structural Design

24.5.1 General

The design of any structure by rational means involves consideration of the uncertainties that arise in regard to the external actions imposed on the structure as well as the strength and response properties of the structural elements. These different uncertainties can be taken into account by introducing probability concepts into the structural design procedure.

In the case of ship structural design, these concepts were introduced by St. Denis and Pierson when determining the ship motions, structural loads, etc. due to operating in a realistic random seaway. At about the same time, other work was being carried out in the area of probabilistic design of structures.

Freudenthal gave a basic application of the probabilistic approach to the safe design of engineering structures, and later he dealt specifically with marine structures. Others have considered the ship problem including Mansour (1972, 1997), Mansour and Faulkner (1973), Stiansen et al (1980), where the theory of structural reliability was applied to ships. Nikolaidis et al (1991, 1993) evaluated uncertainties in stress analysis of marine structures and presented a methodology for reliability assessment of ship structures.

Longitudinal strength analysis has been based mainly on elastic beam theory with emphasis on the maximum expected load (bending moment) and the minimum strength that provides a factor of safety against unspecified failure. It is possible to calculate the probability of failure if we can clearly and completely define a probability distribution for loads (demand) and for strength (capacity). The objective of this section is to discuss the uncertainties in loads (demand) and strength (capacity).

24.5.2 Uncertainties in Loads Acting on Ships

The principal loads acting on a ship's hull may be summarized as follows, with particular reference to longitudinal hull bending:

- Still-water bending moments resulting from uneven distribution of weights and buoyancy in still water.

- Quasi-static bending moments due to relatively long encountered waves.

- Dynamic bending moments caused by wave impacts or high-frequency wave forces.

- Thermal loads induced by uneven temperature gradients.

Other loads not mentioned in the above are internal loads caused by liquid cargoes, machinery or propellers, collision grounding and docking loads, aerodynamic and ice loads.

Quasi-static Wave Bending Moment

Quasi-static wave bending moment has been dealt with using the probabilistic approach, since the waves causing such bending moments could only be described statistically. A specific sea condition can be fully described by its directional spectrum, defining the component wave frequencies and directions present.

Uncertainties arise from:

- Variability in the directional properties of wave spectra, with only limited data available.

- Combined effects of two storms, or sea and swell.

- Variability of spectral shapes for a given significant height.

Referring to Part I Chapter 3, short-term response, can be calculated statistically by linear superposition of the calculated RAO (response amplitude operator) that is the amplitude of the ship response to a unit sinusoidal wave at a frequency. Uncertainties involved in the calculation of RAO'S are due to assumed linearity of response in relation to wave height, inaccuracy of strip theory and effect of variation in weight distribution on motions. In addition,

there are uncertainties in the statistics of response. The use of a simple Rayleigh distribution can result in a bias toward values that are too high in severe seas.

The operation of the ship may also contribute to the uncertainty of wave-induced bending moment, including:

- Cargo distribution and resulting drafts
- Ship headings to the sea
- Ship speed

Still-water bending moments

It is relatively easy to calculate still-water bending moments if the distribution of cargo and other weights is known. However, the still-water bending moments vary between voyages, and in any cases they are seldom recorded. Hence, very little statistical data are available. Estimates can be made on the basis of calculations customarily made for every new ship design

Load Combinations

Correlation exists between the loads discussed in the above. For example, high dynamic loads may often occur in rough seas when large low-frequency loads also occur, but high thermal effects may generally coincide with calm, sunny days when wave-induced loads are relatively mild. It is difficult to combine quasi-static and high-frequency wave-induced loads.

24.5.3 Uncertainties in Ship Structural Capacity

When considering structural failure, separate analyses are necessary for all possible failure modes such as

- Tensile failure
- Buckling and collapse
- Brittle fracture
- Fatigue

Buckling and collapse are an important subject because strength in buckling failure mode is much lower than the tensile failure mode. Brittle fracture failure has been controlled through improved material toughness and design of structural details, workmanship and use of crack stoppers to provide "fail-safe" design. Fatigue failure is an important subject even though fatigue cracks do not normally in themselves threaten the complete failure of the hull girder.

Ultimate failure is complicated by the fact that buckling may occur progressively in different segments of the structure and the first occurrence of a buckle does not usually constitute failure. Loads may successively transfer from buckled areas to those that are still effective.

The objective uncertainties are measurable and include:

- Main dimensions of hull
- Material properties including yield strength, ultimate strength and Young's modulus
- Variations in material thickness and shape dimensions.
- Manufacturing imperfections, including variations in fabrication tolerances, weld quality, alignment, and residual stresses in welds.

- Corrosion, wear and fatigue cracks, which involve "time-dependent strength"

It should be noted that all of the above involve physical uncertainties in the materials used or in the methods of ship construction. Uncertainties may also arise from methods of calculating structural responses, including the effect of boundary conditions, and variability in physical behavior of materials and structures.

The subjective uncertainties required judgement and include (Mansour and Faulkner, 1974):

- Shear lag and other shear effects (considered negligible).

- Major discontinuities; openings, superstructures.

- Torsional and distortional warping.

- "Poisson's ratio" effects, especially at transverse bulkheads and diaphragms.

- Stress redistribution arising from changes in stiffness due to deformations, inelasticity, or both.

- Gross–panel compression nonlinearities; effective width,' inelasticity, residual stresses and shake-out effects (considered negligible).

Other subjective uncertainties not mentioned in the above are residuary strength after ultimate strength of global panel, which may significantly affect ultimate strength and its variability.

24.6 References

1. Ang, A.H.-S and Tang, W. (1975, 1984), *"Probability Concepts in Engineering Planning and Design"*, Volume I & II, John Wiley and Sons, New York.

2. Benjamin, J. and Allin Cornell, C., (1970), *"Probability, Statistics and Decision for Civil Engineers"*, McGraw-Hill, Inc.

3. Mansour, A.E. (1972), "Probiblastic Design Concept in Ship Structural Safety and Reliability", Trans. SNAME, Vol. 80, pp. 64-97.

4. Mansour, A and Faulkner, D. (1973), "On Applying the Statistical Approach to Extreme Sea Loads and Ship Hull Strength", RINA Trans., Vol. 115, pp. 277-313.

5. Mansour, A. E., et al (1997), "Assessment of Reliability of Ship Structures", SSC-398. Ship Structures Committee.

6. Melchers, R.E. (1999), *"Structural Reliability Analysis and Prediction"*, 2nd Edition, John Wiley & Sons Ltd.

7. Nikolaidis, E. and Kaplan, P., (1991), "Uncertainties in Stress Analysis on Marine Structures", Ship Structure Committee Report SSC-363.

8. Nikolaidis, E. and Hughes, O.F., Ayyub, B.M., and White, G.J. (1993), "A Methodology for Reliability Assessment of Ship Structures", Ship Structures Symposium 93. SSC/SNAME, Arlington, VA, pp H1-H10.

9. Stiansen, S.G., Mansour, A.E., Jan, H.Y. and Thayamballi, A. (1980), "Reliability Methods in Ship Structures", J. of RINA.

10. Thoft-Christensen, P. and Baker, M.J., (1982), *"Structural Reliability, Theory and its Applications"*, Springer-Verlag.

This Page Intentionally Left Blank

Part IV

Structural Reliability

Chapter 25   Reliability of Ship Structures

25.1 General

Since researchers first began to apply probabilistic methods in the structural design of ships (Mansour, 1972, Mansour and Faulkner, 1973), a significant amount of achievement has been accomplished. The earliest applications of reliability methods to ship structures focused on overall hull girder reliability subjected to wave bending moments (Mansour, 1974, Stiansen et al., 1980, White and Ayyub, 1985, Guedes Soares, 1996). Recent work in applying reliability methods to the ultimate strength of gross panels using second moment methods (Nikolaidis, et al., 1993) has shown considerable promise. Casella and Rizzuto (1998) presented a second-level reliability analysis of a double-hull oil tanker. Frieze and Lin (1991) assessed reliability for ship longitudinal strength. There is still a continuing effort, which is looking at how these methods and procedures can be used in a system analysis.

There has been a tremendous amount of effort to develop statistical models for load effects (e.g., Guedes Soares and Moan, 1985, 1988, Ochi, 1978, Sikora et al., 1983, Mansour, 1987). Recent research includes the uncertainties associated with loads and load effects (Nikolaidis and Kaplan, 1991), and on loads and load combinations (Mansour et al, 1993).

FPSOs have been used worldwide as an economic solution for the development of offshore oil and gas. Actually many FPSOs are sited at locations with dynamic components of their loading that are less than those arising from unrestricted service conditions. The reliability of FPSO hull girders for the specific-site conditions are quite different with that of oil tanker for unrestricted service conditions. Therefore it is necessary to assess the reliability of FPSO hull girders in order to develop rational design criteria.

As the ocean-going cargo ships, the most catastrophic event of FPSOs is structural failure of hull girders due to extreme bending moments. During its service life, FPSO hull girders predominantly withstand stillwater and wave-induced bending moments. The former is caused by the action of the self-weight, the cargo or deadweight. The latter is a result from the wave action at the specific installation locations. The "Environmental Severity Factors(ESFs)" should be introduced in order to accounting for the specific-site conditions in the wave-induced bending moments (ABS 2000). Because the maximum values of the stillwater and wave-induced bending moments don't occur at the same instant, the stochastic combination method should be used in order to more rationally determine the maximum value of the combined load e.g. Guedes Soares (1990), Mansour (1994) and Wang et al (1996).

In carrying out the reliability assessment relating to the failure of progressive collapse, the limit state function is very complex and may only be expressed implicitly. Among of the methods available for solving such a problem, the response surface method is an effective and

powerful tool, in which the limit state function is approximated by a simple and explicit function at the sampling points, e.g. Bucher (1990) and Liu, et al, (1994).

This Chapter presents a methodology for the time-variant reliability assessment relating to the ultimate strength of the midsection for hull girders subjected to the structural degradations of corrosion and fatigue. It includes three aspects: (1) closed form equations for assessment of the hull girder reliability. (2) load effects and load combination, and (3) time-variant reliability. The progressive collapse analysis of hull girder strength used in the time-variant reliability is a modified Smith's method (Smith, 1977). The modification is to account for corrosion defect and fatigue crack, see Part II Chapter 13.

25.2 Closed Form Method for Hull Girder Reliability

For the vertical bending of the hull girder the limit-state function can be expressed by the following expression for sea going conditions,

$$g(X_i) = M_u - (M_{SW} + M_{WV}) \tag{25.1}$$

where,

M_u = ultimate vertical bending moment

M_{SW} = still water bending moment for sea going condition

M_{WV} = vertical wave bending moment for in sagging or hogging condition

Assuming these load and resistance variables follow normal distribution and have the same COV, we may obtained the following equation based on the Cornell safety index method, Eq. (23.6).

$$\beta = \frac{M_u - (M_{SW} + M_{WV})}{COV \cdot \sqrt{M_u^2 + M_{SW}^2 + M_{WV}^2}} \tag{25.2}$$

Moreover, taking into account the assumptions adopted for modeling of the random variables, Eq. (25.2) shows that the safety index for sea going conditions is inversely proportional to the COV. For an increase of the COV of 50%, the safety index is reduced by 35%.

The Cornell safety index method is also called the Mean Value First Order Second Moment (MVFOSM) concept, where the reliability index reliability index β is defined as the mean of the limit state function divided by its standard deviation.

The limit state function g and reliability index β for different failure modes are

a. For Hull Primary Failure

$$g = M_u - [M_S + k_w(M_w + k_d M_d)] \tag{25.3}$$

$$\beta = \frac{\mu_g}{\sigma_g} \tag{25.4}$$

where,

$$\mu_g = \mu_{M_u} - [\mu_{M_S} + k_w(\mu_{M_w} + k_d\mu_{M_d})] \tag{25.5}$$

$$\sigma_g = \sqrt{\sigma_{M_u}^2 + \sigma_{M_s}^2 + k_w^2 \sigma_{M_d}^2 + k_w^2 k_d^2 \sigma_{M_d}^2 + 2\rho_{M_w M_d} k_w k_d \sigma_{M_w} \sigma_{M_d}} \tag{25.6}$$

where

M_u	= ultimate strength
M_s	= still water bending moment
M_w	= wave bending moment
M_d	= dynamic bending moment
k_w	= load combination factor for still water and wave/dynamic moments
k_d	= load combination factor for wave and dynamic moments
μ_i	= mean of component i
σ_i	= standard deviation of component I

b. For Secondary and Tertiary Failure Mode

$$g = f_u SM - \left[M_s + k_w \left(M_w + k_d M_d \right) \right] \tag{25.7}$$

$$\beta = \frac{\mu_g}{\sigma_g} \tag{25.8}$$

where,

$$\mu_g = \mu_u \mu_{SM} - \left[\mu_{M_s} + k_w \left(\mu_{M_w} + k_d \mu_{M_d} \right) \right] \tag{25.9}$$

$$\sigma_g = \sqrt{\left(\sigma_u^2 \sigma_{SM}^2 + \sigma_u^2 \mu_{SM}^2 + \mu_u^2 \sigma_{SM}^2 \right) + \sigma_{M_s}^2 + k_w^2 \sigma_{M_d}^2 + k_w^2 k_d^2 \sigma_{M_d}^2 + 2\rho_{M_w M_d} k_w k_d \sigma_{M_w} \sigma_{M_d}} \tag{25.10}$$

where

SM	= section modulus
f_u	= ultimate stress
M_s	= still water bending moment
M_w	= wave bending moment
M_d	= dynamic bending moment
k_w	= load combination factor for still water and wave/dynamic moments
k_d	= load combination factor for wave and dynamic moments
μ_i	= mean of component i
σ_i	= standard deviation of component i

25.3 Load Effects and Load Combination

The following sections are based on Sun and Bai (2001) with some modifications. FPSOs hull girders are predominantly subjected to combining actions of stillwater and wave-induced bending moments. Still water bending moment (SWBM) is created from the action of the ship self-weight, the cargo or deadweight and the buoyancy. Differently from ocean-going cargo ships, the SWBM of an FPSO varies more frequently from one load condition to another due

to loading patterns and human action and needs to be considered as stochastic process in long term.

For an FPSO, a Poisson rectangular pulse process in time domain is applied to model the SWBM. Its cumulative distribution cab be fitted by a Raleigh distribution for the sagging condition and by an exponential distribution for the hogging conditions according to Wang, Jiao and Moan (1996), e.g.:

$$F_{M_s}(M_s) = 1 - \exp\left[-\ln(v_s T_0)\left(\frac{M_s}{M_{s,0}}\right)^2\right]$$ (25.11)

for sagging SWBM and

$$F_{M_s}(M_s) = 1 - \exp\left[-\ln(v_s T_0)\left(\frac{M_s}{M_{s,0}}\right)\right]$$ (25.12)

for hogging condition, where M_s is the SWBM of an individual load condition and v_s is the mean arrival rate of one load condition. The specified maximum SWBM in a design lifetime of $T_0 = 20$ years, $M_{s,0}$ is (IACS, 1995)

$$M_{s,0} = \begin{cases} -0.065 C_w L^2 B (C_B + 0.7) & \text{(sagging)} \\ C_w L^2 B (0.1225 - 0.015 C_B) & \text{(hogging)} \end{cases}$$ (25.13)

in which L, B and C_B are the ship length, breadth and block coefficient respectively, and C_w is the wave coefficient given by

$$C_w = \begin{cases} 10.75 - ((300-L)/100)^{3/2} & 100 < L \le 300 \\ 10.75 & 300 < L \le 350 \\ 10.75 - ((L-350)/150)^{3/2} & L > 350 \end{cases}$$ (25.14)

The CDF (Cumulative Distribution Function) for the largest of the individual SWBMs can be found for a total of the $v_s T$ repetitions using the extreme theory,

$$F_{X_s} = \exp[-e^{-\alpha_s(X_s - \mu_s)}]$$ (25.15)

where $X_s = M_s / M_{s,0}$, the parameters α_s and μ_s are given by

$$\mu_s = \sqrt{\frac{\ln(v_s T)}{\ln(v_s T_0)}}, \quad \alpha_s = 2\sqrt{\ln(v_s T_0)\ln(v_s T)} \quad \text{(sagging)}$$

$$\mu_s = \frac{\ln(v_s T)}{\ln(v_s T_0)}, \quad \alpha_s = \ln(v_s T_0) \qquad\qquad \text{(hogging)}$$

Many research efforts have been made on the prediction of VWBM experienced on the ship hulls using linear and nonlinear methods for unrestricted service conditions. VWBM is a naturally stochastic process and can be described by either short-term or long-term statistics. The long-term VWBM is based on the weighted short-term statistics. It is generally accepted

that the long-term VWBM can be modeled as a Poisson process and the peak of each individual VWBM, M_w, can be well approximated by a Weibull distribution.

$$F_{M_w}(M_w) = 1 - \exp\left[-\ln(v_w T_0)\left(\frac{M_w}{M_{w,0}}\right)^{h_w} \right]$$
(25.16)

where v_w is the mean arrival rate of one wave cycle, h_w is the shape parameter varying from 0.9 to 1.1 and reasonably taking 1.0 as a representative value, $M_{w,0}$ is the maximum VWBM in the reference design period $T_0 = 20$years,

$$M_{w,0} = \begin{cases} -0.11(\text{ESF})_s \, C_w L^2 B(C_B + 0.7) & \text{(sagging)} \\ 0.19(\text{ESF})_h \, C_w L^2 B C_B & \text{(hogging)} \end{cases}$$
(25.17)

where $(\text{ESF})_s$ and $(\text{ESF})_h$ are the environmental severity factors for sagging and hogging conditions, which can be taken from 0.5 to 1.0 consistent with the specific installation site (ABS, 2000).

Similar to that of SWBM, the CDF for the largest of the individual VWBMs can be found for a total of the $v_w T$ repetitions,

$$F_{X_w} = \exp[-e^{-\alpha_w(X_w - \mu_w)}]$$
(25.18)

where $X_w = M_w / M_{w,0}$, the parameters α_w and μ_w are given by

$$\mu_w = \frac{\ln(v_w T)}{\ln(v_w T_0)}, \quad \alpha_w = \ln(v_w T_0)$$

Based on *Ferry-Borges* method, the CDF of the combined bending moment is expressed as following (Wang, et al, 1996)

$$F_{M_t}(M_t) = \int_0^{M_t} \frac{f_{M_s}(M_t - u)du}{1 + v_w/v_s [1 - F_{M_w}(u)]}$$
(25.19)

The combined bending moment in a given time T is obtained by

$$F(M_t) = 1 - 1/v_s T$$
(25.20)

For the practical design considerations, load combination factors for SWBM and VWBM, denoted as φ_s and φ_w are introduced

$$M_{t,T} = M_{w,T} + \varphi_s M_{s,T} = M_{s,T} + \varphi_w M_{w,T}$$
(25.21)

The CDF for the largest of the individual combined bending moment can be expressed for a total of the $v_s T$ repetitions,

$$F_{\max}(M_t) = [F(M_t)]^{v_s T} \tag{25.22}$$

25.4 Procedure for Reliability Analysis of Ship Structures

25.4.1 General

Vast amount of publications are available now with regard to the reliability analysis of existing ships since researchers first began to look at the desirability of using probabilistic methods in the structural design of ships in the early 70's. The details of the analysis methods may vary from one paper to another. However, generally speaking, reliability analysis of existing ships should cover the basic steps of next section.

Step 1: Definition of the objective ship and its mission tasks

In order to carry out the reliability analysis of a ship, the basic geometry and scantlings of the ship must be known. Furthermore, the environmental conditions including loading conditions and sea conditions the ship has been exposed over its service life should also be defined.

Step 2: Definition of the limit state functions

Knowledge of the limiting conditions beyond which a ship will fail to perform its intended function will undoubtedly help in assessing more accurately the true margin of safety of the ship. The equations that can represent these limiting conditions are called limit state equations. Establishing the limit state equations is a significant step within the reliability analysis procedure. Generally speaking, there are two categories of limit state equations: serviceability vs. strength. For each category, four different levels of limit states exist. These are:

1. limit state functions for hull girder collapse;

2. limit state functions for stiffened panels;

3. limit state functions for buckling of plates between stiffeners; and

4. limit state functions for fatigue of Critical Structural Details (CSD).

Step 3: Definition of the statistical characteristics of the random variables

Step 4: Selection of the reliability calculation methods

Step 5: Calculate the probability of failure for each failure mode for the given ship

When the limit-state function is complex, a response surface method may be applied to approximate the limit-state surface using a polynomial type function. Using the response surface, a standard FORM/SORM algorithm may then be used to estimate failure probability.

25.4.2 Response Surface Method

The limit state function at time t relating to the ultimate strength failure of an FPSO hull girder is given by

$$g(\mathbf{x}|t) = C_u M_u(t) - C_p[\phi_s M_s(t) + M_w(t)] \tag{25.23}$$

where $M_u(t)$ is the ultimate strength, $M_s(t)$ and $M_w(t)$ are the stillwater and wave-induced moments respectively; C_u and C_p represent the model errors in predicting the hull's ultimate strength and combined total bending moment the ship experiences. The failure probability at the time T is expressed by

$$P_f(T) = \int_0^T \left[\int_{g(\mathbf{x}|t)<0} \cdots \int f_X(\mathbf{x}|t)d\mathbf{x} \right] f_T(t)dt \tag{25.24}$$

where $f_X(\mathbf{x}|t)$ is the joint probability density function; $f_T(t)$ is the probability density function of occurrence time T, which is assumed as a uniform distribution, $f_T(t) = 1/T$. Therefore, Eq.(25.24) can be rewritten by

$$P_f(T) = \frac{1}{T} \int_0^T \left[\int_{g(\mathbf{x}|t)<0} \cdots \int f_X(\mathbf{x}|t)d\mathbf{x} \right] dt \tag{25.25}$$

By defining $P_f(t)$ as a conditional failure probability at time t,

$$P_f(t) = \int_{g(\mathbf{x}|t)<0} \cdots \int f_X(\mathbf{x}|t)d\mathbf{x} \tag{25.26}$$

the failure probability has in a simple form

$$P_f(T_s) = \frac{1}{T} \int_0^T P_f(t)dt \tag{25.27}$$

The response surface method (Bucher, 1990) is applied when the limit state function $g(\mathbf{x}|t)$ is expressed implicitly and has a nonlinear form in order to overcome the expensive computational effort integrating Eq. (25.25) in evaluating the failure probability.

The basic concept of the response surface method is to approximate the original complex and/or implicit limit state function using a simple and explicit function. The accuracy of the results depends highly on how accurately the characteristics of the original limit state are represented by approximate function. The suitability of the response surface obtained relies mainly on the proper location of so-called sampling points. Many algorithms have been proposed to select appropriate sampling points, which promise to yield better response surface fitting. In addition, the basic function shape is also known to be another major factor that influences both the accuracy of the response surface method and the selection of the reliability evaluation method.

Many practical reliability evaluation techniques are available once the failure surface $G(\mathbf{x})$ is defined in an explicit closed form. Among those techniques, first order method is commonly used due to the efficiency with acceptable accuracy. An equivalent linearized limit state at so-called design point is taken and the safety margin of the structural system is determined as the minimum distance from the origin to the original nonlinear limit surface in the independent standard normal space.

In this study, a response surface with a polynomial type function including squared terms but not cross terms is adopted,

$$G(\mathbf{x}) = a + \sum_{i=1}^{r} b_i x_i + \sum_{i=1}^{r} c_i x_i^2 \tag{25.28}$$

where r is the number of basic random variables; $\mathbf{x} = (x_1, x_2, \cdots, x_r)$ is the basic random vector; a, b_i, and c_i are the unknown coefficients that can be determined using $2r+1$ sampling points. The sampling points are selected to be located at the design point $(\bar{x}_1, \bar{x}_2, \cdots, \bar{x}_r)$ and other $2r$ points $(\bar{x}_1, \cdots, \bar{x}_i \pm f\sigma_i, \cdots, \bar{x}_r)$, where f is a parameter determining the upper and lower bounds of selection range. This process should be iterative to guarantee that the sampling points chosen from the new design point include the information from the original failure surface sufficiently. Once the response surface is defined, the failure probability is computed using modified Monte Carlo simulation technique (Sun, 1997).

25.5 Time-Variant Reliability Assessment of FPSO Hull Girders

The time-variant reliability estimation of an FPSO hull girder subjected to the degradations of corrosion and fatigue is studied in this sub-section. The relevant principal particulars of the FPSO are listed in Table 25.1. The midsection is shown in Figure 25.1. Table 25.1 summarizes variable measurements in this assessment. The determination of the various variables is based on the previous studies of FPSOs.

Table 25.1   Principal Particulars of a FPSO

Description	Value
Length, between perpendiculars	194.2 m
Length, for scantling	194.2 m
Breadth, molded	32.0 m
Depth, molded, including box keel	18.0 m
Depth, molded, from base line	16.0 m
Block coefficient	0.816
Transverse web frame spacing	3.7 m

Table 25.2 Variable Measurements

Variable	Description
E	Elastic modulus, normal variable, Mean=2.06×10^5MN/m^2, COV=0.08
σ_y	Yielding stress, normal variable, Mean=315MN/m^2, COV=0.06
Δ	Stiffened panel eccentricity, normal variable, Mean=0.00555m, COV=0.1
W/h_p	Initial center deflection of plating, normal variable, Mean=0.5, COV=0.1
τ_t	Transition time of corrosion, constant, τ_t =3 years
μ_c^d	Steady corrosion rate of the stiffened panels at deck, normal variable, Mean=1.4×10^{-4}m/year, COV=0.1
μ_c^s	Steady corrosion rate of the stiffened panels at side shell and longitudinal bulkhead, normal variable, Mean=1.25×10^{-4} m/year, COV=0.1
μ_c^{ob}	Steady corrosion rate of the stiffened panels at outer bottom, normal variable, Mean=5.4×10^{-5} m/year, COV=0.11
μ_c^{ib}	Steady corrosion rate of the stiffened panels at inner bottom, normal variable, Mean=1.79×10^{-4} m/year, COV=0.16
μ_c^c	Steady corrosion rate of corner elements, normal variable, Mean=5.4×10^{-5} m/year, COV=0.10
C	Material parameter in Paris-Erdogen equation, normal variable, Mean=4.349×10^{-12}, COV=0.206
M	Material parameter in Paris-Erdogen equation, constant, m=3.07
a_0	Initial crack size, normal variable, Mean=1.0×10^{-3}m COV=0.18
Ms	Maximum value of still bending moment, Type I extreme variable, Average arrival period ($1/\nu_s$) =1 day
M_w	Maximum value of wave-induced bending moment, Type I extreme variable, Average arrival rate (ν_w) =10^8 in a 20 years design life
(ESF)$_s$	Environmental severity factor for sagging condition, constant, (ESF)$_s$ =0.80
(ESF)$_h$	Environmental severity factor for hogging condition, constant, (ESF)$_h$ =0.80
C_u	Model error of predicting ultimate strength, normal variable, Mean=1, COV=0.1
C_p	Model error of predicting combined total bending moment, normal variable, Mean=1, COV=0.25(sagging condition)

25.5.1 Load Combination Factors

Since the failure mode under sagging condition is the most prominent one, the results under sagging condition are demonstrated as below.

The parameter analysis of the load combination factors φ_s and φ_w for the FPSO is at first carried out.
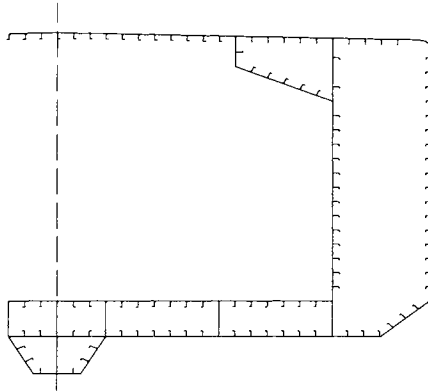
Figure 25.1   FPSO Midsection
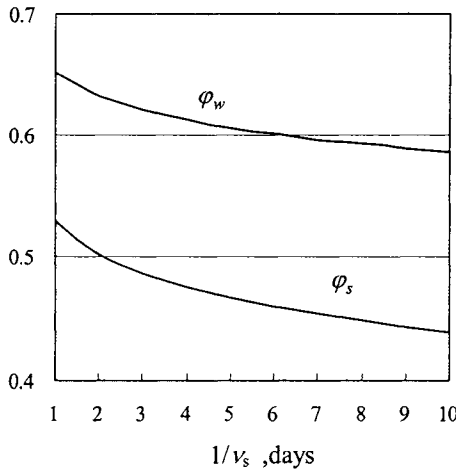
Figure 25.2   Load Combination Factors vs $1/v$

Figure 25.2 shows the effect of the mean arrival period ($1/v_s$) of SWBM on the combination factors, where a total number of 10^8 wave cycles in 20 service years is selected and the environmental severity factors $(EFS)_s$ is taken to 0.80. It can be seen that the load combination factors are sensitive to the mean arrival period of SWBM.

Figure 25.3 shows the dependence of the load combination factors as a time function where the environmental severity factors $(EFS)_s$ is also taken to 0.80. It is demonstrated that the load combination factors gradually decrease with the increase of the service years.
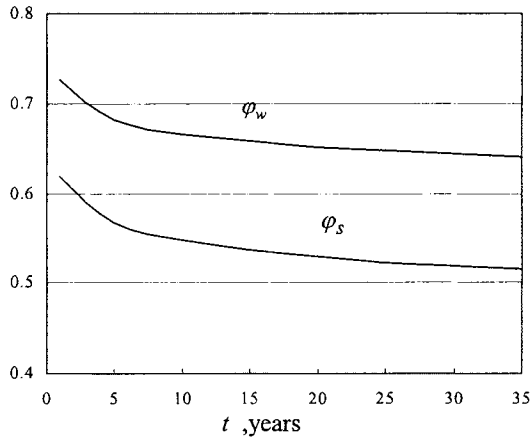
Figure 25.3   Load Combination Factors as a Time Function

Figure 25.4 shows the dependence of the load combination factors with the environmental severity factor where a total number of 10^8 wave cycles in 20 service years and the SWBM mean arrival period $(1/v_s)$ of 1 day are selected. It is shown that the decreasing trend of φ_s is much greater than the increasing trend of φ_w when the environmental severity factor increases. It implies that load combination leads the effect of the environmental severity factor to be small.
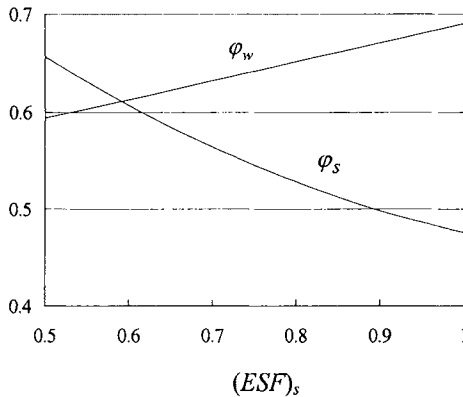
Figure 25.4   Load Combination Fctors vs *ESF*

25.5.2 Time-Variant Reliability Assessment

Figure 25.5 shows the conditional reliability as a time function considering the four cases of degradations. Here the conditional reliability is defined by $R(t)=1-P_f(t)$. For the different service years and mean steady corrosion rates, the reductive ratios of the corresponding conditional reliability index compared to the initial value are listed in Table 25.3.
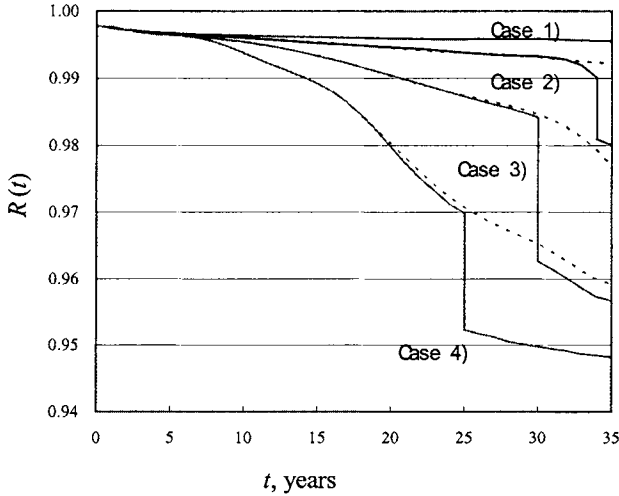
Figure 25.5   Conditional Reliability with Four Cases of Mean Steady Corrosion Rates

Table 25.3   The Reductive Ratios of Conditional Reliability Index

Service year Corrosion	5	10	15	20	25	30	35
Case 1)	95.17%	93.91%	93.29%	92.64%	92.37%	92.45%	91.67%
Case 2)	95.10%	93.11%	91.01%	89.64%	87.88%	86.81%	72.23%
Case 3)	94.76%	91.50%	86.94%	82.39%	78.60%	62.66%	60.26%
Case 4)	94.87%	88.15%	81.09%	72.35%	58.86%	57.99%	57.45%

The conditional reliability of the hull girder is also significantly decreased coincident with the mean ultimate strength. If the reductive ratio 90% of conditional reliability index is selected as reliability threshold in order to maintain the hull reliability level, then the inspections should be made for the Case 3) and Case 4) at about 10th service year. The degradation effect of fatigue cracks seems not to be important to the hull girder reliability before they unsteadily

propagate, but it should be paid attention on their potential disasters during inspections. The unsteady propagation of fatigue cracks might induce to catastrophic event of the FPSO.

Simply adding the extreme values of SWBM and VWBM is quite conservative. It can be found in Figure 25.6, where "LC" and "NLC" represent the load combination and no load combination respectively.
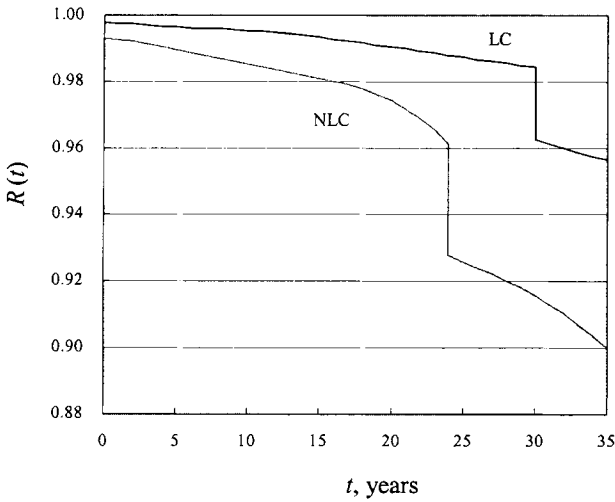
Figure 25.6   Influence of Load Combination on Conditional Reliability
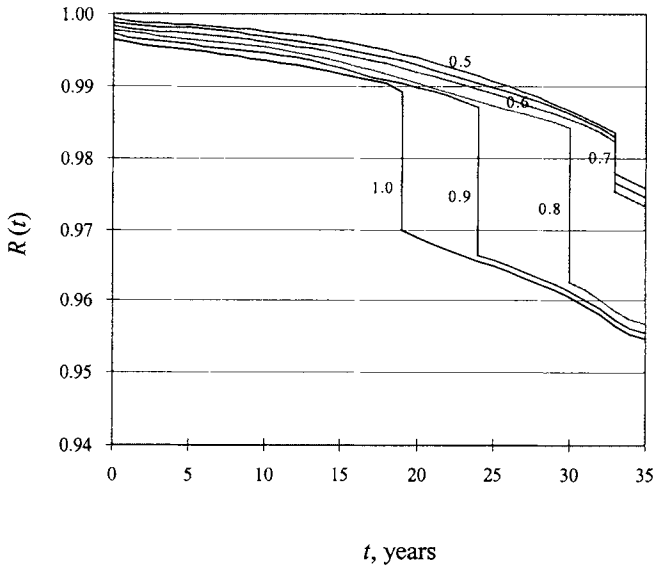
Figure 25.7   Influence of ESFs on Conditional Reliability

Figure 25.7 shows the influence of "Environmental Severity Factors" to the conditional reliability, where the number denotes the value of ESFs. Accuracy measurement of the specific-site installation conditions is very important for the FPSO hull girder design and inspections.

The transition time τ_t is another important parameter relating to the reliability and its effect of different value is shown in Figure 25.8, where the number on the curve denotes the transition years. A relatively larger transition time will keep reliability at relatively higher reliability and postpone the happening of unsteady propagation of fatigue cracks. This result was also obtained by Guedes Soares and Garbatov (1999) who carried out the reliability analysis of maintained, corrosion protected plates.
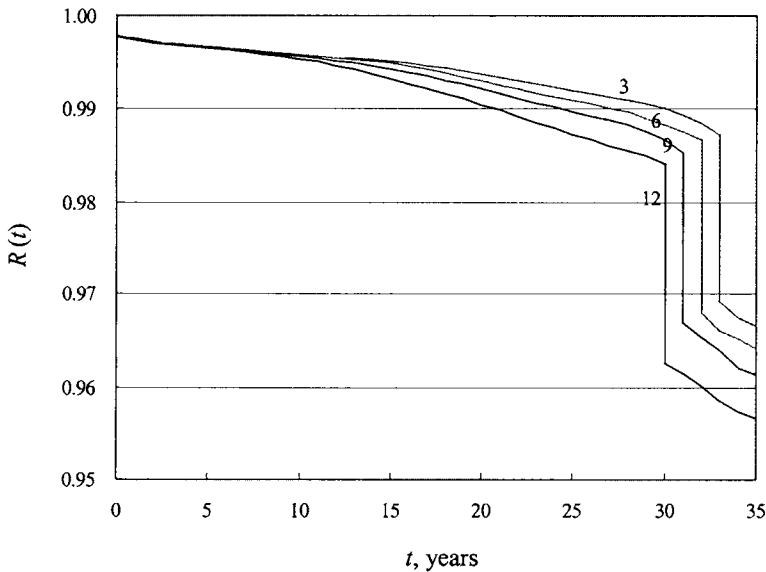
Figure 25.8   Influence of Transition Time on Conditional Reliability

Corrosion wastage depends on many factors, including coating properties, cargo composition, inert gas properties, temperature of cargo, and maintenance systems and practices, and spot-checks may not measure the same location in subsequent spot-checks in normal thickness measurements. This evident makes theoretically constructing corrosion model quite difficult. In the numerical analysis, the mean steady corrosion rates were used, which correspond to the permissible values of corrosion wastage for oil tankers in classification society rules. The coefficient of variation for corrosion rates typically increase with time from 10% at 10th service year to 100% or even larger at 20th service year, but the contribution to the total uncertainty of hull girder ultimate strength is very limited based on the sensitivity analysis (see Figure 25.9).
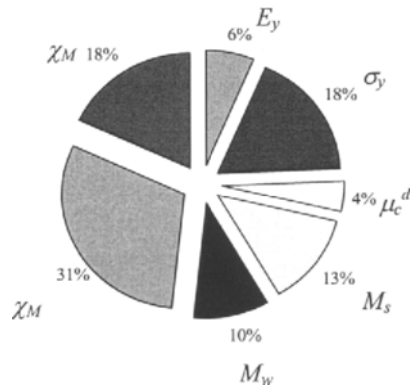
Figure 25.9   Sensitivity Data at 20th Service Year for Nominal Corrosion Rate

Figure 25.10 shows the results of uncertainty analysis of ultimate strength of the hull girder. In this analysis, CRM represents the result from the response surface method. It is found that the coefficient of variation for the ultimate strength is of the upper bound of 10% in any corrosion case considered.

There are several corrosion rate models in the literature. The simplest one among them is the model with constant corrosion rate assumed, which is estimated entirely from observations made as part of normal surveys. Due to the products of corrosion, the corrosion rate decreases with time. But other observations from oil tankers showed that in most cases the corrosion rate appears to increase with time and then keep constant. The reason for this appears to be related to dynamic loading that spill off corrosion products in ocean environments. The corrosion rate model proposed in this section can fit this case. However, much more work for further improvement of corrosion rate model should be done when more data on corrosion wastage becomes available. The rational way to keep the safety level of FPSO hull girders in present practice is to establish risk-based program of inspection planning and reliability-based renewal criteria for corroded components.
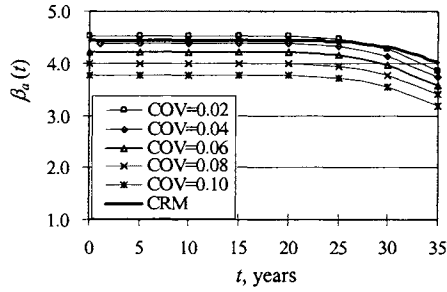
(1) No Corrosion
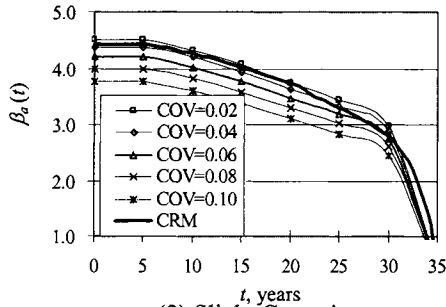
(2) Slight Corrosion
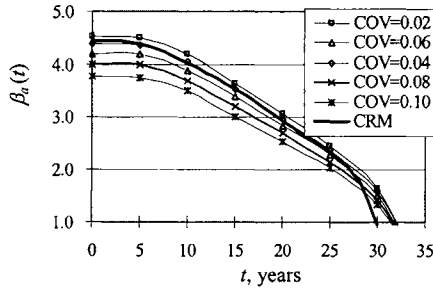
(3) Nominal Corrosion
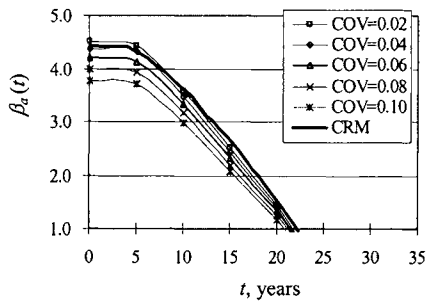
(4) Severe Corrosion

Figure 25.10   Uncertainty Analysis for Ultimate Strength

25.5.3 Conclusions

Time-variant structural reliability assessment of an FPSO hull girder relative to the ultimate strength requires the consideration of the following three aspects: (1) load effects and their combination, (2) the hull ultimate strength, and (3) methods of reliability analysis.

The environmental severity factors are introduced to fit the the wave-induced bending moments accounting for the specific-site conditions. The *Ferry-Borges* method is applied to combine stochastic processes of still-water and wave-induced bending moments and to evaluate time-variation of the maximum combined bending moment.

- The mean value first order second moment method was applied to calculate failure probability of ship structures.

- A procedure for time-variant reliability analysis has been developed.

- An effective response surface approach is used to evaluate the failure function at sampling points. A modified Monte Carlo simulation technique is applied to evaluate the failure probability.

- The time-variant reliability and parametric analysis for an FPSO hull girder are quantified. It is found that the steady corrosion rate, combination of SWBM and VWBM, environmental severity factors and transition time in the present corrosion model are very important in estimating the reliability of the hull girder.

- It is concluded that the load combination factors obtained from this method are dependent on mean arrival rate of SWBM, service lifetime and the environmental severity factors.

25.6 References

1. ABS (2000), "Guide for Building and Classing Floating Production Installations", American Bureau of Shipping.

2. Bucher, C.G., Bourgound, U.A., (1990), "A Fast and Efficient Response Surface Approach for Structural Reliability Problems", Structural Safety, Vol. 7, pp. 57-66.

3. Casella, G., Rizzuto, E., (1998), "Second-level Reliability Analysis of a Double-hull Oil Tanker", Marine Structures, Vol. 11, pp.373-399.

4. Frieze, P.A. and Lin, Y.T. (1991), "Ship Longitudinal Strength Modeling for Reliability Analysis", Proc. of Marine Structural Inspection, Maintenance and Monitoring Symposium, SNAME, Arlington, VA.

5. Ghose D.J., Nappi N.S., Wiernicki C.J., (1995), "Residual Strength of Marine Structures", Ship Structure Committee, SSC-381.

6. Gordo J.M., Guedes Soares C., Faulkner D. (1996), "Approximate Assessment of the Ultimate Longitudinal Strength of Hull Girder", Journal of Ship Research, Vol. 40(1), pp.60-90.

7. Guedes Soares, C., (1984), "Probabilistic Models for Load Effects in Ship Structures", Department of Marine Technology, Norwegian Institute of Technology, Trondheim, Norway, Report No. UR-84-38.

8. Guedes Soares C., (1990), "Stochastic Models of Loads Effects for the Preliminary Ship Hulls", Structural Safety *1990*; 8: 353-368.

9. Guedes Soares, C. and Moan, T., 1985, "Uncertainty Analysis and Code Calibration of the Primary Load Effects in Ship Structures", Proc., 4th International Conference on Structural Safety and Reliability (ICOSSAR '85), Kobe, Japan, Vol. 3, pp. 501-512.

10. Guedes Soares, C. and Moan, T., 1988, "Statistical Analysis of Still-water Load Effects in Ship Structures", Trans. SNAME, Vol. 96, pp. 129-156.

11. Guedes Soares, C., Dogliani, M., Ostergaard, C., Parmentier, G. and Terndrup Pedersen, P., (1996), "Reliability Based Ship Structural Design", SNAME Transactions, Vol. 104, pp.357-389.

12. Guedes Soares, C., Garbatov, Y., (1999), "Reliability of Corrosion Protected and Maintained Ship Hulls subjected to Corrosion and Fatigue", Journal of Ship Research Vol. 43(2), pp.65-78.

13. Guedes Soares, C., Garbatov, Y., (1999), "Reliability of Maintained, Corrosion Protected Plates subjected to Nonlinear Corrosion and Compressive Loads", Journal of Marine Structures, Vol. 12, pp.425-445.

14. IACS (1995), "Requirement S11, Longitudinal Strength Standards", Int. Association of Classification Societies.

15. Liu, Y.W., Moses, F. (1994), "A Sequential Response Surface Method and Its Application in the Reliability Analysis of Aircraft Structural System", Journal of Structural Safety, Vol. 16, pp. 36-46.

16. Mansour, A.E. (1972), "Probiblastic Design Concept in Ship Structural Safety and Reliability", Trans. SNAME, Vol. 80, pp. 64-97.

17. Mansour, A. and Faulkner, D. (1973), "On Applying the Statistical Approach to Extreme Sea Loads and Ship Hull Strength", RINA Trans., Vol. 115, pp. 277-313.

18. Mansour, A.E., (1974), "Approximate Probabilistic Methods of Calculating Ship Longitudinal Strength", Journal of Ship Research, Vol. 18.

19. Mansour, A.E., (1987), "Extreme Value Distributions of Wave Loads and Their Application to Marine Structures", Marine Structural Reliability Symposium, Arlington, VA.

20. Mansour, A.E. (1990), "An Introduction to Structural Reliability Theory", SSC Report SSC-351.

21. Mansour, A.E., Lin, M., Hovem, L., and Thayamballi, A. (1993), "Probability-Based Ship Design Procedure – A Demonstration", SSC Report, SSC-368.

22. Mansour A E. (1994), "Probability Based Ship Design Procedures: Loads and Load Combination", Ship Structure Committee, SSC-373.

23. Mansour, A.E. (1995), "Extreme Loads and Load Combination", J. of Ship Research, Vol. 39, No. 1.

24. Mansour, A. E. and Wirsching, P.H. (1995), "Sensitivity Factors and Their Application to Marine Structures", Journal of Marine Structures, Vol. 8.

25. Mansour, A. E. (1997): "Assessment of Reliability of Ship Structures", SSC Report, SSC-398.

26. Nikolaidis, E. and Kaplan, P. (1991), "Uncertainties in Stress Analysis on Marine Structures", Ship Structure Committee Report SSC-363.

27. Nikolaidis, E. and Hughes, O.F., Ayyub, B.M., and White, G.J. (1993), "A Methodology for Reliability Assessment of Ship Structures", Ship Structures Symposium 93, SSC/SNAME, Arlington, VA, pp H1-H10.

28. Ochi, M.K. (1978), "Wave Statistics for the Design of Ships", Transactions of SNAME, 86: 47-76.

29. Sikora, J.P., Disenbacher, A., and Beach, J.E. (1983), "A Method for Estimating Lifetime Loads and Fatigue Lives for SWATH and Conventional Monohulls", Naval Engineering Journal, ASNE, Vol. 95, No. 4, pp. 63-85.

30. Smith, C.S. (1977), "Influence of Local Compressive Failure on the Ultimate Longitudinal Strength of a Ship Hull", In: Proc. of Int. Symposium on Practical Design of Ships (PRADS'77), Tokyo, Japan, pp. 73-79.

31. Stiansen, S.G. and Mansour, A.E. (1980), "Reliability Methods in Ship Structures", J. of RINA.

32. Sun, H.H., Chen, T.Y., (1997), "Buckling Strength Analysis of Ring-Stiffened Circular Cylindrical Shells under Hydrostatic Pressure", ISOPE-97, pp.361-366, Honolulu.

33. Sun, H.H., Xiao, T.Y. and Zhang, S.K., (1999), "Reliability Analysis based on Ultimate Strength of Midsections for Corroding Ship Primary Hulls", Proc. 18th OMAE/S&R-6007, St. Johns.

34. Sun, H.H. and Bai, Y. (2000), "Reliability of Corroded and Cracked Ships", ISOPE'2000.

35. Sun, H.H. and Bai, Y. (2001), "Time-Variant Reliability of FPSO Hulls", SNAME Transactions, Vol. 109.

36. Wang X., Jiao G., Moan T. (1996), "Analysis of Oil Production Ships Considering Load Combination, Ultimate Strength and Structural Reliability", SNAME Transaction, Vol.104, pp. 3-30.

37. White, G.J. and Ayyub, B, N., (1985), "Reliability Methods for Ship Structures", J. of Naval Engineers, Vol. 97, No. 4.

38. Wirsching P.H. et al. (1997), "Reliability with Respect to Ultimate Strength of a Corroding Ship Hull", Journal of Marine Structures, Vol.10. pp. 501-518.

39. Yamamoto, N.(1998), "Reliability Based Criteria for Measures to Corrosion", Proc.17th OMAE'98.

This Page Intentionally Left Blank

Part IV

Structural Reliability

Chapter 26   Reliability-Based Design and Code Calibration

26.1 General

The most important applications of structural reliability methods is perhaps reliability-based design and calibration of the safety factors in the design codes. These two topics will be addressed in detailed in this chapter.

In structural design, there are always uncertainties involved in determining loads and capacities. Historically, the engineering design process has compensated for these uncertainties by the use of safety factors. However, with reliability technology, these uncertainties can be considered more quantitatively. Specifically, the use of probability-based design criteria has the promise of producing better-engineered designs. For a marine structure, implementation of a probability-based design code can produce a structure having, relative to structure designed by current procedures, (1) a higher level of reliability, or (2) lower overall weight (which means cost savings), or (3) both.

26.2 General Design Principles

General design principles used in practice are outlined in this subsection. Reliability-based design is one of the design methodologies, but it is highlighted as a separate section in this Chapter.

26.2.1 Concept of Safety Factors

Structural safety measures of different kinds are generally used and referred to without always giving a clear picture about their physical meaning. The safety factor concept is frequently applied without giving any corresponding quantitative measure related to the actual structural safety level. Traditional design practice is based on application of some kind of deterministic safety measures. The greater the ignorance about an event, the larger the safety factor should be applied. In principal, the safety factors of design check of components should depend upon the consequence of failure and the type of structural mode.

26.2.2 Allowable Stress Design

ASD criterion has been used since a long time ago by use of explicit design formulae, which can be expressed as

$$\sigma \le o_A \ where \ o_A = \frac{\sigma_L}{\gamma} = \eta \sigma_L \tag{26.1}$$

where σ is the stress in the structures obtained by linear-elastic theory for the maximum loads, σ_A is the allowable stress, σ_L, typically the yield stress, γ is the safety factor, $\eta(=1/\gamma)$ is the usage factor. In the ASD methods the design check is made at a capacity/load effect level below first yield of a component.

Linear elastic analyses are used to describe the structure response characteristics for the given nominal design loading. The complexity of the design format depends on the failure mode considered, i.e. failure in compression, in tension, in buckling, etc. Design codes formulate these equations and provide the safety factors to be used. However, there are some objections to the application of ASD due to differences in the uncertainties with the various loads and resistances, and also due to the over-design.

The ASD design used by AISC is called WSD by API RP2A.

26.2.3 Load and Resistance Factored Design

Due to statistical variability in the applied loads and components resistance and due to certain assumptions and approximations made in design procedure, use of a single safety factor for all load combinations cannot maintain a constant level of structural safety. Partial safety factors may generally reflect the inherent uncertainties in load effects and strength as well as the consequence of failure and safety philosophy

The Load and Resistance Factored Design (LRFD) procedure was issued by the American Institute for Steel Construction (AISC) in 1986. The AISC LRFD criteria were developed under the leadership of T.V. Galambos, see a series of 8 papers published in ASCE journal of the Structural Division, e.g. Ravindra and Galambos (1978).

Further, the American Petroleum Institute (API) has extrapolated this technology for offshore structures with the development of API RP2A-LRFD, in 1989.

Loads acting on the structures can be divided into several types such as functional loads, environmental loads, etc. If the concept of multiple load factors is introduced, the LRFD design criterion can be reformulated as

$$R\left(\frac{f_k}{\gamma_m}, \cdots, \right) \geq S\left(\gamma_{f_i} \psi_i Q_k\right)$$
(26.2)

where γ_{fi} are load factors to account for uncertainties in each individual load Q_i, ψ_i are load combination factors. The safety factor in Eq.(26.2), γ_m, reflects the uncertainty of a given component due to variations in the size, shape, local stress concentrations, metallurgical effects, residual stress, fabrication process, etc. The safety factors applied to loads, γ_f, reflect the uncertainty in estimating the magnitude of the applied loads, the conversion of these loads into stresses, etc.

If R and S are linear functions of f_k and Q_i, respectively, the above format can be written as

$$\phi R(f_k) \geq \sum_{i=1}^{m} \gamma_{f_i} \psi_i S(Q_{ik})$$
(26.3)

ψ_i are load combination factors. In the API - LRFD code, resistance factors $\phi(=1/\gamma_m)$ is defined instead of material factors.

It is emphasized that the safety factors γ_m and γ_{fi} should be seen in conjunction with the definition of the characteristic values of resistance and loads, and the method used to calculate these values. Even if the characteristic values are the same in design codes for different

regions, the safety factors may be different due to the difference in uncertainties involved in resistance and load, difference in target safety levels and difference in environmental and soil conditions.

Comparing LRFD with WSD methods, it is seen that in the LRFD method the loads and capacities are modified by factors representing their statistical uncertainties. This results in a more uniform safety for a wide range of loads and load combinations and component types. Even though the LRFD format is similar in form with ASD format, there exists a substantially different physical interpretation.

The design format should account for the different load conditions and relevant magnitude of uncertainties encountered by structures. As briefly reviewed by Efthymiou et al (1997) that the load and resistance factors in API RP2A LRFD were derived on the basis of calibration to the API-RP2A WSD. The objective was to derive load and resistance factors that would achieve, on average, the same calculated component reliabilities as obtained using API-RP2A WSD. To achieve this objective, reliability analyses were used to derive safety indices for components designed to API-RP2A WSD for a range of gravity and environmental load situations and averaged to obtain the target safety index for the LRFD code.

26.2.4 Plastic Design

Traditionally, Part 2 of the AISC Specification was called Plastic Design. Plastic Design is a special case of limit states design, wherein the limit state for strength is the achievement of plastic moment strength Mp. Plastic moment strength is the moment strength when all fibers of the cross-section are at the yield stress. The design philosophy as per AISC applied to flexural members such as beam-columns. In recent years, Plastic Design became a component of LRFD.

26.2.5 Limit State Design (LSD)

Marine structures are composed of components, e.g. tubular joints, brackets, panels, etc. which are subject to different load conditions including functional loads, environmental loads, accidental loads, etc., and may fail in different failure modes. Usually, the ultimate limit state (ULS) for a specified failure mode is expressed by a mathematical formula in which uncertainties associating with loads, strength and models cannot be avoided.

LSD examines the structural condition at failure, comparing a reduced capacity with an amplified load effect for the safety check.

Besides, LSD covers various kinds of failure modes, such as

- Ultimate limit state (ULS)

- Fatigue Limit state (FLS)

- Accidental limit state (ALS)

The LSD criteria may be formulated in ASD format or LRFD format. The relation between ASD and LSD has been discussed by e.g. Song, Tjelta and Bai (1998), Bai and Song (1997, 1998).

26.2.6 Life Cycle Cost Design

With the application of structural reliability methodology, an optimum life cycle cost (LCC) structural design, meeting complex combinations of economic, operational and safety

requirements may be targeted. These targets may vary both in time and geopolitical location and further, may be continuously affected by technological changes and market forces. To deal with such design targets in structure design, formal procedures of optimization are required to make decisions about materials, configuration, scantling, etc. In the optimal design process, therefore, the key stage is the specification of optimum design targets. General types of design targets may be cost (initial/operational), functional efficiency and reliability.

By using LCC design, it is possible to express the total costs of a design alternative in terms of mathematical expression, which can be generically described as follows:

$$\text{TOTAL (NPV)}=\text{CAPEX(NPV)} + \text{OPEX(NPV)}+\text{RISKEX(NPV)} \tag{26.4}$$

Where,

CAPEX	= the capital expenditure of initial investment
OPEX	= the operational costs
RISKEX	= unplanned risk costs
NPV	= net present value

One main difficulty that often arises is identification of the costs to include accidental situations such as grounding or collision of ships. In this case, safety is the primary design objective while economy takes on the role of important side constraints. One of the ways to deal with this particular situation is introduction of high cost penalty for certain failure modes, e.g. high value of C_F in the following equation

$$C_T = C_I + P_F C_F = C_I + R \tag{26.5}$$

or

$$R = P_F C_F = \sum \left(P_{F_i} C_{F_i} \right) = \sum R_i \tag{26.6}$$

where P_{Fi} is the failure rate of a particular mode i, and C_{Fi} is the cost penalty associated to that failure mode.

26.3 Reliability-Based Design

26.3.1 General

The role of safety factor in traditional deterministic design is to compensate for uncertainties affecting performance. Such safety factors evolved through long term experience. Experience, however, is not always transferable from one class of structure to another, nor can it be readily extrapolated to novel structures. Further, any single class of a traditionally designed structure has been typically found to have a large variability in actual safety levels, implying that resources could perhaps have been more optimally used. Particularly in the context of the present trend toward reliability-based design, reliability methods are suitable to bridge such gaps in traditional design. This is because performance uncertainty can be considered both directly and quantitatively with reliability methodology.

Relative to a conventional factor of safety code, a probability-based design code has the promise of producing a better-engineered structure. Specific benefits are well documented in the literature.

- A more efficiently balanced design results in weight savings and/or an improvement of reliability.

- Uncertainties in the design are treated more rigorously.

- Because of an improved perspective of the overall design process, development of probability-based design procedures can stimulate important advances in structural engineering.

- The codes become a living document. They can be easily revised periodically to include new sources of information and to reflect additional statistical data on design factors.

- The partial safety factor format used herein also provides a framework for extrapolating existing design practice to new ships where experience is limited.

Experience has shown that adoption of a probability-based design code has resulted in significant savings in weight. Designers have commented that, relative to the conventional working stress code, the new AISC-LRFD requirements are saving anywhere from 5% to 30% steel weight, with about 10% being typical. This may or may not be the case for ships and other marine structures.

In reliability-based marine structural design, the effect of uncertainties in loads, strength and condition assessment is accounted for directly. Safety measures are calculated, for assessing designs or deciding on design targets.

26.3.2 Application of Reliability Methods to ASD Format

A design equation may be formulated using ASD format as

$$R_D \geq \eta \cdot S_D \tag{26.7}$$

Alternatively, the safety factor could be referenced to the capacity of the entire structure system Based on characterization of the demands and capacities as being log-normally distributed, the usage factor, η, in ASD can be expressed as (Bea, et al, 1997)

$$\eta = \alpha \frac{B_S}{B_R} \exp[(\beta\sigma - 2.33\sigma_S)] \tag{26.8}$$

where,

η = usage (safety) factor

α = factor that incorporates the interactive dynamic effects – transient loading and dynamic behavior of the system

B_S = median bias in the maximum demand (loading)

B_R = median bias in the capacity of the element

β = annual safety index

σ = total uncertainty in the demands and capacities

σ_S = uncertainty in the annual expected maximum loadings

The number 2.33 in Eq. (26.8) refers to 2.33 standard deviations from the mean value, or the 99th percentile. This is equivalent to the reference of the design loading to an average annual return period of 100 years. In case of installation conditions are defined on the basis of a 10-year return period condition, a value of 1.28 could be used (90th percentile).

The transient/dynamic loading – nonlinear performance factor, α, is dependent on the ductility (strain – deformation – deformation capacity), residual strength (load – stress capacity beyond the yield), and hysteric (cyclic load – deformation – damping behavior) characteristics of the structure. It is also dependent on the transient/dynamic loading.

The safety index can be though of as a type of safety factor; as β gets bigger, the system gets more reliable. The total uncertainty in the demands S and capacities R is determined from

$$\sigma = \sqrt{\sigma_S^2 + \sigma_R^2} \qquad (26.9)$$

where,

$\quad \sigma_S \quad$ = uncertainty in the annual maximum demands

$\quad \sigma_R \quad$ = uncertainty in the capacities of the elements

26.4 Reliability-Based Code Calibrations

26.4.1 General

One of the important applications of structural reliability methods is to calibrate safety factors in design format in order to achieve a consistent safety level. The safety factors are determined so that the calibrated failure probability, $P_{f,i}$ for various conditions is as close to the target reliability level P_f^T as possible. In the following, the various terms and steps involved in a reliability-based code calibration are defined and presented.

26.4.2 Code Calibration Principles

The scope of the structural design code consists of a class of design cases formed by the possible combinations of

- Structures

- Materials

- Environmental and soil conditions

- Failure modes or limit states that the code is meant to cover.

The code objective is the target reliability index corresponding to the safety level aimed at in the design. For simplicity, in the following, the same β_t is assumed for all limit states covered by the scope of code. In practice, however, β_t may vary from one limit state to another, if the consequences of the associated failures are different.

The demand function expresses the frequency of occurrence of a particular point in data space, i.e, of a certain combination of structure, material, geographical location and limit state. The demand function is used to define weighting factor w for the various combinations of structures, materials and limit states with the scope of the code. The weighting factors thus represent the relative frequency of the various design cases within the scope, and their sum is 1.0. the weighting factors are taken as those that representative for the expected future demand. For this purpose, it is common to assume that the demand seen in the past is representative for the demand in the future.

Because the code cannot be calibrated so as to always lead to design which exactly meet the target reliability, a closeness measure needs to be defined. This can be expressed in term of

penalty function for deviations from the target reliability. Several possible choices for the penalty function exist. One that penalizes over and under-design equally on the β scale may be

$$M = \sum_i \sum_j \sum_k \sum_l \left(w_{i,j,k,l} \left(\beta_{i,j,k,l} - \beta_t \right)^2 \right) \qquad (26.10)$$

in which M denotes the penalty, $w_{I,j,k,l}$ is the weighting factor for the design case identified by the index set (i,j,k,l), and $\beta_{I,j,k,l}$ is the reliability index that is obtained for the design case by design according to the code. This expression for the penalty function M may be interpreted as the expected squared deviation from the target reliability over the scope of design cases.

A prime requirement to the calibration of a common set of safety factors for the entire scope of code is then that, over the scope of code, the calibrated set of safety factors shall lead to designs with safety levels as close as possible to the target. The common set of safety factors is therefore determined as the set γ that minimize the penalty function M

$$Minimize\{M\} \qquad (26.11)$$

$$\text{subject to} : \beta_{ijkl} \geq \beta_{min} \qquad (26.12)$$

over the scope of the code.

In which β_{min} is the minimum acceptable reliability index. This can be achieved by means of an optimization technique, and this applies also if another choice of penalty function is made, such as one that is more heavily biased against under-design than against over-design.

26.4.3 Code Calibration Procedure

Combining the calibration principles outlined above with a practical design consideration, the following steps should be in general be considered as the proper reliability based code calibration procedure.

- Step 1: Identify the failure modes for the considered design case

- Step 2: Define design equation

- Step 3: Form Limit State Function (LSF)

- Step 4: Measure uncertainties involved in all random variables in LSF

- Step 5: Estimate failure probability

- Step 6: Determine target safety level

- Step 7: Calibrate safety factors

- Step 8: Evaluate the results

26.4.4 Simple Example of Code Calibration

To demonstrate the code calibration principles and procedure, a simple example is given below.

Problem

Assume that a strength design check for ship structural details in terms of a resistance R and load effect S is given by

$$R_n \geq \gamma \cdot S_n$$

where the characteristic strength, R_C is

$$R_c = 0.85 \cdot \mu_R$$

and the characteristic load effect, S_C, is

$$S_c = \mu_S$$

μ_R and μ_S are mean values. The corresponding coefficients of variation are $V_R=0.1$ and $V_S=0.2$. The standard deviation are given by $\sigma_R = V_R\, \mu_R$ and $\sigma_S = V_S\, \mu_S$. Assume that design check is fulfilled by the equality sign. What value should γ have so that the design check corresponds to a failure probability of 10^{-3} and 10^{-4}, respectively?

Solution

Given

$R_C = 0.85\mu_R$

$S_C = \mu_S$

Applies the equality condition in the design check formula

$R_C = \gamma S_C$

$0.85\mu_R = \gamma\, \mu_S$

$\mu_R/\mu_S = 1.18\,\gamma$

The reliability index, β, is given by

$$\beta = \frac{\mu_R - \mu_S}{\sqrt{\sigma_R^2 + \sigma_S^2}} = \frac{\mu_R - \mu_S}{\sqrt{\left(V_R\mu_R\right)^2 + \left(V_S\mu_S\right)^2}}$$

Then,

$$\beta = \frac{\mu_R\Big/\mu_S - 1}{\sqrt{0.01 \cdot \left(\mu_R\Big/\mu_S\right)^2 + 0.04}} = \frac{1.18\gamma - 1}{\sqrt{0.014\gamma^2 + 0.04}}$$

To reach the failure probability of 10^{-3}

$\Phi(-\beta) = 10^{-3}$

$$\beta = \frac{1.18\gamma - 1}{\sqrt{0.014\gamma^2 + 0.04}} = 3.09$$

Hence,

$\gamma = 1.56$

To reach the failure probability of 10^{-4}

$\Phi(-\beta) = 10^{-4}$

$$\beta = \frac{1.18\gamma - 1}{\sqrt{0.014\gamma^2 + 0.04}} = 3.72$$

Hence,

$$\gamma = 1.76$$

Note that the expression for the reliability index β, assuming μ_R / μ_S follows log-normal distribution, may be defined by:

$$\beta = \frac{\ln(\mu_R / \mu_S)}{\sqrt{V_R^2 + V_S^2}}$$

26.5 Numerical Example for Tubular Structure

26.5.1 Case Description

To demonstrate the calibration procedure, a detailed example is given below, which is directly adopted from Song, Tjelta and Bai (1998). The case study presented in this study is a simple T joint with its geometry and notation defined in Figure 26.1.
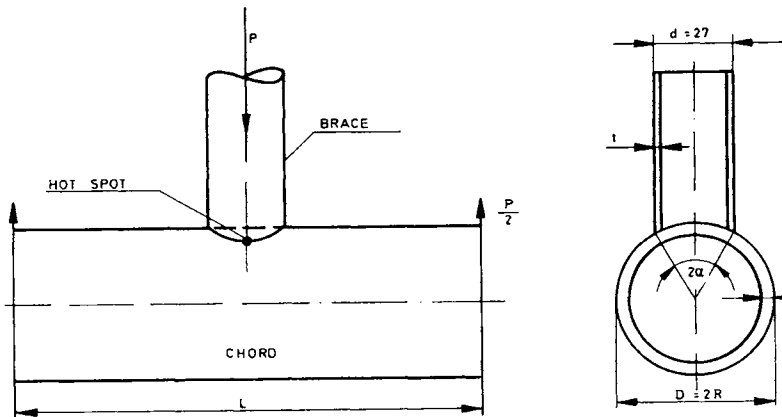
Figure 26.1 Geometric profile of a simple T joint

26.5.2 Design Equations

A simple tubular joint of fixed offshore platforms is shown in Figure 26.2 in which the terminology and geometric parameters are defined. θ is the brace angle measured from chord, g is the gap between braces, t is the brace thickness, T is the chord thickness, d is the brace diameter, D is the chord diameter. The non-dimensional geometrical parameters include diameter ratio ($\beta=d/D$), chord stiffness ($\gamma=D/2T$), wall-thickness ratio ($\tau=t/T$), chord length parameter ($\alpha=L/D$), gap parameter (p=g/D).
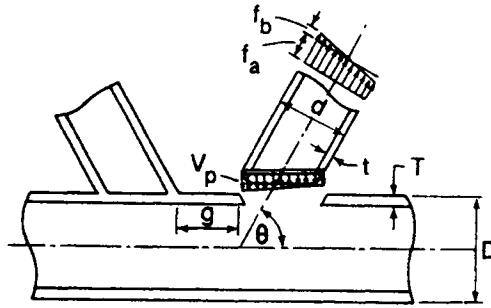
Figure 26.2   Geometric parameters for simple tubular joint connections

According to API RP2A-LRFD, the strength check of simple joints can be performed based on joint capacity satisfying the following

$$P_D < \phi_j P_{uj} \tag{26.13}$$

$$M_D < \phi_j M_{uj} \tag{26.14}$$

where, P_D is the factored axial load in the brace member, P_{uj} is the ultimate joint axial capacity, M_D is the factored bending moment in the brace member, M_{uj} is the ultimate joint bending moment capacity, ϕ_j is the resistance factor for tubular joints.

The ultimate capacities are defined as follows (API, 1993)

$$P_{uj} = \frac{F_y T^2}{\sin \theta} Q_u Q_f \tag{26.15}$$

$$M_{uj} = \frac{F_y T^2}{\sin \theta} (0.8d) Q_u Q_f \tag{26.16}$$

where F_y is the yield strength of the chord member at the joint, Q_f is the design factor to account for the presence of longitudinal factored load in the chord, Q_u is the ultimate strength factor which varies with the joint and load type. Detailed determination of these two factors can be referred to the code (API, 1993).

26.5.3 Limit State Function (LSF)

Generally, the LSF can be expressed as follows for the convenience of reliability-based calibration of safety factors,

$$g(Z) = g[(\gamma_i Q_i), (\phi_j R_j)] \tag{26.17}$$

where Q_i and R_j are sets of random variables of load effect and strength (resistance) respectively; γ_i and ϕ_j are partial safety factors to be calibrated for Q_i and R_j.

LSF can be formed based on failure criteria for the specified case. The failure criterion considered here for simple tubular joint is defined as the exceedance of the static strength in complying with API code check. The LSF based on ultimate static strength criterion can be formulated as

$$g(Z) = \phi_j \frac{F_Y T^2}{\sin \theta} Q_u Q_f - P_D \tag{26.18}$$

$$g(Z) = \phi_j \frac{F_Y T^2}{\sin \theta} (0.8d) Q_u Q_f - M_D \tag{26.19}$$

26.5.4 Uncertainty Modeling

The main topic of the uncertainty analysis is to identify and quantify the different sources of uncertainties that are present and to decide how to take them into account into the subsequent reliability analysis. Uncertainty is measured by the probability distribution function and its statistical values.

Considering uncertainties involved in the LSF, each random variable X_i may be specified as

$$X_i = B_X \cdot X_C \tag{26.20}$$

where X_C is the characteristic value of X_i, and B_X is a normalized variable reflecting the uncertainty in X_i.

Besides model uncertainty discussed above, other major uncertainties considered in this study include follows

Yield strength uncertainty X_y: Uncertainty for yield strength usually depends on the quality of the material used for tubular joints and manufacturing specifications. A normal distribution can be applied to measure this uncertainty with COV=2-5%.

Diameter uncertainty X_d: This is caused by fabrication and measurement. Due to the large enough diameter, the COV of this uncertainty is not expected large.

Wall-thickness uncertainty X_t: This uncertainty is due to fabrication and measurement. The uncertainty in the chord and brace thickness is considered by bias X_t following a normal distribution.

Load uncertainty X_s: This is due to the uncertainties or variability in environmental descriptions and loads calculation. For a sea-state defined by a constant significant wave height and a total number of waves, Rayleigh distribution is usually applied to model the distribution of the largest wave. The COV of the foregoing distributions is a useful parameter characterizing the short-term variability, which may vary with types of storm from 7.5% to 15% (Efthymiou, et al, 1997). The wave loads variability given by COV arises from the natural variability in wave height. The deficiencies in wave theory, force coefficients are also the reasons causing the uncertainty in wave load calculation. From full-scale measurements, it suggests that the wave load recipes are not significant. Based on comparisons of some studies, the wave force model uncertainty is represented by COV=8%. This representation is expected to be on the conservative side (Efthymiou, et al, 1997). This uncertainty is included in the analysis by introducing a bias factor X_S with a COV into the LSF. Presently, a lognormal distribution is applied for this uncertainty.

Ultimate strength uncertainty X_R: The ultimate strength of offshore frame structures are primarily governed by the strength characteristics of members (braces) in compression or tension and the strength of tubular joints under axial loading. For these critical components, the uncertainty in component strength is adequately represented by COV=10%, as indicated by the strength databases both in the US and Europe (Efthymiou, et al, 1997). When a number of members are involved in the collapse mechanism, the uncertainty in system strength reduces.

This implies that provided the method of nonlinear analysis is sufficiently accurate, the variability in system strength is less than 10% for ductile systems.

By introducing those considered uncertainties into LSF, the LSF can be re-expressed simply as

$$g(Z) = X_Y X_t^2 X_R X_m - \phi X_S \qquad (26.21)$$

$$g(Z) = X_Y X_t^2 X_d X_R X_m - \phi X_S \qquad (26.22)$$

The reliability analysis is based on the probabilistic data given in Table 26.1.

Table 26.1   Basic Probabilistic Parameter Descriptions

Random Variable	Distribution	Mean	COV
Model uncertainty, X_m	Lognormal	1.16	0.138
Yield strength uncertainty, X_y	Lognormal	1.14	0.04
Diameter uncertainty, X_D	Normal	1.02	0.02
Thickness uncertainty, X_T	Normal	1.04	0.02
Load uncertainty, X_S	Lognormal	0.90	0.08
Strength uncertainty, X_R	Lognormal	1.05	0.05

26.5.5 Target Safety Levels

When carrying out structural reliability analysis, an appropriate safety should be selected based on factors like consequence of failure, relevant rules, access to inspection and repair, etc., which is termed as target safety level. Target safety levels have to be met in design in order to ensure that certain safety levels are achieved.

Any evaluation of safety levels should be based on information about safety level implied by the design codes and component with historical data on reported failure. The safety level of existing tubular joints designed according to traditional procedures may be a good reference for the target level if the reliability is on average satisfactory. It is important to state that this is related to average failure rate only, as there is expected to be a large variability in the real safety from one tubular joint to another, due to differences and shortcomings in design practices in the past. The target safety level should further be related to the consequences of failure modes as well as the nature of failure, and it may be found that the target reliability level should be increased or even could be decreased concerning specific failure modes.

A target safety level should normally reflect the consequences of failure, safety philosophy, access to inspection and repair, and behavior of the structural components. Safety classes are generally based on mainly the consequences and types of failure, which can be generally divided into low, normal and high safety class depending on the considered platform and components.

Low safety class: where failure of component or tubular joint implies no risk to human safety and environmental damage. When a certain damage is found in this class, its condition can be monitored and no other necessary measures needs to be applied.

Normal safety class: where failure implies negligible risk to human safety, minor danger to the main part of the platform, minor damages to the environment, certain economic loss.

High safety class: where failure implies risk to the total safety of the platform so as to human safety and environmental pollution. High economic loss cannot be avoided.

Table 26.2 Recommended Target Safety Level

Safety Classes	Target	Safety
Low	$P_F = 10^{-2}$	$\beta=2.32$
Normal	$P_F = 10^{-3}$	$\beta=3.09$
High	$P_F = 10^{-4}$	$\beta=3.72$

26.5.6 Calibration of Safety Factors

Besides the direct use of reliability calculation for tubular joint design, representing a full probabilistic design, reliability methods can also be used indirectly for the design purpose based on a calibrated design check with the main goal of obtaining a uniform safety level. The main objective of reliability-based calibration of tubular joint design is to achieve the optimal set of partial safety factors on the basis of a uniform reliability level.
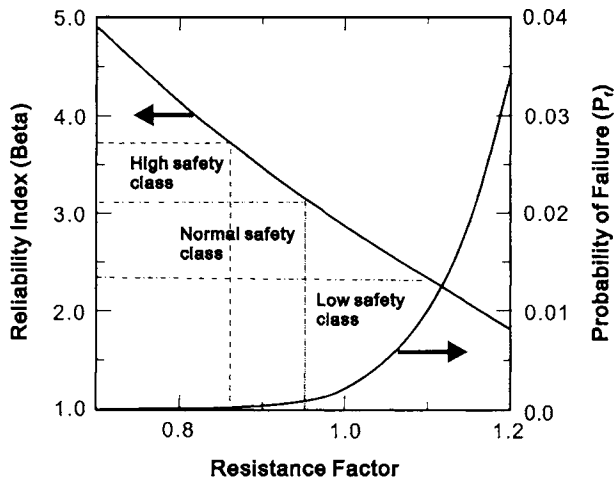
Figure 26.3   Calibration of Safety Factor for Tubular Joint Design

Since the joints have been divided into three classes with low, normal and high safety, different safety factors should be applied according the safety class of the considered joints. The influence of safety factor applied in the design on the reliability index is given in Figure 26.3. It is recommended that safety factors corresponding low, normal and high classes of safety are of 1.1, 0.95 and 0.86 respectively. It must be pointed out that the calibrated safety

based on practical engineering judgment should be applied to the calibrated safety factor. The existing experience with use of safety factors for the specified tubular joints should be considered in the judgment.

26.6 Numerical Example for Hull Girder Collapse of FPSOs

With a reference to Part II Chapter 13 and Part IV Chapter 25, this Section presents a reliability-based calibration of hull girder collapse for FPSO(Sun and Bai, 2001). As an illustration, the bending moment criteria may be expressed as

$$\gamma_s M_s + \gamma_w \varphi_w M_w \leq \phi_u M_u \qquad (26.23)$$

where γ_s, γ_w and ϕ_u are partial safety factors.

The selection of target reliability levels is a difficult task and should be based on the consequences of failure, reliability formulation, and accessibility to inspection and possibility of repair.

There are three methods that have been applied (Mansour, 1997):

(1) Agreeing upon a "reasonable" value in the case of novel structures without prior experience;

(2) Calibrating reliability level implied in currently used design codes (commonly used for code revision);

(3) Cost benefit analysis. Target reliability is chosen to minimize total expected costs over the service life of the structure. This method is preferred but is impractical due to the data requirements of the method.

Mansour (1997) reviewed the sources of information on target reliabilities and suggested that the reliability index for collapse strength of commercial ships be set at 3.5. Guedes Soares et al (1996), suggested that the tentative reliability indices against hull girder collapse are set at 3.7 for the "as built" state and 3.0 for the lower limit of corroded hulls. This is based on their investigation of worldwide causalities and structural safety level implicitly built-in to present ship design practice. The corroded state was defined as such that the section modulus is 90% of the original ("new-built"). Two methods can be used to evaluate the partial safety factors:

γ_s, γ_w and ϕ_u are given by the ratio of the design value of the variables to the corresponding nominal value. The design value is the most likely failure point as calculated by first order reliability method. The following relationships can be derived (Mansour, 1997),

$$\gamma_s = \frac{\chi_s^* M_s^*}{M_s^n}, \gamma_w = \frac{\chi_u^* M_w^*}{M_w^n}, \phi_u = \frac{\chi_u^* M_u^*}{M_u^n}$$

where X^* is design value and X^n is the nominal value;

For a given target reliability index β_0, characteristics for the strength (cov) and probability distribution of load effects, the partial safety factors, and minimum required strength can be determined by first-order reliability method.

Table 26.3 is used to define guidance for the hull girder strength design.

Table 26.3 Variable Reference Measurements

Variable	Description
M_u	Ultimate strength, lognormal variable, mean=undermined, cov=0.10.
M_s	SWBM, Type I extreme variable
M_w	VWBM, Type I extreme variable
φ_w	Load reduction factor
χ_u	Model error of predicting ultimate strength, normal variable, mean=1, cov=0.05.
χ_s	Model error of predicting SWBM, normal variable, mean=1, cov=0.1.
χ_w	Model error of predicting VWBM, normal variable, mean=1, cov=0.24 (sagging condition).
β^0	Target annual reliability index in new-built state β^o =3.7.
β^c	Target annual reliability index in corroded state. β^c =3.0.

Figures 26.4 and 26.5 show the required ultimate strength of a new-built and converted FPSO as a function of the environmental severity factor and the geometrical parameter Ψ defined by the combination of principal particulars, e.g.

$$\Psi = C_w L^2 B(C_B + 0.7)$$ (26.24)

The numerical range of Ψ is between 1.3757×10^8 and 5.2879×10^8, which covers the length of 180~260m, the breadth of 30~46m and the block coefficient of 0.80~0.92 according to the principal particulars of most existing FPSOs (macGregor, 2000). The symbols of A1~A5 in Figure 26.4 and Figure 26.5 represent the values of Ψ with 1.3757×10^8, 2.0884×10^8, 2.8879×10^8, 4.0504×10^8 and 5.2879×10^8 respectively. With the increase of the environmental severity factor or the dimension parameter Ψ, the required ultimate strength increases. The required ultimate strength is approximately a bilinear function of the environmental severity factor and of the geometrical parameter Ψ.

Other results from the present calculations are the partial safety factors. It is found that the resistance factor is slightly dependent on the environmental severity factor and independent of the geometrical parameter Ψ. The relationship between the partial safety factors and the environmental severity factor are shown in Figures 26.6 and 26.7 for new-built and converted FPSO.

In accordance with the results of Figures 26.4 and 26.5, the following two regressive formulas have been obtained: For a new-built FPSO

$$M_u = -0.065(1 + 2.778k_s)C_w L^2 B(C_B + 0.7)$$ (26.25)

For a converted FPSO

$$M_u = -0.060(1 + 2.635k_s)C_w L^2 B(C_B + 0.7)$$ (26.26)

It should be emphasized that the above formulas cannot be interpreted in an absolute way, and the numbers cited have to be considered as guidance only. However, the methodology may be

applied to develop structural design criteria for new-built FPSOs and converted FPSOs, when sufficient data is available.
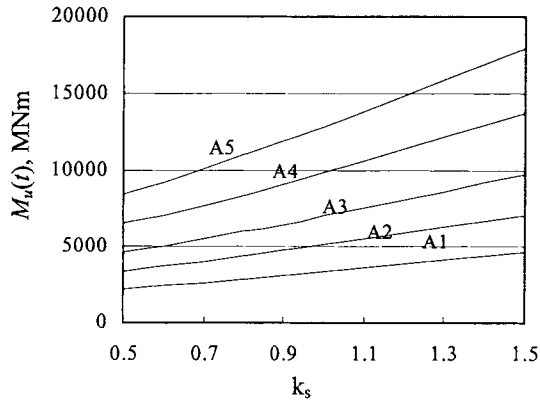
Figure 26.4   Effect of Environmental Severity Factor and Ship's Principal Particulars on Minimum Required Ultimate Strength for a New-Built FPSO
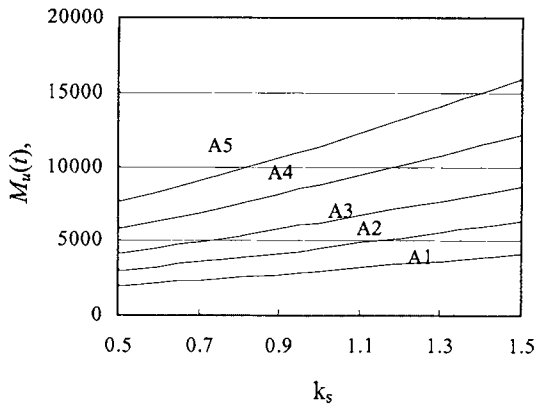
Figure 26.5   Effect of Environmental Severity Factor and Ship's Principal Particulars on Minimum Required Ultimate Strength for a Converted FPSO.
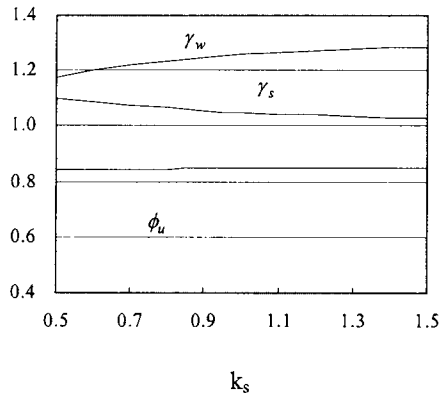
Figure 26.6   Partial Safety Factors vs. k_s for a New FPSO
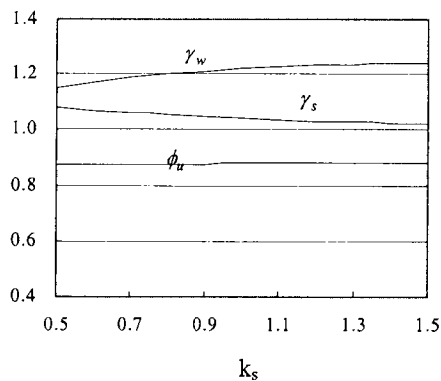
Figure 26.7   Partial Safety Factors vs. k_s for a Converted FPSO

26.7 References

1. AISC (1986), "Load and Resistance Factor Design", in *Manual of Steel Construction*, American Institute of Steel Construction, Chicago

2. API (1989), "Recommended Practice for Planning, Designing and Constructing Fixed Offshore Platforms—Load and Resistance Factor Design", API RP2A-LRFD, American Petroleum Institute, TX.

3. Bai, Y. and Song, R. (1997), "Fracture Assessment of Dented Pipes with Cracks and Reliability-based Calibration of Safety Factors", International Journal of Pressure Vessels and Piping, Vol.74, pp. 221-229.

4. Bai, Y. and Song, R. (1998), "Reliability-Based Limit State Design and Requalification of Pipelines", Proceedings of 17th Offshore Mechanics and Arctic Engineering (OMAE'98), Portugal, July, 1998.

5. Bea, R. and Craig, M. (1997), "Reliability Based Load and Resistance Factor Design Guidelines for Offshore Platforms to Resist Earthquakes", Prof. 16th OMAE, Yokohama, Japan.

6. Birkinshaw, M. and Smith, D. (1996), "The Setting of Target Safety Levels for the Assessment of Offshore Structures", Proc. 6th Int. Offshore and Polar Engineering Conference, USA.

7. Efthymiou, M., Van, J.W., Tromans, P.S. and Hines, I.M. (1997), "Reliability-Based Criteria for Fixed Steel Offshore Platforms", Journal of OMAE, Vol. 119, May.

8. Guedes Soares, C, Dogliani, M., Ostergaard, C., Parmentier, G. and Perdersen, P. Terndrup (1996), "Reliability Based Ship Structural Design", Trans. SNAME, Vol. 104, pp.375-389.

9. MacGregor, J. R., et al, (2000) "Design and Construction of the FPSO Vessel for the Schiehallion Field", Trans. RINA, Vol. 142, pp. 270-304.

10. Mansour, A. E. (1997), "Assessment of Reliability of Ship Structures", SSC-398, Report of Ship Structures Committee.

11. Ravindra, M.K. and Galambos, T.V. (1978), "Load and Resistance Factor Design for Steel", J. of the Structural Division, Vol. 104, pp.1337-1353.

12. Song, R, Tjelta, E and Bai, Y. (1998), "Reliability-based Calibration of Safety Factors for Tubular Joint Design", Proc. 8th International Offshore and Polar Engineering Conference (ISOPE'98), Montreal, Canada, May, 1998.

13. Sun, H.H. and Bai, Y. (2001), "Time-Variant Reliability of FPSO Hulls", SNAME Transactions, Vol. 109.

Part IV

Structural Reliability

Chapter 27 Fatigue Reliability

27.1 Introduction

In conventional strength assessments, the safety of the marine structure is considered under a static maximum design load. However, marine structures are to a large extent affected by stresses that vary over time. The causes of these stresses are the forces generated by a seaway and the propulsion plant, but also changes in the cargo loading.

The failure behavior of a structure subjected to fatigue loading deviates markedly from that of a structure subjected only to static loading. Static loading can give rise to various forms of failure such as yielding, instability or brittle fracture. Such failure occurs under a single extreme load. The damage caused by fatigue loading can be outlined as follows: In the crack initiation phase, microscopic fatigue cracks are formed as the result of an accumulation of alternating plastic deformations. Here local structural changes, precipitation, microstructure changes, etc. can occur. In the further course of the damage, the fatigue crack develops out of one or more microcracks running along slip bands.

Fatigue is a typical failure mode for in-service structures. Proper prediction of the fatigue behavior is of vital importance to maintain a sufficient level of reliability and integrity in structures.

High cycle fatigue is a governing design criterion for certain welded components in marine structures with large dynamic loading, high stress concentration and high stress level due to use of high strength steel, notably braces and brace to deck connections. Fatigue may be of concern for the primary strength of ships. However, most fatigue cracks have been experienced in secondary members, such as transverse frames, especially in joints between longitudinal stiffeners and frames.

A large uncertainty is introduced in fatigue assessment due to various assumptions and hypotheses. Additional uncertainties are due to the lack of the data and inherent random nature exists in the analysis. This necessitates the use of statistical and reliability approaches.

The fundamentals of fatigue strength assessment for ships and other marine structures are explained, e.g. Part 4 of this book, Almar-Naess (1985), Rice et al (1988), Maddox (1991), among others.

27.2 Uncertainty in Fatigue Stress Model

27.2.1 Stress Modeling

The process of computing stresses in a component includes the following steps:

1. Defining and modeling the environment,

2. Translating the environment into forces on the structure,

3. Computing the response of the structure to the environmental loads,

4. Computing nominal stresses in the components, and

5. Computing the stresses to be used for design, e.g., the stress at points of stress concentration.

Assumptions are made at each step, and all of the assumptions contain some uncertainty.

27.2.2 Stress Modeling Error

A simple way to measure the stress modeling error is to define a model uncertainty, with a random variable B, see Part IV Chapters 23 and 24:

$$S_a = B \cdot S$$

(27.1)

where

B = bias that quantities the modeling error

S_a = actual stress

S = estimated stress

Several sources can contribute to the model uncertainty, e.g. Wirsching and Chen (1988):

B_M = manufacturing fabrication and assembly operation

B_S = sea state description

B_F = wave force prediction

B_N = nominal member loads

B_H = estimation of the stress concentration factor (SCF) in stress analysis.

Using these five bias factors, the following representation of B is obtained

$$B = B_M \cdot B_S \cdot B_F \cdot B_N \cdot B_H$$

(27.2)

Assuming that each random variable is lognormally distributed, the mean and the COV of B are respectively

$$\bar{B} = \prod_i \bar{B}_i$$

(27.3)

where i=M, S, F, N, H. and the COV is

$$C_B = \sqrt{\prod_i (1 + C_i^2)} - 1$$

(27.4)

Four levels of refinement of stress analysis are possible, see Table 27.1. Note that the intervals are not symmetric because the lognormal is not symmetric.

Table 27.1 Levels of Uncertainty in Stress Prediction

Level	Coefficient of Variation C_B	Tolerance Level*
1	0.30	0.55 to 1.80
2	0.25	0.61 to 1.65
3	0.20	0.67 to 1.50
4	0.15	0.74 to 1.35
*Assume:	(1) $\tilde{B} = 1.0$; (2) B has a lognormal distribution; and (3) tolerances based on ± 2 standard deviations.	

Some general guidelines regarding the choice of level

Level 1   Use for a safety check expression using the design stress. Default values are assumed for the Weibull shape parameter and the service life. There is little confidence in the estimates of the loads.

Level 2   The Weibull model for long-term stress ranges is used. Reasonable estimates of the parameters are available.

Level 3   The Weibull model for long-term stress ranges is used with good estimates of the parameters obtained from tests on similar ships. The histogram and/or spectral methods with only moderate confidence of the parameters.

Level 4   A comprehensive dynamic and structural analysis of the ship over its predicted service history has been performed as the basis for the input for the histogram or spectral method.

27.3 Fatigue Reliability Models

27.3.1 Introduction

The calculation of the fatigue damage for a structural detail is based on several variables. Each of these variables is to some extent random. In order to account for this randomness, implicit and explicit safety factors are widely used. The safety factors are rather subjective measures that are calibrated based on past experience. Information about the degree of uncertainty of different variables can not be used effectively.

Reliability theory offers a way to include uncertainty information in the fatigue damage calculation. It allows calculating the component reliability, i.e. the probability that a detail has failed at the end of the specified lifetime. Using system reliability it is possible to evaluate the reliability of a system of structural details.

A probabilistic approach to fatigue life prediction consists of probabilistic methods applied in combination with either S-N approach or fracture mechanics approach. Probabilistic analysis in combination with the S-N approach is usually carried out at the structural design stage while the probabilistic analysis of remaining life after inspection is usually based on fracture mechanics (FM) techniques.

This section documents the fatigue reliability models. There are many papers on this subject, e.g. Wirsching (1984), White and Ayyub (1987), Hovde and Moan (1994), Xu and Bea (1997), Wirsching and Mansour (1997).

27.3.2 Fatigue Reliability - S-N Approach

Based on Part III Chapter 19, the cumulative fatigue damage in a period with N_0 cycles can be expressed as

$$D = \frac{N_0}{K} \cdot \frac{S_0^m}{(\ln N_0)^{m/\xi}} \Gamma\left(1 + \frac{m}{\xi}\right) \tag{27.5}$$

where K and m are material parameters, $\Gamma(.)$ is the Gamma function. S_0 and ξ are maximum stress range and Weibull shape parameter for long-term distribution of the stress range. The fatigue failure criterion is defined as

$$D \geq \Delta \tag{27.6}$$

where Δ is the Miner's sum at failure. The uncertainties in the endurance limit N_0 may be considered as a variable X_{N0} following a lognormal distribution with COV ranging from 5% - 20%. Introducing stress modeling parameter B, the limit-state function (LSF) may be written as

$$g_i(Z) = \Delta - \frac{N_0}{K} \cdot \frac{B^m S_0^m}{(\ln N_0)^{m/\xi}} \Gamma\left(1 + \frac{m}{\xi}\right) \tag{27.7}$$

The above LSF may be re-expressed as

$$g_i(Z) = K\Delta \cdot \frac{(\ln N_0)^{m/\xi}}{B^m S_0^m \Gamma\left(1 + \frac{m}{\xi}\right)} - N_T \tag{27.8}$$

where N_T denotes the intended service life.

27.3.3 Fatigue Reliability - Fracture Mechanics (FM) Approach

The probabilistic fracture mechanics is extended from the deterministic Paris-Erdogan's equation for the crack increment per cycle

$$\frac{da}{dN} = C \cdot (\Delta K)^m \tag{27.9}$$

where,

a	= crack depth
N	= number of cycles
C, m	= material constants
ΔK	= K_{max}-K_{min}, range of stress intensity factor, $K = S \cdot \sqrt{\pi \cdot a} \cdot F$
S	= nominal stress in the member normal to the crack
F	= correction factor depending on the geometry of the member and the crack

Initial crack size: Surface defects are usually more dangerous than embedded defects because they are often located at stress concentrations, have a crack-like shape and are oriented normal to the principal stress. The statistical distribution for such defects is the necessary information. The initial crack size is assumed to be independent and treated as a random variable following an exponential distribution:

$$F_{A_0}(a_0) = 1 - \exp\left(-\frac{a_0}{\lambda_0}\right) \tag{27.10}$$

in which, λ_0 is the distribution parameter of initial crack size.

Crack initiation time: For lack of data about the crack initiation time, a simple model is to assume that crack initial time t_0 is some percentage of crack propagation time T_p, and may be expressed as,

$$t_0 = \delta \cdot T_P \tag{27.11}$$

where, δ is a constant, T_P is crack propagation time.

Crack Propagation Prediction: Considering the effect of stress ratio, the modified Pairs law can be rewritten as,

$$\frac{da}{dN} = C\left(\frac{\Delta K}{1-R}\right)^m \tag{27.12}$$

where a is the crack size, N is the number of stress cycles, C and m are parameters depending on material and environment, R is the stress ratio, which depends on stress amplitude in stochastic time history. R is set to 0 in the following analysis. ΔK is the stress intensity factors range and can be estimated from Newman's approximation (Newman and Raju, 1981) given by

$$\Delta K = S\varepsilon_Y Y(a,X)\sqrt{\pi a} \tag{27.13}$$

where S is the stress range and Y(a,X) is a geometry function accounting for the shape of the specimen and the crack geometry, ε_Y is a randomized model uncertainty of geometry function.

By separating variables in Eq.(27.12) and introducing Eq. (27.13)

$$\frac{da}{\varepsilon_Y^m \cdot Y(a,X)^m \cdot (\sqrt{\pi a})^m} = C(\Delta S)^m dN \tag{27.14}$$

Then, the differential equation can be expressed as:

$$\int_{a_0}^{a_N} \frac{da}{\varepsilon_Y^m \cdot Y(a,X)^m \cdot (\sqrt{\pi a})^m} = C\sum_{i=1}^{N}(\Delta S_i)^m = N\sum_{i=1}^{N}\frac{1}{N}(\Delta S_i)^m = NE[(\Delta S)^m] \tag{27.15}$$

Since the stress response induced by sea loads is typically a narrow-band process, the number of stress cycles spent for crack growth N may be defined as

$$N = v_0(r \cdot t - t_0) \tag{27.16}$$

where v_0 is the average zero-crossing rate of stress cycles over the lifetime of the ship, r is the fraction of service time for the ship.

The crack size at the *ith* ship structural detail location at time t can be derived from the above equations with R=0 (Song and Moan, 1998)), as

$$a_i(t) = \Psi^{-1}\left(\Psi(a_{0i}) + C_i v_0 (rt - t_0) \varepsilon_S^m A_i^m \Gamma\left(1 + \frac{m}{\xi}\right) \right) \tag{27.17}$$

where $\Psi(.)$ is the auxiliary function, which is monotonically increasing with the crack size a, expressed as

$$\psi(a) = \int_0^a \frac{da}{\left(\varepsilon_Y Y(a, X) \sqrt{\pi a}\right)^m} \tag{27.18}$$

and

$$A_i = \frac{S_0}{(\ln N_0)^{1/\xi}} \tag{27.19}$$

Assuming that $\ln A_{\backslash i}$ follows normal distribution.

Fatigue failure criterion: When the critical crack size a_C is defined, which may be considered according to the serviceability, the fatigue failure criterion at cycle number N is defined as

$$a_c - a(t) < 0 \tag{27.20}$$

Limit State Function: Based on fracture mechanics, the failure criterion is written in terms of the crack size at time t. The limit state function (LSF) for the *ith* ship structural detail location can thus be written equivalently as (see, e.g. Madsen, 1986)

$$g_i(Z) = \int_{a_{0i}}^{a_{ci}} \frac{da}{\left(\varepsilon_Y Y(a, X) \sqrt{\pi a}\right)^m} - C_i v_0 (rt - t_0) \varepsilon_S^m A_i^m \Gamma\left(1 + \frac{m}{\xi}\right) \tag{27.21}$$

where Z is a set of random variables of material and stress parameters, geometry function, initial crack size, crack growth time, etc. a_{ci} is the critical crack size of the *ith* potential crack site, a_{0i} is the initial crack size at the *ith* crack site which can be calibrated with respect to crack growth part of S-N curve.

Uncertainty in fracture mechanics model: Uncertainties associated with the probabilistic fracture mechanics model include the follows

- initial crack size,
- long-term loading,
- material parameters
- geometry correction factor in stress intensity factor computation, and
- critical crack size.

Initial crack size depends mainly on the material microstructure and fabrication process and the welding quality. Thus, large uncertainty in initial crack size is obvious. In general, the

initial crack size is treated as random variable where the distribution is selected as exponential as given by Eq. (27.10).

The material constants in crack growth analysis are characterized by the two parameters C and m. Due to the uncertainties observed from the experimental studies, C and m should be modeled as random variables. It is generally accepted that C is modeled as a lognormal distributed and m is normal distributed.

The geometry correction factor that is determined by Newman-Raju equation or the hybrid method involves large uncertainty. Its uncertainty is included in the ε_y.

The critical crack size can be selected as a random variable or fixed variable based on serviceability conditions.

27.3.4 Simplified Fatigue Reliability Model – Lognormal Format

For fatigue reliability assessment using lognormal format, uncertainty is introduced as the bias factor in fatigue stress while the other uncertainty associated with fatigue strength are all treated as log normal random variables. This was first developed by Wirsching (1984) and further implemented by Wirsching and Chen (1988).

Eq.(27.8) may be re-written as

$$g_i(Z) = \frac{K\Delta}{B^m \Omega} - N_T \tag{27.22}$$

where the stress parameter is defined as the follows and may be considered as deterministic,

$$\Omega = S_0^m \frac{\Gamma\left(1 + \frac{m}{\xi}\right)}{(\ln N_0)^{m/\xi}} \tag{27.23}$$

There will be a closed form solution for the fatigue failure probability,

$$P_f = P[N \le N_T] \tag{27.24}$$

Assuming the analytical form follows the lognormal format, the reliability index β may be defined as

$$\beta = \frac{\ln\left(\tilde{N}/N_T\right)}{\sigma_{\ln N}} \tag{27.25}$$

$$\tilde{N} = \frac{\widetilde{K\Delta}}{\tilde{B}^m \Omega} \tag{27.26}$$

$$\sigma_{\ln N} = \sqrt{\ln\left[\left(1 + C_K^2\right)\left(1 + C_\Delta^2\right)\left(1 + C_B^2\right)^{m^2}\right]} \tag{27.27}$$

where C_s denotes the COV of each variable.

Uncertainty measures: For the Wirsching's S-N lognormal reliability model, it's necessary to specify the mean and COV of K, B and Δ, which are assumed to be lognormal distributed variables.

The variables B and Δ are used to quantify the modeling error associated with assumption made in the stress analysis and the description of the fatigue strength.

For random variable Δ describing the modeling error associated with Miner-Palgrem hypothesis, the following values for $\overline{\Delta}$ and C_Δ are widely used, $\overline{\Delta} = 1.0$ and $C_\Delta = 0.3$.

For random variable K, it is associated with the uncertainty in the S-N relationship. For the S-N curves established from the fatigue tests, the median value is determined by the experimental tests for different S-N categories while the COV is derived as 0.3-0.6 based on experimental data analysis.

27.4 Calibration of FM Model by S-N Approach

Both S-N curve approach and FM approach have been applied to calculate failure probability:

- Based on the S-N curve and Miner's rule, the LSF can be written as Eq.(27.7), where Δ is the Miner's sum at failure, N_0 is the number of cycles over the design lifetime that causes initiation and propagation. lnK is modeled as a normal distribution.

- Alternatively, a_0 and t_0 used in the FM based LSF Eq. (27.21) can be combined together by neglecting t_0 in the expression and substituting a_0 by $a_{0.eq}$ which is an equivalent initial crack size accommodating crack initiation time.

Accordingly, there is a correlation between these two approaches. This means that the initial crack size used in the FM model may be calibrated to the S-N approach (Song & Moan, 1998).

The numbers of stress cycles to failure can be written as

$$N = KS^{-m} = N_i + N_g = N_i + \int_{a_0}^{a_c} \frac{da}{C\left(\varepsilon_Y Y(a, X)\sqrt{\pi a}\right)^m} \tag{27.28}$$

where a_0 corresponds to the crack size after N_i cycles of crack initiation.

Assuming that $N_i = \delta \cdot N$, the calibration of initial crack size a_0 can be done according to

$$N - N_i = (1 - \delta)N = \int_{a_0}^{a_c} \frac{da}{C\left(\varepsilon_Y Y(a, X)\sqrt{\pi a}\right)^m} \tag{27.29}$$

The median value of the initial crack size a_0 can be calibrated by other variables from Eq. (27.29). It is generally believed that the calibrated a_0 will also depend on the crack initiation period indicated by δ. In the calibration, m may be modeled as a fixed value or a random variable of normal distribution.

In a similar way, the S-N approach can also be calibrated against FM approach. In another word, the crack size can be explicitly included in a S-N curve. No matter which approach is going to be calibrated, the principle of calibration is that the different approaches should yield consistent fatigue life.

27.5 Fatigue Reliability Application - Fatigue Safety Check

27.5.1 Target Safety Index for Fatigue

The basic design requirement is that the safety index describing the reliability of a component exceeds the minimum allowable, or target, safety index.

$$\beta \geq \beta_0 \tag{27.30}$$

The value of β_0 and the statistics on the design variables are used to derive the expression for the target damage level.

For a safety check expression, it is necessary to specify a minimum allowable safety index (or target safety index), β_0. The target safety index for each of the categories was chosen to be compatible with the values selected for other similar applications:

Table 27.2 Target Safety Index (Mansour, 1997)

	Description	Target Safety Index, β_0
Category 1	A significant fatigue crack is not considered to be dangerous to the crew, will not compromise the integrity of the ship structure, will not result in pollution; repairs should be relatively inexpensive	1.0
Category 2	A significant fatigue crack is not considered to be immediately dangerous to the crew, will not immediately compromise the integrity of the ship, and will not result in pollution; repairs will be relatively expensive	2.5
Category 3	A significant fatigue crack is considered to compromise the integrity of the ship and put the crew at risk and/or will result in pollution. Severe economic and political consequences will result from significant growth of the crack	3.0

27.5.2 Partial Safety Factors

An alternative approach to developing probability-based design criteria for the fatigue limit state is to use partial safety factors. Eq. (27.22) may be expressed as

$$N = \frac{K\Delta}{B^m S_e^m} \tag{27.31}$$

Letting the cycles to failure N equal the service life, N_S; and assuming $\widetilde{B} = 1.0$, Eq. (27.31) may be re-written as

$$S_e = \left[\frac{K\Delta}{N_S}\right]^{1/m} \tag{27.32}$$

Considering S_e, Δ, and K are random variables, the following safety check expression may be defined,

$$S_e \le \frac{1}{\gamma_S}\left[\frac{(\gamma_\Delta \Delta_n)(\gamma_K K_n)}{N_S}\right]^{1/m} \tag{27.33}$$

where the subscript n refers to the nominal or design values. Reliability methods may be applied to calibrate the partial safety factors: stress factor γ_S, damage safety factor γ_Δ and material property safety factor γ_K. See Stahl and Banon (2002) for latest development on this subject.

27.6 Numerical Examples

27.6.1 Example 27.1: Fatigue Reliability Based on Simple S-N Approach

Problem

Assuming that the fatigue strength is described by a S-N curve and the fatigue loads are described by a Weibull distribution, then the fatigue damage can be obtained by equation (27.7) given by

$$D = \frac{N_0}{K} \cdot \frac{S_0^m}{(\ln N_0)^{m/\xi}}\Gamma\left(1+\frac{m}{\xi}\right)$$

If only Δ, S_0 and K are considered as random variables, the failure probability may be written as

$$P_f = \int_{g(Z)\le 0} f_X(x)dx \tag{27.34}$$

where

$$g(\underline{Z}) = X_1 - k\frac{X_2^m}{X_3} \tag{27.35}$$

and k is a constant.

Assuming m=3, k=10^6 and X_1, X_2 and X_3 are independent and specified in Table 27.3. Find the distribution of g($\underline{Z}$) and calculate failure probability directly using simple approach.

Table 27.3 Input Data

Random variable	Mean value	COV	Distribution
X_1	1	0	Deterministic
X_2	200	0.2	Lognormal
X_3	$6.93*10^{13}$	0.5	Lognormal

Solution

Before using FORM, it is shown that a simple approach can be applied to calculate P_f in the case. The Eq. (27.51) can be rewritten as

$$g(Z) = \ln X_1 - m \ln X_2 + \ln X_3 - \ln k \qquad (27.36)$$

Since X_1 is deterministic and equal to 1 the following simplification of equation (27.36) can be performed

$$g(Z) = -m \ln X_2 + \ln X_3 - \ln k \qquad (27.37)$$

The random variables X_2 and X_3 are lognormally distributed, which implies that $\ln X_2$, $\ln X_3$ and $g(Z)$ are normal distributions with the following mean and COV values

$$\sigma_{\ln X_2} = \sqrt{\ln(1 + COV_{X_2}^2)} = 0.198$$

$$\mu_{\ln X_2} = \ln \mu_{X_2} - 0.5\sigma_{\ln X_2}^2 = 5.279$$

$$\sigma_{\ln X_3} = \sqrt{\ln(1 + COV_{X_3}^2)} = 0.472$$

$$\mu_{\ln X_3} = \ln \mu_{X_3} - 0.5\sigma_{\ln X_3}^2 = 31.758$$

$$\sigma_g = \sqrt{m^2 \sigma_{\ln X_2}^2 + \sigma_{\ln X_3}^2} = 0.759$$

$$\mu_g = -m\mu_{\ln X_2} + \mu_{\ln X_3} - \ln k = 2.105$$

The reliability index and the failure probability is then

$$\beta = \frac{\mu_g}{\sigma_g} = 2.774$$

$$P_f = \Phi(-\beta) = 2.76 * 10^{-3}$$

27.6.2 Example 27.2: Fatigue Reliability of Large Aluminum Catamaran

The example given here is directly from Song and Moan (1998) to demonstrate the application of fatigue reliability to a large aluminum catamaran. Further details can be referred to their paper.

Description of the Case

The midship section of a catamaran and local structural details in the vicinity of the welds are shown in Figure 27.1 and Figure 27.2. Aluminum alloy 5083 is considered. The material properties are as follows: Young's modulus $E=68.6\times10^3$ MPa, yield strength $\sigma_y=250$ MPa, density $\rho=2700$ kg/m^3. The statistical value of material parameter lnC is taken from Table 27.4 assuming a COV of 0.5. The scale parameter A is determined from implied cumulative damage criterion and given in the Table 27.5. Fatigue parameters K and m are determined from BS8118 code (BSI, 1992). Data for R=0 is applied. Numerical calculations are conducted based on parameters listed in Table 27.6.

Table 27.4 Statistical Value of Material Parameter lnC (Song and Moan, 1998)

	m (BS8118)	logC=a+bm	LnC
R=0, a=-6.74	3.25	-10.12	-23.30
b=-1.04	3.5	-10.38	-23.90
R=0.3 a=-7.09	3.25	-9.8525	-22.69
b=-0.85	3.5	-10.065	-23.18

Table 27.5 Stress Scale Parameter lnA Based on BS8118 (BSI, 1992)

D	S-N characteristic values	Parameter A	LnA
0.1	K=2.09E+11, m=3.25	.27707E+01	.1019E+01
	K=9.60E+11, m=3.5	.35842E+01	.1276E+01
0.3	K=2.09E+11, m=3.25	.38850E+01	.1357E+01
	K=9.60E+11, m=3.5	.49058E+01	.1590E+01

Table 27.6 Probabilistic Parameters for Fatigue Analysis(Song and Moan, 1998)

Variable	Distribution	Mean	COV
Initial crack size, a_0	Exponential	0.02	1.0
Crack initial time ratio, δ	Fixed	0.10	---
Detectable crack size, a_D	Exponential	1.0	1.0
Geometry bias factor, ε_Y	Normal	1.0	0.1
Stress model error, ε_S	Lognormal	1.0	0.1
Material parameter, ln C	Normal	-23.30	0.022
Stress scale parameter, lnA	Normal	1.019	0.10
Crack aspect ratio, a/c	Fixed	0.5	----
Random bias of a/c, $\varepsilon_{a/c}$	Normal	1.0	0.1
Miner's sum at failure, Δ	Lognormal	1.0	0.3
S-N fatigue parameter, lnK	Normal	27.065	0.019
Stress shape parameter, ξ	Fixed	0.95	----
Material parameter, m	Normal	3.25	0.06
Plate thickness, T_H	Fixed	30	----
Plate width, w_P	Fixed	100	----
Stress ratio, R	Fixed	0.0	----
Stress cycles per year, v_0	Fixed	2.5E+6	----
Fraction of a ship at sea, r	Fixed	0.765	----

Note: Correlation between m and lnC is $\rho(m, lnC)=-0.95$; a_0 is calibrated by S-N approach; lnA is estimated based on BS8118 code with D=0.1, K=2.09E+11, m=3.25.

Results and Assessment

Calibration of FM model: S-N curves have been developed based on laboratory tests. On the other hand, there are larger uncertainties in the material parameters that are used in Fracture Mechanics (FM) prediction. It is therefore useful to calibrate the FM material parameters against SN curves. Several analyses were performed with different FM models. Figure 27.3 gives the results of this calibration to achieve a consistent fatigue life based on FM and S-N approaches respectively. It is seen that if an identical parameter m=3.25 is used for FM and S-N, the calibrated results are a_0-EXP(0.02), m-N(3.25,0.06) and ρ(m,lnC)=-0.95 or a_0-EXP(0.007) and fixed m=3.25. If fixed m=3.5 is used for FM and S-N, the calibrated results are a_0-EXP(0.007), or a_0-EXP(0.015), m-N(3.5,0.06) and ρ(m,lnC)=-0.95. However, different m values may be applied for different models. If fixed m=3.5 is used for S-N approach, and m=3.25 is used for FM model, then the calibrated a_0 follows EXP(0.02). It is seen clearly that different calibrated a_0 are available based on the assumptions made. If crack initiation time ratio δ=0.1, this will increase a_0 by about 20% compared to the case with δ=0. If more cycles of N are assumed to be spent in crack initiation, the calibrated a_0 will be expected greater.

Basic parameter studies: Figure 27.3 shows the sensitivity of the reliability at t=4 years, with no inspection based on FORM analysis.

Effect of S-N fatigue parameters: The determination of the fatigue parameters K, m of the S-N formulation depends strongly on how the considered structural details are classified. It is assumed that the implied accumulated damage D equals to 0.1 and 0.3 respectively, corresponding parameters K and m are given in Table 27.8, COV of lnC and lnA are set to 0.5 and 0.1 respectively.

Effect of Weibull shape parameter: Based on preliminary investigations of the long-term distribution, it is assumed that B is 0.95 in this case study. A Parametric study is performed with the results shown in Figure 27.4. It is seen that the shape parameter B is quite influential on the fatigue reliability. Generally, the shape parameter B is in the range of 0.8 - 1.0 for ships. Instead of modeling B as a fixed value, it may be modeled as a stochastic variable. From the results shown in Figure 27.5, it is seen that if 1/B is modeled as normal distribution with μ=1.0526 and COV=0.1, the β will decrease comparing to the results of fixed B. If it is assumed that ρ(1/B, lnA)=-0.8, the effect of B is almost as the same as when B is modeled as fixed.
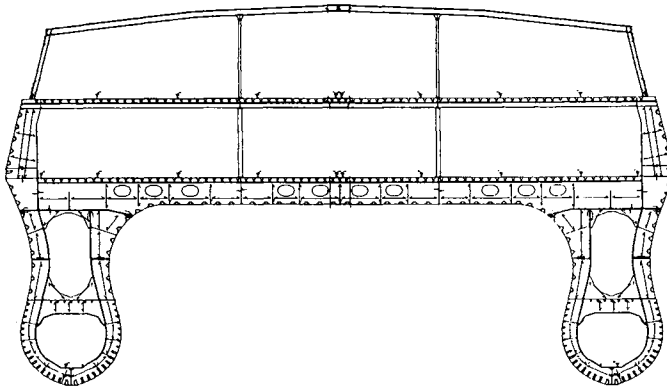
Figure 27.1   Typical Midship Section of A Catamaran (Song and Moan, 1998)
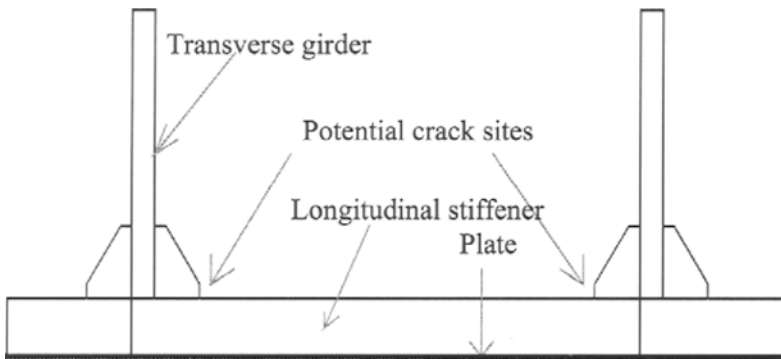
Figure 27.2   Considered Structural Details

Calibration of FM model: a0-EXP(0.02)
—— m-N(3.25,0.06), cc(m,lnC)=-0.95
Calibration of FM model: a0-EXP(0.007)
– – – Fixed: m=3.25
Calibration of FM model: a0-EXP(0.007)
– ·· – Fixed: m=3.5

SN Prediction
—+— D=0.1, m=3.25
—✕— D=0.1, m=3.5
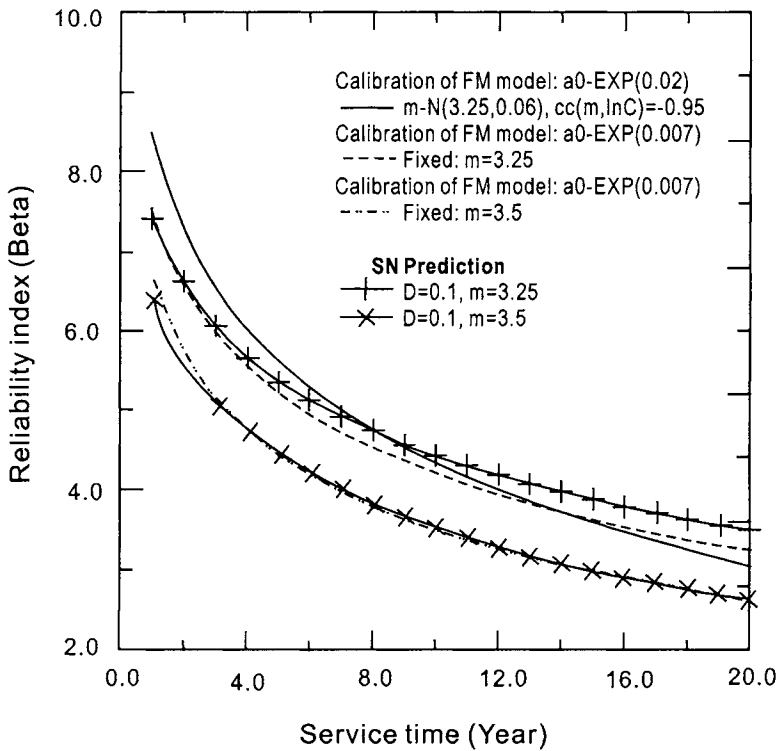
**Figure 27.3   Calibration of FM Model to S-N Approach for Sites with
Cumulative Damage Equal to D=0.1 (cc: correlation
coefficient) (Song and Moan, 1998)**
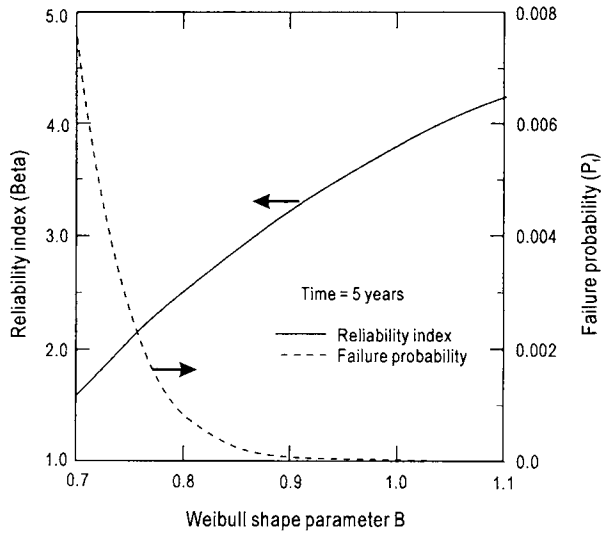
Figure 27.4   Effect of Shape Parameter B on β and P_F of A Component (Song and Moan, 1998)
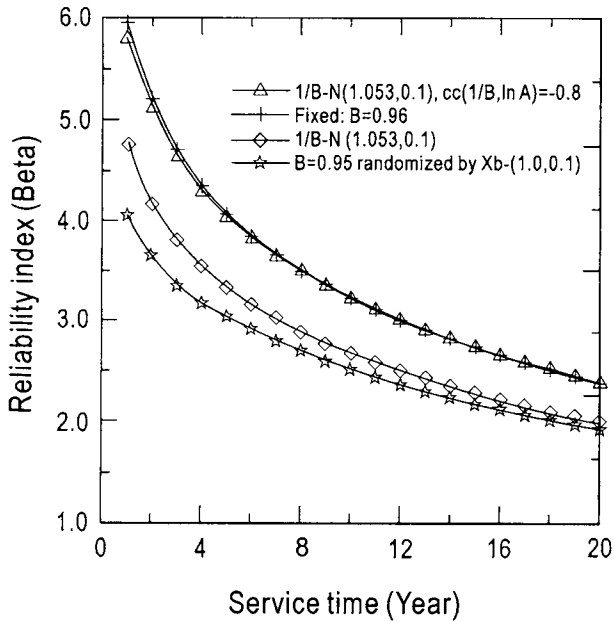
Figure 27.5   Effect of Different Models of Shape Parameter B on β of A Component (cc denotes correlation coefficient) (Song and Moan, 1998)

27.7 References

1. Almar-Næss, A. (ed.) (1985), *"Fatigue Handbook - Offshore Steel Structures"*, Tapir Press, Norway.

2. BSI (1992), "British Standards 8118, Code of Practice for the Structural Use of Aluminum", British Standards Institution, London.

3. Hovde, G.O. & Moan, T. (1994), "Fatigue Reliability of TLP Tether Systems", Proc. 13th OMAE.

4. Maddox, S. (1991), *"Fatigue Strength of Welded Structures"*, Abington Publishing, Cambridge, UK.

5. Madsen, H.O. et al (1986), *"Methods of Structural Safety"*, Prentice-Hall, Inc., Englewood Cliffs.

6. Miner, M.A. (1945), "Cumulative Damage in Fatigue", Transactions of the ASME, J. of Applied Mechanics, Vol. 12, pp. 159-164.

7. Moan, T. and Song, R. (1998), "Implication of Inspection Updating on System Fatigue Reliability of Offshore Structures", the Proc. 17th OMAE, Lisbon, Portugal, 1998.

8. Rice, R.C., et al (1988), "Fatigue Design Handbook, Society of Automotive Engineers", Inc., Warrendale, USA.

9. Song, R. and Moan, T. (1998), "Fatigue Reliability of Large Catamaran Considering Inspection Updating", Proceeding of the 8th International Offshore and Polar Engineering Conference (ISOPE'98), Montreal, Canada, May.

10. Stahl, B. and Banon, H. (2002), "Fatigue Safety Factors for Deepwater Risers", OMAE2002-28405.

11. White, G.J and Ayyub, B.N. (1987), "Reliability Based Fatigue Design for Ship Structures", J. of Naval Engineers, Vol. 99, No. 3.

12. Wirsching, P.H. (1984), "Fatigue Reliability of Offshore Structures", J. of Structural Engineering, Vol. 110, pp. 2340-2356.

13. Wirsching, P.H. and Chen, Y.N. (1988), "Considerations of Probability-Based Fatigue Design Criteria for Marine Structures", J. of Marine Structures, Vol. 1.

14. Wirsching, P.H. and Mansour, A.E. (1997), "Reliability in Fatigue and Fracture Analysis of Ship Structures", Proc. Symposium and Workshop on the Prevention of Fracture in Ship Structures, Edited by Reemsnyder, H., Washington, DC.

15. Xu, T. and Bea, R. (1997), "Marine Infrastructure Rejuvenation Engineering-Fatigue and Fracture of Critical Structural Details (CSD)," JIP report, Marine Technology & Management Group, University of California at Berkeley.

Part IV

Structural Reliability

Chapter 28   Probability and Risk Based Inspection Planning

28.1 Introduction

In-service inspections of marine structures are carried out in order to assure structural integrity. To optimize the in-service inspections, it is necessary to deal with the uncertainties in design, fabrication and damage detection as well as the adequacy of examining only limited amount of critical elements. Many efforts have been devoted to reliability updating through inspection and repair, see Moan (1993, 1997), Xu and Bea (1987). Moan and Song (1998), Song and Moan (1998) have studied inspection updating based on system consideration. Uses of probability-based inspection in other engineering fields are given by e.g. Yazdan and Albrecht (1990).

Risk assessment can be used as a valuable tool to assigning priorities among inspection and maintenance activities. A throughout discussion of risk assessment is given in Part V of this book. This Chapter shall present the following:

- Concepts of Risk Based Inspection
- Reliability Updating Theory for Probability Based Inspection
- Risk-Based Inspection Examples
- Risk-Based Optimum Inspection

28.2 Concepts for Risk Based Inspection Planning

In general, the dimensions of risk can be considered in the following three main categories:

- Personnel risk

     Fatality risk

     Impairment risk

- Environmental risk

- Asset risk

     Material (structural) damage risk

     Production delay risk

Risk is defined as

$$R=f(P_f,C) \tag{28.1}$$

where, P_f is the failure probability; C is the consequence of the failure.

A more general expression of the risk for practical calculation is given by

$$R = \sum \left(P_{f_i} \cdot C_i \right)$$
(28.2)

Then, the risk-based inspection can be planned by minimizing the risk.

$$\min\{R\}$$
(28.3)

The development of a system-level, risk-based inspection process includes the prioritization of systems, subsystems, and elements using risk measures, and definition of an inspection strategy (i.e., the frequency, method, and scope/sample size) for performing the inspections. The process also includes the decision about the maintenance and repair following inspections. Finally, there is a strategy for updating the inspection strategy for a given system, subsystem, or component/element, using the results of the inspection that are performed.

Figure 28.1 illustrates the overall risk-based inspection process which composed of the following four steps:

- Definition of the system that is being considered for inspection

- Use of a qualitative risk assessment that utilizes expert judgement and experience in identifying failure modes, causes, and consequences for initial ranking of systems and elements in inspection.

- Application of quantitative risk analysis methods, primarily using an enhanced failure modes, effects, and criticality analysis (FEMCA) and treating uncertainties, as necessary, to focus the inspection efforts on systems and components/elements associated with the highest calculated safety, economic, or environmental risk.

- Development of the inspection program for the components, using decision analysis to include economic considerations, beginning with an initial inspection strategy and ending with an update of that strategy, based on the findings and experience from the inspection that is performed.

Several feedback loops are shown in Figure 28.1 to represent a living process for the definition of the system, the ranking of components/elements, and the inspection strategy for each component/element. A key objective is to develop a risk-based inspection process that is first established and then kept up to date by incorporating new information from each subsequent inspection.

```
                              ┌─────────────────────────────────────────┐
                              │        System Definition                 │
                              │  * Defines System, System Boundary,      │
                              │    and fitness for purpose criteria      │
                              │  * Collect Information                    │
                              └─────────────────────────────────────────┘

                              ┌─────────────────────────────────────────┐
                              │   Risk Analysis                          │
                              │   * Define Failure Modes                 │
                              │   * Define Failure Criteria              │
                              │   * Identify Consequence                 │
                              │   * Rank Subsystem e.g. stiffened panel  │
                              │   * Rank Components/Elements              │
                              └─────────────────────────────────────────┘

         ┌───────────────────────────────────────────────────────────────────────┐
         │  (1) Failure Modes, Effects, and Critically Analysis                   │
         │      * Redefine Failure Modes                                          │
         │      * Redefine Failure Causes                                         │
         │      * Redefine Failure Consequence                                    │
         │      * Assess Failure Probabilities for the Fitness for Purpose        │
         │      * Assess Consequences                                             │
         │      * Risk Evaluation                                                 │
         │      * Risk Based Ranking                                              │
         └───────────────────────────────────────────────────────────────────────┘

Risk
Analysi
         ┌───────────────────────────────────────────────────────────────────────┐
         │  (2) Development of Risk Based Inspection Program                      │
         │      * Choose Potential Inspection Strategies                          │
         │        (Frequency, Methods, Sampling Procedures)                       │
         │      * Define Potential for Damage States                             │
         │      * Define Potential Damage for Inspection Damage                   │
         │      * Estimate Effect of Inspection on Failure Probabilities          │
         │      * Choose Inspection Strategy and Perform Inspection               │
         │      * Perform Sensitive Studies                                       │
         │      * Choose Appropriate Inspection, Maintenance,                     │
         │        Repair (IMR) System                                            │
         └───────────────────────────────────────────────────────────────────────┘
```

Figure 28.1   Risk-based Inspection Process (Xu et al, 2001)

28.3 Reliability Updating Theory for Probability-Based Inspection Planning

28.3.1 General

Baysian models have been applied to reliability updating for probability-based inspection planning. This Section shall present two major approaches that have been developed in the pat 30 years.

Updating Through Inspection Events to update the probability of events such as fatigue failure directly, (Yang, 1976, Itagaki et al, 1983, Madsen, 1986, Moan, 1993 & 1997). A simplified Bayesian method that only considers crack initiation, propagation and detection as random variables and independent components in a series system was proposed by Yang (1976) and Itagaki et al (1983).

Updating Through Variables to re-calculate failure probability using the updated probability distributions for defect size etc. (Shinozuka and Deodatis, 1989). The change in reliability index is caused by the changes in random variables. The distribution of a variable can be updated based on inspection events. When the variables are updated, the failure probability can be easily calculated using the updated variables. However, if several variables are updated based on the same inspection event, the increased correlation between the updated variables should be accounted for.

The approach for updating through inspection events will be further explained in the next subsection.

28.3.2 Inspection Planning for Fatigue Damage

Fatigue failure is defined as the fatigue crack growth reaches the critical size, e.g. wall thickness of the pipe. Based on fracture mechanics, the criterion is written in terms of the crack size at time t. By integrating Paris law, the limit state function can be written as, (See Part IV Chapter 27 of this book, Madsen et al, 1986)

$$g(Z) = \int_{a_0}^{a_c} \frac{da}{\left(\varepsilon_Y Y(a,X)\sqrt{\pi a}\right)^m} - C\nu_0 t \varepsilon_S^m A^m \Gamma\left(1 + \frac{m}{\xi}\right) \tag{28.4}$$

where, $Y(a,X)$ is the finite geometrical correction factor, ε_S is the stress modeling error, ε_Y is randomized modification factor of geometry function, ν_0 is the average zero-crossing rate of stress cycles over the lifetime, $\Gamma(.)$ is the Gamma function.

Basically, two most common inspection results are considered here, namely: no crack detected, and crack detected and measured (and repaired), see Madsen et al (1986).

No Crack Detection

This means that no crack exists or the existing crack is too small to be detected. This inspection event margin for the *ith* detail can be expressed as,

$$I_{no,i}(t_i) = a_D - a_i(t_i)$$

$$= \Psi(a_D) - \Psi(a_{0i}) - C_i \nu_0 t_i \varepsilon_S^m A_i^m \Gamma\left(1 + \frac{m}{\xi}\right) > 0 \tag{28.5}$$

in which, $a(t_i)$ is the crack size predicted at inspection time t_i, a_D is the detectable crack size.

The detectable crack size a_D is related to a specified inspection method and modeled as a stochastic variable reflecting the actual probability of detection (POD) curve. Among several formulations of POD available, the commonly used exponential distribution is selected in this case:

$$P_D(a_D) = 1 - \exp\left(-\frac{a_D}{\lambda}\right)$$

(28.6)

where λ is the mean detectable crack size.

Crack Detected and Measured

If a crack is detected and measured for a weld detail i, this inspection event can be written as

$$I_{yes,i}(t_I) = a_m - a_i(t_I)$$

$$= \Psi(a_m) - \Psi(a_0) - C_i \nu_0 t_I \varepsilon_S^m A_i^m \Gamma\left(1 + \frac{m}{\xi}\right) = 0$$

(28.7)

where, a_m is the measured crack size at time t_I and regarded as a random variable due to uncertainties involved in sizing. $\Psi(a)$ is a function reflecting the damage accumulation from zero to crack size a and is defined as (Paris and Erdogn, 1963, Newman and Raju, 1981),

$$\Psi(a) = \int_0^a \frac{da}{\left(\varepsilon_Y Y(a, X)\sqrt{\pi a}\right)^m}$$

Repair Events

The inspection itself does not increase the reliability of the structures, but it makes possible to take the necessary corrective actions like repair if a crack is detected. After repair, it is assumed that the material parameters and initial crack size follow the previous models but are statistical independent. This repair event based on crack detected and measured is the same as given by Equation (28.7), i.e. $I_R = I_{yes}$. After repair the failure event also needs to be modified as discussed below.

Reliability Updating Through Repair

If a crack is detected, measured and repaired, statistical properties of the material are expected to be the same magnitude but statistically independent. Weld defects, a_R, after (underwater) repair depends upon the repair and post-repair treatment methods (grind, a_{Rg} or weld, a_{Rw}). Here it is assumed to follow the same model as a_0. The new safety margin after repair, $M_R(t)$, becomes

$$M_R(t) = \int_{a_R}^{a_c} \frac{da}{\left(\varepsilon_Y Y(a, X)\sqrt{\pi a}\right)^{m_R}}$$

$$- C_R \nu_0 (t - t_R) \varepsilon_S^{m_R} A^{m_R} \Gamma\left(1 + \frac{m_R}{\xi}\right)$$

(28.8)

where, t_R is the repair time. Parameters a_R, C_R, m_R are assumed to follow the previous models but are statistically independent.

Updated failure probability for repaired structural details is written as

$$P_{F,up} = P\Big[M_R(t) \le 0 \Big| I_R(t_R) = 0\Big] \qquad t > t_R \tag{28.9}$$

It should be mentioned that an alternative way to consider repair effect is to update the random variables in equation (28.8) based on inspection events first. Then, the reliability can be estimated through repair safety margin by introducing initial crack size a_R depending upon repair methods applied.

28.4 Risk Based Inspection Examples

The methodology presented in Part IV Section 25.5 could be extended to risk-based inspection planning (Sun and Bai, 2001). As an example, the risk is defined as:

Risk=(Consequence of failure)×(Likelihood of failure)

where consequence of failure can be measured by:

C1: Loss of hull, cargo and life, which is the most serious consequence;

C2: Minor oil spill, serviceability loss and salvage;

C3: Unscheduled repair and serviceability reduction.

and likelihood of failure may be divided into three categories:

L1: Rapid corrosion rate;

L2: Nominal corrosion rate;

L3: Slow corrosion rate.

In the present analysis, it is assumed that all components with corrosion wastage larger than the critical size with certain probability of detection (POD) will be replaced and after that, their state will be recovered to the original.

The inspection are made in each year (Annual Survey), 2.5 years (Intermediate Survey) and 5 years (Special Survey) based on the survey strategy by classification societies. The four levels of POD for thickness measurement are considered, i.e. 60%, 80%, 90% and 95% under the inspection condition that POD is 99.9% when the thickness of corroded component reaches 75% of the original one.

The tentative reliability indices against hull girder collapse (one of most serious consequence of failure) are set at 3.7 for the "new-built" state and 3.0 for the lower limit of corroded hulls.

Figure 28.2 shows the time-variant reliability with the risk of C1 and L1 combination.

It can be seen that thickness measurement and renewal for the components with POD of less than 80% should be carried out in each Annual Survey after the 10th service year in order to meet the annual reliability index over the lowest limit of safety level. Figure 28.3 demonstrates the time-variant reliability with the risk of C1 and L2 combination.
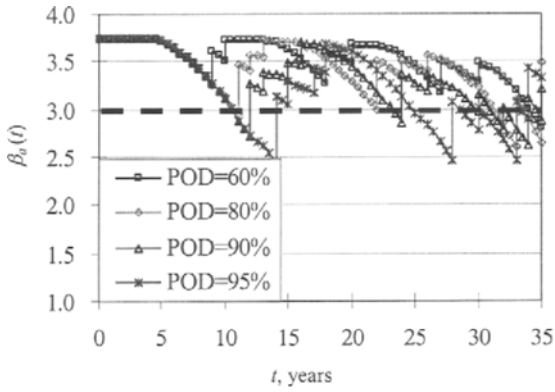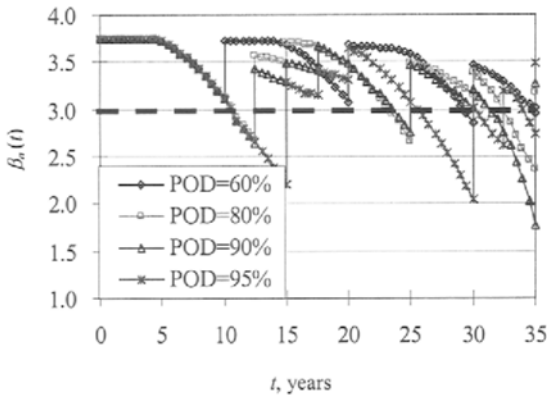
(1) Annual Survey

(2) Intermediate Survey
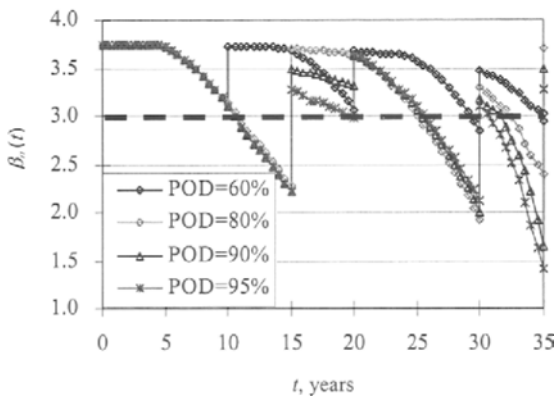
(3) Special Survey

Figure 28.2   Time-Variant Reliability with Risk of C1 and L1 Combination
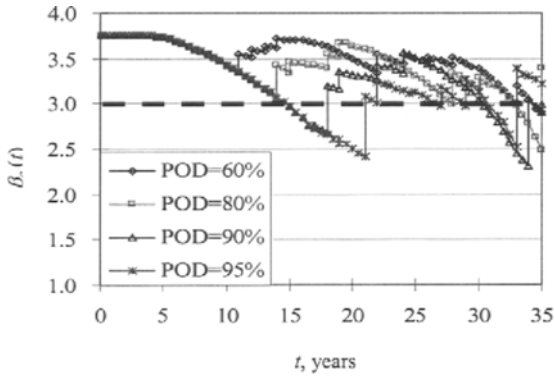
(1) Annual Survey
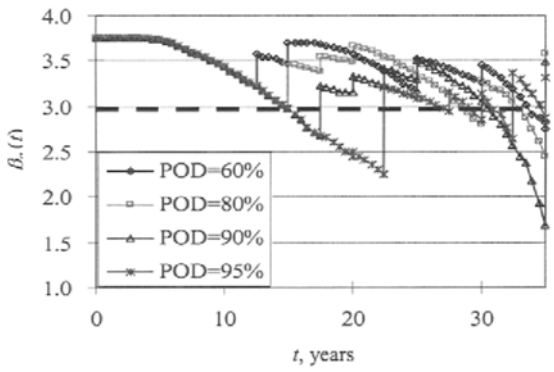
(2) Intermediate Survey
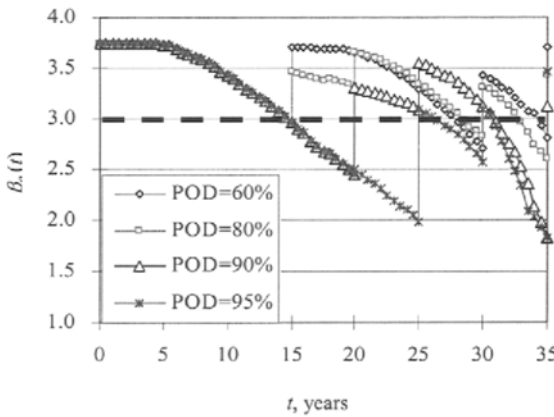
(3) Special Survey

**Figure 28.3   Time-Variant Reliability with Risk of C1 and L2
              Combination**
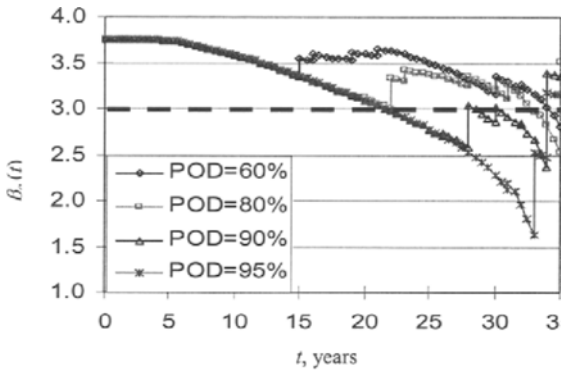
(1) Annual Survey
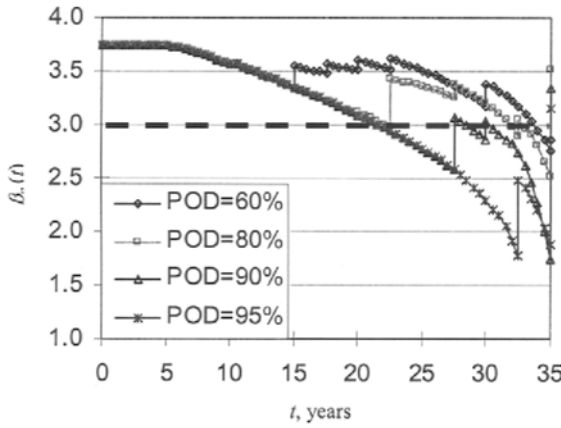
(2) Intermediate Survey
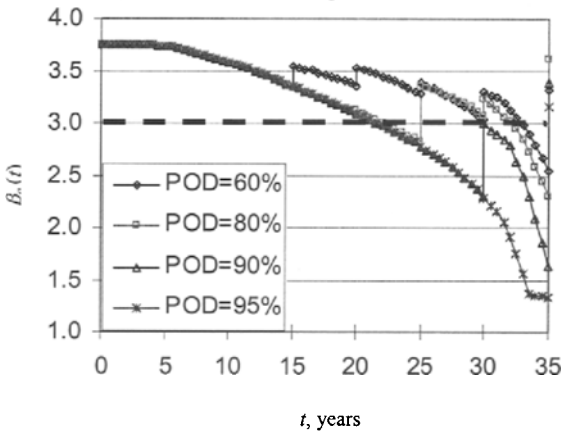
(3) Special Survey

Figure 28.4   Time-Variant Reliability with Risk of C1 and L3 Combination

It can be seen from the above figure that thickness measurements and renewal for the components with POD of less than 80% should be carried out in order to guarantee the annual reliability index over the lowest limit of safety level during the first 20 service years. They may be done in Special Survey No.3 during the first 20 service years, but should be implemented in Annual Survey if the FPSO is required to keep in service over 20 service years.

Figure 28.4 shows the time-variant reliability with the risk of C1 and L3 combination. From this figure, it is found that the annual reliability index is always greater than the lower limit of safety level and thickness measurement may not be necessary during the first   20 service years, but the thickness measurement and then renewal for the components with POD of less than 80% in Intermediate Survey should be carried out if the FPSO is required to keep in service over 20 service years.

From the above example, we conclude that the inspection planning is dependent on the consequence of failure (lower limit of safety level), corrosion rate, ship age and probability of detection (POD). The requirements of inspection gradually more demanding with the increase of the consequence of failure (lower limit of safety level), corrosion rate and ship age and with the decrease of POD. The latter usually makes thickness gauging and judgement more difficult.

28.5 Risk Based 'Optimum' Inspection

This Sub-section is based on Xu et al (2001). Experience with in-service inspections of ship and offshore structures have adequately demonstrated that there are two categories of damages:

- those could have been or were anticipated (natural, predictable)

- those could not have been anticipated (human caused, unpredictable)

A substantial amount (if not a majority) of damages falls in the second category - unpredictable and due to the 'erroneous' actions and inaction's of people.

Quantitative inspection analyses (e.g. probability or risk based inspection methods and programs) can help address the first category of defects by providing insights of when, where, and how to inspect and repair. However, such an analysis cannot be relied upon to provide information that addresses the second category of defects. Expert observation and deduction (diagnostic) techniques must be used to address the second category of defects.

Such recognition techniques lead to the development of the 'optimum' inspection method (Xu et al, 2001). The overall objective of the 'optimum' inspection method is to develop an effective and efficient safety and quality control system in the life-cycle management of the structural systems.

Inspection Performance

Inspection performance is influenced by the vessel, the inspector, and the environment.

The vessel factors can be divided into two categories: design factors and condition/maintenance factors. Design factors, including structural layout, size, and coating, are fixed at the initial design or through the redesign that may accompany repair. Condition/maintenance factors reflect the change in a vessel as it ages, including the operation history and characteristics of individual damages/defects (crack, corrosion, bucking), its size, and its location.

The person (inspector) who carries out an inspection can greatly influence the inspection performance. Performance varies not only from inspector to inspector, but also from inspection to inspection with the same inspector based on his mental and physical condition. Factors associated with the inspector include experience, training, fatigue, and motivation.

The environment, in which the inspection is carried out, has a major influence on performance. The environmental factors can be divided into two categories: external factors which cannot be modified by inspection procedures and procedure factors that can be modified. External factors include weather and location of the vessel, that is, whether the inspection is performed while underway, while in port, or while in dry-dock. Procedural factors reflect the condition during the inspection (lighting, cleanliness, temperature, ventilation), the way in which the inspection is conducted (access method, inspection method, crew support, time available), and the overall specification for inspection (inspection type).

Inspection Strategies

Inspections, data recording, data archiving (storage), and data analysis should all be a part of a comprehensive and optimum inspection system. Records and thorough understanding of the information contained in these records are an essential aspect of inspection programs.

Inspection is one part of the 'system' that is intended to help disclose the presence of 'anticipated' and 'unanticipated' defects and damage. Development of inspection programs should address:

- Elements to be inspected (where and how many?)

- Defects, degradation, and damages to be detected (what?)

- Methods to be used to inspect, record, archive, and report results (how?)

- Timing and scheduling (when?)

- Organization, selection, training, verification, conflict resolution, and responsibilities (who?)

- Objectives (why?)

- Where and How Many?

- The definition of the elements to be inspected is based on two principal aspects:

- Consequences of defects and damage

- Likelihood of defects and damage

The consequence evaluation essentially focuses on defining those elements, and components that have a major influence on the quality and safety of a FPSO. Evaluation of the potential consequences should be based on historical data (experience) and analysis to define the elements that are critical to maintaining the integrity of a FPSO. The likelihood evaluation focuses on defining those elements that have high likelihood's of being damaged. Experience and analyses are complementary means of identifying these elements.

What?

A substantial amount (if not the majority) of the damage is unpredictable and due to the unanticipated 'erroneous' actions and inaction's of people.

Current experience also indicates that the majority of damage that is associated with accidents (collisions, dropped objects) is discovered after the incident occurs. About 60% of damages due to fatigue and corrosion are detected during routine inspections. However, the balance of 40% is discovered accidentally or during non-routine inspections.

How?

The methods to be used in FPSO inspections are visual. In one form or another, these methods are primarily focused on getting an inspector close enough to the surface to be inspected so that he can visually determine if there are significant defects or damages. However, ultrasonic gauging, magnetic particle, radiographic, and other nondestructive methods, are sometimes necessary for structures.

When?

There are no general answers to the timing of inspections. The timing of inspections is dependent on:

- The initial and long-term durability characteristics of the FPSO structure

- The margins that the operator wants in place over minimums so that there is sufficient time to plan and implement effective repairs

- The quality of the inspections and repairs

- The basis for maintenance – 'on demand' (repair when it 'breaks or leaks' or 'programmed' (repair or replace on standard time basis)

Who?

Experience has adequately demonstrated that the single most important part of the inspection system is the inspector. The skills, knowledge, motivation, and integrity of the inspector are critically important. Equally important are the organizational influences exerted on the inspector, the procedures and processes that he is required to follow, the environments in which he must work, and the support hardware/systems that are provided to perform his work. Thus, the inspector is significantly influenced by 1) organizations, 2) procedures, 3) hardware (facilities), and 4) environments.

Much has been learned about how to improve the effectiveness and efficiency of the inspector. It is important that the inspector be recognized as a part of the system, as new inspection systems are designed.

Why?

The inspection should have objectives at several levels: first, it should provide the general information and knowledge about the in-service structures for fitness for purpose evaluation. Second, it should detect the damage/defects so effective and efficient maintenance and repair programs can be implemented to correct these damages/defects (quality control and assurance). Third, it is a safety control tool to prevent the failure or loss of the in-service structures during the inspection interval (safety control and assurance).

The inspection strategies (when, where, how, who) for different level objectives should be different. The first level inspection should select typical elements/components to provide general information about the in-service structures for fitness for purpose evaluation. Less detailed inspections are frequently associated with long-term maintenance and repair programs. The second level (quality control) inspection should focus on the critical components/elements in order to detect as many damage/defects as possible. It is associated with the short-term maintenance and repair program. The third level inspection (safety control) is used to prevent the most critical damage/defects or errors to ensure a safe operation during the inspection interval. It is the most detailed and difficult inspection, which identifies safety-related predictable or unpredictable damages/defects and errors. Every inspection practice for a specific fleet should be a combination of these three different inspection strategies.

The value of the inspection for objectives of different levels should also be different. The value of the first level inspection is about the decision on whether or not the existing structure can fulfill the purpose for extended service. The value of the second level inspection is about the decision of whether or not we should change the maintenance and repair program. The value of the third level inspection is about the decision of whether or not we should take any intermediate actions. Value analysis (value of information) can help make these decisions.

'Optimum' Inspection Method

The 'optimum' inspection method can be proactive (focused on prevention) or it can be reactive (focused on correction). It should have four functions:

- Assess the general conditions of the in-service offshore structures

- To confirm what is thought: to address the intrinsic damages/defects that can be prediction based results from technical analyses

- To disclose what is not known before inspection; to address damage/defects that cannot be predicted based on technical analyses

- To control the predictable and unpredictable damages

- To develop a high quality maintenance and repair program

The 'optimum' inspection program should begin with the design of the structure (conception), proceed through the life of the structure, and conclude with its scrapping (life cycle). The optimum inspection program should include not only the hull structure, but its equipment, and its personnel as well. The optimum inspections should become the means to assess the general conditions of the whole structure. The optimum inspections are also the means to detect unpredictable flaws and damages of the structural elements, and permit appropriate measures to be taken to preserve the safety and integrity of the structure. The optimum inspections are also the means to assure that all is going as expected, that the structural elements are performing as expected, and that corrosion protection and mitigation (e.g. patching pits, renewing locally excessively corroded plates) is maintained.

The 'optimum' inspection method starts from the survey for the intrinsic damage that is common for the class of structures. Based on experience, the inspection for the intrinsic damage can be conducted in a rational way. The existing risk-based inspection method discussed in earlier Sections, is the framework for the intrinsic damages/defects for the structural system. The probability-based inspection method can be applied to specific

elements/components based on the results of risk-based inspection. For the extrinsic damage of each individual structure, the knowledge-based diagnosis method should be developed. The systematic knowledge-based diagnosis process is a potential means to identify the extrinsic damages.

Knowledge systems routinely do diagnosis reasoning using three methods: model-based diagnosis, heuristic classification, and case-based reasoning. Our system uses a combination of each of these methods:

Model-Based Diagnosis (MBD) to identify the details of a large class of possible problems, heuristic classification to identify the presence of a set of idiosyncratic problems, and Case-Based Reasoning (CBR) to compare observation with previously identified cases.

An 'optimum' inspection method could include:

- Developing a standard task checklist to ensure that relevant data and tasks are not lost because of distractions or workload

- Performing global surveys to develop situation awareness for potential expected and unexpected damage and defects

- Inspecting high likelihood of damages or defect 'parts' and high consequence parts. If something 'suspicious' is found, the inspection is intensified by model-based diagnosis, heuristic classification, and case-based reasoning until root causes (not symptoms) are determined

- Periodic inspections, decreasing the time between inspections as the rate of degradation or likelihood of defects and damage increase

- Inspecting after accidents or 'early warning' signals are detected

- Implement the long-term and short-term maintenance and repair strategies based on the inspection results

- Update the IMMR (Inspection, Maintenance, Monitoring, and Repair) plan based on the survey results and the results from maintenance and repair

- Performing inspections that are independent from the circumstances that cause potential defects and damage

- Using qualified and experienced inspectors that have sufficient resources and incentives to perform quality inspections

Prior to the commencement of any general survey, a standard checklist and procedure should be established from the Structural Life-Cycle Information Management System, in order to carry out an effective evaluation of the structure's general condition:

- Structural drawing

- Operating history and conditions

- Previous damage/defects inspection results

- Condition and extent of protective coatings

- Classification status, including any outstanding conditions of class

- Previous repair and maintenance work

- Previous information on unpredictable damage or defects

- Expert's judgment and comments

- Relevant information from similar structures

With this information and previous inspection guidelines regarding critical elements/subsystems in the structural systems considered to be sites of potential damage/defects based on historical data, analyses results, and expert's judgment, it is possible to target the appropriate inspection strategies for the potential areas within the structure for general survey and the initial scope of the inspection. After completing the initial inspection to determine the general condition of the system, the inspector can develop situation awareness to identify some potential unpredictable critical damage/defect sites. Further knowledge-based diagnosis should be conducted for these suspicious areas. The knowledge-based diagnosis is conducted along with detailed inspections.

Inspection Data System

Little thought has been given to the efficient gathering of data and information, even less thought to what is done with this data and information when it is obtained, and far less thought given to the archiving, analysis, and reporting of the data. The interfaces in the data gathering, archiving, analysis, and reporting activities have received very little systematic thought. Current work has not been able to identify a single coherent and optimum, inspection data system.

Advances in information technology have resulted in better ways to use information for the management of safe and efficient ships and offshore structures. The integration of stand-alone systems combined with improved information recording, organization, and communication, offers substantial benefits for the life-cycle management of ship and offshore structures. A life cycle Structural Information Management System (SMIS) is intended to facilitate the life-cycle management. This includes areas from design and construction as well as operations including Inspection, Maintenance, Monitoring, and Repair (IMMR). The inspection data system is a component of the IMMR module in SMIS.

The general objectives of an inspection data system are:

- Collect inspection data

- Store the data

- Provide means for logic inspection data management

- Allow for the organization of the inspection data in a form suitable for fitness or purpose analyses, and failure analyses

- Analyze the data

- Show trends of the information such as damage/defects associated with structural integrity

- Communicate and report the data

Once a structure is ready for service, a series of inspections are scheduled according to inspection programs. The objective and scope of the internal tank inspections are defined. The access methods and data recording methods are chosen, and the inspections are performed. The inspection results including corrosion gauging, cracking, status of coating, and corrosion protection systems, as well as other structure/equipment defects are updated into the corresponding database. Using the inspected data, maintenance and repair strategies can be developed and the repairs are finally carried out.

28.6 References

1. Itagaki, H., Akita, Y., and Nitta, A (1983), "Application of Subjective Reliability Analysis to the Evaluation of Inspection Procedures on Ship Structures", Proc. Int. Symp. On the Role of Design, Inspection and Redundancy in Marine Structural Reliability, National Academic Press, Nov.

2. Madsen, H.O. et al (1986), "*Methods of Structural Safety*", Prentice-Hall, Inc., Englewood Cliffs.

3. Moan, T., (1993), "Reliability and Risk Analysis for Design and Operations Planning of Offshore Structures", Proc of the 6th Intl. Conf. on Struct. Safety and Reliability, ICOSSAR'93.

4. Moan, T., (1997), "Current Trends in the Safety of Offshore Structures, Keynote Lecture", Proc. 7th ISOPE, Vol. VI, Honolulu, USA.

5. Moan, T. and Song, R. (1998), "Implication of Inspection Updating on System Fatigue Reliability of Offshore Structures", Proceedings of 17th Offshore Mechanics and Arctic Engineering (OMAE'98), Portugal, July.

6. Newman, J.C. and Raju, I.S. (1981), "An Empirical Stress Intensity Factor Equation for Surface Crack", Engng. Frac. Mech., Vol. 15, 185-192.

7. Paris, P.C. and Erdogan, F. (1963), "A Critical Analysis of Crack Propagation Laws", J. of Basic Engng, Trans. ASME, Vol. 85.

8. Shinozuka, M. and Deodatis, O. (1989), "Reliability of Marine Structures under Bayesian Inspection".

9. Song, R. and Moan, T. (1998), "Fatigue Reliability of Large Catamaran considering Inspection Updating", Proceeding of the 8th International Offshore and Polar Engineering Conference (ISOPE'98), Montreal, Canada, May.

10. Song, R. and Zheng, P. (1999), "Reliability Assessment of Offshore Structures at Cold Phase Considering Inspection Effect", Proceeding of the 9th International Offshore and Polar Engineering Conference (ISOPE'99), Brest, France, May.

11. Sun H. and Bai, Y. (2001), "Time-Variant Reliability of FPSO Hulls", SNAME Transactions, Vol. 109.

12. Xu, T. and Bea, R. (1997), "Marine Infrastructure Rejuvenation Engineering-Fatigue and Fracture of Critical Structural Details (CSD)," JIP report, Marine Technology & Management Group, University of California at Berkeley.

13. Xu, T., Bai, Y., Wang, M. & Bea, R.G. (2001), "Risk based Optimum Inspection of FPSO Hulls", OTC12949, May 2001.

14. Yang, J.N., (1976), "Inspection Optimization for Aircraft Structures Based on Reliability Analysis", Journal of Aircraft, AAIA Journal, Vol. 14, No. 9, pp. 1225-1234.

15. Yazdan, N. and Albrecht, P. (1990), "Probabilistic Fracture Mechanics Application to Highway Bridges", Engng. Frac. Mech., Vol. 37, pp. 969-985.

Part V: Risk Assessment

This Page Intentionally Left Blank

Part V

Risk Assessment

Chapter 29 Risk Assessment Methodology

29.1 Introduction

29.1.1 Health, Safety and Environment Protection

In recent years, the management of health, safety and environmental protection (HSE) became an important subject for the design and construction of marine structures. The objective of design projects is to engineer safe, robust and operable structural systems at minimum life cycle cost. The HSE target is to have an injury/illness free work place in the design and construction process (Toellner, 2001). In addition, attention has been given to ergonomics and noise control for health protection (ASTM, 1988, 1995). Some of the other important subjects in HSE are for instance, emergency response, evacuation, escape and rescue, fire protection and medical response. From the viewpoint of the environmental protection, the leakage of hydrocarbon from pipelines and risers, tankers and facilities shall meet the required standard. On many deepwater offshore projects, an environmental impact assessment is conducted. Air emission and discharges of waste are controlled.

Risk assessment is a tool for the management of safety, health and environmental protection.

29.1.2 Overview of Risk Assessment

Risk assessment is more and more applied in managing safety, environmental and business risk. The purpose of this chapter is to discuss the basic procedures for the risk assessment, as shown in the flowchart in Figure 29.1 (NTS, 1998). Furthermore, this chapter explains risk concepts and risk acceptance criteria. More information may be found from NORSOK standard (NTS, 1998), Arendt et al (1989), Avens (1992, 1994), Guedes Soares (1998).

Risk assessment was initially developed by the nuclear engineering community as "probabilistic safety assessment" (NRC, 1983). It has been also applied by the chemical industry as "quantitative risk assessment (QRA)" for risk management of chemical process and chemical transportation (CCPS, 1989, 1995, Arendt et al, 1989). In recent years, it has been accepted by the marine and offshore industry, see Vinnem (1999) and CMPT (1999). Applications to engineering systems in general are discussed in Wilcox and Ayyub (2002). An extensive list of the recently published papers on marine risk assessment may be found in ISSC (2000).

As shown in Figure 29.1, the main steps of a risk assessment are:

- Planning of risk analysis
- System description
- Hazard identification
- Analysis of causes and frequency of initiating events

- Consequence and escalation analysis
- Identification of possible risk reducing measures

Each of the above steps is further explained in the below.

```
                    ┌──────────────────┐
                    │  Risk Analysis   │
                    └──────────────────┘
                              │
                              ▼
                    ┌──────────────────┐
            ┌──────▶│ System Definition │◀──────┐
            │       └──────────────────┘        │
            │                 │                  │
            │                 ▼                  │
┌─────────────────┐  ┌──────────────┐  ┌─────────────────┐
│      Risk       │  │    Hazard    │  │  Risk Reducing  │
│   Acceptance    │  │Identification│  │    Measures     │
└─────────────────┘  └──────────────┘  └─────────────────┘
          │            │          │              ▲
          │            ▼          ▼              │
          │   ┌────────────┐  ┌────────────┐     │
          │   │ Frequency  │  │Consequence │     │
          │   │  Analysis  │  │  Analysis  │     │
          │   └────────────┘  └────────────┘     │
          │            │          │              │
          │            ▼          ▼              │
          │        ┌──────────────┐             │
          │        │ Risk Picture │             │
          │        └──────────────┘             │
          │                 │                    │
          │                 ▼                    │
          │          ╱──────────────╲            │
          └─────────▶│      Risk     │───────────┘
                     │   Evaluation  │
                      ╲──────────────╱
                              │
                              ▼
                     ┌──────────────┐
                     │ Further Risk │
                     │   Reducing   │
                     └──────────────┘
```
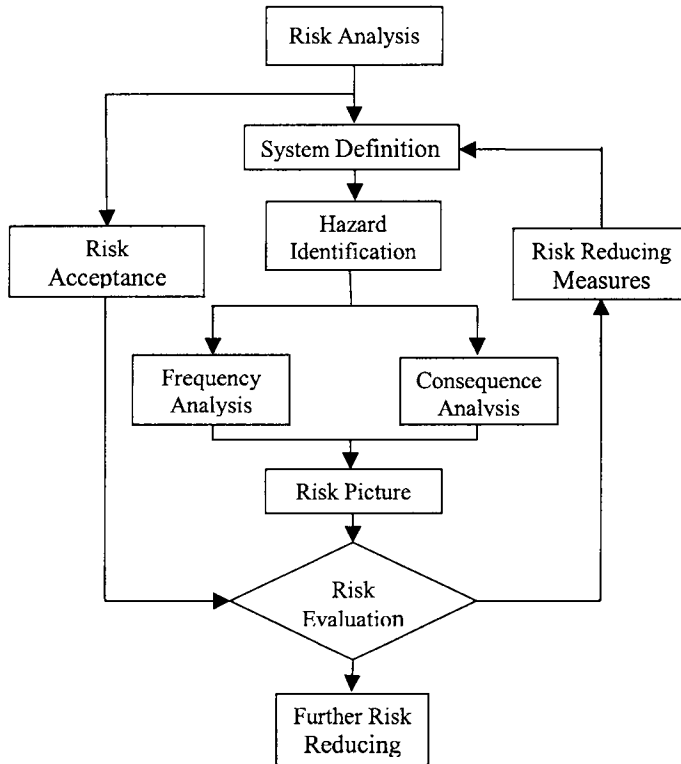
Figure 29.1   Risk Estimation, Analysis, and Evaluation

The risk assessment provides a qualitative/quantitative measure of risk. Through hazard identification, it is possible to separate critical hazards from un-critical ones. The process of risk reducing measures may control risk through cost-effective design and procedure improvements.

29.1.3 Planning of Risk Analysis

Risk analyses are carried out as an integrated part of the design and construction project, so that these analyses form part of the decision-making basis for the design of safe, technical sound, cost-effective and environmental friendly facilities.

Risk analyses are also conducted in connection with major facility modifications, such as change of installation sites and/or decommissioning/disposal of installations, and in connection with major changes to the organization and manning level.

The purpose and scope of work for the risk analysis should be clearly defined in accordance with the needs of the activity. The risk acceptance criteria need to be defined prior to the initiation of risk analysis. It will be helpful to involve operational personnel in the project execution. For the activity related to the design and construction of ships, mobile offshore drilling units and floating production installations, applicable regulations, classification rules, and industry standards/specifications may be useful.

When a quantitative risk analysis is carried out, the data basis should be appropriately selected. A sufficiently extensive data basis is a must in order to draw reliable conclusions. In some situations, comparative risk studies may lead to more meaningful conclusions.

To quantify accident frequency or causes, it is particularly important to establish a reliable data basis. The data basis should be consistent with relevant phases and operations. The analysis model shall comply with the requirements to input data and assumptions, etc. The quality and depth of the frequency, escalation and consequence modeling determine how detailed conclusions may be made for the systems involved in the analysis. The level of accuracy in the results may not be more extensive than what is justifiable based on the data and models that are used for the quantification of frequency and consequence. For instance, risk may not be expressed on a continuous scale when the estimation of frequency and/or consequences is based on categories.

29.1.4 System Description

The next step in a risk assessment is a detailed study of the system used, including a general description of the system's structure and operation, functional relationship between the elements of the system, and any other system constraints. The description of the system includes the technical system, the period of time, personnel groups, the external environment, and the assets to which the risk assessment relates, and capabilities of the system in relation to its ability to tolerate failures and its vulnerability to accidental effects

29.1.5 Hazard Identification

Hazard identification establishes the foundation on which subsequent frequency and consequence estimates are made. The hazard identification yields a list of accidental situations that could result in a variety of potential consequences. The potential hazards are identified in order to avoid ignorance of the potential hazardous accidents in the risk assessment. Identification of hazards also includes a ranking of the significance of each hazard in relation to the total risk. For the subsequent analysis, hazards are roughly classified into critical hazards and non-critical hazards. The criteria used in the screening of the hazards should be stated. The evaluations made for the classification of the non-critical hazards should be documented.

There are several approaches for hazard identification and the success in using these techniques depends on the knowledge and information available. Possible data and tools for the hazard identification are literature review, check-lists and accident statistics, HAZOP (HAZard and OPerability) studies, FMEA (Failure Mode and Effect Analysis). Safety audit, brainstorming and experience from previous projects may be useful. It is also important to involve operational personnel.

29.1.6 Analysis of Causes and Frequency of Initiating Events

Analysis of possible causes of initiating events gives the best basis for identifying measures that may prevent occurrence of these events and thus prevent accidents. Frequency assessment methods include:

- historical data,
- fault tree analysis,
- event tree analysis,
- failure mode and effect analysis (FMEA), and
- human reliability analysis.

It is important to include the contributions from human and operational factors.

In many cases, frequency may be estimated through direct comparison with experience or extrapolation from historical data. However, in most risk assessment, the frequencies are very low and therefore must be synthesized involving:

- appropriate probabilistic mathematics,
- development of basic failure data from available industry data, and
- determination of the combinations of failures and circumstances that can cause the accidents.

29.1.7 Consequence and Escalation Analysis

This term is used in a wide sense, including estimation of accidental loads and consequence modeling, modeling of escalation, and estimation of response to accidental loads. The distinction between cause analysis and consequence analysis may vary somewhat according to the purpose and the nature of the analysis. The most relevant methods for the escalation analysis include:

- event tree analysis,
- fault tree analysis, and
- simulation/ probabilistic analysis.

The consequence analysis involves the following:

- To characterize the release of material or energy due to the hazards being identified using experiments and the analysis models that have been developed for consequence analysis,
- To measure/estimate the release/propagation of the material/energy in the environment on the target of interest,
- To quantify the safety, health, environmental and economical impacts on the target of interests, in terms of the number of fatalities and injuries, amount of materials released to the environment, and the dollar values lost.

Like frequency estimates, there are large uncertainties in the consequence estimates due to differences in time-dependent meteorological conditions, basic uncertainties in physical and chemical properties, and model uncertainties.

In any case, examining the uncertainties and sensitivities of the results to changes in assumptions and boundary conditions may provide great perspective. It is necessary to put a

third to a half of the total effort of a risk assessment into the consequence evaluation, depending on the number of different accident scenarios and accidental sequence being considered.

29.1.8 Risk Estimation

A general expression of risk "R" is:

$$R = \sum f(p, C) \tag{29.1}$$

where p and C denote frequency and consequence of accidents respectively. The risks due to all possible events shall be summed up for all situations considered in the analysis. The results of an uncertainty analysis can be presented as a range defined by upper and lower confidence bounds and the best estimates. It should also be kept in mind that potential severe accidents usually generate greater concern than smaller accidents, even though the risk (product of frequency and consequence) may be equivalent.

The estimated frequencies and consequences are integrated into presentation format on an absolute basis compared to a specific acceptance criterion, or on a relative basis to avoid arguments regarding the adequacy of the absolute numbers.

When evaluating risk estimates, it is recommended to calculate the importance of various components, human errors and accident scenarios to the total risk. It may be useful to calculate the sensitivity of the total risk estimates to changes in assumptions, frequencies or consequences. Through these exercises, the major risk contributors may be identified, and on which risk-reducing measures can then be taken.

29.1.9 Risk Reducing Measures

Risk reducing measures include frequency reducing and consequence reducing activities, and their combinations. The measures may be of technical, operational, and/or organizational nature. The choice of types of measures is normally based on a broad evaluation, where risk aspects are in focus. Emphasis should be put on an integrated evaluation of the total effects that risk-reducing measures may have on risk. Possible coupling between risk reducing measures should be communicated explicitly to the decision-makers, if alternative measures are proposed. Priority is normally given to the measures that reduce the frequency for a hazardous situation to initiate and develop into an accident event. In order to reduce consequence, measures should be taken in the design of load bearing structures and passive fire protection, etc. Layout arrangements shall be suitable for the operations and minimize the exposure of personnel to accidental loads.

In selecting risk reducing measures, consideration is given to their reliability and the possibility of documenting and verifying the estimated extent of risk reduction. Consequence reducing measures (especially passive measures such as passive fire protection) will often have a higher reliability than frequency reducing measures, especially for the operating conditions.

The possibility of implementing certain risk reducing measures is dependent on factors such as available technology, the current phase in the activity, and the results of cost benefit analysis. The choice of risk reducing measures shall therefore be explained in relation to such aspects.

29.1.10 Emergency Preparedness

Emergency preparedness is also a part of the risk assessment. The goal of emergency preparedness is to be prepared to take the most appropriate action to minimize its effects and to transfer personnel to safer place in the event that a hazard becomes a reality (NTS, 1998 & Wang, 2002). In the UK, it is not legal to operate an offshore installation without an accepted operational safety case, which is a written submission prepared by the operator for the installation.

29.1.11 Time-Variant Risk

Risk, R(t), is a function of time, and may be denoted as the production of the time-variant probability, p(t) and time variant consequence, C(t):

$$R(t) = \sum \{p(t) \times C(t)\} \tag{29.2}$$

The time rate of change of risk may be written as:

$$\frac{dR(t)}{dt} = \sum \left\{ \frac{dp(t)}{dt} \times C(t) + p(t) \times \frac{dC(t)}{dt} \right\} \tag{29.3}$$

The above equation shows that the most significant measures to reduce risks are to reduce the probability of largest consequence events and to reduce the consequence of the highest probability events. In incremental form, the effect of risk reducing measures may be expressed as:

$$dR(t) = \sum \{dp(t) \times C(t) + p(t) \times dC(t)\} \tag{29.4}$$

Negative value of dR(t) means the overall risk level has been reduced, due to reduced probability, reduced consequence or a combination of both.

29.2 Risk Estimation

29.2.1 Risk to Personnel

The risk to personnel is often expressed as fatality risk, sometimes also as risk in relation to personnel injury. An estimate of the personnel injured in accidents is often required as input to emergency preparedness analysis.

Individual Risks

The most common measure of fatality risk is the risk to individuals. PLL (Potential Loss of Life) is calculated according to Eq.(29.5) below:

$$PLL = \sum_N \sum_J f_{nj} \times c_{nj} \tag{29.5}$$

where,

f_{nj} = Annual frequency of accident scenario n with personnel consequence j

c_{nj} = Annual number of fatalities for scenario n with personnel consequence j

N = Total number of accident scenarios in all event trees

J = Total of personnel consequence types, usually immediate, escape, evacuation and rescue effects

FAR (Fatal Accident Rate) and AIR (Average Individual Risk) express the IR (Individual Risk). The FAR value expresses the number of fatalities per 100 million exposed hours for a defined group of personnel. The AIR value indicates the fatality risk per exposed person onboard. Further, FAR or AIR may be based on total offshore hours (8760 hours per year) as the following equations.

$$FAR = \frac{PLL \times 10^8}{Exposed\ hours} = \frac{PLL \times 10^8}{POB_{ev} \times 8760}$$

(29.6)

$$AIR = \frac{PLL}{Exposed\ Individuals} = \frac{PLL}{POB_{ev} \times \dfrac{8760}{H}}$$

(29.7)

where,

POB_{ev} = Average annual number of manning level

H = Annual number of offshore hours per individual

Society Risks and f-N Curves

Experience has shown that society is concerned about the effects of accidents on the society as a whole. Therefore, some measure of risk to society, i.e. the total effect of accidents on the society, is required. This is what the GR (Group Risk) accomplishes. Group risk is often expressed in terms of an "f-N" curve (f = frequency, N = number, i.e. measurement of consequence), see Figure 29.2.
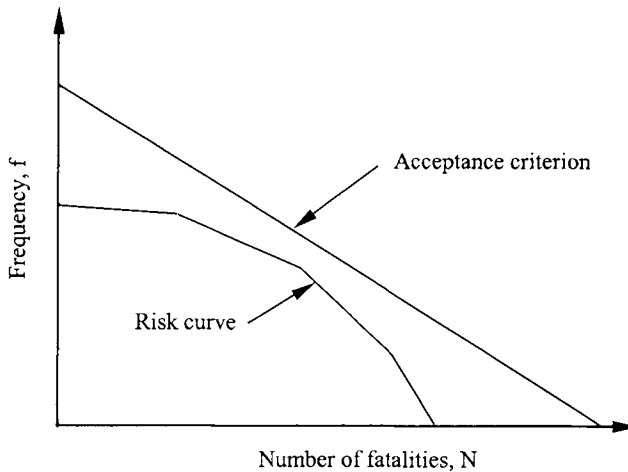

Figure 29.2   F-N Curve

The f-N curve expresses the acceptable risk level according to a curve where the frequency is dependent on the extent of consequences, such as number of fatalities per accident. The

calculation of values for the f-N curve is cumulative, i.e. a particular frequency relates to "N or more" fatalities.

29.2.2 Risk to Environment

The assessment of environmental risk includes establishment of release duration distribution, simulation of oil spill for relevant scenarios, estimation of the effects on environmental resources and restoration time. The overall principle to estimate environmental risk is (NTS, 1998):

*   VECs (Valued Ecological Component) are identified.

*   Assessment is focused on "most vulnerable resources".

*   Damage frequency is assessed for each VEC.

*   Restoration time is used to measure environmental damage.

The environmental damage may have the following categories based on restoration time:

*   Minor - environmental damage with recovery between 1 to 12 months,

*   Moderate - environmental damage with recovery between 1 to 3 years,

*   Significant - environmental damage with recovery between 3 to 10 years,

*   Serious - environmental damage with recovery in excess of 10 years.

29.2.3 Risk to Assets (Material Damage and Production Loss/Delay)

The risk to assets is usually referred to, as material damage and production loss/delay. The material damage can be categorized as the local, one module, several modules, or total loss. The production delay is categorized by the delay time: up to 1 to 7 days, 1 week to 3 months, 3 months to 1 year, above 1 year etc.

In order to estimate the risk for asset damage and production delay, the distribution for duration of accidental events shall be established, and response is calculated in the form of equipment and structures.

29.3 Risk Acceptance Criteria

29.3.1 General

How safe is safe enough? Risk acceptance criteria define the overall risk level that is considered as acceptable, with respect to a defined period of the activity. They are a reference for the evaluation of the need for risk reducing measures and therefore should be defined prior to initiating the risk analysis. Further, the risk acceptance criteria shall reflect the safety objectives and the distinctive characteristics of the activity.

The risk acceptance criteria may be defined in either qualitative or quantitative terms, depending on the expression for risk. The basis for their definition includes:

*   Governmental legislation applicable to safety in the activity,

*   Recognized industry standards for the activity,

*   Knowledge of accidental events and their effects,

*   Experience from own and past activities.

According to the purpose and the level of detail for the risk analysis, the acceptance criteria may be:

- High level criteria for quantitative studies,
- Risk matrices and the ALARP principle,
- Risk comparison criteria.

Fischhoff et al (1981) identified and characterized various methods for the selection of risk acceptance criteria. They indicated that values, beliefs and other factors all influence the selection of risk acceptance criteria. The complexity of defining risk acceptance criteria should be explicitly recognized, due to uncertainty about their definition, lack of relevant facts, conflicting social values, and disagreements between technical experts and the public. The selection of risk acceptance criteria is subject to a rigorous critique in terms of philosophical presuppositions, technical feasibility, political acceptability, and the validity of underlying assumptions about human factors.

29.3.2 Risk Matrices

The arrangement of accident frequency and the corresponding consequences in a matrix (see Figure 29.3) may be a suitable expression of risk where many accidental events are involved or where single value calculations are difficult. The matrix is separated into three regions as follows:

- Unacceptable risk.
- Acceptable risk.
- A region between acceptable and unacceptable risk, where evaluations have to be carried out in order to determine whether further risk reduction is required or whether more detailed studies should be conducted.
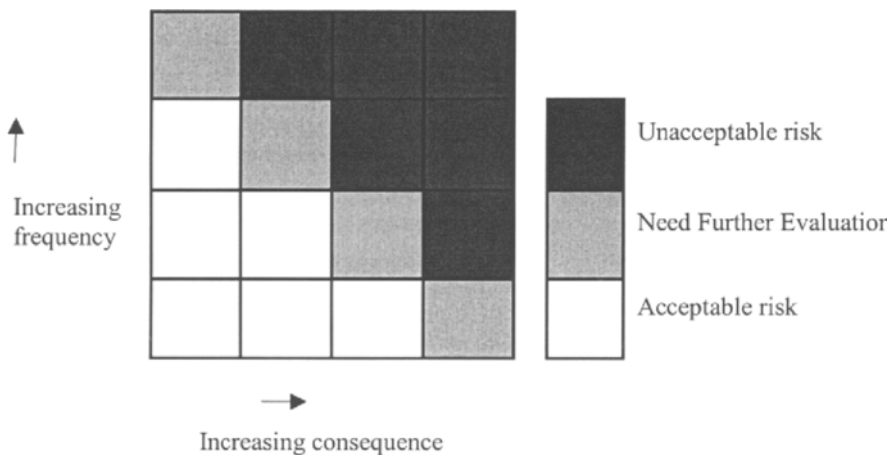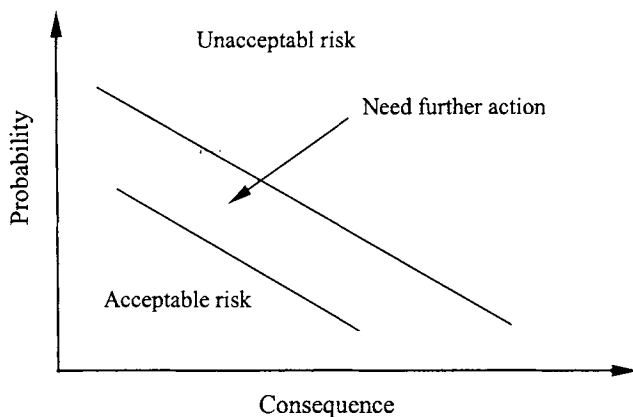

Figure 29.3   Risk Matrix

Figure 29.4   Risk Matrix in Terms of Continuous Variables

The limit of acceptability is set by defining the regions in the matrix, which represent unacceptable and acceptable risk. The risk matrix may be used for qualitative as well as quantitative studies. If frequency is classified in broad categories such as rare and frequent and consequences in small, medium, and catastrophic, the results from a qualitative study may be shown in the risk matrix. The definition of the categories is particularly important in the case of qualitative use.

The categories and the boxes in the risk matrix may be replaced by continuous variables, implying a full quantification. An illustration of this is shown in Figure 29.4.

The following are examples of situations where the use of a risk matrix is natural:

*   Evaluation of personnel risk for different solutions such as integrated versus separate quarters.
*   Evaluation of risk in relation to operations such as exploration drilling.
*   Evaluation of risk in relation to a particular system such as mechanical pipe handling.
*   Evaluation of environmental risk.

29.3.3 ALARP-Principle

The ALARP ("As Low As Reasonably Practicable", see Figure 29.5) principle is sometimes used in the industry (UK HSE, 1993). The use of the ALARP principle may be interpreted as satisfying a requirement to keep the risk level "as low as possible", provided that the ALARP evaluations are extensively documented. In the ALARP region, (between "lower tolerable limit" and "upper tolerable limit"), the risk is tolerable only if risk reduction is impracticable or if its cost is grossly disproportionate to the improvement gained. The common way to determine what is practicable is to use cost-benefit evaluations as a basis for the decision on whether certain risk reducing measures should be implemented. A risk may not be justified in any ordinary circumstance, if it is higher than the "upper tolerable limit". The "upper tolerable limit" is usually defined, whereas the "lower tolerable limit" may sometimes be left undefined. This will not prohibit effective use of the approach, as it implies that ALARP evaluations of risk reducing measures will always be required. The ALARP principle used for risk

acceptance is applicable to risk to personnel, environment, and assets. Trbojevic (2002) illustrated the use of the ALARP-principle in design.
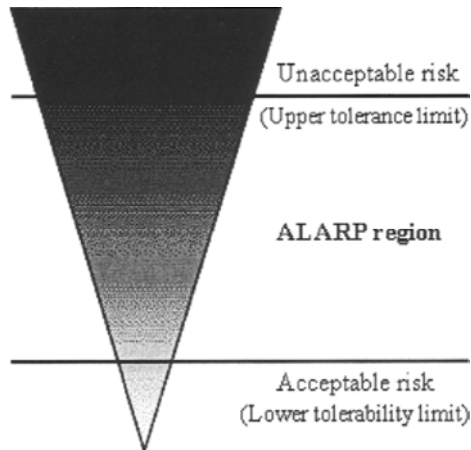
Figure 29.5   The ALARP-Principle

29.3.4 Comparison Criteria

This type of criteria is suitable in more limited studies that aim at comparing certain concepts or solutions for a particular purpose with established or accepted practice. The criteria are suitable in relation to operations that are often repeated such as drilling and well interventions, heavy lift operations, diving, etc. The use of the comparison criteria requires that the basis of the comparison be expressed precisely.

The formulation of the acceptance criterion in this context may be that the new solution shall not represent any increase in risk in relation to current practice.

Examples of comparison criteria are:

- Alternative design (or use of new technology) for fire water system shall be at least as safe as conventional technology
- The risk level for the environment shall not be higher compared to the existing solution
- Alternative solution shall be at least as cost effective as the established practice

This type of risk acceptance criteria is also suitable for risk to personnel, environment, and assets.

29.4 Using Risk Assessment to Determine Performance Standard

29.4.1 General

LR (1999) published guidelines for classification using risk assessment techniques to determine performance criteria. The risk assessment methodology used in LR (1999) is similar

to that described in Section 29.1 to Section 29.3 of this Chapter. LR (1999) guidelines additionally included the following:

- A "critical element" is a part of the installation, or a system, sub-system or component, which is essential to the safety and integrity of the installation in relation to the identified hazards.

- "Performance standards" are statements that can be expressed in qualitative or quantitative terms, of the performance required of a critical element in order that it will manage the identified hazards to ensure the safety and integrity of the installation.

- "Verification" is the confirmation by a process of examination of the design, manufacturing, construction, installation and commissioning of the critical elements in order o demonstrate that they meet the required performance standards. The verification may be used for new construction and in-service installations.

- "Inspection and maintenance plan" is the Owner/Operator's program of scheduled inspection and maintenance activities that ensure the required performance standards continue to be met in service, to maintain the safety and integrity of the installation against the identified hazards.

29.4.2 Risk-Based Fatigue Criteria for Critical Weld Details

An example application is the determination of fatigue acceptance criteria for critical weld details and the development of corresponding inspection and maintenance plan, as below:

- Critical elements (weld details) are identified in relation to the fatigue failure through screen analysis based on simplified fatigue assessment. The consequence of failure may also be accounted for in relation to reduction to the safety and integrity of the installation.

- In the design phase, performance standards (fatigue acceptance criteria) may be established in quantitative terms, of the condition required for a weld detail, in order to ensure that it will not experience the fatigue failure that threatens the safety and integrity of the installation.

- A verification process is applied for new construction projects to confirm that the selected critical elements (weld details) meet the pre-defined performance criteria (fatigue acceptance criteria).

- For an in-service installation, a program is established to schedule and plan inspection and maintenance activities that ensure the required fatigue criteria are met against the fatigue failure. Verification is conducted to confirm that the identified critical weld details continue to meet the pre-defined fatigue criteria.

29.4.3 Risk-Based Compliance Process for Engineering Systems

Due to the difficulty in developing prescriptive requirements for all possible system designs, governmental regulations and industry design codes provide provisions for design equivalency of alternate designs to the existing requirements. Wilcox, R. and Ayyub, B.M. (2002) proposed a risk-based compliance approval process to deal with new concepts and special classes of engineering designs by establishing safety equivalency to current standards and existing accepted designs. Risk is used as an overall performance measure to assist in making decisions for a system design. The risk-based compliance approval methodology aids in identifying critical factors for evaluating the minimum level of performance necessary for approval. The process may also be suitable for assessing conventional engineering systems

and performing safety calibration. The risk acceptance criteria may be established through the calibration of existing codes and safety goals. Testing and monitoring programs improve the understanding of system performance, help control risk, and improve quality in manufacturing and operational phases.

29.5 References

1. ASTM (1988, 1995) "ASTM F1166-95a: Standard Practice for Human Engineering Design for Marine Systems, Equipment and facilities", American Society of Testing and Materials.

2. Aven, T. (1994), "On Safety Management in the Petroleum Activities on the Norwegian Continental Shelf", Journal of Reliability Engineering and System Safety, Vol. 45, pp. 285-291.

3. Aven, T. (1992), *"Reliability and Risk Analysis"*, Elsevier, England.

4. CCPS (1989), *"Guidelines for Chemical Process Quantitative Risk Analysis"*, Center for Chemical Process Safety, American Institute of Chemical Engineers.

5. CCPS (1995), *"Chemical Transportation Risk Analysis"*, Center for Chemical Process Safety, American Institute of Chemical Engineers.

6. Arendt, J.S., Lorenzo, D.K., Lusby, A.F., (1989), *"Evaluating Process Safety in the Chemical Industry – A Manager's Guide to Quantitative Risk Assessment"*, Chemical Manufactures Association.

7. CMPT (1999), *"A Guide to Quantitative Risk Assessment of Offshore Installations"*.

8. Fischhoff, B., Lichtenstein, S., Slovic, P., Berby, S.L. and Keeney, R. (1981), *"Acceptable Risk"*, Cambridge University Press.

9. Guedes Soares, C., (1998), *"Risk and Reliability in Marine Technology"*, A.A. balkema, Rotterdam, The Netherlands.

10. ISSC (2000), "Risk Assessment", Proceedings of the International Ship and Offshore Structures Congress, Nagasaki, Japan.

11. LR (1999), "Guidelines for Classification using Risk Assessment Techniques to Determine Performance Criteria", Part 1A of the LR Rules and Regulations for the Classification of a Floating Offshore Installation at a Fixed Location, Lloyd's Register.

12. NRC (1983): "PRA Procedures Guide – A Guide to the Performance of Probabilistic Risk Assessment for Nuclear Power Plants", NUREG/CR-2300, Nuclear Regulatory Commission, Jan. 1983.

13. NTS (1998), "Risk and Emergency Preparedness Analysis" NORSOK Z-013, Norwegian Technology Standards, March 1998.

14. Toeliner, J. (2001), "Safety Partnerships with Contractors: A Hoover/Diana Project Success Story", OTC 13080.

15. Trbojevic, V.M. (2002), "ALARP Principle in Design", Proceedings of OMAE Conference.

16. UK HSE (1992), "Safety Case Regulations", Health and Safety Executives, HMSO.

17. Vinnem, J.E. (1999), *"Quantified Risk Assessment – Principles, Modelling and Applications of QRA Studies"*, Kluwer Academic Publishers.

18. Wang, J. (2002), "A Brief Review of Marine and Offshore Safety Assessment", SNAME Journal of Marine Technology, Vol. 39(2), pp. 77-85.

19. Wilcox, R. and Ayyub, B.M. (2002), "A Risk-Based Compliance Process for Engineering Systems", SNAME Annual Conference Proceedings and Transactions.

Part V

Risk Assessment

Chapter 30   Risk Assessment Applied to Offshore Structures

30.1 Introduction

Use of offshore risk assessment started in the late 1970s, based on the methodologies and data from the nuclear power generation industry. Following the Alexander L. Kielland accident in 1981 that resulted in total loss of the platform and 123 fatalities, the Norwegian Petroleum Directorate issued their guidelines that required quantitative risk assessment be carried out for all new offshore installations in the conceptual design phase (NPD, 1992). Another significant step was the Safety Case Legislation in the UK in 1992, following the Piper Alpha accident that resulted in total loss of the platform and 165 fatalities in 1988 (UK HSE, 1992, 1995).

There are several types of offshore risks, e.g.

- structural and marine events
- collisions
- fires
- dropped objects
- blowouts
- risers/pipelines leaks, process leaks
- transport accidents

Risk due to structural failure is discussed in Part IV. Risks associated with blowouts, riser/pipeline hydrocarbon leaks, process leaks, transport accidents are discussed by CCPS (1995) and CMPT (1999). Reference is made to specialized books (e.g. Vinnem 1999) on the basic methodologies for risk evaluation such as

- Hazard Modeling and Cause Analysis,
- Fault Tree Analysis, Event Tree Analysis, and
- Failure Mode and Effect Analysis.

In the following sections, discussions will be made on risks associated with collision, explosion, fire and dropped objects, including:

- Overview
- Frequency analysis
- Loads and consequence analysis
- Risk reduction

30.2   Collision Risk

The ship/platform collision is one of the main risk contributors in the offshore exploration and production activities. The most frequently occurred collisions are impacts between offshore supply vessels and platforms. In most situations this type of collisions only causes minor damage to the platforms.

30.2.1 Colliding Vessel Categories

The first step in evaluating the collision risk is to specify the different types of vessels that may collide with an offshore platform. Collision hazards due to the field related supply vessels are characterized with high frequency and low consequence. The passing vessels may lose their power and drift resulting in collisions with the platforms. In the North Sea, merchant vessels represent the greatest hazard, since they are often large and thus have considerable impact energy in a collision with the platforms. Further, in some areas the merchant traffic can be very busy. Table 30.1 summarizes the colliding vessel categories, based on information in Vinnem (1999). In the following Sections, only the external passing vessel collision is evaluated.

Table 30.1   Colliding Vessel Categories

External Traffic		Field related Traffic	
Merchant	Merchant ship	Offshore (To/from field itself)	Standby vessel
Naval	Surface ship	Offshore (To/from field itself)	Supply vessel
Naval	Submarine	Offshore (To/from field itself)	Working vessel
Fishing	Trawler	Offshore (To/from field itself)	Offshore tanker
Offshore (To/from another field)	Standby vessel	Floating units	Storage vessel
Offshore (To/from another field)	Supply vessel	Floating units	Flotel / Barge
Offshore (To/from another field)	Offshore tanker	Floating units	Drilling unit
Offshore (To/from another field)	Tug	Floating units	Crane / Diving vessel

30.2.2 Collision Frequency

Based on the collision risk model proposed by Haugen (1991), the passing vessel collisions can be sub-divided into two groups:

- Powered collisions: Vessels are steaming towards the platform while the navigator might not be aware of the situation.

- Drifting collisions: Vessels are out of control and drift towards the platform under the influence of environmental conditions.

The overall collision frequency can therefore be expressed as:

$$P_{CP} = P_{CPP} + P_{CPD}$$

(30.1)

where,

P_{CP} = Frequency of passing vessel collision

P_{CPP} = Frequency of powered passing vessel collision

P_{CPD} = Frequency of collision due to a passing vessel in drift

The frequencies of powered and drifting vessel collisions are generally dependent on the location of ship routes relative to the platform. This information may be obtained by assessing a database of ship routes or by performing a localized survey for the area.

Powered Ship Collision

A powered ship collision may occur when the following three conditions are met:

- The ship is on a collision course to the platform.

- The navigator is not aware of the situation early enough before the ship reaches the platform.

- The ship and the platform both fail to normalize the situation.

The basic mathematical expression for powered ship collision frequency can thus be written as:

$$P_{CPP} = N \cdot P_{CC} \cdot P_{FSIR} \cdot P_{FPIR}$$

(30.2)

where,

N   = Annual number of passing vessels

P_{CC} = Probability of passing vessel on a collision course

P_{FSIR} = Failure probability of ship initiated recovery

P_{FPIR} = Failure probability of platform initiated recovery

The probability of being on a collision course, P_{CC}, is a geometric factor. It is based on the composition and position of the traffic flow. For a vessel, which has not taken pre-planning to avoid a site, it may be assumed that the vessel will be normally distributed about the route center. The fraction of vessels on a collision course can be found based on the route details and the collision diameter presented by the platform. For a vessel that has taken deliberate steps to avoid a platform or to use it for position fixing, re-modeling is needed to modify the traffic distribution. A skewed distribution can normally be observed instead of normal distribution.

The ship-initiated recovery from a collision course is divided into two cases: Early recovery and late recovery. Early recovery is a normal operation under sound command. The ship is recovered from a collision course in the early recovery zone. Late recovery occurs under the condition that early recovery fails. This reflects recognition of an emergency situation and quick response recovery. The failure frequency of ship-initiated recovery may be calculated by fault trees involving a number of factors, such as watch-keeping failure mode, visibility, vessel type and size categories, traffic-planning group, and vessel flag etc.

The platform-initiated recovery is to alert the ship in time by platform or standby vessel to prevent a collision. The failure probability of platform-initiated recovery is highly dependent on the reason for the failure of ship-initiated recovery. It may be estimated by event trees based on whether the following actions are taken in time:

- Identification of the vessel as a possible threat

  Attempt to inform the vessel on radio/VHF

- Standby vessel reaches position alongside the coming vessel
- Correct avoidance action by the vessel

Drifting Vessel Collisions

A drifting vessel collision will occur if the following conditions are all satisfied:

- The vessel loses propulsion.
- The vessel drifts towards the platform.
- The vessel fails to recover from its collision course due to either failure of external assistance or failure of its own recovery measures.

Based on information of the rate of propulsion failure, vessel sizes, types, and flags, the likelihood of a vessel drifting can be estimated. The likely positions of vessel when in drift can be determined by using the route pattern. The metocean data for the location is then used to determine the probability of the vessel drifting towards the platform.

External assistance includes e.g. towing the drifting vessel away, its failure probability depends on factors such as the relative size of vessel and the location of towing tug. Collision avoidance by vessel's own measures depends on the probability of a drifting vessel regaining power (e.g. by restarting engines) or avoiding collision by steering with the rudder.

The above discussions have been based on research on collision between ships and fixed platforms (Haugen, 1991 and Vinnem, 1999). For new types of floating structures like FPSO, additional considerations are necessary, e.g. on collision during offloading operation.

Chen and Moan (2002) suggested that the collision probability of FPSO-tanker offloading operation, is the product of the probability of tanker uncontrolled forward movement (in the initiating stage), and the probability of recovery failure initiated from tanker and FPSO conditioned on the tanker uncontrolled forward movement (in the recovery stage). The probability of uncontrolled forward movement in the initiating stage is predicted as the sum of the probability of tanker *powered* forward movement and the probability of tanker *drifting* forward movement. The drift forward movement is a low probability and low consequence event. The probabilistic model for tanker powered forward movement involves a complex man-machine interaction, human factors and their interaction.

30.2.3 Collision Consequence

A number of factors may influence the collision consequences, e.g.:

- Mass and velocity of colliding vessel
- Collision geometry
- Criteria that were applied for the structural design of the platform
- Platform topology
- Fender and reinforcement on platform

The most critical factors in the above list are the vessel mass and velocity that determine the impact energy level. Further, the collision geometry is also an important factor, since it will influence the energy distribution between the vessel and the platform. The following distinctions of collision geometry are made for a jacket structure:

- *Impact on the vertical column or bracing:* Vessel hitting a column or bracing will result in a high proportion of energy being absorbed by the platform, and thus leading to large plastic deformations.

- *Glancing bow:* Considerable amount of kinetic energy may be retained on the vessel after collision if hit is a glancing bow, possibly resulting from last minute evasive actions.

- *Rotation of vessel:* Kinetic energy may be transferred to the vessel rotation, thus only a limited amount of energy is absorbed by the platform.

- *Contact spot on vessel:* The contact spots on the vessel are important. If a 'hard spot' is hit on the vessel (e.g. heavily framed curvatures such as bulb, stern), high puncture loads may be generated.

The collision response and consequence for the platform may be predicated using non-linear finite element analysis (Bai and Pedersen, 1993), see Part II Chapter 14 of this book.

30.2.4 Collision Risk Reduction

When considering risk reduction measures, the type of vessel representing the greatest risk to the platform needs to be analyzed. For the passing vessel collision, the risk reduction measures are:

- Improving the information distribution for the platform's site. This measure can increase the probability of the platform being located, and subsequently ships may pre-plan their voyage to avoid collision.

- Warning to the incoming ships as early as possible if they come along a collision course. Calling the vessel on VHF/radio and actively using a standby vessel to intercept the incoming vessel are also effective risk reduction measures.

The collision consequence reduction measures include the use of rubber fenders and protection nets on the platform, which are standard design practice.

30.3 Explosion Risk

A gas explosion is a process with a rapid increase of pressure caused by the combustion of premixed fuel and air. Gas explosions can occur inside the process equipment or pipes, in buildings or modules, in open process areas or in unconfined areas. The design of topside structures to resist explosions and fires requires special considerations such as (Burgan and Hamdan, 2002),

- Characteristics of the explosion such as overpressure and gas velocities,

- The response of the structure including high strain rate material property design data for use in explosion resistant design,

- Performance requirements of the structure such as strength, deformation limits and load shedding,

- Elevated temperature material property design data for use in fire engineering,

- Analysis techniques for fire and explosion design,

- Design methods based on codified rules and advanced techniques such as risk-based methods.

The explosion load may be categorized by its maximum overpressure. For instance,

- if the overpressure is smaller than 0.2 bar, it is typically an 'insignificant' explosion;
- if the overpressure is larger than 2 bar, it is considered to be a severe explosion.

In the Piper Alpha accident, an explosion due to ignited gas leakage set off an uncontrolled fire, which in the end led to the total loss of the platform. In the last few years, large-scale tests were conducted to study explosion modeling. The test results revealed that the blast loads due to explosion had been significantly underestimated previously, and these loads cannot be pre-designed in many cases. Therefore, the explosion risk picture may be even more severe than previously thought.

30.3.1 Explosion Frequency

If the gas cloud formed by the gas leak is outside the flammable concentration range, or the ignition source is lacking, no explosion will occur. Subsequently the gas cloud will dilute and disappear. Thus, three factors may influence the explosion occurrence, i.e. gas leak sources, ventilation/dispersion, and ignition sources. The overall explosion frequency can be expressed as:

$$P_{EP} = P_{Leak} \cdot P_{GC} \cdot P_{ignition} \tag{30.3}$$

where,

P_{EP} = Frequency of explosion

P_{Leak} = Probability of gas leakage

P_{GC} = Probability of gas concentration

$P_{Ignition}$ = Probability of ignition

Gas leak sources are important for the gas dispersion. Generally, the following aspects need to be considered:

- Location of the leak source, in a 3-dimensional space
- Gas composition and characteristics, i.e. temperature and specific weight
- Leak rate
- Direction of flow from the leak source
- Unrestricted gas jet or diffuse gas leak

The ventilation conditions also have considerable influence on the dispersion of a gas leak and the resulting gas cloud. Most platforms have natural ventilation, implying that the dispersion of a gas leak will be strongly dependent on the wind speed and direction.

The actual location of the ignition point may vary considerably depending on the type of ignition source. The ignition sources are generally identified as one of the following three types:

- *Rotating equipment:* Major equipment units, with a discrete distribution related to the location of each unit.
- *Electrical equipment:* A high number of possible sources, may be described as a continuous distribution.

- *Hot work:* usually possible in most locations, such as welding; may be described as a continuous distribution over the area.

The frequency of explosion events may be estimated using an event tree analysis. For example, given a medium gas leak, a number of conditions may be considered to determine the possible explosion events. Then the calculation of event frequencies in the event tree will establish the explosion frequencies for all explosion cases. This simple event tree assumes that all ignitions of the gas leak lead to explosions. A more detailed event tree will differentiate more explicitly between ignition causing an explosion or just causing a fire.

30.3.2 Explosion Load Assessment

Since 1990s gas explosions have been subjected extensive research and load characteristics include (Burgan and Hamdan, 2002):

- Experimental studies at scales representative of offshore scenarios,

- Computer simulation models,

- Formal explosion model evaluation protocols, either phenomenological or based on computational fluid dynamics.

In order to determine the explosion loads (blast loads), an exceedance function needs to be established for each structural element. This exceedance function may be defined as "The annual frequency of exceeding a specified overpressure load as a function of the overpressure level", based on analysis of uncertainties and probability distributions for variables such as:

- Location and direction of the leak source

- Flow rate of the leak

- Wind direction and speed

- Ignition source and strength

Distribution for the location and the direction of the leak are usually based on geometric considerations. Distributions for the flow rates can be derived using hole size distributions that are usually available from the leak statistics. Wind data can be obtained from the environmental criteria. These variations will generate input scenarios to dispersion simulations e.g. by Computational Fluid Dynamics (CFD). Non-relevant dispersion scenarios need to be eliminated later. Then explosion simulations (e.g. by CFD) can be carried out to determine the blast loads. When blast loads for all the cases have been simulated, the blast load distribution can be generated from a combination of simulated blast loads and scenario frequencies.

30.3.3 Explosion Consequence

Calculating the explosion loads on a structure and estimating responses involve the following calculations:

- hydrocarbon release,

- explosion overpressure loads as a function of time,

- structural response to the time dependent overpressure loads.

- secondary blast effects, such as missiles, flying objects, etc.

The consequence of an explosion is also dependent on the space and environment in which the gas cloud is contained. Therefore, it is natural to classify explosions into the following three categories (Vinnem, 1999):

- *Confined Explosion (internal explosion)*, occurs within tanks, process equipment, pipes, and closed rooms etc. For this kind of explosion, the combustion process does not need to be fast in order to cause serious pressure build-up.

- *Partly Confined Explosion*, occurs inside partially opened buildings. Typical cases are compressor rooms and offshore modules. The explosion pressure can only be relieved through the vent areas, or if the surrounding enclosure fails.

- *Unconfined Explosion*, occurs in open areas such as process plants. A truly unconfined, unobstructed gas cloud ignited by a weak ignition source may produce low overpressures. In a process plant, there are local areas, which are partly confined and obstructed. These areas are causing high explosion pressures. However, if an unconfined gas cloud detonates, the explosion pressure will be as high as 20 bar independent of confinement and obstructions.

Depending on the amount of the explosion loads, the types of damage on structures include:

- Direct catastrophic failure,

- Considerable damage which may be further extended by the subsequent fire,

- Little or no damage to structures, but causing critical failure of safety systems and thereby preventing control of the fire,

- Damage to passive fire protection, thereby reducing the survivability of structural members,

- Damage to process equipment, thereby causing immediate escalation of the accident.

The damages to the structures may be predicted using simplified analysis (such as single degree of freedom model for dynamics) and simulated using non-linear finite element analysis, based on a methodology that is similar to collision analysis discussed in Part II Chapter 14 of this book. The explosion consequence is also dependent on the overpressure loading duration in relation to the natural period of the structure being subjected to the explosion loads, for instance,

- Impulsive loads with duration that is shorter than the natural period of the structure,

- Dynamic loads with duration that is comparable with the natural period of the structure,

- Quasi-static loads that are applied slowly.

The overpressure time history should be properly modeled in the explosion consequence analysis as it may significantly affect the analysis results.

The acceptance criteria (performance requirements) include strength criteria for structural failure and deformation criteria for operating critical equipment.

30.3.4 Explosion Risk Reduction

To reduce the risk of explosion, the first priority is to reduce the frequency of its occurrence. This may be achieved by the following three measures (Vinnem, 1999):

Prevent Gas Leakage

The most effective action for the prevention of gas leakage is to reduce the number of sources for potential leakage, e.g., the number of flanges. This may be easily accomplished for a new platform. However, it is generally more difficult for existing platforms. The number of gas leakage may also be reduced by:

- improving the maintenance quality in the process area,

- selecting high quality material for gaskets, and

- following up the minor leakage to identify trends and unwanted tendencies.

Prevent Ignitable Concentrations

The next step to reduce explosion risk is to prevent the formation of any ignitable atmosphere, e.g., through extensive natural ventilation. In the design phase, good natural ventilation is normally provided. During operation, ventilation may have been purposely reduced, e.g. by temporary equipment being installed or left in the openings, or to improve the working environment. It is therefore a difficult trade-off between the increased natural ventilation and the deteriorated working conditions. Mechanical ventilation systems may be effective for small gas leakage. However, for massive gas releases, the forced ventilation is generally insufficient.

Prevent Ignition

The next option is to prevent an explosive atmosphere from being ignited. Several actions are possible in this aspect. The first action is to reduce the extent of hot work activities. This has been applied successfully on many installations where it has been proven that a variety of tasks may be done in a 'cold' manner. The second action is to improve maintenance of 'ex-proof' equipment. Attention should also be given to so-called 'continuous sources', i.e. potential ignition sources that are constantly active, such as a lighted flare.

The following measures are effective to reduce explosion consequence.

Prevent High Turbulence

Turbulence is caused by the interaction of the flow with obstacles such as cable trays, pipe racks, etc. The turbulence may increase the burning rate dramatically due to the wrinkling of the flame front by large eddies and the turbulent transport of heat and mass at the reaction front. A number of basic design rules may help prevent the high turbulence, e.g. optimization of the equipment arrangement, avoidance of multiple equipment pieces, and optimization of the location of pipe racks relative to likely ignition sources.

Prevent High Blockage

Small sized objects may have the largest effect on module congestion, and in turn lead to high overpressure. The mitigation measures are therefore to: 1) remove temporary installations, containers, small obstacles, and weather cladding; 2) arrange vessels in a way, which minimizes blockage of the most likely path of the flame front.

Avoid Human Activities from Explosion Potential

The location of control rooms, transportation, and accommodation facilities should be well away from modules with explosion potentials.

Install Fire and Blast Barriers

Escalation caused by explosions can be limited by fire and blast barriers between modules and areas. However, the barriers themselves may cause problems for keeping ventilation and introduce more blocks. The construction/repair of such barriers may involve extensive hot work. This measure is therefore more effective in the early design stage.

Active Deluge on Gas Leakage

Leakage may be deluged out without causing any explosions or fires. Deluge may be particularly effective in preventing so-called runaway flame accelerations. It may also lead to a reduction of the peak overpressure.

The most critical aspect in the use of deluge is that it must be triggered prior to ignition, e.g. on detection of a gas leak. Modeling of ignition has shown that the most likely interval between release and ignition is two to three minutes. Thus deluge activation has to be within the first half minute in order to be effective.

Improve Resistance of Equipment and Structures

The last possibility of reducing an explosion consequence is to improve the resistance of equipment and structures to blast loads. However, it is not cost-effective to design structures for the worst explosion case. Therefore this approach may be quite expensive.

30.4 Fire Risk

In the offshore risk assessment, usually two types of fire risk are considered: the topside fire and the fire on sea. The following sections mainly deal with the topside fire. Further, the smoke effect analysis and the structural response under the fire are normally integrated into the fire risk assessment.

The distinction between what is classified 'fire' and what is called 'explosion' is relatively subjective. The total loss of the fixed platform 'Piper Alpha' was initiated by a small explosion, but the damage was primarily due to fire.

30.4.1 Fire Frequency

Fire frequency analysis is very similar to explosion frequency analysis. The overall fire frequency can be expressed as:

$$P_{FP} = P_{Leak} \cdot P_{GC} \cdot P_{Ignition} \tag{30.4}$$

where,

P_{FP} = Frequency of fire

P_{Leak} = Probability of gas leakage

P_{GC} = Probability of gas concentration

$P_{Ignition}$ = Probability of ignition

The flammable gas/air concentration range determines whether it is explosion or fire for a given ignition. Further, fire scenarios are mainly caused from the following sources: blowout, riser failure, pipeline failure, process equipment failure, and dropped object. The uncontrolled hydrocarbon flow (blowout or riser failure) is considered as the main fire risk contributor to the structures. Further, dropped objects may contribute to fire only when they lead to the

rupture of hydrocarbon containing equipment. Under certain conditions, structural failure or collision impact may also lead to fires. Their final consequences are largely dependent on the escalating sequences.

30.4.2 Fire Load and Consequence Assessment

A brief overview of some important aspects in the fire consequence analysis is made below.

Fire Types and Characteristics

Despite the fact that a fire originates from combustion reactions, the process of a fire may largely depend on the factors that are not directly involved in combustion. Fires are therefore usually separated into the following types:

- Ventilation controlled fires in enclosed units (closed or partly closed)

- Fuel controlled fire in enclosures

- Pool fires in open areas or in modulus

- Jet fires

- Fires in running liquids

- Fire balls

- Gas fires (premixed, diffuse)

Other types of fire may occur in electrical equipment or in the accommodations or on sea. These 'non-hydrocarbon' fires are not included here.

Burgan and Hamdan (2002) gave a list of research publications on fire and explosion load characteristics, structural response analysis and performance requirements. The fire load may be converted into thermal loads (time-temperature curves) acting on the structural members. Some of the time-temperature curves are available in the literature in a form suitable for use in design. The temperature-time history for a given structural member is affected by the applied heat load, the shape of the member (for heat transfer) and the use of any passive fire protection material.

Table 30.2 summarizes the main characteristics that need to be determined for these fire types.

Table 30.2 Fire Load Characteristics

Jet Fire	Diffuse Gas Fire	Pool Fire	Fire on Sea
Hole size	Release rate	Pool size	Spreading
Release velocity	Duration of leak	Wind direction	Wind direction
Direction	Air supply	Duration of fire vs. leak	Wind speed
Duration of leak		Air supply	Pool breakup
Air supply			

Fire Response Analysis Procedures

The assessment of fire response of structures has the following calculations:

- releases of hydrocarbons (combustion, radiation and convection),
- fire loads,
- structural time-temperature distribution,
- structural response to temperature distribution.

Each of these calculations may be conducted using simplified methods or nonlinear finite element simulations. Simplified calculations may be performed in the form of hand calculations or computer spreadsheets. The weakness of the simplified calculations is its inability to account for redistribution of structural internal forces during the fire. However, the simplified calculations are normally more conservative and may be calibrated against experimental results.

Smoke Effect Analysis

Smoke does not affect structural elements, but it is one of the major hazards to personnel in fires, especially in oil fires. The smoke effects are e.g.:

- Reduced visibility,
- Pain and injury to the personnel due to temperature of the smoke,
- Incapacitation or death due to toxic or irritating components in the smoke.

Knowledge of smoke production, smoke flow, and impact of smoke on people and facilities is available from literature, laboratory tests, and experience of real fires such as the fire on Piper Alpha platform. By proper CFD codes, the smoke effects analysis in a fire scenario can be performed, and the results can be compared to the threshold values in above three areas.

Structural Response to Fire

Simplified methods for structural response to fire have been derived based on results from fire tests and fire engineering codified methods. The sophisticated computer models are based on finite element methods, that calculate the temperature increase in a structural member based on a given temperature exposure curve and the thermal properties of the materials which are also temperature dependent.

The consequences of fire include i.e.,

- 'Minor damage' and 'Significant damage' do not reflect much damage to the main and secondary structures (support structure, main deck structure, and module structure), but rather to tertiary structures and to their equipment.
- The higher consequences, i.e. 'Severe damage' and 'Total loss', will on the other hand, involve considerable damage to the main and secondary structures.

The performance requirements are applied for the protection of the primary structure and safety critical structures and systems. They are defined as strength (for structural failure) and deformation limits (to ensure that support to safety critical structures and performance of blast/fire wall are not compromised).

30.4.3 Fire Risk Reduction

Fire risk reduction measures may be considered in the following four aspects, see Vinnem (1999) for more details:

Leak prevention

Adopt welded connections

Flange types with reduced leak probability

Leak detection

Gas detection

Fire detection

Emergency shutdown system

Blowdown system

Ignition prevention

Hot work procedures

Explosion-protected equipment

Maintenance of electrical equipment

Escalation prevention

Installation layout

Segregation of areas

Active fire protection, e.g. deluge water system, CO_2 system, etc

Passive fire protection, e.g. H-60, H-30 segregation, etc.

30.4.4 Guidance on Fire and Explosion Design

A probabilistic approach has been proposed in the new NORSOK guidance documents (Pappas, 2001) and in a new engineering handbook published by Corrocean (Czujko, 2001). Walker et al (2002) presented a guidance document based on the risk matrix approach described in API RP 2A (21st edition). The API risk classification method has been applied to fire and explosion engineering. Methods are proposed to enable the derivation of a dimensioning explosion overpressure that may be applied to a static or dynamic analysis to assess the structure against the ductility level explosion. Two levels of explosion loading are suggested for explosion assessment by analogy with earthquake assessment.

For the "Ductility Level" explosion, a performance standard such as the one below is typical: "In the case of an explosion event at least one escape route must be available after the event for all survivors. For a manned platform a temporary refuge of safe mustering area must be available to protect those not in the immediate vicinity of n explosion and to survive the event without injury".

For the "Design Level" explosion, it is required that the primary structure remains elastic, with the essential safety systems remaining functional. The explosion overpressure is the cumulative overpressure distribution for the installation, showing the probability that a given overpressure will not be exceeded. The explosion overpressure may then be expressed as a function of the return period (years).

30.5 Dropped Objects

The hazards of dropped objects are mainly caused from falling crane loads. Also, various cases of crane boom fall or entire crane fall have been documented. The risk picture of the crane accidents in the North Sea shows that several fatalities have occurred when an entire crane was toppled overboard. The equipment has been damaged due to falling objects. The subsea wellheads have been damaged as a result of BOPs (Blow out Preventers) falling during exploration drilling.

30.5.1 Frequency of Dropped Object Impact

The frequency of dropped object impact is defined as follows (Vinnem, 1999):

$$P_{DOI} = \sum_I N_i \cdot P_{Di} \cdot \sum_J P_{H\,ij} P_{F\,ij} \qquad (30.5)$$

where,

P_{DOI}	= Occurrence probability of dropped object impact
N_i	= Annual number of lifts per load category i
P_{Di}	= Probability of load dropped from crane for load category i
P_{Hij}	= Probability of equipment j being hit by falling load in category i, given that the load is dropped
P_{Fij}	= Probability of failure of equipment j given impact by load in category i

Annual Lift Number and Load Distribution

Table 30.3 presents two representative load distributions for simultaneous drilling and production and for normal production. Typical numbers of crane operations per crane during one year on an installation are also shown.

Table 30.3   Typical Crane Load Distribution (based on Vinnem, 1999)

Load Categories	Load Distributions (%)	
	Simultaneous Drilling and Production	Normal Production
Heavy or multiple drill collars	22.2	0
Other Heavy (> 8 tons)	0.3	0.7
Medium Heavy (2-8 tons)	27.1	33.6
Light (< 2 tons)	50.5	65.7
Number of Lifts per year	20884	8768

Probability of Dropped Load

The probability of dropped loads during operations depends on the characteristics of the load and environmental conditions. Typically, only one average frequency may be estimated, i.e. an average drop frequency per lift or per crane year.

A typical frequency of dropped loads is in the order of 10E-5 to 10E-4 loads dropped per crane per year. For critical lifting operations, particular emphasis is placed on adhering to strict procedures. The dropped load frequency for this so called 'procedure lift' may be typically 30%-70% lower than the value for a 'normal' crane operation.

Probability of Hitting Objects

A dropped crane load may hit three types of objects. Each of them with the worst consequences is presented below.

The probability of hitting is usually based on geometrical considerations reflecting the areas over which the lifting is performed. Lifting over the process area is usually prohibited by operational procedures unless special restrictions are implemented. If a load is dropped under

such circumstance, it may be a critical event. The probability of topside equipment being hit may be expressed as follows:

$$P_{Hij} = \frac{A_{lij}}{A_{tot-i}} \cdot f_{crit}$$

(30.6)

where,

A_{lij} = Area of equipment j over which loads in category i may occasionally be lifted

A_{tot-i} = Total area of hydrocarbon equipment over which load category i may be lifted

f_{crit} = Ratio of critical area to total area over which lifting is performed

The probability of hitting structural components or subsea equipment can be determined in similar equations based on areas over which the lifting is performed.

30.5.2 Drop Object Impact Load Assessment

In principal, two cases need to be considered regarding the falling objects from the crane:

- Loads that are dropped on the equipment, structures, deck, or other locations which are above the sea surface.

- Loads that are dropped into the sea and possibly hit structures in the water or subsea equipment on the sea bottom.

The first case has only one phase, i.e. the fall through air. The second case has three phases, falling through the air, impact with the sea surface, and the fall through the water. Idealized calculations to determine the impact velocities in these three phases are briefly presented below. The drift caused by the currents may also be taken into account when calculating the most probable landing point on the seabed.

Fall through the Air

A falling object will accelerate towards the sea surface in accordance with the force of gravity. The impact velocity V_1 can be determined by:

$$V_1 = \sqrt{2gh}$$

(30.7)

where,

h = Height from which the drop occurs

g = Gravity acceleration

Impact with the Water

A falling object may hit the sea surface and proceed through the water with the velocity V_2, as determined by Eq. (30.8). The integral represents the loss of momentum during the impact with the water surface.

$$V_2 = V_1 - \int_0^t \frac{P(t)}{M} dt$$

(30.8)

where,

M = Object mass

$P(t)$ = Impact force

Fall through the Water

After the impact, the object will accelerate from V_2 towards its terminal velocity V_t in the water.

$$V_t = \sqrt{\frac{2(W - O)}{C_d \cdot A \cdot \rho}}$$

(30.9)

where,

W	= Gravity force (in air)
O	= Buoyancy force
ρ	= Density of sea water
A	= Cross section area
C_d	= Shape coefficient of the object depending on the Reynolds number

It is also known that an object will tend to oscillate sideways during the fall through water. These oscillating movements are determined by the impact angle with the water surface and the external shape of the object. Bar-shaped objects with large surface areas will oscillate more than massive and spherical objects. An oscillating object will have a lower terminal velocity than a non-oscillating object.

30.5.3 Consequence of Dropped Object Impact

The consequences of an impact are dependent on how a falling load actually hits the equipment (topside or subsea) or a structural component, i.e. velocity of the falling mass, hitting spot, impact angle, impact time, and contact area. Calculations are often made for ideal situations. It is often natural to distinguish falling loads between long cylindrical objects and bulky objects, because they have a different drop rate, trajectory/velocity in water, and effect on the structure/equipment.

Table 30.4 Consequences of Hitting Objects

Topside equipment	May cause loss of integrity of hydrocarbon containing equipment and possibly lead to a process fire.
Structural components above or in the water	May cause structural failure or loss of stability or buoyancy.
Subsea equipment	May cause loss of containment of production (hydrocarbon containing) equipment, possibly lead to a significant oil spill.

Topside equipment such as pressure vessels, separators, are obviously vulnerable to the dropped object's impact. Subsea production systems and pipelines are also very sensitive to dropped objects. Some calculations have indicated that a falling load with a mass of 2 tons could easily damage an actuator on the subsea production system. The same loads applied to a pipeline may cause pipeline damage and leakage. For structural components, the following component parts are often of interest: a) Topside structure, b) Module support beams, c) Supporting structure, and d) Buoyancy compartments.

30.6 Case Study – Risk Assessment of Floating Production Systems

30.6.1 General

A risk assessment may be conducted as part of the offshore field development and includes the following,

- All critical elements are appropriately selected and the corresponding performance standards are adequately defined for the life cycle of the FPS in terms of its functionality, availability, structural integrity, survivability, dependency and influence on the other critical elements. It should e demonstrated that the critical elements fit for purpose and meet the performance standards.

- Risk acceptance criteria are defined prior to the execution of risk assessment, and to provide a level of safety that is equivalent to that defined in the prescriptive rules and codes.

- All hazards with a potential to cause a major incident have been identified, their risks are evaluated and measures have been taken (or will be taken) to reduce the risk to the level that complies with the risk acceptance criteria.

Type of risks for FPS depends on the type of vessel used and the geographical region it is sited. FPSOs used in the North Sea are mainly new vessels with turret system. The offloading tankers come to empty the storage tanks at frequency (approximately) once per week. The offloading tankers may represent a collision hazard to the FPSO with medium frequency and potentially high consequence. So far FPSOs in the west Africa offshore are mainly based on spread mooring system and a single point mooring for oil export. FPSOs used in other geographical regions are mainly based on converted tankers.

In the following, an FPSO (Floating Production Storage and Offloading) for the Gulf of Mexico is chosen as an example to illustrate methods of risk assessment. The methods illustrated in this section may also be applied to other types of floating production systems such as TLPs, Spars and semi-submersibles.

A risk assessment of FPSO may include evaluation of the following systems:

Process Systems

The process systems include, e.g.:

- Process plant with three-stage separation, gas compression for export and gas turbine-driven power generation on deck

- piping, pressure vessels in production and storage facilities

- cargo tanks and crude pumping systems, offloading systems and its operation

Process risk is mainly initiated by loss of hydrocarbons containment that might escalate to explosion and fire accidents. The risk assessment of process systems may be conducted using a conventional offshore QRA approach (Wolford, 2001),

- Development of isolatable sections

- Summarize the loss of containment frequency by using a parts count approach

- Identifying spatial interactions that could lead to escalation

Leak frequencies may be derived primarily from generic databases that are available to the offshore industry. Emergency detection and process control response to a loss of containment event should be accounted for.

API RP 14J (1993) has been used by the industry for the design and hazards analysis for facilities on offshore production installations. This RP mainly deals with the prevention of fire risk due to hydrocarbon ignition. Methodologies for hazard analysis are recommended. The API methodologies can be applied to assess explosion risk as well. Guidance is given on the risk management through platform equipment arrangement, hazard mitigation and personnel evacuation. Detailed check-lists are given in its appendix on facility layout (and emergency response/medical, escape and rescue), process equipment, safety and electrical systems, fire and gas leakage protection and mechanical systems, etc.

Marine Systems

The marine systems may include, e.g.:

- marine systems, such as cargo tanks, crude pump room, boilers and engine room, power generation/supply systems, ballast system and wing tanks,
- escape and evacuation system and equipment

The risk assessment of marine systems is similar to that for process systems. The exception is the scope of marine system risk is broader than the loss of hydrocarbon containment. The majority of the marine system risk is fire due to fuel leakage and electrical systems. However, there is a lack of FPSO fire initiator frequency data for the appropriate quantification of fire risk.

Structural Systems

The structural systems may include, e.g.:

- hull structures, especially the moonpool area that accommodates the turret if there is one
- position mooring systems, such as moorings and anchors, and/or dynamic position systems
- risers and flowlines
- topside structures
- helideck and helicopters operation
- flare system

The structural system risk is covered in Part IV of this book.

30.6.2 Hazard Identification

In an FPSO risk assessment, the primary objective of the hazard identification is to identify and register the hazardous events that may escalate into accidental events. The hazard identification task may be relatively coarse and subjective in the conceptual design phase, and become more specific in the detail design phase. A partial list of the typical hazards is given below.

- explosions/fires in cargo and ballast tanks

  The explosion and fire in cargo ballast tanks may result in hull structural failure and cause oil spill.

- explosions/fires in engine room and/or pump room

The explosions/fires in engine room and/or pump room may cause loss/delay of production, and escalate to cargo tanks.

- collisions from shuttle tanker or other vessels

Shuttle tankers, supply vessels and pass-by vessels may collide into the FPSO due to failure of position mooring systems, errors in navigation or offloading operation, power failure etc.

- dropped objects

Dropped objects may cause damage to structures leading to loss of buoyancy and cause damages to equipment and subsea flowlines leading to hydrocarbon leaks and personnel injuries/fatalities.

- extreme weather

The weather conditions may be more severe than that considered in the design. Waves whose height is lower than the 100 year return design wave height but with more vibration sensitive wave periods may cause larger vessel motions and green water impacts.

- green water

Green water can induce impacts loads on the forecastle, topsides along the deck edges of the vessel, and may cause damage/impair of evacuation tunnels.

- structural failure such as corrosion defects and fatigue cracks

Fatigue may be induced by wave loads and due to poor design of structural details. Corrosion defects may be found in cargo tanks, piping and pressure vessels.

- rupture in risers, flowlines and leaks in offloading hose

Failure of risers, flowlines and offloading hose may be caused by corrosion, fatigue and accidental loads.

- failure of station-keeping capacity

A partial failure of the station-keeping system may lead to damages to risers resulting in gas leakage and fires. Loss of station keeping capacity may lead to collisions and grounding (in shallow water).

30.6.3 Risk Acceptance Criteria

A risk matrix approach defined in Part V Chapter 29 may be used as the risk acceptance criteria and it consists of failure frequency and consequence.

The failure frequency may be classed into high, medium, low and remote, each of them is defined below.

- High – an accident that occurred at least once in the past year and expected to occur again to the system, e.g. frequency > 0.1

- Medium – an accident that might occur at least once in the life cycle of the system, no one would surprise if the accident occurs, e.g. 0.01<frequency<0.1

- Low – an accident is considered unlikely to occur. However, similar accidents have occurred once or twice in the industry worldwide, e.g. 0.0001<frequency<0.01

- Remote – an accident is credible, but not expected to occur in the life cycle of the system, e.g. frequency <0.0001.

The consequences of failure may depend on the type of risks considered, e.g. personnel risks, economical risks and environmental risks. An example category of failure consequences is given below,

- Catastrophic – fatality or disability injury; major loss of the FPSO or long-term loss of its production; serious oil and gas release resulting in long-term damage to the environment.

- Critical – severe injury; major damage to the FPSO or its production; significant oil and gas release.

- Significant – non-severe injury; some damage to the equipment and systems and minor loss of production; oil/gas release requiring regulatory notification.

- Minor – no injury; minimum component failure and no loss of production; record-able event but no regulatory involvement.

The physical phenomena to be considered in consequence modeling include:

- Release modeling, multi-phase, near field flow regime and internal-pressure time history

- Thermal radiation effects to humans and equipment from jet fires and pool fires.

- Explosion over-pressure that impacts human and equipment

- Evacuation of personnel on board

30.6.4 Risk Estimation and Reducing Measures

If risks are unacceptably high, measures are to be taken to eliminate/reduce the risks. Examples of the approaches to reduce risks are,

- modify the design to eliminate the hazard,

- reduce the frequency of occurrence of an initiating event,

- reduce the frequency of the events that may cause an initiating event to become an accidental event of unacceptable consequences,

- reduce the exposure of personnel and equipment to the hazard,

- implement strict operational procedures, safety procedures and emergency response program.

More specifically major risk estimation and reducing measures include the following,

Process Leakage

Process systems are often the main contributor to personnel risk. The gas compression has the highest leakage frequency followed by the fuel gas system and the gas dehydration system. Most of leakage is small, e.g. less than 10 mm equivalent hole size. The process leaks may lead to explosions and fires. Pollution from process leaks is limited by the process shutdown and isolation system, unless an explosion with subsequent fire escalates to the cargo tanks and threatens the overall integrity of the vessel. The process leak may be reduced by: relocating process control center to within the accommodation, installing a protected escape route from bow to stern, installing additional gas detectors in the process area.

Offloading and Shuttle Tanker Risk

There are two types of oil offloading systems, namely tandem assisted offloading and single point mooring. The former is used with turret moored FPSO and the later is applied with

spread moored FPSO. The main hazards associated with tandem assisted offloading are collision between shuttle tankers and FPSO and oil spillage from hose rupture. Loading hose rupture can occur during connection of transfer hose and offloading phases, due to structural defects, fatigue loading, excessive tension/pressure or extreme fishtailing. Fatigue cracks may develop in offloading risers in harsh environment. Failure of single point mooring system may lead to failure of the transfer risers if the transfer risers are structurally supported by the single point mooring system.

Examples of the approaches to reduce risks are,

- improving the ability to detect the failure and to activate the shutdown system,

- monitoring traffic and mooring hawser and deck watches,

- improving personnel training and preparedness to face accidental situation (Karsan, et al 1999),

- isolating oil offloading risers (hoses) from the buoy of the single point mooring system from structural redundancy point of view,

- use of standby vessels that can perform a variety of operations from providing emergency towing to assisting with the mooring and hose lifting operations (Daughdrill and Clark, 2002),

- designing offloading system with adequate redundancy.

Daughdrill and Clark (2002) outlined several published guides on offloading:

- "Offshore loading safety guideline with special relevance to harsh weather zones" by Oil Companies International Marine Forum (OCIMF) in 1999,

- "Ship to ship transfer guide (petroleum), 3rd Edition" by OCIMF in 1997,

- "The training and experience of key DP personnel", by International Marine Contractors Association (IMCA) in 1996,

- "Risk minimization guidelines for shuttle tanker operations worldwide at offshore locations" by INTERTANKO (International Association of Independent Tanker Owner) in 2000.

To predict the relative motion (surging and yawing) and probability of collisions between FPSO and shuttle tankers in tandem offloading operation, Chen et al (2002) presented a simulation-based approach based on a time-domain simulation code SIMO. The collisions are modeled in two stages: the initiating stage and the recovery stage. The initiating stage is the situations where something could possibly go wrong to cause tanker uncontrolled forward movement, while the recovery stage is the initiation by tanker to avoid collision after the occurrence of the initiating stage. In the probabilistic model for the initiating stage, Chen at al (2002) integrated technical events, human actions and their interactions. The SIMO simulation models are calibrated for a typical North Sea FPSO and a DP shuttle tanker. The extreme values for the simulated relative distance and heading between FPSO and tanker are analyzed by fitting with statistical models. Chen et al (2002) estimated that the frequencies of excessive surging and yawing can both be in the order of 10E-3 per year. Sensitivities to various technical and operating factors are studied, and measures are identified to minimize the probability of collision.

Marine System Risk

Only cargo tank system for oil storage is considered herein. The cargo tanks are provided with inert gas system and crude oil washing system. Explosion and fire may occur in cargo tanks although there is a lack of incident data for the frequency quantification. A cargo tank explosion may cause structural damage and damage to the process plant. This would probably result in a hydrocarbon leak from process system and a possible subsequent fire in the process area. Immediate fatalities are mainly due to the effect of the explosion in the process area. Smoke may be a treat to personnel safety. The potential risk reduction measures are: improving procedures for tank intervention,

- improving reliability of the inert gas system,

- installing thrusters to allow the vessel to change heading (to avoid fire engulf the accommodation) and,

- improving the fire/blast protection of the front wall of the accommodation (Nesje et al, 1999).

Collision Risk

The wing tanks of the vessel ballasted with water would provide dual barrier against puncturing of the cargo tanks. Measures for collision avoidance and consequence reduction include radar surveillance, having a standby vessel, developing hazard management plans and installation of thrusters to reduce target for a drifting vessel on a collision course. Protection of risers, offloading lines and fluid transfer lines shall be designed to meet the energy absorption requirements.

MacDonald et al (1999) provided an overview of the ship/FPSO collision risks and presented methodologies that can be applied to quantify the frequency and consequences of these events. Measures that have potential to reduce the risk of ship collision are highlighted focusing on the scenarios most likely to result in pollution, loss of life and asset and production loss/delay.

Explosion Risk

In the detail design phase, explosion risk is estimated and effort is made to minimize explosion overpressures. Hydrocarbon lines, riser/fluid transfer lines are appropriately routed such that possible leakage on main decks is minimized.

Fire Risk

Jet fires and pool fires may represent risks to equipment. The design fire duration is determined considering the ability of personnel to escape to a safe location and the reduction of the pollution of hydrocarbon to the environment.

Dropped Object Risk

The design criteria for equipment protection depend on the size and location of the lifts and the frequency of their operations. Normally a dropped object study is conducted as part of the detail design in which credible dropped weight and the loads acting on the equipment are calculated, structural response and failure frequency are estimated.

30.6.5 Comparative Risk Analysis

Risk assessment may also be applied in a comparative risk analysis that compares a particular design with other designs that have been accepted to have adequate level of safety. For

instance, Gilbert et al (2001) presented a study to compare the risks of FPSO, which have never been used in the Gulf of Mexico, with the risks for existing deepwater floating production systems (TLP and Spar) in the Gulf of Mexico, and a shallow-water jacket serving as a hub and host to deepwater platforms. The whole production systems were considered, from the wells through the transport of product to the shore. Three risk measures were assessed and analyzed for each system in a 20-year production life: the total number of the human fatality risk, the total volume of oil spilled as a measure of the chronic environmental risk and the maximum volume spilled in a single incident. It was concluded that there are no significant difference in the fatality risks, environmental risks among of the four types of systems studied. The study has been very useful for the regulatory agency and offshore industry to accept the use of FPSO in the Gulf of Mexico.

30.6.6 Risk Based Inspection

Three fundamental questions are to be answered in the planning of risk-based inspections (Xu, 2001),

- what should be inspected ?
- how much effort should be made on individual components or details ?
- when the inspection should be conducted ?

The key step in inspection planning is the ranking of the components for inspection. A rating system should be created including analysis of frequency and consequence and the detection of defects through inspection. The frequency analysis may be based on databases for failure frequency and analytical methods or a combination of the databases and analysis.

The consequence of failure to be considered in inspection of the FPSO structures include the following,

Structures including vessel hull and topside structures

- catastrophic – loss of stability and structural integrity or leading to downtime of more thn one year;
- critical – loss of structural integrity that requires excessive dry dock repairs or down time of between 6 months and one year;
- severe – moderate structural damage that requires minor dry dock repirs or downtime of between 1 months and 6 months;
- minor – minor damage that requires a quick onboard repair or a down time of less than one month.

Mooring systems and the thruster system that assists the station keeping system

- catastrophic – resulting in a big loss of asset or downtime of more than one year
- critical – resulting in major collision and grounding with downtime of between 6 month and one year;
- severe – leading to minor collision and downtime between 1 month and 6 months.
- minor – leading to repair or replacement of one line at site and two or more lines damaged.

Import/export systems such as risers, flowlines and offloading systems

- catastrophic – resulting in major oil spill or fire due to the leakage of oil and gas

- critical – leading to moderate oil spill and downtime of above 6 months

- severe – ruptures in the pipe require repair and replacement and downtime of 1 to 6 months

- minor – repair or replacement of the riser, flowline and offloading systems that cause shut-down of less than one month.

For generic methodologies for risk-based inspection, reference is made to API RP 580 (API, 2002). This newly developed RP contains the following Sections:

- Introduction to risk-based inspection

- Screen and boundary identification

- Data and information collection for RBI assessment

- Identifying deterioration mechanisms and failure modes

- Assessing likelihood of failure

- Assessing consequences of failures

- Assessing risk

- Risk management with inspection activities

- Other risk mitigation activities

- Reassessment and updating RBI assessment

- Roles, responsibilities, training and qualification

- RBI documentation and record keeping

The formulation for probability and risk-based inspection has been given in Part IV Chapter 28. The effectiveness of inspection depends on the degradation mechanism and rate, inspection scope/frequency and detection capability as well as the usefulness of the mitigation.

For FPSO, the biggest benefit from the use of risk-based inspection is perhaps the reduced loss of production.

30.7 Environmental Impact Assessment

In many situations, an environmental impact assessment must be conducted prior to the execution of an offshore field development. The results of the environmental impact assessment may be used to minimize the environmental impact from development and operation of the oil/gas field. The scope of an environmental impact assessment may depend on the geographical regions and the characteristics of the field, and may for example include the following:

- Investigate distribution, population size and biology of key species of fish, birds and mammals

- Evaluate food webs and tropical interactions, energy transfer in the ecosystem,

- Assess environmental toxins in sediments, benthic organisms and fish

- Develop oil spill modeling

- Establish databases with relevant environmental data

From environmental protection point of view, the following items should be considered (Gudmestad et al, 1999):

- Discharge from drilling operations such as mud and cuttings

- Produced water handling

- Ballast water storage tanks

- Selection of chemicals considering environmental data for toxicity, degradability and potential for bio-accumulation

- Loading operations to reduce possibility for oil spills during loading

- Tanker oil transport to avoid oil spills

- Oil spill contingency plan, e.g. in-situ burning, bioremediation etc.

- Waste handling

- Emission to air of CO_2, No_x, and SO_x

30.8 References

1.   API RP 14J (1993), "API Recommended Practice for Design and Hazard Analysis for Offshore Production Facilities", American Petroleum Institute.

2.   API RP 580 (2002), "Risk-Based Inspection", American Petroleum Institute.

3.   Bai, Y. and Pedersen, P. Terndrup, "Elastic-Plastic Behavior of Offshore Steel Structures Under Earthquake Impact Loads", International Journal of Impact Engineering, 13(1), pp. 99-115.

4.   Burgan, B.A. and Hamdan, F.H.(2002), "Response of Topside Structures to Fires and Explosions: Design Considerations", Offshore Technology Conference, OTC 14130.

5.   CCPS (1995), *"Chemical Transportation Risk Analysis"*, Center for Chemical Process Safety, American Institute of Chemical Engineers.

6.   Chen, H. and Moan, T. (2002), "Collision Risk Analysis of FPSO-Tanker Offloading Operation", 21st Int. Conference On Offshore Mechanics and Arctic Engineering (OMAE), OMAE2002-28103.

7.   Chen, H. and Moan, T., Haver, S. and Larsen, K. (2002), "Prediction of Relative Motion and Probability of Contact Between FPSO and Shuttle Tanker in Tandem Offloading Operation", 21st Int. Conference On Offshore Mechanics and Arctic Engineering (OMAE), OMAE2002-28101.

8.   CMPT (1999), *"A Guide to Quantitative Risk Assessment of Offshore Installations"*.

9.   Czujko, J. (2001), "Design of Offshore Facilities to Resist Gas Explosion Hazard, Engineering Handbook", Corrocean.

10. Daughdrill, W.H. and Clark, T.A. (2002), "Consideration in Reducing Risks in FPSO and Shuttle Vessel Lighting Operations", Offshore Technology Conference, OTC 14000.

11. Gilbert, R.B., Ward, E.G. and Wolford, A.J. (2001), "A Comparative Risk Analysis of FPSOs with Other Deepwater Production Systems in the Gulf of Mexico", Offshore Technology Conference, OTC 13173.

12. Gudmestad, O.T. et al (1999), "*Basics of Offshore Petroleum Engineering and Development of Marine Facilities with Emphasis on Arctic Offshore*", ISBN 5-7246-0100-1.

13. Haugen, S (1991), "Probabilistic Evaluation of Frequency of Collision between Ships and Offshore Platforms", Dr.ing Thesis, Division of Marine Structures, NTNU, MTA-report 1991:80.

14. Karsan, D.I., Aggarwal, R.K., Nesje, J.D., Bhattacharjee, S., Arney, C.E., Haire, B.M. and Ballesio, J.E. (1999), "Risk Assessment of Tanker Based Floating Production Storage and Offloading (FPSO) System in Deepwater Gulf of Mexico", OTC 11000.

15. Lassagne, M.G., Pang, D.X. and Vieira, P. (2001), "Prescriptive and Risk-Based Approaches to Regulation: The Case of FPSOs in Deepwater Gulf of Mexico", OTC 12950.

16. MacDonald, A., Cain, M., Aggarwal, R.K., Vivalda, C. and Lie, O.E., (1999), "Collision Risks Associated with FPSOs in deep Water Gulf of Mexico", OTC 10999.

17. Nesje, J.D., Aggarwal, R.K., Petrauskas, C., Vennem, J.E., Keolanul, G.L., Hoffman, J. and McDonnell, R. (1999), "Risk Assessment Technology and its Appliction to Tanker Based Floting Production Storage and Offloading (FPSO) Systems", OTC 19998.

18. NPD (1992), "Regulations Relating to Implementation and use of Risk Analysis in the Petroleum Activities", Norwegian Petroleum Directorate, Stavanger, Norway.

19. NTS (1998), "NORSOK Standard for Design of Steel Structures Annex A, NORSOK N-004", Rev.1, Norway.

20. Pappas, J. (2001),"The NORSOK Procedure on Probabilistic Explosion Simulation", Paper 5.5.1, ERA Conference, "Major Hazards Offshore", London, 27-28 Nov. 2001.

21. Saubestre, V., Khalfi, J-P., Paygnard, J-C. (1995), "Integrated Fire Analysis: Application to Offshore Cases", OMAE-95, Copenhagen

22. UK HSE (1992), "Safety Case Regulation", United Kingdom Health and Safety Executives.

23. UK HSE (1995), "Prevention of Fire and Explosion, and Emergency Response Regulation", United Kingdom Health and Safety Executives.

24. Vinnem, J.E. (1999), "*Quantified Risk Assessment – Principles, Modelling and Applications of QRA Studies*", Kluwer Academic Publishers.

25. Walker, S., Corr, B., Tam, V., O'Connor, P. and Bucknell, J. (2002), "New Guidance on Fire and Explosion Engineering", 21st Int. Conf. On Offshore Mechanics and Arctic Engineering (OMAE), OMAE2002-28623.

26. Wolford, A.J., Lin, J.C., Liming, J.K., Lidstone, A. and Sheppard, R.E. (2001), "Integrated Risk based Design of FPSO Topside, Structural and marine Systems," OTC 12948.

27. Xu, T., Bai, Y., Wang, M. and Bea, R. (2001),"Risk-based Optimum Inspection of FPSO". OTC 12352.

Part V

Risk Assessment

Chapter 31   Formal Safety Assessment Applied to Shipping Industry

31.1 Introduction

Shipping is a traditional industry in which safety has been an issue for hundreds of years. Meanwhile, accidents have often led to the recognition of the need for measures to control risks at sea. For example, the Titanic disaster in 1912 in which 1430 lives were lost, led to the first International Conference on Safety of Life at Sea (SOLAS), that are international standards and regulations to prevent such causalities. The capsizing of the liner Andrea Doria prompted the United States delegation to attend the 1960 International Safety Conference and introduced the concept that ship safety should be measured as the extent of damage a ship could survive. A Growing public concern over the devastating consequence of marine pollution due to several oil tanker accidents prompted the organization of the MARPOL conventions of the 1970s. The Exxon Valdez disaster in 1990 resulted in the use of double hull tankers mandated by IMO. These incidents indicate the everlasting necessity for introducing the modern risk assessment techniques in the commercial shipping industry.

The nuclear industry developed probabilistic safety assessment in 1960s. In 1970s, the chemical industry used Quantitative Risk Assessment (QRA). Due to industry self-regulation, since 1980s the offshore industry has applied QRA in Norway after the Alexander accident, and then in the UK due to the Piper-Alpha accident.

In 1993 a particular type of risk management framework in the ship safety regime was proposed by the UK to IMO, referred to as the Formal Safety Assessment (FSA). The FSA has been taken as a priority item on IMO Maritime Safety Committee's agenda in the conferences since then. IMO uses the FSA process for rulemaking and issued FSA interim guidelines in 1997 (IMO, 1997) and guidelines in 2001. Being a tool designed to assist maritime regulators, FSA is not intended for application to individual ships, but for use in a generic way for shipping in general. The main elements introduced by FSA are: a formalized procedure, an audible process, communicated safety objectives, and priorities based on cost effectiveness. These have made the FSA a more rational risk assessment approach for the regulatory purposes in shipping industry.

It should be recognized formal safety assessment is applied to safety issues common to a specific ship type (e.g. a bulk carrier or a high-speed craft) or a particular hazard (e.g. collision, grounding, fire etc.). A safety case approach used in the UK offshore industry is applied to a particular offshore installation.

A comprehensive summary of the recently published work on marine risk assessment was given by Yoshida et al (2000) in the ISSC report for Specialist Committee V1 "Risk Assessment".

The following Sections in this Chapter deal with the FSA. The major functional components of FSA are outlined, and followed by a detailed description of each component. A case study in the FSA regime is then briefly presented for illustrative purpose. The inclusion of human and organizational factors within FSA is also discussed. Finally, the challenges, limitations, and concerns regarding FSA application in shipping industry are discussed.

31.2 Overview of Formal Safety Assessment

As a risk based methodology, in some aspects FSA is similar to the Safety Case regime used in the UK Continental Shelf. A safety case should be applied to a particular offshore installation. However, FSA is applied as a whole to shipping or to safety issues common to a ship type, such as tankers or high-speed passenger vessels. This type of application is due to a number of reasons, for example, the unique feature of the shipping industry: there is no single regulator, no single culture, and no uniformed education & qualification system existing in maritime industry worldwide. FSA is a tool for rule-making at IMO to make decision process more rational and to provide a proactive approach comprising technical and operational aspects. IMO interim FSA Guidelines state that "FSA can be used as a tool to help in the evaluation of new safety regulations of making a comparison between existing and possibly improved regulations, with a view to achieving a balance between the various technical and operational issues, including the human element, and between safety and costs". The FSA may be used to develop "performance-based" rules stating safety objectives and functional requirements and rational "prescriptive standards" based on the performance-based rules.

The main characteristics of the Formal Safety Assessment are presented below:

- A systematic approach considering the ships as socio-technical systems. The system may consist of hardware, environment, human organizations, operations, and procedures.

- Hazards are identified proactively through the hazard identification process. A large number of different hazard identification approaches may be put into use.

- Risks associated with various hazards are described and analyzed. The risk is a composite of the likelihood and consequences of the potential undesirable events arising from a hazard. The risk analysis covers a certain time-span, i.e. the operational life, and may involve various quantitative or qualitative tools to perform likelihood and consequence calculations.

- Once a risk is quantified, it is then necessary to determine if the risk is acceptable, based on the predefined acceptance criteria. When the risk is acceptable, a cost/benefit analysis may be followed to compare the costs for preventive/protective measures with the benefits.

- The above mentioned basic elements are integrated into a risk model, where the objective is to recommend the most cost effective, preventive, and mitigating measures for risk management.

The functional components in a Formal Safety Assessment are shown in Figure 31.1 below. Being a risk based approach it may look quite similar to the offshore QRA procedures. However, the actual content of each step as well as the methods and tools used may be different from offshore applications. This is described in more detail in Section 31.3.

The types of risks to be considered include:

- risk to human safety

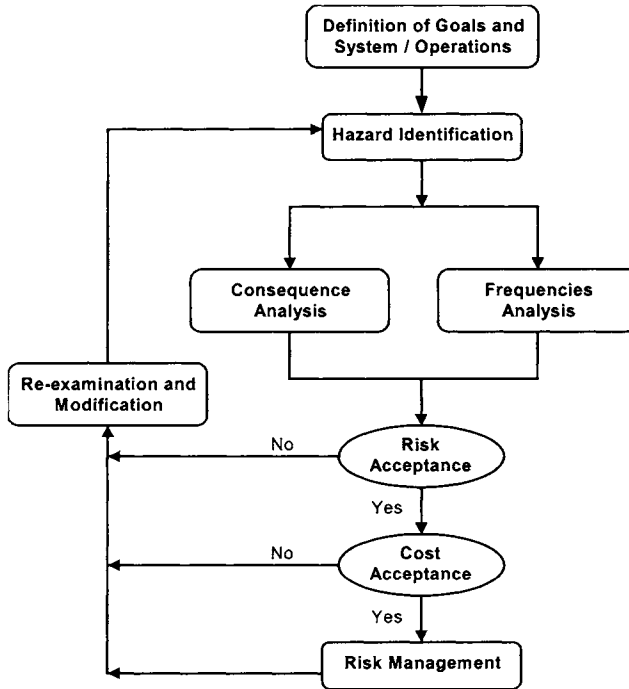- risk to the environment
- risk to property

Figure 31.1   Functional Components in Formal Safety Assessment

31.3 Functional Components of Formal Safety Assessment

31.3.1 System Definition

A detailed system description is essential to the risk assessment. Such description usually consists of a hierarchical structure, including all hardware, people, procedures, and environment, being described in a 'top-down' manner. The hardware that comprises a generic ship is the most basic layer in the system definition. The interface between hardware and human operators, i.e. the so-called man-machine interface, forms the second layer. The external environment could be considered as the third layer. The overall safety is influenced by the hardware, individuals & organization, and external environment, which may vary during the ship life cycle. Therefore, in the following Sections we shall discuss the ship's hardware, the stakeholders (interested parties), and the ship's life cycle.

The Ship Hardware

The ship hardware can be roughly decomposed into two categories: structure and machinery.

The ship structure has been traditionally divided into three sub-categories: hull girder, internal structure, and superstructure. Structural elements play various roles in maintaining the integrity of the ship. Structural failure may lead to cracking, localized flooding, or even ship breaking apart in extreme cases. A considerable progress has been made in the past few decades to analyze the capacity of complex ship structures using modern FEM tools, see Part II Chapter 13. However, uncertainties concerning construction errors and defects, and uncertainties in the load prediction still exist.

The ship machinery consists of many sub-systems: i.e. power generation system, propulsion system, steering and maneuvering system, navigation and communication system, cargo-fuel-ballast handling, mooring and anchoring, monitoring, and emergency response system. The integrity of these systems is vital to the operation of the ship. Improper operation or accidental system failure can directly trigger accidents, which may lead to the loss of cargo, human life, and/or severe environmental pollution.

The Stakeholders

A generic ship may involve the following stakeholders: Crew, Ship-owner/Charter, Classification society, Builder, Cargo and cargo owner, Passengers, the Insurer, the Port, and Coastal States. Various stakeholders may have different views of the safety, as well as the cost/benefits derived from the changes of the shipping safety. The interaction among these parties is complex, and will significantly influence the safety of shipping.

The Ship Life Cycle

A ship may be originated by the owner's decision to build a new ship, with characteristic dimensions that satisfy functional requirements. The second stage is the design stage. Specifications for the structures and machinery of the ship are determined. The third stage is the building stage. It consists of construction, launching, and outfitting the ship by yard. The fourth stage consists of normal operations. A typical new ship can be in service for thirty or more years, and FSA will emphasize on the normal operation. During the ship's service life, it will have four principal activities: open ocean navigation, waterway navigation, port operation, and dry-dock operation. These are described in detail below.

- Open Sea Navigation: The largest percentage of time in the whole life of any large ship is spent in transit on open sea.

- Waterway Navigation: This is usually the second most frequent activity in a ship's life cycle. As a large ship approaches (or leaves) a harbor, it is common for the ship to pick up a pilot who has greater familiarity with all aspects of the waterway leading into the harbor.

- Port Operations: The port is where cargo or passengers are loaded or discharged. Many accidents have occurred in ports relating to the transfer of cargo. Different ships may involve different types of operation, and therefore different duration's.

- Dry-dock Operations. Ships dry-dock at regular intervals for the purpose of inspection, repair, and maintenance. The dry-docking can involve inspections by an agent of the classification society, and inspections by the owner.

- The last stage is the scrapping stage. Ships may be finally scrapped in a repair yard at the end of their life.

31.3.2 Hazard Identification

In the FSA regime, a hazard is broadly defined as a situation with the potential to cause harm to human life, the environment and property. Hazards become a problem when they develop into accidents, generally this occurs through a sequence of events. There are two features for ship hazards as described below.

A ship hazard characteristic is that it is more difficult to achieve ideal levels of separation from the onboard hazards, since command and control facilities, living/working areas, fuel, propulsion, power generation plants, and emergency systems are within the ship.

Another characteristic of ship hazards is that, at different phases of the operation, the ship could experience different kinds of hazards.

A hazard identification is performed by selected professionals and the purpose of hazard identification is to identify all conceivable and relevant hazards. Typically a team of 6 to 10 experts, including naval architects, structural engineers, machinery engineers, surveyors, human factor engineer, marine officers and meeting moderator, provide the necessary expertise for the topic under study. The hazards are identified using historical incident databases and expertise of the team. Several analysis methods are available, including FMEA, HAZOP etc. The identified scenarios are ranked by their risk levels, and prioritizing hazards are given a focus and may be subjected to more detailed analysis.

For a generic ship and its associated sub-systems, the following important hazard categories are identified. Each of these categories is complex, resulting from a large number of different factors. After hazard identification, hazard ranking may be performed to prioritize the hazards, based on rough estimates of the risk associated with each identified hazard.

Collision and grounding
Fire
Explosion
Loss of structural integrity

Loss of power
Hazardous material
Loading errors
Extreme environmental condition

Collision and Grounding

Collision occurs when a ship strikes another ship or other object. It is a high consequence hazard for oceangoing ships. Grounding occurs when the ship bottom is penetrated by the sea bottom or underwater rocks. Collision and grounding are a low probability, high consequence event, especially for tankers, Amrozowicz (1997). The assessment of grounding and collision risk includes:

- Frequency of occurrence of the grounding and collision accidents

- Consequence in terms of structural damages, oil outflow and environmental/economical impact due to the oil spill

Wennick (1992) investigated the frequency of occurrence of collision and grounding in channel and port navigation using the "statistical method" and the "causal method". The "statistical method" uses historical incident records to estimate accident frequencies while the "casual method" establishes the relationship between the contributing factors and the occurrence of the accidents. While the "casual method" may be used to study the impact of

changes in the physical plan on the risk of collision and grounding, it needs to be calibrated with the "statistical method".

Sirkar et al (1997) proposed a risk assessment approach that account for the consequence of collisions and groundings. Their model for tanker environmental risk includes calculation of the accident probability, oil outflow analysis using probabilistic methods, and estimation of consequences using spill response simulation. Like offshore environmental risk analysis, the volume of oil spill is not the best measure of the environmental risk. Instead, the effect of oil spill should be used, see Part V Section 29.1.7. In Sirkar et al (1997), the probability of damage and oil outflow analysis is based on a simplified probabilistic oil outflow methodology. They proposed a method for calculating probability distributions of damage extents and locations by simulating structural response in grounding and collision in a large number of accident scenarios using a Monte Carlo approach. In the Monte Carlo Simulations, the input variables include the accident scenarios (e.g. vessel characteristics, grounding types), and the initial distributions defined based on historical data and expert judgment.

The principal underlying cause in this category is lack of information, for example, an imprecise knowledge of one's own position at a given time, uncharted obstacles, inaccurate position and speed of nearby vessels will all pose the threats mentioned above. Severe weather, human error, often in the form of miscommunication or an otherwise occupied pilot, and inappropriate speed, all play an important role in causing consequential damages.

Fire

Fire is a ship hazard of higher consequence. It is estimated that more than a third of all ship-board deaths during the period 1987-1992 are due to fire accidents (Hessler, 1995). To protect from the fire effects, detection and alarm systems notify the crew to take appropriate fire fighting actions and alert the passengers to evacuate from the dangerous area. Early detection of fire is vital. Once a fire has started, it is difficult to extinguish and it can easily escalate. Sometimes it may be difficult to reach a fire site due to the confined nature of quarters on board ships, limited access to the burning area, and other factors such as toxic smoke. Inadequate training of the crew in fire fighting procedures may also pose a problem.

To reduce fire growth and spread, material and product performance testing are used to set limits on the heat release, on the thermal properties of structural boundaries and on the use of restricted combustible materials. These testing requirements provide containment of the fire in the origin area and minimize the impact of the fire on the means of escape or to the access for fire fighting. The system design to facilitate passenger evacuation can play an important role for timely passenger evacuation and fire fighting.

Fires that start in the engine room are often linked to a leak in the fuel line, lubricating oil or hydraulic fluid, with subsequent ignition. Electrical short circuits are another cause. Regions such as the galley, laundry rooms, recreational and storage areas contain many combustible materials such as cooking oils, sugars, flour etc. Crew may sometimes fail to recognize these commonplace hazards. NK (1994) issued guidance to protect engine room fire based on a series of risk assessment study. Arima et al (1994) summarized the engine room fire causality data. About 0.1 % of ships were damaged by the engine room fire, and the same amount due to fire in hull compartments. 75% of engine room fire occurred when ships were underway, in which 50% of the ships became uncontrollable.

Explosion

A number of explosions that occurred in the past were initiated on crude carriers in ballast tanks after the cargo had been unloaded. Crude oil contains many volatile constituents that can create a highly explosive mixture in air. Inert Gas Protection techniques such as pumping pure nitrogen or carbon dioxide in the tanks as they are being emptied, or shortly after, to remove the oxygen has offered greater protection than before. Communication and strict adherence to protocols are vital duties, which will avoid explosions during venting operations.

Human error resulting in inadequate precautions is another factor. A number of explosion accidents actually originated from mistakes or violations in the operational procedure, e.g. smoke, illegal short cut in procedure, etc.

Loss of Structural Integrity

Loss of structural integrity is a traditional concern for classification societies. Hull failure may result from faulty designs, construction, maintenance, or operation related factors. Furthermore, the introduction of new technologies and new ship types may constantly lead to new problems.

The maintenance of aging ships may not be perfect. It is impossible to inspect some areas of the ship and register the condition of all the structural members since their condition can never be known with certainty. Cyclic loading due to waves causes the structural components to fatigue over time. The degree to which fatigue degrades the load-bearing capacity of the vessel can not be estimated accurately. Corrosion is also a likely problem. All the above mentioned possibilities may lead to the loss of the ship's structural integrity.

Loss of Power

The loss of engine power at sea is potentially dangerous. Without power, steering the ship becomes impossible since the rudder becomes ineffective with no propeller race or forward speed. The vessel may then collide with another vessel or obstacle, or drift under the wind, waves, currents, and subsequently the ground. In heavy seas, the vessel can possibly broach and founder with no way of pointing into or running with the waves.

Power failure may result from mechanical failure of the engine, generator breakdown, a boiler or crankcase explosion, engine room fire, etc. One known initiator of power loss is contamination of the fuel supply by water. Seawater passing through damaged fuel tank ventilators caused BRAER (crude oil tanker) to lose power and drift aground off Scotland where its cargo was then spilled.

Hazardous Material

The risks associated with cargo such as crude oil or liquefied natural gas are obvious. However, the danger of materials such as powered aluminum, certain types of flour, etc. may not be readily apparent. The international community has set regulations on known hazardous substances. For instance, containers carrying hazardous substances require a bold diamond shaped label marking them 'Dangerous and Hazardous' and displaying a code that indicates the contents precisely.

There is a possibility of mishandling containers during port operations, causing breaking or leakage. If a leak occurs inside a container for whatever reason, it may stay unnoticed for a time. Undetected release of toxic substances may pose a threat to the crew and cleanup on board at sea can be difficult.

Romer et al (1993) presented a risk assessment of marine transport of dangerous goods based on historical data that consist of 151 accidents in the period of 1986 to 1991. Their paper gave frequencies for various kinds of accidents, FN curves and frequencies and size of spills.

Loading Errors

Improperly loaded cargo may adversely affect the ship's stability, as well as put undue strain on the hull and subsequently increase the failure probability at sea. In rare cases, a vessel can sink due to improper loading.

Vessels such as ore carriers are susceptible to payload shifts during periods of rough seas. While for container ships, container lashings can become loosened or broken, causing containers to shift or move freely. This will not only jeopardize ship stability, but also pose a threat to personnel, machinery, or the hull. There is also an economic intention to fill the vessel to its maximum capacity, especially for a short time period. However, some overloaded fishing vessels have foundered due to this reason.

Extreme Environmental Condition

Many ships were lost at sea during the extreme weather. The ocean is a hazardous environment for both man and ships.

The crew is likely to lose their lives overboard if they go on deck during a sea storm. Secured components may also be broken and cause damage to the equipment. This typically happened for BRAER tanker, where pipes stored on the deck broke free and damaged the vents serving the diesel fuel tank during a storm. This led the diesel fuel to be contaminated with seawater and finally, the power in the vessel was lost. The vessel then drifted ashore under a prevailing current, leading to a significant oil spill. The heavy weather may also lead to tiredness and seasickness of the crew; this therefore increased the likelihood of operational errors. Rough seas may pose other hazards as well, e.g. loss of visibility, position, or communications, which potentially increase the risk of grounding and colliding.

31.3.3 Frequency Analysis of Ship Accidents

The risk associated with an event is a function of two quantities: the likelihood of the event and the consequence from that event. Therefore, the frequency analysis forms an essential part in the risk estimation. CCPS (1995) listed ocean-going vessel failure modes (e.g. collision, grounding, fire and explosion and material/equipment failure), discussed parameters influencing accident rates and hazards release probabilities, and suggested procedures for failure (release) frequency calculations.

For ship accidents, sometime sufficient historic data are available for some critical events. One of the best sources of data is the U.S. Coat Guard's vessel casualty file for U.S. waterways, the Marine Casualty Information Reporting Systems (USCG, 1992). The frequency can then be derived simply from the past data. However in most cases, a frequency analysis may not be so straightforward and it must examine the contributing factors that lead to the actual accident. In this process, it is necessary to break the compound event into individual events and put them together in a logic sequence to model how the hazards are developing into accidents via different failure paths.

After a synthesis of individual events according to certain scenarios, the occurrence probability of the accident may be quantified by using the fault-tree technique and the event-tree technique. Normally, the fault tree is used to explore the causes of a critical event, while

the possible outcome of the event is traced down by using the event tree. The frequency of initiating events may be drawn from historical data, for example, failure rates, mean time between repairs, or accident and incident frequencies, and then be modified based on expert judgment according to the actual system. Sometimes data for similar accidents from other industries may be applied if they are sufficiently relevant. In all, obtaining adequate data to avoid ship hazards, can be a problem and sometimes the lack of data can make the quantitative risk analysis rather difficult, if not totally impossible.

31.3.4 Consequence of Ship Accidents

The consequence is conditional depending on the probability of the accident. The general consequences from ship accidents are measured in the following terms:

- Loss of human life
- Loss of cargo
- Damage to ship or other ships
- Damage to the environment

A unique feature for shipping is that different ship stakeholders may see, feel, and judge differently to the above mentioned consequences.

Loss of Human Life

When quantifying the consequence of loss of lives, analysts may ask a sensitive question of how much the loss of a human life will cost, for the purpose of making risk comparisons. Historically, the only way loss of human life can be compensated for, after an accident, is through monetary means. There are well-defined procedures for such compensation. Such monetary values should not be regarded as what a human life is 'worth'; rather they indicate what the benefit is to a stakeholder if a life has been saved.

Typically, there is a difference made between loss of life for ship operating personnel and passengers, since the former are supposed to know the increased risk level they are taking while the latter are not. As a result, the potential consequence of loss of a passenger ship may be very large.

Random losses of human life in small numbers per accident may appear to be accepted by society, but this is not the case for massive losses. The latter type of accidents will inevitably come under public scrutiny and investigation, and may end up with some new regulations. The consequences in this respect are then far beyond the monetary terms.

Loss of Cargo

Loss of cargo occurs in many marine accidents. Usually the shipper obtains insurance for the transport of cargo, and in case of a loss, the shipper will be directly compensated by the insurer. Reimbursement of the value of the cargo is normally the extent of the consequences. In some cases, where the time to deliver the cargo is critical, reimbursement of the value of cargo may not compensate the shipper for the total consequences of the loss. The intangible part of the loss is difficult to assess and may vary from case to case.

Damage to Ship or Other Ships

The consequences of loss or damage to the ship also involve tangible and intangible components. If any of the ships involved are not totally lost, then the tangible costs are simply

those that are incurred in getting the ships to a repair yard and completing the repairs. If the ship alone is lost entirely, then the tangible cost is simply the replacement cost for the ship.

There are many intangible consequences involved in the loss or damage of a ship and these can be more significant than the tangible cost. These are primarily business consequences due to the loss of the operation of the ship or loss of the entire ship.

Damage to the Environment

There are many ways in which a ship can damage the environment, the most obvious being the unintentional spillage of oil as a result of an accident. This can happen as a result of many types of accidents including grounding, collision, fires, or explosions. The effects that oil will have on the environment depend on the amount of oil released, the ecological fragility of the local area, the wind, waves and currents at the time of the accident and during the attempted cleanup, etc.

From the Amoco Cadiz, Exxon Valdez, and Braer accidents, we have seen that the associated costs can be very high, even tens or hundreds of times larger than the value of the ship and cargo put together.

31.3.5 Risk Evaluation

Risk estimation can identify the areas with high risk, the main contributors to risk specific hazards. The total risk to human safety, business and the environment may then be estimated.

The first thing relating to the risk evaluation is the pre-defined acceptable (target) risk levels for human safety, business, and the environment. Then, the obtained risk values can be evaluated according to the target levels. Unacceptable risks will lead to a modification of the system and a need to perform the previous steps involved in risk assessment, again. The determination of the target levels may be difficult; therefore, they may initially be based on values obtained from the risk analyses of existing ships.

The well-known ALARP principle is also applicable to the FSA. It requires that risks be reduced as low as reasonably practicable. To apply ALARP, the bounds of risk tolerability need to be defined. If the risk is broadly acceptable, no specific actions may be required. However if the risk is between certain levels, they will ordinarily be tolerated if they are reduced to as low as reasonably practicable, i.e. the cost to reduce the risk further is grossly disproportionate to the benefit gained. This will involve a cost benefit analysis.

31.3.6 Risk Control and Cost-Benefit Analysis

There are two methods to control risk, namely,

*   preventive approach: to reduce the frequency of an initiating event,

*   mitigating option: to reduce the severity of the failure

The actions for controlling risk include applications of engineering and implementation of procedures. The practical risk control approaches should be investigated and their ability to reduce risk be documented. The effect of risk control actions can be determined by repeating risk analyses and comparing the results to the original case. The benefits are the avoidance of accidents and these can be measured by evaluating the avoidance of harm to people, damage to property, environment, and other costs. To achieve a balance, the benefits of a risk control measure must be considered and compared to the cost of its implementation. This is done through a cost benefit analysis.

In a cost benefit analysis the costs associated with the risk control option or package of options are estimated considering both public cost (enforcement, inspection, etc.) and commercial sector cost (e.g. capital cost, compliance cost, etc.). A similar exercise is undertaken to estimate benefits, which for ships may include reduced environmental cleanup costs, increased vessel life, the value of saved lives, etc. The net present value of each option or option package is calculated by subtracting the benefits from the costs. Sensitivity analysis may be conducted around key assumptions to estimate the level of confidence that can be attached to the computed net value of each option package. Risk control options may be ranked based on their cost-effectiveness. The final step in a formal safety assessment is "decision making", which gives recommendations for safety improvement. The selection of risk control options for the decision-making is based on the cost-effectiveness and the principles of ALARP (As Low As Reasonably Practicable). Intolerable risk shall be controlled regardless of costs. "Reasonable" means that the costs are to in gross disproportion to the benefits.

31.4 Human and Organizational Factors in FSA

IMO (1997) recommends a balanced approach between human and technical factors reflecting their contributions to the safety of the overall system considered. IACS (1999) proposed Draft Guidance on Human Reliability Analysis (HRA) within Formal Safety Assessment (FSA). The HRA guidance was developed to assist the incorporation of HRA in the FSA process. It provides references and summaries of various HRA techniques.

The majority of ship incidents and accidents appear to have a human factor component, e.g. error in loading, error in operating machinery, etc. It is therefore necessary to integrate the human and organizational factors (HOF) into the FSA. To this end, it is essential to include HOF expert and operational experience in FSA team.

The consideration of HOF can be done in one of two ways. The first and probably the less difficult way is to treat human behavior at a phenomenological level, to determine the probability of an improper human decision (behavior) to be made with respect to each one of the critical aspects of the operation. The second and more difficult way involves the underlying causes of the improper human decision. The following example is used to illustrate the first approach.

In a shipboard fire, many of the initiation probabilities may be a direct result of humans, like smoking. Humans may also affect the progress of the fire, by fighting it manually or using fire suppression equipment. Such influences can be incorporated in the FSA. For example, the effects of humans on fire initiation may be implicitly included in the actual historical data. Differences in crew training and safety discipline may be accounted for by using different probabilities assigned to the event tree in the risk analysis. Human errors of commission or omission can also be similarly incorporated. However, it is generally very difficult to quantify the effects of different human and organizational factors accurately.

31.5 An Example Application to Ship's Fuel Systems

The above mentioned Formal Safety Assessment method can be applied to the ship's fuel system to identify appropriate risk control measures that reduce the potential for fire and failure or to mitigate the consequence.

A possible approach starts with the description of a generic ship fuel system. This consists of

defining the essential features of the components fitted to all fuel systems and the fuel processing plant, and would include both high and low pressure areas.

Casualty data arising from failures of fuel systems would then be collected and categorized into relevant hazard categories (Fire, Hardware failure, etc.). Any of the existing worldwide databases for reliability data associated with marine parts, e.g. rotating and reciprocating fuel pumps, piping, and connections may be used. Hazard and Operability Studies (HAZOP) could be employed to identify areas in the generic fuel systems that are most prone to failure. A fault tree could then be constructed to structure the information and assess the failure frequency. The event tree is then used to model the possible consequence.

The output of the above exercise would be a prioritized list of issues contributing to the frequency of occurrence of each accident category, combined with the severity of the consequences. A cost benefit analysis of an engine room fire or downtime, weighted against the benefits provided by increased reliability, would provide supplemental information for the decision-making.

31.6 Concerns Regarding the Use of FSA in Shipping

FSA may be a tool to support the development of rational regulations (such as IMO), enable focusing on important issues and justifying a modification or development of a regulation is reasonable. It offers a better insight in hazard identifications and scenarios developments. Indeed FSA is a more systematic approach to managing risk.

Although many elements of the approach described in previous Sections are well established in other contexts, their applications to the shipping industry in a generic way are relatively new and unproven.   Trial applications are being undertaken, with the intention of accumulating relevant results and experience. The development of suitable mechanisms and procedures in which the FSA process can be applied by the IMO committees in future decisions are also being considered.

Useful risk estimation data include: incident statistics, equipment reliability, structural reliability, human reliability and fleet (exposure) data. The cost data are related to the estimation of investment costs, operating costs, inspection and maintenance costs and the cost for clean-up, pollution etc. In many cases, data are insufficient to do an appropriate estimation of risk.

As with all risk assessments, the results obtained are dependent on data and also on judgement in interpreting the data and anticipating industry trends, the impact of changes in technology, the potential for future accidents, etc. The results of an FSA study are therefore dependent upon both the availability of relevant data and qualified analysts that can undertake rational judgements. The quality of a FSA is as good as the data provided, expertise used and mathematical models applied. There are many challenges in collecting and interpreting risk data. In many cases, it is found that the data has not been recorded or not in the way that enables FSA. Mathematical modeling and computer simulations may be the alternatives to the data. An expert's opinion may be a necessary substitute or complement of statistical data. In undertaking such an effort, one may find that those with long experience and good background in relevant specialties may lack familiarity with expressing their judgments in probabilistic terms. The subjectivity of FSA based on incomplete information is a great concern. A study of required and existing databases pertinent to marine risk analysis is needed and a plan for a systematic collection of additional data needs to be developed and implemented.

31.7 References

1. Amrozowicz, M.D., Brown, A., Golay, M. (1997), "A Probabilistic Analysis of Tanker Groundings". ISOPE 1997, Honolulu, USA.

2. Arima, T. et al (1997), "Basic Investigation on Formal Safety Assessment – Risk Analysis of Fire in Ship Engine Rooms", Class NK Technical Bulletin.

3. CCPS (1995), *"Chemical Transportation Risk Analysis"*, Center for Chemical Process Safety, American Institute of Chemical Engineers.

4. Hessler, B.(1995), "Training Ship's Crew for Effective Fire Fighting and Emergency Incident Command", The Institute of Marine Engineers, May, 1995.

5. IACS (1999), "Draft Guidance on Human Reliability Analysis (HRA) within the Formal Safety Assessment", IMO MSC 71/Wp.15/Add.1.

6. IMO (1997), "MSC/Circ. 829 & MEPC/Circ. 335, Interim Guidelines pn the Application of Formal Safety Assessment (FSA) to the IMO Rule-Making Process", International Maritime Organization.

7. Kristiansen, S. (1995), "An Approach to Systematic Learning from Accidents", The Institute of Marine Engineers.

8. Marine Accident Investigation Branch (1993), "Report of the Chief Inspector of Marine Accidents into the Engine Failure and Subsequent Grounding of the Motor Tanker BRAER at Garths Ness, Shetland, Southampton, UK".

9. NK (1994), "Engine Room Fire, Guidance to Fire Prevention", Nippon Kaiji Kyokai (Class NK).

10. Pålsson, I., Swenson, G. (1996), "Formal Safety Assessment – Introduction of Modern Risk Assessment into Shipping." Report: 7594, Swedish National Maritime Administration, SSPA Maritime Consulting.

11. Romer, H., Brockhoff, L., Haastrup, P. and Styhr Petersen, H.J. (1993), "Marine Transport of Dangerous Goods, Risk Assessment based on Historical Accident Data", Journal of Loss Prevention in the Process Industries, Vol. 6(4).

12. Sirkar, J., Ameer, P., Brown, A., Goss, P., Michel, K., Nicastro, F. and Willis, W. (1997), "A Framework for Assessing the Environmental Performance of Tankers in Accidental Groundings and Collisions", Transactions of SNAME.

13. Skjong, R., Vivalda, C. (1998), "Use of Risk Assessment within the Maritime Industry". EU RORO, MARIN, Wageningen, The Netherlands.

14. USCG (1992), "The Marine Casualty Information Reporting Systems (CASMAIN), 1981-1991", The U.S. Coat Guard.

15. Wennick, C.J. (1993), "Collision and Grounding Risk Analysis for Ships Navigating in Confined Waters", Journal of Navigation, Vol. 45 (1), pp. 80-91.

16. Yoshida, K. et al (2000), "Risk Assessment", Proceedings of ISSC-2000, Nagasaki, Japan.

This Page Intentionally Left Blank

Part V

Risk Assessment

Chapter 32   Economic Risk Assessment for Field Development

32.1 Introduction

32.1.1   Field Development Phases

An offshore field development project generally consists of four main phases, i.e., exploration, development, operation, and decommission. An illustration of the development phases (mainly the first three), along with the main activities, duration, and the cost in each phase is shown in Figure 32.1.

TIME	EXPLORATION	DEVELOPMENT	OPERATION
GRANTING OF PERMIT 1 2 3 4 5 6 7 8 9 10 11 12 13 14 15 16 17 18 19 20 21 22 23 24 25 26 … DECOMMISSION	Geology & Geophysics / Exploration & Appraisal well	Reservoir Engineering & Simulations / Develop Transport Installations / Geophysics / Drilling produ. Wells	Production build up / Reservoir Engineering (continued) / Maximum Production / (continued) / Decline
Share of Technical Cost	10 to 20%	40 to 60%	20 to 50%

Figure 32.1   Field Development Phases

The exploration phase starts after the field license is awarded. If an oil & gas field is discovered based on the results from exploration drilling, the concept screening and feasibility studies of the field will be carried out. Technical feasible and commercial optimum solutions are identified. The exploration phase concludes with the authority approval of the Plan for Development and Operation (PDO).

The development phase starts with the conceptual engineering, which is based on the recommendations of the PDO. The final field development concept is then fixed, along with the operation philosophy, safety, and environmental programs, etc. Subsequently, the whole project is executed systematically: engineering, procurement, construction, and installation. Meanwhile, production wells are being drilled if pre-drilling is recommended.

The operation phase typically has a period of 20 years. The production will initially increase and reach its maximum, and then it gradually declines. Meanwhile, reservoir engineering will continue to maximize the production, based on updated reservoir information. The decommission phase is at the end of the field life. The platform is abandoned and removed from the site.

32.1.2   Background of Economic Evaluation

Economic evaluation is carried out throughout the life cycle of a field development project. Net Present Value (NPV) and Internal Rate of Return (IRR) are the two most basic decision criteria. Recently, Life-Cycle Cost (LCC) criterion is frequently used in decision-making, and it is actually derived based on NPV.

Before and during the exploration, economic evaluation is mainly applied to assess whether or not the required investment in this project is profitable enough. An exploration decision is like a major gamble: a large field may be discovered, or at the other extreme, no oil or gas found at all. However, the costs incurred in individual explorations are relatively low compared to the total cost of field development if the exploration is successful. The economic evaluation is repeated at each stage during the exploration, and the results could culminate in a final decision to invest in developing the discovery. Classic economic evaluation methods by using Net Present Value (NPV) or Internal Rate of Return (IRR) are preferred in this phase. The definitions of NPV and IRR are provided in Appendix I.

Once the project is approved and is ahead in the development and operation phases, the Life Cycle Cost (LCC) approach is preferable. In the LCC model, all of the relevant economic implications of a decision and the effects on the operating company may be considered. For example, by using the LCC model, the total cost of a production facility could be expressed by the sum of the following cost elements (NORSOK O-CR-0002):

- Capital costs (CAPEX)
- Operating cost (OPEX), which covers operation and maintenance
- Cost of deferred production

The initial capital expenditure of the facility is then not the only criterion for decision-making. Instead, the optimum design concept is chosen as the one that provides the minimum life cycle cost.

32.1.3   Quantitative Economic Risk Assessment

The economic risks involved in the field development projects vary, and may include (1) technical risks (which may ultimately have their economic impact), (2) commercial risks (associated mainly with cost and income variables), (3) potential natural disaster, and so on. Uncertainties may include: (1) reservoir information such as production profiles, recoverable oil and gas, (2) cost parameters such as cost of fabrication, transportation, installation, and cost of operation, maintenance, (3) financial variables such as interest rate, oil price, etc. A systematic economic risk assessment is therefore needed to assess the impact of risks and

uncertainties associated with the whole field development project, and to subsequently provide the necessary support for decision-making.

By adopting probabilistic analysis tools, an economic risk assessment could treat the exiting uncertainties and assess risks in a quantitative manner. Accordingly, probabilities of failure events, as well as the importance and sensitivity measures for each uncertainty could be provided. Comparing to simple 'best case' and 'worst case' estimates in traditional deterministic economic evaluations, these results could provide better support for decision-making and help reduce the overall uncertainties involved in a field development project.

A quantitative economic risk assessment methodology is presented in this Chapter. It is a generalization of various published economic risk studies, e.g. by, Skjong et al (1988), Bitner-Gregersen et al (1992), Cui et al (1998), Odland (1999) and Bai et al (1999). Five major steps are proposed as follows.

- Identify the field development phase that is to be studied. This has been discussed in Section 32.1.1.

- Identify which decision should be made during the development phase, e.g. starting exploration, comparing early production concepts, evaluating different final development concepts, operation and maintenance strategies, and so on.

- Define the decision criteria and subsequently set up the limit state functions, e.g. by setting a certain target NPV or IRR value, or the minimum LCC.

- Model economic risk by obtaining statistical data for each parameter in the limit state functions and calculating the failure probability. Both simulation and analytical reliability methods may be used. Parameters in limit state functions can be classified as cost and income variables. They can be expressed in terms of statistic distributions or deterministic values.

- Perform sensitivity studies and propose economic risk reductions and uncertainty reducing measures in order to improve the decision-making process.

32.2 Decision Criteria and Limit State Functions

32.2.1 Decision and Decision Criteria

Various decisions and decision criteria are involved in different phases of an offshore field development project. Below are three major examples, which occurred in exploration, development, and operation phases respectively.

A. Should the field be developed now?

Will the development project be at least as profitable as alternative investment opportunities? Will a development based on existing technology be acceptable in relation to the utilization of resources, e.g. oil recovery factor, gas utilization, safety, and environment? Is the timing right with regard to infrastructure? The IRR or NPV may be suitable in this context.

B. Given that the field is under development, how should it be developed?

Different field development concepts may be feasible. Both the value of production, the CAPEX, the OPEX, and the phasing of income and costs should be considered in a realistic and balanced way. The NPV may be the most suitable criterion in this context

C. How should the project be carried out?

For day-to-day execution of the project, including the selection of equipment and services from contractors, it is necessary to use criteria that can be easily related to the consequences of such decisions. LCC may be a suitable criterion in this context.

32.2.2 Limit State Functions

The limit state functions in a probabilistic analysis are defined based on NPV or IRR. LCC criterion could virtually be traced down to NPV criterion.

If the event is the achievement of a specified internal rate of return in this project, the limit state function can be formulated as:

$$G(\mathbf{X}) = \sum_{n=6}^{30} \frac{I_n(\mathbf{X})}{(1+irr)^{n-1}} - \sum_{n=1}^{30} \frac{C_n(\mathbf{X})}{(1+irr)^{n-1}}$$

(32.1)

The total period of 30 year is considered in Eq.(32.1). I_n denotes the income generated in the nth year and C_n is the cost in the nth year. Both I_n and C_n are functions of input variables (basic variables) expressed in the equation by X. A negative value of the function G(X) implies that the internal rate of return is less than the *irr*.

The limit state function for the decision criteria based on the net present value is similarly:

$$G(\mathbf{X}) = \sum_{n=6}^{30} \frac{I_n(\mathbf{X})}{(1+irr)^{n-1}} - \sum_{n=1}^{30} \frac{C_n(\mathbf{X})}{(1+irr)^{n-1}} - \mathrm{npv}$$

(32.2)

In this case, the function G(X) is negative if the net present value is less than the value npv for a corporate rate of return *irr*.

32.3 Economic Risk Modeling

The cost variables are related to the cost of design, construction, installation, and operation (including maintenance). The income variables, however, are related to the reservoir size and characteristics, oil and gas prices, currency fluctuations, inflation and interest changes, and taxation rules. Modeling the uncertainties associated with income and cost variables is therefore the core of economic risk modeling.

A typical North Sea oil and gas field project in the development and operation phase is chosen as a representative case to illustrate the economic risk modeling. These are adapted from Bitner-Gregersen, et al (1992). These data are listed only for the illustrative purpose, and should be updated specifically for each project considered. The field is assumed to be in production for 25 years after 5 years of construction and installation period. The decision criteria are based on the IRR or NPV, and limit state functions are subsequently defined in the form of Eqn. (32.1) and Eqn. (32.2). Modeling of cost variables, income variables, and their uncertainties are described in the following Sub-sections.

32.3.1 Cost Variable Modeling

An overview of the costs during development and operation phases are presented below (Odland, 1999):

- Facility Costs

- – Topsides
- – Substructure
- – Well/Riser system
- – Export/Import system
- – Project management and insurance
- • Drilling Costs
  - – Platform wells
  - – Pre-drilling
- • Operation and Maintenance Costs
  - – Personnel and catering
  - – Well maintenance
  - – Logistics
  - – Land organization and insurance

Costs of Facilities and Drilling

The costs associated with facilities mainly occur in the platform design, construction, and installation phases. Each cost center has a base value B_i and several influencing cost variables.

For example, the cost of template material is a product of the template weight and the cost of template material per unit weight. In order to establish the uncertainties in the cost variables, the analysts are to assess factors and multiply the best estimates to give the 10%, 25%, 50%, 75%, and 90% fractile of the variables. The lognormal distribution is thus used for all cost variables and the distribution parameters are then determined by a least-square fit of the distribution to the data points.

Some cost variables enter more than one cost center. As an example, it is likely that if the amount of material exceeds the base estimate, then the number of man-hours spent to weld the material will also exceed the base estimate. The correlation should be accounted for properly. The correlation coefficients may be given based on an understanding of the interplay between different cost variables and experience in the form of existing data. All costs are distributed over time as a result of a scheduling program.

Costs of Operation and Maintenance

Additional costs occur for production, processing, and transportation during the production phase as discussed earlier. These costs are divided into each product, e.g. oil, gas, and liquefied natural gas (LNG).

32.3.2 Income Variable Modeling

The income variables are grouped into three categories as described below:

- • Reservoir size and production profiles
- • Oil and gas prices
- • Taxes, inflation and interest rates

Reservoir Size and Production Profile

At the time the decision is made to start the construction of a platform, large uncertainties are present with respect to the total recoverable volume, the time it takes to reach full production, and the production profile. The uncertainty varies depending on the geological properties, the amount of geophysical exploration and the number of test wells. In order to model the production rate as it evolves in time, an analytical expression (Skjong, 1988) for the production rate is adopted:

$$V(t) = \frac{V_{tot} b^{ab+1}}{\Gamma(ab+1)} t^{ab} \exp(-bt)$$

(32.3)

where V(t) is the production rate at time t, V_{tot} is the total recoverable volume, a and b are parameters describing the production profile, and Γ is the Gamma function. By letting V_{tot} be a random variable, the uncertainty in the recoverable volume can be modeled. By letting a and b be random variables, the uncertainties involved in how early the maximum production rate can be reached and the production profile modeled.

Prices of Oil, Gas, and LNG

The uncertainties in the price of oil, gas, and LNG in a long period of time (5 – 30 years) are obviously very large. A simplified model is applied here. The mean value of the oil price 5 years from now is assumed to be 23 USD per barrel, and it is assumed to change with inflation for the total period. The price in each year is randomized by applying a lognormal distribution with 20% coefficient of variation. Therefore, there is a 10% probability of oil price to be less than 17.5 USD per barrel and a 10% probability of the oil price to be larger than 29.4 USD per barrel.

It is likely that the oil price in one year is highly correlated to the price in the next year, and the correlation becomes less for the years further into the future. This is modeled by a correlation of 0.7 between values in two successive years.

Taxes, Inflation, and Interest Rates

The tax on the net profit is assumed to be 50.8%, plus an additional tax for oil companies of 30% to 85% of the net profit. The tax on assets is 0.5% and the depreciation period is 6 years, starting from the year the investment is made. Results are given for both consolidated and unconsolidated situations. For the consolidated case, a tax deduction that cannot be used due to a negative profit is used by the company elsewhere and credited to the project.

The inflation rate is assumed constant at 6%. The financing of the project is planned with 50% equity capital and 50% loans. The interest rate on the loan is assumed constant at 10%. The financing model can easily be made more realistic, for example with loans in different currencies, and with different uncertain developments in the exchange rates.

32.3.3 Failure Probability Calculation

After formulating the limit state function based on IRR or NPV criteria, the probability of getting a negative value in the limit state function can be computed by Monte Carlo simulations or by applying analytical reliability methods (FORM and SORM). The simulation methods represent basic calculation techniques that are often used to verify the results obtained by analytical methods.

The probability, P_E, of a desirable or undesirable event, based on a limit state function (or performance function) G(X) is defined in Eq. (32.4). The sign of the limit state function is selected in such a way that a negative value corresponds to not achieving the desired goal.

$$P_E = P(G(X) \leq 0)$$ (32.4)

Corresponding to the event probability, the reliability index β_R is defined as:

$$\beta_R = -\Phi^{-1}(P_E)$$ (32.5)

where Φ is the standardized normal distribution function. The probabilistic analysis procedure can also treat situations where several criteria must be fulfilled simultaneously.

32.4 Results Evaluation

32.4.1 Importance and Omission Factors

The importance factor, α_i, indicates the fraction of the total uncertainty arising from uncertainty in a variable. For the FORM analysis, the reliability index is increased by a factor $1/\sqrt{1-\alpha_i^2}$ (called omission factor), if the uncertainty in variable i, is ignored and the variable is replaced by its mean value (50% fractile) as a deterministic variable. These importance measures would provide useful guidance in a process of choosing which variables to collect further data for, to reduce the overall uncertainty.

The importance of the different sources of uncertainty may be obtained from the FORM method. The total uncertainty of the project gets three major contributions: Facilities (design, construction and installation) and drilling (34.2%), Reservoir size and production profile (41.8%), and Oil price (20.3%). It is of particular interest to note the importance of the time it takes to reach the maximum oil production. This clearly indicates that the economic result of the project is dependent on good engineering, planning, and quality control. It is also observed that within the assumed model, the project result is not dominated by uncertainties in the oil price.

The use of the omission factors is illustrated by studying the well pre-drilling cost. Assume a fixed price contract (a deterministic value) for pre-drilling which corresponds to 50% of its original distribution. This changes the reliability index β by a factor $1/\sqrt{1-\alpha_{30}^2}$. For the consolidated IRR analysis with an IRR = 11.3% (10% fractile, worst case), the reliability index is changed from 1.28 to 1.34. The corresponding failure probability is then 9%. This means that with a fixed price contract for pre-drilling, the probability of not achieving an internal rate of return of 11.3% is reduced from 10% to 9%.

32.4.2 Sensitivity Factors

During decision-making, the following question is often asked: "What is the effect of changing this parameter?" Such question can be answered by using sensitivity measures, which give the change in event probability (through change in reliability index) to an increment $\Delta\theta$ in any input parameter θ, whether it is a statistical distribution parameter or a deterministic parameter.

It has been shown that the time to reach the maximum oil production is very important to the final project result. The consolidated IRR analysis is used to demonstrate the use of sensitivity factors for this variable. The analysis is for an IRR = 11.3% corresponding to 10% fractile. From FORM analysis, the change of the reliability index due to a change of the mean time to reach the maximum production rate from 2.5 years to 1.5 years is:

$$\beta_{new} = \beta_{old} + \left(\frac{\mathrm{d}\beta}{\mathrm{d}\mu_{62}}\right)\Delta\mu_{62} = 1.28 + (-0.15)(-1.0) = 1.43$$

(32.6)

The corresponding failure probability is 0.076, i.e. the probability of not achieving an internal rate of return of 11.3% is reduced from 10% to 7.6%.

The effect of reducing the uncertainty in the time to reach maximum production can also be studied. If the standard deviation can be reduced from 1.5 year to 0.5 year, the change of reliability index is:

$$\beta_{new} = \beta_{old} + \left(\frac{\mathrm{d}\beta}{\mathrm{d}\sigma_{62}}\right)\Delta\sigma_{62} = 1.28 + (-0.044)(-1.0) = 1.32$$

(32.7)

The corresponding failure probability is 0.093, i.e. the probability of not achieving an internal rate of return of 11.3% is reduced from 10% to 9.3%.

32.4.3 Contingency Factors

In the FORM and SORM analysis, the 'design point' X* is obtained, which gives the most likely values of the input parameters if the performance function is not fulfilled:

$$X_i^* = F_{X_i}^{-1}\left(\Phi(\beta_R a_i)\right)$$

(32.8)

where $F_{Xi}()$ is the distribution function for X_i and a_i is an output for the coordinates of the design point. The contingency measures (factors) for different variables are the ratios between the design point value and the mean value (or another base value selected before hand).

The contingency factors depend on the probability level, i.e. the confidence in achieving the desired event. In traditional deterministic analyses, base values are multiplied by contingency factors to check whether or not the required performance is achieved, but the selection of contingency factors was not done in a rigorous manner. The probabilistic analysis however, can provide a consistent calibration of contingency factors for any desired confidence level.

32.5 References

1.   Bai, Y., Sørheim, M., Nødland, S. and Damsleth, P.A. (1999), "LCC Modelling as a Decision Making Tool in Pipeline Design", OMAE '99.

2.   Cui, W., Mansour, A.E, Elsayed, T. and Wirsching, W. (1998), "Reliability based Quality and Cost Optimisation of Unstiffened Plates in Ship Structures", Proc. of PRADS '98, Edited by M.W. C. Oosterveld and S. G. Tan, Elsevier Science B.V

3.   Bitner-Gregersen, E.M., Lereim, J., Monnier, I., Skjong, R. (1992), "Economic Risk Analysis of Offshore Projects", Journal of Offshore Mechanics and Arctic Engineering, Vol. 114, August.

4. Gudmestad, O.T. et al (1999), *"Basics of Offshore Petroleum Engineering and Development of Marine Facilities with Emphasis on Arctic Offshore"*, ISBN 5-7246-0100-1.

5. Lereim, J. (1989), "Uncertainty Modelling of Project Economy in the Light of Company Strategy", 13th International Expert Seminar on Integration of Projects into the Company Organization, April 1989, Switzerland.

6. NTS (1996), "NORSOK O-CR-0002", Norwegian Technology Standards Institution, (available from: www.nts.no/norsok).

7. Odland, J. (1999), *"Lecture Note for 81063 – Development of Offshore Oil and Gas Fields, (Part 6: Cost, Economics and Decision Criteria)"*, Dept. of Marine Structures, Norwegian University of Science and Technology.

8. Park, C.S. and Sharp-Bette, G.P. (1990), *"Advanced Engineering Economics"*, John Wileys & Son, Inc.

9. Skjong, R., Lereim, J. and Madsen, H.O., (1988), "Economic Risk Analysis of Offshore Field Development Project", Proceedings of the 9th International Cost Engineering Congress, Norway.

APPENDIX A: Net Present Value and Internal Rate of Return

For more information on engineering economics, references is made to Park and Sharp-Bette, (1990) on general items and Gudemestad et al. (1999) on offshore field development applications. A profitability criterion which is frequently used in decision-making for offshore field development projects, is Net Present Value (NPV) where cash inflows and out-flows are compared at the same point in time (today). Internal Rate of Return (IRR) is also used. An investment project is profitable if its IRR exceeds the required discount rate that is cost of capital.

Notation:

n = Time, measured in discrete compounding periods

I = Market interest rate, or opportunity interest rate

C_0 = Initial investment at time 0, a positive amount

C_n = Expense at the end of period n, $C_n \geq 0$

= Revenue at end of period n, $I_n \geq 0$

N = Project life

F_n = Net cash flow at the end of period n ($F_n = I_n - C_n$; if $I_n \geq C_n$, then $F_n \geq 0$; if $I_n < C_n$, then $F_n < 0$)

Net Present Value (NPV)

Consider a project that will generate cash receipts of In at the end of each period n. The present value of cash receipts over the project life, I, is expressed by:

$$I = \sum_{n=0}^{N} \frac{I_n}{(1+i)^n} \tag{A.1}$$

Assume that the cash expenses (including the initial investment C_0 associated with the project) at the end of each period are C_n. The present value expression of cash expenses, C, is:

$$C = \sum_{n=0}^{N} \frac{C_n}{(1+i)^n}$$

(A.2)

Then the NPV of the project [denoted by NPV(i)] is defined by the difference between I and C, i.e.

$$NPV(i) = \sum_{n=0}^{N} \frac{I_n - C_n}{(1+i)^n} = \sum_{n=0}^{N} \frac{F_n}{(1+i)^n}$$

(A.3)

A positive NPV for a project represents a positive surplus, and we should accept the project if sufficient funds are available for it. A project with a negative NPV should be rejected, because we could do better by investing in other projects at the market interest rate i or outside the market.

Internal Rate of Return (IRR)

The IRR is another time-discounted measure of investments similar to the NPV criterion. The IRR of a project is defined as the rate of interest that equates the NPV of the entire series of cash flows to zero. The project's IRR, is mathematically defined by:

$$NPV(irr) = \sum_{n=0}^{N} \frac{F_n}{(1+irr)^n} = 0$$

(A.4)

Note that Eqn. (A.4) is a polynomial function of *irr*. A direct solution for such a function is not generally possible except for projects with a life of four periods or fewer. Therefore, two approximation techniques are generally used, one using iterative procedures (a trial-and-error approach) and the other using Newton's approximation to the solution of a polynomial.

Part V

Risk Assessment

Chapter 33　Human Reliability Assessment

33.1　Introduction

The human reliability analysis plays an important role in the reliability analysis of a man-machine system. Accidents such as Bhopal, Three Mile Island, Chernyobl, and Piper Alpha disasters, have actually demonstrated human failures and their catastrophic consequences that could have on a system. According to studies made by Moore (1994), approximately 65% of all catastrophic marine-related accidents are the result of compounded human and organizational errors during operation. In a risk assessment, there is therefore a distinct need for properly assessing the risks from human errors and for ways to reduce system vulnerability to human impact. These can be achieved via Human Reliability Assessment (HRA). The HRA may be applied in many fields, e.g. in design, fabrication, installation and operation etc.

Early research on human factors by the nuclear power industry was summarized by Swain (1989) whose work has also been extensively used to improve human performance in the chemical industry (Lorenzo, 1990). Lorenzo (1990) illustrated examples of error-likely situations, suggested strategies for improving human performance and developed human reliability analysis techniques. An extensive list of past publications may be found from these two books.

For the offshore industry, Bea (1994, 1995) studied the role of human error in design, construction and reliability of marine structures. For more information on this subject, readers may refer to recent publications, Bea (2001, 2002). Human and Organizational Factors are also considered to be an important part of the formal safety assessment introduced by IMO (1997) and IACS(1999) for the shipping industry, see Part 6 Chapter 31.

This Chapter deals with general principles for HRA (Kirwan (1994), and specific application to offshore industry (Bea, 2001, 2002). The HRA has three principle steps: Human Error Identification (identify what errors can occur), Human Error Quantification (decide how likely the errors are to occur), and Human Error Reduction (reduce the error likelihood), see Figure 33.1.

In the following Sections, an overview of the HRA process is given first. Then each major step is discussed with emphasis on how to identify, assess, and reduce human errors.
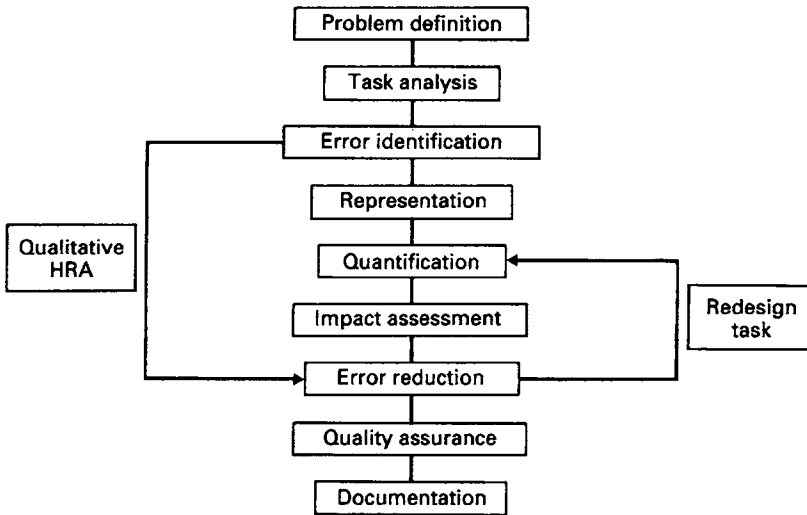
Figure 33.1   The HRA Process (Kirwan, 1994)

33.2 Human Error Identification

33.2.1 Problem Definition

The essence of the HRA problem definition is to set the scope of the analysis, decide what types of human interaction should be dealt with, and find out the existing constraints within which the HRA must work.

Five common types of human interactions may appear in HRA studies. The most usual type involves the human response to a system demand, usually arising as a result of some system failure. This type of human interaction has been the focus of many risk studies, since these events are often where the system most clearly relies on human reliability to reach a safe state. The remaining four types that the HRA analysts may also consider are: a) maintenance and testing errors; b) human error-related initiators; c) response failures; d) final recovery actions and mitigating strategies.

The resources available, in terms of funds, expertise, prior studies, and software, will constrain the HRA. Another major constraint, which interacts with the resource, is the project-life-cycle stage. The earlier the life-cycle stage, the more difficult the task- and human-error-identification phases will be, since much of the required detail concerning operator tasks and equipment will not be available.

33.2.2 Task Analysis

Task analysis is a fundamental approach describing and analyzing how the operator interacts with a system itself and with other personnel in that system (Kirwan and Ainsworth, 1992). HRA must first have a definition of how a task should be carried out, and this requires a task analysis. The task analysis defines a model of

- what should happen during a correct performance,
- which is then applied to the HRA techniques as a basis to identify what errors can occur at various steps in the task execution,
- how likely such errors are to occur, and
- whether or not the task is adequately safe (quantitatively or qualitatively).

The Task Analysis in HRA mainly consists of two stages: data collection and task representation. Once data have been collected and verified, the task must be formally described and represented, to illustrate what should happen in a correct performance.

33.2.3 Human Error Identification

In Reason (1990), the human errors are classified into three classes:

- Slips and lapses – e.g. pressing the wrong button, or forgetting a step in a long procedure. These are the most predictable errors and are usually characterized by inaccurate performances. The main characteristic of this error class is that the intention is correct but the execution is wrong.

- Mistakes – e.g. misunderstanding by the operator of what is happening. The characteristic is that the intention is incorrect, which leads to erroneous actions.

- Violations – these errors involve some types of deviation from rules or procedures and consequently contain a risk-taking element. There are generally three basic types. The first is the routine violation e.g. taking an 'illegal' short cut during a procedure or corner-cutting an operation. The second is the situational violation, which appears as the only way to carry out a task practically under such situation, e.g. staff shortages. The third is the extreme violation, e.g. someone tries to test how far the system can be pushed in a normal operation, or disable safety interlocks, etc.

It should be noted that a brand of errors which has yet to be properly classified is the errors which affect an organization, and which do so at a higher level. These management-related errors, which can have a severe effect on safety levels, are the main reasons for ongoing research.

The following is a list of some well-known approaches for human error identification, Kirwan and Ainsworth (1992).

HUMAN HAZOP	Human error hazard and operability study (Kletz, 1974)
SRK MODEL	Skill-, Rule-, and Knowledge-based approaches (Rasmussen et al, 1981)
THERP	Technique for human error rate prediction (Swain & Guttmann, 1983)
SHERPA	Systematic human error reduction and prediction approach (Embrey, 1986)
GEMS	Generic error modeling system (Reason, 1987, 1990)
HRMS	Human reliability management system (Kirwan, 1990)

However, no single technique addresses the full potential human error on one system. Instead, there are only tools, which deal with particular types or subsets of potential human error. It is note-worthy that slips and lapses may have been identified adequately by above-mentioned HEI techniques, while other areas of human involvement (particularly mistakes and violations, etc.) may not. There is clearly a need for new methods, which attempt to deal with cognitive errors especially, as well as completing validations and tests of these methods.

33.2.4 Representation

Representations should integrate the identified human contributions to risk with other relevant contributions (hardware, software and environmental) in a logical and quantifiable format. Representation allows the overall risk level of the system to be accurately assessed, and enables the HRA analyst to see the relative human contributions, see Section 33.3.2 "impact assessment").

There are two basic issues that need to be considered in Representation. The first issue is the format of the representation, usually two formats are applied, i.e. the fault tree and the event tree. The second issue is about the level of decomposition in representation, i.e. when to stop breaking down human errors into yet more detailed causes.

33.3 Human Error Analysis

33.3.1 Human Error Quantification

Once the potential human-errors have been represented, the next step is to quantify the likelihood of the human errors involved. The human error probability (HEP) is defined as:

$$HEP = \frac{Number\ of\ errors\ occured}{Number\ of\ opportunities\ for\ error\ to\ occur}$$

In reality, there are few such recorded human error probability data, due to difficulty in estimating the number of opportunities for error in the realistically complex tasks and unwillingness to publish data on poor performance.

The human error quantification techniques therefore rely on expert judgement or on a combination of data and psychologically based models, which evaluate the effects of major influences on human performance. The major techniques in the field of human error quantification are listed below (Kirwan 1994).

APJ   Absolute probability judgement (Seaver and Stillwell, 1983)
THERP   Technique used for human error rate prediction (Swain and Guttmann, 1983)
SLIM-MAUD   Likelihood of success index method using multi-attributed utility
                decomposition (Embrey et al, 1984)
HEART   Human error assessment and reduction technique (Williams, 1986)

Human error dependence is an important issue when representing human errors and quantifying their frequencies. For example, the response to the first alarm and the response to the second alarm, it is obvious that if the same operator is involved in both actions, then the error associated with each of these events are unlikely to be independent. Dependence at this level may be dealt with by the use of conditional probabilities.

33.3.2 Impact Assessment

Once the human error probabilities (HEPs) have been quantified and assigned to the various events in the fault trees, the overall system risk level can be evaluated mathematically, i.e. the top-event (accidental) frequencies will be calculated. It is also at this point that the relative contributions of individual human errors, as well as the contribution from human error as a

whole, to accident frequencies are determined. This can be done, e.g. by the fault-tree-cut-set analysis.

Then, the calculated accident frequencies will be compared against predefined accident criteria. If the frequencies are violating the criteria, the individual events (human, hardware, software or environmental – or any combination) that make a great impact on the accident frequencies must be identified. It is these high-impact events that must be targeted for risk reduction. The risk levels must then be re-calculated accordingly, until the required levels of acceptable risk are achieved, or until the risk levels are as low as reasonably practicable (ALARP principle). In practice, this is an iterative process.

33.4 Human Error Reduction

33.4.1 Error Reduction

Human Error Reduction will be implemented if the impact of human error on the system's risk level is significant, or it may be desirable to improve the system's safety level even if the target risk criteria have been met. There are a number of methods of error reduction (Kirwan, 1994).

- Consequence Reduction
- Error Pathway Blocking
- Error Recovery Enhancement

In practice, HRA analysts often give serious consideration to an error-recovery-enhancement process, since this technique is easy to implement, e.g. by slight modification to procedures, or team training. It is also advisable even in cases where risk levels are satisfactory.

33.4.2 Documentation and Quality Assurance

In this final stage of HRA, assumptions made, methods used and results obtained are to be documented. All of the assumptions made by the HRA team shall be made clear to the project team who will run the system. In addition, the assessment should ideally be seen by the operators as a document whose use will extend over the whole lifetime of the system itself, rather than as a document that is simply put in the archives once its immediate purpose has been served.

The quality assurance (QA) in a HRA includes the assurance that a quality HRA has been carried out (i.e. the objectives have been achieved within the scope of the project and without errors), and the assurance that human-error reduction measures remain effective and that the error-reduction potential is realized.

33.5 Ergonomics Applied to Design of Marine Systems

In recent years, attention has been given to ergonomics and noise control in equipment design, as for the workplace, in order to minimize design-induced human errors and maximize productivity by reducing human fatigue and discomfort. ASTM (1988, 1995) issued "Standard Practice for Human Engineering Design for Marine Systems, Equipment and Facilities" in 1988 and updated it in 1995. The ASTM standard has been used by the oil and gas industry in the design of offshore structures.

ABS (1998) issued "Guidance Notes on the Application of Ergonomics to Marine Systems", which cover the following topics:

- Alarms, displays, control actuators and their integration

- Valve mounting heights and orientations

- Labeling for panels, piping/electrical systems, component/hazard identifications

- Stairs, vertical ladders, walkways and platforms

- Accommodation spaces, ventilation, temperature, humidity, noise, illumination and noise

- Applications of ergonomics in design

The Guidance Notes suggested 4 steps for the application of ergonomics in design, including the following:

- Step 1 is to define what are the tasks required of human to operate the equipment/system being design? For instance, is the human required to stand or sit to perform the operation? Must the human take the visual information being displayed and communicate with others to finish the task?

- Step 2 is to identify who are the users for the equipment/system to account for the difference in height and other physical dimensions between sex, race and origin. Normally the design is made for the 5th percentile to 95 percentile persons.

- Step 3 is to determine the environmental factors such as temperature, noise to optimize human performance.

- Step 4 is to determine the worst case operating scenario, e.g. the extreme temperature and noise.

The target of these 4 steps process is to design the right shape, size, arrangement, layout, labeling, color etc. so that the human may safely and effectively conduct the task defined in step 1.

33.6 Quality Assurance and Quality Control (QA/QC)

Quality Assurance (QA) is those practices and procedures that are designed to help assure that an acceptable degree of quality is maintained. Quality Control (QC) is associated with the implementation and verification of the QA practices and procedures.

As a general reference on quality, reference is made to Bergman and Kjefsjo (1994). This book discusses the importance of quality for survival in business, and control of quality in design and production phases to meet customers expectation. It concluded with discussions on how leadership may influence the process and improve quality continuously.

Bea et al (1997) gave a comprehensive discussion on QA/QC strategies, and its applications in jacket structures and operating safety of offshore structures and in-services inspection & repair, trends in Norwegian offshore operations. They also outlined the international safety management (ISM) code, their proposed safety & quality information systems.

QA/QC procedures include those:

- Put in place before the activity (prevention)

- During the activity (self-checking, checking by team colleagues and verification by activity supervisors)

- After the activity (inspection)

- After the manufacturing (testing)

- After the marine structure has been put in service (detection)

As will be discussed in the next section, QA/QC procedures are an important part of the process to reduce human errors.

33.7 Human & Organizational Factors in Offshore Structures

33.7.1 General

Bea (2001, 2002) defined an offshore structure system as six major interactive components and identified the associated malfunction:

- **Operating teams:** people who have direct contacts with the design, construction, operation, maintenance and decommissioning of the system. The single leading factor in operation malfunction is communications. Other malfunctions include intentional infringements, ignorance, not suited or not trained for the activities, excessively fatigued and stressed and mistakes.

- **Organizations:** groups that influence how the operating personnel conduct their operations and provide the resources for the conduct of these operations. The organizational malfunctions include ineffective communication, inappropriate goals and incentives etc.

- **Procedures and Software:** formal and informal, written and unwritten practices that are to be followed in performing operations. Inaccurate and incorrect procedures, software and their documentation may cause human errors.

- **Hardware/Equipment:** structures and equipment on which and with which the operations are performed. Poorly designed structures and equipment are difficult to construct, operate and maintain, and may invite human errors.

- **Environments:** wind, temperature, lighting, ventilation, noise, motion and sociological factors (e.g., values, beliefs, morays) all may have significant effects on the performance characteristics of the operating teams and organizations.

- **Interfaces:** among the foregoing.

The offshore structure system is measured in two types of criteria:

- Quality: which is a combination of serviceability, safety, durability and compatibility

- Reliability: the likelihood of developing acceptable quality from design phase to decommissioning.

The quality management system consists of three basic components:

- Quality Management Procedures: documentation that specify the requirements and procedures for quality management.

- Assessors: the people from the system (operators, mangers, engineers, regulators) and counselors who have extensive experience with the system and operations.

- Evaluation: The quality assessment team assigned grades (normal, best, worst etc,) for each of the component factors as well as recommendations for improvement.

The quality management system may be implemented to reduce the likelihood and consequence of the malfunctions and increase the detection and correction of malfunctions. The system risk analysis may be conducted to characterize the human and organizational factors and their effects on the performance of a system using a couple of tools such as

- HazOp (Hazard Operability) and FMEA (Failure Mode and Effects Analysis) etc.
- Probabilistic Risk Analysis:
- Quantitative Risk Assessment:
- Structural Reliability Assessment:

33.7.2 Reducing Human & Organizational Errors in Design

To assure the quality in the design of offshore structures, there are three approaches for risk management:

- Proactive: reduce incidence of malfunctions.
- Reactive: increase detection and correction of malfunctions, and
- Interactive: reduce occurrence and effects of malfunction.

Several approaches may be applied to reduce human errors:

- **Organizations Change:** (1) avoiding compromise of the quality and reliability assurance while the management is seeking greater productivity and efficiency. (2) preventing loss of corporate memory due to corporate down-sizing because it has been a cause in many cases of structural failure. (3) establishing policies that positively improving human performance (e.g. reward people for self improvement and accomplishment). (4) developing a safety culture.

- **Improving Performance of Operating Teams:** (1) training people to avoid mistakes and incorrect communications that may cause failures. (2) taking QA/QC measures to prevent errors, detect errors and correct them. Self-check, independent check and third-party check may be useful for the QA/QC measures.

- **Hardware/Equipment Change:** (1) providing equipment compatible with fundamental human capabilities (e.g. labels that can be read from reasonable distance). (2) eliminating opportunities for human errors (e.g. controls and displays can be simplified to minimize potential confusion and to provide clearer information.).

- **Procedure Improvement and Software Verification:** (1) ensuring current and accurate procedures are used (2) eliminating errors embedded in the procedures and guidelines (3) avoiding use of the guidelines out of their validity envelopes. (3) applying 3rd party verification of the software.

- **Environmental Change:** providing an environment (comfortable temperature, adequate lighting, and limited noise) compatible with the physical requirements of the human conducting the operation.

33.8 References

1. ABS (1998), "Guidance Notes on the Application of Ergonomics to Marine Systems", American Bureau of Shipping, January.

2. ASTM (1988, 1995) "ASTM F1166-95a: Standard Practice for Human Engineering Design for Marine Systems, Equipment and facilities", American Society of Testing and Materials.

3. Basra, G. and Kirwan, B. (1996), "Collection of Offshore Human Error Data". OTO Report 95-037, HSE books.

4. Bea, R.G. (1994), "The Role of Human Error in Design, Construction and Reliability of Marine Structures", Ship Structures Committee, SSC-378.

5. Bea, R.G. (1995), "Quality, Reliability, Human and Organization Factors in Design of Marine Structures", OMAE-1995.

6. Bea, R.G. et al (1997), "Quality Assurance for Marine Structures", Report of Specialist Panel V.1", the International Congress of Ship and Offshore Structures.

7. Bea, R.G., (2001), "Human Factors and Risk Management of Offshore Structures", Proceedings of the International PEP-IMP Symposium on Risk and Reliability Assessment for Offshore Structures", Mexico City, Dec. 3-4, 2001.

8. Bea, R.G. (2002), "Human & Organizational Factors in Design and Operation of Deepwater Structures", OTC 14293.

9. Bergman, B. and Klefsjo, V. (1994), "Quality – from Customer Needs to Customer Satisfaction", Studentlitteratur, ISBN 91-44-46331-6.

10. Cacciabue, C., et al (1989), "COSIMO: A Cognitive Simulation Model in Blackboard Architecture: Synergism of AI and Psychology". In the Proceedings of the Cognitive Science Approaches to Process Control Conference, Italy.

11. IACS (1999), "Draft Guidance on Human Reliability Analysis (HRA) within the Formal Safety Assessment", IMO MSC 71/Wp.15/Add.1.

12. IMO (1997), "MSC/Circ. 829 & MEPC/Circ. 335, Interim Guidelines pn the Application of Formal Safety Assessment (FSA) to the IMO Rule-Making Process", International Maritime Organization.

13. Lorenzo, D.K., (1990), "A Manager's Guide to Reducing Human Errors – Improving Human Performance in the Chemical Industry", Chemical Manufacturers Association.

14. Moore, W.H. (1994), "The Grounding of Exxon Valdez: An Examination of the Human and Organizational Factors", Marine Technology, Vol.31, No.1, Jan. 1994, pp. 41-51.

15. Kirwan, B. and Ainsworth, L. K. (1992), "*A Guide to Task Analysis*", Taylor & Francis, UK

16. Kirwan, B. (1994), "*A Guide to Practical Human Reliability Assessment*", Taylor & Francis, UK

17. Kletz, T. (1974), "HAZOP and HAZAN – Notes on the Identification and Assessment of Hazards", Institute of Chemical Engineers.

18. Rasmussen, J., Pedersen, O. M., Carnino, A., Griffon, M., Mancini, C., and Gagnolet, P. (1981), "Classification System for Reporting Events Involving Human Malfunctions", Report Riso-M-2240, DK-4000, Riso National Laboratories, Denmark

19. Reason, J. (1990), *"Human Error"*, Cambridge University Press, UK

20. Reason, J. (1997), *"Managing the Risks of Organizational Accidents"*, Ashgate, UK

21. Swain, A. D. (1989), "Comparative Evaluation of Methods for Human Reliability Analysis", ISBN 3-923875-21-5, GRS-71

22. Swain, A. D. and Guttmann, H. E. (1983), "A Handbook of Human Reliability Analysis with Emphasis on Nuclear Power Plant Applications", Nureg/CR-1278, with Addedum #1 to Nureg/CR-1278 in Sept. 1985 by Swain, A.D., US Nuclear Regulatory Commission (USNRC), Washington DC-20555.

23. Woods, D. D., et al (1987), "An Artificial Intelligence based Cognitive Model for Human Performance Assessment", NUREG/CR-4852, USNRC, Washington DC.

Part V

Risk Assessment

Chapter 34   Risk Centered Maintenance

34.1 Introduction

34.1.1 General

Offshore maintenance covers engineering tasks for various offshore facilities and equipment, from the seabed to the topside. The tasks include routine maintenance, inspection and repair of these facilities, and modifications / enhancements to the plant and the equipment.

The maintenance of offshore facilities presents many unique difficulties, which are not usually encountered in inland applications. This is mainly due to factors such as:

- Statutory requirements for safety are very restrictive
- Improper maintenance often results in big losses in terms of safety, environment protection, production, materials damage, and reputation in case of breakdown
- Maintenance costs are relatively high due to high costs of manpower, offshore storage, transportation between onshore and offshore, etc.
- It is much more difficult to perform a maintenance task in the splash zone and subsea
- Maintenance activities are often restricted by seasons (e.g. adverse weather conditions)
- Logistics offshore can be the greatest problem to be resolved for an actual maintenance task to be carried out

Therefore, operators for offshore installations usually establish good maintenance programs to ensure that the production programs are met in terms of safety, reliability, availability, quality, and quantity of supplies.

Scheduled (proactive) maintenance includes two major classifications:

- *Preventive Maintenance*: Maintenance task frequencies are determined from a known relationship between time (number of cycles, usage, age etc.) with reliability (survival probability with respect to wear-out, corrosion, fatigue etc.).
- *Predictive Maintenance*: Condition-based maintenance tasks are scheduled based on the achievement of certain routinely measured conditions. The P-F interval is defined as the distance from the point where we can find potential failure to the point where failure actually occurs (Moubray, 2000). Condition-based maintenance tasks must be conducted at intervals less than the P-F interval.

This chapter describes the application of risk analysis to maintenance of facilities on offshore installations. It mainly consists of Preliminary Risk Analysis (PRA) and Reliability Centered

Maintenance (RCM). The basic concept, principles and applications of PRA and RCM are introduced for the development of an effective preventive maintenance program for offshore facilities. PRA and RCM are methods that have been used for the development and optimization of maintenance strategies in a structured and systematic way. They have been widely used in the past years in many industries like nuclear power plants, aircraft's, and the offshore industry.

34.1.2 Application

This chapter is conceived to be a guide for the development and optimization of maintenance strategies. The roles of PRA and RCM in the maintenance process are illustrated in Figure 34.1 (Rausand and Vatn, 1997). As shown in the figure, PRA analyses shall be performed for screening and rating maintainable items.
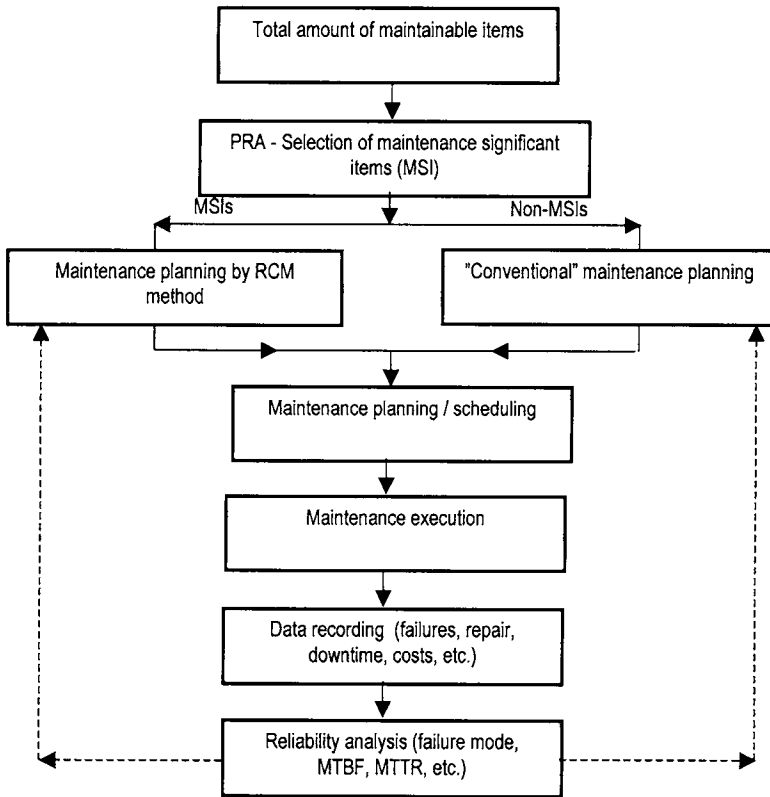
Figure 34.1   The Roles of PRA and RCM in Maintenance Processes

The RCM analysis is then carried out on the items where preventive maintenance is recommended. This means that RCM process should focus on maintenance-significant-items (MSI), while the remaining items can be assigned with maintenance tasks by the more traditional methods. However, all planned maintenance tasks will ultimately be integrated in a common maintenance planning and control system.

34.1.3 RCM History

RCM was first formulated for the commercial aircraft industry in the late 1960s (Jones, 1995, Rausand and Vatn, 1997). It started as a result of using of reliability methods by two US airliners to analyze the data they collected. For instance they plotted the probability of failure of components against age. To their surprise, it was found that only about 10% of the whole range of units became less reliable with advancing age. This was not because the intervals were not short enough, or inspections were not sufficiently thorough. Rather, it was contrary to expectations, for many items, the frequency of failures did not increase with operating age. Consequently, a maintenance policy based exclusively on some maximum operating age would, have little or no effect on the failure rate, no matter what the age limit was. This forced them to re-think the basis for preventive maintenance (PM), which at that time consisted of time-based overhauls with a considerable cost.

The Federal Aviation Agency (FAA) that is responsible for regulating airline activities in the USA, was frustrated, because it was not possible for airlines to control the failure rates of certain engines by any feasible changes in the PM policy. As a result, in 1960 a task force was formed, consisting of representatives from both the FAA and the airlines, to investigate the capabilities of preventive maintenance.

The task resulted in a FAA / Industry Reliability Program, which was issued in November 1961. The program was directed specifically at propulsion engine reliability. Further work during the 1960s in the development of PM programs for new aircrafts, showed that more efficient programs could be developed through the use of a logical decision processes. This work was performed by a Maintenance Steering Group (MSG-1, 1968), that consists of representatives from the aircraft manufactures, airline companies, and the FAA.

This group developed the first version of RCM, and it was issued as a handbook in 1968. This new maintenance philosophy was designated MSG-1, and was used as basis for development of the PM program for Boeing 747 (Jumbo-jet). In due time, the RCM-concept was further developed for use by the aircraft industry. Two revisions were made, an MSG-2 document issued in 1970, and an MSG-3 in 1980.

After the initial use of the wide-bodied aircraft (Boeing 747, DC 10, L1011 Tristar) the method was adapted and used by a European aircraft industry (Concorde, Airbus A300) and the latest type of aircraft from USA (e.g. Boeing 757, 767).

In the early 1970s, the US Navy started to apply the RCM methodology to both new and in-service aircrafts. Shortly thereafter, the Naval Systems Command applied RCM to surface ships, and in 1980 RCM became the required method for defining PM programs for all new Naval surface ships. The Canadian Navy then followed the same steps. The US Army and the Air Force also adopted the RCM approach.

In 1983 a pilot study was initiated to testing the reliability of the method for nuclear power plants by the Electric Power Research Institute (EPRI). They evaluated whether a maintenance method that has been successfully applied in aircrafts and ships may also be suitable for nuclear power plants. From a system point of view all are highly redundant complex and have high reliability. They are all regulated by governmental agencies (the airlines are monitored by FAA, the military has Congress, and nuclear power plants are controlled by the Nuclear Regulatory Commission). EPRI (1985) documented that RCM applications to nuclear power plants are promising. Several labor and material intensive maintenance tasks that were performed at specified time intervals before applying RCM were now performed only when

the equipment degraded to a certain measurable conditions. Savings were achieved through reduced maintenance costs and enhanced reliability.

RCM Applications to maritime industry, solar receiving plants and coal mining are discussed in Jones (1995).

34.2 Preliminary Risk Analysis (PRA)

34.2.1 Purpose

The purpose of a PRA process can be summarized as follows:

- Screen operating units within a plant used to identify areas of higher risk

- Assign a risk level to each equipment item based on a consistent methodology

34.2.2 PRA Procedure

The application of PRA in offshore installations is a qualitative approach. It uses the same concepts of consequence and frequency as the quantitative analysis described in the previous chapters, except that it requires less detail and can be conducted fairly quickly. While the results it yields are not as precise as those of the quantitative analysis, it provides a basis for rationalizing maintenance efforts based on potential risks associated with each item.

The analysis first categorizes the failure consequences within the area, and then failure frequency. Tables 34.1 and 34.2 illustrate examples of relevant definitions.

After the categories of consequences and frequencies have been defined, they are combined in a risk matrix to produce a risk rating, as shown in Figure 34.2.

The probability category is determined by evaluating factors that may affect the occurrence of failures. Each factor can be weighted, and their combination results in the probability. The factors that may affect probability are:

- Potential damage mechanisms

- Current equipment condition

- Nature of the process

- Equipment design basis

Appropriateness of basis services like lube, cleaning, and inspection

Table 34.1 Classification of Failure Consequences

Consequence Categories	Consequences to Health, Safety, or Environment
I – Catastrophic	May cause deaths, or severe impact on the environment
II – Critical	May cause severe injury, or severe occupational illness, or major impact on the environment
III – Marginal	May cause minor injury, or minor occupational illness, or minor impact on the environment
IV – Negligible	Will not result in a significant injury, or occupational illness, or provide a significant impact on the environment

Table 34.2 Classification of Failure Probabilities

Frequency Categories	Nominal Range of Frequency per Year
A – Often	$> 10^{-1}$
B – Likely	10^{-1} to 10^{-2}
C – Unlikely	10^{-2} to 10^{-3}
D – Incredible	$< 10^{-4}$
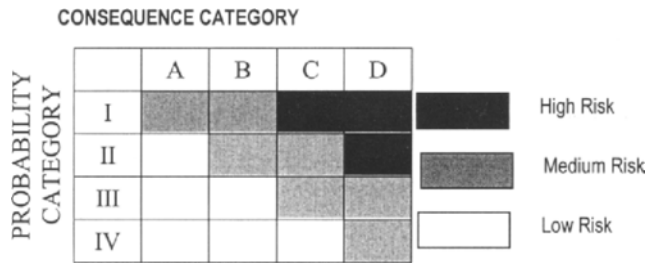
Figure 34.2 Qualitative Risk Matrix

The consequence category may be determined by considering the factors that may influence the magnitude of a hazard like:

- Inherent tendency that a failure may occur

- Operating conditions

- Possibility of escalation from minor to serious conditions

- Engineered safeguards in place

- Degree of exposure to damage

When the resulted categories of failure consequence and frequency are plotted on the risk matrix, they give an indication of the level of risk for the unit being evaluated.

The PRA process will result in assigning each unit with a risk rating: high, medium, or low. The risk rating is often called criticality. The relevant PRA process is also called a criticality analysis. The resulting risk rating may be used to group maintenance items into three categories:

- Items with a risk rating of high or medium: The items with medium risk ratings shall be further analyzed by RCM process in order to reduce the risk as low as reasonably practicable (ALARP), which shall be detailed in the following Sections.

- Items with a low risk rating: These items fall in the acceptable risk region. They may therefore be maintained using traditional maintenance methods or even "break-down" maintenance strategies.

- Items with high-risk rating belong to the unacceptable risk region: These items shall be subject to further detailed analysis regarding design, engineering, risk, and/or maintenance. The possible decisions include change of design/engineering and adding protection measures and redundancy, and development of various preventive maintenance measures such as condition monitoring, inspection, etc.

34.3 RCM Process

34.3.1 Introduction

According to the Electric Power Research Institute (EPRI), RCM is:

"A systematic consideration of system functions, the way functions can fail, and a priority-based consideration of safety and economics that identifies applicable and effective PM tasks."

RCM is defined as a process for determining what must be done to ensure that any equipment/facility continue to do whatever its users expect it to do. The main focus of RCM is hence on the system functions, and not on the system hardware.

34.3.2 RCM Analysis Procedures

Before an actual RCM analysis is initiated, an RCM project team shall be established. The team shall include at least one person from the maintenance function and one from the operation function, in addition to an RCM specialist who serves as the facilitator for the RCM process.

The RCM team shall define the objectives and the scope of work. Requirements, policies, and acceptance criteria shall be clarified with respect to health, safety, and the environment (NPD, 1991). RCM analysis typically focuses on improving the PM strategy. It is however, possible to extend the analysis to cover topics like corrective maintenance strategy, spare parts, etc. The RCM team shall clearly define the scope of the analysis. An RCM analysis process may be carried out as a sequence of activities, as the 6 steps described in the following (Rausand and Vatn, 1997, Jones, 1995):

Step 1: System Selection and Definition

The first question in the RCM analysis is "Which systems shall be analyzed by the RCM process ?". This question is normally answered before the RCM analysis project is approved because clear reasons are needed to justify initiation of an RCM analysis. The reasons can be, for example, some systems have failed too often and/or have resulted in serious consequences in terms of safety, environmental protection, and production.

The system is divided into sub-systems that are not over-lapped each other. The level of technical hierarchy may be defined as:

- Plant: A logical grouping of systems that function together to provide an output by processing various input of raw materials and feed stock. E.g. an offshore oil and gas production platform may be considered as a plant.

- System: A logical grouping of subsystems/main equipment that will perform a series of main functions, which are required by the plant. Examples of the systems are water injection and gas compression systems on an oil and gas production platform.

- Subsystem/main equipment: A logical grouping of equipment/units that mainly perform one function, e.g. one water injection package and one gas compressor.

- Equipment/instrument: A grouping or collection of components which can perform at least one significant function as stand-alone items, e.g. pumps, valves, and pressure indicators.

- Component: The lowest level at which equipment can be disassembled without damage or destruction to the items involved, e.g. an impeller in a pump, a bearing in a gas compressor.

It is very important that the RCM team decides on which level the analysis shall be carried out in the initial phase of the RCM process. There are some constraints for this issue, for example, the project's time schedule, the availability of information regarding failures, the maintenance efforts and costs, available experience, and know-how on the systems involved. In an ideal situation, an RCM analysis should be performed from the system level down to the component level. The analysis of functions and functional failures should be applied to all the levels above the component level. The failure modes and reasons should be applied to the component level.

Step 2: Functional Failure Analysis

Functional failures are the different ways a subsystem can fail to perform its functions. The tasks of a functional failure analysis are:

- To identify and describe the required functions for systems, subsystems, and equipment

- To describe input interfaces required for the system to operate

- To identify the ways in which the system might fail to function

A system may have different functions that can be categorized in different ways, e.g.:

- Based on importance:

  - Main (essential) function: These are the functions required to fulfill the main design service. An essential function is often reflected in the name of the item. An essential function of a pump is, for example, is to pump fluid.

  - Auxiliary functions: These are the functions that are required to support the essential functions. They are usually less obvious than the essential functions, but may, in certain cases, be as important as the essential functions. An auxiliary function of a pump is containment of the fluid.

- Based on functionality:

  - Protective functions: which, for example, provide protection for safety, environment.

  - Information functions: which comprise condition monitoring, various gauges, alarms, etc.

  - Interface functions: which apply to the interfaces between the item in question and other items.

Note that the classification of functions should only be used as a checklist to ensure that all relevant functions are revealed. A system may generally have several operational modes, and

several functions for each operating mode. The essential functions are often obvious and easy to establish, while the other functions may be rather difficult to reveal.

The identified system functions may then be represented by functional diagrams of various types. The most common diagram is the so-called functional block diagram. A simple functional block diagram of a pump is shown in Figure 34.3.
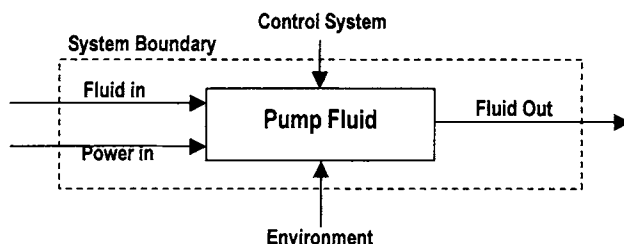
Figure 34.3   Functional Block Diagram for a Pump

As shown in Figure 34.3, a functional diagram includes all inputs (control signals and power supplies) and outputs. It is generally not required to establish functional block diagrams for all system functions. The diagrams are, often considered as efficient tools to illustrate the input/output interfaces of a system boundary.

The last task of the functional failure analysis is to identify and describe how the system functions may fail. In most of the RCM references, functional failures may be classified into three groups:

- Total loss of function: In this case, a function is not achieved at all, or the quality of the function is far beyond what is considered acceptable.

- Partial loss of function: This group may be very broad, and may range from the nuisance category to almost the total loss of the function.

- Erroneous function: This means that the item performs an action that was not intended, often it performs the opposite of the intended function.

Step 3: Failure Modes and Effects Analysis (FMEA)

The dominant failure modes are developed from a failure modes and effect analysis. The FMEA identified specific conditions that need to be prevented by preemptive maintenance. After having defined system functions and functional failures, the next logical step is to identify failure modes, which may cause each identified functional failure. For example, a functional failure analysis identified that a booster pump was designed to increase water from 5 bar at the inlet to 25 bar at the outlet. Sometimes it is not able to deliver water to 25 bar. Therefore, it has a functional failure – partial loss of function. In the FMECA step, the tasks are to find out what may cause this functional failure and what maintenance methods may be cost-effective enough to prevent the failure.

System: Performed by:

Ref. Drawing no: Date:

Description of unit			Failure Mode	Failure Effects								Criticality	Failure Cause	Failure Mechanism	Failure Characteristic	Maintenance Methods	Recommended Interval
MSI	Operation	Function		Failure Severity				Failure Likelihood									
				S	E	P	C	S	E	P	C						

Figure 34.4   Example of an RMECA Form

A variety of FMECA forms are used in the RCM analysis. An example of the FMECA forms is shown in Figure 34.2. The various columns in the form are discussed below:

MSI: the item number (tag number).

Operational mode: for example running or standby.

Function: e.g. a function of standby water supply pump is used to start pump upon demand.

Failure mode: the manner by which a failure is observed and is defined as non-fulfillment of one of the equipment functions.

Failure severity: described in terms of the "worst case" impacts on safety, environmental protection, production loss/delay and other economic costs. The severity classes may be defined using an approach that is similar to the consequence categories for qualitative risk analysis.

Failure likelihood: defined as the "worst case" probability of failure. In this stage, qualitative classes are appropriate. The relevant likelihood classes can be defined using a procedure that is similar to the probability categories for qualitative risk analysis.

Criticality: can be derived by combining the relevant failure severity and likelihood. The procedure is similar to determining risk levels of systems, sub-systems, and equipment. However, the difference is that criticality considers failure modes.

The information described so far should be considered for all failure modes. A screening process is now appropriate, giving only critical failure modes.

For the critical failure modes the following fields are required:

Failure cause: For each failure mode there may be more than one failure cause. Note that all components should be considered at this step. A "fail to close" failure of a safety valve may for example be caused by a broken spring in the actuator.

Failure mechanism: Examples of failure mechanisms are fatigue, corrosion, and wear.

Failure characteristic: Failure propagation may be categorized as:

- Gradual failure: The progress of failure propagation can be measured by inspection or condition monitoring techniques.

- Aging failure: The failure propagation is age-dependent, i.e. a wear-out process.

- Sudden failure: Random failure that may not be detected by condition monitoring measures.

Maintenance method: May hopefully be found by the logic decision applied in Step 5. This field shall be completed in Step 5.

Recommended task interval: The identified maintenance action should recommend an estimated time interval, which shall be performed in Step 5.

Step 4: Selection of Maintenance Methods

Decision logic is designed and used to guide the RCM team through a question-and-answer process. The input to the decision logic is the dominant failure mode identified in Step 1. The design of decision logic is based on the principle: preventive maintenance measures should be specified whenever they exist and are cost-effective against a critical failure.

There are generally three reasons for applying a preventive maintenance task:

- To detect failures at their early stage in order to have more time to plan and execute preventive measures

- To prevent equipment to fail with serious consequences

- To discover hidden failures

Only the critical failure modes shall be subjected to preventive maintenance. The selection of appropriate maintenance methods is dependent on the following factors:

- Failure causes and mechanisms

- Failure characteristics

- Detection techniques

The basic maintenance methods may be classified as follows:

- Scheduled on-condition task

- Scheduled overhaul

- Scheduled replacement

- Scheduled function test

- Run to Failure

Scheduled on-condition task is a scheduled inspection or condition monitoring of an item at regular intervals to find potential failures. The following criteria shall be met:

- Potential failure condition can be clearly defined

- Potential failures can be detected by a condition monitoring technique

- There is a reasonable consistent time interval for failure detection and prevention.

Scheduled overhaul can be applied to an item at or before a certain specified age limit. An overhaul task may be applicable to an item when the following criteria are met:

- There is an identifiable age after which the item's failure rate increases rapidly
- Failure resistance of the item can be restored by overhaul

Scheduled replacement is a scheduled elimination of an item or its parts at or before a certain age limit. A schedule replacement program can be applied under the following circumstances:

- There exists an identifiable age after which the item's failure rate increases rapidly
- Failure resistance of the item can be restored by replacing the item or its parts

Scheduled function test is a scheduled inspection of a hidden failure, which is normally an on-demand failure. A SFT may be performed on an item under the following conditions:

- A functional failure is not evident to the operating crew during the normal duty
- No other type of preventive tasks are as cost-effective

Run to failure is a deliberate decision allowing an item to run to failure. The main reason for run to failure may be that no other preventive tasks are possible or as cost-effective

The criteria given for using the preceding tasks serve only as guidelines for selecting a suitable preventive task. An example of the RCM decision logic is illustrated in Figure 34.5. Note that this is a simplified version of the decision logic. Such decision logic can not cover all situations. For example, a hidden function with aging failures may be prevented by a combination of scheduled replacements and function tests.
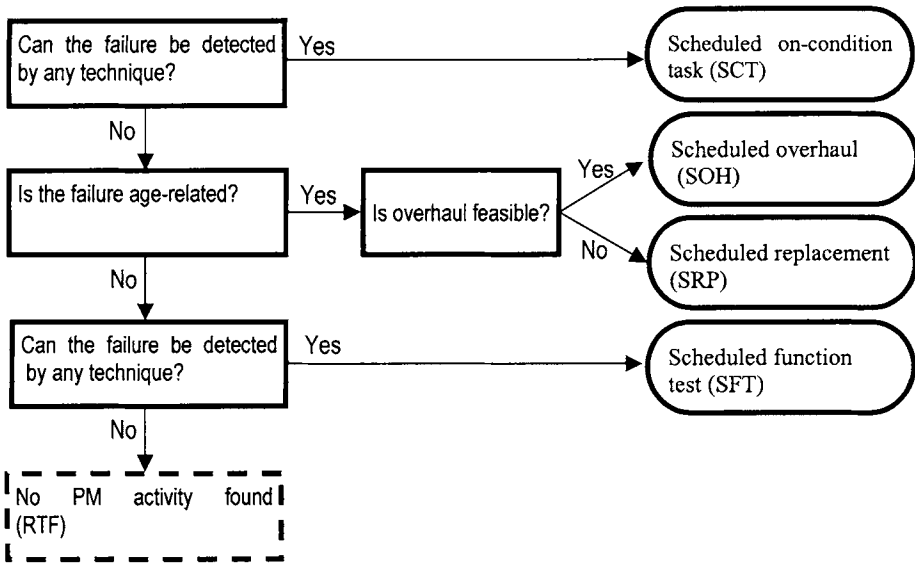
Figure 34.5   RCM Decision Logic

Step 5: Determination of Maintenance Task Intervals

After selecting preventive maintenance methods for each critical failure mode, the next step is to determine the time interval for each selected maintenance task.

The shorter the activity interval, the higher the maintenance cost. On the other hand, the longer the activity interval the higher the risk of failure to occur. The optimal interval should mathematically be set at the minimum of the sum of the failure risk and maintenance costs. This is typically the task of a benefit-cost analysis. The maintenance cost is more or less easy to estimate. Unfortunately, the benefit of a maintenance task is difficult to assess since it depends on the following parameters:

- Risk: failure consequence and likelihood, possibly causing an impact on:
  - Safety
  - Environment
  - Production and/or services
  - Material damage
  - Reputation
- Risk reduction by the maintenance task, which depends on:
  - Failure causes
  - Failure mechanism and distribution
  - Characteristics of the maintenance task such as SCT, SOH, SRP, or SFT

The optimization of maintenance task intervals usually requires a quantitative analysis. The detailed description of the optimization process is not within the scope of this book.

Step 6: Implementation of Maintenance Tasks

Implementation is not a direct task of an RCM analysis. However, in most cases, the results of an RCM analysis shall be implemented. A necessary basis for the implementation is that the organizational and technical functions fully understand and support the results of the RCM analysis.

The maintenance actions recommended by an RCM analysis are usually failure-oriented. In practice, maintenance work orders are normally issued on equipment packages or modules. Therefore, the maintenance actions resulting from the RCM analysis should be grouped into maintenance program packages with a description of where, when, and what to do.

The necessary resources and skills are then allocated to implement the maintenance tasks.

A more comprehensive discussion of RCM may be found in Moubray (2000) including the RCM decision diagram, implementing RCM recommendation, applying the RCM process and measure RCM achievements. The implementation process includes:

- All the RCM recommended maintenance tasks are approved by the managers with the overall responsibility for the equipment/facility.
- All Routine task descriptions are upgraded in detailed task instructions clearly and concisely.
- Routine task descriptions are incorporated into work packages.

- The work packages are implemented in systems that ensure the work is done.

34.3.3 Risk-Centered Maintenance (Risk-CM)

Risk-Centered Maintenance (Risk-CM)

RCM began in U.S. commercial aviation industry for maintenance for highly redundant aircraft. Criticality class in a RCM is categorized with respect to safety, operation/production, economics and hidden failure. The difference between Risk-CM and RCM is that the criticality class in RCM is replaced with a direct evaluation of risks in Rick-CM (Jones, 1995). The direct risk evaluation gives a more complete description of the hazards than the coarser assessment (criticality class). This Risk-CM involves independent estimation of frequency and consequence for each failure mode, providing the ranking mechanism based on risk concept. When risks are calculated for individual failure modes, it is possible to rank priority for maintenance tasks based on the risks. Qualitative risk assessment may be fairly adequate for Rick-CM as comparative risks are sufficient for priority ranking. It is not require to accurately estimate absolute risks. Consistency between the risk evaluations is rather important. There are however, two difficulties in applying Risk-CM (1) risk concept is still not fully accepted by the industry in some areas (2) there is indeed a lack of data for the adequate evaluation of risks, in particular for some new applications on which little industry experience exists.

Operational Risk Assessment

Operational risk assessment is performed on process critical equipment and facilities. Its objective is to focus maintenance resources (money and manpower) in the plants that have highest risk. Operational risk assessment starts with data gathering and evaluation. The data used for operation risk assessment are usually collected during the equipment/facility operations. There are three major contributors to the operational risk, namely:

- *Equipment*: It is no doubt that the equipment is a major contributor to operational risk. Equipment is operated by human to produce products. Maintenance activities are performed on equipment.

- *Production*: Loss production (including scheduled maintenance and turnaround) and product quality below standards are an operational risk. Production loss may be due to equipment failure, lack of raw material supplies, shortage in packaging, shipping and storage.

- *Human*: Humans are the key contributors to operational risk. People often cause system failure and make up costs when equipment fails and production reduced, e.g. in terms of labor costs.

Human Contribution to Risk

People are an integral part of plant operation and maintenance, and take the main liabilities. There are two types of human errors (Jones, 1995):

- *Active errors*: result in instantly observable effects.

- *Latent errors*: Have consequences that are not realized for relatively long period of time until they combine with other factors that result in accidents.

Machine operation used to be more hands on activities. As computer promoted people to higher level, the information people receive is computer displays in control room. Latent failures are generally major players in these situations.

Fatigue and other human factors such as drinking and driving make great contribution to risks. Fatigue induced risks become larger when control responsibilities are concentrated in a few people.

34.3.4 RCM Process - Continuous Improvement of Maintenance Strategy

It can be seen from the preceding Section that the RCM process is a systematic process used to make decisions about the maintenance strategy. It is a powerful tool for developing the initial maintenance strategy by rationalizing maintenance efforts. It should also be used for continuous improvement of the existing maintenance strategy. In fact, the full benefit of RCM is achieved when the operation and maintenance experience is fed back into the analysis process.

The process of updating the RCM analysis results is important due to the following facts:

- An RCM analysis is usually based on many assumptions due to lack of reliability data

- The operation conditions and equipment status are changing over time

- Real reliability data, knowledge, and know - how's, are growing with time

The maintenance strategy should be updated continuously using RCM processes. The continuous improvement may follow the steps presented below:

- Assign criticality to equipment, components, and failures based on historical data, e.g. failure consequences, maintenance costs, etc.

- Compare the updated criticality with that developed from the early RCM study and update or replace the assumptions with the historical reliability data

- Perform cost-benefit analyses to identify where the modification of the existing maintenance strategy may increase reliability and reduce the costs

- Modify the existing maintenance strategy to increase the cost-effectiveness of the maintenance strategy

34.4 References

1. EPRI (1985), *"Application of Reliability-Centered Maintenance to Component Cooling Water System at Turkey Point Units 3 and 4"*, EPRI NP-4271, October.

2. Jones, R.B. (1995), *"Risk-Based Management – A Risk Centered Approach"*, Gulf Publishing Company, Houston.

3. Moubray, J. (1992), *"Reliability Centered Maintenance"*, Industrial Press, Inc.

4. MSG1(1968): *"747 Maintenance Steering Group Handbook: Maintenance Evaluation and Program Development (MSG-1)"*, Air Transport Association, July.

5. NPD (1991), "Regulations Concerning Implementation and Use of Risk Analysis in the Petroleum Activities", Norwegian Petroleum Directorate, 1991.

6. Rausand and Vatn (1997), *"Reliability Centered Maintenance"*, NTNU.

SUBJECT INDEX